

UNCLASSIFIED

AD 405 923

DEFENSE DOCUMENTATION CENTER

FOR

SCIENTIFIC AND TECHNICAL INFORMATION

CAMERON STATION, ALEXANDRIA, VIRGINIA



UNCLASSIFIED

NOTICE: When government or other drawings, specifications or other data are used for any purpose other than in connection with a definitely related government procurement operation, the U. S. Government thereby incurs no responsibility, nor any obligation whatsoever; and the fact that the Government may have formulated, furnished, or in any way supplied the said drawings, specifications, or other data is not to be regarded by implication or otherwise as in any manner licensing the holder or any other person or corporation, or conveying any rights or permission to manufacture, use or sell any patented invention that may in any way be related thereto.

ASD-TDR-63-260

405923

**T
&
A**

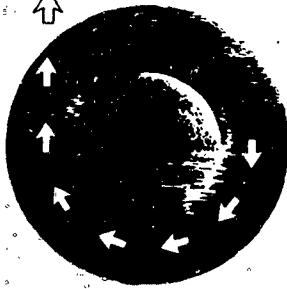
**Proceedings of the First Space Vehicle
Thermal and Atmospheric Control Symposium**



TECHNICAL DOCUMENTARY REPORT NO. ASD-TDR-63-260



April 1963



Flight Accessories Laboratory
Aeronautical Systems Division
Air Force Systems Command
Wright-Patterson Air Force Base, Ohio

405 923

Project No. 6146

BDC
RECEIVED
JUN 13 1963
TISIA A

NO.OTS

**Best
Available
Copy**

NOTICES

When Government drawings, specifications, or other data are used for any purpose other than in connection with a definitely related Government procurement operation, the United States Government thereby incurs no responsibility nor any obligation whatsoever; and the fact that the Government may have formulated, furnished, or in any way supplied the said drawings, specifications, or other data, is not to be regarded by implication or otherwise as in any manner licensing the holder or any other person or corporation, or conveying any rights or permission to manufacture, use, or sell any patented invention that may in any way be related thereto.

ASTIA release to OTS not authorized.

Qualified requesters may obtain copies of this report from the Armed Services Technical Information Agency, (ASTIA), Arlington Hall Station, Arlington 12, Virginia.

Copies of this report should not be returned to the Aeronautical Systems Division unless return is required by security considerations, contractual obligations, or notice on a specific document.

Foreword

This report consolidates the technical presentations and papers from the Space Vehicle Thermal and Atmospheric Control Symposium, sponsored by the Aeronautical Systems Division on 12 and 13 Feb 1963. Effort in this area is supported under Project 6146, "Flight Vehicle Environmental Control." E. B. Thompson of the Environmental Control Section, Flight Accessories Laboratory, acted as Symposium Program Manager and monitor of this report.

On behalf of the Aeronautical Systems Division, acknowledgement is made to the Chairmen, the various committees, the speakers and authors, and the attendees for their excellent response and interest before, during and after the symposium. The Aeronautical Systems Division is proud to have provided this opportunity for competent exchange of technical information, an exchange in which we hope you will continue to take part.

Abstract

This report presents various papers concerning Space Vehicle Thermal and Atmospheric Control Systems. Papers include those presented or submitted by both industry and Governmental Agencies for the first Space Vehicle Thermal and Atmospheric Control Symposium held on 12 and 13 February 1963. The symposium was sponsored by the Flight Accessories Laboratory, Aeronautical Systems Division of the Air Force Systems Command. The specific areas include: (1) Analysis of environmental control systems by application of digital computer techniques, (2) Methods for Synthesizing Environmental Control Systems, (3) Atmosphere Control Problems in long duration space vehicle missions, (4) Control of contaminants present in closed atmospheres, (5) Various techniques for recovering oxygen from carbon dioxide, such as carbon dioxide reduction by hydrogen and photosynthesis, (6) Heat transfer in pool boiling as affected by an electric field, (7) Various techniques of thermal analysis of structures, (8) A general computer program for the determination of radiant-interchange geometric configuration factors, and (9) Temperature control systems for satellites and probe vehicles.

Publication Review

Publication of this technical documentary report does not constitute Air Force approval of the report's findings or conclusions. It is published only for the exchange and stimulation of ideas.

FOR THE COMMANDER:


WILLIAM C. SAVAGE
Chief, Environmental Branch
Flight Accessories Laboratory

TABLE OF CONTENTS

Proceedings of the First Space Vehicle Thermal and Atmospheric Control Symposium

Section I

	Page
Introduction	2
Session I - Environmental Control Systems	
Thermal and Atmosphere Control for Manned Interplanetary Vehicles, J. Smith, R. Jagow, and L. A. McKellar, Lockheed Aircraft Corporation, Sunnyvale, California.	5
Methods for Synthesis of Optimal Environmental Control Systems, R. A. Paselk, North American Aviation, Downey, California.	41
Analysis of Thermal and Atmospheric Control Systems for Space Vehicles by Application of Digital Computer Techniques, Frederick H. Green, AiResearch Manufacturing Division, Garrett Corporation, Los Angeles, California.	83
Environmental Control Systems for a Manned Maneuverable Space Vehicle, E. P. Gebhardt, The Martin-Marietta Corporation, Denver, Colorado	117
Section II - Atmosphere Control Subsystems	
The Development of an Engineering Model Carbon Dioxide Reduction System, G. A. Remus, J. D. Zeff, and R. A. Bambenek, Mechanics Research Division, General American Transportation Corporation, Niles, Illinois.	161
Control of Organic Contaminants in Closed Atmospheres, Jack G. Christian, and J. Enoch Johnson, U. S. Naval Research Laboratory, Washington, D. C.	185
Oxygen Recovery System Integration for Long-Range Space Missions C. S. Coe and Jean Rousseau, AiResearch Manufacturing Division, Garrett Corporation, Los Angeles, California.	205

TABLE OF CONTENTS (Continued)

	Page
The Application of Chemically Regenerative Atmospheric Control Systems, J. G. Krisilas and J. W. Smylie, Aerospace Corporation, Los Angeles, California.	237
Photochemical Reactions Significant in Atmosphere Regeneration Processes, Dr. J. P. Allen, Aeronautical Systems Division, Wright-Patterson Air Force Base, Ohio.	299
Session III - Radiation and Thermal Analysis	
Space Radiator Experiment, Carl J. Feldmanis, Aeronautical Systems Division, Wright-Patterson Air Force Base, Ohio.	311
A General Computer Program for the Determination of Radiant-Interchange Geometric Configuration Factors, K. A. Toups, North American Aviation, Downey, California.	393
Heat Transfer in the Presence of an Electric Field, Dr. Harry Y. Choi, Tufts University and Dynatech Corporation, Cambridge, Massachusetts.	439
Thermal Analysis of Structures Including Radiation in an Enclosure, R. A. Knezek and G. J. French, Chance Vought Corporation, Dallas, Texas.	475
A Transient Thermal Analysis Digital Computer Program, R. Cannizzaro, Aeronautical Systems Division, Wright-Patterson Air Force Base, Ohio, W. Niehaus and R. Criss, Aeronca Manufacturing Company, Middletown, Ohio.	501
Session IV - Thermal Control Subsystems	
Effect of Electrical Potential on Boiling Heat Transfer, Dr. Michael Markels, Jr., and Dr. Robert L. Durfee, Atlantic Research Corporation, Alexandria, Virginia.	531

TABLE OF CONTENTS (Continued)

	Page
Thermoelectric Temperature Control in Satellites, C. Usiskin, Astro-Electronics Division, Radio Corporation of America, Princeton, New Jersey.	559
Selection of a Temperature Control System for a Mars Probe, C. V. Dohner, General Electric Company, Philadelphia, Pennsylvania.	581
Dynamic Response of Temperature Control Systems by the use of Digital Computer, F. I. Honea, North American Aviation, Downey, California.	609

Section II.

Associated Technical Papers

Transient Heat Transfer Analysis of Systems Involving Fluid Flow, John C. Grafton, North American Aviation, Downey, California.	651
The Condensing - Ejector Refrigeration System for Space Vehicles, Clarence A. Kemper and George A. Brown, Joseph Kaye & Company, Inc., Cambridge, Massachusetts.	673
Contamination Pattern in the Enclosed Atmospheres of Mercury Spacecraft, R. A. Saunders, U. S. Naval Research Laboratory, Washington, D. C.	709
Concurrent Cathodic Reduction of Carbon Dioxide and Anodic Production of Breathing Oxygen, R. E. Shearer, J. C. Kingland, and C. A. Palladino, Mine Safety Appliances Research Corporation, Callery, Pennsylvania.	725
Choice of an Atmosphere for an Extended Space Mission, Robert S. Thomas, Lockheed Missiles and Space Company, Palo Alto, California.	733

TABLE OF CONTENTS (Continued)

	Page
Thermal Environment Requirements in Manned Spacecraft, J. E. Janssen, Minneapolis-Honeywell Regulator Company, Hopkins, Minnesota.	761
Lithium Perchlorate Candles - A Lightweight Solid Chemical Oxygen Source, R. C. Oliver, Aeronutronic Division of Ford Motor Company, Newport Beach, California.	779
The use of Electric Fields to Orient Dielectric Liquids in a Zero Gravity Environment, Dr. John M. Reynolds, Dynatech Corporation and Massachusetts Institute of Technology, Cambridge, Massachusetts.	795
Means of Creating Simulated Variable Gravity Fields for the Study of Free Convective Heat Transfer, David A. Kirk, Aeronautical Systems Division, Wright-Patterson Air Force Base, Ohio.	821
Analytical and Experimental Investigation of Self-Thermostatic Effects, T. M. Olcott, and M. Ratner, Lockheed Missiles and Space Company, Palo Alto, California.	843
Spacecraft Thermal Control Using Cryogenic Hydrogen, G. M. Hall, and A. F. Knights, Walter Kidde and Company, Belleville, New Jersey.	877
Section III	
List of Attendees	899

ASD-TDR-63-260

SECTION I

Proceedings of the First
Space Vehicle Thermal and Atmospheric Control Symposium

Introduction

Edward B. Thompson

The Symposium on Space Vehicle Thermal and Atmospheric Control was conducted to present the complex requirements of environmental control systems for aerospace vehicles and those applied research efforts being conducted by Government and industry to meet these requirements. The intent was to stimulate thinking and technical discussion in problem areas encountered in the design and performance of environmental control systems. Accordingly, the symposium provided a unique opportunity for the productive exchange of ideas.

The provision of thermal and atmosphere control for flight vehicles entered a new sphere of technical problems with the advent of earth-orbital satellites and cislunar and planetary probes. The space environment with its singular conditions of zero gravity and near total vacuum introduced entirely new criteria for designing vehicle thermal and atmosphere control systems. The lack of an external atmosphere dictates that all vehicle waste heat ultimately be rejected by radiation heat transfer since no convective or conductive medium exists. In addition, respiratory supplies of oxygen for manned vehicles must be carried as stores unless atmosphere regeneration from carbon dioxide to oxygen can be accomplished of oxygen imposes a severe weight penalty. The lack of gravity is a hindrance to all phase separation processes occurring in the environmental control subsystems, since no normal body forces exist to effect liquid/gas separation. This presents serious difficulties in designing, for example, a vapor cycle system for vehicle cooling or water electrolytic cells for producing oxygen. These problems and many associated ones must be solved before practical thermal and atmosphere control systems for all types of space vehicles can be realized.

Col. John R. Hood, Deputy for Technology at the Aeronautical Systems Division, gave the welcome address. Mr. Peter R. Murray, Technical Director for the Deputy for Technology, presented the keynote address.

The Symposium proceedings which follow contain all the papers on which presentations were based as well as papers that were not presented. The papers are grouped according to symposium session and each is followed by the questions and answers it generated during the session discussion period. Every effort was made to faithfully reproduce the question and answer discussions as they actually occurred and persons participating are acknowledged wherever possible. The proceedings are concluded with a list of the names and addresses of all personnel attending the Symposium.

SESSION I
ENVIRONMENTAL CONTROL SYSTEMS

CHAIRMAN
WILBERT J. UHL, Jr.

**THERMAL AND ATMOSPHERIC CONTROL
FOR MANNED INTERPLANETARY VEHICLES**

by

J. B. Smith

R. B. Jagow

L. A. McKellar

**Lockheed Missiles and Space Co.,
Sunnyvale, California**

ASD-TDR-63-260

THERMAL AND ATMOSPHERIC CONTROL

FOR

MANNED INTERPLANETARY VEHICLES

J. M. Smith

R. B. Jagow

L. A. McKellar

INTRODUCTION

The development of efficient and reliable thermal and atmospheric control systems will be a major factor in establishing the feasibility of manned interplanetary flight.

It is the intent of this paper to explore some of the problems facing the thermal and atmospheric control system designer, as well as some of the presently considered solutions, in the areas of: atmosphere regeneration, trace contaminant removal, and thermal control, for a mission of approximately a year's duration involving orbital flights around Venus at altitudes ranging from 150 to 10,000 nm.

ATMOSPHERE REGENERATION

With the propulsion systems presently being considered for early manned interplanetary flights, mission durations of a year or longer are not uncommon. For such missions the weight saving achievable through the use of an atmosphere regeneration system is truly significant.

At the present time a physico-chemical regeneration system is favored, over a biological system, on the basis of weight, volume, power and availability.

In the following discussion a typical physico-chemical system is described, the weight savings associated with various processes of the system are presented, resulting increases in complexity and safety hazard are examined, and conclusions are drawn regarding the desirability of including the various processes in a system for an interplanetary vehicle.

TYPICAL SYSTEM

The atmosphere regeneration system selected for discussion includes atmospheric water vapor recovery, regenerative carbon dioxide removal, water recovery from urine followed by electrolysis, the reduction of carbon dioxide to methane and water, and the reduction of methane to carbon and hydrogen.

A specific system has been selected primarily to provide the basis for a discussion of potential weight savings vs. resulting increases in complexity. However, the system chosen includes subsystems which, for the most part, have proven feasibility and are the subject of present hardware development efforts.

In the selected system water vapor is condensed from the airstream, collected, and passed through charcoal and microbe filters. Potable water is provided by this method with a minimum of processing equipment.

Carbon dioxide removal is provided by a regenerable solid adsorbent system.

Two silica-gel beds and two Molecular Sieve beds are provided to: dehumidify the incoming air, remove carbon dioxide from the dry air, and rehumidify the processed air before returning it to the cabin. While one Molecular Sieve bed is removing carbon dioxide, the other is being desorbed by the combined action of a heater and a vacuum pump which exhausts to a carbon dioxide accumulator.

Urine is processed by the vapor-compression distillation method. The urine is evaporated in a distillation tank, and the resulting water vapor is compressed and passed through a condenser submerged in the evaporating liquid. The heat of evaporation is provided by the heats of condensation and compression. A chemical agent is added to the urine in the distillation tank to reduce odor, bacterial growth, and to minimize residue carryover. The condensed water vapor is passed through a series of filters before storage.

The recovered water is electrolyzed to provide: (1) oxygen to meet metabolic and leakage requirements, and (2) hydrogen for carbon dioxide reduction. The recovered water is mixed with an electrolyte and pumped through an electrolytic cell, gas separators, and temperature control equipment. Hydrogen and oxygen separated from the electrolyte are stored in high-pressure storage tanks.

Carbon dioxide reduction is accomplished in a Sabatier reactor to form methane and water. Hydrogen stored during the electrolysis process, and carbon dioxide stored during desorption of the carbon dioxide removal system, are reacted over a catalyst at elevated temperatures. The resulting methane, water, and unreacted gases are cooled to remove the majority of the water

vapor. The condensed water vapor is filtered and delivered to the cabin water supply system. With the Sabatier reactor high reduction efficiencies can be obtained with moderate temperatures.

The reduction of methane is accomplished in a high temperature reactor. The dehumidified exhaust gases from the Sabatier reactor are heated in a regenerative heat exchanger and passed over a catalyst. The catalyst is heated electrically to maintain the required reaction temperature. Carbon is deposited on the catalyst and the hot exhaust gases (mostly hydrogen) are passed through the regenerative heat exchanger to the inlet of the Sabatier reactor.

YIELD VS. COMPLEXITY

Weight savings are achieved with the selected atmosphere regeneration system because:

atmospheric water vapor recovery, urine regeneration, the reduction of carbon dioxide, and the reduction of methane reduce the requirements for stored water

the regenerable carbon dioxide removal system eliminates the need for an expendable absorbent such as lithium hydroxide

urine regeneration followed by electrolysis of the product water reduces the need for stored oxygen

On the other side of the ledger, the weight penalties for these subsystems include: fixed system weight, weight of expendables (such as chemicals, catalysts, filter materials, etc.), and the weight attributable to the power required.

Figure 1 presents the weight savings for various steps in closing the selected atmosphere regeneration system. The reference weight is the total weight of a closed system which includes all of the atmosphere regeneration processes shown on the abscissa of Figure 1. The ordinate of this figure represents the weights which must be added to the reference weight for systems embodying various regenerative features. For example, if the system were completely open its weight would be 15,800 lb. greater than the reference system. The introduction of atmospheric water vapor recovery reduces the weight difference to 9550 lb., the additional inclusion of the regenerable carbon dioxide removal feature reduces the weight difference to 6400 lb., etc. The weights shown do not include any provisions for redundancy, spare parts, or tools, and a power penalty of 100 lb/KW was assumed.

Table 1 shows the material balance assumed for the calculations.

TABLE 1
HUMAN MATERIAL BALANCE

Input	lb/man-day	Output	lb/man-day
Dry food	1.32	Carbon dioxide	2.25
Water in food	0.91	Water vapor	5.30
Drinking water	7.06	Urine	3.36
Oxygen	1.91	Feces	0.29
Total	11.20	Total	11.20

Atmospheric water vapor recovery provides the largest weight saving, with a

minimum increase in system complexity. The regenerative carbon dioxide removal, urine reclamation and electrolysis, and carbon dioxide reduction processes each add substantially to system complexity but provide weight savings commensurate with the increased complexity. The additional complexity resulting from inclusion of the methane reduction process is comparable to that for the carbon dioxide reduction process, but the weight saving is relatively small.

It is recognized that the effects of increased complexity can be offset by suitable redundancy and maintenance provisions. Indeed, a considerable weight allowance for redundancy and spare parts could be made without significantly altering the weight savings shown in Figure 1, since the fixed equipment weight for any of the regenerative processes shown does not exceed 4% of the weight saved by that process. A thorough reliability analysis to determine the weight of redundant systems, spare parts, tools and repair equipment required for each subsystem, to obtain a reliability commensurate with that of the open system, would assist greatly in drawing conclusions concerning the value of each step in closing the system. The value of each one of these processes must also be assessed in the light of: (1) the amount of time and effort required of the crew to control the process and to maintain the equipment, and (2) the safety hazards incurred.

In summary, inclusion of the atmospheric vapor recovery, regenerable carbon dioxide removal, and urine reclamation and electrolysis processes in the atmosphere regeneration system for an interplanetary vehicle seems clearly desirable. The advisability of including the carbon dioxide reduction process is not obvious on the basis of presently available information, and the

desirability of including the methane reduction process is extremely questionable.

TRACE CONTAMINANTS

Unless the trace contaminant removal system can maintain suitably low contamination levels it will be necessary to purge the cabin periodically, a procedure which will result in significant weight penalties. The need for more complete contaminant removal increases with mission duration for two primary reasons: (1) cabin leakage should be exceedingly small, consequently, this avenue of contaminant loss is expected to be of minimal significance, and (2) the effects on the crew of exposure to contaminants is a function of concentration and time of exposure which both increase with mission duration. While it appears that satisfactory removal systems can be designed on the basis of present information, the nature of the problem is such that considerable empirical verification will be required before it can be stated with assurance that the problem is indeed solved. The following discussion summarizes the major problems and the solutions presently being considered in this vital area.

TYPES AND SOURCES

The types of contaminants expected are gases, vapors, bacteria, ions, aerosols, and particulate matter, arising from the following sources:

Respiration, perspiration, and elimination (a)

(a) Quantitative, but highly variable, data on evolution rates for contaminants arising from respiration, perspiration, and elimination are typified by those given in Ref. 1.

- . Outgassing of materials and equipment
- . Ionizing radiation, and operation of high voltage equipment and fluorescent lights
- . Dust, lint, and metallic residue remaining after fabrication, and arising from various operations
- . Food preparation

The contaminants found in a submarine atmosphere are frequently referred to in discussions of this problem. While there are similarities between the submarine and spacecraft contamination problems, it is expected that spacecraft operations will be sufficiently restrictive that we will not be faced with contaminants from smoking, shoe polishing, food frying, painting en-route, etc. It is also expected that equipment can be better isolated from the cabin so that contaminants from batteries, fuels, lubricants, etc., can be minimized. On the other hand one would expect to encounter more ions, ozone, ammonia, methane, etc., from operations peculiar to a space vehicle, including exposure to cosmic radiation and solar flares, and the operation of atmosphere regeneration equipment. The severity of the contamination problem can be greatly reduced if a "contaminant reduction" policy is established in the design phase and is followed through to, and including, vehicle operations.

The actual determination of evolution rates for the various contaminants in a specific vehicle is largely an empirical process which will require long-term testing of prototype space cabins.

ALLOWABLE CONCENTRATIONS

The concentration of contaminants in the space cabin must be maintained below levels which might cause physical damage, a significant impairment of crew performance, or a fire or explosion hazard.

The data on limits for physical damage (Ref. 2) have for the most part been determined for hazardous industrial operations. Under such conditions individuals subject to toxic materials have time for elimination and recovery between work periods. Consequently, there is considerable uncertainty regarding the applicability of such data in submarine or spacecraft situations. An additional question arises in regard to the possibility of additive, synergistic and antagonistic effects in the presence of multiple contaminants. Animal tests, such as those reported in Ref. 3, involving continuous exposure to various contaminants as well as mixtures of contaminants will aid in answering these questions.

REMOVAL TECHNIQUES

Activated carbon exhibits high retentivities for a wide variety of gasses and vapors (Ref. 4). There are, however, some notable exceptions including ammonia, methane, hydrogen, and carbon monoxide. The majority of these, along with bacteria and most aerosols, can be removed in a catalytic (hopcalite) burner operating at a temperature of about 700°F. Ammonia can be removed by inclusion of a bed containing hydrated cobaltous chloride on pumice. A wide variety of contaminants can be removed by combining various adsorbents with appropriate chemical compounds (Ref. 5). Particulate matter

and ions will be effectively removed by a combination of micronic filters and either grounded or oppositely charged screens.

Anticipated contaminants, their sources, and appropriate removal techniques are summarized in Table 2. It is recognized that any such list is necessarily incomplete; additional sorbents may well become necessary as more data are obtained from the operation of ground prototype vehicles for extended periods.

THERMAL CONTROL

Satisfactory performance of both crew and equipment is vitally dependent upon achievement of the required degree of thermal control. The design of the thermal control system must take into account the maximum variations in: (1) internal energy dissipation and, (2) the absorption and rejection of energy by the vehicle exterior surfaces.

The following discussion deals with practically attainable surface characteristics, degradation of these characteristics in the space environment, resulting equilibrium temperatures for a Venus-orbiting vehicle, and systems which might be used to provide the necessary control over the internal temperatures of such a vehicle.

SURFACES

Maximum flexibility in thermal design dictates the achievement of practical surface systems approximating four basic thermal control surfaces;

TABLE 2
REMOVAL TECHNIQUES FOR
SOME EXPECTED CONTAMINANTS

<u>Contaminant</u>	<u>Sources</u>	<u>Removal Technique</u>
Indole	Excreta	} Activated carbon
Skatole	Excreta	
Hydrogen sulfide	Flatus	
Mercaptans	Flatus	
Urea	Urine	
Aldehydes	Electrical insulation, cooking	
Freons	Cooling loop	
Ozone	Ionizing radiation	
Butyric acid	Perspiration	
Valeric acid	Perspiration	} Catalytic oxidation
Hydrogen	Electrolysis, CO ₂ reduction	
Carbon monoxide	Respiration, CO ₂ reduction	
Methane	Flatus, CO ₂ reduction	
Glycol	Water-thinned paints	
Bacteria	Crew	
Aerosols	Many, organic and inorganic	
Particulate matter	Many and varied	Filter
Ions	Ionizing radiation	Grounded or oppositely charged screens
Ammonia	Urine	Hydrated CoCl ₂ on pumice

the solar reflector, the solar absorber, the flat reflector, and the flat absorber (Refs. 6 and 7). In addition, these systems must possess adequate stability in the space environment.

The following discussion will be limited to solar reflectors for two reasons:

(1) stable solar reflectors are essential to the operation of spacecraft in the vicinity of the inferior planets due to the increased solar radiation encountered, and (2) of the four basic systems, solar reflectors are most susceptible to environmental damage in space.

Low α_s/ϵ Surfaces

The two basic methods presently in use for achieving solar reflectors, or low α_s/ϵ (solar absorptance/infrared emittance) surfaces are:

White dielectric high-emittance surfaces (paints, ceramics,
and adhesive-backed films)

Second-surface mirrors

Some examples of these systems are listed in Table 3, together with remarks on environmental stability and ease of production. The importance of production problems, and the potentially degrading effects of the pre-launch and ascent environments are discussed in Refs. 7, 8, and 9.

Before reviewing the effects of the space environment, a few comments on mirror-type thermal control surfaces may be of interest. The second-

TABLE 3

CANDIDATE SOLAR-REFLECTOR THERMAL CONTROL SURFACE SYSTEMS

Class	Material	Initial Values		Space Stability Ranking	Cure	Remarks
		C_s	ϵ			
White Organic Paints	Kemacryl Lacquer; White No. M49WC 12 (Sherwin-Williams)	0.27 \pm 0.04	0.89 \pm 0.03	3	(1)	In use on IMSC vehicles
White Semi-organic Paints	Fuller 517-W-1 Gloss White Silicone (W.P. Fuller Co.)	0.26 \pm 0.03	0.84 \pm 0.04	2	(2)	In use on IMSC vehicles
White Semi-organic Films (adhesive-backed)	Dow-Corning TiO ₂ - pigmented Silicone Paint	0.21 \pm 0.03	0.83 \pm 0.03	1	(1)	Under development by IMSC and Dow-Corning
White Inorganic Coatings	Dow-Corning TiO ₂ - pigmented Silicone Film	0.12 \pm 0.03	0.86 \pm 0.04	1	(1)	Under development by IMSC and Dow-Corning
White Inorganic Coatings	IMSC Lithafrax- pigmented Silicate Paint	0.11 \pm 0.03	0.86 \pm 0.03	1	(2)	In use on IMSC vehicles; further development on improved formulations underway
Second-Surface Mirrors	1 mm thick sapphire, polished on both faces. Silver vacuum deposited on back by Optical Coating Laboratory, Inc	0.10 \pm 0.02	-	1		This data to indicate possible C_s values for the class. Second sur- face mirrors are utilized on Mariner II.

(1) Room temperature cure.

(2) Elevated temperature cure.

surface mirror consists of a material, transparent to solar radiation, with a metallized back surface. Solar radiation is reflected from the carefully prepared and protected metal surface, resulting in a low α_s . With properly chosen materials, and with sufficient thickness for opacity in the far infrared, the solar-transparent material will have an emittance of 0.80 - 0.90.

Environmental Effects

Allowance for the degradation of thermal control surfaces is an extremely important consideration in the design of a thermal control system. A space vehicle encounters a wide variety of environmental conditions; however, only those constituting a probable hazard to thermal control surfaces will be considered here.

Ultraviolet radiation. The most damaging environmental condition which can be adequately evaluated in the laboratory is the near ultraviolet component of solar radiation. This is arbitrarily defined herein as the 2200 to 4000 Å band (Ref. 7), and is estimated to contain nine percent of extraterrestrial solar radiation (Ref. 10). The effect of this radiation is evaluated by exposing surface specimens in a vacuum of 10^{-6} to 10^{-7} Torr to ultraviolet energy from a water-cooled mercury-argon high pressure AH-6 lamp (Ref. 11). Measurements of α_s and ϵ are made before and after exposure.

Data showing the exponential nature of the degradation is presented in Figure 2. Data points are not shown in the interest of clarity; the spread of measured α_s for a given exposure is $\pm 10\%$ or less. The dashed lines represent extrapolations which are based on the observed exponential increase of α_s with exposure. A flux density of one "sun" is defined as the total flux density of solar radiation in space at one astronomical unit from the sun, of wavelengths between 2200 and 4000 Å, irrespective of spectral distribution within that band.

It should be noted that the time scale of ultra-violet degradation estimated on the basis of this data may be in error by a factor of two or more, due primarily to lack of knowledge of the wavelengths of photons causing the damage. Since the AH-6 lamp (or any other intense ultraviolet source) does not duplicate the solar spectrum, information on this wavelength dependence is required for precise prediction of ultraviolet degradation. Investigations are being initiated at IMSC to obtain this data; until this information is available, usage of the admittedly unsatisfactory exposure parameter of "sun-hours" will probably continue.

The damage caused by ultraviolet exposure will be heightened by the increased flux density of solar radiation as the spacecraft travels toward Venus or Mercury. There is experimental evidence of a rate dependence for the ultraviolet damage of some materials (i.e., an exposure to six "suns" for ten hours does not produce the same effect as an exposure to one "sun" for sixty hours). However, generally an error of less than twenty percent in α_s is incurred if one assumes a linear relationship between

damage rate ($d \alpha_g/dt$) and flux density for variations from one to six "suns". The solar flux density at Venus is about 1.9 times that at Earth; at Mercury it is about 6.8 times that at Earth. If precise predictions of damage are required, one must determine the dependence of damage rate upon intensity and take this into account.

In making ultraviolet degradation predictions for calculations in this paper both rate-dependences and possible time-scale errors have been ignored.

Penetrating radiation. For thermal control surfaces of the vehicle under consideration, the most important source of penetrating radiation damage is expected to be solar flares. Solar flare protons can cause both radiation damage and sputtering; pertinent data are reviewed in References 10 and 12. While they are not considered to imperil thermal control surfaces of earth-satellites, solar flares are worthy of greater attention at the orbits of inferior planets. At the orbit of Venus the flux is estimated to be 2.0 to 2.5 times greater than at the orbit of Earth; at Mercury it is suspected to be 6 to 15 times greater.

The thicknesses of thermal control materials which determine the thermal radiative behavior range from a few microns for metals to 2-10 mils for paints and ceramics. An exception to this statement is the solar-transparent material of a second-surface mirror, which must maintain its transparency to solar energy; this could be as thick as 1/16 inch in some designs.

All incident particles will have some probability of altering the radiative behavior of the materials, but the largest dose will be from protons of energies less than approximately 20 mev. These particles can be expected to have a high probability for interaction with thermal control materials within the thicknesses mentioned above. Low energy electrons could represent a greater threat to thermal control surfaces if present in solar flares in large numbers. The fluxes and energy spectral of solar flare electrons are not well-known at present, however (Ref. 10, 12).

In any case, candidate thermal control surfaces for missions to the inferior planets should be subjected to low energy (≤ 20 mev) proton bombardment before final approval. It is expected, however, that the damaging effects of ultraviolet radiation will be proved to overshadow degradation caused by penetrating radiation.

Volatilization. Due to the low particle densities in space the potential problem of volatilization must be considered (Ref. 9). However, it is our experience at LMSC that materials developed for resistance to the effects of ascent heating, ultraviolet radiation, and penetrating radiation are also generally stable in vacuum.

Thermal stress. The last environmental effects worthy of mention are those of thermal stress and, if appropriate, thermal cycling. Such tests are performed routinely in vacuum at LMSC. In the near future, they are to be combined with the ultraviolet tests mentioned earlier. Such tests should be of particular importance for vehicles orbiting Mercury; surface-substrate systems must not fail due to differential thermal expansion.

EQUILIBRIUM TEMPERATURES

Equilibrium temperatures for the various surfaces of a hypothetical vehicle for a Venus-orbiting mission were calculated. Such data are useful in determining what types of thermal control systems might be used.

Mission and Vehicle Data

A Venus mission consisting of a 110 day Earth-to-Venus transfer, 10 day Venus orbit, and a 250 day Venus-to-Earth transfer was selected for study. A rotating interplanetary vehicle comprising a re-entry module, an operations module, and a power and control module was assumed. The power and control module acts as the hub of the rotating vehicles with the remaining two modules on the ends of two opposing spokes. The operations module, consisting of a cylindrical section with two hemispherical ends, was the only portion of the vehicle for which equilibrium temperatures were computed. The crew occupies the operations module during the major portion of the mission.

Two orientations were assumed for the transfer periods and for Venus orbit in order to determine the sensitivity of equilibrium temperatures to this parameter. For the transfer periods, the operations module was assumed to be oriented with one hemispherical end continuously facing the sun, or with the axis of the cylinder perpendicular to the solar vector. For Venus orbit, it was assumed that the axis of the cylinder was locally vertical, or locally horizontal and perpendicular to the orbit plane. In all cases

the module was assumed to be rotating. The Venus orbit was assumed to be in the ecliptic plane at altitudes of 10,000, 3200, and 150 nm.

Assumptions and Calculation Methods

Average equilibrium temperatures were determined by equating the absorbed and emitted energies. The use of average temperatures as a guide is quite reasonable since the vehicle is rotating and temperature-time variations around an orbit do not generally affect the thermal control system significantly.

Solar absorptance values for white silicate paint were taken from Figure 2. The infrared emittance was assumed constant at a value of 0.86. The solar flux was assumed to vary inversely as the square of the distance from the sun.

Transfer periods. During these periods the only absorbed energy is that arising from solar radiation. Solar view factors were determined by taking the ratio of the projected area normal to the solar vector, to the total area of the surface being considered.

Venus orbit. Absorbed fluxes during Venus orbit were determined by the method presented in Ref. 6. The solar reflectivity of Venus (0.76) was taken from Ref. 13. Venus planetary emission (50.8 Btu/hr-ft^2) was determined from temperature data from Ref. 14. Solar, albedo, and planetary-emission view factors were determined for several positions around an orbit, thereby allowing a determination of the average heat flux absorbed during an orbit.

Calculation results. The resulting equilibrium temperatures, shown in Figure 3, are useful in determining the heat rejection capability of the module surfaces, since at a given temperature:

$$q_r = \sigma \epsilon (T_s^4 - T_{eq}^4)$$

Where:

$$q_r = \text{Net heat rejection rate, Btu/hr-ft}^2$$

$$\sigma = \text{Stefan-Boltzmann constant, Btu/hr-ft}^2\text{-}^{\circ}\text{R}^4$$

$$\epsilon = \text{Surface emittance}$$

$$T_s = \text{Surface temperature, }^{\circ}\text{R}$$

$$T_{eq} = \text{Surface equilibrium temperature, }^{\circ}\text{R}$$

Throughout the entire mission equilibrium temperatures are sufficiently low that the rejection of sizeable heat loads is possible at reasonable surface temperatures. For example, at an average surface temperature of 60°F the horizontally oriented operations module orbiting at 150 nm can reject approximately 17.5 watts/ft². The module could well have a total surface area of 1000 ft², resulting in a total heat rejection capability of approximately 17.5 KW. Heat rejection in the vertical orientation would be slightly greater.

During the transfer periods heat rejection capability would be substantially increased by orienting the module with its axis parallel to the solar vector. However, since the Venus-orbiting phase is the critical design condition there is nothing to be gained by so restricting the vehicle orientation during the transfer periods.

It should be noted that the calculations were based on nominal values of all parameters, consequently some reduction in heat rejection capability must be considered due to uncertainties in these parameters.

The shape of the curves for Venus-to-Earth transfer results from the assumed trajectory which takes the vehicle more than one astronomical unit from the sun before it returns to Earth.

SYSTEMS

It is possible to specify the exact nature of the thermal control system only after assembling a considerable amount of information on internal loads, allowable temperature variations, equipment locations, etc., and performing the necessary analysis to determine the inter-relationship of all the variables. The time variation in vehicle equilibrium temperatures, however, is a useful tool in predicting the general nature of the system which might be used.

If the necessary internal heat loads can be rejected from the vehicle surfaces at sufficiently low temperatures then the problem is one of either (1) properly regulating the flow of energy from the interior of the vehicle to these exterior surfaces or (2) controlling the radiative characteristics of these surfaces. If such a procedure is not possible, as may be the case with large externally absorbed heat fluxes, then evaporative and/or heat pump systems are required.

Evaporative cooling systems, wherein an expendable coolant absorbs the load and is vented to space, have general usefulness for cooling during ascent, emergencies, and re-entry, but are not applicable to long-term operation involving substantial heat loads. In cases where heat must be rejected at elevated temperatures for long periods, the heat pump system will provide a weight saving over the evaporative system at some point in time of operation.

Since low altitude manned planetary orbital flights, except around Mercury, can be made without resorting to the use of a heat pump, the following discussion will focus on systems which regulate internal-to-external heat flow, or external radiative characteristics. Such systems include (1) variable external surface properties (α_s and/or ϵ), (2) variable internal-to-external thermal resistance, and (3) controlled internal heating.

Variable α_s and/or ϵ

Systems which vary the solar absorptance and/or infrared emittance of the vehicle exterior can compensate for changes in incident flux and internal heat generation. Examples of these are thermo- and phototropic surfaces, and shutter systems. A detailed treatment of such surfaces and devices is presented in Ref. 15. It has been our conclusion, from theoretical analysis, that such systems are not generally applicable to close temperature control of vehicles experiencing significant changes in internal power dissipation.

Variable Internal-to-External Resistance

The internal-to-external thermal resistance can be varied to compensate for changes in internal heat generation and externally absorbed flux. This resistance may be radiative, conductive, convective, or some combination thereof. Examples are: the conduction-radiation switch, infrared radiation shutters, and fluid circulation systems. LMSC has done experimental work on a conduction-radiation switch (Ref. 15) and a fluid circulation system (Ref. 16). A resistance ratio of approximately 18 to 1 has been achieved with the switch device. Considerably greater resistance ratios can be achieved with the fluid circulation system but with the added complications of a fluid-filled space radiator and a pumping system. This system does, however, represent a present state-of-the-art solution to thermal control for a wide variety of manned interplanetary missions.

Internal Heating

This approach to thermal control involves selection of sufficiently low internal-to-external thermal resistances so that under the combined conditions of maximum internal heat generation and maximum external flux the internal temperature will not exceed its maximum allowable value. At lower levels of internal heat generation and external heat flux, heat is added internally at a rate sufficient to maintain the internal temperature above its minimum allowable value. Such systems, employing electrical heaters, have been used for satellite thermal control.

An improvement over the electrical heater approach would be the utilization of excess heat from less temperature-sensitive equipment. For example, certain items of equipment which have fairly wide allowable temperature ranges might be used to supply the energy required for close control of other equipment and areas occupied by the crew. A variable-resistance thermal link would be required between the heat source and the item to be closely controlled.

The feasibility of this method of thermal control depends on a number of variables which are difficult to generalize such as equipment location, power dissipation, and power duty cycle. Consequently, it is not possible to conclude in a general way that such a system will or will not work. Such a conclusion must await an analytical study based on a particular vehicle design. If such an approach can be made to work it will have obvious advantages over the fluid circulation system.

CONCLUSIONS

The utilization of an atmosphere regeneration system in a manned interplanetary vehicle will result in substantial weight savings for a year-long mission with a three man crew. Physico-chemical rather than biological regeneration systems are favored at this time on the basis of weight, volume, power, and availability.

By comparing the weight reduction with the increased complexity for each of the regenerative features of one physico-chemical system, it seems

clearly desirable to include the atmospheric water vapor recovery, regenerable carbon dioxide removal, and urine reclamation and electrolysis features. The advisability of including the carbon dioxide reduction process is not obvious on the basis of present information, and the inclusion of the methane reduction process is extremely questionable.

Design of the trace contaminant removal system is hampered by a lack of data on the types and evolution rates of contaminants to be encountered in a specific spacecraft, and the allowable concentrations for continuous exposure to these contaminants. Considerable empirical investigation will be required to obtain the required information in these areas. A "contaminant reduction" policy should be implemented early in the design phase to reduce the severity of the problem, however, removal of the majority of the contaminants should be satisfactorily accomplished with a system including activated carbon, a catalytic oxidation unit, hydrated cobaltous chloride on pumice, and suitable particulate filters and ion traps. Additional sorbents may well become necessary as more data are obtained from the operation of ground prototype vehicles for extended periods.

Satisfactory thermal control can be achieved for low altitude Venus orbital missions by using a variable-flow fluid circulation system in conjunction with radiators coated with a white silicate paint developed at IMSC. An internal-heating type system, utilizing equipment power dissipation to control internal temperature, may prove to be a simple and reliable substitute for the fluid circulation system.

REFERENCES

1. C. Clemedson, "Toxicological Aspects of the Sealed Cabin Atmosphere of Space Vehicles," Astronautik, Vol. 1, Issue 4, 1959, pp. 133-158.
2. "Threshold Limit Values for 1960," Archives of Environmental Health, August 1960, Vol. 1, pp. 140-144.
3. C. Sandage, Tolerance Criteria for Continuous Inhalation Exposure to Toxic Material, ASD-TR-61-519 (I), October 1961, Dayton, Ohio.
4. F. H. Munkelt, "Air Purification and Deodorization by Use of Activated Carbon," Refrigeration Engineering, Vol. 56, September, 1948.
5. A. B. Ray, "Role of Activated Carbon in Practical Control of Atmospheric Contamination," Proceedings of the United States Technical Conference on Air Pollution, McGraw-Hill, 1952, New York.
6. W. G. Camack and D. K. Edwards, "Effect of Surface Thermal Radiation Characteristics on the Temperature Control Problem in Satellites," Surface Effects on Spacecraft Materials, ed. F. J. Clauss, John Wiley & Sons, New York.
7. L. A. McKellar, "Effects of Spacecraft Environment on Thermal Control Materials Characteristics," Spacecraft Thermodynamics Symposium, ed. G. A. Etemad, Holden-Day, Inc., San Francisco, 1962, pp. 99-128.
8. R. E. Gaumer and L. A. McKellar, Thermal Radiative Control Surfaces for Spacecraft, Lockheed Missiles and Space Co. report LMSD 704014, Sunnyvale, California, March 1961.
9. K. Goetzel and J. B. Singletary, ed., Space Materials Handbook, Lockheed Missiles and Space Co., Sunnyvale, California, January 1962.
10. F. S. Johnson, ed., Satellite Environment Handbook, Stanford University Press, Stanford, California, 1961.
11. R. E. Gaumer, F. J. Clauss, M. E. Siber, and C. C. Shaw, Materials Effects in Spacecraft Thermal Control, Lockheed Missiles and Space Co. report LMSD 704019, Sunnyvale, California, November 1960.
12. D. K. Bailey, "Time Variation of the Energy Spectrum of Solar Cosmic Rays in Relation to the Radiation Hazard in Space," Journal of Geophysical Research, Vol. 67, No. 1, January 1962.
13. G. P. Kuiper, "Planetary Atmospheres and Their Origin," The Atmospheres of the Earth and Planets, University of Chicago Press, Chicago, Ill., 1952, p. 308.
14. W. M. Sinton and J. Strong, Astrophysical Journal, 131, 470-490, 1960.
15. T. M. Olcott and M. Ratner, "Analytical and Experimental Investigation of Self-Thermostatic Effects," Space Vehicle Thermal and Atmosphere Control Symposium, Wright-Patterson Air Force Base, Ohio, Feb. 12-13, 1963.

16. J. M. Smith, R. B. Jagow, and G. R. Werth, "Thermal and Atmospheric Control in Bioastronautic Systems," Spacecraft Thermodynamics Symposium, ed. G. A. Etemad, Holden-Day, Inc., San Francisco, California, 1962.

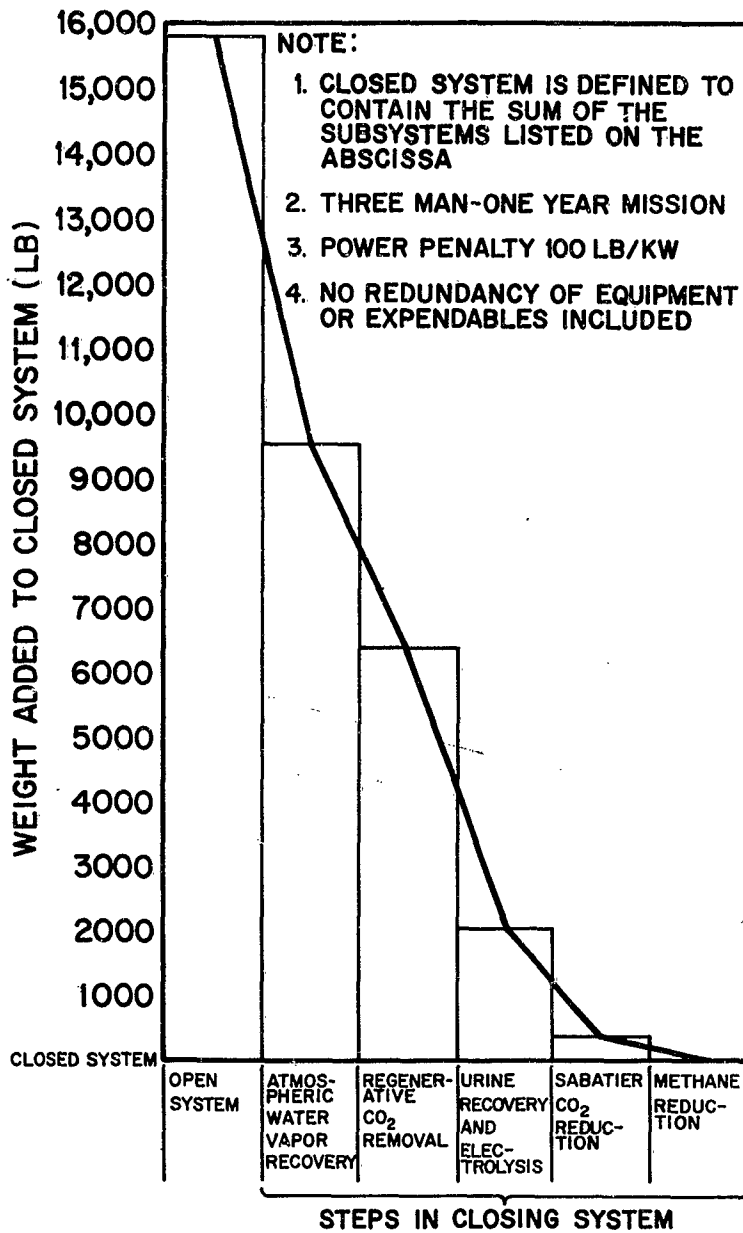


FIG.1 COMPARISON OF WEIGHT SAVINGS FOR VARIOUS STEPS IN CLOSING AN ATMOSPHERE REGENERATION SYSTEM

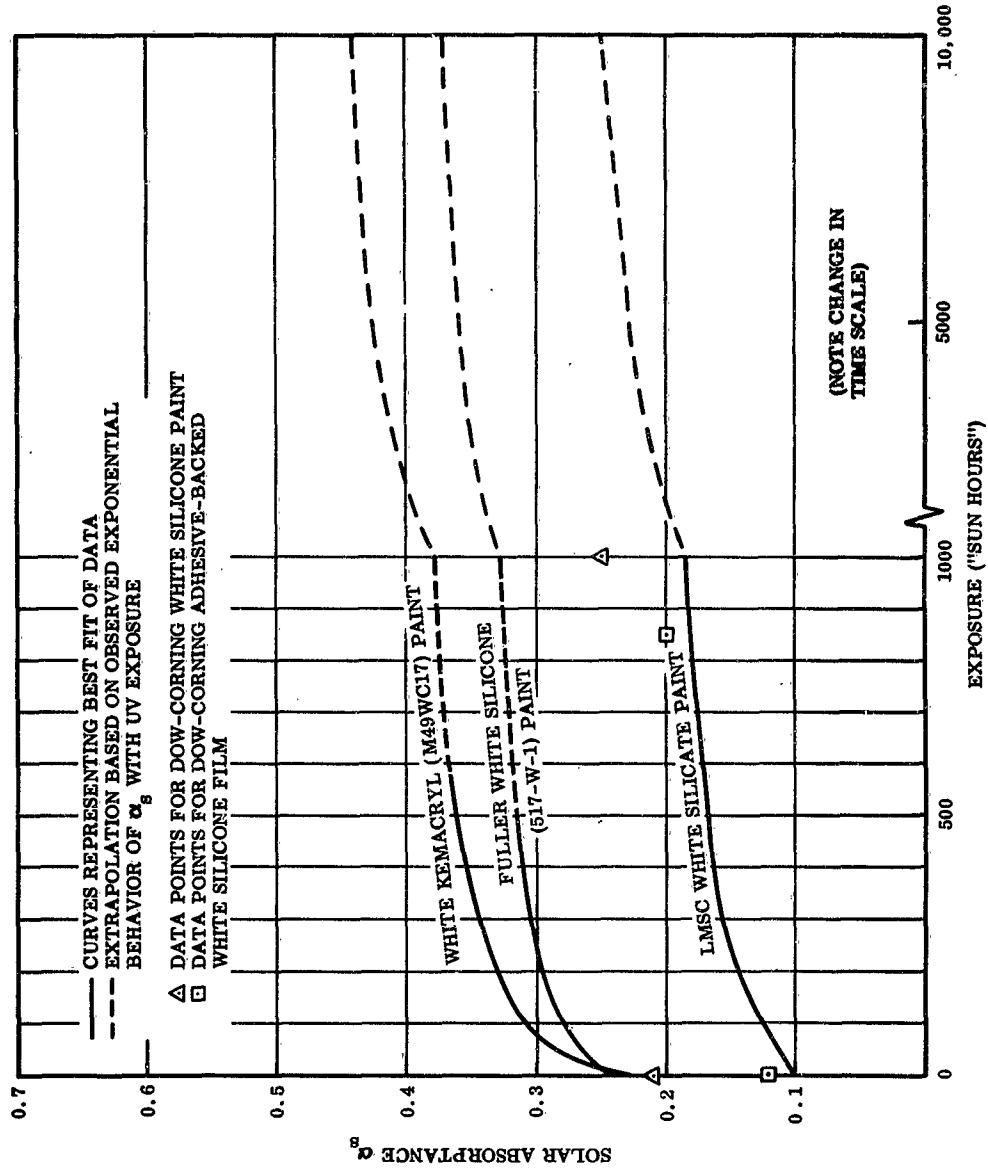


FIG. 2 EFFECT OF NEAR ULTRAVIOLET RADIATION IN VACUUM ON THE SOLAR ABSORPTANCE α_s OF CANDIDATE WHITE SURFACES

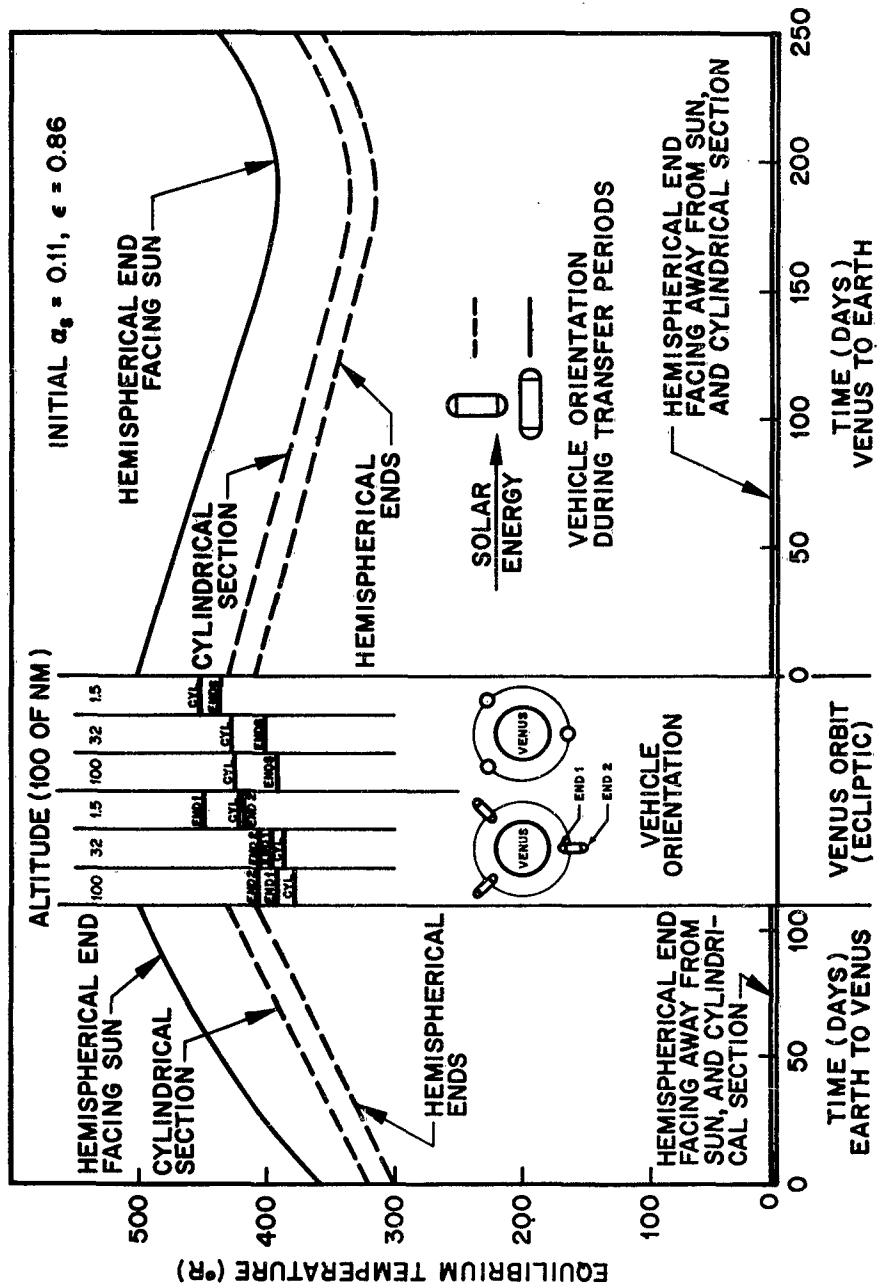


FIG. 3 ROTATING VEHICLE EQUILIBRIUM TEMPERATURES FOR VENUS MISSION

QUESTION AND ANSWER PERIOD

SESSION I - Environmental Control Systems

First Paper-- "Thermal and Atmospheric Control for Manned Interplanetary Vehicles" by Mr. J. M Smith, Lockheed Aircraft.

QUESTION: (H.C. Nordwall, North American Aviation) What leakage rates were used in your analysis and were the variable α/E used in the thermal analysis?

ANSWER : (Mr. Smith) We did not assume specific rates in the analysis. It turned out that there was approximately .64 pounds per manday of oxygen generated in excess of metabolic requirement. Consequently, this would be available for leakage. On the variable Alpha over E problem we assumed that absorption degraded as the result of UV exposure but that emittance remained constant. We did not have a variable Alpha over E system operating on the vehicle.

QUESTION: (A. Rakowski, Walter Kidde & Company) Have you considered handling feces in detail in the analysis?

ANSWER : (Mr. Smith) In this analysis we have assumed the feces to be unusable, so they didn't enter into a weight trade off. They still have to be disposed of, of course, and the answer is that we didn't look at this problem in detail.

QUESTION: (R.A. Saunders, Naval Research Lab.) Have the trace contaminants, or contaminant types mentioned, actually been detected in the spacecraft atmosphere or is their presence only assumed?

ANSWER : (Mr. Smith) It was assumed on the basis of observed contaminants and submarine simulator tests. A number of contaminants from submarines were not included because they seem to be peculiar to submarine operation.

QUESTION: (Bart Bartholemew, Atlantic Research Corporation.) What percentage of burning of methane was achieved at 700 degrees Fahrenheit?

ANSWER : (Mr. Smith) We have not tested these devices, however 30 per cent conversion at these temperatures has been reported in the literature.

QUESTION: (M. Rand, Avco) Are the values of Alpha .19 and E .86 on the last slide assumed data or have such values been attained in reality?

ANSWER : (Mr. Smith) Well, we attained the .11 Alpha and E .86 initially before degradation. The value of .19 used on the final curve was a degraded surface and we assumed an exposure to obtain .19. The .19 turned out to be the value that the Venus vehicle would have had during its orbital flight period.

QUESTION: (R. Van Vliet, ASD) On what surface did you find an intensity effect for UV radiation?

ANSWER : (Mr. Smith) Well, just about all of the white paints that we tested.

QUESTION: (Anonymous) Did you check the decrease in Alpha Sub S caused by dark fading?

ANSWER : (MR. SMITH) Here I presume you mean the bleach, due to exposure due to atmosphere, and this is eliminated by testing in a vacuum and rather rapidly getting the specimen into the measuring device.

QUESTION: (R.N. Bailey, Sundstrand Aviation) Would you please elaborate on the operation of the oxidation catalyst referred to in your talk; specifically type, or types

of active surfaces, operating temperatures; thirdly, are extra reactions such as oxygen added to assure complete combustion?

ANSWER : (Mr. Smith) On the first case I am not familiar with the exact type of surface. I am sure that you will want to spread the catalyst over as much surface as possible. The catalyst used is hopcalite which is a mixture of oxides of manganese, cobalt, copper and silver. The operating temperatures are around 700 degrees Fahrenheit and no oxygen is added. The oxygen in the atmosphere is used for the oxidation.

**METHODS FOR THE SYNTHESIS OF OPTIMAL ENVIRONMENT
CONTROL SYSTEMS**

by

R. A. Paselk

**North American Aviation
Downey, California**

METHODS FOR THE SYNTHESIS OF OPTIMAL ENVIRONMENT CONTROL SYSTEMS

Robert A. Paselk

INTRODUCTION

The natural environment of space is lethal. Escape, recovery, or rehabilitation is not possible even after short durations of exposure. Thus, the manufacture and retention of an artificial environment is critical, its requirements are exacting, and no uncertainty can exist as to performance of function. Mission and vehicle considerations also require that the selection, sizing and arrangement be optimum for every vital material, process and component of the system. Further, technology has produced an enormous array of new materials and processes which must be considered if an optimum is to be achieved and progress is to be continued. Thus, the development of methods for the rapid and accurate selection and optimization of complete systems from competitive alternates is probably the most needed technology today. Such development must be guided by practical considerations involving the best utilization of human skills and facilities available.

Achievements of the last decade, as well as those expected for the future, seriously alter the character of problems which must be dealt with by the environment control systems engineer and his associates. Frequently in the analysis of complex systems, the number of variables to be considered and the volume of calculations to be performed are so great as to require the use of high speed computing equipment. Under these circumstances it is very easy for the practical systems designer to lose all feeling for the problem and to use the results from the machine computations indiscriminately or with confusion. If this happens, the design synthesis is created essentially without benefit of the designer's experience and possibly without his having a clear understanding of the factors and interrelationships involved. Thus, the volume of uninterpreted data must be reduced if human evaluation and decision capabilities are to be used at their maximum. Optimum selection from the many possible alternates must be reduced to a simple, straightforward, and economical practice.

On the other hand, computers have many capabilities other than high speed, which are not being adequately used. If problems and instructions are introduced properly, a computer can handle many areas better than their human manager and at the same time can be restricted from making decisions best accomplished by experienced engineers and programmers. Logical decisions, simple learning, parametric organization of data, equation development from empirical data, graphical and bar chart print-outs are examples.

The intent of this paper is to show that practical approaches are available for the synthesis of optimum, or near-optimum, systems. It will be demonstrated that difficult and

accurate selections can economically be made under conditions of uncertainty, both with and without the use of computers. Although this work is preliminary in nature and the need for additional development is apparent, positive conclusions can nevertheless be drawn relative to the methods developed so far.

The paper consists, first, of a discussion of the philosophy underlying the methods for system synthesis and optimization. This is followed by a brief description of the methods and their utility. Finally, an example is given of the application of the methods to environmental control systems and components.

The studies reported in this paper were performed at the Los Angeles Division of North American Aviation, in conjunction with the research and development of advanced vehicles. Most of the analytical development has taken place within the past two years, although many of the ideas have germinated during the author's earlier experiences in design of aircraft and space environmental control systems.

PHILOSOPHY OF APPROACH

In the effort to develop an orderly and rational method of system synthesis and optimization, a number of new concepts and approaches have been developed and combined with common practices to yield a total approach. Some of these concepts represent the basic elements upon which the development of a total synthesis method depends; thus, it is appropriate that they be introduced briefly.

Synthesis and Optimization

Synthesis of optimal systems is concerned with the conception, description, assembly, integration, and selection of processes and systems to optimum criteria.

Synthesis may be defined for purposes of this study as "a set of methods for the identification, description, and assembly of materials, processes, etc, into a total system which fulfills the requirements imposed by performance, design, manufacturing and operational criteria".

Optimization, when used in relation to systems, implies the selection, sizing, and integration of a particular system from many possibilities and variations based on one or more criteria regarded as a sound basis for selection.

Synthesis may be accomplished without considering optimization. Optimization is, therefore, an additional restraint to synthesis, applied by unique operations which maximize or minimize variables or choices.

An optimum, in a mathematical sense, is single-valued. That is, only a single solution or solution set will result when specific numerical criteria are imposed. Any variation in criteria or alteration in the mathematical function after a solution is completed, will destroy the optimization.

An optimum, in a philosophical sense, can be treated as numerically multivalued, thus permitting multiple choice and variation within specified limits to accommodate criteria which cannot be specified numerically. This is one of the most important concepts of this study. Total optimization is not possible unless all criteria can be accommodated, and the philosophy presented herein recognizes that criteria which cannot be accurately quantified will always exist. Thus, optimization must include both the genius and weakness of human judgment.

Three classes of optimization operations are considered, and are indicated in figure 1.

- (1) Best selection from an array of alternates, primarily concerned with type of material, process, configuration, etc.
- (2) Minimum or maximum value of a variation, usually continuous and primarily concerned with sizing of components.
- (3) Best arrangement in a circuit.

These considerations lead to the necessity of establishing specific criteria for optimization of environmental control systems. This problem will be discussed in detail in the following section.

Criteria for Optimization

Criteria for system optimization must be distinguished from requirements. Criteria for optimization must be variable and a function of one or more system variables. Weight and power, for example, vary with most system variables. Requirements, on the other hand, are fixed, altered only by compromise or to satisfy a desire to increase the latitude of usefulness of the product. Neither of these are true variations since both alter the basic problem statement. Other fixed value quantities are terminal boundary conditions such as the

environments and limits of various types.

Optimization criteria must also be quantified when optimization is to be accomplished by numerical methods. Further, all optimization criteria must be related to a common denominator or one of the criteria being considered.

Weight, volume, and power are the key criteria which may be related and treated numerically, particularly when the total vehicle and mission problem statement is used in the formulation of relationships.

Reliability, performance, mission environment, and material limits must be regarded as requirements and are fixed.

Cost, producibility, service factors, etc, cannot be quantitatively related to weight, for example, except by the use of arbitrary weighting coefficients which, when considered collectively, yield a total effect commonly called a "figure of merit".

The weighting or "figure of merit" concept has been discarded, due to uncertainty as to the worthiness of the arbitrary numbers chosen, as well as the incompleteness of the weighting list. Weight, power, and volume have been selected, then, as the only criteria which will be quantitatively evaluated and treated by numerical optimization techniques.

Allowable Deviations From Optimum

Allowance for deviation from a quantitative minimum is desired due to the use of weight or its equivalent as a sole criterion for optimization. This can be accomplished by allowing a controlled deviation from the minimum to encompass more choices. The methods for introducing controlled deviations from the minimum solution are shown in figure 1. In the case of selection of system components, processes, or arrangements, several alternates which are within a specified tolerance of a minimum weight choice, may be considered as equivalents permitting the systems engineer to include other factors in his selection.

When a selection has been made, dimensions or proportions may be varied to a limited extent to permit optimization of an installation.

If the requirement is known only approximately as in the case of mission parametric studies, many solutions and variations may be viewed collectively against both weight and requirement, as shown in figure 2, giving a clear picture of the selection problem to the systems engineer.

Figure 2 shows a hypothetical selection problem where each alternate includes an allowable variation in weight or requirement as a condition for choice.

Thus, each appears as a band on the plot; the common regions (intersections) of each band permitting alternate choices. Note that the number of available choices vary from one to three, depending on the region of the requirement. An inadequate number of choices can readily be rectified by enlarging the allowable deviation for weight.

Thus, the deviation from minimum may be varied if necessary to encompass as many choices as are required until nonweight-oriented criteria such as cost, reliability, and other factors are fulfilled. If a substantial weight deviation exists between a minimum weight choice and another choice based on some other criteria, a problem area is signalled, establishing a basis for further development or research planning.

The above are some of the basic philosophies which establish the foundation for developments. The reader is referred to the more extensive coverage appearing in References 1 and 2. A generalized survey of methods reviewed from the literature is also included in Reference 3.

Assembly Levels

For purposes of analysis and design, it is expedient to consider the stepwise development of a system. The "assembly level" breakdown used in the present development is closely related to the natural sequence of steps in the physical assembly of a system: materials are assembled into functional components; components into loops, circuits, etc; circuits into subsystems; subsystems into functional systems; systems into vehicles, etc. The set of assembly levels used in the present work is indicated in figures 3 and 4.

Figure 3 illustrates the relationship of component to branch, circuit, and system similar to typical practice. All components have vehicle linkage and some are in themselves branch and circuit linkages.

Associated with each assembly level is a set of requirements and a set of restraints as illustrated in figure 4. Certain of these requirements and restraints affect only the one level with which they are associated. The effects of other requirements and restraints are propagated to other levels, both up and down the assembly level scale as shown.

The study of specific interrelations between assembly levels is of particular value for determining which decisions

can be made at which level. It is desirable to make all of the decisions which are immediately apparent at all levels in order to allow decision making at each level to be as independent of other levels as possible. Matching of all requirements and restraints at all levels is fundamental to synthesis.

Unifunctional Groups

Most atmospheric control circuits are complex series-parallel arrangements serving several functional requirements such as removal of CO₂, moisture, heat, particles removal, etc. All processes and components affect the state of the circulating gas due to fluid friction, thermal, and mass exchanges. All processes include friction, most processes have thermal effects, and many are affected by humidity. Except for the above, most processes have very minor effects on the state of the circulating gas other than the alteration of the state which dictated the inclusion of the process.

This condition allows treating processes whose primary function is the alteration of mass (other than water), independently of each other as shown in figure 5. By the expedient of assigning to each process the circuit weight increases caused by heat and moisture increments due to process reaction, and by including the source requirement data affecting the process, the process may be separated from the circuit to form a pseudo or equivalent circuit. When applied to a whole circuit a transformation is accomplished, and a parallel circuit consisting of separated single or unifunctional groups is formed.

This technique is believed to be useful as a basis for circuit synthesis, and preliminary trials with the method have been reasonably successful. Its value will not be fully tested, however, until this study has explored the circuit level more fully. Figure 5 shows a process combined with the requirement and all influences on the vehicle and the balance of the circuit.

The artificial arrangement resulting is a closed loop where the sum of pressure drops, temperature changes, humidity change and process variable change are each equal to zero.

Characterization

A most important operation is the development of mathematical models or component characterizations which are particularly adapted to synthesis and optimization considering weight and performance.

Format is particularly important if the task of selection and optimization is to be accomplished economically and with understanding. The following formats were developed.

Installed Weight General Format

A characterization equation, to be useful for selection and assembly, must include the total effects of usage if a common denominator for comparison is to be obtained.

Since every component added to a vehicle adds weight and requires power (at least propulsive), structure, and volume the total influence of a component installation cannot be evaluated without including all of them.

This can be accomplished by relating power, volume, installation structure weights, and vehicle weight growth factors, at least to component weight, thus:

$$\begin{aligned}
 * \text{ Installed Weight} &= \text{Component Weight} + \frac{\text{Power}}{\text{Weight}} \text{Equiv. } (W_{IP}) + \frac{\text{Volume}}{\text{Weight}} \text{Equiv. } (W_V) + \\
 &\quad \frac{\text{Installation}}{\text{Weight}} \text{Structure } (W_I) + \frac{\text{Weight}}{\text{Growth}} \text{Factor}
 \end{aligned}$$

Influence Parameter Format

The influence of the insertion of a component (or process) on total circuit or system weight is also added to complete the model. When system effects are added to the equation an influence or decision format is accomplished since alternate components having differing effects on the circuit and vehicle have a common basis for comparison.

Thus,

$$\text{Total Influence Weight} = \text{Installed Weight} + \text{System Increments}$$

If a process adds heat the system weight increment may be represented, for example, by

$$W = K_q(q)$$

where q is the heat added by the process.

The use of influence parameters is valuable in technical decisions, particularly those based on phenomena which are

expressible as mathematical statements. This involves the arrangement of equations into a form in which the various influences, such as pressure levels, temperature levels, fluid properties, geometrical factors, and other such variables are collected together into parameters which can be evaluated as a unit or resolved by a single decision. This procedure facilitates making specific decisions at lower assembly levels, since effects of variations at higher levels frequently have identical effects on alternates being considered at the lower level. The formulation of parameters is useful for the organization of equations for optimization. Further, optimization is useful in grouping related variables and the combining of separated influences parameters into total influence or decision parameters.

Coefficients representing unknown values of high assembly-level variables can be introduced into the characterization equations and grouped as parameters, subject to interpolation, change, and decision at the higher assembly level. Coefficients which are altered by vehicle and mission can be adjusted during each preliminary design phase and finally set just prior to release of a final design. Frequent adjustment would result in numerical changes in total weight, but will not, in many cases, influence type selection and identification of problem areas.

The desired format is shown in the following word equation and is organized into parametric groupings, the objective being to permit evaluation of each parameter for influence on result, and to make decisions where possible. Obviously, before such an objective can be accomplished, data must be obtained on influence coefficients and experience accumulated to establish the relative independence of outside variations and uncertainties. The greater the number of choices of excellence which can be made, the more certain the quality of the selection and the result. As an example of such a parameter, consider (density) x (conductivity) for insulation, a property parameter in this case. Insulation can be selected since the lower value of this parameter will always be in the direction of the optimum design, providing space limitations and temperature service limits are not exceeded. In general, an equation may contain parametric groupings according to assembly level as follows:

$$W_C = f \left[\begin{array}{l} \text{constants, properties \&, local} \\ \text{limits} \qquad \qquad \qquad \text{statepoints} \end{array} \right. ,$$

$$\left. \begin{array}{l} \text{branch} \qquad \qquad \text{circuit} \qquad \qquad \text{system} \\ \text{parameters} \quad , \quad \text{parameters} \quad , \quad \text{requirements} \end{array} \right. ,$$

$$\left. \begin{array}{l} \text{vehicle parameters,} \qquad \text{mission parameters,} \\ \text{power coefficients,} \quad , \quad \text{flight periods,} \\ \text{and environment} \qquad \qquad \text{and environment} \end{array} \right]$$

The choice of parameters and size of each grouping should be such that a numerical value is established when a single and conventional system design decision is made. Until that time, the form of the expression should indicate the directional and proportional influence of each parametric group on system weight.

Additional Format Considerations

Equations may also be written in ideal, limit, or reference formats, depending on purpose. The objective is to show the relationship of one particular numerical data set to another set having a desirable or limiting character. See Reference 1 for detailed developments relating reliability potential to temperature limits, for example.

Equations may be written in error record or uncertainty format, which merely introduces a memory of crude approximations and allows for the assessment of the influence of uncertainty or error on choice at a higher assembly level.

In addition to the above, a major emphasis was placed in the study on the use of analogies (such as heat-transfer to mass-transfer) for the purpose of keeping the number of types of equations to a minimum. Process variations were treated as coefficients to be established from detailed theoretical developments, empirical data, or supplier quotations.

Additional developments in the organization, classification, and categorization of processes and assembly levels, as well as in the development of formats, is covered in Reference 1.

Parametric Optimizations

Optimization reduces the number of variables describing the dimensions or other characteristics of a component or process tending to force solutions to ideal proportions, etc. The remaining variables are regrouped and frequently can be organized into convenient parameters, each representing the influence of a single design or configuration decision. Using the heat exchanger again as an example, the minimum weight equation takes on a new form best represented by a word equation as follows for each core, fluid and vehicle installation.

$$\left[\frac{\text{Weight}}{UA} \right]_{\min} = \left[\begin{array}{c} \text{Core} \\ \text{Parameter} \end{array} \right] \left(\begin{array}{c} \text{Fluid} \\ \text{Parameter} \end{array} \right) \left(\begin{array}{c} \text{Vehicle} \\ \text{Power} \\ \text{Parameter} \end{array} \right) \Bigg]_{\text{Side a}}^n$$

$$\left[\begin{array}{c} \text{Core} \\ \text{Parameter} \end{array} \right] \left(\begin{array}{c} \text{Fluid} \\ \text{Parameter} \end{array} \right) \left(\begin{array}{c} \text{Vehicle} \\ \text{Power} \\ \text{Parameter} \end{array} \right) \Bigg]_{\text{Side b}}^m$$

The core parameter, however, may still contain fluid and vehicle density effects, treated collectively as a pseudo-core density.

Parameter optimization may be accomplished at low assembly levels using localized independent variables which occur at no higher level, but numerical optimization relative to many specific higher assembly level variables cannot be accomplished. Assigning values to such variables is, however, useful in determining their general effect and magnitudes of the result, as illustrated in the following section.

APPLICATIONS OF METHOD

Evidence of the practical value of approaches discussed may be obtained by application to a variety of processes and circuits.

Application studies were made in References (1) and (2) and included the development of characterizations in the desired format, optimization of weight and power for heat exchangers, chemisorbers, catalytic reactors, ducting, and simple loops.

Characterization Examples

The typical method of format development is shown in figure 6 for the heat exchanger and in figure 7 for one type of catalytic burner, and illustrate a surprising difference from conventional formulation. Details of the development and examples of application are presented in the text of Reference 1. The utility of this format for decision and synthesis is not apparent until optimization is accomplished using Reynolds number as the independent parameter.

Component Optimization Examples

Optimization is not usually straightforward due primarily to nonlinearities existing in the equations. Numerical evaluations are highly desirable to determine the influence of

each variable and to gain preliminary knowledge of the character of the solution.

General solutions may be developed when the effects of minor variables are understood, and a suitable method for accounting for them can be developed, including substitution of empirical relations having good accuracy over a wide range of variation.

Examples of catalytic reactor, chemisorber and heat exchanger optimizations are shown in figures 8, 9, 10, 11, and 12, and were developed in Reference 1.

The first three figures are representative of cases where requirements, flow, and temperatures can be assumed and it is desired to determine the influence of geometry and permissible variance in the region of minimum weight. In all three cases, Reynolds number, representative of cross-sectional area, was chosen for the optimization in order to keep Reynolds number, friction, heat and mass-transfer factors grouped together.

Figure 10 is a more involved problem, representing optimizations involving two independent variables (Reynolds number both sides) thus yielding two dependent solutions, one for the air side and one for the water side. The nearly abrupt change in the curve is due to transition and is not shown accurately in this region since the minimum occurred elsewhere. The plot does, however, provide a basis for testing the proximity of the solution to a discontinuity. Also shown are variations in the solution as affected by fluid fill and vehicle volume penalties. It may be noted that this effect is very significant and will be considered more thoroughly in the section on selection which follows.

Figure 11, also developed in Reference 1, is a generalized solution applicable to chemisorbers, catalytic reactors and many other processes which can be reduced to the type of equation shown. It is presented to illustrate

- (1) the reduction of variables by relating the independent variable to a generalized component-system parameter
- (2) the small weight error of a generalized approximation which can be applied to a large number of cases.

Figure 12 shows that the final weight parameter for these cases may be related reasonably accurately to a combined component-system parameter (e), with the independent variable (x) in this case now absent. The accuracy is essentially constant for all values of e greater than 2, thus useful over many orders of magnitude.

Such an equation may be regarded as a preoptimization. It is very useful in the selection process, an operation regarded as the most important operation in the system synthesis process, as well as in assembly since the resulting equation is a combined form representative of a higher assembly level.

Example of Process Section From Several Alternatives

Application of Methods to Heat Exchangers

A primary objective in the development of synthesis methods is the optimum selection of a process out of a large array of alternates, with a minimum of information regarding the remaining portions of the branch, circuit, and vehicle.

A method has been developed which fulfills these objectives and evidence of validity has been obtained using heat exchangers as a test example.

The selection solution follows from the comparison of a large array of cores with specified fluids and vehicle factors using the preoptimized heat exchanger equations. Circuit flow and temperature conditions are held constant, but not specified numerically, for the comparison. This solution applies exactly for circuits where flow and temperature conditions are established by processes other than heat flow. For the thermal control circuit, flows will optimize at higher values for heat exchangers having higher weights, thus the process rank orders developed in the solution will not be affected.

The format of the preoptimized heat exchanger equation is

$$\left(\frac{W_T}{UA}\right)_{ij}^n = (\text{constant}) \left[(C_i^n + C_j^n) (\rho l)_i + (\rho l)_j \right]^m$$

where C_i is a function of core configuration and fluid properties for side i , and $(\rho l)_i$ is a function of core properties, fluid and vehicle density for side i .

Also

$$UA = \frac{W_{Cp} \Delta T}{\log \text{ mean temp difference}}$$

For fixed flows and circuit temperatures UA is constant.

Holding fluid and vehicle density and one side (j) fixed for a comparison, an array of cores (i) can be established in a specific minimum to maximum rank order.

Further, both sides may be paired in all possible combinations and displayed in a matrix.

Computer Program; Example of Selection Process

A designer-monitored computer program was developed including a number of solutions besides that required for the solution for the pair of heat exchanger surfaces whose combined weight would be a minimum. The following operations developed, with notations as to method of operation:

- (1) Data organization into influence parameters and calculation of values (designer, computer).
- (2) Calculation of minimum solutions from preoptimization equations (computer).
- (3) Calculation of all solutions including the minimum from the origin equation to permit
 - (a) display of effects of deviation from the optimum value of the independent variable (Reynolds number or dimension) upon weight (computer)
 - (b) a test of solution accuracy of the pre-optimized equations (computer)
- (4) Calculation of the weights and rank order of the side (i) array normalized to a arbitrary standard obtained from prior analysis for side (j). The standard is used to yield the best first approximation of minimum weight pairs. The rank order resulting when applied to both sides is used to organize the pair matrix for printout (computer).
- (5) Calculation of all weights of both arrays in pairs.
- (6) Comparison of independent-side rank orders with pair rank orders.
- (7) Improvement of the standard if a new minimum is included in the array being tested, providing reliability and other criteria are also met (designer-monitored).
- (8) Plotting of input data, interim and final results in graphical and tabular form, arranged for direct comparison (computer).
- (9) Evaluation of results and decision (designer).

Figures 13 through 18 shows the results of calculations for thirteen plate-fin heat exchanger cores extracted from Reference 4. Cores were established in two arrays, one for air and one for water. Solutions were developed for vehicle densities ranging from 1 to 100 lbs per cubic foot including an uncertainty factor of 500 percent, as well as for power penalties ranging from .05 to .2 pounds/foot-pounds per second*, a range typical of space applications..

Vehicle densities were varied to determine the influence of a strong but uncertain variable on the choice of a minimum, as well as on the consequence of making a poor assumption as to the magnitude of that variable.

Figure 13 is a cathode ray tube reproduction of machine calculated values illustrating the intersection method used to obtain the minimum and is strictly a work chart; thus, no attempt has been made to separate the confusion of curves. Two cases have been marked heavily to illustrate the method. This technique differs from the gradient search technique for finding the minimum of a curve in that it uses two equations obtained by differentiation and establishes the minimum from their intersection. This technique is considerably faster than the gradient method, even by machine, and especially valuable where many cases are involved and where the formulation of parameters developed in the differentiation are useful for interpretation, and reduction of printout volume.

The intersections of two curves for thirteen cases (only 2 shown) established thirteen solution values. Such an analysis was repeated for an array of thirteen secondary side variations; thus a total of 169 cases.

When the weight solution for one side is normalized to a standard, a preliminary rank order is made as shown in the CRT tabulation of figure 14. Weight results are grouped into sets. Group number 1 contains the minimum and all solutions within 5 percent. Group numbers 2 through 5 contain all other solutions within 5 to 25 percent of the minimum. Those in excess of 25 percent of the minimum are shown as "x" and may be considered as undesirable and discarded. All cores within 25 percent of the minimum are also shown on the CRT Bar Chart of figure 15. "X" again indicates discard.

The result of all combinations (169) were also developed for CRT reproduction shown on figure 16. Columns and rows of the matrix were arranged according to the rank orders forecast by the independent rank order solutions for the water and air sides. A test of the accuracy of forecasting pair rank orders from the preliminary per-side rank orders occurs when no

* 37 to 148 lbs/kw

deviation in rank order exists within the matrix. In theory, deviations must exist whenever the data introduced differs by an amount which is smaller than the error created by the introduction of the arbitrary standard. The most significant results of the matrix are clearer when the matrix is reduced, as shown on figure 17 by (1) combining rows and columns which are within 5 percent since these may be regarded as equivalent choices, (2) by notation of the minimum as well as results which are within 25 percent of the minimum, (3) by deleting all values in excess of the minimum set which also conform to the rank order forecasted, and (4) by noting exceptions and their variance. Results obtained were as follows:

- (1) Only 5 exceptions to the per side forecast resulted. The most severe deviation was within 18 percent of the weight required to correct the rank order to the forecast value. All five were safely out of the region of interest since they were at least 125 percent heavier than the minimum.
- (2) No equivalents within 5 percent of the minimum occurred. A total of 18 pair combinations existed, however, within a 25 percent variation from the minimum, representing some degree of selection.
- (3) The total range of the weight parameter was 33 to 159, a ratio of nearly 5 to 1.

The result represents a remarkable accuracy for the prediction of single and pair core choices with minimum data, since only the type of fluid on both sides and vehicle density information were required in addition to core data.

It should also be noted that if the array were much larger, and the characteristics of cores much closer, a greater number of rank order shifts would occur, but the differences in weight would also be less.

In any case, if results were to deviate a great deal from the first trial, the standard can be adjusted and the solution normalized to an exact conclusion for the minimum pair and close equivalents. This process in itself gives the program a learning capability since the constant improvement of the standard provides a memory of best core characteristics from all previous solutions and is constantly adjusting in the direction of state-of-the-art.

Uncertainty and Consequence

The flow of rank order position with vehicle density is

shown for the most competitive cores on figure 18. Note that core number 9 remains within the top 10 percent over the entire range, whereas number 3 is the best at high values and out of the range of consideration at low values. The consequence of a very poor guess is more severe if number 3 is chosen than if number 9 is chosen. Note also that core number 1 improves, then regresses, thus is never competitive, a fact which permits further reduction of the competitive list.

This example provides at least preliminary evidence of a major improvement in speed and economy over conventional approaches, particularly where a requirement exists for a more accurate discrimination of alternates than the quick evaluation of an experienced design specialist.

It is believed that this development is new, unique, accurate, and practical. It is also believed that the method has captured to a significant extent the qualities of assessment, decision, learning, and the benefit of prior experience. It combines many of the capabilities of the experienced design specialist and the systems engineer.

Branches and Circuits Analysis

In addition to the effort described, approaches to the solution of loops, branches and circuits have been studied. Although optimization and synthesis approaches to the higher levels of assembly have been generated at a very preliminary level and appear promising, they have not yet been reported due to lack of confirmation as to accuracy or practical value.

Machine programs have been developed and examples tested for some simple loops, however, particularly those associated with thermal control. The formulations and solution methods have been highly generalized in order to permit solution of a large variety of processes and circuit arrangements.

Figure 19, the optimization of flow and operating state for a simple closed loop, is representative of the approach. In this case a minimum weight solution results from balancing the circuit load and requirement state (in the cabin for example) with the process and circuit ducting. The best balance of process and duct configuration for least total weight, yields a specific solution of loop flow and return state. Some of the parameters and variables used are weight (W), required concentration (C_1), return concentration (C_2), generated constituent (ΔM), ducting parameter (K_D), process parameter (K_p), loop flow (w_g).

SUMMARY OF DEVELOPMENTS

Basically, the developments consisted of

- (1) Circuit synthesis and breakdown, which encompassed
 - (a) Synthesis and decision planning.
 - (b) Organization of circuits into an assembly level scale, each level representing an assembly of a lower level.
 - (c) Development of arguments and criteria for selection and decision.
 - (d) Transformation of circuits into single function groups, each group representative of a requirement, a process and all circuit and vehicle factors which influence or which are influenced by the inclusion of that function.
 - (e) Concepts for the reduction of variables within each group by the application of restraints transposed from several assembly levels, combining variables which are process related, and by optimization of local independent variables.
 - (f) Selection from an array of competitive alternates with minimum data and conditions of uncertainty.
 - (g) Concepts for decision based on an analysis of consequence associated with trial decisions.
 - (h) Possibilities for optimum arrangement by analytical method.
 - (i) Possibilities for multicircuit synthesis.

ANTICIPATED APPLICATIONS

The approaches developed and results obtained are adaptable to the rank-ordering, selection, and optimum sizing of many types of processes, loops, and circuit arrangements. Approaches are not limited in their application to environment control systems, nor to space environments.

Considerable work is required, however, beyond the scope of present planning. Probably the element of greatest importance is the complete reorientation of traditional approaches to the subject, since the results of this

investigation have yielded a total approach which is neither fish nor fowl when compared with highly developed theoretical and machine analysis approaches or with strictly empirical or intuitive design approaches.

Specific studies needing further effort are:

1. Selection methods for many other specific processes.
2. Branch and loop studies at higher circuit levels including the combining of circuits at the cabin level.
3. Optimum circuit arrangement.

Some work is planned in these areas in Phase IV of the T & A contract but is limited to general development. Additional effort of considerable magnitude is required for specific processes and arrangements. Results are expected to have applicability for a long time to come, thus should be worthy of pursuit.

ACKNOWLEDGEMENTS

I wish to acknowledge the assistance and helpful criticism given by my colleagues at the Los Angeles Division of North American Aviation, Inc. who assisted me in the areas of computing, development and editing, and in particular to Grace Taylor, Leon Shafer, Bruce Truett, and Gordon Campbell.

REFERENCE

1. ASD Technical Report 61-176, Part II, Integration, and Optimization of Space Vehicle Environmental Control Systems, April 1962 to be published
2. ASD Technical Report (to be published), Part III, Integration, and Optimization of Space Vehicle Environmental Control Systems
3. Glasser, S., and Stelzriede, Mr., ASD TR 61-176, Integration and Optimization of Space Vehicle Environmental Control Systems, Part I (1961)
4. Technical Report No. 49, Department of Mechanical Engineering, Stanford University, The Heat Transfer and Flow Friction Characteristics of Five Offset Rectangular and Six Plain Triangular Plate-Fin Heat Transfer Surfaces, November 30, 1960

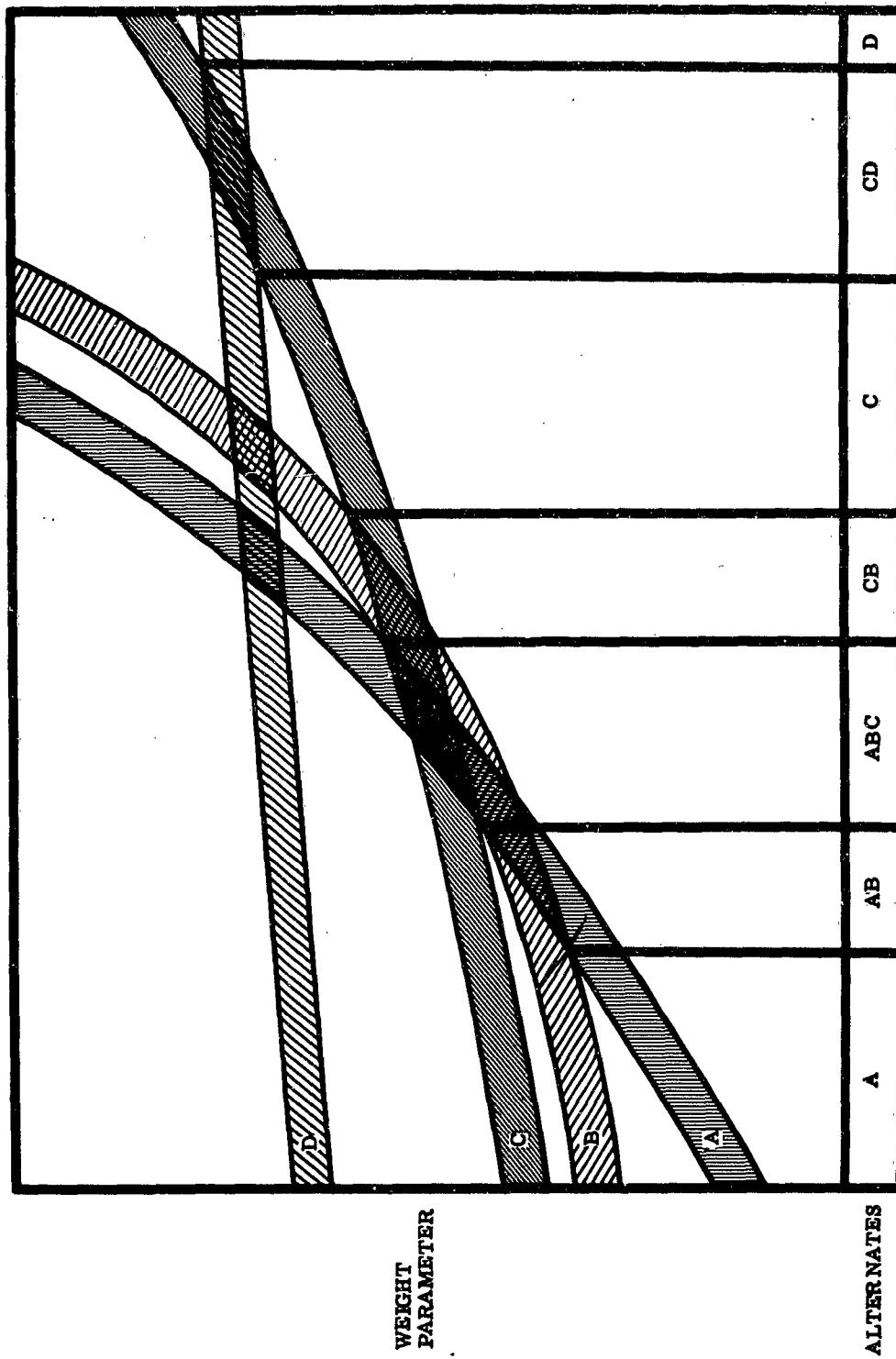


Figure 2. Effect of Tolerance on Multiple Choice

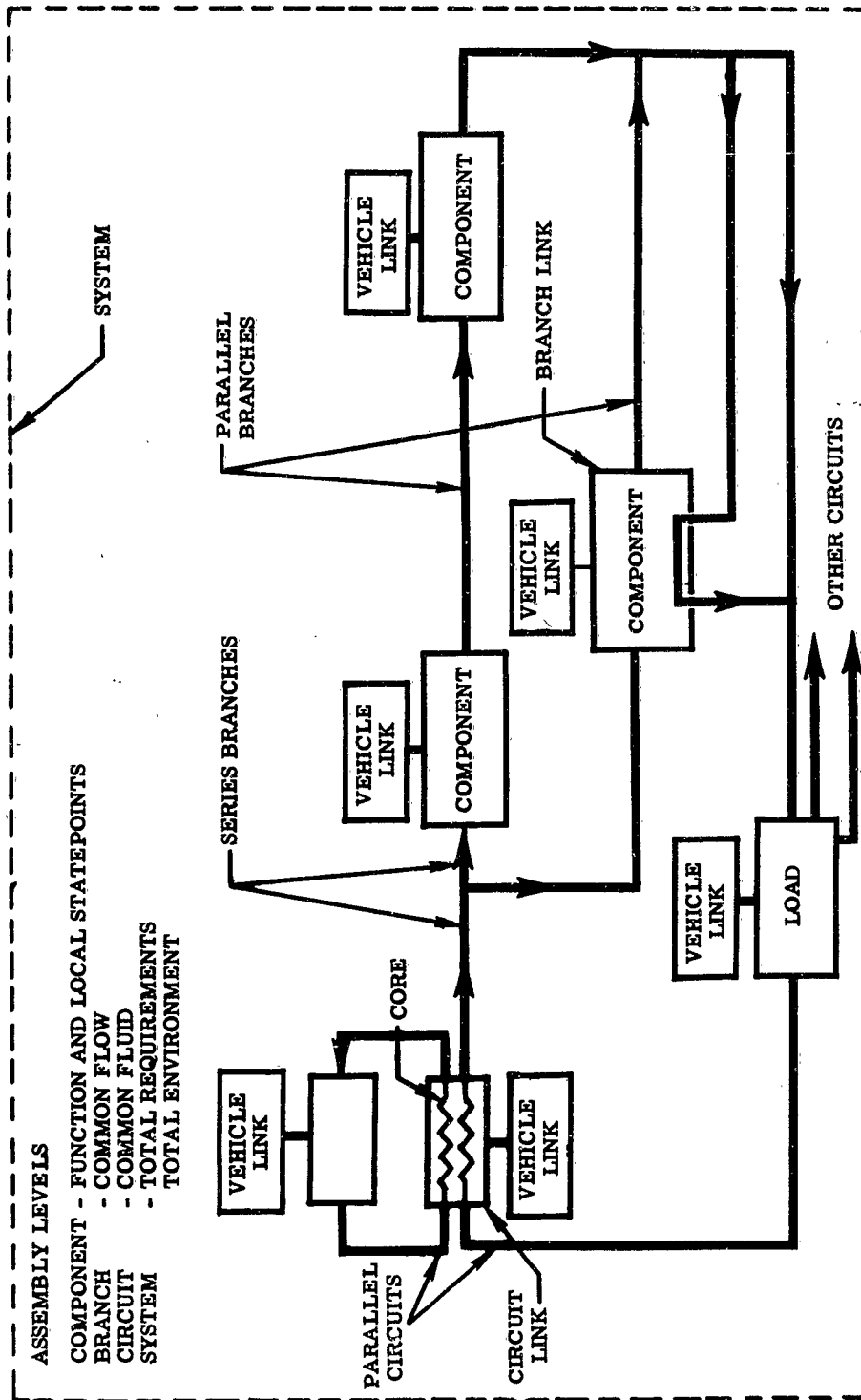


Figure 3. General Schematic Assembly Levels and Links

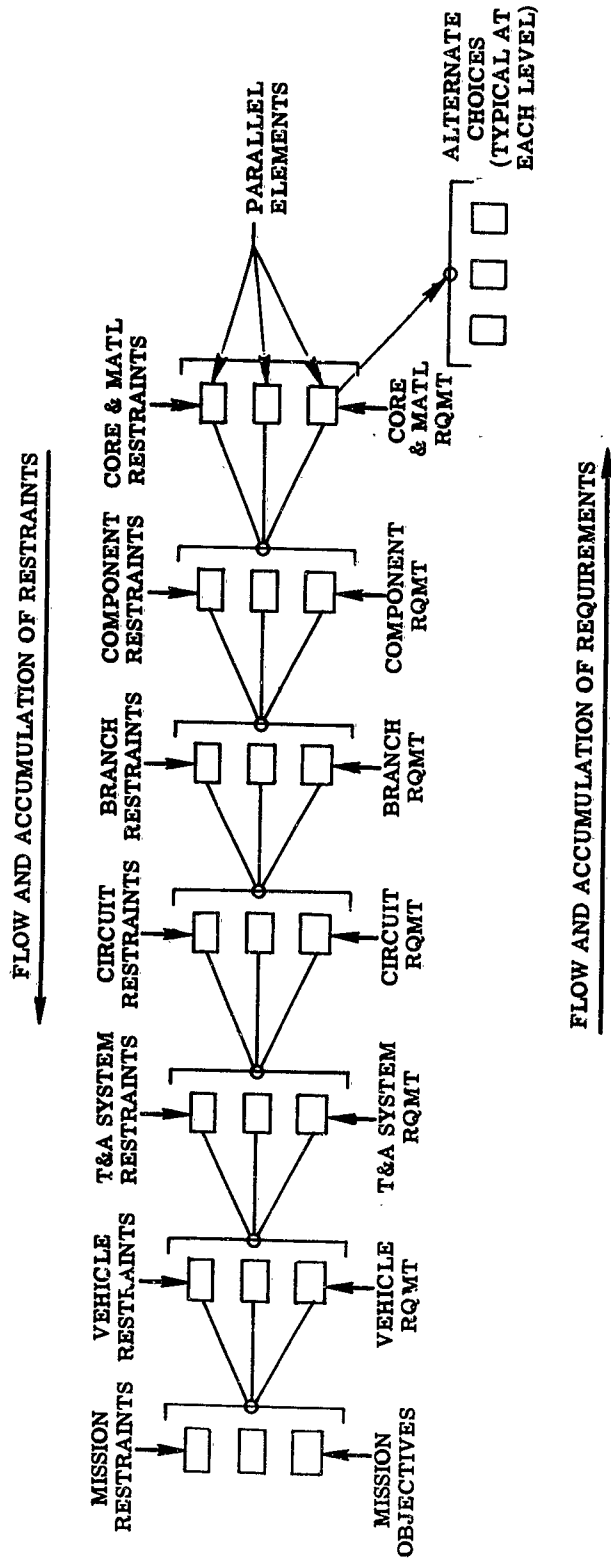


Figure 4. Synthesis Versus Assembly Level

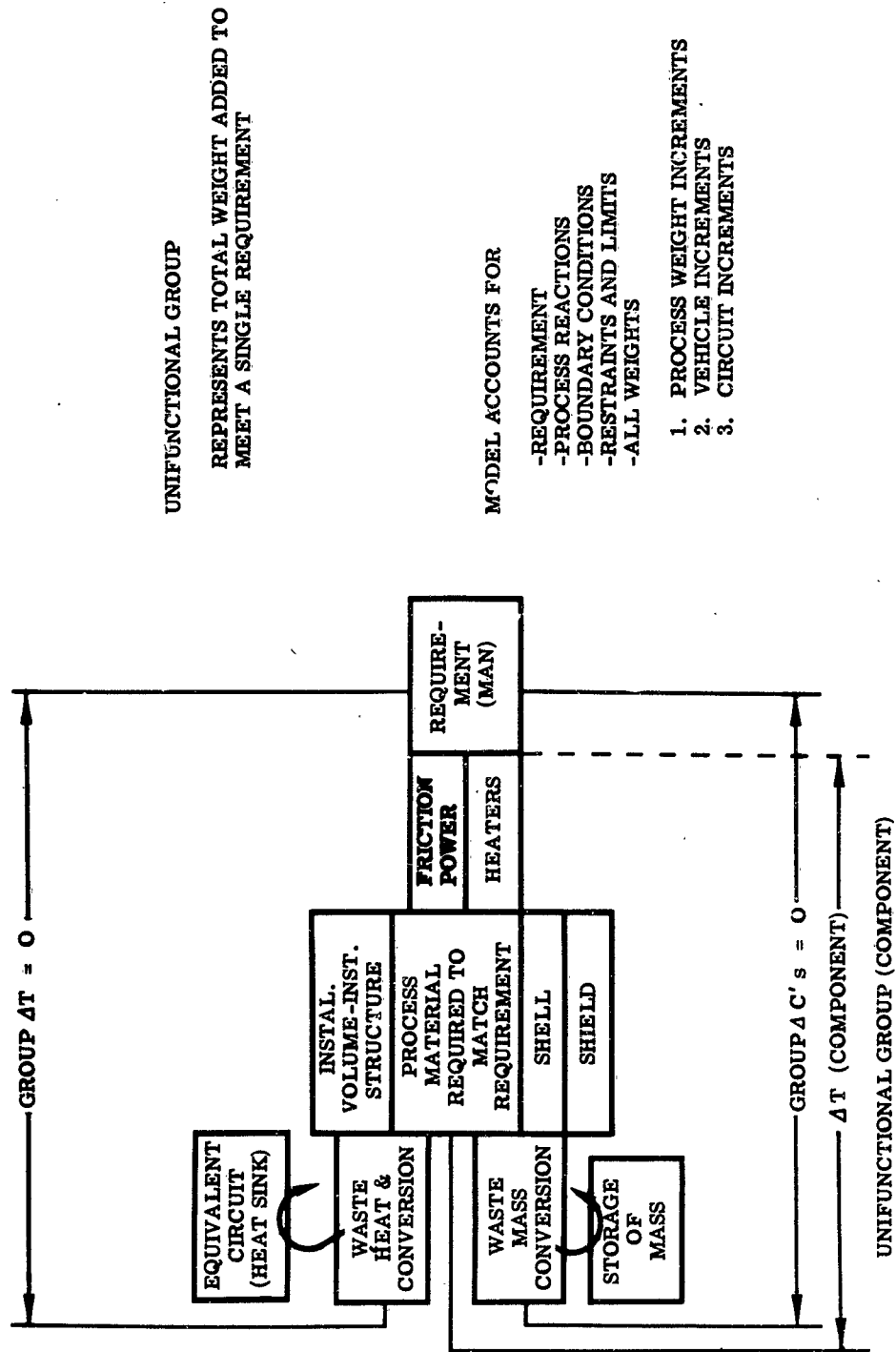


Figure 5. Circuit Synthesis

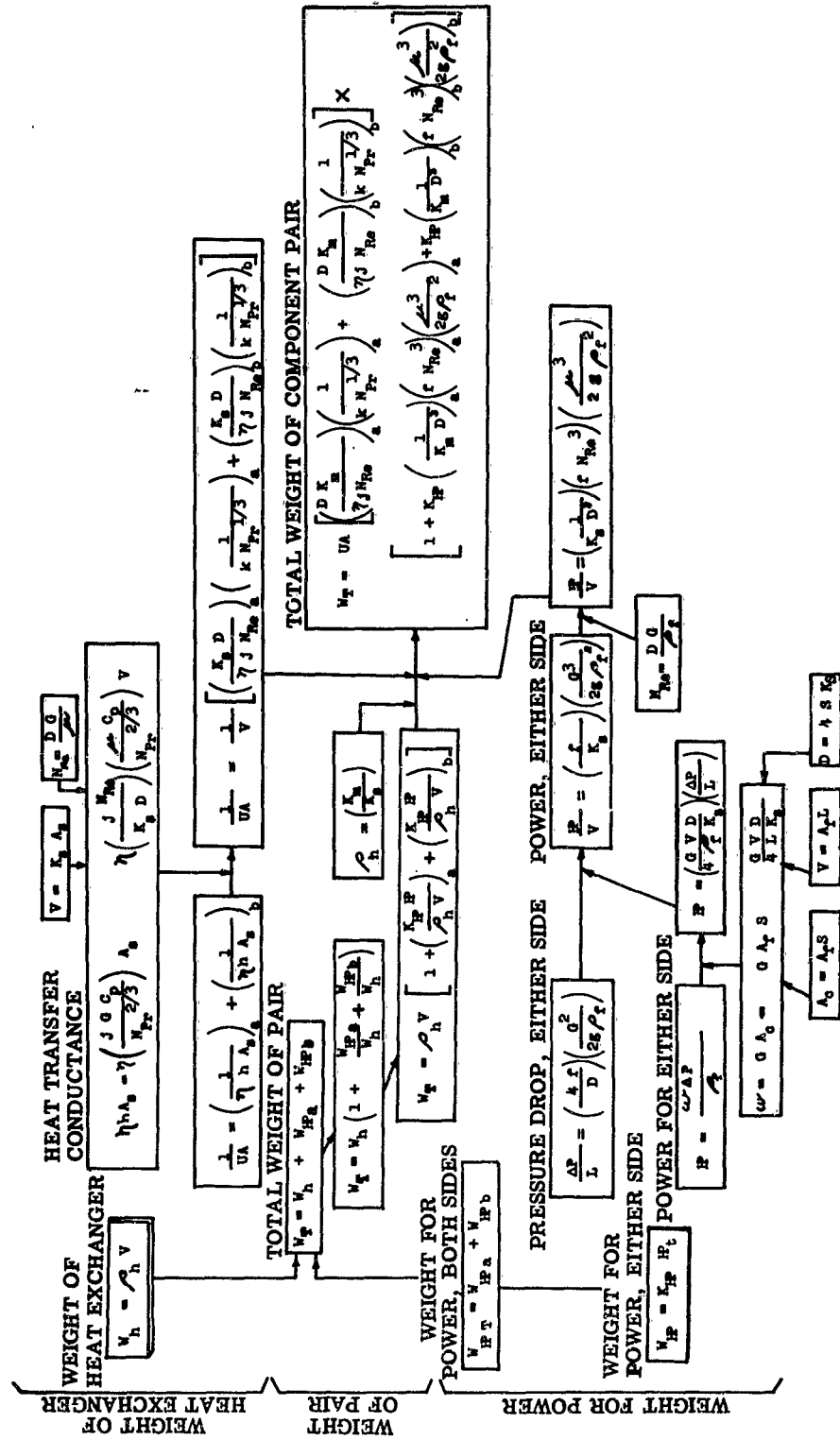


Figure 6. Characterization of Heat Exchanger-Power Pair

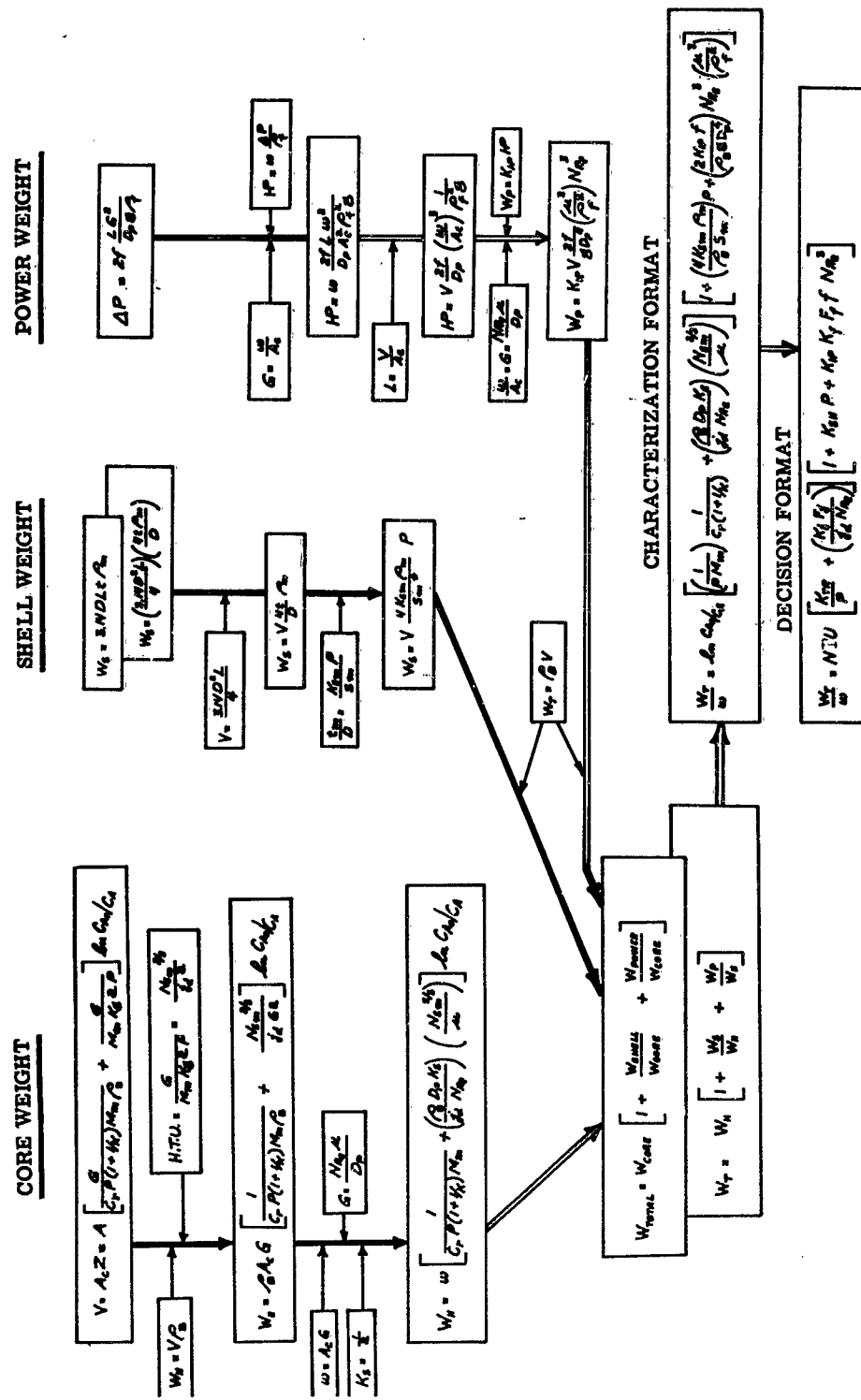


Figure 7. Catalytic Burner Characterization

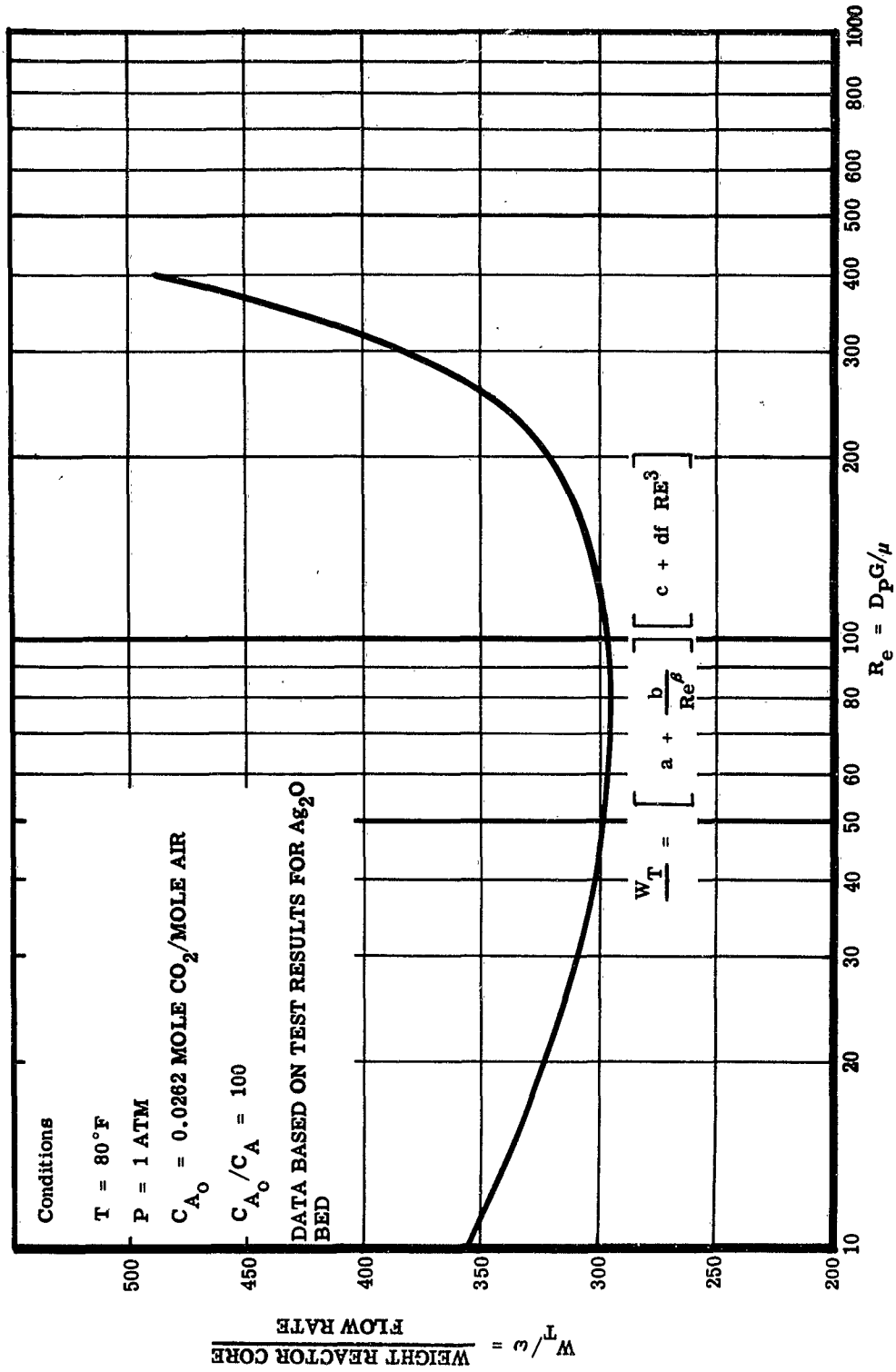


Figure 8. Chemisorber Optimization Example

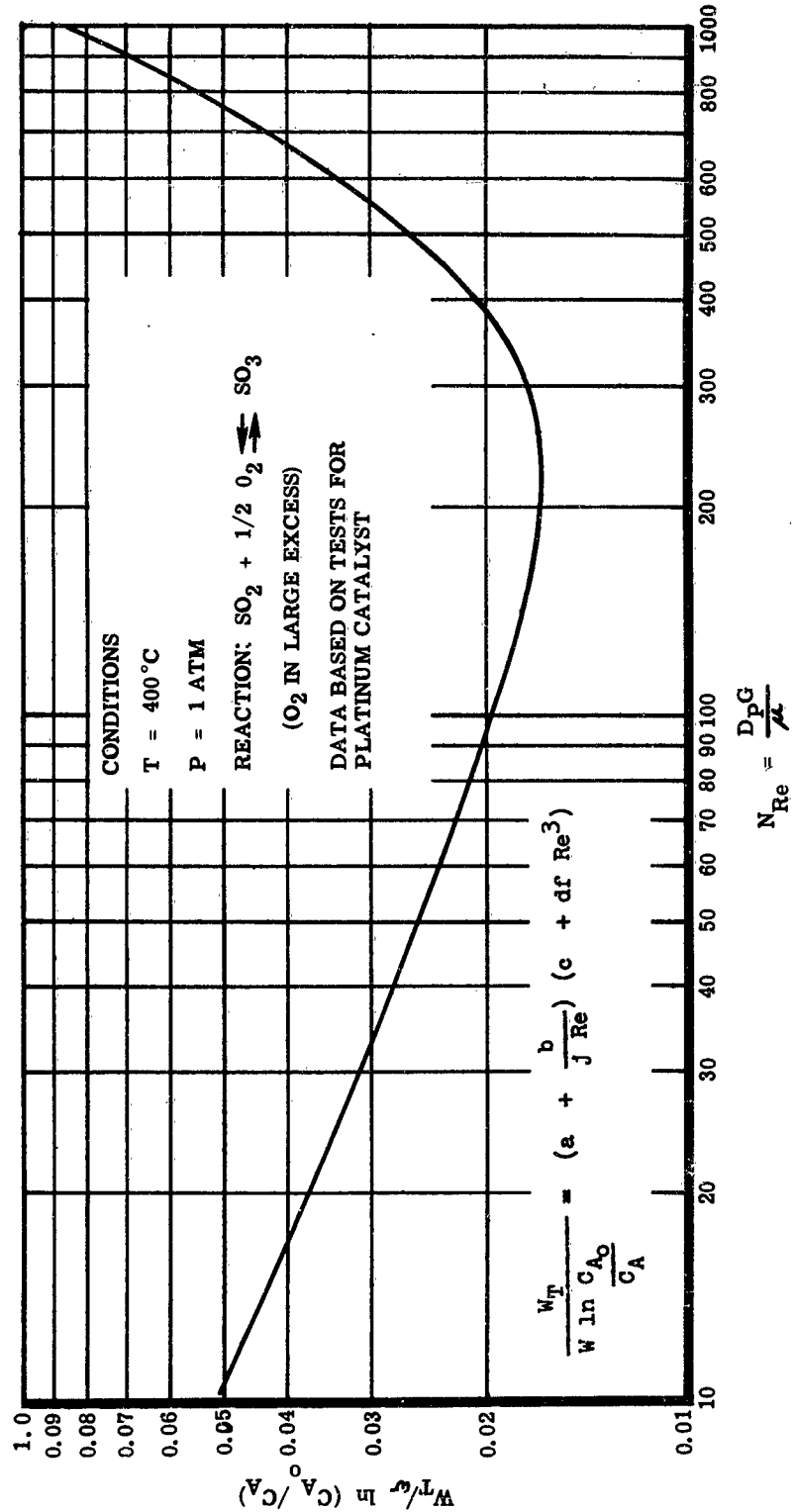


Figure 9. Catalytic Burner Optimization Example

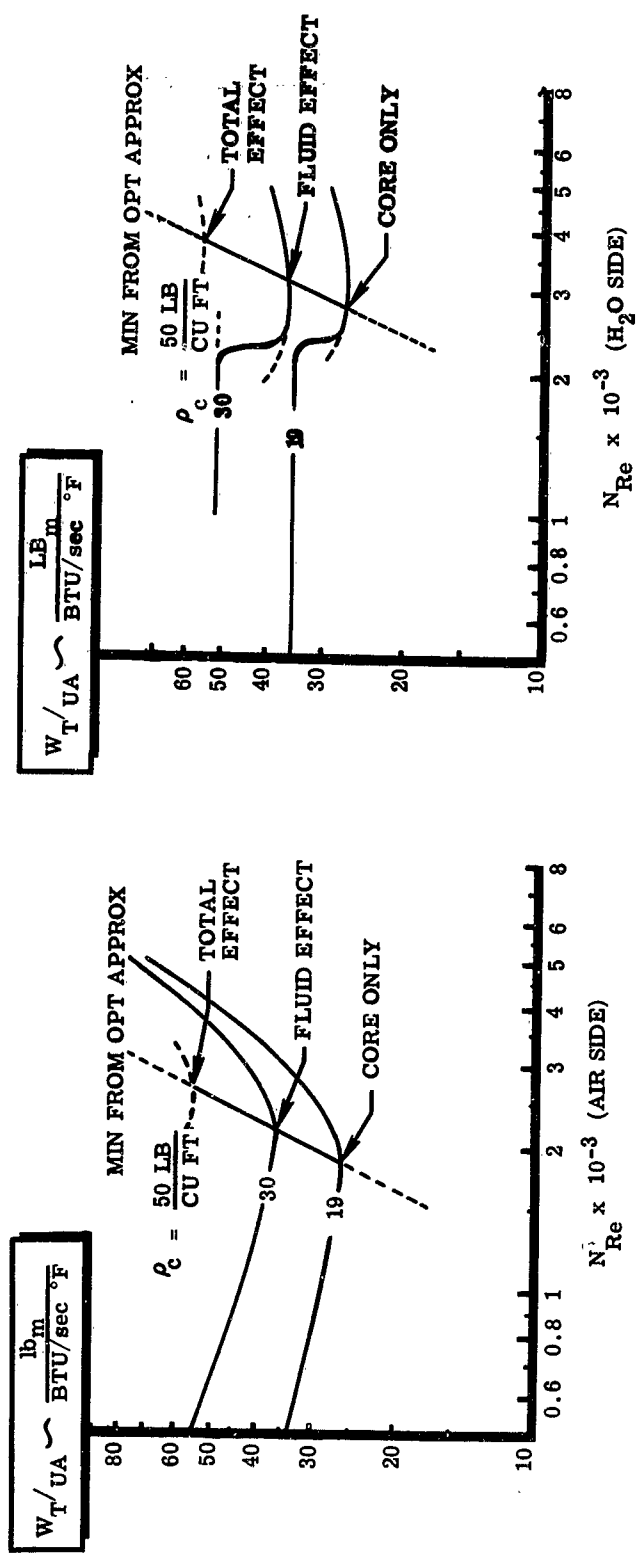


Figure 10. Heat Exchanger Optimization Example Showing Fluid and Vehicle Volume Effect (Total Density)

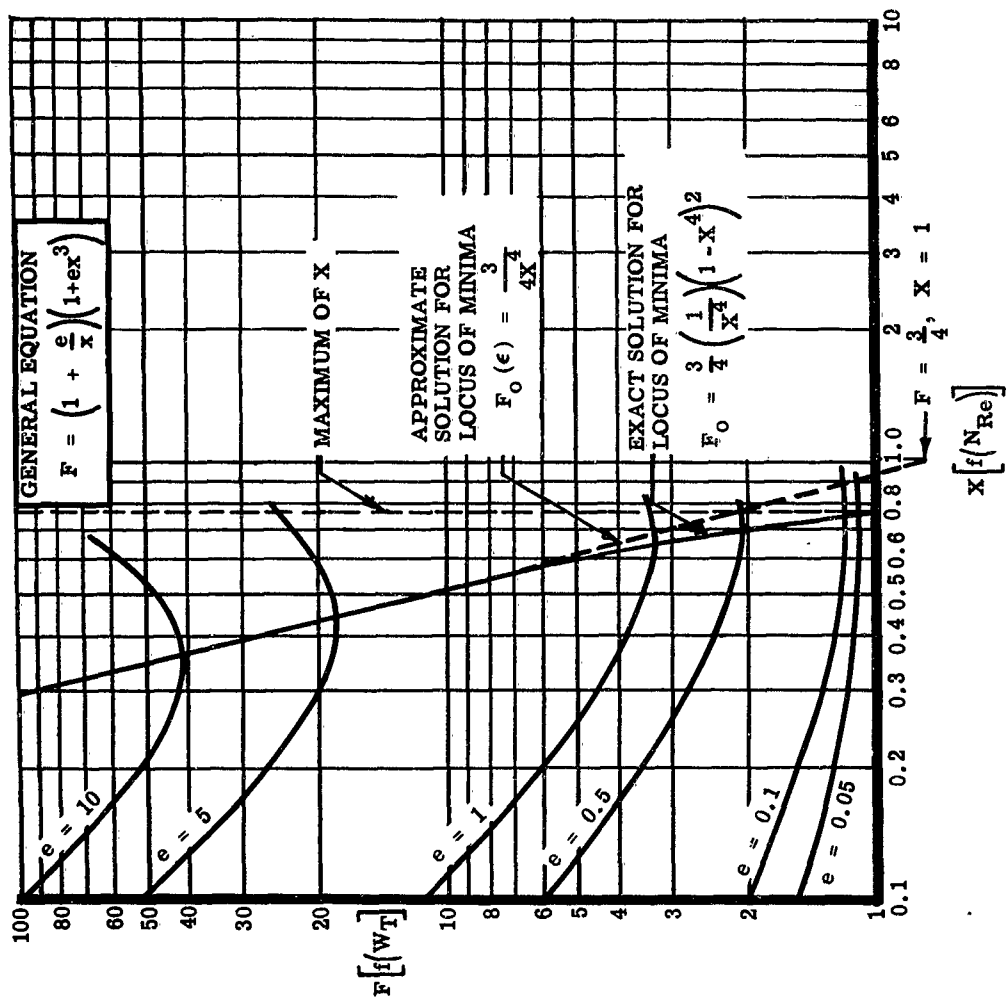


Figure 11. Exact Versus Approximate Solutions of Minima Catalytic Burner or Chemisorber

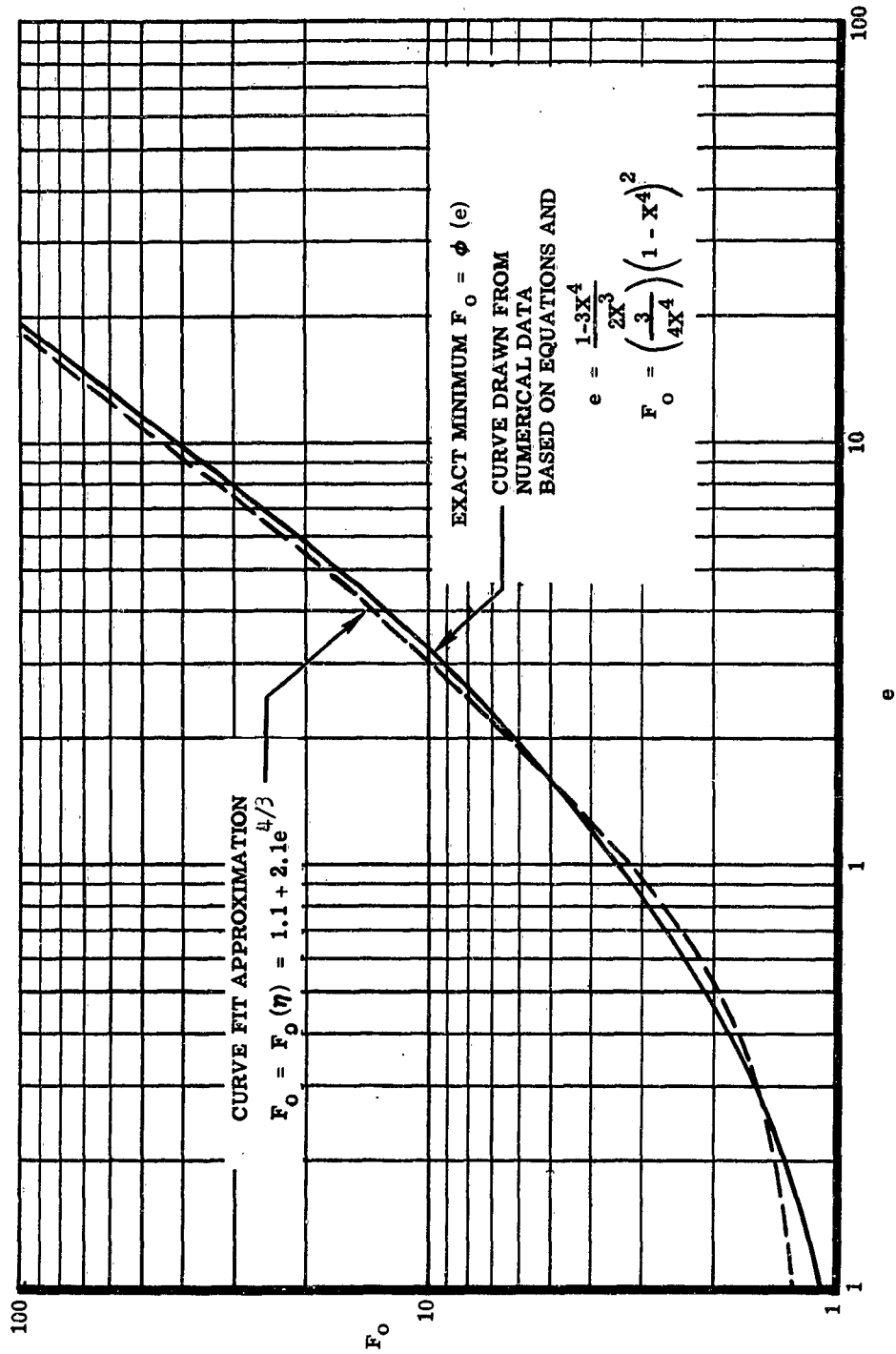


Figure 12. Curve Fitting of Minima to Eliminate a Variable

1175-40
016 - 016

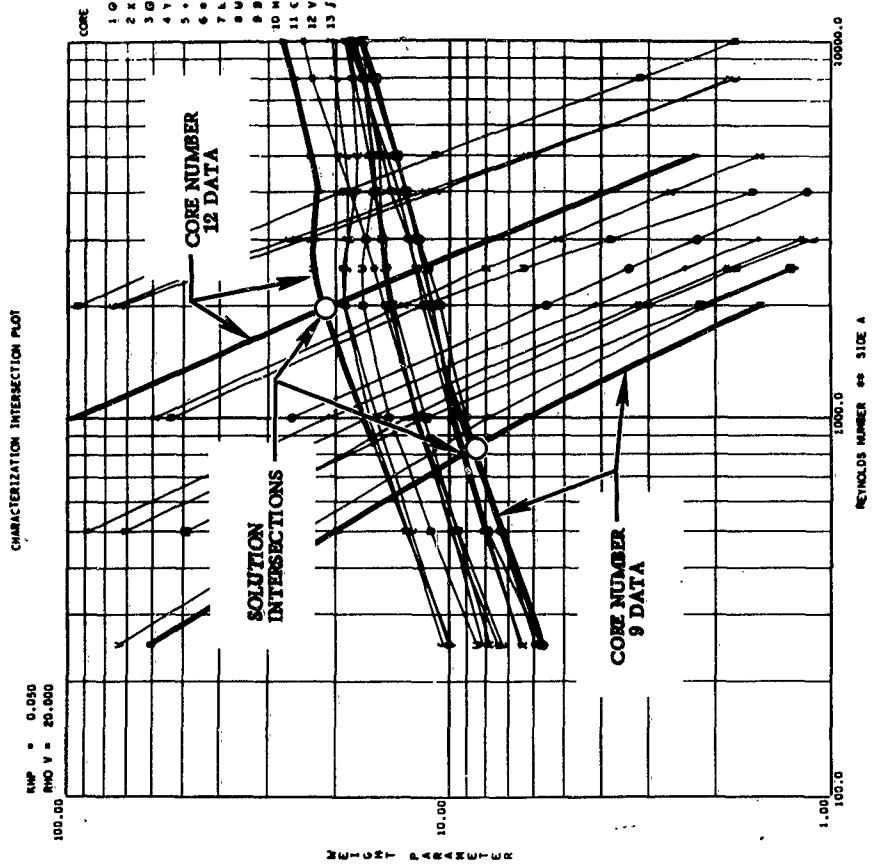


Figure 13. CRT Reproduction - Working Chart Showing Method of Solution by Intersection

1175-01
010-010

BANK ORDER
WT. TABLE

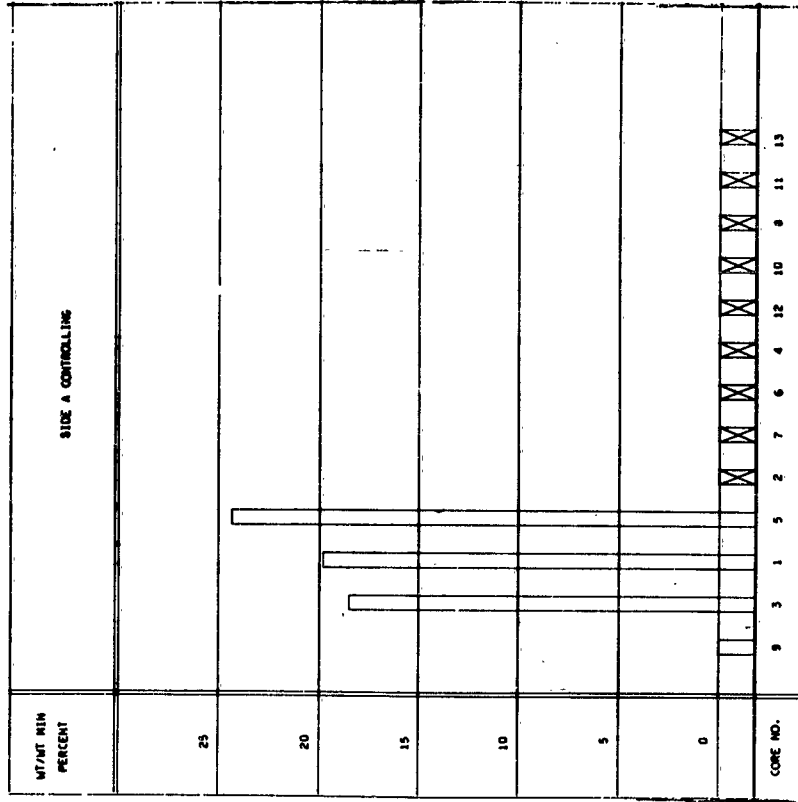


Figure 14. CRT Reproduction Showing Weight Results and Preliminary Rank Order

1173-08
017-017

RANK ORDER
WT. TABLE

RANK ORDER NO.	STAGE A CONTROLLING	
	CORE NO.	INT/UM3 VALUES
1	9	33.805
4	3	40.052
	1	40.501
5	5	42.037
X	2	51.261
	7	53.831
	6	55.669
	4	67.193
	12	67.317
	10	75.152
	8	80.199
	11	90.231
	13	93.028

Figure 15. CRT Reproduction Showing Weight Results of Best Solutions

OPTIMIZED WEIGHT PER UNIT UA
(PRE-OPT. METHOD)

SIDE 8 CORE NO IN RANK ORDER	SIDE 4												
	9	3	1	5	2	7	6	4	12	10	8	11	13
7	33.0	40.4	40.2	42.2	51.6	54.0	56.4	67.0	66.2	74.6	79.2	89.3	92.1
12	36.1	43.7	43.6	45.6	55.3	58.6	60.4	71.0	70.6	79.1	84.7	94.6	97.8
3	39.3	46.4	45.7	47.6	58.4	66.1	62.3	75.7	76.6	84.6	93.7	102.2	106.6
11	38.2	46.1	45.6	47.6	57.9	63.1	62.4	74.7	74.6	83.4	90.2	100.0	103.6
13	40.3	48.3	47.8	49.9	60.5	65.9	65.0	77.6	77.5	86.4	93.5	103.3	107.1
9	46.0	52.0	51.2	53.0	64.8	76.1	69.2	81.4	87.0	93.7	106.1	112.9	119.4
4	45.1	51.6	50.8	52.9	64.4	74.6	68.1	82.9	85.3	92.6	106.2	111.6	117.6
5	47.2	53.0	52.1	53.9	65.7	76.1	69.2	84.7	88.8	95.4	108.6	115.3	122.0
1	50.9	55.8	54.9	56.6	68.2	82.8	72.1	88.6	93.7	99.9	114.3	120.6	128.0
2	55.9	60.1	59.2	60.8	74.1	90.0	76.8	94.4	101.3	108.7	122.9	129.3	137.4
6	48.1	57.3	57.2	59.5	70.6	73.6	75.9	88.5	87.4	97.4	103.3	114.2	117.7
8	56.4	60.4	59.5	61.1	74.5	90.0	77.1	94.8	102.3	107.4	123.9	130.2	136.5
10	67.3	70.3	69.5	70.9	85.9	106.5	87.7	108.1	120.5	122.7	141.9	146.9	159.0

Figure 16. CRT Reproduction Showing Pair Weight Results
in Rank Order Format

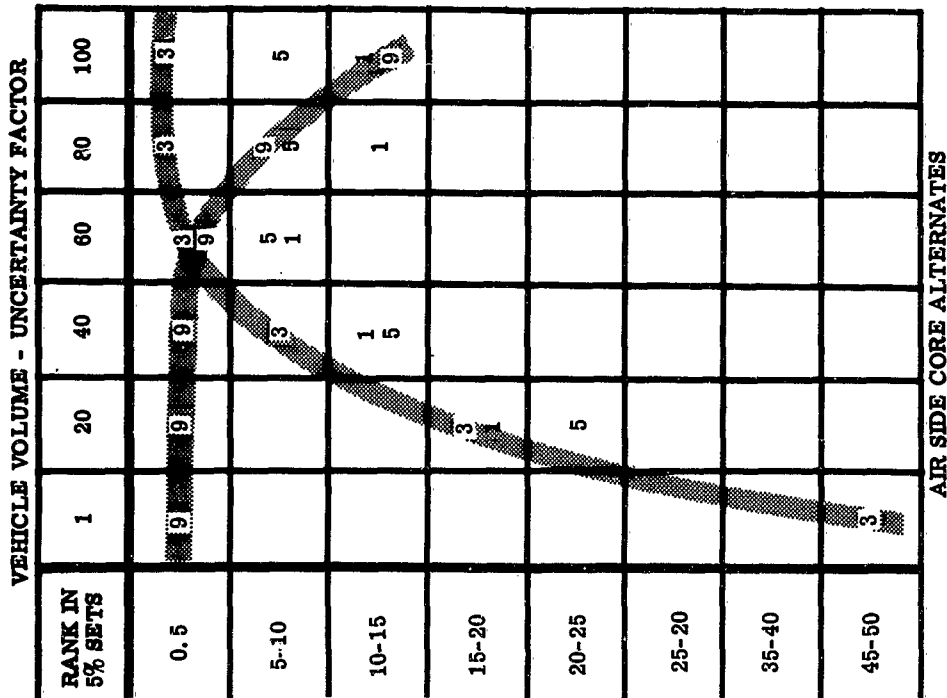
AIR SIDE CORE NUMBER (5% SETS)

WATER SIDE NUMBERS	9	3 1 5	2	7 6	4 12	8	11 13
7	1.0	1.22					
12	1.10						
3 11	1.19						
13 9	1.22						
4	1.40						
5 1							
2							
8				2.24	2.65	2.95	3.13
6							
10							4.82

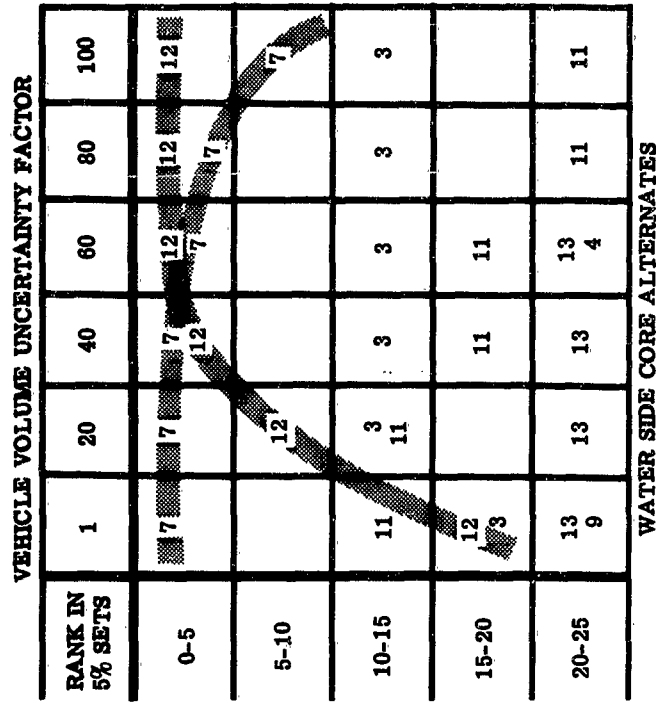
Annotations:

- SOLUTIONS WITHIN 25% OF MINIMUM (points to cell 3, 11)
- FOR DATA NOT SHOWN IN SAME ORDERS CONFORM (diagonal across middle)
- ENTRIES DEVIATING OVER 5% FROM PREDICTION (points to row 8)
- MAX DEVIATION 18% (points to cell 8, 4)
- MAX WEIGHT (points to cell 10, 8)

Figure 17. Normalized Weights With Near Equal Rows and Columns Combined



AIR SIDE



WATER SIDE

Figure 18. Influence of Vehicle Design Uncertainty on Selection

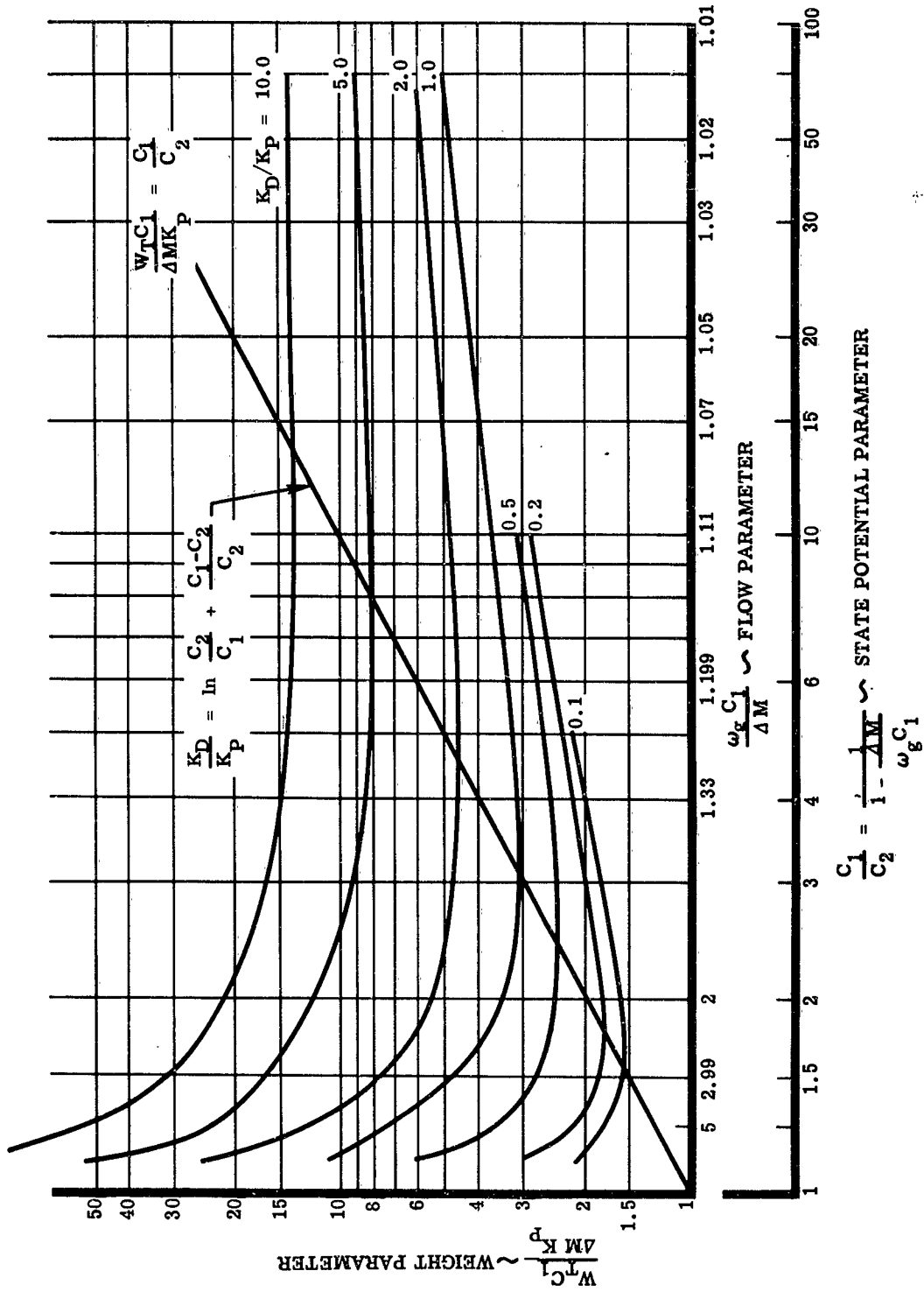


Figure 19. Simple Closed Loop Optimization (Process, Ducting and Source)

Second Paper -- "Methods for Synthesis of Optimal Environmental control Systems," by R.A. Paselk, North American."

QUESTION: (S.N. Berliner, ITEK Corporation) Were optimized weights for core only for the heat exchanger, or did the analysis include header ducting?

ANSWER : (Mr. Paselk) The heat exchanger analysis included weights for the core, the headers contained fluids, vehicle weight increment due to volume displacement. Ducting is not included with the heat exchanger, but is partially optimized separately, then optimized in a loop containing fluid ducting and heat exchanger as well as a load.

QUESTION: (Mr. H. Cohan, Lockheed) Have you investigated the use of highbred digital analogue machines in evaluating the importance of parameters?

ANSWER : (Mr. Paselk) I think the answer is: Not as a total computing system. We have used the 1620 in conjunction with plotters, and we have used the 7090 in conjunction with the cathode ray tube and photo process for print-outs. We do however in the formulation of a problem, we have used analogue techniques but we have solved the analogue equations by digital methods.

**ANALYSIS OF THERMAL AND ATMOSPHERIC
CONTROL SYSTEM FOR SPACE VEHICLES BY
APPLICATION OF DIGITAL COMPUTER TECHNIQUES**

by

F. H. Green

**The Garrett Corporation
AiResearch Manufacturing Division
Los Angeles, California**

ANALYSIS OF THERMAL AND ATMOSPHERIC
CONTROL SYSTEMS FOR SPACE VEHICLES BY
APPLICATION OF DIGITAL COMPUTER TECHNIQUES

SECTION I

OPTIMIZED SYSTEM PERFORMANCE

A thermal and atmospheric control system for a space vehicle consists of a number of different components which may be arranged relative to the air flow path in many different ways. Each such arrangement is referred to as a circuit. The basic requirements for a circuit are that it must have a minimum of three components. First, there must be a load to be modified. This load may represent the change in the atmosphere caused by the presence of an occupant of the space module or it may represent the load caused by the presence of equipment to be cooled or otherwise modified. The second necessary component of a circuit is a means of circulation. This component may be a fan, or an axial flow or radial flow compressor. The third necessary element is a piece of equipment which modifies the air flowing in the circuit in at least one manner.

Typical circuits, utilizing three components, are shown in Figure 1. For example, Figure 1(a) shows a circuit consisting of a load, a circulator, and a filter. Such a circuit would be useful only in removing dust particles and aerosols from the air flowing in the circuit. Figure 1(b) shows a similar circuit utilizing a catalytic oxidizer. The catalytic oxidizer is composed of a catalyst which has the ability to oxidize certain low-molecular-weight compounds, such as hydrogen, carbon monoxide, and methane, producing carbon dioxide and water. Such a device will work at low temperatures with hydrogen, but requires a relatively high temperature with methane. Figure 1(c) shows a circuit which incorporates activated charcoal. Activated charcoal works on the principle of physical adsorption on the surface, and has the ability to adsorb most compounds of molecular weight higher than approximately 30. These compounds include most body odors and hydrocarbons which might get into the vehicle. Figure 1(d) shows the use of lithium hydroxide as a method of removing carbon dioxide. Figure 1(e) shows the use of a heat exchanger to

lower or raise the dry bulb temperature of the air passing through the circuit. Figure 1(f) shows the use of a moisture absorber to remove moisture from the air in the circuit.

Each of the circuits performs only one of the following categorized functions: (1) removal of dust, (2) removal of low-molecular-weight contaminants, (3) removal of high-molecular-weight contaminants, (4) removal of carbon dioxide, (5) change of temperature, and (6) removal of water. It is not so apparent that there is also a need for circulation to provide mixing of the air in the module of the space vehicle. Circulation can be eliminated if natural convection is available. The familiar example here, of course, is the use of steam radiators for heating a building. However, at the low-g or zero-g values likely to be present in a space vehicle, natural convection will either be very weak or entirely absent and, therefore, it can not be relied upon for circulation. Also, many of the designs for space vehicles of the future are of such physical shape that they would not be well adapted to natural convection; forced circulation would be required. In addition, unless a reasonable amount of power is used to move the air through the various circuit components, the components, themselves, will have to be very large.

It would appear logical to arrange all of the elements of the circuit in series in the manner shown in Figure 2. For ease of computation we have separated two heat exchanger functions which are actually contained within the same single exchanger. That is, we have defined a temperature control heat exchanger and a water-condensing heat exchanger. By this we mean that the temperature control heat exchanger reduces the temperature to the dew point of the entering air, but no condensation takes place in that heat exchanger. The water-condensing heat exchanger further reduces both the temperature and the dew point to the point necessary to satisfy the conditions of the general circuit.

To review the functions occurring in Figure 2, the load is added to the air, including dust, low-molecular-weight contaminants such as methane, high-molecular-weight contaminants such as body odors, carbon dioxide, heat, and moisture. The air passes, first, to the filter where the dust is removed; then to the circulator which increases the temperature and pressure, and

provides the force for circulating the air; then to the catalytic oxidizer which removes the low-molecular-weight methane; then to the activated charcoal which removes the higher-molecular-weight odors; to the lithium hydroxide which removes the carbon dioxide, but, in so doing, adds both heat and moisture to the air; to the temperature control heat exchanger which brings the air down to the inlet dew point; and to the water-condensing heat exchanger which now takes out an amount of water equal to that added by the load, plus that added by the catalytic oxidizer and the lithium hydroxide. This water is now in the form of fog which must be coalesced and removed from the airstream in the water separator. The air, now at a lower temperature and lower moisture content, and relatively free of contaminants, passes back to the load for reuse. This series circuit, as described here, is essentially that used in Project Mercury, except that the Project Mercury circuit does not include a catalytic oxidizer. The Project Mercury circuit, however, also includes a second circuit similar to Figure 1(e) for additional temperature control in the capsule, particularly just previous to re-entry.

It is well to elaborate on the total function of the water control and temperature control heat exchanger combination. Although in an actual vehicle, this is quite likely to be built as a single unit, it is much better, mathematically, to consider it as two separate pieces of equipment. Figure 3 shows the temperature and moisture content of the air at all points in the circuit. The separate functions of the two heat exchanger sections are readily distinguished. The air enters the first section at a temperature of 148°F and is reduced to the dew point of 54.5°F. From the original dew point of 54.5°F, the air is further cooled in the second section to a final dew point of 40°F. Although the process in the first part of the heat exchanger is relatively simple, that in the second part of the heat exchanger is more complex, since the temperature of the air and the amount of moisture removal both affect the size of the heat exchanger surface which is required for removal of each Btu.

To look at the entire picture, consider Figure 4 which shows the relative effect of the various elements in the thermal and atmospheric control system on the various parameters of the flow circuit and on the overall system

parameters of volume, weight, and power input. Note that there are four types of loads: metabolic load for people, equipment load, which would also include heat flow through the walls of the vehicle, and supply and leakage loads relative to the gases themselves. Of the various parameters, note that it is desirable to keep separate account of water vapor, carbon dioxide, nitrogen, and oxygen, and record, for each point in the circuit, the temperature, pressure, total weight flow rate, and the dimensions, volume, weight, and direct power input to each component. A distinction in the method of computing described here is that the direct power input, at each component where electrical or other high-grade energy is used, is the only consideration in the circuit. The "equivalent" power is not used since it is believed that this is a far more difficult method of handling the problem.

If we are going to study all possible circuits for a space vehicle, then we note (Figure 4) that there are nine circuit elements which can be arranged three or more at a time. This would lead to $9! + 8! + 7! + 6! + 5! + 4!$ arrangements. It would be relatively impractical to attempt to solve all of these, even with a high-speed computer. Fortunately, many of the arrangements are not practical. For example, by definition the temperature control heat exchanger must either be used alone or must precede the water-condensing heat exchanger. The reverse is not acceptable. The water separator must follow the water-condensing heat exchanger unless we are going to fog up the cabin.

In the original design of this program, it had been planned that the machine would make the various choices relative to different types of air conditioning circuits and would explore all of the feasible possibilities. It would be necessary, however, to place many restrictions on the $409,104$ possible arrangements of the 9 circuit elements. It did not appear worthwhile to write a complex program merely to inform the machine which restrictions to observe. As an example of this, consider the catalytic oxidizer. Present thinking is to the effect that this device requires only about 2 to 5 percent of the total flow in order to perform its function. Further indications are that the pressure drop of the device will be high, even at this very low flow. Therefore, the catalytic oxidizer should be placed in the circuit where its pressure drop will cause the least difficulty. The actual method of doing this, which seems to be best in most cases, is to place the

device around the circulator as shown in Figure 5, so that the full circulator pressure drop is available. This arrangement ensures that the output of the catalytic burner, which does have some odor, will go through the activated charcoal. Many other considerations led to the conclusion that it was far easier to specify the relatively modest number of combinations which would be feasible and then actually try each one of those separately as an individual problem.

The program, as currently established, permits use of 18 different system elements. Of these elements, one must be the load and one the circulator. One or more of the other elements may be chosen from the remaining 16 elements. To permit rearranging the order of the elements without interfering with the program itself, a table of values of NFROM and NTO is established as shown in Figure 6. The relative locations of the elements in this circuit are from the first to the highest number used, which may be as high as 18. The numbers fed into the machine for each location represent the previous element and the following element; that is, if the air flows from the load to the circulator and then to the filter, this being the circuit shown in Figure 1(a), the load being numbered 1, the circulator 2, and the filter 4, then, at the fourth (filter) positions in the NFROM and NTO matrices there will be NFROM = 2, representing the circulator, and NTO = 1, representing the load. A similar arrangement is used throughout this particular case. The next case may have an entirely different arrangement. In other words, the filter might be located between two different elements, and this would be readily shown by the input matrix. As written now, the matrix allows computation of up to seven different circuits during one machine run, with complete freedom for use of any desired arrangement of elements.

To clarify the handling of the data where the various elements of the circuit may be arranged differently for each case, and to avoid too many special features in the program, use is made of the device of establishing the output or DATOUT matrix with the elements arranged in the same order as in the input matrix, and all desired values are referred to this output matrix. That is, if the input matrix calls for the sequence load, filter, and circulator, then these will be the first three items appearing in the output

matrix. The output matrix for one solution is shown on Figure 7. It will be noted that 14 different parameters applying to the elements and the system appear relative to each component. By definition, such parameters as temperature, pressure density, and the five flow rates apply to the conditions at the outlet of the component. Such items as area, length, volume, weight, direct power input, and pressure drop apply to the individual unit computed for the stated conditions. Since each element subroutine takes its input from the DATOUT matrix and returns its output to the DATOUT matrix before the next subroutine starts, thus updating the matrix each time the circuit goes through the loop, it is possible to have a relatively straightforward program which permits rearrangement of the elements without change of any subroutines. The specific dimensions of the parameters shown in the DATOUT output matrix are as follows:

1. Temperature, °F
2. Pressure, in. of water, absolute
3. Total weight flow rate, lb per hr
4. Water vapor weight flow rate, lb per hr
5. Carbon dioxide weight flow rate, lb per hr
6. Oxygen weight flow rate, lb per hr
7. Nitrogen weight flow rate, lb per hr
8. Pressure drop or rise, in. of water
9. Gas density, lb per cu ft
10. Significant flow cross-section, sq in.
11. Significant flow length, in.
12. Volume in cubic inches
13. Component weight in lb
14. Direct electrical power input in watt-hr per hr

In the actual operation of the circuit, certain quantities must be given: the metabolic heat loads, both sensible and latent; the range of air flows to be studied; and the desired limiting temperature from the heat exchanger combination. The reason for making this last quantity an input is that the environmental control system, in general, is dependent on some external heat sink; variations in this will cause great variation in the circuit performance. The circuit starts computation with the given loads; takes the

average of the weight flow range set in the input; and, using this resulting outlet temperature from the load, provides this input and the given pressure and other conditions to the first element; determines the changes which will occur in that element; goes to the second element and determines those changes; and so on around the circuit. When the question of pressure is considered, the matter is handled readily by merely establishing that each time around the circuit the pressure rise in the circulating device must equal the sum of all the other pressure drops in the circuit. In order to get the cycle started the first time, initial values are fed into the program. Even if inaccurate, these approximate values will not interfere with the program operation.

When the program reaches the heat exchanger complex, it determines, first, the dew point of the incoming air which, of course, is a function of the quantity of the moisture available and of the total pressure and density of the air stream. This dew point is, by definition, the outlet air temperature of the temperature control heat exchanger, and the inlet air temperature for the water-condensing heat exchanger. The outlet temperature of the water-condensing heat exchanger is one of the given items. Thus, the air side of the heat exchanger is fully defined. On the liquid side of the circuit, it is merely required that the temperature of the inflowing liquid be defined and the available rate of flow and specific heat of that liquid.

The program then computes the conditions in the temperature-control heat exchanger for which the drop in dry bulb temperature in that heat exchanger, plus the drop in the water-condensing heat exchanger, will equal the total temperature increase of all the other elements in the circuit. This approaches the ideal condition where the circuit will be fully balanced, or optimally designed, relative to the heat exchanger and also relative to the circulator. Any less specific assumption than this would lead to a rather chaotic output and very little chance of actually reaching a solution.

The quantity of moisture present and the amount of carbon dioxide present in the circuit are allowed to adjust themselves to meet the specified conditions: The output of the water-condensing heat exchanger will represent saturated air at a known temperature; and the output of the lithium

hydroxide removing device will contain a particular partial pressure of carbon dioxide. Typically, for chemical-type carbon dioxide removal systems, a partial pressure of 1/2 millimeter mercury may be used. In going around the circuit, the system computation has determined volumes, weights, and power inputs for each element in the system. The optimizing SOBER routine now takes over and, utilizing a weight/power penalty quantity which can be inserted into the program, it looks for a minimum sum, S , of weight and power weight penalty with a possible maximum limitation on volume. The actual quantity minimized is $S = \alpha \sum \text{POWER} + \beta \sum \text{WEIGHT}$, wherein the relative importance of power and weight may easily be redefined by changing the input values of α and β .

The subroutine SOBER selects and identifies the proper parameters for the given arrangement and varies the parameters in the direction of minimum S , subject to the constraints imposed on the affected elements. For fixed increments of the parameters, the criterion of convergence is based on a repeatable oscillation of the value of S about the minimum point. When this happens, the sizes of the increments are decreased by a constant proportion and another search in a finer mesh is conducted. The increment sizes are reduced a third time before the solution is considered final. In case the variables do not define a "convex" function in the neighborhood of the optimum point, or in case of other difficulties, the program then simply selects the minimum design out of 100 trial combinations of the parameters. A flag is set up to indicate whether a solution is obtained by means of a normal exit or by means of a truncated exit.

The usual amount of time required to completely design a system on an IBM 7090 is less than one minute, including optimization. It should be noted that the print-out contains information on all 14 of the parameters for up to 18 circuit elements, together with such additional parameters as total weight, total power, and weight-power penalty total.

The system which has been designed is optimum for only the one given set of conditions. Since any real system may operate at many other imposed conditions, it is desirable to continue the analysis to determine operation at off-design points and under transient inputs. Both of these functions are described in the next section of this paper.

SECTION 2

TRANSIENT SYSTEM PERFORMANCE

Analysis of transient performance of atmospheric control systems may be defined as the determination of the detail performance of a given system (arrangement of components) based upon a given set of imposed time-varying conditions. For the analysis to have validity and usefulness, the influence of the system performance upon the conditions of the atmosphere in a conditioned space must be included in the analysis. The total process can be presented as shown in Figure 8.

In the transient analysis process, the starting point is the previously determined atmospheric control system for a compartment of a space vehicle. The transient computer program then determines the performance of the system, and the resulting characteristics of the conditioned atmosphere as a function of elapsed time. A typical system may contain 10 different pieces of equipment, each with its own performance pattern. The definition of the resulting atmosphere will require determination of at least the pressure, temperature, humidity, carbon dioxide content, and oxygen content. The resulting amount of calculation necessary to determine the effect of a change in heat load or an increase in leakage is so large that the use of digital computer techniques is essential and economical.

The program is described by expanding Figure 8, as shown in Figures 9 and 10, to define, in detail, all the elements of program input and output. The performance of the environmental control system, itself, is covered in Figure 9. The determination of the conditioned atmosphere which will result is outlined in Figure 10.

For comparison with the discussion in Section I of this report, Figure 11 has been prepared similar to Figure 4 to indicate the relative effect of transients on the system parameters in relation to the design conditions.

In Figures 9 and 10 it is shown that the Final Program Output (column H) is the state of the conditioned atmosphere of the space vehicle at a specific time. The state definition includes the temperature, the total pressure, the partial pressures of oxygen, nitrogen, carbon dioxide, and water vapor, and the mass of each of these four gases present.

To obtain this result, the given system, or specific arrangement of atmospheric control components, is fully defined in the optimizing program as specified in column A of Figure 9. In addition, the Imposed Conditions (column B) are those for which the performance of the system is optimum.

If one or more of the Imposed Conditions (column B) is varied as a function of time, the specific System Performance Results (column D) will be computed by the program. In this computation it is assumed that (a) the system, itself, has no time lag, (b) the variation in performance for off-design points can be arbitrarily stated for each component of the system, and (c) performance is constant throughout the chosen time interval. (In plotting results, it is assumed that the computer performance is that result at the end of the time interval.) The length of the time interval is at the discretion of the program user. It should be short enough so that the step-wise results will closely approach a smooth curve, and long enough to avoid excessive computer time.

To apply the program to the atmosphere in a compartment of a space vehicle, it is necessary to define the Original Conditioned Atmosphere (column E, Figure 10) at the point when Time = 0. Next, it is specified that one or more of the Time-Dependent Conditions (column F) varies with time. There may

be a continuous, though not necessarily constant, variation; in which case, the program computes the resulting conditions. There may be a single change in one, or more, conditions taking place instantaneously (as when the heat load is suddenly increased), in which case the system determines the resulting effect, which will often reach a constant value after a certain period of time (approach an asymptote).

The effect of the Time-Dependent Condition (column F, Figure 10) on the Original Conditioned Atmosphere, which is assumed to have a time lag, will be to establish the Imposed Conditions (column B) necessary to determine System Performance Results (column D).

The System Performance Results (column G, Figure 10) are then used in conjunction with the Original Conditioned Atmosphere (column E) to obtain the Modified Conditioned Atmosphere (column H) with a separate set of answers being obtained for the end of each time interval.

SECTION 3

COMPRESSOR PERFORMANCE

It is assumed that the optimized circuit contains a compressor and driving motor so designed that the combination operates at its peak efficiency at the design flow rate and pressure rate. The design flow rate is the flow rate in the optimized circuit, and the design pressure rise is numerically equal to the sum of all the series pressure drops in the circuit. Figure 12 shows the actual performance of a compressor-driving motor combination when handling oxygen at a pressure of 5 psia and a density of 0.0272 lb per cu ft. In the specific case where the compressor volume flow rate (measured at the inlet to the compressor) is 23 cu ft per min, Figure 12 indicates a pressure rise of 11 inches of water, compressor motor power input of 68 watts, and an overall peak efficiency of 51 percent. Upon examining the efficiency curve, it was apparent that it would be closely approximated, at volume flows other than the design, by the equations

$$ER = 1 - (1 - VR)^2 \text{ for values of } VR \text{ less than } 1.0 \quad (1)$$

$$ER = 1 - (VR - 1)^2 \text{ for values of } VR \text{ greater than } 1.0 \quad (2)$$

in which

$$ER = \frac{\text{Efficiency at off-design point}}{\text{Efficiency (maximum) at design point}}$$

$$VR = \frac{\text{Volume flow rate at off-design point}}{\text{Volume flow rate at design point}}$$

The pressure drop curve is approximated by the equations

$$\Delta PR = (ER/VR) \left[1 - 0.33 (1 - VR) \right] \text{ for values of } VR \text{ less than } 1.0 \quad (3)$$

$$\Delta PR = 1 - 0.85 (VR - 1) \text{ for values of } VR \text{ greater than } 1.0 \quad (4)$$

in which

$$\Delta PR = \frac{\text{Pressure rise at off-design point}}{\text{Pressure rise at design point (maximum efficiency)}}$$

In the transient analysis program, the compressor efficiency and pressure rise at the design point are given in the input at the values established in the optimizing program. The corresponding volume flow rate is computed from input data. For transient volume flow rates which are less than the design rate by more than 2 percent and not more than 50 percent, Equation(1) is used to find the new efficiency, and Equation(3) is used to find the new pressure rise. For transient volume flow rates which are greater than the design flow rate by more than 2 percent and not more than 70 percent, Equation(2) is used to find the new efficiency, and Equation(4) is used to find the new pressure rise.

The new pressure rise is now compared with the required pressure rise, which is the sum of all the other pressure drops in the circuit. If the two agree within ± 0.3 in. H₂O, it is assumed that the compressor and circuit are matched. If they do not agree within the above limits, then the weight flow rate in the circuit is adjusted by approximation formulas, the circuit is recomputed using the new compressor efficiency and weight flow, and the pressure rise is again compared with the sum of the pressure drops. This continues until a solution is reached or the number of tries exceeds the preset limit.

SECTION 4

HEAT EXCHANGER PERFORMANCE

It will be remembered that the optimizing program computed the heat exchanger as two separate sections to correspond to the two different types of cooling necessary on the air side. The temperature control heat exchanger section lowered the temperature of the air from the original dry bulb temperature to the original dew point temperature, thus acting as a dry heat exchanger on the air side. The water-condensing heat exchanger section further reduced the dry bulb temperature of the air from the inlet dew point to the desired outlet dew point temperature. This section also condensed to liquid water that amount represented by the difference in moisture content of the air at the inlet dew point and that amount at the outlet dew point.

The combined performance of the two heat exchanger sections, then, is that necessary to provide a certain drop in dry bulb temperature and to remove water at a rate equal to the water input. This cooling and condensing process requires a coolant fluid supply at a temperature lower than the required outlet dew point. The coolant fluid flows through the water-condensing heat exchanger section and then through the temperature control heat exchanger section. Typical air and liquid temperatures and water vapor contents for the two exchanger sections are as shown at the top of Figure 13. The relative values of UA indicate that $\frac{0.497}{0.497 + 1.660} = 23.1$ percent of the heat exchanger is being used for the temperature control section, and the balance, 76.9 percent, is being used for the water-condensing section. This checks closely with the optimizing program heat exchanger section volumes of 16.9 and 57.9 cu in. which give proportions of 22.6 percent and 77.4 percent.

The preceding considerations are based on assumptions that each section of the heat exchanger acts in pure counter-flow, that each section has a constant value of U, and that the areas of surface in each section (x-axis dimensions in Figure 13) are related to the computed core volumes in the same degree.

Figure 13 is based on a total UA, for both sections, of 2.157. If a different problem is given for the heat exchanger, as shown on the bottom half of Figure 13, then the known items for any one trial will be inlet air temperature, dew point temperature, inlet coolant temperature, and total UA for both sections. By means of an iterative process, the program computes the outlet air temperature and outlet moisture content, together with the intermediate and outlet coolant temperatures which are consistent with the same Σ UA as in the optimizing program. As shown on the bottom of Figure 13, the result will be a shift in the relative sizes of the two heat exchanger sections, and a new outlet air temperature and moisture content, both of which then become inputs to the remainder of the program in a continuation of the transient analysis process.

If the original heat exchanger designs are relatively accurate, as by means of the PFV program, then the effect of the simplifying assumptions, described above, should be very small in relation to the whole problem. To give warning of solutions where the analogy might have been carried too far, the program checks, and prints out notice if either section becomes less than half or more than twice the proportionate size which it had in the optimizing program. A notice is also printed if the total heat transfer exceeds the 50 to 200 percent limit. Neither of these notices stops the calculation, since extreme transients may still be desired, even if the answers are of reduced accuracy.

CIRCUITS WITH 3 COMPONENTS

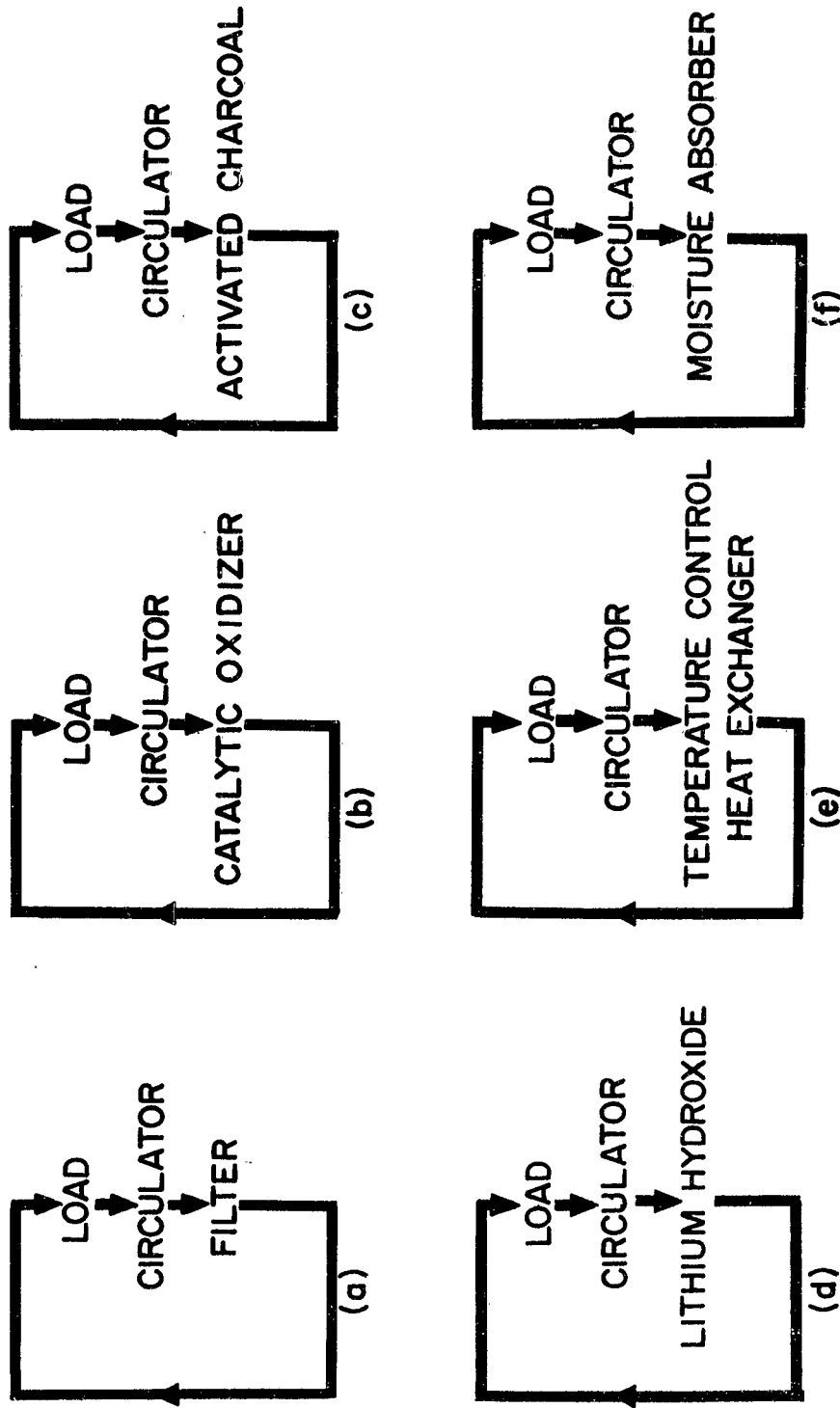


Figure 1. Circuits with Three Components

SINGLE CIRCUIT-SERIES

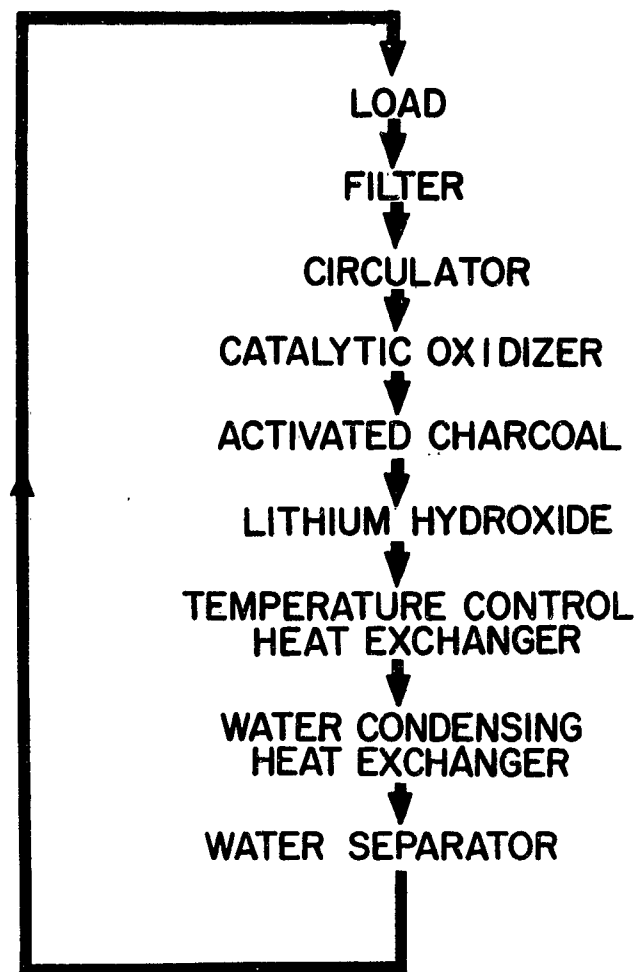


Figure 2. Single Circuit-Series

PARAMETERS	LOADS				CIRCULATOR	
	METABOLIC EQUIPMENT	SUPPLY	LEAKAGE	COMPRESSOR OR FAN	FILTER AND DUCT	
Temperature	Given Increase	Given Increase	Minor Change	Minor Change	Increase	
Pressure	Given Decrease	Given Decrease	Supply maintains pressure constant	Leakage compensated by supply	Increase	Decrease
Total Weight Flow Rate (Sum of Next 4 Flow Rates)	Given Increase		Weight flow rate maintained nearly constant	Leakage compensated by supply		
Water Vapor Weight Flow Rate	Given Increase			Minor Decrease		
Carbon Dioxide Weight Flow Rate	Given Increase			Minor Decrease		
Oxygen Weight Flow Rate	Given Decrease	Minor Decrease	Supply maintains oxygen partial pressure constant	Given Decrease		
Nitrogen Weight Flow Rate			Supply maintains total pressure constant	Given Decrease		
Pressure Drop	Computed	Computed			Press. Rise Equal to Sum Press. Drop	Computed
Density	Decrease	Decrease	Increase	Decrease	Increase	Decrease
Cross Section Area						Variabl
Flow Length						Given
Component and System Volume					Increase	Increase
Component and System Weight					Increase	Increase
Component and System Power Input					Increase	Increase



Figure 4. Effect of Elements on Optimum System Parameters

		ELEMENTS							
		CIRCULATOR					COMPONENTS		
LEAKAGE		COMPRESSOR OR FAN	FILTER AND DUCTS	CATALYTIC OXIDIZER	ACTIVATED CHARCOAL	LITHIUM HYDROXIDE	TEMPERATURE CONTROL HEAT EXCHANGER	WATER CONDENSING HEAT EXCHANGER	WATER SEPARATOR
	Minor Change	Increase		Increase		Increase	Decrease To Inlet Dew Point	Decrease To Required Dew Point	Outlet Given
maintains constant	Leakage compen- sated by supply	Increase	Decrease	Decrease	Decrease	Decrease	Decrease	Decrease	Decrease
flow rate nearly constant	Leakage compen- sated by supply			Given		Decrease		Decrease	Decrease
	Minor Decrease			Minor Increase		Increase		Decrease	
	Minor Decrease			Minor Increase		Decrease			
maintains partial constant	Given Decrease								
maintains pressure constant	Given Decrease								
		Press. Rise Equal to Sum Press. Drop	Computed	Computed	Computed	Computed	Computed	Computed	Computed
	Decrease	Increase	Decrease	Decrease	Decrease	Decrease	Increase	Increase	Increase
			Variable	Given	Variable Same for Both Components		Variable Same for Both Components		Variable
			Given	Given	Variable (Limited)	Variable (Limited)	Variable	Variable	Given
		Increase	Increase	Increase	Increase	Increase	Increase	Increase	Increase
		Increase	Increase	Increase	Increase	Increase	Increase	Increase	Increase
		Increase		Increase					Minor Increase

Figure 4. Effect of Elements on Optimum System Parameters



CIRCUIT WITH MIXING CHAMBER

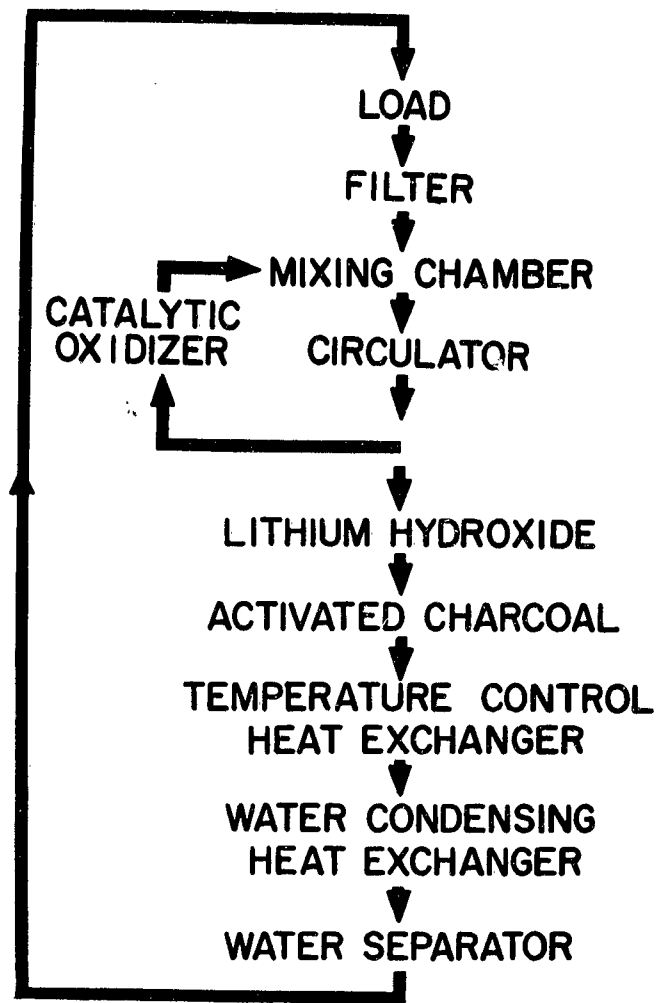


Figure 5. Circuit with Mixing Chamber

		COMPONENT NO. N =															
		1	2	3	4	5	6	7	8	9	10	11	12	13	14	15	
COMPONENT DESCRIPTION																	
TABLE	CASE NO.																
NFROM	I = 1	4	1														
	Fig. 1a				2												
	I = 2	10	4	1	2	5	6	7	8	9							
	Fig. 2																
	I = 3	10	11	1	2	7	2	6	8	9	4						
	Fig. 5																
	I = 1	2	4	1													
	Fig. 1a																
	I = 2	4	5	2	6	7	8	9	10	1							
	Fig. 2																
	I = 3	4	5	11	7	8	6	9	10	1	2						
	Fig. 5																
	NTO																

Figure 6. Nfrom and Nto Table -(N is Component Number, I is Case Number)

SYSTEM ANALYSIS

FIRST SEVEN CASES

DEC. 14, 1962

CONDIT

CASE NO. 1

SUM	POWER	WEIGHT	ALPHA	BETA		
2.3834E 02	2.7790E 02	7.1597E 01	6.0000E-01	1.0000E 00		
WF	DP-TCHE	DP-WCHE	A-FILTER	IAFR	L-L.H.	ILH
6.3804E 01	-1.2994E 00	-1.4191E 00	1.9609E 02	1	8.4182E 00	1
		H IN	C IN	H OUT	C OUT	
		TCHE 168.66870	39.62739	54.54305	47.95145	
		WCHE 54.44794	35.00000	40.01203	39.62739	
TMP1 4.3656E-02	VP13 5.8142E 00	VP14 3.3748E 00				
ELEMENT	TEMP. DP	PRESSURE DENSITY	WF A	H2O L	CO2 V	
SUIT LOAD	8.5000E 01 -8.5782E 00	1.2691E 02 0.	6.4701E 01 0.	1.5204E 00 0.	4.7989E 0.	
COMPRESSOR	1.4517E 02 1.6815E 01	1.4346E 02 0.	6.6208E 01 0.	1.5688E 00 0.	5.0685E 2.7940E	
FILTER	8.5000E 01 -2.7014E-01	1.2664E 02 2.4917E-02	6.4701E 01 1.9609E 02	1.5204E 00 1.0000E 00	4.7989E 2.3531E	
CAT. OXIDZER	2.6614E 02 1.6815E 01	1.6027E 02 2.5364E-02	1.5070E 00 0.	4.9543E-02 0.	2.7483E 2.2500E	
ACT. CHARCOAL	1.6867E 02 -2.2247E-01	1.4040E 02 2.3934E-02	6.4513E 01 1.5259E 02	1.6646E 00 2.9491E-01	1.7424E 4.5000E	
LITH. HYDRO.	1.6867E 02 -2.8363E 00	1.4062E 02 2.5364E-02	6.4518E 01 1.5259E 02	1.6646E 00 8.4182E 00	1.7424E 1.2845E	
TEMP CONTROL H.E.	5.4448E 01 -1.2994E 00	1.3910E 02 2.3896E-02	6.4513E 01 4.5672E 00	1.6646E 00 3.6947E 00	1.7424E 1.6874E	
WATER COND. H.E.	4.0000E 01 -1.4191E 00	1.3768E 02 2.8931E-02	6.3796E 01 1.5240E 01	9.4881E-01 3.7966E 00	1.7424E 5.7861E	
WATER SEPARATOR	4.0000E 01 -2.0863E 00	1.3549E 02 2.9441E-02	6.3762E 01 1.5583E 01	9.4901E-01 1.0000E 00	1.6989E 4.3114E	
MIXING CHAMBER	8.8856E 01 0.	1.2664E 02 0.	6.6208E 01 0.	1.5688E 00 0.	5.0685E 0.	

Figure 7. Typical Output

SYSTEM ANALYSIS

FIRST SEVEN CASES

DEC. 14, 1962

CONDITION 1

CASE NO. 1

JM	POWER	WEIGHT	ALPHA	BETA			
34E 02	2.7790E 02	7.1597E 01	6.0000E-01	1.0000E 00			
	DP-TCHE	DP-WCHE	A-FILTER	IAFR	L-L.H.	ILH	
34E 01	-1.2994E 00	-1.4191E 00	1.9609E 02	1	8.4182E 00	1	
	H IN	C IN	H OUT	C OUT			
TCHE	168.66870	39.62739	54.54305	47.95145			
WCHE	54.44794	35.00000	40.01203	39.62739			
VP1	4.3656E-02	VP13 5.8142E 00	VP14 3.3748E 00				
ELEMENT	TEMP. DP	PRESSURE DENSITY	WF A	H2O L	CO2 V	LMW W	HMW E
BIT LOAD	8.5000E 01 -8.5782E 00	1.2691E 02 0.	6.4701E 01 0.	1.5204E 00 0.	4.7989E-01 0.	10.0000E-03 0.	5.0000E-03 0.
MPRESSOR	1.4517E 02 1.6815E 01	1.4346E 02 0.	6.6208E 01 0.	1.5688E 00 0.	5.0685E-01 2.7940E 02	0. 6.5682E 00	0. 2.6238E 02
FILTER	8.5000E 01 -2.7014E-01	1.2664E 02 2.4917E-02	6.4701E 01 1.9609E 02	1.5204E 00 1.0000E 00	4.7989E-01 2.3531E 02	0. 4.5572E 00	0. 0.
T. OXIDZER	2.6614E 02 1.6815E 01	1.6027E 02 2.5364E-02	1.5070E 00 0.	4.9543E-02 0.	2.7483E-02 2.2500E 02	1.0000E-03 6.7500E 00	0. 1.5423E 01
T. CHARCOAL	1.6867E 02 -2.2247E-01	1.4040E 02 2.3934E-02	6.4513E 01 1.5259E 02	1.6646E 00 2.9491E-01	1.7424E-01 4.5000E 01	0. 1.6467E 01	5.0000E-04 0.
TH. HYDRO.	1.6867E 02 -2.8363E 00	1.4062E 02 2.5364E-02	6.4518E 01 1.5259E 02	1.6646E 00 8.4182E 00	1.7424E-01 1.2845E 03	0. 3.1808E 01	0. 0.
MP CONTROL H.E.	5.4448E 01 -1.2994E 00	1.3910E 02 2.3896E-02	6.4513E 01 4.5672E 00	1.6646E 00 3.6947E 00	1.7424E-01 1.6874E 01	0. 4.8927E-01	0. 0.
TER COND. H.E.	4.0000E 01 -1.4191E 00	1.3768E 02 2.8931E-02	6.3796E 01 1.5240E 01	9.4881E-01 3.7966E 00	1.7424E-01 5.7861E 01	0. 1.3802E 00	0. 0.
TER SEPARATOR	4.0000E 01 -2.0863E 00	1.3549E 02 2.9441E-02	6.3762E 01 1.5583E 01	9.4901E-01 1.0000E 00	1.6989E-01 4.3114E 01	0. 3.5773E 00	0. 1.0000E-01
KING CHAMBER	8.8856E 01 0.	1.2664E 02 0.	6.6208E 01 0.	1.5688E 00 0.	5.0685E-01 0.	1.0000E-03 0.	0. 0.

Figure 7. Typical Output

107

2

Program Input			Optimizing Program Output
A	B	C	D
Given Component Arrangement or System	Imposed Conditions	Component Characteristics	System Performance Results
<u>EQUIPMENT</u>	Power-Weight Ratio	Separate Modifiable Subroutine for Each Component See Fig. 4 & Fig. 11 for Qualitative Presentation	Weight Flow Rate
Circulation	Temperature In		Temperature Out
Ducts	Sensible Heat Load		H ₂ O Out
Filters	Latent Heat Load		CO ₂ Out
CO ₂ Removal	CO ₂ Load		p O ₂ Out
HMW Removal	Weight Flow Rate Limits		Component Dimensions
LMW Removal	Volume Flow Rate Limits		Component Weights
Temperature Control	Total Pressure		Component Power Consumed
Water Vapor Removal	p O ₂		
<u>PROPERTIES</u>			
Dimensions			
Weight			
Power Input			
Efficiency			
Performance			
Air Pressure Drop			
Air Temperature Change			

Figure 9. Performance of Environmental Control System

Program Input		From Optimizing Program Output	Final Program Output
E	F	G	H
Original Conditioned Atmosphere	Time- Dependent Conditions	System Performance Results	Modified Conditioned Atmosphere
Mass O ₂	O ₂ - Leak	p O ₂ Out	Mass O ₂
Mass N ₂	O ₂ - Consumed	Temp Out	Mass N ₂
Mass H ₂ O	O ₂ - Supply	H ₂ O Out	Mass H ₂ O
Mass CO ₂	CO ₂ - Load	CO ₂ Out	Mass CO ₂
Temperature	N ₂ - Leak	Weight Flow	Temperature
Total Pressure	N ₂ - Supply		Total Pressure
p O ₂	(Time Interval)		p O ₂
p N ₂			p N ₂
p H ₂ O			p H ₂ O
p CO ₂			p CO ₂
Volume			

Figure 10. Determination of the Conditioned Atmosphere of Space Vehicle - Which Will Result

PARAMETERS	CONDITIONED ATMOSPHERE			LOADS		
	STABILIZED CONDITIONS AT TIME = 0	TIME DEPENDENT VARIABLES	METABOLIC	EQUIPMENT	SUPPLY	LEAKAGE
Temperature	Given	Varies	Varies with SHL change	Varies with SHL change	Minor Change	Minor Change
Pressure	Given	Varies	Computed Decrease	Computed Decrease	Supply attempts to increase pressure to constant	Leakage to be compensated
Total Weight Flow Rate (Sum of Next Four Flow Rates)			Computed		Supply tends to maintain weight flow rate constant	Leakage to be compensated
Water Vapor Weight Flow Rate	Atmospheric content given	Atmospheric content varies	Varies with LHL change			Computed Decrease
Carbon Dioxide Weight Flow Rate	Atmospheric content given	Atmospheric content varies	Varies with LHL or SHL change			Computed Decrease
Nitrogen Weight Flow Rate	Atmospheric content given	Atmospheric content varies			Supply attempts to maintain total pressure constant	Computed Decrease
Oxygen Weight Flow Rate	Atmospheric content given	Atmospheric content varies	Given Decrease	Minor Decrease	Supply attempts to maintain oxygen partial pressure constant	Computed Decrease
Pressure Drop			Varies	Varies		
Air Density	Computed at given conditions	Computed at variant conditions	Decrease	Decrease	Increase	Decrease
Cross Section Area (Same as Optimum)						
Flow Length						
Conditioned Atmosphere, Component, and System Volume	Given Volume					
Conditioned Atmosphere, Component, and System Weight	Given computed mass of atmosphere at given conditions	Varies				
Component and System Power Input						



Figure 11. Assumed Eff in Relation

ELEMENTS	CIRCULATOR				COMPONENTS				
	LEAKAGE	COMPRESSOR OR FAN	FILTER AND DUCTS	CATALYTIC OXIDIZER	ACTIVATED CHARCOAL	LITHIUM HYDROXIDE	TEMPERATURE CONTROL HEAT EXCHANGER	WATER CONDENSING HEAT EXCHANGER	WATER SEPARATOR
	Minor Change	Increase Varies		Varies		Varies with CO ₂ change	Decrease to inlet dew point	Decrease to attainable dew point	Varies
empt e pres- instant	Leakage tends to be compensated by supply	Increase Varies (See ΔP)	Decrease	Decrease	Decrease	Decrease	Decrease	Decrease	Decrease
ids to eight con-	Leakage tends to be compensated by supply					Decrease		Decrease	Decrease
	Computed Decrease			Minor Increase		Varies with CO ₂ change		Varies with LHL or SHL change	
	Computed Decrease			Minor Increase		Decrease			
empt n to- re	Computed Decrease								
empt n oxy- l pres- ant	Computed Decrease								
		Press. rise equal to sum press. drops	Varies	Varies	Varies	Varies	Varies	Varies	Varies
	Decrease	Increase	Decrease	Decrease	Decrease	Decrease	Increase	Increase	Decrease
			No Change	No Change	No Change	No Change	Total length is unchanged		No Change
		No Change	No Change	No Change	No Change	No Change	Total volume is unchanged		No Change
		No Change	No Change	No Change	No Change	No Change	Total weight is unchanged		No Change
		Varies with performance requirements		Varies with performance requirements					No Change

2

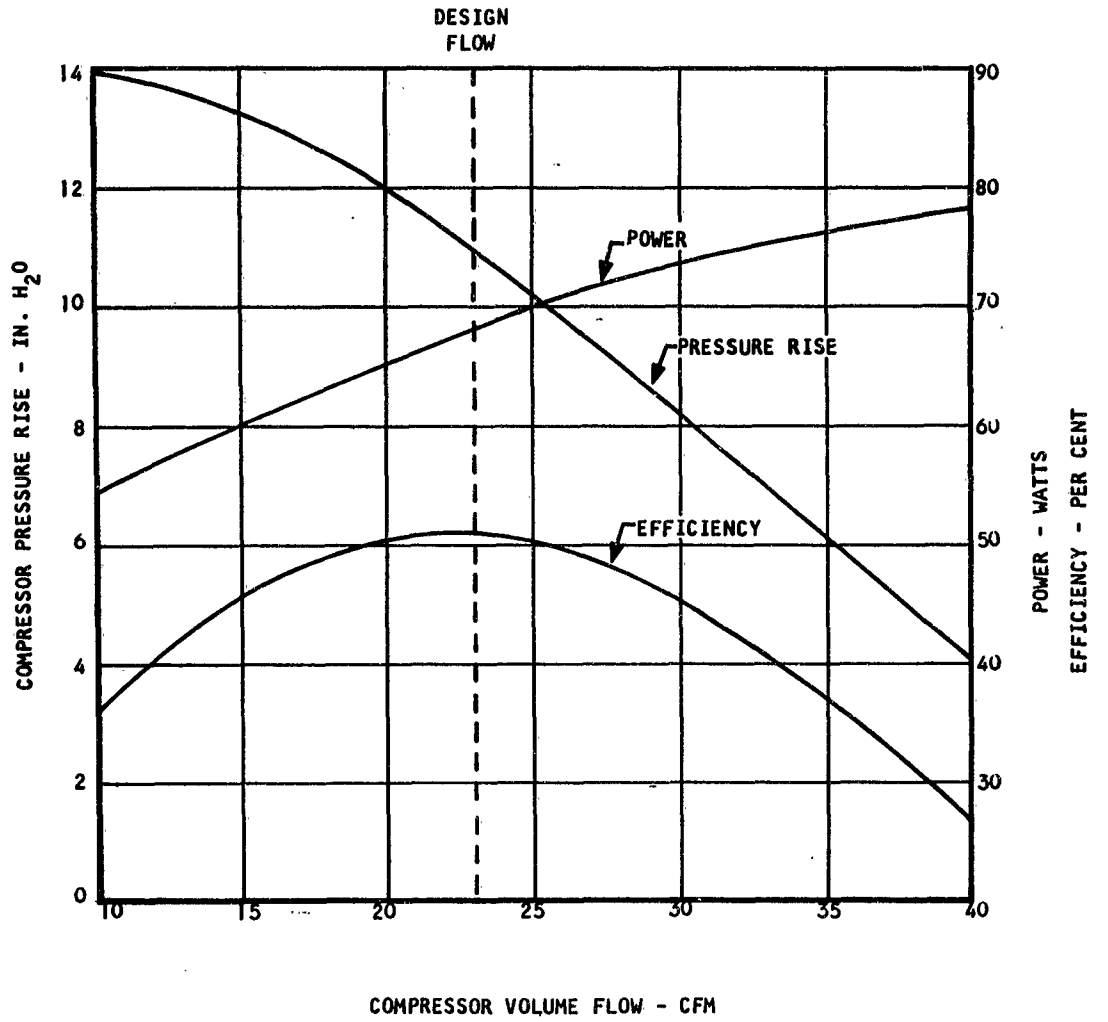


Figure 12. TYPICAL COMPRESSOR PERFORMANCE

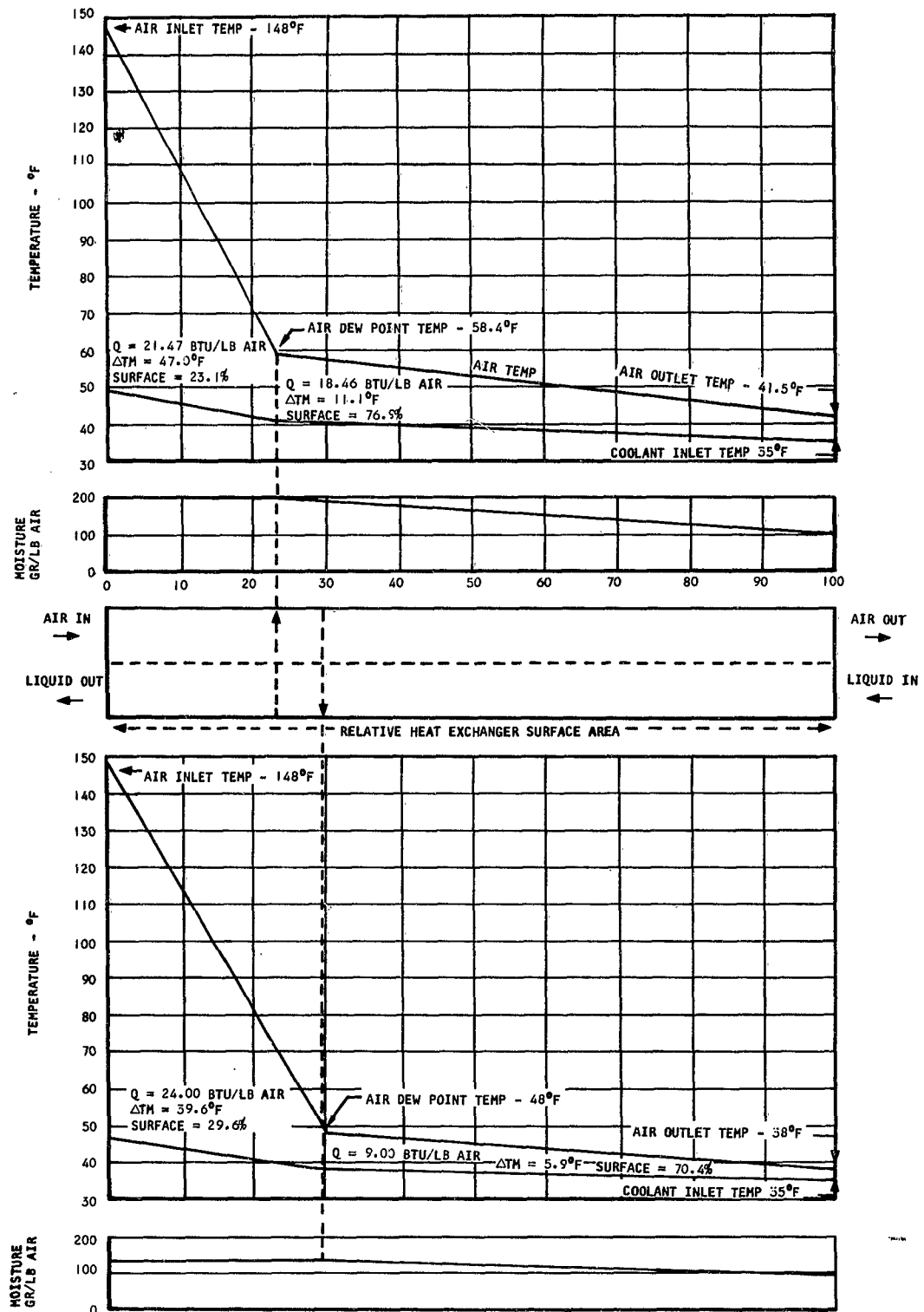


Figure 15 METHOD OF ESTIMATING OFF-DESIGN PERFORMANCE OF HEAT EXCHANGER

Third Paper -- "Analysis of Thermal and Atmospheric Control Systems for Space Vehicles by Application of Digital Computer Techniques," by F.H. Green, AiResearch.

QUESTION: (John Smylie, Aerospace Corporation) It was mentioned in the talk on the slide covering the properties of the airstream that some of the properties consisted of over one pound of water per pound of dry air. That seems pretty high, even in a reduced pressure. Should the decimal point be moved?

ANSWER : (Mr. Green) I admit fully that point problems can occur, however the error was mine in not explaining that all of the values shown for flow rate are pounds per hour, so that to find the amount of water per pound of dry air you would have to perform a little division or perhaps a little further than that. The reason for keeping track of total weight during this circuit is this makes the overall mathematics fairly straight forward with less chance of error. If you want to have a printout of such a thing as range of water per pound or something of this sort, this readily could be added to the program.

QUESTION: (Anonymous) Is it possible in your optimization program to take into account that some data, such as weight and power are involved in the circuit used by the coolant to carry heat from the heat exchanger to the heat sink.

ANSWER : (Mr. Green) This probably will not be too apparent in the paper itself. It will be apparent in the technical documentary report which shows the basic setup of these equations. Currently there is no equation for electrical energy used relative to the heat exchanger, but it will be a fairly simple matter to add an equation to this particular sub-routine. It might be presumed, for example, that you were using the heat exchanger design which comes within the so

called plate thin fin sub-routine which is another subject of one of the technical documentary reports developed under this overall thermal and atmospheric study but every equation that is used is spelled out in the technical documentary report and it is fairly apparent where to go from there to sub-routines since the same symbols are used both in the equations, the original equation and the sub-routines.

QUESTION: (Emil Schmidt, Atlantic Research) You stated that pressure drop was too high in a catalytic oxidizer. What is your basis for this statement? What is your idea of proper pressure drop level?

ANSWER : (Mr. Green) The problem from the system point of view in a catalytic oxidizer is to keep the overall power level low, and this calls for a high effectiveness, regenerative heat exchanger, and in order to keep system weight low, it calls for a very small weight circuit. This seems to be best handled by assuming that the catalytic oxidizer can have a high pressure drop. You wish to recover in a regenerative heat exchanger all of the necessary temperature rise. If you take, say, air at 140 degrees and then heat it up to 750 degrees, this would be a tremendous waste of energy unless you could recover in a regenerative heat exchanger most of that energy. At the same time, if you come up with a combination of catalytic oxidizer, plus heat exchanger that weighs more than about two pounds everybody will hold up their hands in horror, regardless of whether you can prove anything by it or not. It doesn't make very much difference. This is one of those cases where people are just not going to want to put too much weight in this device. So the best thing we know now, you have to pass only perhaps one-half to one pound per hour per man through the oxidizer and this means, why not make it very small and put it in a place where you can relatively afford to have a high pressure drop in it; this being primarily a matter of packaging in the heat exchanger, rather than the catalytic material itself.

**ENVIRONMENTAL CONTROL SYSTEMS FOR A MANNED MANEUVERABLE
SPACE VEHICLE**

by

E. P. Gebhardt

**The Martin-Marietta Corporation
Denver, Colorado**

ASD-TDR-63-260

**Environmental Control Systems For A
Manned Maneuverable Space Vehicle**

E. P. Gebhardt

INTRODUCTION

The stated objectives of the present Mercury program include 1) placing a manned spacecraft in orbit around the earth, 2) investigating man's performance and ability to survive in a space environment, and 3) recovering the man and spacecraft safely. All of these objectives have been attained. The third objective was attained through the use of a ballistic-type re-entry with water landing and recovery. This technique requires precise disorbit control and allows little or no maneuvering in the landing pattern, with no alternate choice of landing site. The use of a vehicle configuration having the capability of generating aerodynamic lift during the re-entry and atmospheric flight phases would increase its versatility and thus would represent a highly desirable characteristic from the operational standpoint.

Another desirable feature for this class of space vehicle would be the ability to rendezvous with other vehicles in orbital flight. Solution of the rendezvous problem is a planned objective of the Gemini program. If the rendezvous capability is incorporated into a configuration of the lifting-body type, the resulting vehicle can perform various logistics and inspection missions of relatively short duration, and then re-enter the earth's atmosphere, maneuver at low altitude, and land in the manner of a conventional, high-performance aircraft.

The internal thermal and atmosphere control problems of this vehicle configuration and its potential missions indicate the need for a review of the applicable environmental control techniques and an assessment of the weight, power, and volume penalties associated with representative hardware.

ENVIRONMENTAL CONTROL SYSTEM FUNCTIONS

The environmental control system for a space vehicle is required to provide a controlled, life-supporting atmosphere for the crew and a controlled thermal environment for the heat-generating components of other subsystems in the vehicle. Specific functions to be performed by the system include 1) breathing oxygen supply, 2) carbon dioxide removal, 3) water vapor removal, 4) odor removal, and 5) heat rejection.

In order to investigate the alternate techniques available for performing these functions, a vehicle configuration, a mission definition, an environmental control system design philosophy, and an applicable set of design criteria and design specifications must be established.

VEHICLE CONFIGURATION

The vehicle configuration upon which subsequent environmental control discussions are based is the lifting-body. General characteristics of this configuration are depicted in Fig. 1. This shape and similar shapes have been shown experimentally to be capable of generating lift-to-drag ratios on the order of 1 to 1.3 at supersonic speeds and as high as 3.5 at subsonic speeds. These lift-to-drag ratios result in the attainment of a cross-range capability of 750 nautical miles and landing speeds on the order of 170 knots.

MISSION DEFINITION

A vehicle of this type could be used to rendezvous with and inspect (or perform maintenance of) various earth-orbiting satellites. It could be used to perform a logistics function by rotating crews and resupplying earth-orbiting space stations. A four-man space station crew-rotation and resupply mission is selected for the environmental control system investigations. This mission requires the vehicle to carry a fresh crew of four men and their associated equipment and supplies to an earth-orbiting space station, and to return the relieved crew and a quantity of scientific equipment to earth. The total mission duration is 36 hours, and the mission profile is estimated to be that shown in Table 1.

ENVIRONMENTAL CONTROL SYSTEM DESIGN PHILOSOPHY

Because of the relatively short duration of the mission and the number of critical phases with respect to the crew (such as launch, rendezvous, crew transfer, and re-entry), it is desirable to include pressure suits as integral components of the environmental control system. In addition, a "back-pack" life support system should be incorporated into the suit to act as a backup in an emergency and also to facilitate the crew transfer operation.

Primary considerations in the selection of components for thermal and atmosphere control are the weight, volume, and power penalties imposed on the vehicle by the various techniques available. No method for performing the stated environmental control

functions should be considered if its use appears to be incompatible with the chosen vehicle configuration and its assumed mission.

ENVIRONMENTAL CONTROL SYSTEM DESIGN CRITERIA

Criteria for environmental control system design are primarily functions of 1) the physiological requirements of the crew, and 2) the heat loads imposed on the vehicle internal atmosphere resulting from crew, operating equipment, and vehicle external environment during all phases of the mission.

Crew Physiological Requirements

Physiological requirements of the crew are defined in terms of metabolic heat production, oxygen consumption, carbon dioxide production, water vapor production, urine and feces production, odor and noxious gas production, and food and drinking water consumption. Values of these factors are determined as a function of the size and weight of a crew member, his activity level, type of clothing worn, and the condition of the cabin atmosphere in terms of the temperature, pressure, composition, and ventilation rate. Calculated metabolic data for an Air Force 95th percentile man, clothed in a ventilated pressure suit, and exhibiting an activity level that is compatible with the assumed mission, is shown in Table 2.

Electrical Heat Loads

In addition to the heat load on the cabin atmosphere resulting from crew metabolism, heat is generated by power-consuming components of the vehicle's various subsystems. The heat rejection requirements of this equipment generally follow the power demand schedule and can therefore be determined and described as a function of the mission profile. From the power demand schedule, average equipment heat rejection rates were established and are shown in Table 3.

External Heat Loads

A heat load is also imposed on the cabin atmosphere because of the aerodynamic heating of the vehicle structure during ascent and re-entry, and because of thermal radiation from the sun and earth when the vehicle is in orbital flight.

Typical stagnation point heating rates during ascent and re-entry are shown on Fig. 2 and 3, respectively. Heating rates on other portions of the vehicle are generally on the order of 10 to 20 percent of the stagnation point values. Total heat flux received by the vehicle in orbital flight (sum of the direct solar, earth-reflected solar, and earth-emitted) was calculated, and typical values are shown in Fig. 4. In this calculation the vehicle configuration was approximated by considering it to be made up of six plane areas and by calculating the total heat flux to each area as a function of the vehicle's position in orbit.

The magnitude of the external heat load is obtained from the structural heat balance using the above heating rates. Obviously, this load varies with time. Nominal design values can be established, however, for major phases of the mission profile. These values are shown in Table 4.

ENVIRONMENTAL CONTROL SYSTEM DESIGN SPECIFICATIONS

Since an artificial atmosphere will be established in the vehicle and the environmental control system will be required to maintain it, acceptable values of its total pressure, composition, temperature, relative humidity, carbon dioxide level, etc., must be specified. Values of these parameters used in this study are summarized in Table 5.

THERMAL AND ATMOSPHERE CONTROL TECHNIQUES

Alternate approaches can be considered for the heat rejection, breathing oxygen supply, carbon dioxide and water vapor removal functions of the environmental control system for this vehicle configuration and mission.

Heat Rejection

The available methods for rejecting heat from a manned space vehicle are those employing either a low-temperature radiator or an expendable heat sink. The only acceptable location for a radiator on this vehicle configuration was found to be on the upper surface just aft of the canopy (refer to Fig. 1). This location could accommodate a radiator surface area of only 80 square feet. The heat balance on the radiator is given by

$$Q_R = Q_{EXT} + Q_{INT}$$

$$\text{or } \epsilon \sigma A_R T_R^4 = q_{EXT} A_R + Q_{INT} \quad [1]$$

where

- Q_R = net heat radiated (Btu/hr);
- Q_{EXT} = external heat load on radiator (Btu/hr);
- Q_{INT} = internal heat load on radiator (Btu/hr);
- ϵ = emissivity of radiator surface;
- σ = Stefan-Boltzmann constant (Btu/hr-ft²-°R⁴);
- A_R = radiator surface area (ft²);
- T_R = radiator surface temperature (°R);
- q_{EXT} = external heat flux (Btu/hr-ft²).

Solving equation [1] for the required radiator temperature (T_R) gives

$$T_R = \left[\frac{1}{\epsilon\sigma} \left(q_{EXT} + \frac{Q_{INT}}{A_R} \right) \right]^{\frac{1}{4}} \quad [2]$$

The required radiator temperature was determined using values of q_{EXT} from Fig. 4, while the value of Q_{INT} was assumed to be constant and equal to the sum of the human (Table 2) and electrical (Table 3) heat loads. The results of the calculation are shown in Fig. 5, where required radiator temperature is plotted as a function of vehicle position in orbit. This figure shows that the radiator could not be used during the sunlit portion of each orbit because of the excessive radiator temperatures required. Therefore, the low-temperature radiator as a means for thermal control was not considered feasible for this vehicle and its assumed mission.

Investigation of the expendable heat sink technique for thermal control shows that water appears to be the best heat sink. For instance, the heat of vaporization of water boiling at 70°F is about 1054 Btu/lb. This requires a pressure of about .36 psia; or, it means that boiling water at altitudes above about 82,000 feet could be used as a means for thermal control in this vehicle. Cryogenic hydrogen and oxygen can also be considered as expendable heat sinks for thermal control if they are already required aboard the vehicle as the power system working fluids. The heat sink capacity of hydrogen, which is heated from liquid temperature (-423°F) to a temperature of 70°F at a constant pressure of one

atmosphere, is about 1880 Btu/lb. The heat sink capacity of oxygen, which is heated from liquid temperature (-297°F) to a temperature of 70°F at a constant pressure of one atmosphere, is about 172 Btu/lb. The quantity of hydrogen and oxygen required depends upon the method of integrating the power and cooling functions in the vehicle. When water is considered as the heat sink, no possibility exists for integrating power and cooling functions.

Breathing Oxygen Supply

Only storage methods are considered for breathing oxygen supply. These are 1) high pressure gas storage at cabin temperature, 2) supercritical storage at near-cryogenic temperature, and 3) storage of a solid chemical source of oxygen such as potassium superoxide. The first method allows reasonably low container weight and volume penalties for the quantity of oxygen required for this mission. The second method can be competitive, however, if power system oxygen is also required, and both can be stored in a common container. Method three is also considered to be competitive because of its additional ability to perform the carbon dioxide removal function.

Carbon Dioxide Removal

Since only storage methods of breathing oxygen supply will be investigated, the carbon dioxide removal methods need not include the requirement for collection of carbon dioxide. Applicable carbon dioxide removal methods are 1) physical adsorption using molecular sieves (regenerable), 2) chemical combination with lithium hydroxide (non-regenerable), and 3) chemical combination with potassium superoxide (non-regenerable).

Water Vapor Removal

The best method for removing respired and perspired water vapor from the atmosphere (humidity control) is by condensation in a heat exchanger followed by sponge or centrifugal separation. If cryogenic fluids are on board the vehicle, they can be used as the condenser heat sink. However, when no cryogenic fluids are available, water must be used.

ENVIRONMENTAL CONTROL SYSTEM COMPARISONS

Various systems can be postulated and compared when the following are considered: 1) the given vehicle configuration and its mission, 2) the established environmental control system

design philosophy, design criteria, and design specifications, and 3) the suggested alternate choices of thermal and atmosphere control methods. Eight systems are shown schematically in Fig. 6 through 13 and are described as follows:

System 1 - In this system, heat is transferred from the circulating cabin atmosphere to a water boiler by means of a heat exchanger and coolant loop. The water is caused to boil at 45°F by maintaining a constant pressure of about .1 psia in the boiler. Humidity control is accomplished in the water vapor removal loop by a condensing heat exchanger and a centrifugal water separator. Water, boiling at 35°F, is used as the heat sink. Carbon dioxide and odors are removed in a combined lithium hydroxide and activated charcoal cannister. Breathing oxygen is supplied from a high pressure gas storage container.

System 2 - This system is the same as System 1 except that carbon dioxide is removed by a regenerable adsorber. The unit contains two silica gel beds for pre-drying the process flow and two artificial zeolite beds for adsorbing carbon dioxide. One pair of beds (one silica gel and one artificial zeolite) is on-stream adsorbing, while the other pair is being desorbed. The artificial zeolite bed is desorbed by venting to space, and the silica gel bed is desorbed by purging with the warm process gas from the on-stream artificial zeolite bed. Odors are removed in a separate activated charcoal cannister before the process gas is returned to the cabin.

System 3 - This system is also the same as System 1 except that the oxygen supply and carbon dioxide removal functions are combined by using a potassium superoxide cannister to liberate oxygen and remove carbon dioxide. This reaction requires control of the temperature and humidity of the process gas so that proper ratio of oxygen produced to carbon dioxide removed is maintained. Since water vapor is consumed in the reaction, a humidifier is used downstream of the potassium superoxide cannister.

System 4 - The thermal control and water vapor removal functions are accomplished in this system by using the heat sink capacity of the power system working fluids -- hydrogen and oxygen. Hydrogen is stored supercritically and is delivered to the power system combustor through a heat exchanger in the cabin atmosphere coolant loop. Thermal pressurization and delivery of the hydrogen are accomplished by returning warm hydrogen from the heat exchanger to the storage container. Oxygen is also stored supercritically and is delivered to the power system combustor through a heat

exchanger in the water vapor removal loop. Thermal pressurization and delivery of the oxygen are accomplished by returning warm oxygen from this heat exchanger to the storage container. Additional heat is supplied to each storage container by means of internal electrical heaters. Breathing oxygen is stored with the power system oxygen and is withdrawn at a point between the storage container and the power system combustor, where it has been warmed to 60°F. In this system the cooling load determines the required power system performance. At an expansion ratio of 200:1, an expander inlet temperature of 660°F, and a mixture ratio of 0.32, the specific fuel consumption is 2.56 lb/hp-hr for a power output of 3.0 horsepower.

The carbon dioxide removal and odor removal functions were accomplished using lithium hydroxide and activated charcoal as in System 1.

System 5 - This system is the same as System 4 except that carbon dioxide is removed by a regenerable adsorber, and odors are removed by a separate activated charcoal cannister, as in System 2.

System 6 - The thermal control and water vapor removal functions are accomplished in this system using the cooling capacity of supercritically stored hydrogen, which is also the power system working fluid. Because of the manner in which the hydrogen is used for both power and cooling, a power output of 3.0 horsepower is obtained and all of the cooling is accomplished with a specific fuel consumption of only 1.0 lb/hp-hr. The power system uses a low temperature hydrogen expansion cycle with three stages of expansion, interstage reheating, preheating and afterheating. The over-all expansion ratio is 125:1, and the expander inlet temperature is 50°F.

Carbon dioxide and odors are removed in a combined lithium hydroxide and activated charcoal cannister. Breathing oxygen is supplied from a high pressure gas storage container.

System 7 - This system is the same as System 6 except that a regenerable adsorber (silica gel and artificial zeolite) and a separate activated charcoal cannister are used to remove carbon dioxide and odors as in System 2.

System 8 - This system is also the same as System 6 except that the oxygen supply and carbon dioxide removal functions are accomplished with potassium superoxide as in System 3.

Temperatures, enthalpies, specific humidities, relative humidities, and specific volumes of the atmosphere at various points in the systems were determined with the aid of the psychrometric chart. Numbers and letters on the psychrometric chart of Fig. 14 refer to flow stations in System 1 (refer to Fig. 6). Values of atmosphere properties at the designated points in System 1 are listed in Table 6 along with assumed values of flow rates and pressure drops.

All of these systems were analyzed to determine the performance required from the major components. This data was then used to estimate the weight, volume, and power penalties associated with each system. Weight, volume, and power estimates for each system (including power system) are listed in Tables 7 through 14 and are summarized in Table 15.

CONCLUSIONS

For this vehicle configuration and its assumed mission, the least weight penalty is incurred when the power and cooling requirements are met with an integrated system using cryogenic hydrogen as the working fluid. System 8 represented 37.8 percent less weight penalty to the vehicle than the lightest non-integrated system (System 1), while consuming essentially the same power and occupying only 1.7 percent more space. The atmosphere control techniques used in System 8 were 1) potassium superoxide for oxygen supply and carbon dioxide removal, and 2) condensation and centrifugal separation for water vapor removal.

Table 1 Crew Rotation Mission Profile

Mission Phase		Time
Ascent	From launch to 100,000 ft	.05 hr
	100,000 ft to 100 n mi parking orbit	.15 hr
Orbit	Waiting in 100 n mi parking orbit	24.00 hr
	Transfer to 257 n mi servicing orbit	.75 hr
	On station plus waiting to disorbit	9.70 hr
	Disorbit to 400,000 ft.	.45 hr
Re-entry	400,000 ft to 100,000 ft	.54 hr
Landing	100,000 ft to earth	.36 hr
Total		36.00 hr

Table 2 Metabolic Data for an Air Force 95th Percentile Man

Heat Production Rate (Total)	655 Btu/hr
Latent	165 Btu/hr
Sensible	490 Btu/hr
Oxygen Consumption Rate	2.585 lb/day
Carbon Dioxide Production Rate	3.028 lb/day
Water Production Rate (Total)	8.340 lb/day
In Perspiration and Respiration	3.762 lb/day
In Urine	4.578 lb/day
Drinking Water Consumption Rate	7.500 lb/day
Dry Food Consumption Rate	1.920 lb/day

Table 3 Average Electrical Heat Loads

Guidance	1230 Btu/hr
Flight Control	205 Btu/hr
Instrumentation	410 Btu/hr
Communications	614 Btu/hr
Lighting and Controls	683 Btu/hr
Line Losses	683 Btu/hr
Total	3825 Btu/hr

Table 4 Nominal External Heat Loads

Ascent Phase	2700 Btu/hr
Orbital Phase	
Sunlight (60% of orbit)	900 Btu/hr
Shadow (40% of orbit)	-3000 Btu/hr
Re-entry Phase	6000 Btu/hr

Table 5 Environmental Control System Design Specifications

Cabin Total Pressure	6.0 psia
Oxygen Partial Pressure	3.6 psia
Nitrogen Partial Pressure	2.4 psia
Cabin Temperature	70 - 80°F
Cabin Relative Humidity	30 - 50 %
Maximum Carbon Dioxide Concentration	7.6 mm.hg

Table 6 Assumptions and Calculated Atmosphere Properties for System 1

<u>Assumptions:</u>									
Temperature at 3 = 50°F									
Relative Humidity at 3 = 90%									
Flow Rate in Water Vapor Removal Loop = 152 lb/hr									
Pressure Drop in Water Vapor Removal Loop = 6 in. H ₂ O									
Flow Rate in Carbon Dioxide Removal Loop = 80 lb/hr									
Pressure Drop in Carbon Dioxide Removal Loop = 4 in. H ₂ O									
Flow Rate in Suit Loop = 264 lb/hr (66 lb/hr/suit)									
Pressure Drop across Suit = 3 in. H ₂ O									
Pressure Drop in Primary Circuit = 6 in. H ₂ O									
Blower Efficiencies = 60%									
<u>Calculated Properties (refer to Fig. 6 and 14):</u>									
Flow Rate at 6 = 367 lb/hr for Temperature and Specific Humidity at 7 = 60°F and 114 grains/lb, respectively.									
Station Property ↘	1	2	3	n	o	y	z	b	d
Enthalpy (Btu/lb)	36.7	39.6	29.0	31.8	22.2	30.8	36.3	30.4	37.8
Specific Humidity (grains/lb)	114	114	114	114	85	114	114	114	131
Temperature (°F)	83.5	95.5	50.0	62.0	39.5	58.0	82.0	56.5	76.0
Relative Humidity (%)	28	20	90	59	100	68	30	70	42
Specific Volume (cu ft/lb)	32.8	33.5	30.8	31.5	30.0	31.2	32.7	31.2	32.4
Note: Values shown are for sunlit portion of 257 n mi orbit.									

Table 7 Weight, Volume, and Power Estimates for System 1

Item	Weight (lb)	Volume (in. ³)	Power (watts)
<u>Primary Circulation Loop</u>			
Blower	10.0	230	708
Particle Filter	1.0	170	-
Valves and Ducting	52.5	11,850	-
<u>Thermal Control Loop</u>			
Atmosphere to Coolant Heat Exchanger	20.0	430	-
Water Boiler and Water	255.0	5,150	-
Coolant Pump and Coolant	5.0	110	10
Valves and Piping	6.0	72	-
<u>Water Vapor Removal Loop</u>			
Blower	2.0	15	125
Condenser and Water	70.0	1,440	-
Water Separator	5.0	240	-
Valves and Piping	5.0	50	-
<u>Carbon Dioxide Removal Loop</u>			
Blower	1.0	6	42
Lithium Hydroxide Cannister	48.0	1,700	-
Valves and Piping	1.0	8	-
<u>Oxygen Supply</u>			
Oxygen and Container	40.0	700	-
Pressure Regulator and Piping	1.0	15	-
<u>Suit Loop</u>			
Blowers	8.0	24	108
Suits	100.0	6,050	-
Valves and Piping	6.0	50	-
<u>Power System</u>			
Power Components	46.0	3,450	-
Fuel, Oxidizer and Tankage	426.0	8,750	-
Totals	1108.5	40,510	993

Table 8 Weight, Volume, and Power Estimates for System 2

Item	Weight (lb)	Volume (in. ³)	Power (watts)
<u>Primary Circulation Loop</u>			
Blowers	10.0	230	720
Particle Filter	1.0	170	-
Valves and Ducting	52.5	11,850	-
<u>Thermal Control Loop</u>			
Atmosphere to Coolant Heat Exchanger	20.0	430	-
Water Boiler and Water	270.0	5,450	-
Coolant Pump and Coolant	5.0	110	10
Valves and Piping	6.0	72	-
<u>Water Vapor Removal Loop</u>			
Blower	2.0	15	125
Condenser and Water	70.0	1,440	-
Water Separator	5.0	240	-
Valves and Piping	5.0	50	-
<u>Carbon Dioxide Removal Loop</u>			
Blower	1.0	6	150
Carbon Dioxide Adsorber	75.0	4,850	-
Odor Removal Cannister	6.0	20	-
Valves and Piping	1.0	8	-
<u>Oxygen Supply</u>			
Oxygen and Container	40.0	700	-
Pressure Regulator and Piping	1.0	15	-
<u>Suit Loop</u>			
Blowers	8.0	24	108
Suits	100.0	6050	-
Valves and Piping	6.0	50	-
<u>Power System</u>			
Power Components	46.0	3,450	-
Fuel, Oxidizer and Tankage	464.0	9,550	-
Totals	1194.5	44,780	1,113

Table 9 Weight, Volume, and Power Estimates for System 3

Item	Weight (lb)	Volume (in. ³)	Power (watts)
<u>Primary Circulation Loop</u>			
Blowers	10.0	230	710
Particle Filter	1.0	170	-
Valves and Ducting	52.5	11,850	-
<u>Thermal Control Loop</u>			
Atmosphere to Coolant Heat Exchanger	20.0	430	-
Water Boiler and Water	258.0	5,200	-
Coolant Pump and Coolant	5.0	110	10
Valves and Piping	6.0	72	-
<u>Water Vapor Removal Loop</u>			
Blower	2.0	15	125
Condenser and Water	70.0	1,440	-
Water Separator	5.0	240	-
Valves and Piping	5.0	50	-
<u>Carbon Dioxide Removal Loop</u>			
Blower	1.0	6	50
Potassium Superoxide Cannister	60.0	5,750	-
Humidifier	1.0	50	-
Pump, Valves, and Piping	1.5	12	5
<u>Suit Loop</u>			
Blowers	8.0	24	108
Suits	100.0	6,050	-
Valves and Piping	6.0	50	-
<u>Power System</u>			
Power Components	46.0	3,450	-
Fuel, Oxidizer and Tankage	426.0	8,750	-
Totals	1084.0	43,949	1,008

Table 10 Weight, Volume, and Power Estimates for System 4

Item	Weight (lb)	Volume (in. ³)	Power (watts)
<u>Primary Circulation Loop</u>			
Blowers	10.0	230	712
Particle Filter	1.0	170	-
Valves and Ducting	52.5	11,850	-
<u>Thermal Control Loop</u>			
Atmosphere to Coolant Heat Exchanger	9.0	430	-
Coolant to Hydrogen Heat Exchanger	12.0	570	-
Coolant Pump and Coolant Valves and Piping	2.0 3.0	100 30	50 -
<u>Water Vapor Removal Loop</u>			
Blower	2.0	15	125
Atmosphere to Oxygen Heat Exchanger	1.0	50	-
Condenser	1.5	100	-
Water Separator	5.0	240	-
Valves and Piping	5.0	50	-
<u>Carbon Dioxide Removal Loop</u>			
Blower	1.0	6	42
Lithium Hydroxide Cannister	48.0	1,700	-
Valves and Piping	1.0	8	-
<u>Suit Loop</u>			
Blowers	8.0	24	108
Suits	100.0	6,050	-
Valves and Piping	6.0	50	-
<u>Power System</u>			
Power Components	40.0	2,550	-
Fuel, Oxidizer and Tankage	659.0	77,000	50
Pressure Regulator, Valves and Piping	10.0	30	-
Totals	977.0	101,303	1,087

Table 11 Weight, Volume, and Power Estimates for System 5

Item	Weight (lb)	Volume (in. ³)	Power (watts)
<u>Primary Circulation Loop</u>			
Blowers	10.0	230	730
Particle Filter	1.0	170	-
Valves and Ducting	52.5	11,850	-
<u>Thermal Control Loop</u>			
Atmosphere to Coolant Heat Exchanger	9.0	430	-
Coolant to Hydrogen Heat Exchanger	12.0	570	-
Coolant Pump and Coolant Valves and Piping	2.0	100	50
	3.0	30	-
<u>Water Vapor Removal Loop</u>			
Blower	2.0	15	125
Pre-cooler	1.0	50	-
Condenser	1.5	100	-
Water Separator	5.0	240	-
Valves and Piping	5.0	50	-
<u>Carbon Dioxide Removal Loop</u>			
Blower	1.0	6	150
Carbon Dioxide Adsorber	75.0	4,850	-
Odor Removal Cannister	6.0	20	-
Valves and Piping	1.0	8	-
<u>Suit Loop</u>			
Blowers	8.0	24	108
Suits	100.0	6,050	-
Valves and Piping	6.0	50	-
<u>Power System</u>			
Power Components	40.0	2,550	-
Fuel, Oxidizer and Tankage	700.0	82,000	50
Pressure Regulator, Valves and Piping	10.0	30	-
Totals	1051.0	109,423	1,213

Table 12 Weight, Volume, and Power Estimates for System 6

Item	Weight (lb)	Volume (in. ³)	Power (watts)
<u>Primary Circulation Loop</u>			
Blowers	10.0	230	715
Particle Filter	1.0	170	-
Valves and Ducting	52.5	11,850	-
<u>Thermal Control Loop</u>			
Atmosphere to Coolant Heat Exchanger	9.0	430	-
Coolant Pump and Coolant Valves and Piping	3.0	150	50
	5.0	50	-
<u>Water Vapor Removal Loop</u>			
Blower	2.0	15	125
Condenser	2.0	140	-
Water Separator	5.0	240	-
Valves and Piping	5.0	50	-
<u>Carbon Dioxide Removal Loop</u>			
Blower	1.0	6	42
Lithium Hydroxide Cannister	48.0	1,700	-
Valves and Piping	1.0	8	-
<u>Oxygen Supply</u>			
Oxygen and Container	40.0	700	-
Pressure Regulator and Piping	1.0	15	-
<u>Suit Loop</u>			
Blowers	8.0	24	108
Suits	100.0	6,050	-
Valves and Piping	6.0	50	-
<u>Power System</u>			
Power Components	120.0	12,120	-
Fuel and Tankage	297.0	4,070	25
Totals	716.5	38,068	1,065

Table 13 Weight, Volume, and Power Estimates for System 7

Item	Weight (lb)	Volume (in. ³)	Power (watts)
<u>Primary Circulation Loop</u>			
Blowers	10.0	230	730
Particle Filter	1.0	170	-
Valves and Ducting	52.5	11,850	-
<u>Thermal Control Loop</u>			
Atmosphere to Coolant Heat Exchanger	9.0	430	-
Coolant Pump and Coolant Valves and Piping	3.0	150	50
	5.0	50	-
<u>Water Vapor Removal Loop</u>			
Blower	2.0	15	125
Condenser	2.0	140	-
Water Separator	5.0	240	-
Valves and Piping	5.0	50	-
<u>Carbon Dioxide Removal Loop</u>			
Blower	1.0	6	150
Carbon Dioxide Adsorber	75.0	4,850	-
Odor Removal Cannister	6.0	20	-
Valves and Piping	1.0	8	-
<u>Oxygen Supply</u>			
Oxygen and Container	40.0	700	-
Pressure Regulator and Piping	1.0	15	-
<u>Suit Loop</u>			
Blowers	8.0	24	108
Suits	100.0	6,050	-
Valves and Piping	6.0	50	-
<u>Power System</u>			
Power Components	120.0	12,120	-
Fuel and Tankage	308.0	4,220	25
Totals	760.5	41,388	1,188

Table 14 Weight, Volume, and Power Estimates for System 8

Item	Weight (lb)	Volume (in. ³)	Power (watts)
<u>Primary Circulation Loop</u>			
Blowers	10.0	230	717
Particle Filter	1.0	170	-
Valves and Ducting	52.5	11,850	-
<u>Thermal Control Loop</u>			
Atmosphere to Coolant Heat Exchanger	9.0	430	-
Coolant Pump and Coolant Valves and Piping	3.0	150	50
	5.0	50	-
<u>Water Vapor Removal Loop</u>			
Blower	2.0	15	125
Condenser	2.0	140	-
Water Separator	5.0	240	-
Valves and Piping	5.0	50	-
<u>Carbon Dioxide Removal Loop</u>			
Blower	1.0	6	50
Potassium Superoxide Cannister	60.0	5,750	-
Humidifier	1.0	50	-
Valves and Piping	1.5	12	-
<u>Suit Loop</u>			
Blowers	8.0	24	108
Suits	100.0	6,050	-
Valves and Piping	6.0	50	-
<u>Power System</u>			
Power Components	120.0	12,120	-
Fuel and Tankage	297.0	4,070	25
	<u>689.0</u>	<u>41,457</u>	<u>1,075</u>
Totals	689.0	41,457	1,075

Table 15 Summary of System Weight, Volume, and Power Estimates

System		Weight (lb)	Volume (cu ft)	Power (kw)
1	Non-Integrated, H ₂ O Heat Sink, Lithium Hydroxide CO ₂ Removal, High Pressure Gaseous O ₂ Supply, H ₂ O Vapor Condensation	1108	23.4	0.99
2	Non-Integrated, H ₂ O Heat Sink, Regenerable CO ₂ Removal, High Pressure Gaseous O ₂ Supply, H ₂ O Vapor Condensation	1194	25.9	1.11
3	Non-Integrated, H ₂ O Heat Sink, Potassium Superoxide CO ₂ Removal and O ₂ Supply, H ₂ O Vapor Condensation	1084	25.4	1.01
4	Integrated, H ₂ -O ₂ Heat Sink, Lithium Hydroxide CO ₂ Removal, O ₂ from Power System Supply, H ₂ O Vapor Condensation	977	58.7	1.09
5	Integrated, H ₂ -O ₂ Heat Sink, Regenerable CO ₂ Removal, O ₂ from Power System Supply, H ₂ O Vapor Condensation	1051	63.3	1.21
6	Integrated, H ₂ Heat Sink, Lithium Hydroxide CO ₂ Removal, High Pressure Gaseous O ₂ Supply, H ₂ O Vapor Condensation	716	22.0	1.07

Table 15 (concl)

	System	Weight (lb)	Volume (cu ft)	Power (kw)
7	Integrated, H ₂ Heat Sink, Regenerable CO ₂ Removal, High Pressure Gaseous O ₂ Supply, H ₂ O Vapor Condensation	760	23.9	1.19
8	Integrated, H ₂ Heat Sink, Potassium Superoxide CO ₂ Removal and O ₂ Supply, H ₂ O Vapor Condensation	689	24.0	1.07

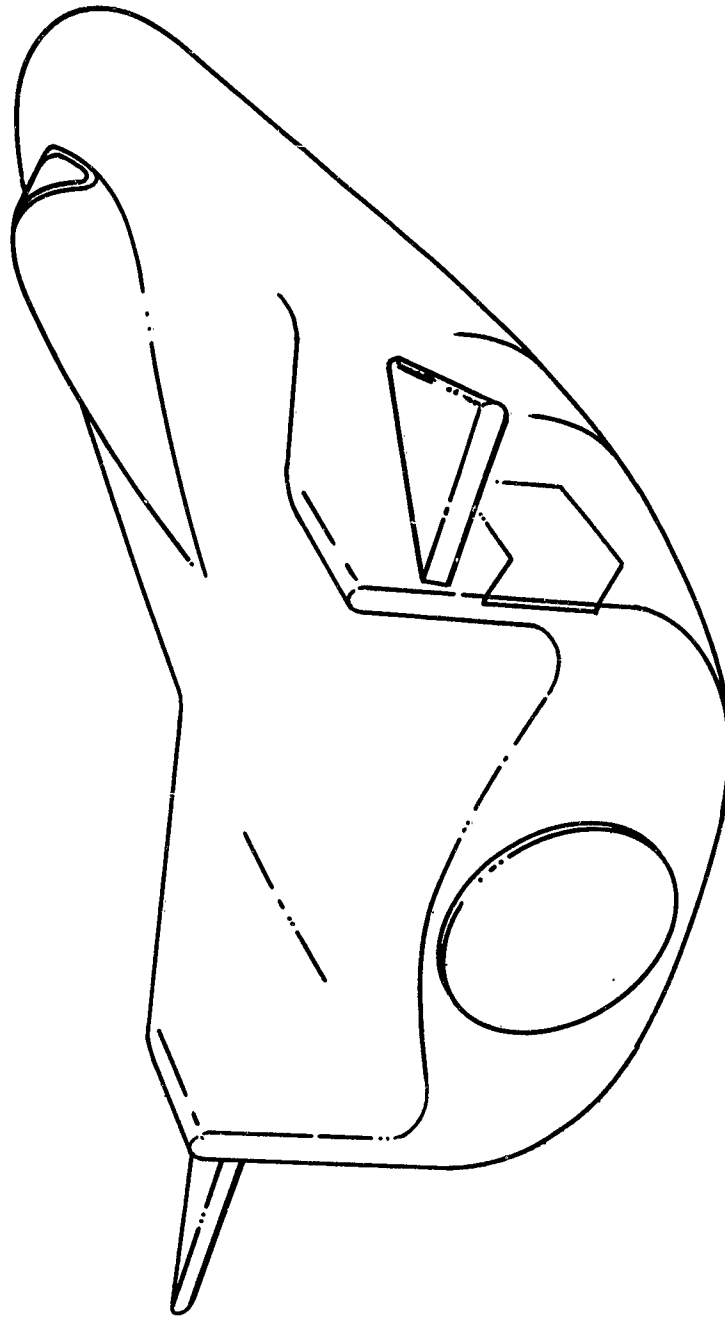


Fig. 1. Lifting-Body Configuration

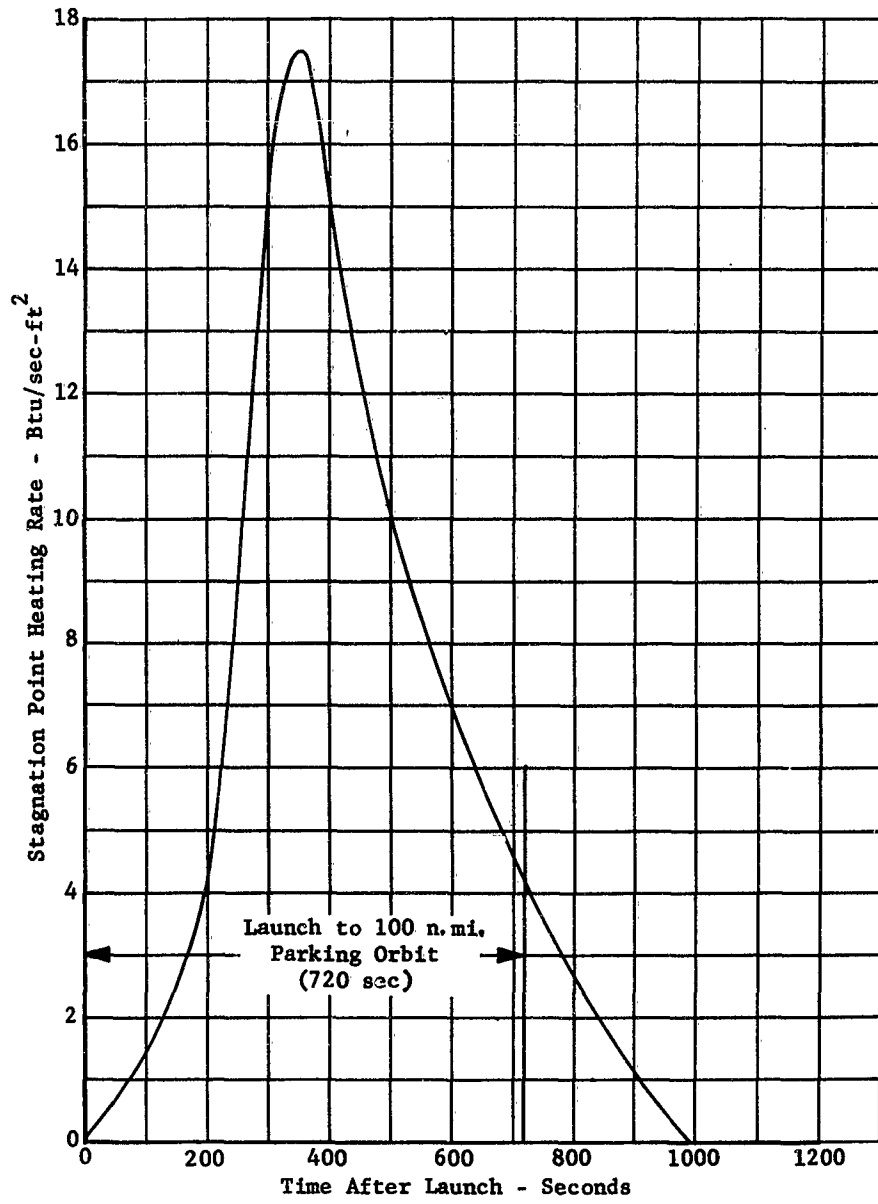
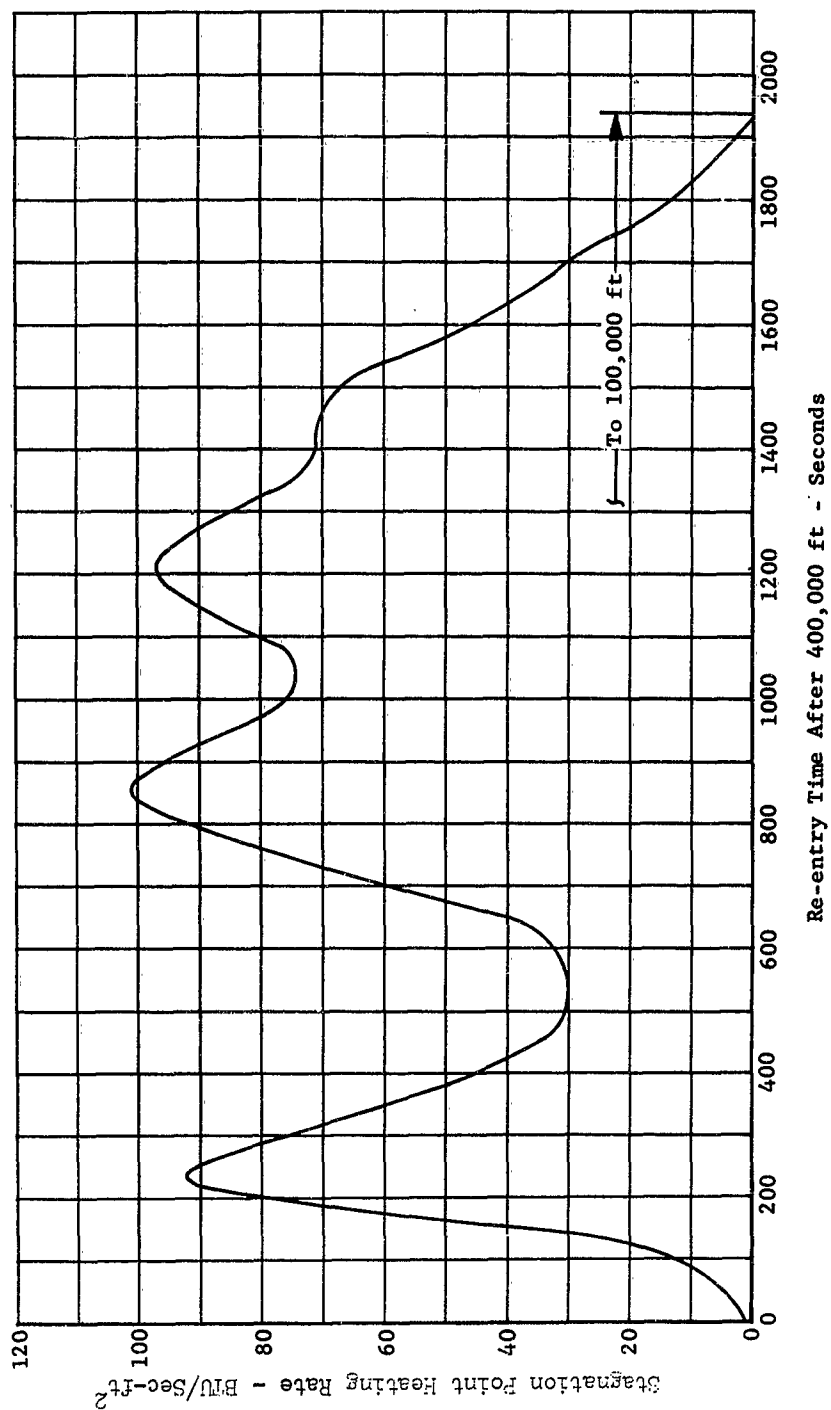


Fig. 2 Typical Stagnation Point Heating Rates During Launch



Re-entry Time After 400,000 ft - Seconds

Fig. 3 Typical Stagnation Point Heating Rates During Re-entry

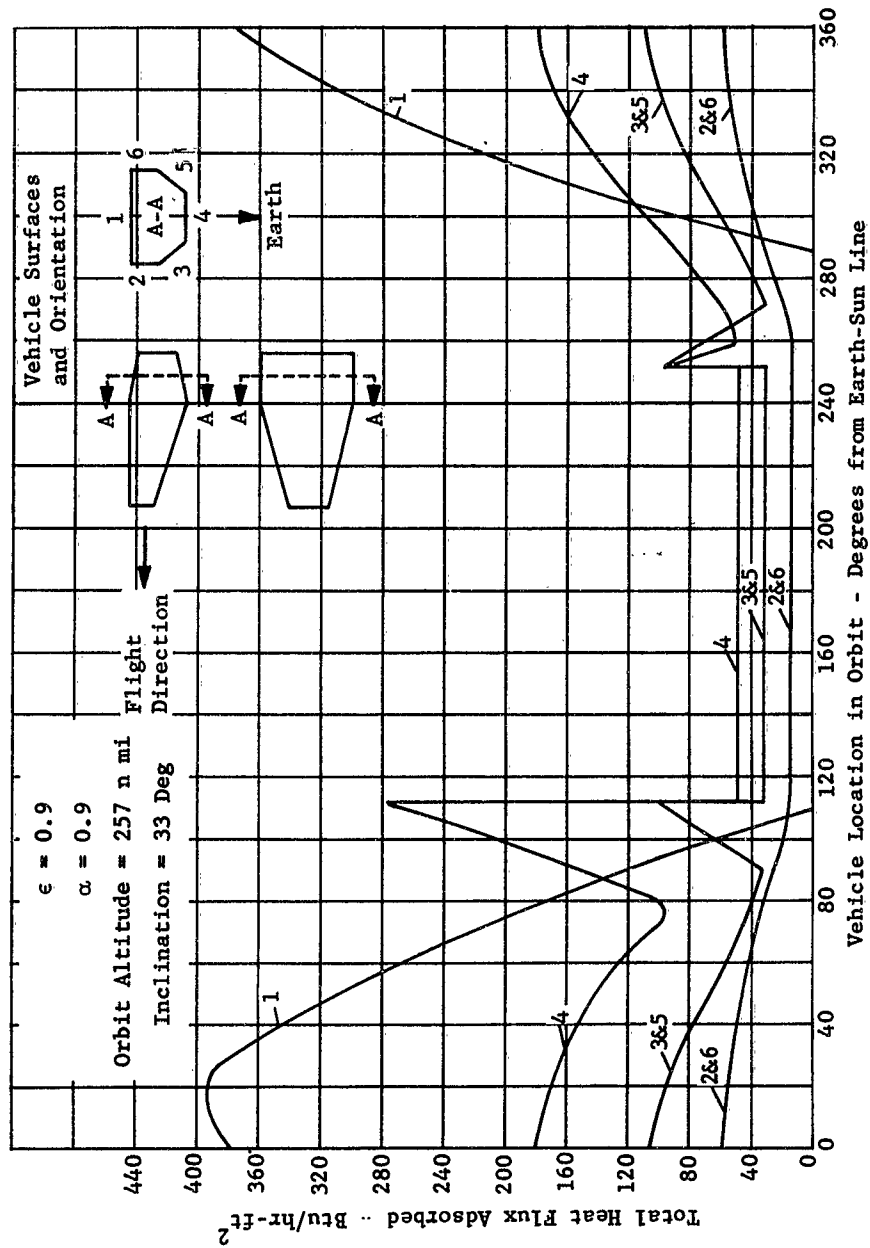
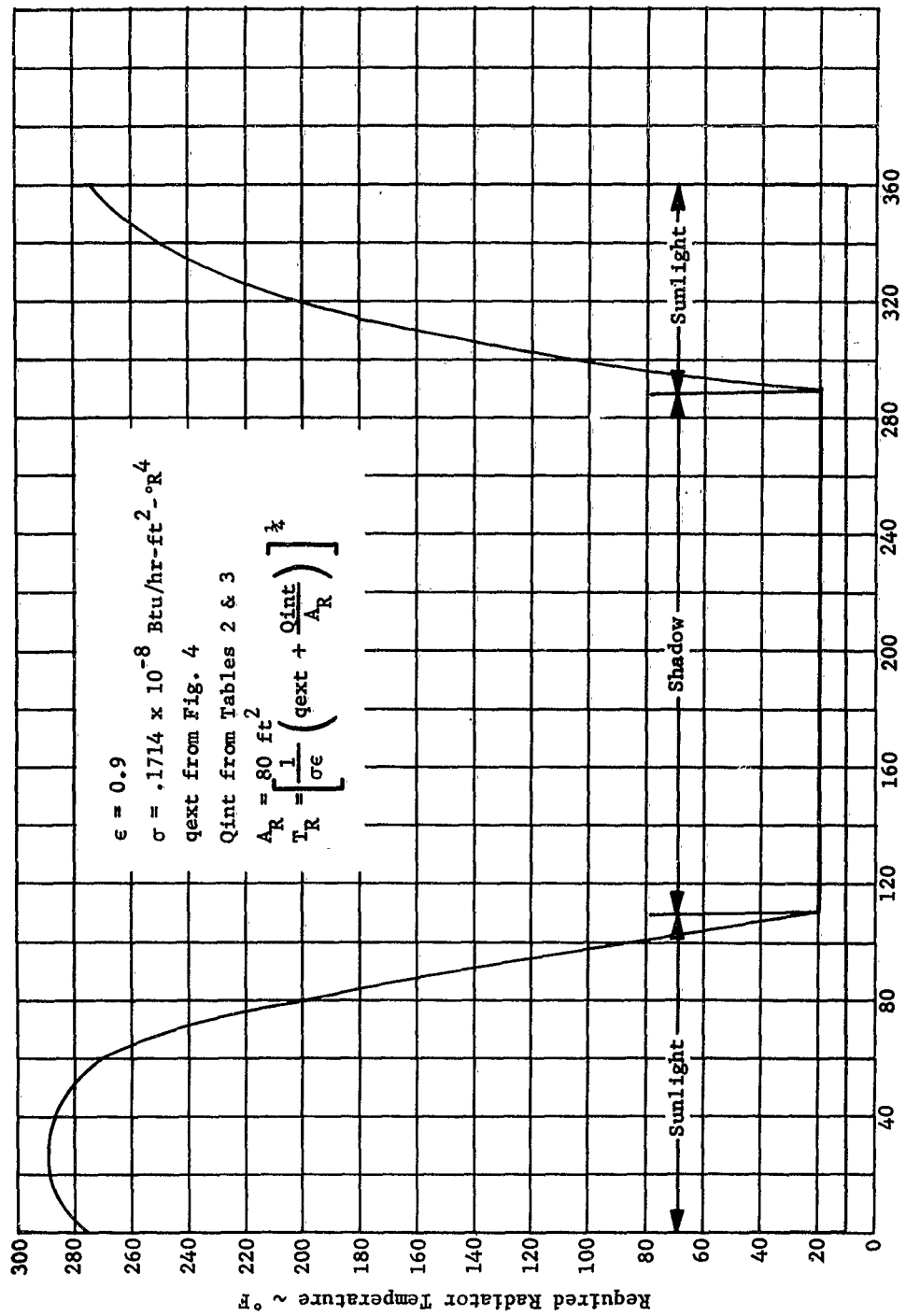


Fig. 4 Total Heat Flux Adsorbed During Orbital Flight



Vehicle Location in Orbit-Degrees from Earth-Sun Line
 Fig. 5 Required Radiator Temperature vs Vehicle Position in Orbit

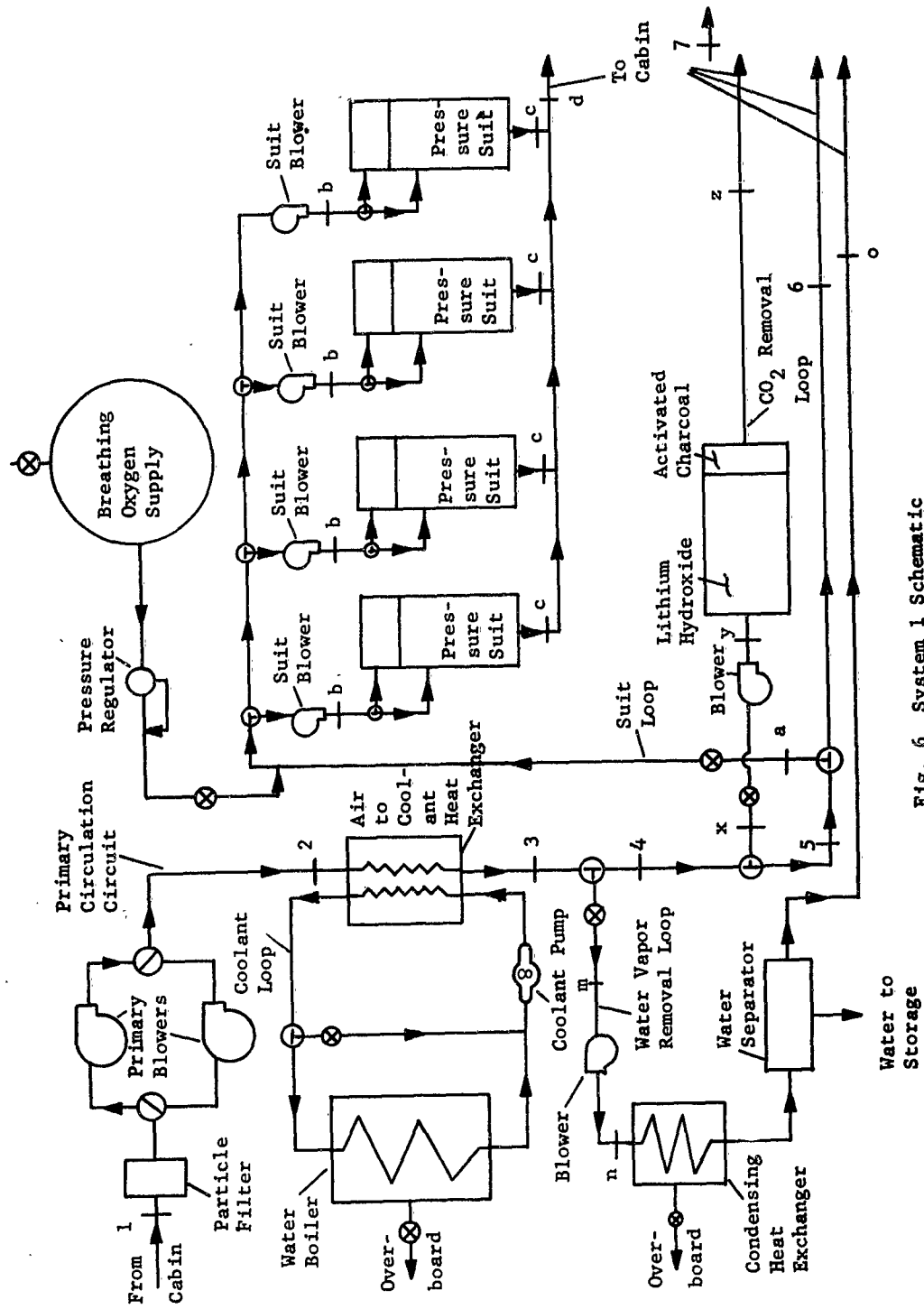


Fig. 6 System 1 Schematic

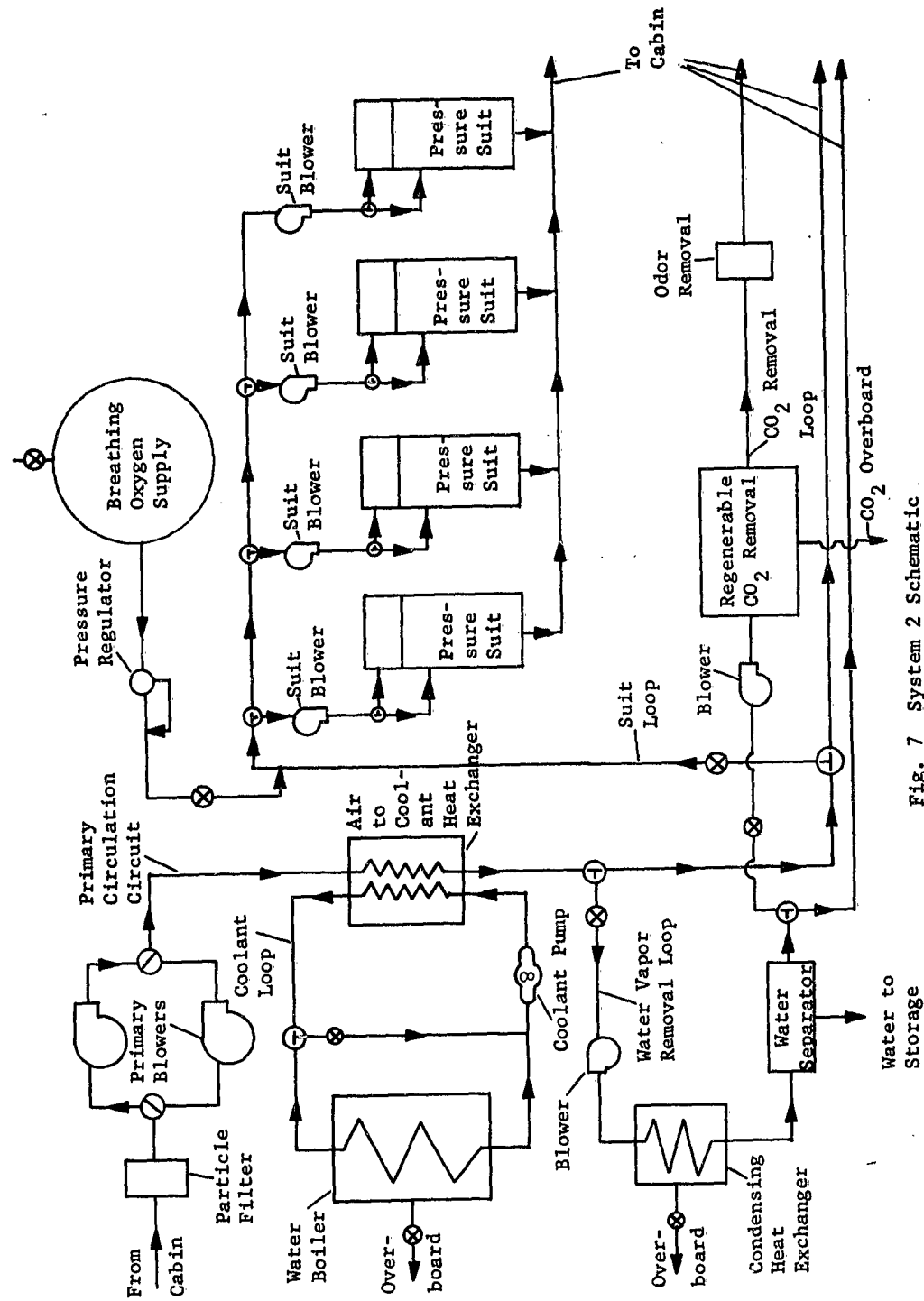


Fig. 7 System 2 Schematic

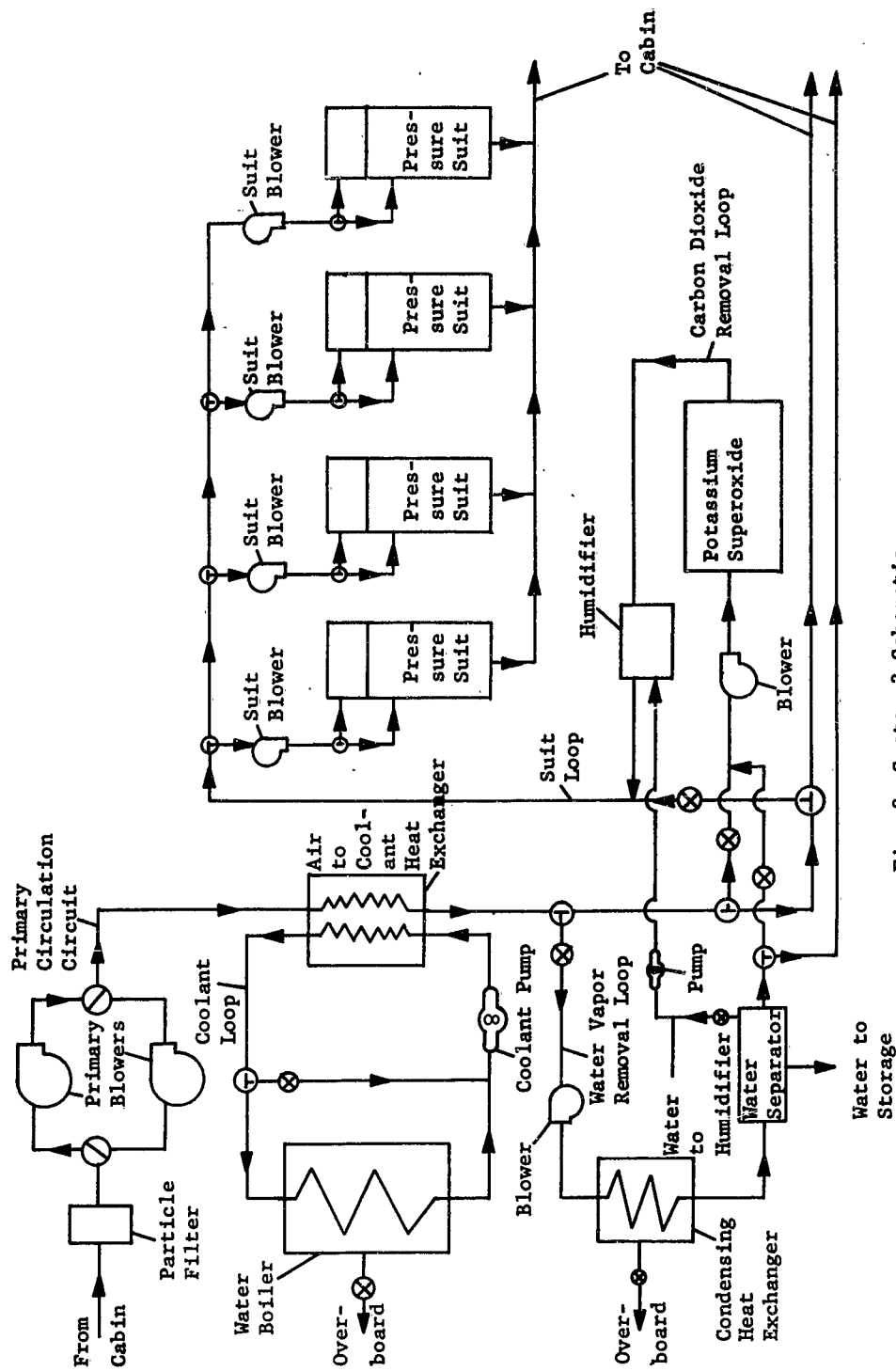


Fig. 8 System 3 Schematic

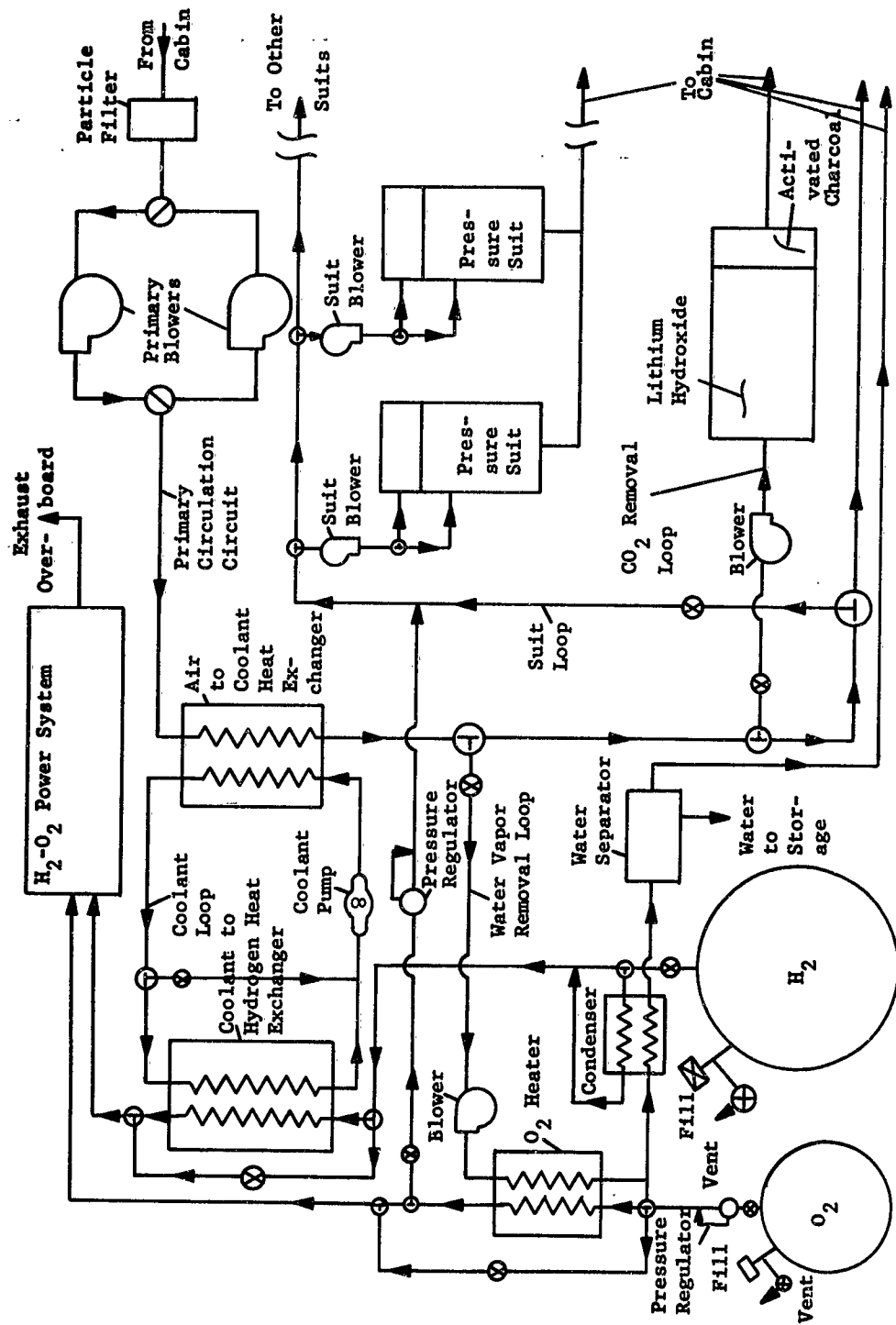


Fig. 9 System 4 Schematic

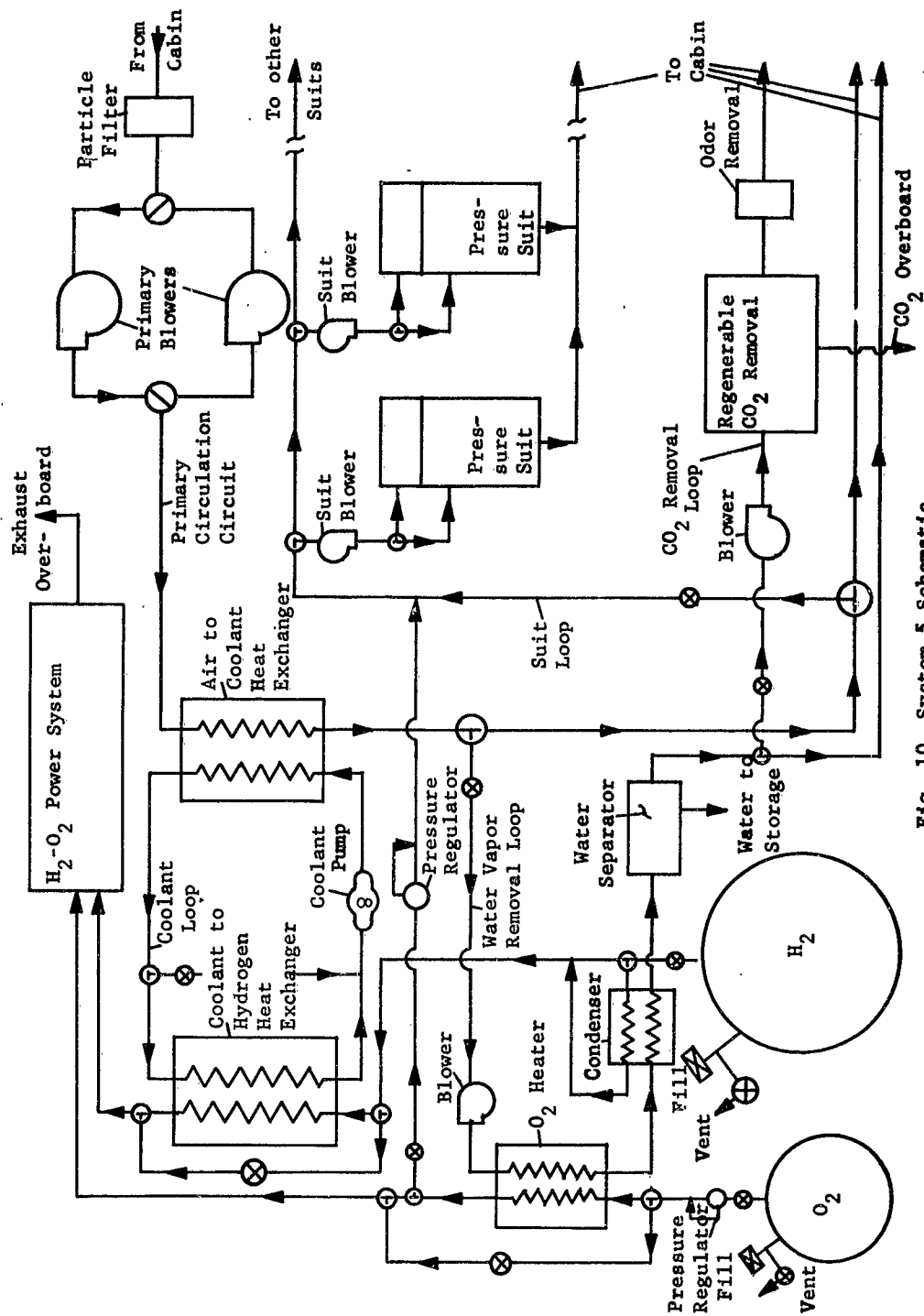


Fig. 10 System 5 Schematic

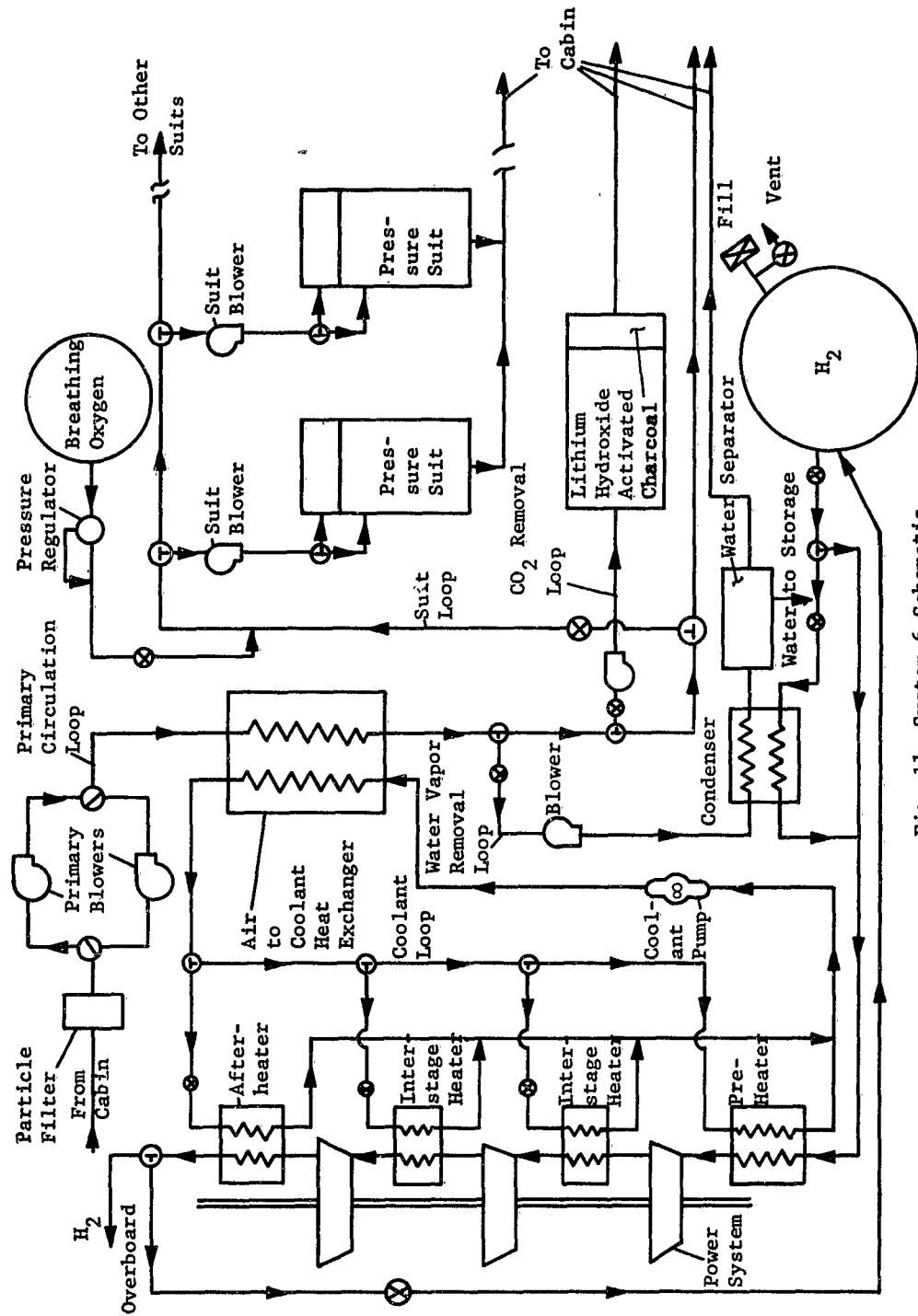


Fig. 11 System 6 Schematic

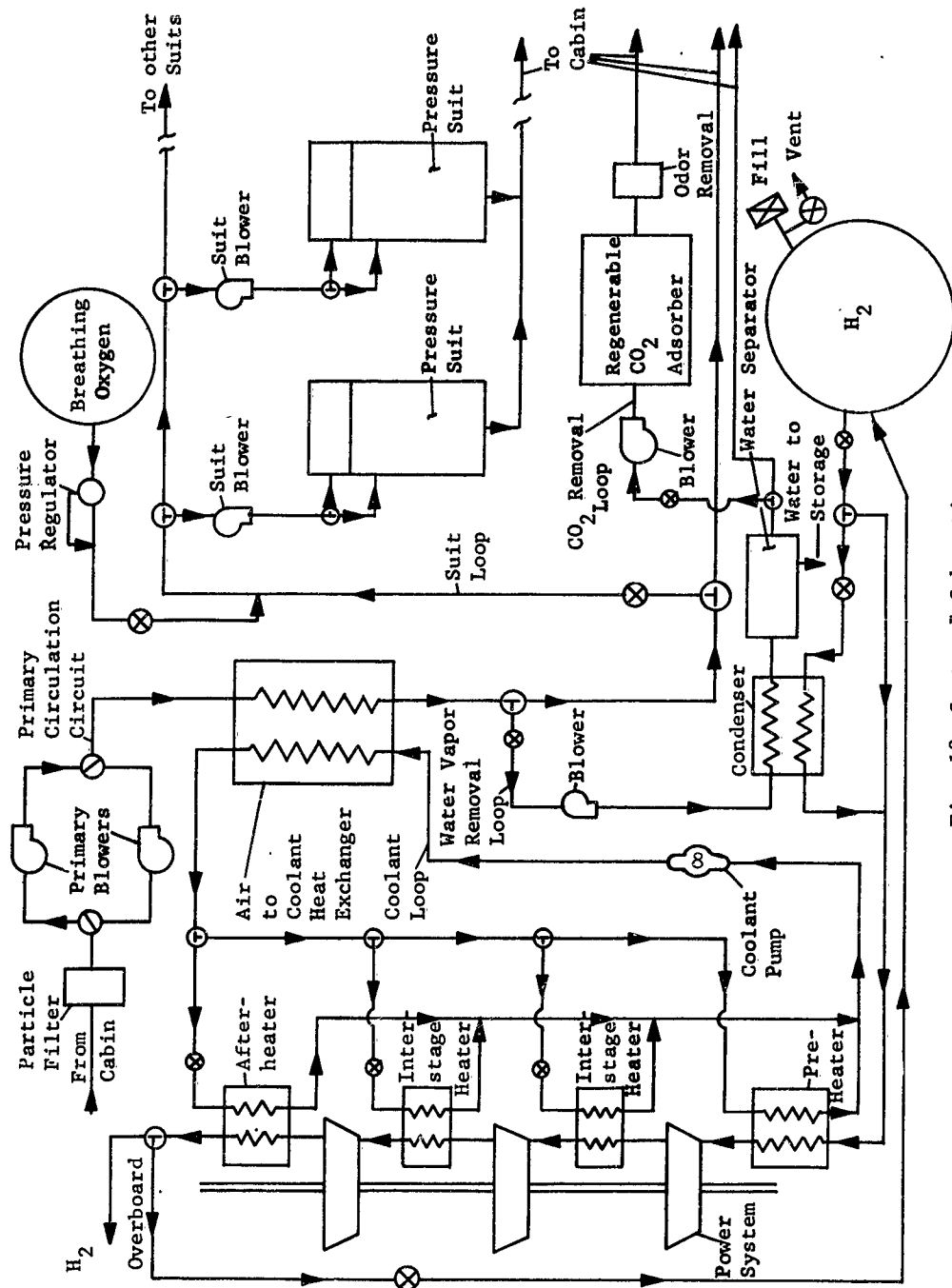


Fig. 12 System 7 Schematic

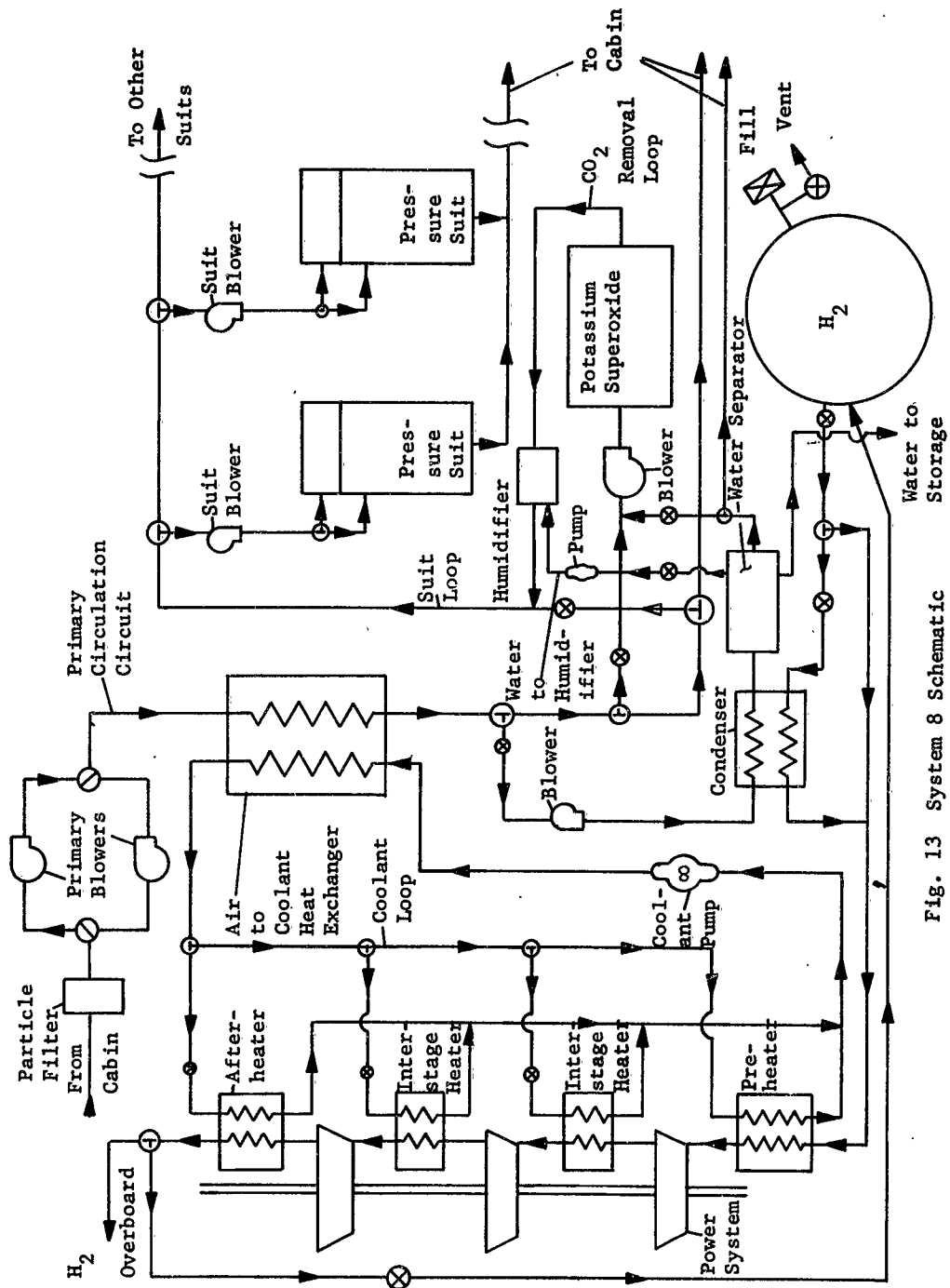


Fig. 13 System 8 Schematic

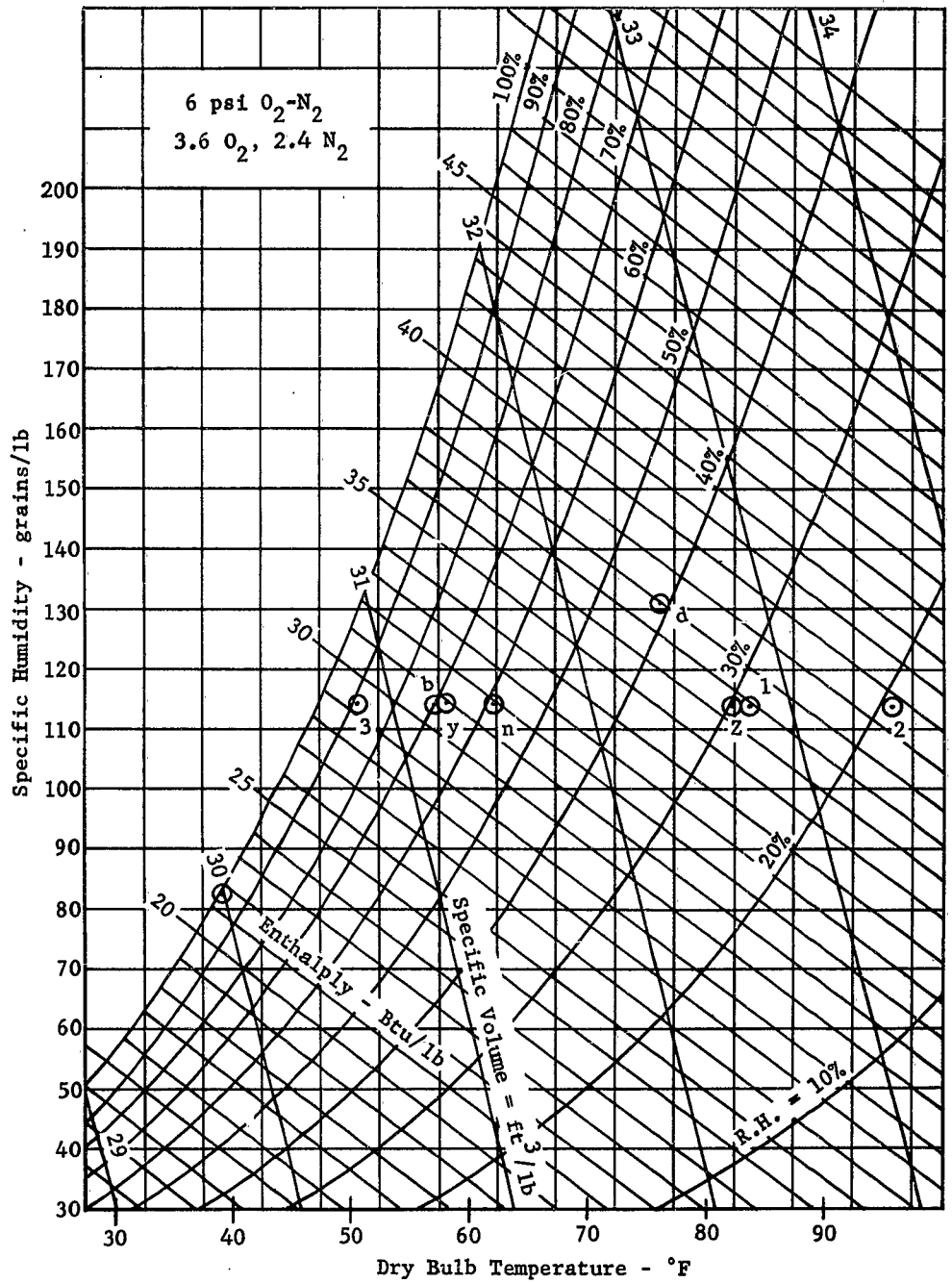


Fig. 14 Psychrometric Chart

Fourth Paper -- "Environmental Control Systems for a Manned Maneuverable Space Vehicle," by E.P. Gebhardt, Martin.

QUESTION: (John Smylie, Aero Space Corporation) Did you consider an expendable radiator for heat loads except in re-entry?

ANSWER : (Mr. Gebhardt) The consideration of the radiator, of course, was for the orbital phase of the mission and we considered only skin interval radiators. If we had considered an expendable radiator it would not be compatible with logistics in the operational capability of the vehicle. I'm a little bit biased for this vehicle and its mission for radiators to be giving so many reasons, for my reasons for rejecting it in this study may not be too convincing. (Laughter.) It's okay for long-term space stations but this is the only possibility that you have.

QUESTION: (Anonymous) The second question is not signed but it is on the radiator also. It says: Based on 80 square feet of radiator area what is an unacceptably high temperature for the heat load and external flow conditions?

ANSWER : (Mr. Gebhardt) I calculated heat and balance on this radiator of 80 square feet, and the temperatures required to reject the heat during the sunlit portion of the orbit was over 200 degrees Fahrenheit. Of course they were lower when the vehicle went into its shadow.

QUESTION: (Mr. Peeples, McDonnell) Was additional oxygen provided along with potassium superoxide to make up leakage?

ANSWER : (Mr. Gebhardt) I guess here I was a little optimistic in assuming a zero leakage cabin all the way through.

However, we are going to have leakage and this would be handled by a separate container of a mixture of oxygen and nitrogen gas probably under high pressure storage.

QUESTION: (Mr. Bailey, Sundstrand) Was the power requirement that I showed tabulated there?

ANSWER : (Mr. Gebhardt) That required only for the environmental control system came out about one Kilowatt. The vehicle power level was around 3 Horse Power for all the systems compared.

QUESTION: (Mr. Bailey, Sundstrand) Was the power requirement, that required to power the environmental control system, or that required from the power system to supply sufficient cooling, referring to the integrated system.

ANSWER : (Mr. Gebhardt) Well, as I said, the power level for all systems was around 3 Horse Power and in the fourth and fifth systems where the hydrogen and oxygen power system was used, the heat could be dropped into the hydrogen only between the storage container and the combustor, so the cooling mode would determine this flow rate of hydrogen. This came out to specific fuel consumption for the entire system of almost 2.6 pounds per Horse Power per hour. Whereas the last three integrated systems, using the low temperature, hydrogen expansion cycle with the three stages of expansion and interstage leakage, could dump heat into the hydrogen between the storage container and the first stage of the expansion, between the two stages, and then after the final stage, and could absorb almost twice as much heat by this alternate expansion and reheat cycle, so that the resulting specific fuel consumption was only about one pound per Horse Power per hour for the low temperature hydrogen expansion cycle.

QUESTION: (Mr. Day, McDonnell) What degree of optimization or verification was made of the systems before comparison?

ANSWER : (Mr. Gebhardt) Preliminary calculations were accomplished to show or attain the types of techniques that applied to the short term mission. These calculations showed that we should not be regenerating oxygen from carbon dioxide and so on. It was more determined that we were in the category of storage techniques.

QUESTION: (Mr. Day, McDonnell) Were these concepts partially developed or experimentally verified?

ANSWER : (Mr. Gebhardt) All of the techniques that we have assumed in the various systems were postulated for comparison. Hardware is in existence for all of these. Some of the hardware has actually flown in orbit, like the lithium hydroxide canister for CO₂ removal, and water boiling for thermal control and some of the other techniques. Hardware is in existence beyond the laboratory stage.

QUESTION: (Mr. Lambert, United Controls) What kind of difficulties do you anticipate in maintaining fuel (Hydrogen & Oxygen) storage pressure when dumping heat back into the tanks?

ANSWER: (Mr. Gebhardt) Of course, I think the supercritical storage technique for cryogenics which requires heat addition when fluid is withdrawn to maintain pressure beyond the critical value is going to require fairly sensitive control mechanism to balance the fuel withdrawal requirement with the variations in power and cooling load schedules.

SESSION II
ATMOSPHERE CONTROL SUBSYSTEMS

CHAIRMAN
AARON SHAFFER

**THE DEVELOPMENT OF AN ENGINEERING
MODEL CARBON DIOXIDE REDUCTION SYSTEM**

by

C. A. Remus

J. D. Zeff

R. A. Bambenek

**General American Transportation Corporation
Mechanics Research Division
Niles, Illinois**

THE DEVELOPMENT OF AN ENGINEERING
MODEL CARBON DIOXIDE REDUCTION SYSTEM¹

C. A. Remus
J. D. Zeff
R. A. Bambenek

INTRODUCTION

A three-man, carbon dioxide reduction system capable of converting expired CO₂ to water and elemental carbon automatically under manned aerospace flight conditions has been developed by the MRD Division of GATC for the Aerospace Medical Division, United States Air Force. The system weighs 190 pounds (not including power source), occupies 6.5 cubic feet, and requires 950 watts of electrical power.

The development program included an analytical study of process variables and an experimental study of a laboratory model to delineate the design of the system.

The testing of the system to date has shown a capability of converting 0.365 pounds of CO₂/hr to H₂O (higher than required for 3-man capacity). Most suitable process conditions found are: a reaction temperature of 1300°F, a recycle rate of 3.0 SCFM, and a reaction pressure of 15 to 25 psia.

The system can be operated continuously for 24-30 hours without carbon removal from the reactor. Iron in the form of expanded screening was found to be the most appropriate catalyst.

Recommendations for a smaller and lighter weight system requiring less power are included, and for integrating the reduction system with a solid electrolysis system for producing breathing oxygen from the formed water vapor.

In the closed environment of space vehicles one of the most important requirements for supporting human life is a continuing supply of oxygen for breathing. Under normal conditions each crewmember in breathing will consume approximately two pounds of oxygen per day and will convert this to carbon dioxide. Depending on the number of crewmembers and the duration of the mission the weight of oxygen required for breathing could become a significant factor in the payload weight if all of the required oxygen had to be stored initially aboard the vehicle. However, if a system were available for recovering the oxygen from carbon dioxide the payload penalty would involve only the weight of the recovery system rather than the weight of oxygen required.

¹ Acknowledgement on the final page describes the supporting agency and project personnel.

Various systems have been suggested for recovering oxygen from carbon dioxide, but the one which appears most favorable is a three-step system. The three steps consist of (1) carbon dioxide removal and collection from the vehicle atmosphere, (2) carbon dioxide reduction with hydrogen to water and solid carbon, and (3) electrolysis of the water formed to regenerate hydrogen for the reduction step, and to return oxygen to the vehicle atmosphere for breathing. This three-step system was believed most favorable because of the potential advantages of high recovery efficiency, low weight, and a minimum of process steps.

OBJECTIVE

The major objective of the project discussed herein has been to develop and fabricate a working engineering model to accomplish the second step of the overall process, namely, to reduce carbon dioxide to water. This project consisted of three phases, namely, (1) analytical, (2) experimental, and (3) engineering model fabrication and testing. All three phases will be discussed, but the last phase will be emphasized because this phase covers the actual final test results and operation of the engineering model.

SCOPE

The scope of the project was to perform a theoretical analysis and an experimental evaluation on the carbon dioxide reduction unit developed by the Battelle Memorial Institute, under a previous Air Force contract, to determine its performance characteristics. Then from this analysis and evaluation an improved engineering model was to be designed and fabricated that is capable of supporting a three-man crew by reducing a minimum of 0.33 pounds of carbon dioxide per hour. The model was to be designed to operate automatically under aerospace flight conditions, be readily maintainable, and require minimum power, weight, and volume.

ANALYTICAL

According to chemical equilibrium theory an equation may be written for the reaction system of carbon dioxide and hydrogen, which will relate the volume concentrations of these gases with the gaseous volume concentration of the water formed at equilibrium conditions. This equilibrium equation is as follows, where "x" denotes the volume fraction, P the reaction pressure, and K the equilibrium constant which is a function of temperature and thermodynamic properties of the reactants and products:

$$(x_{\text{H}_2\text{O}})^2 / (x_{\text{CO}_2})(x_{\text{H}_2})^2 P = K_1 \quad (1)$$

Although carbon results from the reaction it does not appear in the equilibrium statement in equation (1), because it is formed as a solid rather than a gas. However, the carbon does cause other effects in that it initiates side-reactions with hydrogen and carbon dioxide to produce methane and carbon monoxide, respectively. These gases will all be present at theoretical equilibrium, and equilibrium equations for the reactions are as follows:

$$(x_{\text{CO}})^2 P / (x_{\text{CO}_2}) = K_2 \quad (2)$$

and

$$(x_{\text{CH}_4}) / (x_{\text{H}_2})^2 P = K_3 \quad (3)$$

These equations establish the relation between the volume fractions of the five gaseous components present at simultaneous equilibria for the reactions representing the chemical system.

In the reacting system the ratio of oxygen atoms to hydrogen atoms remains constant with the restriction that no material is added or removed during the reaction, and may be expressed as follows:

$$\frac{O}{H} = \frac{CO_2 + CO + H_2O}{2x_{\text{H}_2} + 2x_{\text{H}_2O} + 4x_{\text{CH}_4}} \quad (4)$$

The sum of the volume fractions is unity:

$$x_{\text{CO}_2} + x_{\text{CO}} + x_{\text{H}_2O} + x_{\text{H}_2} + x_{\text{CH}_4} = 1 \quad (5)$$

The five volume concentrations and the O/H ratio are unknowns, but only five equations were developed. An IBM 1620 computer analysis was made and series of data were developed as general solutions.

The results of the equilibrium analysis as graphically depicted in Figures 1 and 2 showed that the amount of carbon dioxide reduced by hydrogen is (1) maximized when the O/H ratio = 0.5, (2) increased at lower temperatures, (3) increased at higher pressures, and the effect of increased pressure is more pronounced at higher temperatures.

EXPERIMENTAL

The experimental phase consisted of testing and evaluation of the carbon dioxide reduction unit built by the Battelle Memorial Institute. This system was composed primarily of a stainless steel reactor tube filled with a catalyst and the accessory equipment for pumping reaction gases through the system. A flow diagram of the system is shown in Figure 3. During operation of the system carbon dioxide and hydrogen feed gases were heated to 1300°F and passed through the catalyst zone which was filled with iron in the form of steel wool. In later experiments the iron was in the form of screening material. The feed gases reacted within the catalyst and water and carbon were formed. Carbon remained in the catalyst zone, while water vapor, by-product CH₄ and CO, and un-reacted CO₂ and H₂ passed out of the reactor. These gases and the water vapor were cooled, and water was removed from the gas stream by a condenser. The by-product and unreacted gases were returned to the reactor inlet and were heated along with fresh carbon dioxide and hydrogen feed gases for further reaction.

It was necessary to recycle unreacted CO_2 and H_2 gases because only a small fraction of the carbon dioxide feed would react in a single pass through the reactor. If the outlet gases were discharged and not reprocessed a considerable amount of recoverable oxygen would be lost.

In addition, if the by-product CH_4 and CO could be fed in appropriate amounts into the reactor along with fresh CO_2 and H_2 , then from equilibrium considerations no further CH_4 and CO would form, and the overall reaction would result in the formation of only water and carbon. Thus it was highly advantageous to recycle the by-product and unreacted gases. With this type of system the reactor could reach conversion and recovery efficiencies of 100%, since all of the oxygen in the carbon dioxide could be recovered, at least in the form of water.

Although the recycle characteristic of the system allows for recovery of all of the oxygen in the carbon dioxide feed, various other characteristics govern the quantity or the rate at which oxygen may be recovered. These other characteristics were the objects of study in the experimental phase.

The experimental factors tested were (1) Reaction temperature, (2) Reaction Pressure, (3) Gas flow rate through the reactor, (4) Catalyst Material, (5) Catalyst Configuration, (6) Inlet Gas Composition.

The experimental parameters were varied and evaluated in a series of thirty-four tests. The results of these tests showed the following:

- a. Conversion capacity increased with temperature increase. The reaction appeared to stop below approximately 600°F . Holding all other parameters constant, the three-man conversion capacity objective was achieved at approximately 1300°F .

These results are in contrast with the results of the theoretical study of equilibrium factors which indicated that CO_2 conversion is favored by a temperature decrease. This contrast shows the definite influence of kinetics upon the chemical reaction.

- b. The reaction pressure may vary between 1 and 9 psig without loss of capacity. This is in general agreement with the theoretical analysis.
- c. Capacity increases approximately directly with recycle gas flow rate between flow rates of 1.0 and 3.0 scfm.
- d. Pure iron appeared to be the most suitable catalyst material.
- e. The catalyst configuration was required to minimize and obstruction to flow, to provide a maximum catalyzing surface area, and to retain its structural integrity throughout the reaction. Iron metal in the form of screen material in one-inch squares appeared satisfactory for these requirements.
- f. The optimum inlet recycle gas composition appeared to be approximately 10% CO_2 , 40% H_2 , 35% CH_4 , and 15% CO . This is equivalent to an O/H ratio of approximately 0.17 as compared to 0.50 shown in the

theoretical analysis, again indicating the dominant influence of kinetic effects.

ENGINEERING MODEL FABRICATION AND TESTING

The engineering model of the carbon dioxide reduction system consists of the reactor and carbon collector, a counter-current heat-exchanger water condenser, a mechanical water separator, a recycle gas pump, and the carbon dioxide and hydrogen feed subsystem with overall controls and instrumentation. Visual indicators were included for verifying proper system operation.

The reactor is an insulated twelve-inch long by six-inch diameter stainless steel tube filled with iron catalyst in the form of 1-inch-square screens. The catalyst requires preconditioning with pure hydrogen at 1300°F for twenty-four hours. Inside the reactor is an electrical heater which is externally removable from the reactor core without disassembling the entire reactor. Attached to the lower end of the carbon collector is an insulated twenty-inch long by four-inch diameter tube with a dual purpose safety and manual valve at the bottom for periodic carbon removal. The reactor and carbon collector are mounted on aluminum support angles and plates.

The heat-exchanger and water condenser are both counter-current concentric tube heat transfer coils, wrapped in a continuous helix around the carbon collector. The water separator consists of a fourteen-inch long by four-inch diameter cylinder with a double end piston alternately compressing and releasing a water-absorbing sponge at each end; the piston is moved back and forth by an electrical motor driven rack and pinion gear assembly. The recycle pump is an electrically driven sliding-vane, positive-displacement pump, enclosed in pressure-tight containers to avoid the use of dynamic seals.

The variable controls in the CO₂ reduction system are the reaction temperature control, the hydrogen partial pressure control, and the carbon dioxide partial pressure control. The instrumentation components in the system are system inlet and outlet pressure gauges, reactor inlet and outlet temperature indicators, carbon dioxide composition indicator, heater element indication on-off switch and circuit breaker, recycle-pump indicating on-off switch and fuses, and water-separator indicating on-off switch and fuse.

A drawing of the assembled engineering model and the control panel are shown in Figure 4, while a block-type flow diagram is shown in Figure 5, illustrating the major components of the system and pressures, temperatures and composition at various points in the system. During operation a mixture of CO₂, H₂, CH₄, and CO gases is continuously circulated in and out of the reactor in a closed loop. Water formed by the reaction of CO₂ and H₂ is continually removed and CO₂ and H₂ which have reacted are continually replaced. Carbon formed by the same reaction either remains in the catalyst where the reaction takes place, and is removed when the catalyst is removed, or is blown free from the catalyst section and into the carbon collector for periodic removal by blow-down with excess hydrogen gas. A pictorial type flow diagram showing the actual path of the gases in each component of the system is illustrated in Figure 6.

Starting at point A on either diagram the mixture of gases enters the inlet side (annulus) of the counter-current heat-exchanger at approximately

100°F and 7.5 psig, at a flow rate slightly over 3 scfm. The composition by volume of these gases is 45-50% H₂, 5-7% CO₂, 25-40% CH₄ and 0-20% CO. Some water vapor is present, approximately 0.5 to 1.0% by volume, corresponding to the outlet composition of the water-saturated gas stream leaving the water condenser.

The gas mixture leaves the heat exchanger and enters the reactor at approximately 950°F and 5.5 psig. Within a central riser inlet tube the gas is heated further by an electric heater to 1300°F. The gases reverse flow direction and pass through a large annulus containing the iron catalyst where in the reaction to form water and carbon takes place. By the time the gases have passed through the catalyst the temperature has dropped to 1150°F. These reacted gases then enter the outlet side (center tube) of the heat exchanger at this temperature, and still at 5.5 psig.

The gases leave the heat exchanger and enter the water condenser at approximately 200°F and 2.5 psig. Sufficient cooling of the gases occurs to condense 75% of the water present in the gas stream. The gases, with entrained water droplets, leave the condenser at 50°F and 1.5 psig, and enter the water separator.

In the water separator the entrained water droplets are trapped in sponges while the gases pass through for further recycling. The gases leaving the water separator pass into a mixing tank which is mounted integrally with the recycle pump.

A carbon dioxide partial pressure detector cell is located in the recycle pump mixing tank. The signal from the detector is used to operate an on-off solenoid feed valve which adds CO₂ to the gas stream entering the reactor to maintain CO₂ partial pressure as required by the dynamic operating equilibrium in the system. System total pressure is transmitted to a pressure regulator which controls the hydrogen feed supply and adds H₂ as required to the gas stream entering the reactor. Together these two subsystems add CO₂ and H₂ in the correct amounts to replace CO₂ and H₂ which reacted to form water and carbon. The complete gas mixture enters the pump at 50°-60°F and 1.5 psig, and leaves the pump at 150°F and 7.5 psig. This returns the loop to the original starting point A.

The engineering model of the carbon dioxide system was tested in two phases. The reactor and heat-exchanger condenser were initially tested separately without the final water separator, recycle pump and system controls. The object of the first phase was to determine the operating characteristics of the reactor proper and the effectiveness of the internal heating system, including both preheating from the heat-exchanger and final heating by the electrical heater element.

In the second phase of testing all system components were assembled and tested as a unit. In this phase the behavior of the recycle pump, water separator and system controls was observed under the demands of actual operation, rather than under simulated conditions for each component.

Briefly, the first phase showed that the reactor would provide slightly in excess of the required 3-man conversion capacity, that the heat-exchanger worked well at over a 90% operating efficiency, that the internal heater

element provided in excess of the needed heating capacity, and that the system could be operated at the required conversion rate for at least 17 hours based on available carbon storage capacity within the catalyst. It was also found that the reactor operating temperature radically affects the conversion rate, since a drop from 1300°F to 950°F lowered the rate from 3.1 to 0.8 man-capacity.

The second phase showed that the recycle pump and automatic system controls operated properly, that the reaction proceeded as well at outlet pressure of 1.5 psig as at 5.8 psig, that the water-separator required re-design, and that the system could be run continuously for 21 hours at the required conversion rate using about 80% of the available carbon storage volume within the catalyst. These runs also showed that no carbon could be blown out of the catalyst into the carbon-collector even at recycle rates as high as 3.5 scfm.

The total weight of the engineering model is 190 pounds, compiled as follows:

<u>Insulated Reactor and Heater</u>	35 lbs
<u>Canister Plus Catalyst</u>	4
<u>Insulated Carbon Collector</u>	52
<u>Heat-Exchanger - Condenser</u>	21
<u>Recycle Pump and Motor with Mixing Tank</u>	21
<u>Water Separator</u>	11
<u>Feed System</u>	6
<u>Instrumentation and Controls</u>	14
<u>Piping</u>	6
<u>Support Frame</u>	20
	190 lbs Total

The average power requirement for the system in normal operation is 975 watts, compiled as follows:

<u>Heater</u>	650 watts
<u>Recycle Pump</u>	230
<u>Water Collector</u>	10
<u>Instrumentation and Controls</u>	85
	Total 975 watts

The volume occupied by the total system is as follows:

$$4'-8" \text{ high} \times 1'-2" \text{ deep} \times 1'-4" \text{ wide} = 6.5 \text{ ft}^3$$

SUMMARY

The results of the analytical, experimental and engineering model test phases showed that the unit developed operated reliably, automatically and continuously at over the required conversion capacity. The conversion rate appears to be governed mainly by kinetic rather than equilibrium effects. The operating characteristics were as follows for the engineering model.

1. Operating Temperature	1300°F
2. Operating Pressure	2 to 9 psig
3. Operating Capacity	0.365 lbs CO ₂ /hr (10% in excess of required)
4. Catalyst Material	Iron metal preconditioned for 24 hours with H ₂ at 1300°F
5. Catalyst Configuration	One-inch squares of screen material
6. Inlet Gas Composition	5% CO ₂ , 50% H ₂ , 25% CH ₄ , 20% CO
7. Recycle Gas Flow Rate	3.0 to 3.5 scfm
8. Reactor Size (3-man)	6-inch diameter x 12-inch length.

Further developments could be made to reduce the weight, size and power required for operation. Several areas which show promise are tubular or strip catalyst configurations to permit continuous carbon removal, a lighter weight honeycomb-type heat-exchanger, a centrifugal type water separator, a combined water separator electrolysis-cell, and an auxiliary or modified reactor heater for shortening start-up time.

ACKNOWLEDGEMENT

This project was initiated by the Life Support Systems Laboratory of the 6570th Aerospace Medical Research Laboratories, Aerospace Medical Division, Wright-Patterson Air Force Base, Ohio. The research was conducted under Contract AF 33(616)-8223, Project No. 6373, "Equipment for Life Support in Aerospace", and Task No. 637302, "Respiratory Support Equipment". This work was monitored by Messrs. R. E. Bennett and C. M. Meyer of the Life Support Systems Laboratory.

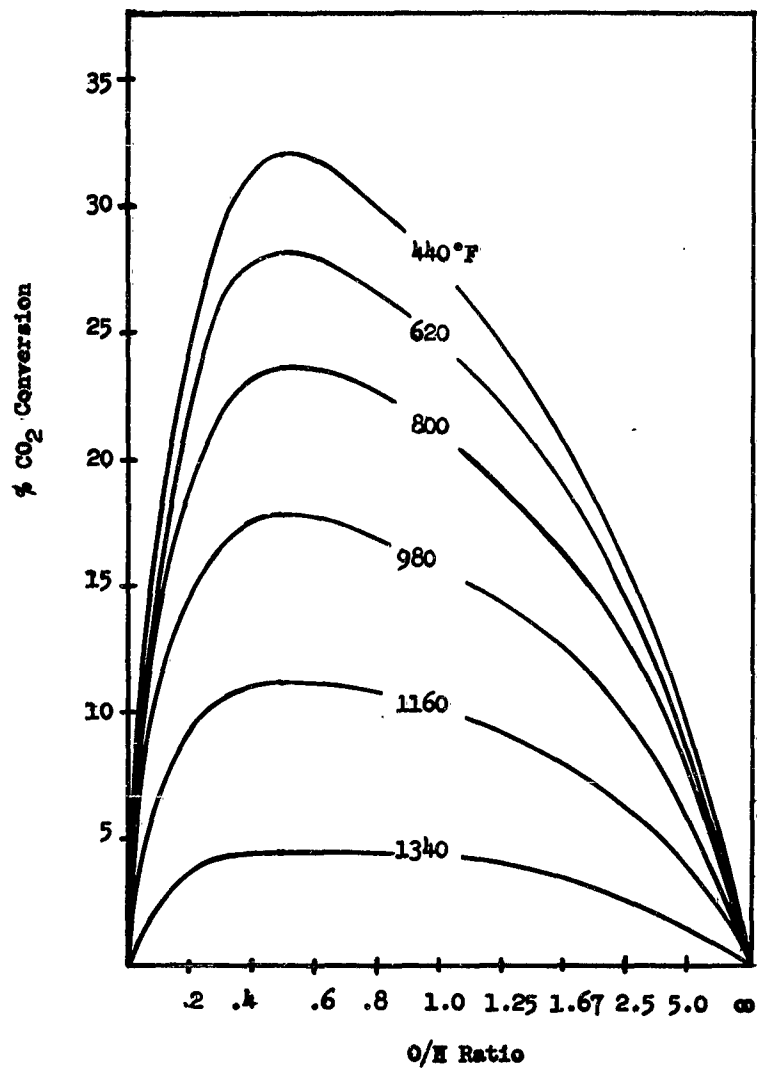


Figure 1 CO₂ % CONVERSION VS. O/H RATIO 9 PSIG

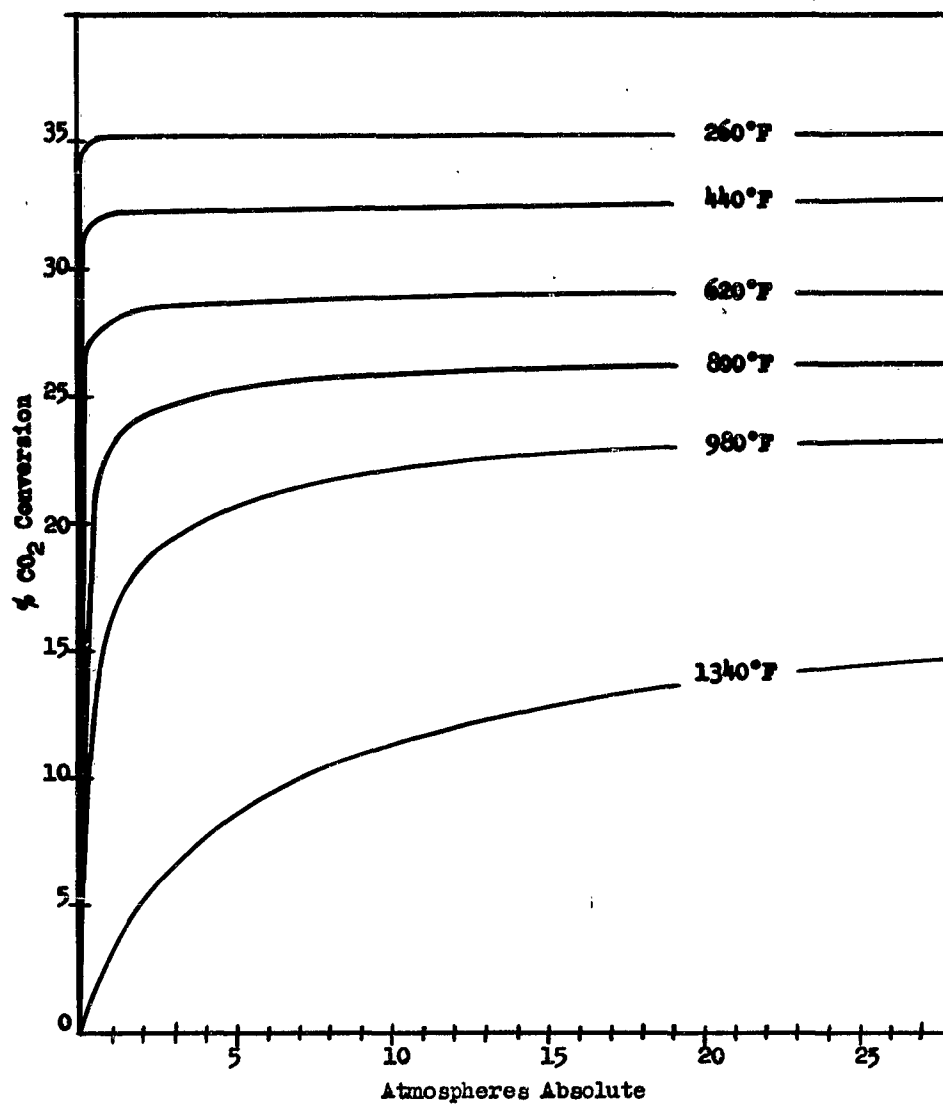


Figure 2 CO₂ % CONVERSION VS. REACTION PRESSURE, O/H RATIO, 0.5

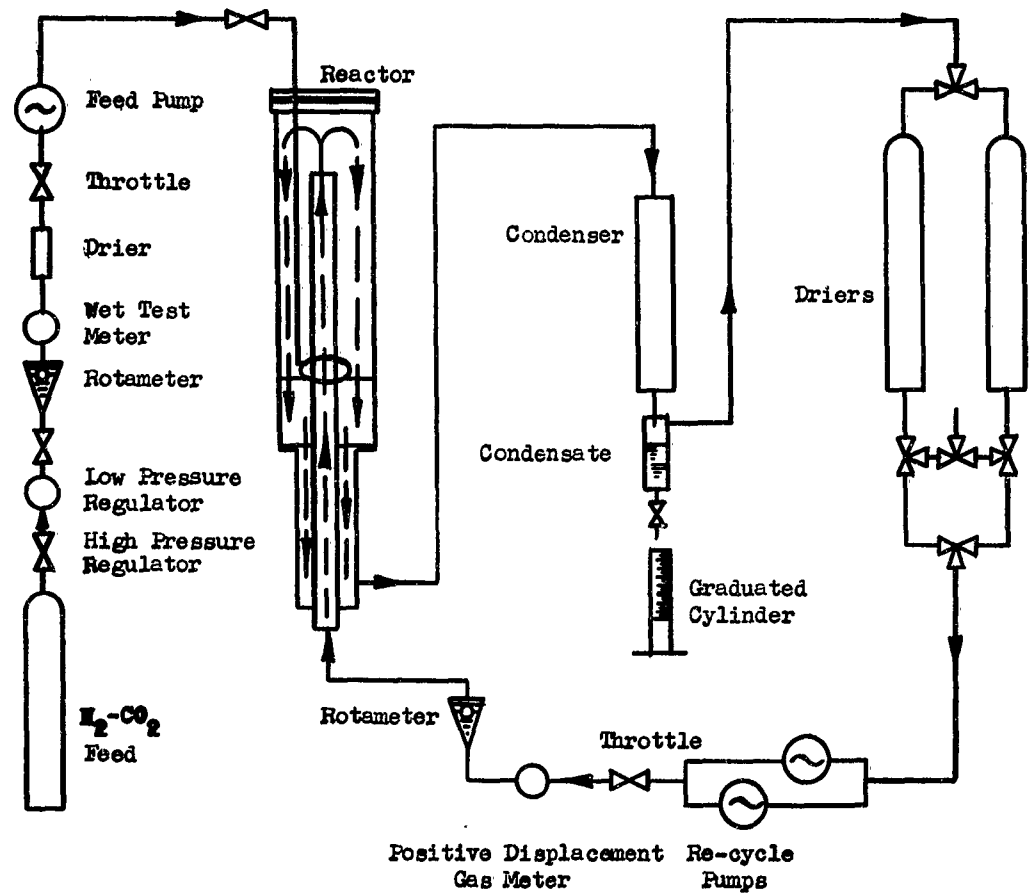


Figure 3 BATTELLE CO_2 SYSTEM FLOW DIAGRAM

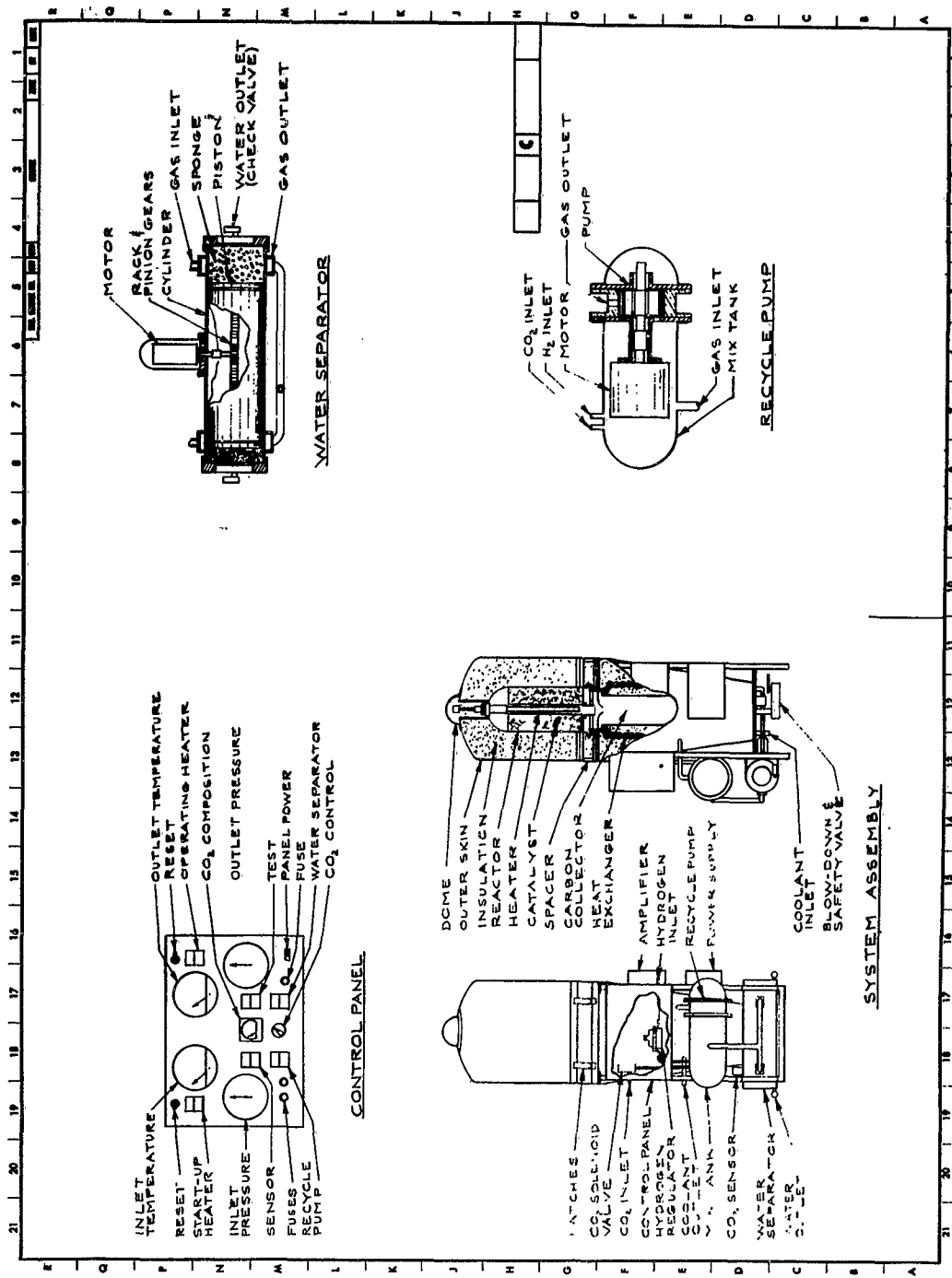


Figure 4 ASSEMBLED ENGINEERING MODEL AND CONTROL PANEL

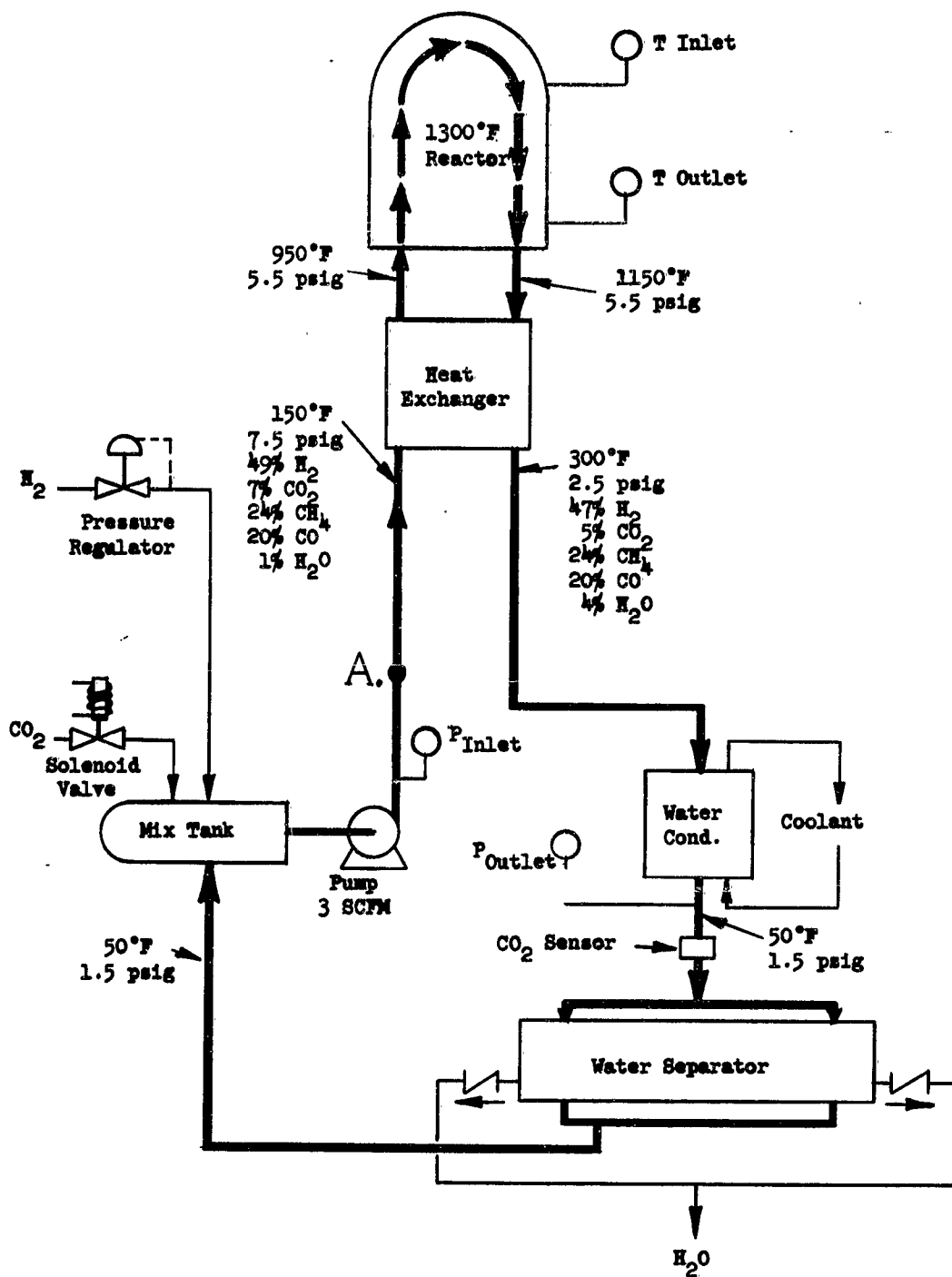


Figure 5 ENGINEERING MODEL, BLOCK FLOW DIAGRAM

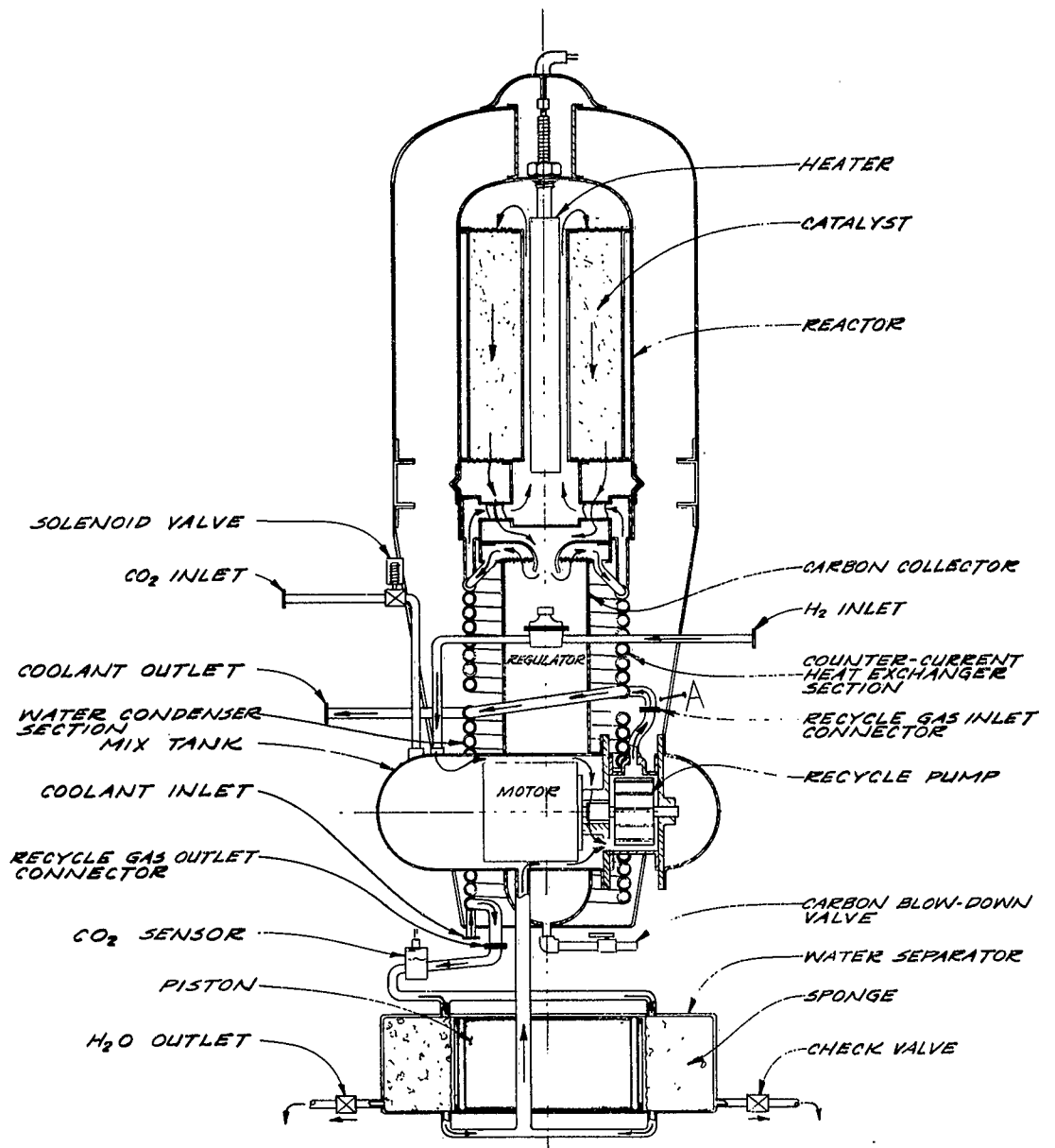


Figure 6 ENGINEERING MODEL PICTORIAL FLOW DIAGRAM

QUESTION AND ANSWER PERIOD

SESSION II -- Atmosphere Control Subsystems

First Paper -- "The Development of an Engineering Model Carbon Dioxide Reduction System," by G. A. Remus, J. D. Zeff and R.A. Bambenek. (Presented by G.A. Remus, Mechanics Research Division, General American Transportation Corp.)

QUESTION: (Mr. Shaffer, AiResearch Co.) Are you positive-- let me put it this way: What chance do you think there is of this carbon forming reaction floating out of the reactor into the water separator and gumming up the whole works when you conduct water out?

ANSWER : (Mr. Remus) That particular comes to mind when we were putting the system together. I wonder if I could have one of my slides back again? Is the slide operator gone? There is another question that would involve one of the slides. The gases first have to pass out of the bottom of the reactor down into this provisional carbon collector chamber that we put on the bottom of the reactor. This chamber was fitted with a nozzle which would accelerate the gases, and the carbon if there are any carbon particles in the gas as it passes through the nozzle, and force them down into the bottom of this collection chamber. We felt that they would stay in this collection chamber if they were forced down to the bottom. The particles would have a particular velocity (the same as the gas passing through the nozzle) but once the gas stream passed through the nozzle it could expand and slow down. The particles would supposedly continue on to the bottom and stay there. Also at the top of this carbon collection chamber we had a screen and a stainless steel filter to prevent any particles that might flow up to the top from getting into the inlet of the heat exchanger. So we did consider the problem and it didn't occur until the catalyst material very effectively trapped all of the carbon that was formed. We couldn't

get it out of there no matter how we tried. There were two cards here that asked approximately the same question and they dealt with: Why the conversion was carried on at 1300 degrees and 40 degrees Fahrenheit instead of 440 degrees Fahrenheit which was indicated as more or less a most desirable temperature from the analytical study.

ANSWER : (Mr. Remus) Well the analytical study was based completely on equilibrium equations, not on kinetics and as it turned out the equilibrium analysis told us one thing but the experimental data told us exactly the opposite. This indicated that the reaction is controlled mostly by temperature and by the kinetic features. We did not attempt to make a theoretical analysis on the kinetics reaction. It was too complicated. The only reason we did the equilibrium analysis at all was to give us some insight into what would be theoretically the best mixture to feed to the reactor to get the maximum conversion. Incidentally, when we did this, we varied the temperature to see what effect this might have, if any, and it gave the effect shown in the graph but again this was just from equilibrium. That question came from a Mr. Jahn from Boeing.

QUESTION: (Mr. William Bigler, United Aircraft Corp.)
How sensitive is the catalyst poisoning?

ANSWER : (Mr. Remus) The catalyst appeared to be relatively insensitive. I operated the reactor for a total of about a hundred hours, the final reactor, and had no catalyst poisoning. The rate of conversion did not decrease during this hundred hour period, although there was no way, really, of telling if any poisons were introduced. Probably there were very few because I used bottled gases. But one of the things that leads us to suspect that the catalyst is not easily poisoned is as follows: One batch of catalyst was reduced with hydrogen at 1300 degrees Fahrenheit. The catalyst was then left sitting out in the lab in an open container

purposely to see if this would affect the catalyst since it had been reduced. We then put the catalyst into the reactor and ran it to see if there were any difference between these runs and the runs where the catalyst was reduced followed by a test reaction. The catalyst seemed to be stable as far as poison was concerned but then again there were no excessive amounts of poison in our laboratory atmosphere.

QUESTION: (Mr. Bigler) Might not problems of gas separation make this reduction system unattractive as compared to reductions with only one gaseous product; for instance, ionic bulk electrolysis?

ANSWER : (Mr. Remus) Well, I really don't quite know what is meant here but there is no need to separate gases in the system. Carbon dioxide and hydrogen are fed into one point of the loop, the recycle loop, water comes out at another point. Once the system has gotten to an operating equilibrium where there are the appropriate quantities of methane and carbon monoxide, hydrogen and carbon dioxide gases in the recycle loop, methane and carbon monoxide are not formed and the system functions more or less as a continuous process. The carbon dioxide and hydrogen gas enter one side and water comes out of the other side. The solid carbon collects, and that is a problem, how to get that out of the system? But there is no need for separating gases as such in the system.

QUESTION: (Mr. Bigler) Would one type of carbon dioxide reduction system serve for all missions?

ANSWER : (Mr. Remus) I assume--I don't know if this is the correct assumption--that he means, "Would this particular system serve for all missions?" Well, it was not for short or intermediate duration missions. It is too heavy on power requirement and the missions are too excessive. If he means, would one other type of reduction system serve for all missions, I don't know. Maybe it would.

QUESTION: (Mr. Bigler) Is the formation of iron carbide possible in this process?

ANSWER : (Mr. Remus) When the carbon was removed from the reactor, we found that it was magnetic and even the smallest was magnetic, so more than likely there are iron carbides formed. Actually the carbon that is formed is some sort of a carbide rather than pure carbon. This we base only on the fact that every particle of carbon that we would find, even the smallest, was attracted by a magnet. There are no carbon oxygen compounds formed because the atmosphere is a highly reducing atmosphere.

QUESTION: (Mr. Bigler) Will the presence of dissolved gases in the condensed water terminate the electrolytically produced oxygen?

ANSWER : (Mr. Remus) Well, they could contaminate the oxygen, but if this were the case we could pass the oxygen through a catalytic burner and convert whatever contaminants were in there (and these contaminants would be either methane, carbon monoxide or carbon dioxide) convert them into more carbon dioxide and pass them into cabin atmosphere where, as carbon dioxide, they would again be removed and sent through the system again.

QUESTION: (Mr. Duffy, Battelle Memorial Institute) What carbon dioxide detector was used in the flight system?

ANSWER : (Mr. Remus) We used a Beckman sensor. It has an electrolytic type jell--rather an electrolyte jell in the type of sensor that senses the carbonate in the jell solution.

QUESTION: (Mr. Duffy) Also, what is its sensitivity and accuracy?

ANSWER : (Mr. Remus) I don't really know. I would say

that it was sufficient to accomplish the control feature that we required. We were measuring partial pressures in the vicinity of 50 millimeters on down of carbon dioxide and I would say that it was accurate within plus or minus 5 millimeters in that range, but this was sufficient to control or keep the control where we wanted it.

QUESTION: (Mr. Ginwalla, Northern Research Engineering Corporation) Did you measure the reactor heat transfer?

ANSWER : (Mr. Remus) No, we did not. The only part of the heat transfer problem that we were interested in was how well our heat exchanger performed. This we did measure, but we didn't measure the heat transfer across the reactor itself. The effect of a catalyst's size, we didn't measure this but qualitatively. One of the catalysts that was used in the beginning was a very fine mesh steel wool, because this is what the people at Battelle had used too. We calculated the surface area of the steel wool and then replaced the surface area by using these metal screens, little squares. The diameter of the steel wool was about a thousandth of an inch in diameter, the screen wire was around a thirty-second of an inch, qualitatively they both performed the same. The surface area seemed to be the criteria rather than the actual dimension of the catalyst.

QUESTION: (Mr. Ginwalla) Did you measure catalyst poisoning which would occur in a real system?

ANSWER : (Mr. Remus) No, we didn't measure the effect of poisoning of the catalyst as described in an earlier question.

QUESTION: (Mr. Ginwalla) Do you have any data on carbon formation?

ANSWER : (Mr. Remus) I don't know quite what he means by this. The carbon that was formed was not pure carbon. It

was probably carbide. Quantitatively there were about 350 grams of catalyst in the reactor. The amount of carbon that would fill the reactor was only about 800 grams. We feel that the catalyst could have been used over again. So that the amount of carbon formed in the program, say of the catalyst, is something we were not able to find out. This is something we would have to determine if we could remove carbon continuously from the catalyst.

QUESTION: (Mr. Fred Morris, Hamilton Standard) Has there been any experimental investigation of the effects of oxygen, nitrogen or other impurities in the carbon dioxide?

ANSWER : (Mr. Remus) If there were oxygen in the carbon dioxide feed it would be reduced immediately to water. If it were nitrogen in the feed it would build up and effectively cut down the capacity of the unit and the feed would have to be purged to remove the nitrogen again. I don't know what impurities, for instance hydrocarbons; they could possibly build up also in the reactor and have to be purged. They might however, if they were high enough chain of hydrocarbons, they might decompose, but I wouldn't say for sure.

QUESTION: (Mr. Morris) Can such effects be predicted at this time?

ANSWER : (Mr. Remus) We don't know.

QUESTION: (Mr. Pollara, ISOMET Corporation) What carbon to catalyst ratio is expressed in the batch method?

ANSWER : (Mr. Remus) We did not measure this. We could not measure it in the system we had. Again this was the problem involving carbon removal. The catalyst will probably last for a much longer time than the amount of time that it takes up to fill up the catalyst.

QUESTION: (Mr. Pollara) On a continuous basis?

ANSWER : (Mr. Remus) It is the same answer.

QUESTION: (Mr. Pollara) Is the oxygen recovered by the Isomet procedure?

ANSWER : (Mr. Remus) No, it is based on phosphorous pentoxide.

**CONTROL OF ORGANIC CONTAMINANTS IN CLOSED
ATMOSPHERES**

by

J. G. Christian

J. E. Johnson

**U. S. Naval Research Laboratory
Washington, D. C.**

ASD-TDR-63-260

CONTROL OF ORGANIC CONTAMINANTS IN
CLOSED ATMOSPHERES

by

Jack G. Christian
and
J. Enoch Johnson

INTRODUCTION

With the advent of the nuclear submarine, extended submergences completely isolated from the surface became feasible. Such prolonged isolation requires not only that oxygen be supplied to the crew and the carbon dioxide from their breathing be removed, but also carbon monoxide from smoking and hydrogen from batteries must be eliminated. Further, organic materials such as paint solvents, fuel vapors and the like must be removed since otherwise the concentration of these organic vapors could build up to excessive values. It has been calculated that the evaporation of one gallon of diesel fuel into the atmosphere of a closed submarine having a free volume of 85,000 ft³ would produce a hydrocarbon concentration of 1350 mg/m³, or 218 ppm, using 150 for the average molecular weight. Some of the contaminant organic vapors and aerosols are removed by beds of activated carbon and electrostatic precipitators, but the main system for removal of organic vapors is that of catalytic combustors.

Hopcalite is an oxidation catalyst which was first used during World War I for the oxidation of carbon monoxide in

gas masks (1). Fortuitously when this catalyst is operated at higher temperatures it also catalyzes the oxidation of hydrogen and organic compounds. The work reported here was carried out to determine the efficiency of hopcalite at various temperatures for catalyzing the combustion of vapors of several structural types of hydrocarbons, oxygenates, halogenides, nitrogen-containing organics as well as aerosols of several oils (2,3,4). It was important to study these variables because of the differences in toxicity and ease of combustion among the many organic constituents of submarine air.

APPARATUS AND PROCEDURE

A laboratory scale unit was built which duplicates ship-board combustors as to catalyst bed depth, and space velocity. The furnace temperature was controlled by a rheostat. A schematic diagram of this apparatus is shown in Figure 1.

The hydrocarbons studied were the Phillips pure grade containing not less than 99 mol percent. The lubricating oil and the triarylphosphate ester used in the aerosol work were commercial mixtures. The carbitol used was shown to contain 15% ethylene glycol by means of gas chromatography. A correction was made for this glycol content in calculating the theoretical CO_2 which would be obtained upon complete combustion. The Freons used were Dupont products.

Known mixtures of the liquid organics with air were prepared by diverting a portion of the CO_2 -free air stream

through a weighed bubbler containing the fluid under study and recombining it with the main air stream. Known mixtures of gases with air were prepared by allowing a flow of the subject gas controlled by a fine needle valve through a rotameter or soap bubble flowmeter to mix with the main air stream. Aerosols were produced using an apparatus described by J. K. Thompson (5).

The carbon dioxide was measured dynamically using a LISTON-BECKER model 15-A non-dispersive infrared analyzer. Calibration was done by comparison with tank breathing air of known CO₂ content. In the case of compounds containing halogens, nitrogen or phosphorus, analysis of the furnace effluent for compounds of these elements were made as appropriate.

Gas chromatography was used to compare the halogenide concentration of the furnace influent with that of the effluent. This technique was also used to compare concentrations of the gaseous hydrocarbons and to measure nitrous oxide in the furnace effluent.

RESULTS

1. Hydrocarbons

The higher hydrocarbons, hexane and above, are converted to practically the theoretical amount of carbon dioxide at temperatures of 300-350°C as shown in Table I. Several aromatic compounds, benzene and 1, 2, 4 - trimethylbenzene, which are

known to be resistant to uncatalyzed vapor phase oxidation, seemed to be somewhat more resistant to hopcalite-catalyzed oxidation than the n-paraffins. While oxidation of these compounds was essentially complete at 300°C, the efficiency dropped rapidly below this temperature. The paraffin, 2,2-dimethylbutane, showed similar behavior. Methane exhibited marked resistance to oxidation as Table II shows. The combustion efficiency was about 2% at 300°C and 30% at 400°C. The combustion efficiency for ethane dropped from 12% at 315°C to 6% at 260°C. For propane the drop was from about 25% at 315°C to 11% at 260°C.

Gas chromatographic and infrared studies of the furnace effluent collected during incomplete combustion of methane revealed only carbon dioxide and methane. In other words, once oxidation of the molecule is begun, it proceeds completely and no partial oxidation products are formed. Hexane also formed no partially oxidized products when studied under conditions of incomplete combustion at lower temperatures. This is important since in many cases partially oxygenated products such as aldehydes and acids are more baneful than the parent compound.

2. Oxygenates

Methanol, ethylene glycol, carbitol (diethylene glycol monoethyl ether) and o-cresol were found to be practically completely oxidized over hopcalite at 300-350°C as shown in Table III.

3. Halogenides

The extent of decomposition at 315°C of the halogen compounds studied ranged from slight in the case of Freon-12 (dichlorodifluoromethane) to extensive in the case of methyl chloroform (1,1,1-trichloroethane). In the case of a bromine containing compound, Freon 114B-2 (Dibromotetrafluoroethane), there was an apparent retention of some of the bromine and most of the fluorine on the catalyst since photometric analysis of the furnace effluent failed to account for the amount of these halogens expected for the amount of Freon 114B-2 disappearing. During one eight hour run the apparent decomposition of Freon 114B-2 fell from 30% to about 5%.

Methyl chloroform as such almost completely disappeared upon passage over hopcalite at 315°C. In addition to the small amount of undecomposed methyl chloroform detected in the furnace effluent by gas chromatography, three additional products were detected. One was vinylidene chloride (1,1-dichloroethylene), another was trichlorethylene (1,1,2-trichloroethylene) and the third, present in much smaller amounts, was not identified. The data are shown in Table IV. Although some Freons seem rather resistant to oxidation under the conditions studied, the production of even small amounts of halogen acids presents problems. Not only are these gases physiological irritants, but they cause metal corrosion. For this reason, in any system where catalytic combustion is used, selection of the Freon or similar compound is important and suitable means must be provided for scrubbing out of the acids formed.

4. Nitrogen compounds

Table V shows that all the nitrogen compounds studied formed nitrous oxide in greater or lesser amounts when admitted into the hopcalite furnace. At 315°C ammonia was converted to nitrous oxide in 70% yield while less than 3% of the initial ammonia was detected in the effluent. Higher furnace temperatures diminished the yield of nitrous oxide. During a separate run with the inlet ammonia concentration at 350 ppm, less than 5 ppm of nitrogen dioxide (NO₂) was measured in the furnace effluent.

Monoethanolamine produced nitrous oxide in 19% yield at 315°C. Raising the furnace temperature diminished the yield as in the case of ammonia. Reducing the furnace temperature to 260°C seemed to increase the production of nitrous oxide slightly.

Nitrous oxide was formed in 16% yield from morpholine and 17% yield from pyridine at 315°C. All the organic nitrogen compounds studied produced essentially the theoretical amount of carbon dioxide at 300-350°C.

5. Aerosols

Aerosols of dioctyl phthalate (DOP), a petroleum base lubricating oil (Navy Symbol 2190) and a commercial triaryl phosphate fluid (TAP) were oxidized quantitatively at 300°C as shown in Table VI. Phosphatic material from the oxidation

of relatively high concentrations of TAP aerosol (20-60 μ g/l) was retained essentially quantitatively on the surface of the catalyst granules with no apparent loss in catalytic activity toward hydrocarbons. When extremely high concentrations of TAP aerosol (>60 μ g/l) were introduced into the catalyst bed, some unchanged liquid TAP emerged from the furnace exit and some impairment of the efficiency of the catalyst for hydrocarbon combustion was experienced. A catalyst thus treated appeared to undergo at least a partial regeneration of its activity upon continued exposure to hydrocarbon vapors.

DISCUSSION AND SUMMARY

Catalytic combustion using hopcalite catalyst has been shown to be an efficient method for the destruction of a number of organic vapors and aerosols of many structural types. Operation of the catalytic reactor at temperatures around 300°C or slightly less provided for essentially complete destruction of most of the hydrocarbons, oxygenates, aerosols and nitrogen-containing compounds studied. Certain lower molecular weight hydrocarbons such as methane, ethane and propane are more resistant to oxidation. The Freons studied, with the exception of the bromine-containing 114B-2, suffered but little decomposition at about 300°C. Methyl chloroform on the other hand suffered essentially complete destruction at 300° with the formation of three organic products which were detected in the furnace effluent. All nitrogen-containing compounds studied yielded

more or less nitrous oxide and the organic nitrogen compounds formed the theoretical amount of carbon dioxide.

Thus a catalytic combustor containing hopcalite and operated at moderate temperatures provides a good system for the complete combustion of many organic compounds with minimum decomposition of Freons. A great advantage of this system is that even though oxidation may not be 100%, no partially oxidized fragments were found in the effluent gas.

REFERENCES

1. Lamb, A. B., Bray, W. C., and Frazer, J. C. W., "The Removal of Carbon Monoxide from the Air", J. Ind. Eng. Chem. 12, 213-21 (1920)
2. Johnson, J. Enoch, Christian, Jack G., and Carhart, H. W., "Hopcalite-Catalyzed Combustion of Hydrocarbon Vapors at Low Concentrations", J. Ind. Eng. Chem. 53, 900-02 (1961)
3. Christian, Jack G. and Johnson, J. Enoch, "Catalytic Combustion of Aerosols", presented before the Petroleum Division of the American Chemical Society on 11 September 1962 at Atlantic City, N. J.
4. Christian, Jack G., "Catalytic Combustion of Freons," Chapter 13 in "Second Annual Progress Report, The Present Status of Chemical Research in Atmosphere Purification and Control on Nuclear-Powered Submarines," Piatt, V. R. and White, J. C., NRL Report 5814, August 29, 1962.
5. Thompson, J. K. Report of NRL Progress, July 1956, p. 14-17

TABLE I

Combustion of Hydrocarbons Over Hopcalite

<u>Compound</u>	<u>Percent of Theoretical CO₂ Found</u>		
	<u>350°C</u>	<u>300°C</u>	<u>200°C</u>
Benzene	92	87	74
1,2,4-Trimethylbenzene	100	98	55
t-Butylbenzene	96	96	86
n-Hexane	97	97	77
n-Decane	96	98	89
2,2-Dimethylbutane	98	84	40
Octene-1	94	89	83
Cyclohexane	91	--	--

TABLE II
Combustion of Lower Hydrocarbons
Over Hopcalite

Compound	Temperature °C	Percent of Theoretical CO₂ Found
Methane	400	30
	300	2
Ethane	315	12
	260	6
Propane	315	25
	260	11

TABLE III

Combustion of Oxygenated Compounds Over Hopcalite

	Vapor Conc.		% of Theor. CO ₂		
	mg/m ³	ppm	350 °C	300 °C	200 °C
Methanol	130	97	98	98	95
Carbitol	40	7	100	82	79
Ethylene glycol	7	3	100	100	100
o-Cresol	86	20	100	99	83

TABLE IV
Products From the Hopcalite
Catalyzed Combustion of Methyl Chloroform

<u>Compound</u>	<u>Retention Time (Minutes)</u>	<u>Amount in Effluent</u>
Vinylidene chloride [CH ₂ = CCl ₂]	2 1/2	much
Methyl chloroform [CH ₃ CCl ₃]	5	very little
Trichloroethylene [CHCl = CCl ₂]	11	much
Unknown	16	little

- NOTES: (1) Beckman GC-2A Instrument
(2) UCON HB200 Column at 70°C
He pressure 30 psig

TABLE V
Hopcalite - Catalyzed
Oxidation of Nitrogen Compounds

Compound	Inlet Concentration (ppm)	N ₂ O Formed (% Theoretical)
Ammonia	140	70
Monoethanolamine	19	20
Morpholine	35	16
Pyridine	40	17

- NOTES: (1) Space Velocity 21,000 hours⁻¹ and temperature 315°C
- (2) Raising the furnace temperature diminished the yield of N₂O from MEA and ammonia

TABLE VI

Combustion of Aerosols Over Hopcalite at 300°C

Substance Studied	Aerosol Conc. [$\mu\text{g}/\text{l.}$]	Extent of Conversion to CO_2
Lubricating oil	100-150	100%
DOP	40-100	100%
TAP	20-60	ca. 115%

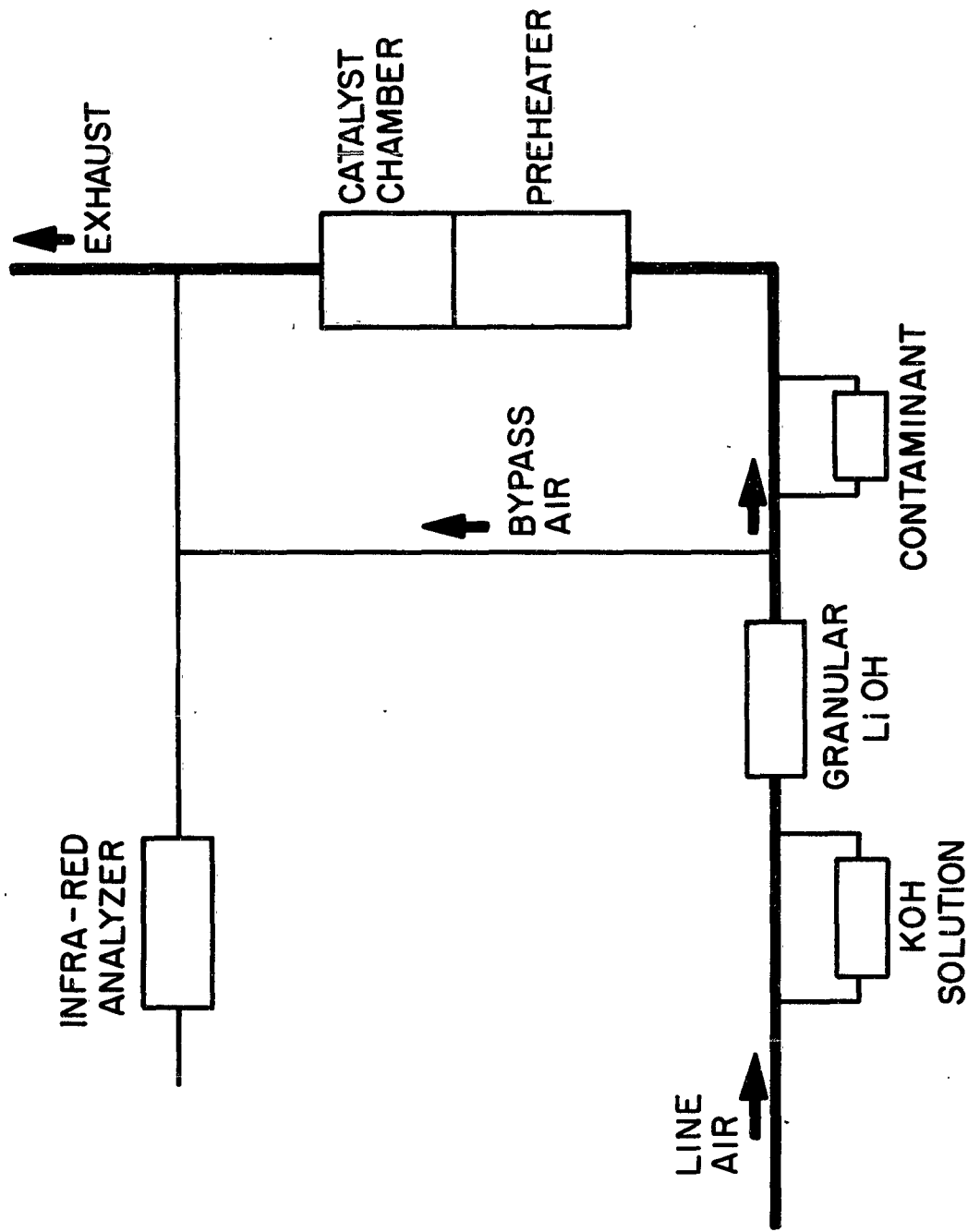


Figure 1. Schematic of Laboratory Scale Unit

Second Paper -- "Control of Organic Contaminants in Closed Atmospheres," by Jack G. Christian, U.S. Naval Research Laboratory.

QUESTION: (Mr. J.D. Zeff, American Transportation) How did you select the concentrations of contaminants you worked with and did you use the H₂ flame detector for all of your tests?

ANSWER: (Mr. Christian) The concentrations selected were nearest possible to those found aboard submarines. When this was not practical, and this was usually because they were too low in nuclear submarines, we chose the lowest concentration that we could immediately work with and measure, whether it was produced concentrations or measured concentrations. We didn't use a hydrogen flame detector because we only bought the detector about a year ago and anyway it is not good for every thing.

QUESTION: (Mr. W.W. Thayer, Douglas Long Beach) Approximately how long must the contaminants be kept in contact with the catalyst to get the performance desired?

ANSWER : (Mr. Christian) Well, I gave the space velocity in the paper and you can calculate that out. It's in the micro seconds range--pretty fast; one cubic inch through a one inch cross section of catalyst at bed depth.

QUESTION: (Mr. R.M. Byke, Douglas Aircraft, Santa Monica) Wouldn't even small amounts of freon decomposition products be dangerous in a relatively small volume spacecraft due to their toxicity?

ANSWER : (Mr. Christian) Yes.

QUESTION: (Mr. Pollara, ISOMET Corporation) Do you get any HF by the catalytic decomposition of the freons?

ANSWER : (Mr. Christian) Yes.

QUESTION: (Mr. R.B. Jagow, Lockheed, Palo Alto) Based on your experimental studies, are there any physical and/or chemical properties of a contaminant that can be used to predict the ability of a hopcolite bed to effectively reduce it?

ANSWER : (Mr. Christian) Not based on our studies.

QUESTION: (Mr. J.B. Werner, Lockheed) Reference to slide on combustion to CO₂ over hopcolite, how does efficiency reaction vary with flow rate over the bed?

ANSWER : (Mr. Christian) Better at the slow rate.

QUESTION: (Mr. Werner) What velocity was used for the indicated results?

ANSWER : (Mr. Christian) 1 CFM.

QUESTION: (Mr. Werner) Also, length of bed?

ANSWER : (Mr. Christian) Five inches.

(Mr. Shaffer) I think the space velocity was given about 21 thousand hours to the minus one.

(Anonymous) Yes, reciprocal hours.

**OXYGEN RECOVERY SYSTEM INTEGRATION
FOR LONG-RANGE SPACE MISSIONS**

by

C. S. Coe

J. Rousseau

**The Garrett Corporation
AiResearch Manufacturing Division
Los Angeles, California**

OXYGEN RECOVERY SYSTEM INTEGRATION
FOR LONG-RANGE SPACE MISSIONS

C. S. Coe and J. Rousseau

INTRODUCTION

For space missions of duration longer than a few months, it becomes necessary to consider the recovery of oxygen from carbon dioxide in order to conserve weight. The actual weight saving attainable for any given mission depends on the results of a trade-off study which considers the atmospheric gas supply system weight, the oxygen recovery system weight, and the power requirements. In this presentation, attention is directed not to this trade-off study but rather to the performance requirement of several oxygen recovery processes when considered in relation with other vehicle systems and overall material balance.

The life support systems of interest here include the food supply, water management, and waste management systems. Atmospheric gas supply, humidity control, and carbon dioxide management are considered part of the atmospheric control system. Life support systems, as they affect the vehicle material balance, are briefly discussed in the following paragraphs.

LIFE SUPPORT SYSTEMS

Food Supply

Food planning for missions of extended duration is more involved than the establishment of a simple metabolic balance for the astronaut. Because of the important effect food preparation has on the morale of the crew, a wide variety of foods must be stored aboard the space vehicle. Food can be stored in several forms, such as dehydrated, frozen, canned, fresh, or precooked. For prolonged missions, a mixture of these food types could be made available to the astronauts with somewhat elaborate food storage and preparation facilities. Storage weight and volume can be greatly reduced by the use of dried foods. In the past decade, considerable progress has been made in the development of palatable dried foods. It is to be expected that this development will accelerate in the next few years to such an extent that, even for prolonged missions, a large portion of the

food supply will be in dried form. On a dry-food basis, it is estimated that 1.32 lb of food per man-day is sufficient to satisfy the nutritional requirement of the astronauts.

Water Management System

Four sources of water are available to a space vehicle water recovery system: the humidity removed from the cabin atmosphere; the water used for washing; urine; and the water contained in the feces. The degree of pollution of the water from the four sources varies considerably. In view of this, it might be advisable not to mix the water from all four sources, but rather to have a separate water recovery for each single source. In this manner, if a bactericide is used in the wash water, it is not necessary to remove the bactericide; the water recovered can be reused for washing. In addition, water intended for washing purposes does not require purification to the same degree as that intended for drinking and food preparation.

Water from the environmental control system (ECS) dehumidifier can be expected to be relatively pure and essentially free of solid impurities, since its source is water vapor condensed from the atmosphere. However, the possibility of contamination by bacteria and dissolved gases may require some processing of the water in order to render it safe and palatable for drinking. The amount of water recovered from the humidity control system will vary greatly with the perspiration rate of the astronauts, and with the amount of water evaporated during food preparation and washing.

The composition of urine is very complex. The solids in urine amount to about 5 percent by weight, approximately half of this being urea. The solids found in urine are amino acids, electrolytes, minor minerals, hormones, organic acids, pigments, vitamins, and various miscellaneous compounds. Urine production rate is dependent on the diet, the liquid intake, the perspiration rate, and the metabolic activity of man. However, the average rate of urine production over long periods of time aboard a space vehicle is anticipated to be about 3.0 lb per man-day.

The wash water can contain an effective bactericide and detergent to control bacteria on the skin and increase the efficiency of soil removal. Selection of these materials is extremely important, since the wash water

must have no irritating effect on any portion of the body. When drying, the water must not leave deleterious or uncomfortable residue. The bactericide must be able to destroy the common types of bacteria that may be encountered in washing. It is estimated that at least 4.0 lb of water per man-day will be sufficient for the purpose of washing on extended missions.

The composition and amount of feces produced depend upon the composition of the diet and the physical condition of the individual. Usually about 0.33 lb of feces are produced per man per day; the water content is 70 to 85 percent. Reclamation of the water from the feces is the function of the waste management system. It is estimated that by drying, filtration, or filtering under pressure, about 85 percent of the water contained in the feces can be extracted for purification in the water recovery system.

Man-Material Balance

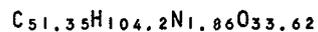
Figure 1 depicts overall man-material balance on a dry food basis. The water vapor production (2.2 lb/day) by respiration and perspiration is based on a perspiration rate corresponding to a shirt-sleeve atmosphere. The urine, feces, and carbon dioxide production rates represent the average values quoted in Reference 1. These values are based on a daily requirement of 3000 kilocalories per man-day, or 1.32 lb of dry food of the following composition:

- 15 percent protein
- 20 percent fat
- 65 percent carbohydrate

Assuming the following approximate composition of these food elements,

Protein	$C_4H_9O_2N$
Fat	$C_{16}H_{32}O_2$
Carbohydrate	$C_6H_{12}O_6$

the overall food composition can be assigned the empirical formula



Metabolism of 1.32 lb of this compound produces about 0.97 lb of water, with a portion of the hydrogen and oxygen present remaining in the waste products. This water is termed metabolic water, and appears as an excess of the man-water output over the input. The metabolic water is the product of the oxidation of combined hydrogen by combined oxygen and also by atmospheric oxygen. Details of the overall metabolic process occurring in man are shown in Table I. Recovery of the combined hydrogen or combined oxygen as water is not complete because of the loss of both elements in solid food wastes. Loss of such elements in this manner is estimated to be about 8 percent. It should be pointed out that the metabolic water production rate is independent of the rate of water vapor generated by perspiration and respiration.

Vehicle Material Balance

Certain losses are incurred in the recovery of water from the four sources mentioned previously, so that the net excess water is lower than the metabolic water production. The rate of excess water production can be estimated by assuming a separate water recovery system is used for each of the four water sources. Here, the following efficiencies are assumed:

TABLE I
MAN METABOLIC WATER BALANCE

Metabolic Conditions	Rate (lb/man-day)
Oxygen consumption	2.0
Food requirement (dry)	1.32
Carbon dioxide generation	2.25
Water vapor production	2.20
Urine production	3.0
Fecal output	0.33
Oxygen converted to carbon dioxide: $\frac{(2.25)(32)}{44} =$	1.637
Oxygen converted to water: $2.0 - 1.637 =$	0.363

TABLE I (Continued)

Metabolic Conditions	Rate (lb/man-day)
Water generated from oxygen: $\frac{(0.363)(18)}{16} =$	0.41
Fecal water: $0.33 - 0.10 =$	0.23
Solid waste from food: $0.33 - 0.23 =$	0.10
Carbon in food converted to carbon dioxide: $\frac{(2.25)(12)}{44} =$	0.614
Hydrogen in food converted to water: $\frac{(0.363)(2)}{16} =$	0.046
Metabolic water production: $1.32 - 0.614 - 0.046 - 0.10 + 0.41 =$	0.97
Total water output: $2.2 + 3.0 + 0.23 =$	5.43
Water intake requirement for balance: $5.43 - 0.97 =$	4.46
Fecal water reclamation	0.85
Fecal water recovery	0.95
Water recovery from urine (after removal of the solids)	0.98
Water recovery from humidity	0.99
Water recovery from wash water	0.99

The surplus water production aboard the vehicle is then calculated to be 0.636 lb per man-day on a dry-food basis. On a wet-food basis, the water surplus is increased by that amount which is contained in the food. The oxygen that is recoverable from the carbon dioxide, 1.636 lb/man-day, is not sufficient to make up the metabolic requirement of the crew. An additional 0.364 lb/man-day of oxygen must be generated from the excess water of the water management system to effect overall balance. It is interesting to note that even in these conditions water is overproduced at the rate of 0.227 lb/man-day. Oxygen could also be recovered from this water by electrolysis, thus making it unnecessary to recover all the oxygen from the carbon dioxide and, therefore, relieving somewhat the efficiency required from the oxygen recovery system. The amount of oxygen which can be applied for this purpose is, however, limited by the vehicle leakage rate.

Leakage of atmospheric gases from the cabin must be considered in establishing vehicle material balance. Leakage can occur as a result of the following: (1) Leakage takes place through seals around viewing ports and doors, and around lines routed from pressurized areas to unpressurized areas; (2) Cabin atmosphere is lost through operation of airlocks which allow personnel to leave the pressurized areas of the vehicle; (3) Accidental cabin decompression can result from cabin puncture by meteorites.

Although normal leakage can be reduced to a minimum by careful sealing of the pressurized cabin, the quantities of gas required for cabin pressurization and airlock operation generally increase with the mission duration. An extensive study of each particular mission, together with actual vehicle design considerations, is necessary to determine what gas supply arrangement is optimum. As an example, consider a 4-man cabin where 2,000 ft³ of air (40 percent O₂, 60 percent N₂) at 10 psia is provided. One complete repressurization would require 45 lb of oxygen and 56.3 lb of nitrogen. In addition, upon cabin decompression, 1.5 lb of carbon dioxide and 1.15 lb of water vapor would be lost.

A comprehensive study of the leakage problem is beyond the scope of this paper. A general treatment of the problem is given in Reference 2. From the data shown, it appears that refrigerated cryogenic storage of oxygen offers the best solution for cabin repressurization and air-lock operation. Normal oxygen gas leakage of about 0.2 lb per man-day or lower can be made up, as will be shown, by electrolysis of the excess water produced within the vehicle. This solution appears attractive since water is continuously overproduced while oxygen continuously leaks out of the vehicle. An oxygen leakage rate of 0.2 lb per man-day corresponds to about 75 percent per month of the gas contained in a 400 ft³ per man cabin at 10 psia, and to a total gas loss of 180 lb per man per year. These values are given here as an illustration of the weight that could be expended by sealing the cabin for leakage reduction.

OXYGEN RECOVERY SYSTEMS

Oxygen can be generated aboard a space vehicle from two sources: (1) by reduction of the carbon dioxide generated metabolically by the occupants, (2) by electrolysis of the excess water from the water management system. Several methods of oxygen recovery from carbon dioxide offer possibilities. Most of these processes, however, involve the production of water from which the oxygen is ultimately recovered by electrolysis. Therefore, depending on the water content of the food supply and on the cabin oxygen leakage rate, complete recovery of the oxygen from the carbon dioxide may not be necessary nor desirable.

Seven processes are discussed and evaluated in the light of the efficiency requirement established by overall vehicle material balance. These processes include:

1. Sabatier reaction without methane processing
2. Sabatier reaction with methane pyrolysis
3. Sabatier reaction with further reaction of carbon dioxide and methane
4. Direct hydrogenation to carbon and water
5. Catalytic decomposition at low pressure
6. Direct electrolysis
7. Fischer-Tropsch synthesis reaction

The efficiency requirement for the process is based on the following assumptions and data:

1. All the excess water available from the water management system is assumed to be electrolyzed. On a dry-food basis, this excess water is taken as 0.636 lb per man-day, as derived previously. On a wet-food basis, the excess water is increased by the amount of water present in the food.
2. Only a normal or average oxygen leakage rate from the cabin is considered. If a two-gas atmosphere is considered, the total leakage rate would be higher.

3. The metabolic rates of interest are as follows (see Figure 1):

CO₂ production rate: 2.25 lb/man-day

O₂ consumption rate: 2.0 lb/man-day

The Sabatier Process without Methane Processing

The Sabatier process involves the catalytic hydrogenation of carbon dioxide to produce methane and water according to the equation



Electrolysis of product water is subsequently carried out to liberate oxygen for breathing, and hydrogen for recycle to the Sabatier reaction.

The methanation reaction is favored by high pressures and low temperatures. Substantially complete conversion is attained at temperatures of 450°F, and below, under atmospheric pressure. Supported nickel catalysts are effective in the Sabatier reaction; carbon dioxide conversion rates of 0.27 lb per lb of catalyst per hour are readily obtained, and carbon monoxide is not formed in stoichiometric mixtures. Indications are that catalyst life can be reactivated by partial oxidation. Conversion efficiencies in excess of 95 percent have been reported (see Reference 3).

Oxygen recovery proceeds in two steps defined by the reactions:

a. Methanation of carbon dioxide



b. Electrolysis of water



The hydrogen produced in step "b" is recycled in step "a" while the oxygen is discharged in the cabin atmosphere. Defining E as the excess water available from the water management system in lb per man-day, and L as the cabin oxygen leakage rate in lb per man-day, material balance can be expressed algebraically as follows:

1. The cabin oxygen requirement is satisfied if

$$y = \frac{2 + L}{32} \quad (4)$$

2. Water vehicle balance is achieved if

$$2y = 2x + \frac{E}{18} \quad (5)$$

3. If all the hydrogen necessary in step "a" for the methanation of the carbon dioxide is to be produced by water electrolysis according to step "b", the following inequality must hold:

$$2y \geq 4x \quad (6)$$

This condition is only met if

$$E \geq \frac{9}{16} (2 + L) \quad (7)$$

This equation is plotted in Figure 2. If the leakage is greater than shown, hydrogen must be stored aboard the vehicle or oxygen is overproduced. The reaction under these conditions may not be desirable for long mission durations.

The reaction efficiency requirement, assuming all the water available is electrolyzed, is plotted in Figure 3 against the water content of the food for various leakage rates. The plot is only given for the region where oxygen is not overproduced, and where enough hydrogen is produced by water electrolysis to effect methanation of the carbon dioxide. The efficiency plot is based on the hydrogen reacted, since this element is the limiting factor in this case. The amount of carbon dioxide reduced is also shown in Figure 3. The reaction efficiency is defined here as $(\frac{2x}{y})$.

The plot shows that under conditions of low vehicle water excess the Sabatier process alone is insufficient to provide for the cabin oxygen requirement. Further processing of the methane is necessary in these conditions.

The Sabatier Reaction with Methane Pyrolysis

Recovery of hydrogen from the methane is an important final step in the oxygen recovery process by the Sabatier reaction. This hydrogen, together with that produced electrolytically, can be recycled to the Sabatier reaction, thus broadening considerably the application range of the process. One method

of recovering hydrogen from the methane produced in the Sabatier reaction involves the catalytic pyrolysis of the methane to form carbon and hydrogen. The reaction is expressed as follows:



Equilibrium data indicate that temperatures of at least 1000°F are essential to obtain any significant methane decomposition. The reaction is endothermic, requiring 2340 Btu per lb of methane decomposed at 1000°F and 1 atmosphere pressure. It is possible that rapid removal of carbon from the reaction zone may increase conversion above the equilibrium value. Catalysts can also be used to increase the rate of decomposition.

In addition to the high temperature levels at which the reaction takes place, cracking of the methane presents serious problems. One problem is the separation of the carbon from the catalyst because of strong surface adhesion. Another problem is the low reaction yield requiring recycling of the methane for high conversion efficiency. The system is further complicated by the separation of the product hydrogen from the unreacted methane.

The oxygen recovery process efficiency requirement by Sabatier reaction, methane pyrolysis, and water electrolysis can be calculated on the basis of vehicle material balance. The complete process is defined by the following steps:

- a. Methanation of carbon dioxide



- b. Pyrolysis of methane



- c. Electrolysis of product water



In this system, the hydrogen produced by methane pyrolysis and water electrolysis is recycled to achieve methanation. The three reactions are related by the following necessary conditions for material balance:

The cabin oxygen requirement imposes the condition for oxygen balance,

$$z = \frac{2 + L}{32} \quad (12)$$

where L is the oxygen leakage rate from the cabin. Overall vehicle water balance requires that the sum of excess water produced aboard the vehicle, E, and the methanation reaction product water, 2x, be electrolyzed.

$$2z = 2x + \frac{E}{18} \quad (13)$$

The hydrogen produced in steps "b" and "c" must be sufficient to effect carbon dioxide methanation (step "a"). This condition yields

$$2z + 2y = 4x \quad (14)$$

Combining Equations 12, 13, and 14 yields

$$y = \frac{2 + L}{32} - \frac{E}{18} \quad (15)$$

and
$$x = \frac{2 + L}{32} - \frac{E}{36} \quad (16)$$

Noting that the maximum value of x corresponds to complete methanation of the carbon dioxide ($x_{\max} = 2.25/44$), and that y reaches a maximum when equal to x, the efficiency requirement of the methanation and pyrolysis reactions for material balance can be calculated for any value of the cabin leakage rate and water excess produced within the vehicle, by the relations

$$\eta_{\text{Sabatier}} = \frac{x}{(2.25/44)} \quad (17)$$

and
$$\eta_{\text{pyrolysis}} = \frac{y}{x} \quad (18)$$

Minimum efficiencies of the methanation and pyrolysis reactions are plotted in Figure 4 against the water content of the food for various oxygen leakage rates from the cabin. This plot was prepared assuming complete water electrolysis and hydrogen balance according to Equations (13) and (14). The pyrolysis reaction efficiency requirement is much lower than that of the Sabatier reaction. The amount of oxygen produced electrolytically in this case is constant for any leakage rate and equal to the total cabin requirement (metabolic and leakage).

Recycle of the unreacted methane might be necessary under very low food water content. However, at a food water content of about 20 percent, the oxygen recovery system can be opened since the unreacted methane and carbon dioxide are exhausted from the system.

The Sabatier Reaction with Further Reaction of Methane and Carbon Dioxide

Another method of recovering the hydrogen from the methane offers possible solutions. The method involves the catalytic reaction of methane and carbon dioxide to produce carbon and water according to the relation

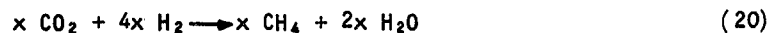


Electrolysis of the product water yields oxygen for the cabin, and hydrogen for recycling in the Sabatier reaction. Only mildly exothermic, this reaction liberates 142 Btu per lb of carbon dioxide at 100°F and is relatively independent of pressure. Conversion, however, is favored by low temperature. At 100°F, the equilibrium conversion is calculated to be 83 percent. Little experimental work has been accomplished for this reaction; however, early studies indicated that formation of carbon monoxide might constitute a problem.

A second problem in this process involves the separation of solid carbon from the catalyst. Here, it may be necessary to sacrifice the catalyst in order to accomplish removal without introducing carbon particles into the cabin atmosphere.

As for the other processes discussed thus far, the efficiency requirement of the reactions involved in oxygen recovery can be established by vehicle material balance considerations. The complete process is defined by the three following steps:

- a. Methanation of carbon dioxide



- b. Reaction of carbon dioxide with the product methane



- c. Electrolysis of water



The following relations are dictated by material balance:

1. Oxygen balance requires that

$$z = \frac{2 + L}{32} \quad (23)$$

2. Vehicle water balance is established without any water wasted or stored if

$$2z = 2x + \frac{E}{18} \quad (24)$$

3. The hydrogen produced by water electrolysis should be sufficient to effect carbon dioxide methanation. This can be expressed by

$$2z \geq 4x \quad (25)$$

4. A fourth necessary condition dictates that the methane used in step "b" can not exceed that produced in step "a"; i.e.,

$$x \geq y \quad (26)$$

5. Finally, the amount of carbon dioxide reacted in steps "a" and "b" can not be greater than that produced in the cabin; this is expressed by

$$x + z \geq \frac{2.25}{44} \quad (27)$$

It should be noted that, when solving the above equations, y cannot assume negative values. It should also be borne in mind that the methanation reaction can be accomplished more readily than the reaction of step "b". The equations were solved first for $y > 0$; in this case, the hydrogen production is assumed balanced such that

$$z = 2x = \frac{2 + L}{32} \quad (28)$$

$$x = \frac{2 + L}{64} \quad (29)$$

and
$$y = \frac{2 + L}{64} - \frac{E}{36} \quad (30)$$

When $y = 0$, the following expressions are obtained:

$$z = \frac{2 + L}{32} \quad (31)$$

$$x = z - \frac{E}{36} = \frac{2 + L}{32} - \frac{E}{36} \quad (32)$$

Graphical solutions of these equations, for $y > 0$ and $y = 0$, are given in the form of reaction efficiencies in Figure 5. These factors are plotted against the water content of the food for various leakage rates. It should be noted that the condition requiring hydrogen balance makes the methanation reaction efficiency relatively low at the lower values of the food water content.

Recycle of the unreacted products of the methane-carbon dioxide reaction might be necessary at low food water content and high oxygen leakage rates. However, it is estimated that conversions of at least 60 percent can be achieved in one pass through the catalyst bed. Therefore, even if only a slight amount of water is present in the food, recycling would not be required.

Hydrogenation of Carbon Dioxide to Carbon and Water with Electrolysis of the Product Water

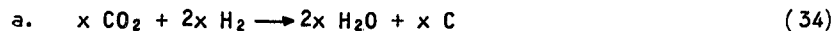
At elevated temperatures and over a variety of catalysts, carbon dioxide can be hydrogenated to water and carbon as shown in the equation



This reaction appears to incorporate both the reversed water gas and the reversed water gas shift reactions. The reaction evolves 921 Btu per lb of carbon dioxide reacted. Iron has been found to be an effective catalyst for the process which takes place at an optimum temperature of about 1100°F. At this temperature level, conversion amounts to about 30 percent per pass, so that recycle is necessary. Carbon monoxide is stated to be a component of the recycle gas. Since product water is removed as a liquid by condensation and transported to an electrolysis cell, little danger exists for introduction of this toxic gas into the cabin. Methane may also be a component of the recycle gas, depending on the reaction conditions.

The carbon produced in the reaction forms on the catalyst surface and its separation from the catalyst presents a problem. Steel wool has been found to be an excellent catalyst for this process. Due to the difficulties of separating the carbon from this catalyst, it will probably be the practice to employ two reactors operating in parallel, discarding the catalyst mass when the reactor pressure drop increases above a predetermined value. Other forms of iron catalyst might prove easier to cleanse and be more attractive for long mission durations than expendable steel wool. A second problem arises from the necessity of recycling hot product gases in a system that must remain leakproof over a long period of time.

The reaction efficiency requirement for this process can be calculated in the same manner as for the other processes discussed previously. The equations describing the complete oxygen recovery process can be written as



The necessary conditions for water, oxygen, and hydrogen balance determine the amount of carbon dioxide to be reduced. The cabin oxygen demand is satisfied by the condition

$$y = \frac{2 + L}{32} \quad (36)$$

where L is the oxygen leakage rate from the cabin in lb per man-day. The vehicle water balance is established if the total amount of water electrolyzed, 2y, is equal to the sum of the product water, 2x, and the water management system surplus. This is expressed algebraically by

$$2y = 2x + \frac{E}{18} \quad (37)$$

where E is the surplus water from the vehicle water management system in lb/man-day. By combining Equations (36) and (37), the following expression for x is obtained:

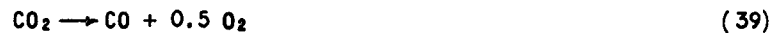
$$x = \frac{2 + L}{32} - \frac{E}{36} \quad (38)$$

The hydrogen produced by water electrolysis must be sufficient to achieve carbon dioxide reduction in accordance with Equation (34). From examination of Equation (37), it is found that excess hydrogen is produced when excess water is available from the water management system. Since this is always the case, hydrogen is continuously evacuated overboard or stored for other uses. The hydrogen excess is found to be equal to $(E \times 2/18)$ lb per man-day.

The efficiency of the reduction reaction defined as $\frac{44x}{2.25}$ is plotted in Figure 6 as a function of the water content of the food and the cabin oxygen leakage rate. By examining Figure 6, it can be seen that, for food water content higher than 80 percent and zero leakage condition, recycle of the reaction products is not necessary. In this case, the process is of particular interest.

Catalytic Decomposition of Carbon Dioxide at Low Pressures

The direct thermal decomposition of carbon dioxide is difficult because of the large thermal energy input involved (3850 Btu per lb of carbon dioxide at 67°F). In addition, the rate of decomposition is only appreciable at high temperatures. If the reaction is conducted at low pressure over suitable catalysts, decomposition of carbon dioxide to carbon monoxide and oxygen occurs in low yields. This process occurs as follows:



Metals of the platinum group have been suggested as catalysts for this reaction. A conversion of about 5 percent has been obtained at 1 psia and 3500°R; higher conversion is possible at lower pressures and higher temperatures. The carbon monoxide can be pyrolyzed catalytically after separation from the product oxygen. This reaction proceeds at a good yield at temperatures of about 900°F, according to the equation



Iron carbide and the product carbon, itself, have successfully been used as catalysts.

The process overall reaction can be written as



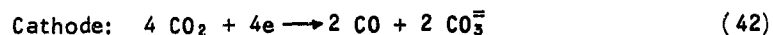
This process is attractive because oxygen is produced directly without the intermediate formation of water which requires an electrolytic cell for ultimate recovery of the oxygen. However, the low pressures associated with the decomposition of the carbon dioxide introduce some problems, and the low efficiency of this reaction considerably complicates the system since recycling is necessary. Separation of the oxygen formed from the unreacted carbon dioxide and carbon monoxide in the first reaction also presents difficulties. Freezeout and low-temperature adsorption have been proposed for separating carbon dioxide and carbon monoxide, respectively, from the product oxygen. Oxygen admitted to the cabin must be treated in a catalytic burner to ensure that traces of carbon monoxide are oxidized. It is possible that low pressures may be necessary to effect desorption of carbon monoxide from the adsorbents used in the separation of this material. Low pressures in all cases must be supplied by internal equipment; the use of space vacuum is not considered desirable.

Based on the overall reaction, the process efficiency requirement, as a function of the water content of the food and the cabin leakage rate, is the same as plotted in Figure 6. However, the quantities of water electrolyzed for oxygen recovery might be much lower depending on the method employed to separate the product oxygen from the unreacted carbon dioxide and carbon monoxide.

Direct Electrolysis of Carbon Dioxide

Direct electrolysis of carbon dioxide is an attractive process for recovery of oxygen from carbon dioxide because it requires no reaction with hydrogen; also, the electrolytic products (oxygen and carbon monoxide) are discharged at different electrodes, automatically effecting separation. Two principal processes are currently being studied for carbon dioxide electrolysis. The processes differ by the electrolyte employed. The first process involves electrolysis in a fused mixture of alkali metal carbonates. Here,

carbon monoxide appears at the cathode and oxygen at the anode. Electrode reactions are believed to accord with the following equations:



In addition to these electrolytic reactions, pyrolysis of carbon monoxide occurs at the elevated temperature of the cell (900°F - 2000°F) to produce carbon dioxide and carbon so that the overall reaction follows the equation



The addition of catalysts is desirable to accelerate this reaction. The theoretical energy requirement, assuming a decomposition potential of 1 volt, is 1.52 kw-hr per lb of carbon dioxide. In practice, voltages of about 1.7 must be applied to initiate decomposition. Efficiencies of the order of 25 percent have been obtained for this process, indicating an overall expenditure of electrical energy of 6 kw per lb of oxygen.

In the present state of development of the process, the disadvantages include high weight and volume penalties. Operation at elevated temperature may lead to shortened equipment life. Separation of solid carbon from the molten electrolyte also involves problems in a zero gravity field.

The second approach to direct electrolysis of carbon dioxide involves the use of solid-state semiconductors. Metallic oxides, in which a portion of the cations are replaced by ions of lower valence, contain lattice defects and allow the diffusion of oxygen ions through the crystal lattice and, therefore, behave as solid electrolytes under the proper conditions. Preliminary tests have indicated that some electrolysis does occur in thorium oxide-lithium oxide solid solution at temperatures in the range 800°F-1700°F. Carbon monoxide is produced from carbon dioxide in the cell, when 4 volts is applied at the electrodes. Much work remains to be accomplished, however, before the feasibility of cells of this type is established. At present, it is believed that the pyrolysis of carbon monoxide produced in the cell may be advantageously accomplished in a separate unit to produce carbon and carbon dioxide as shown in Equation (45).

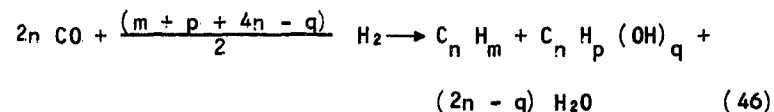


Catalysts could conceivably be incorporated in the solid electrolyte to effect this reaction in situ. Carbon formation in the solid electrolyte may pose a problem.

In this case, the reaction efficiency requirement is based on Equation (41) and is given by Figure 6.

Fischer-Tropsch Process

The Fischer-Tropsch process is normally associated with the commercial production of liquid hydrocarbons by the reaction of carbon monoxide and hydrogen over a promoted iron or cobalt catalyst. The overall reaction can be represented approximately by the equation:



In addition to hydrocarbons and water, oxygenated organic compounds may also be produced, depending on the reaction conditions.

For space vehicle applications, the reaction must be adapted to utilize carbon dioxide in place of carbon monoxide. This could be accomplished in two steps by employing the initial reaction of hydrogen and carbon dioxide to form carbon monoxide and water as shown in Equation (47).



The carbon monoxide would then be reacted with hydrogen over a Fischer-Tropsch catalyst. There are indications that carbon dioxide will react directly with hydrogen over some Fischer-Tropsch catalysts, under certain conditions, to form hydrocarbons and water. The reaction apparently proceeds through carbon monoxide as an intermediate step.

The advantages of the Fischer-Tropsch catalysts for reclamation of oxygen from carbon dioxide in space vehicles include the following:

1. Liquid hydrocarbons are formed which may be more readily separated from the catalysts than solid carbon.
2. Reasonable variations in the H_2/CO_2 ratio can be tolerated without seriously affecting the nature of the reaction products.

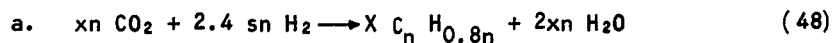
Fischer-Tropsch catalysts are usually promoted iron or cobalt, supported on kieselguhr or alumina. Promoters include thoria, ceria, and magnesia. Alkalization with potassium carbonate increases the hydrocarbon yield. The cobalt catalyst is effective at atmospheric pressure while the iron catalyst, without special treatment, requires pressures in the range of 10-20 atmospheres for satisfactory synthesis performance.

The Fischer-Tropsch catalyst is effective at about 380°F and the heat evolved in the reaction depends on the type of hydrocarbon formed. For liquid hydrocarbons of low H/C ratio, a heat release of about 700 to 900 Btu per lb of carbon dioxide reacted is expected.

To conserve hydrogen, it is desirable to form hydrocarbons of low H/C ratio. Condensed olefinic and aromatic hydrocarbons appear to be a possibility in this direction, and it is estimated that hydrocarbons of average composition $C_n H_{0.8n}$ can be produced.

The single bed Fischer-Tropsch process, converting carbon dioxide directly into water and hydrocarbons, appears desirable for space vehicle applications, although much development work remains to be done in this area. Separation of the hydrocarbon oil from the product water may be accomplished by fractional condensation, although this might present problems in a zero-gravity environment.

The following equations summarize the reactions involved in the recovery of oxygen by means of the Fischer-Tropsch synthesis:



Assuming the entire cabin oxygen requirement is supplied by water electrolysis, then

$$y = \frac{2 + L}{32} \quad (50)$$

The vehicle water balance is expressed by

$$2y = 2x + \frac{E}{18} \quad (51)$$

If all the hydrogen for the Fischer-Tropsch synthesis, as shown in Equation (45) where n is equal to 1, is to be produced by electrolysis of water, then the following inequality can be written:

$$2y \geq 2.4x \quad (52)$$

This condition is possible only if

$$E \geq \frac{3}{16} (2 + L) \quad (53)$$

The Fischer-Tropsch efficiency requirement for material is the same as that plotted in Figure 6 as a function of the food water content and the cabin oxygen leakage rate. It appears that recycle of the unreacted products might be necessary at high leakage rate and low food water content.

CONCLUSIONS

Based on the analysis presented, it is apparent that the required efficiency of a process for recovery of oxygen from metabolic carbon dioxide in a space cabin is a function of the vehicle leakage rate and the water content of the food. Assuming a reasonable control of leakage, then the food water content, both from combined hydrogen and oxygen and from liquid water present, can be electrolyzed to recover oxygen for breathing, and hydrogen for use in reduction processes for oxygen recovery.

Table II summarizes the efficiency requirements of the processes considered in this presentation. Of the processes studied, the Sabatier process is attractive because of its simplicity and high conversion rates. Processing of methane to recover hydrogen for recycle to the methanation reactor must be employed, however, when food water content less than about 4.0 percent is used. The process recommended at this time for methane processing involves its reaction with a portion of the incoming carbon dioxide to produce carbon and water. Conversions in this process are expected to be sufficiently high to avoid recycling.

The Fischer-Tropsch process also appears attractive for oxygen recovery in future space missions, since it has the advantage of being a single-step process. Adaptation of this process to space vehicles remains to be initiated.

TABLE 2
 OXYGEN RECOVERY SYSTEM - MATERIAL BALANCE SUMMARY

Type of Food Process	Dry Food		50 Percent Water in Food			
	Reaction Efficiency (percent)	CO ₂ Overboard (lb/man-day)	H ₂ O Electrolyzed (lb/man-day)	Reaction Efficiency (percent)	CO ₂ Overboard (lb/man-day)	H ₂ O Electrolyzed (lb/man-day)
CO ₂ + 4 H ₂ → CH ₄ + 2 H ₂ O 2 H ₂ O → 2 H ₂ + O ₂		IMPOSSIBLE WITHOUT ADDITIONAL H ₂ SUPPLY		90.8	0.207	2.36
CO ₂ + 4 H ₂ → CH ₄ + 2 H ₂ O CH ₄ → C + 2 H ₂ 2 H ₂ O → 2 H ₂ + O ₂	93.4 63.4	0.1485	2.36	58.1 0	0.943	2.36
CO ₂ + 4 H ₂ → CH ₄ + 2 H ₂ O CO ₂ + CH ₄ → 2 C + 2 H ₂ O 2 H ₂ O → 2 H ₂ + O ₂	64.6 83.1	0.1485	2.36	58.1 0	0.943	2.36
CO ₂ + 2 H ₂ → 2 H ₂ O + C 2 H ₂ O → 2 H ₂ + O ₂	93.4	0.1485	2.36	58.1	0.943	2.36
n CO ₂ + 2.4n H ₂ → C _n H _{0.8n} + 2n H ₂ O 2 H ₂ O → 2 H ₂ + O ₂	93.4	0.1485	2.36	58.1	0.943	2.36

NOTE: Oxygen leakage rate, 0.1 lb/man-day

REFERENCES

1. Breeze, R. K., Space Vehicle Environmental Control Requirements Based on Equipment and Physiological Criteria, ASD-TR-61-161, Part I, December 1961.
2. Atmospheric Control Systems for Space Vehicles, ASD-TDR-62-527, Part II, in preparation.
3. Rydelek, R., Investigation of Integrated Carbon Dioxide Hydrogenation Systems, ASD-TDR-62-581, October 1962.

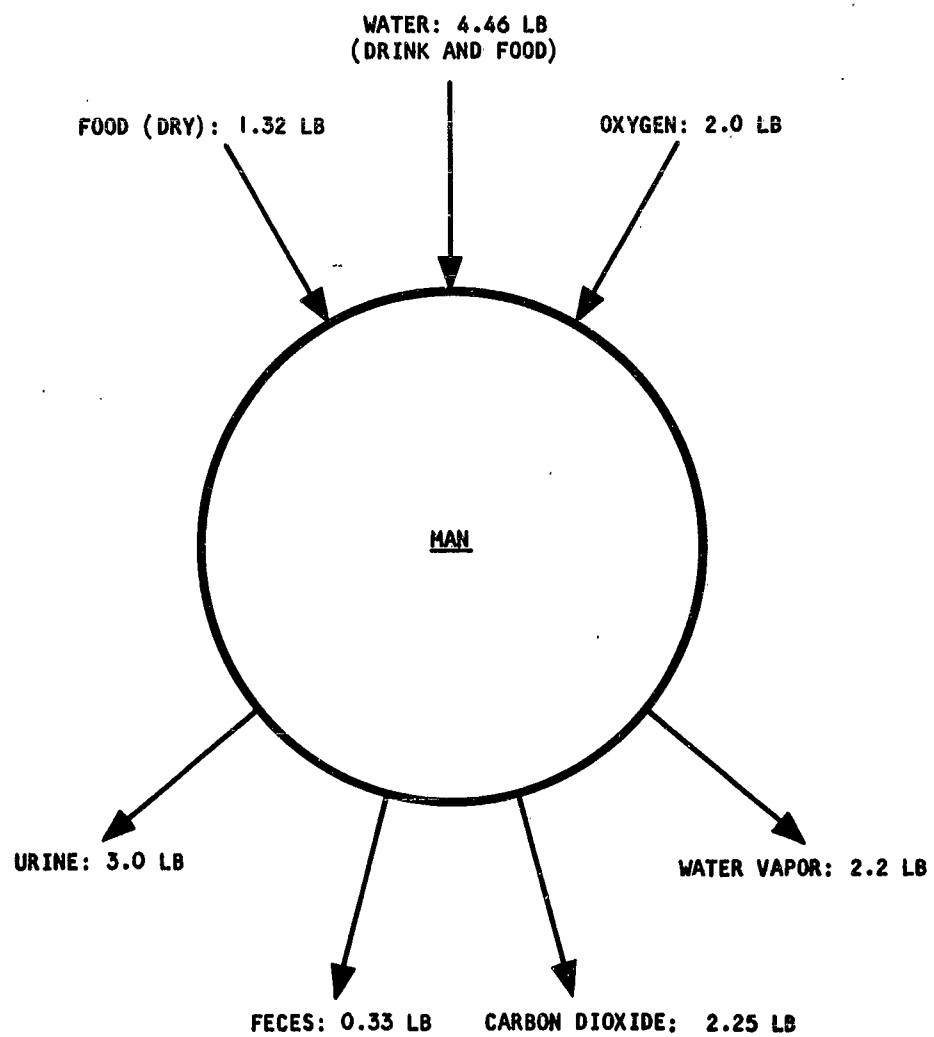


Figure 1. Man Metabolic Material Balance

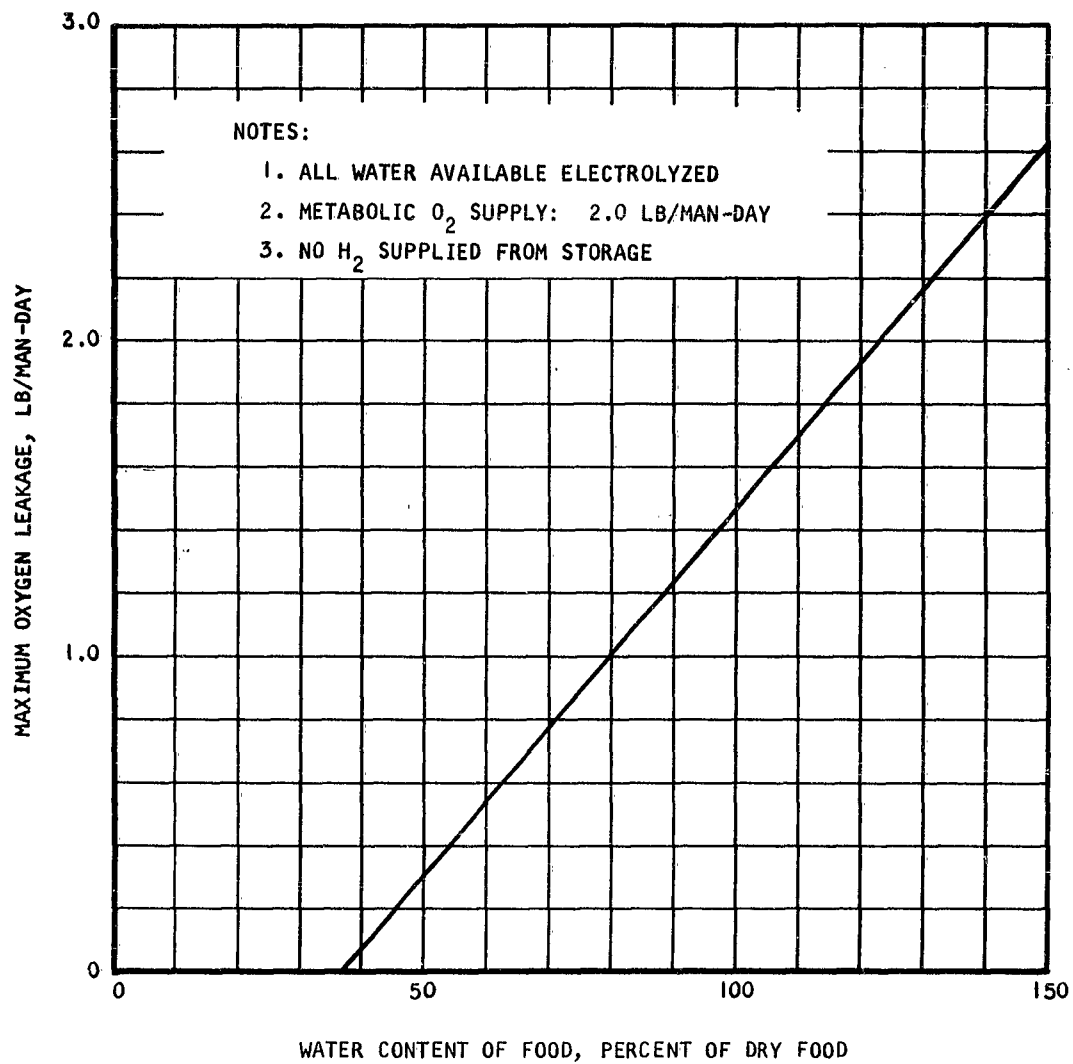


Figure 2. Maximum O_2 Leakage Rate for Complete Material Balance Using Methanation for Oxygen Recovery

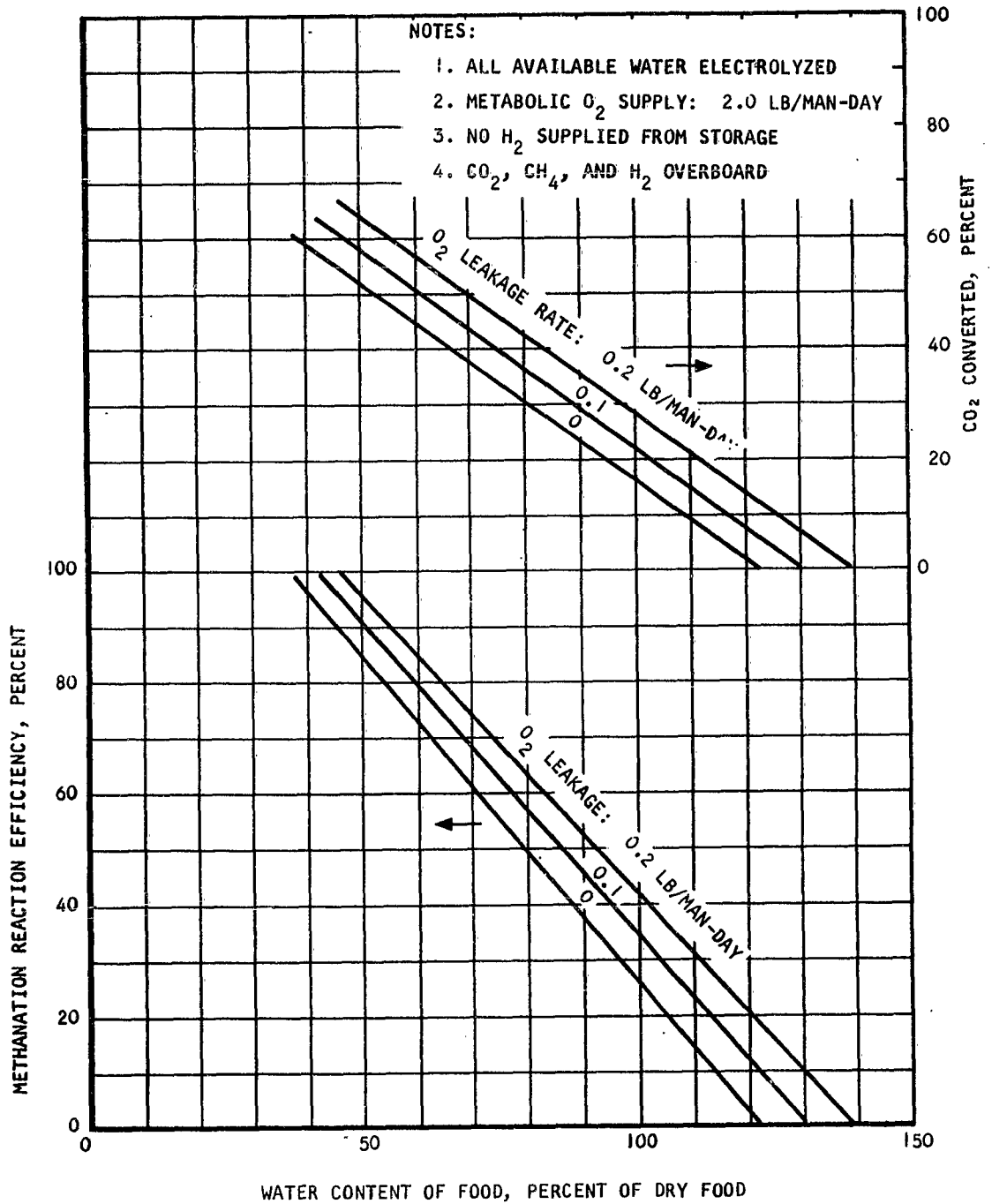


Figure 3. Efficiency Requirement of O₂ Recovery Process (CO₂ Methanation)

NOTES:

1. ALL AVAILABLE WATER ELECTROLYZED
2. METABOLIC O_2 SUPPLY: 2.0 LB/MAN-DAY
3. NO H_2 SUPPLIED FROM STORAGE
4. CO_2 , CH_4 , C, AND H_2 OVERBOARD

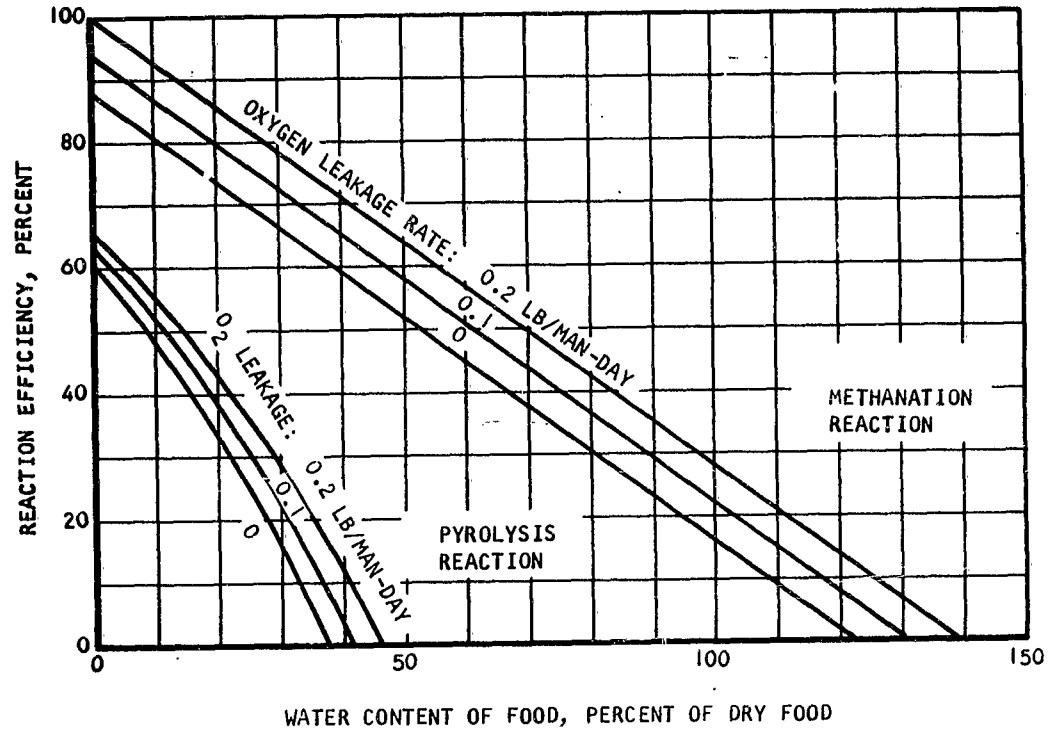


Figure 4. Efficiency Requirement of O_2 Recovery Process (CO_2 Methanation, and CH_4 Pyrolysis)

NOTES:

1. ALL WATER AVAILABLE ELECTROLYZED
2. METABOLIC O_2 SUPPLY: 2.0 LB/MAN-DAY
3. NO H_2 SUPPLIED FROM STORAGE
4. CO_2 , CH_4 , C, AND H_2 OVERBOARD

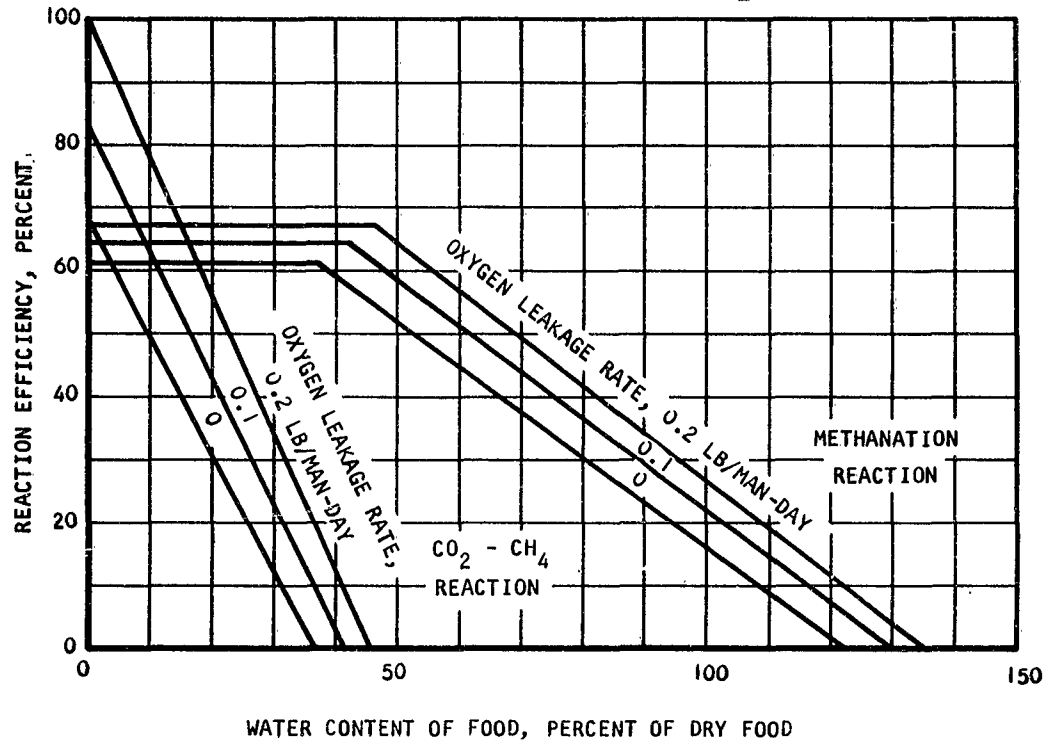


Figure 5. Efficiency Requirement of O_2 Recovery Process (CO_2 Methanation, and $CO_2 - CH_4$ Reaction)

NOTES:

1. ALL WATER AVAILABLE ELECTROLYZED
2. METABOLIC O_2 SUPPLY: 2.0 LB/MAN-DAY
3. NO H_2 SUPPLIED FROM STORAGE
4. CO_2 , CH_4 , C, AND H_2 OVERBOARD

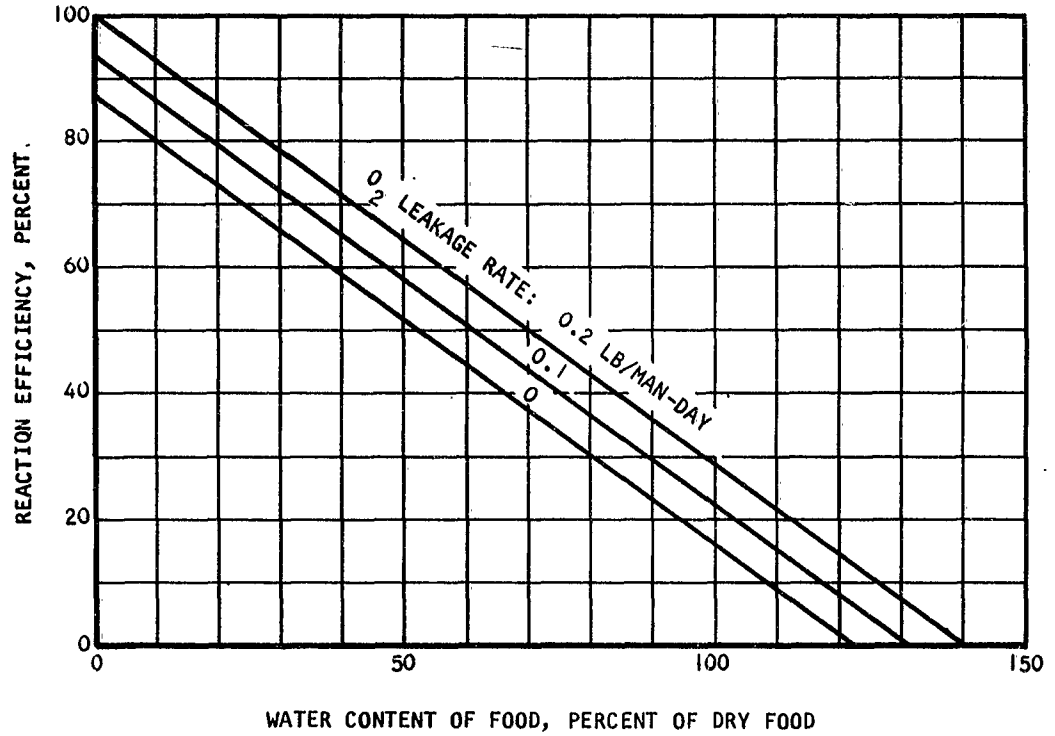


Figure 6. Efficiency Requirement of O_2 Recovery Process
(Direct Hydrogenation of CO_2 to Carbon and Water)

Third Paper -- "Atmospheric Control Problems in Long Range Space Missions," by C.S. Coe & Jean Rousseau, AiResearch Mfg. Co. (Presented by Mr. Coe.)

QUESTION: (Mr. Shear, Mine Safety Research Corp.) Can you give us any comparison of efficiency of CO₂ conversion process, such as direct hydrogenation followed by water electrolysis, carbonite electrolysis, and of course, Sabatier reaction?

ANSWER : (Mr. Coe) Well, actually the only process that we have had any direct experience with is Sabatier. We feel that we can achieve 98 to 100 per cent conversion electrolysis. Based on our studies of the literature, we feel that electrolysis of water should be 65 to 70 per cent; possibly as the state of the art advances, even greater than this. Now our figures that we have derived for carbonite electrolysis is something like 20 to 25 per cent efficient. The direct hydrogenization is something that Mr. Remus could give a better answer to. We have been using the value of 30 per cent conversion efficiency. The Fischer-Tropsch process we feel will approach a hundred per cent efficiency; as to the direct decomposition of oxide processes, our studies and calculations--empirical studies--indicate possibly 20 per cent efficiency per pass.

**THE APPLICATION OF CHEMICALLY
REGENERATIVE ATMOSPHERIC CONTROL SYSTEMS**

by

J. G. Krisilas

J. W. Smylie

**Aerospace Corporation
Los Angeles, California**

The Application of Chemically Regenerative Atmospheric Control Systems

J. G. Krisilas and J. W. Smylie

I. INTRODUCTION

As mission times and the complement of manned spacecraft increase, a point will be reached in the not too distant future where the penalties for the use of expendable or open cycle atmospheric control and life support systems will be excessive. The development of regenerative atmospheric control and life support systems becomes imperative in order to alleviate the weight and resupply penalties associated with expendable systems. In this paper, life support is defined to mean sustenance supply (food and water) while atmospheric control is defined to mean the supply of oxygen and the removal of CO_2 , water vapor and toxic gases from the cabin environment. It is technically feasible and practical to recover and make reusable several products from these regenerative systems. Waste water will be the first item to be recovered for reuse. A water reclamation system will not impose large penalties to the space vehicle and, although more than one method appears promising, these systems pose only relatively straightforward engineering design problems. The generation of breathing oxygen from expired carbon dioxide will probably be the second major development. However, carbon dioxide reclamation systems will impose significant penalties to the vehicle, and system design is neither simple nor straightforward. A substantial engineering effort will be required to develop a spaceborne carbon dioxide reclamation and oxygen generation system for space vehicle use. This paper summarizes the published theoretical studies and experimental effort expended on chemically regenerative atmospheric control systems by industrial and governmental agencies through the fall of 1962, evaluates two of the most feasible systems, and recommends directions for further development work. Although emphasis is placed on inorganic systems on the basis of their potential availability, vehicle compatibility, weight, and power requirements, a short discussion of expendable and biological systems is also included for comparison.

Several excellent studies on regenerative atmospheric control systems have been presented in the past. The most complete collection of these studies is contained in Reference 1. These studies relied chiefly on analytical evaluation since experimental results were usually not available. This paper

incorporates experimental results (which are still quite limited) that are presently available and considers the effects of several aspects of vehicle design such as leakage, water recovery system efficiency, the the use of by-products, in order to make more accurate estimates of the carbon dioxide reclamation system penalty to the vehicle.

II. CANDIDATE SYSTEMS

The following systems were evaluated on the basis of their potential availability, vehicle compatibility, weight and power requirements:

1. Hydrogen reduction
 - A. Hydrogen carbonization (sometimes called water gas shift)
 - B. Methanization (sometimes called Sabatier)
2. Lithium oxide reduction
3. Lithium hydride reduction
4. Sodium reduction
5. Direct thermal decomposition
6. Direct electrical decomposition
7. Irradiation
8. Algae systems
9. Higher plants
10. Hydrogen reduction bacteria
11. Artificial photosynthesis

The various regenerative atmospheric control systems were compared on a weight and power requirement basis. The following assumptions were made.

a. Regenerative atmospheric control systems will be used for longer duration missions which preclude the use of open cycle oxygen-hydrogen fuel cells for the power supply. Therefore, it was assumed that if electrolysis was required to generate oxygen, the electrical power system would consist of

either a solar or a nuclear energy source which would provide no surplus water for make-up supply to the atmospheric control system. In addition, the power penalty would be fixed weight independent of mission time. A weight penalty of 300 lb/kw was assumed for this portion of the study. The system selection is, in general, not dependent on this assumption because the lighter weight systems also require less power. The possible exception is the direct electrical decomposition of carbon dioxide, but the performance of this system cannot be accurately predicted from the data available at this time.

b. Complete recovery of CO_2 will not supply all of the breathing oxygen required. Therefore, regenerative system evaluation must include consideration of how the balance of breathing oxygen will be supplied. If all metabolic water can be recovered, there will be enough surplus water to generate the required breathing oxygen plus some left over for leakage make-up. It was assumed, for the purpose of this evaluation, that the efficiency of the water reclamation system was great enough to provide the breathing oxygen make-up, approximately 0.42 pound of water per man-day. (Approximately one pound of water per man-day is produced from food and oxygen in excess of the liquid water consumption.)

c. The penalty of the carbon dioxide collection system was not included because more than one method might be considered and all of the closed systems require a similar carbon dioxide recovery system. This would add the same penalty increment to each curve and reduce the effectiveness of a comparison study.

III. SELECTION OF SYSTEMS

A brief description of the candidate systems is presented below. Figure 1 shows the relative comparison of these systems. The literature was used extensively in determining these weights which included some planned improvements for systems under development. It is evident that hydrogen carbonization and methanization enjoy a considerable power and weight advantage over the other candidate systems. In addition, both have been advanced beyond laboratory devices into engineering component and system development. The detailed analysis of the two hydrogen reduction systems selected is presented in the next section and a detailed discussion is presented following the analysis section.

A. Hydrogen Carbonization

This system, shown in the simplified schematic of Figure 2, is based on an iron catalyzed reaction at moderately high temperatures (1100 - 1400°F) which is sometimes called the reversed water gas shift. Several of these systems have been fabricated, ranging from experimental laboratory models to full scale three-man prototypes. Although the experimental models require considerable power, the reactions involved are exothermic and it is probable that both the power requirement and the weight of the reactor system can be reduced significantly in an actual space application. A detailed discussion of the system characteristics is presented in a later section of the paper. This system was selected for detailed analysis due to the favorable penalty comparison shown in Figure 1 and the present advanced development status of this system.

B. Methanization

This system is based on a moderate temperature (300 - 600°F) nickel catalyzed reaction which proceeds to almost complete conversion of carbon dioxide and hydrogen into methane and water in a one-step reactor (Reference 2). The system is shown schematically in Figure 3. The methanization system can be operated as a partially open system with the methane either discarded from the vehicle or stored for use as a jet reaction control fuel. The system can also be operated as a closed cycle by recovering the hydrogen from the methane. It is similar to the hydrogen carbonization system in that the water electrolysis cell will be the major penalty element of the system.

This system was selected for detailed analysis due to the favorable penalty comparison shown in Figure 1. Further detailed discussion of this system is presented in a later section of this paper.

C. Lithium Oxide Reduction

Lithium oxide reduction is the nearest inorganic system competitor to the hydrogen reduction systems. One of these cells was built by Mine Safety Appliance Research Corporation and delivered to the Navy for evaluation (Reference 3).

In this process lithium carbonate is formed by adding carbon dioxide to a molten lithium oxide solution. The lithium carbonate is then electrolyzed to form oxygen, carbon and lithium oxide. A comparison of the free energies of formation (Reference 4) with the reactions that probably take place shows that the power consumption for this device will always be greater than that required for the electrolysis of water. Although this system shows some promise because of its proved feasibility, it was not evaluated in detail because of its high power consumption which cannot apparently be substantially reduced.

D. Lithium Hydride and Sodium Reduction Systems

These systems were originally proposed because of their high rates of reaction and the efficient electrolysis of the molten metallic hydroxides. The power requirements (Reference 5), however, are quite high as shown in Figure 1. Some results on a sodium cell have been reported in Reference 8, but they were not sufficient to make a comparative analysis. A comparison of the free energies of formation show that the power requirements for the electrolysis of these compounds will not be competitive with the electrolysis of water. These systems were not selected for detailed analysis due to the high power requirement and the complexity of designing a liquid metal circulation loop.

E. Direct Thermal Decomposition

The direct thermal decomposition of carbon dioxide into its elements, carbon and oxygen, is an interesting prospect since it is a reversible one-step process. This system is the theoretical minimum energy method for producing oxygen from carbon dioxide. It was not evaluated in detail because the solutions to the engineering problems of separating the oxygen from the products of reaction and the development of a highly reliable system operating at the high temperatures required are not apparent at this time.

F. Irradiation

Carbon dioxide will decompose when subjected to nuclear radiation bombardment. The discussion by Foster and McNulty (Reference 6) indicates that excessive volume would be required for this system. The results of

reported experiments using almost pure carbon dioxide also indicate low conversion rates and the production of substantial quantities of carbon monoxide in addition to possible carbon suboxides (Reference 7). At any rate, not enough data is available to permit a comparative analysis of this system.

G. Direct Electrical Conversion

A solid state electrical device for recovering oxygen from carbon dioxide is described in Reference 8. Some of the reported values from this reference were used to determine the weight shown in Figure 1. Since the information in the reference is more qualitative than quantitative, the penalty shown in Figure 1 was extrapolated from data that made the assessment of accuracy difficult. Comparison of the free energies of formation, however, shows that the energy required for the reduction of carbon dioxide to carbon monoxide and oxygen, which is apparently the way this cell operates, will require considerably more power than the electrolysis of water for equal quantities of oxygen produced. There is also the additional problem of reducing the carbon monoxide. There was not enough information available to permit a detailed analysis of this system at this time.

H. Algae Systems

Due to the large range of performance estimates made for algae systems, it was necessary to analyze them in some detail. The values shown in Figure 1 agree with what might be called rather optimistic estimates. These values are as low as one can get without running into severe temperature and concentration control problems. A solar illuminated algae system would appear competitive with the inorganic systems when the carbon dioxide removal subsystem is included as part of the system's penalty. This may not be the true situation since the potentially large structural weight required for deployment and support of the solar illumination chambers was neglected in this analysis. In general, solar illumination is not compatible with a large range of missions; nor is it clear that the system could be made reliable when the illumination chambers are exposed to interplanetary dust erosion and meteorite damage. In addition, algae itself may not be compatible with direct

solar radiation. For these reasons, the solar illuminated algae system was discounted as a competitor with the inorganic systems at this time.

The high power requirement for artificial illumination also removes the algae system from competition with inorganic systems.

One problem that makes an algae system appear questionable for any long term mission is the system mass balance. More algae is produced than can be used in the crew diet (Reference 9), but a nutrient must be supplied in addition to the carbon dioxide to produce this algae. This implies that large quantities of nutrient must be supplied and large quantities of algae must be disposed of for a long term mission. If urine is used for this nutrient, a deficit occurs in the water management system. In other words, an algae-man system is not a compatible closed system unless the algae can be made more digestible than past experiments indicate (Reference 9).

I. Higher Plants

Higher plants require more power, larger volumes and greater weight than algae systems. They are, therefore, not competitive with the chemically regenerative atmospheric control systems.

J. Hydrogen Reduction Bacteria

Various simple life forms can use hydrogen and almost any form of human waste including carbon dioxide as a nutrient. Excess water will be formed during their normal growth. The water can be recovered and electrolyzed to provide oxygen while the hydrogen is returned to the culture. The tentative weight and power estimate for this system (Reference 5) makes it appear competitive with inorganic systems. Not enough information is available, however, to include a detailed analysis in this paper. It may not be feasible to control this system and the net mass balance may be unfavorable as is apparently the case for algae systems.

K. Artificial Photosynthesis

Artificial photosynthesis has not been accomplished yet, but the knowledge of the photosynthetic process is accumulating so rapidly that the

effect of artificial photosynthesis on regenerative atmospheric control systems must be considered (Reference 10). Artificial photosynthesis could lead to the development of more efficient and reliable organic systems whether whole plants or plant derivatives are used, and it might even lead to a compact low temperature inorganic system using the photosynthesis process. It may even be possible in the future to design a system to reverse the metabolic action of man on food and oxygen for a truly closed life support system. The research work on photosynthesis should be closely followed by the space vehicle life support system designer in the future.

IV. DESIGN ANALYSIS

A series of parametric equations were developed for estimating the performance of the two hydrogen reduction atmospheric control systems being compared. These equations are presented in Table I in terms of design parameters. The nomenclature is presented in Appendix A. The derivation of these equations is shown in Appendix B.

Penalty equations I, II, and III predict the performance of the closed hydrogen reduction systems (either a closed methanization system or the hydrogen carbonization system); Equation IV defines the penalty associated with the open methanization systems and Equation V represents a stored oxygen supply with no oxygen generation. Equations I through III can be used for both the hydrogen carbonization system and the closed methanization system since there are no essential differences between the penalties associated with either of these systems. The parameter in Equations I through III is the make-up material supply. Equation I includes the weight of a stored oxygen supply. Equation II includes the weight of hydrogen peroxide storage in which the hydrogen peroxide is reduced to oxygen and water; the water is subsequently electrolyzed into hydrogen and oxygen. The cooling penalty associated with the heat of decomposition of the hydrogen peroxide was found to be negligible and was therefore not included. Equation III includes the weight of a water make-up supply which is electrolyzed into oxygen and hydrogen.

Table 1. Summary of Penalty Equations*

Closed Regeneration System (Carbonization or Closed Methanization)
Using Stored Oxygen for Make-Up

$$I. \quad \frac{W_T}{N_P} = n_c W_c (W_r + P_r N_1 + C_r N_2) + (n_c W_c \frac{36}{44} + w_2) (W_e + P_e N_1 + C_e N_2) \\ + \left\{ -N_8 + [N_4] \left[W_b + W_f - \frac{16}{18} (n_c W_c \frac{36}{44} + w_2) \right] \right\} t$$

Closed Regeneration System (Carbonization or Closed Methanization)
Using Stored Hydrogen Peroxide for Make-Up

$$II. \quad \frac{W_T}{N_P} = n_c W_c (W_r + P_r N_1 + C_r N_2) \\ + \left\{ n_c W_c \frac{36}{44} + w_2 + \left[1 - \frac{16}{34} N_6 \right] \left[\frac{W_b + W_f - \frac{16}{18} (n_c W_c \frac{36}{44} + w_2)}{\frac{16}{18} (1 - N_6 \frac{16}{34}) + N_6 \frac{16}{34}} \right] \right\} (W_e + P_e N_1 + C_e N_2) \\ + \left\{ -N_8 + [N_5] \left[\frac{W_b + W_f - \frac{16}{18} (n_c W_c \frac{36}{44} + w_2)}{\frac{16}{18} (1 - N_6 \frac{16}{34}) + N_6 \frac{16}{34}} \right] \right\} t$$

Closed Regeneration System (Carbonization or Closed Methanization)
Using Water for Make-Up

$$III. \quad \frac{W_T}{N_P} = n_c W_c (W_r + P_r N_1 + C_r N_2) + \frac{18}{16} (W_b + W_f) (W_e + P_e N_1 + C_e N_2) \\ + \left\{ -N_8 + [N_3] \left[(W_b + W_f) \frac{18}{16} - \frac{36}{44} n_c W_c - w_2 \right] \right\} t$$

Open Methanization System Using Water for Make-Up

$$IV. \quad \frac{W_T}{N_P} = \frac{44}{64} (W_b + W_f) (W_r + C_r N_2) + \frac{72}{64} (W_b W_f) (W_e + P_e N_1 + C_e N_2) \\ + \left\{ \left[\frac{36}{64} (W_b + W_f) - w_2 \right] [N_3] - N_8 \right\} t + \\ \text{for } n_c W_c \geq \frac{44}{64} (W_b + W_f)$$

Non-Regenerative Stored Oxygen System

$$V. \quad \frac{W_T}{N_P} = N_7 + (W_b + W_f) N_4 t$$

*The nomenclature is defined in Appendix A

Although the developed equations contain a number of terms, they are all rather simple and similar. The first complete term on the right represents the penalty associated with the reactor. It is made up of a coefficient representing the rate of carbon dioxide being processed, multiplied by the specific weight penalty of the reactor. The specific penalty of the reactor is made up of three terms representing the fixed weight, the power penalty equivalent weight and the cooling penalty equivalent weight.

Similarly, the second complete set of terms represents the penalty associated with the electrolysis cell. The coefficient representing the rate of water being processed is determined by a mass balance to meet the vehicle oxygen requirements, the water available from the reactor, the excess water from the water management system and water which may be provided as a constituent of the make-up material. The form of the coefficient varies due to the type of make-up material used, but it still represents the weight rate of water being electrolyzed. The specific weight penalty of the electrolysis cell is made up of fixed weight penalty, power equivalent weight penalty, and cooling equivalent weight penalty.

The third complete term is made up of the time-dependent penalty. The packaging coefficient, pounds of system per pound of useful product times the daily usage of the make-up material less the make-up material already available, is the time-dependent weight penalty. A time credit term is shown, N_8 , if the by-products of the atmospheric regeneration system are used in another system.

The penalty of the carbon dioxide collection system was not included for two reasons. The recovery system is not well defined since more than one method might be considered. All of the closed systems require a carbon dioxide recovery system which would add the same penalty increment to each curve and reduce the effectiveness of a comparison study. The open cycle methanization system would not necessarily require the same carbon dioxide recovery system since it does not require the high purity of the closed systems, but the difference in this requirement will not affect the weight comparisons.

The stored system (Equation V of Table 1) will have even less stringent requirements for a carbon dioxide recovery system, but very few, if any, vehicles will be in the range where a selection between a stored system and a regenerative system is not clear. Vehicles requiring a regenerative atmospheric control system must have a closed cycle power system. The same requirements which dictate a closed power cycle, such as long duration operation and minimum resupply, will also dictate that a regenerative atmospheric control system be used.

These equations may be used in a number of ways. The preliminary environmental control designer uses the equivalent weight for trade-off studies; the weights engineer require the absolute weights which can be found by setting the specific power penalty, N_1 , and the cooling penalty, N_2 , equal to zero; and the power systems designer needs a power load which can be obtained by setting $t = W_r = W_e = N_2 = 0$, and $N_1 = 1$.

This study used this set of equations to determine the effect of a single design parameter on the equivalent weight penalty of the system. The most important parameters, as shown in Appendix B, are the water recovery system performance the electrical power system, the leakage rate, the breathing oxygen supply and mission duration. Figures 4 through 14 show the system's takeoff weight penalty as a function of these parameters. Table 2 shows the nominal values of parameters and constants used in the analysis.

Figures 4 through 14 illustrate the general conclusion that accurate equivalent weight penalties for regenerative atmospheric control systems can only be determined when the design parameters of the mission and vehicle are carefully defined.

Figures 4 and 5 show the effect due to power system penalty on the equivalent penalty of the carbon dioxide recovery system for 100 days and 200 days operation. The closed system using hydrogen peroxide storages is the lightest system for the particular set of average parameters held constant. This is not as pertinent as the large variation on all of the systems caused by changing the power system penalty. Since the selection of a power system is normally

Table 2. Nominal Value of Parameters.

		<u>Closed</u>	<u>Methanization</u>
n_c	Carbon dioxide concentrator recovery efficiency, per cent	94	94
W_b	Breathing oxygen rate, lb/man-day	2.0	2.0
W_c	Expired CO ₂ rate, lb/man-day	2.3	2.3
W_r	Reactor specified weight, lb reactor/lb CO ₂ processed per day	20	12
P_r	Reactor specific power, watts/lb CO ₂ processed per day	75	0
C_r	Reactor circuit cooling loss, watts/lb CO ₂ processed per day	100	50
N_1	Specific power penalty, lb/watt	0.1	0.1
N_2	Specific cooling penalty, lb/watt	0.04	0.04
W_l	Oxygen leakage rate, lb/man-day	0.4	0.4
W_e	Electrolysis cell specific weight, lb/lb water electrolyzed per day	23	23
P_e	Electrolysis cell specific power, watts/lb water electrolyzed per day	125	125
C_e	Electrolysis cell specific cooling, watts/lb water electrolyzed per day	50	50
W_2	Water surplus from water management system, lb/man-day	0.4	0.4
N_3	Specific system weight of water storage system, lb/lb of H ₂ O	1.07	1.07
N_4	Specific system weight of oxygen storage system, lb/lb of oxygen	1.5	N/A
N_5	Specific system weight of H ₂ O ₂ storage system, lb/lb H ₂ O ₂	1.12	N/A
N_7	Fixed weight of oxygen supply system, lb/man	6.0	N/A

narrowed to one or two systems early in the preliminary design phase of a particular vehicle, it is not too difficult for the environmental control system designer to cover all possibilities.

Figures 6 and 7 illustrate the effect of loss of cabin gases for a 100 and 200-day mission. The variation again can be several hundred pounds and the leakage rate is not as easy to pin down as the power system. The designer has only a limited control on leakage rates through the design of the vehicle closures. This rate can be determined by testing during hardware construction and checked by testing the entire vehicle. The number of decompression events can never be reliably predicted and this is the largest unknown factor in leakage rates. A decision will be required in the preliminary design phase as to the number of allowable decompressions before the mission is to be aborted. The crew has some control over leakage rate in the duration of extra-vehicular activity. Figures 6 and 7 both reflect the advantage shown by the methanization system for increased leakage rates. A significant advantage only occurs for a combination of relatively large leakage rates and short mission durations. The maximum allowable leakage rate must be defined for a particular vehicle before the weight of the oxygen supply system can be determined.

Figures 8 and 9 show the effect of breathing rate. The systems' weights follow the same trends as for the leakage rates, with the methanization favored at higher breathing rates and shorter mission durations. The crew activity level must be defined before this requirement can be determined. The crew has considerable control over this requirement and might even compensate for slightly abnormal leakage rates by reducing their personal activity.

The effect of the water balance from the water management system (the difference between water available and the water required by the crew) is shown in Figures 10 and 11 for various make-up oxygen supply systems for 100 and 200-day missions. The variation is again several hundred pounds. This balance must be determined to a greater degree of accuracy than is possible by analytical techniques. It would be discouraging to abort a long duration mission at midpoint simply because the water management system efficiency degraded a few percentage points. It is imperative than an extensive

long duration water management test program be a part of the vehicle development if full advantage is to be taken of a potential water surplus.

Figures 12 and 13 show the takeoff weight of the various systems plotted as a function of time for two leakage rates. Figure 12 shows a small range where the open cycle methanization is the lightest system. Figure 13 shows that if lower leakage rates can be maintained, there is no regime where the methanization system will be the lightest system for the particular set of "average" design parameters selected. This occurs because the electrolysis cell penalty is larger for the open methanization system than for a closed system using hydrogen peroxide storage. Half of the oxygen obtained from the hydrogen peroxide is obtained without electrolysis while all of the oxygen from the methanization comes from the electrolysis of water which requires a larger electrolysis cell. This difference in electrolysis requirements offsets the lighter methanization reactor for all mission durations at the lower leakage rates.

Figures 12 and 13 reflect the weight of stored material, but if resupply is considered a separate plot of materials shown in Figure 14 may be quite useful.

These curves illustrate the importance of specifying the design parameters of the vehicle and mission, almost to the point of naming the crew members and their physiological characteristics before a satisfactory determination of the oxygen supply system weight can be made. Perhaps this can be illustrated more graphically by taking a combined set of the worst conditions for the methanization system and comparing this to the best conditions for a stored system. This resulted in a cross-over point at 380 days with both systems having an equivalent weight penalty of 1180 pounds per man.

V. DISCUSSION OF REGENERATIVE SYSTEMS

A more complete and detailed description of the two promising regenerative atmospheric control systems is required in order to understand the inter-relationship between these systems and their various components, such as the electrolysis unit, the CO₂ collector, etc., and between these systems and the over-all vehicle considerations, such as leakage, etc.

The minimum theoretical energy required to separate carbon dioxide into its elements with 100 per cent mass conversion and no energy losses would be approximately 1.55 kw-hr of energy to produce one pound of free oxygen. If a power system using stored chemicals for an energy source is utilized to supply the energy for this conversion, it must have a specific fuel consumption less than 0.65 lb/kw-hr for the ratio of oxygen produced to fuel supplied to be greater than one. None of the space power systems being developed have specific fuel consumption rates lower than 0.65 lb/kw-hr, although a hydrogen concentration fuel cell has been suggested which would have a theoretical specific fuel consumption lower than this (Reference 11). For this reason a carbon dioxide regeneration system can be justified only when solar or nuclear energy is used as the energy source for the electrical power system. The only exceptions to this arise when direct thermal decomposition of the carbon dioxide or biological systems are considered, but they must utilize solar energy directly to be competitive. It is also interesting to note that a water reclamation system will probably not be required until this transition in power systems is made since hydrogen-oxygen fuel cells will provide sufficient water for meeting the crew requirements.

A. Hydrogen Carbonization System

The hydrogen carbonization system is based on a circulating gas loop in which carbon dioxide is reduced to water and elemental carbon by heated hydrogen.

The system operation is relatively simple. The hydrogen-carbon dioxide mixture is preheated through a regenerative heat exchanger before entering the reactor. Some of the carbon dioxide is reduced to water and carbon in the reactor. The reaction products include unreacted hydrogen, carbon dioxide, methane and sometimes carbon monoxide. The iron catalyst also serves as the carbon collector. The reaction products are cooled through the regenerative heat exchanger and a condenser. The water is collected from the condenser and transported to the electrolysis cell. The electrolysis cell returns the hydrogen to an accumulator for reuse in the system and oxygen can be stored or used as produced. The dehumidified

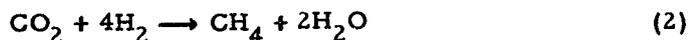
process stream is reheated through a regenerative heat exchanger and re-admitted to the reactor. Although the reaction is an exothermic process, the reactor must be supplied with a net heat input due principally to the large heat loss in the condenser.

When only considering the feed gas and the products removed from the reactor loop, the operation of the system can be described by the following equation:



This is the desired reaction, but the formation of water retards the conversion. The water must be continuously removed to force the reaction to continue to the right.

Examination of the gases in the recirculating loop shows that other reactions are taking place. Inclusion of all the probable reactions that are actually taking place will not add to the understanding of the over-all problem and the following two side reactions will account for most of the by-products:



Some of the earlier studies rejected this process for lack of data, the high temperatures required, the fact that the above side reactions would dominate the process, and that the process is hazardous (References 2, 12, 13) (see Equation 3). Other studies showed this process to be promising and development work was initiated.

The success of this system is dependent upon the CO_2 reactor design and the ability to conserve the heat in the recirculating loop. As mentioned above, the over-all process is exothermic, but the recirculating gases must be cooled to condense the water and then reheat before then re-enter the reactor. On the basis of the analysis and results of the tests made on systems built by Battelle and the Mechanics Research Division of General American Transportation Company for the Aerospace Medical Laboratories, reasonable

design improvements could reduce the net heating power to 80 watts/man and the circulating power to 25 watts/man. This may appear to be a difficult objective when compared to the 216 watts/man heating power and 76 watts/man circulating power used in the development model (Reference 16). The funds only allowed limited optimization and the system operated at approximately 125 per cent design capacity. For example, improvement in the development model performance may be gained by a reduction in the recirculating gas flow to 80 per cent which would lead to a circulating power reduction of almost 50 per cent. Substitution of a compact plate and fin heat exchanger instead of the coiled tube exchanger used should also result in another substantial reduction. Substituting a more effective lightweight, low conductivity insulation for the industrial mediumweight insulation used should reduce the reactor heating power by a large factor while reducing the weight at the same time. Therefore, these modifications which would be incorporated into an operational flight model, should show the improvements noted above. In addition, only slight improvement in the reactor conversion efficiency will reduce both the pumping and heating power required by significant amounts.

The reactor temperatures, between 1100 and 1400°F, are well within the limits of stainless steel construction and the reducing atmosphere will tend to retard corrosion. The iron catalyst may be regenerated with excess hydrogen, or it may be discarded since the catalyst weight is a small fraction of carbon deposition weight.

The water electrolysis cell will be required to supply oxygen from the water produced in the reactor. Excess water (0.42 lb/man-day) from the water reclamation system can be fed to the cell to provide the breathing oxygen balance.

Hydrogen will be produced in excess of the quantity required to balance the reactor requirements due to the water from the water management system. The hydrogen could be useful as a jet reaction fuel, as a purge

gas for removing carbon from the reactor, as a means of reactivating the reactor catalyst, or even used in a hydrogen concentration cell to produce electrical power.

An almost pure supply of carbon dioxide is required at approximately 10 to 20 psia depending on reactor design. If water vapor is present in the carbon dioxide or hydrogen feed, it will reduce the capacity of the system although the water is removed in the first complete pass. Small quantities of oxygen will reduce reactor capacity, but should not be an explosion hazard unless present in large amounts. Inert trace contaminants can probably be allowed to build up and be expelled when the carbon is removed from the reactor.

This system has the following promising points:

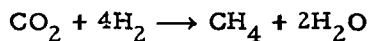
- a. It is almost a closed cycle system, requiring only water from the water management system to balance the oxygen supply.
- b. It has been proven operationally feasible in full scale prototype models.
- c. No technical breakthroughs will be required to develop a reliable flight model.

These reasons were considered to be sufficient to justify a detailed penalty and performance analysis.

B. Methanization System

1. Open Cycle

The methanization system, shown in a simplified schematic in Figure 3, also uses hydrogen as a reducing agent in the carbon dioxide reactor; but, as the name implies, methane is formed in the following reaction:



The water can then be electrolyzed to provide breathing oxygen. The reaction is a relatively low temperature (300 to 600°F) nickel catalyzed reaction that

can be essentially carried to completion (greater than 95 per cent conversion) (Reference 12) in a one-step reactor. The addition of water (1.13 lb/man-day) to the electrolysis cell allows the methane to be discarded or used for some other purpose. Since it is difficult to justify a "free" supply of more than 0.42 pounds of water per man-day, the balance of water required (0.71 lb/man-day) must be charged to the carbon dioxide system. However, use of this system will still result in a reduction of the time-dependent penalty of the oxygen supply system over that of an expendable system by at least 1.29 lb/man-day (2.00 lb O₂ minus 0.71 lb H₂O).

The methane forming reaction is an exothermic process which will require active cooling to prevent the reactor from exceeding the most favorable reaction temperatures. The reactor shell will probably not exceed 350°F which indicates that aluminum can be used for the bulk of this component. Methane along with surplus carbon dioxide is a by-product of the open methanization cycle. The combination of gases might be useful as a jet reaction fuel.

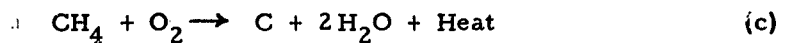
When this system is operated as a partially open system as described, it provides the following advantages over the hydrogen-carbonization system.

- (1) Low temperature exothermic system requiring only start-up heating power.
- (2) No carbon deposition problems since carbon is never formed.
- (3) Simple system requiring no recirculation of by-products.
- (4) Smaller, lighter weight reactor due both to lower temperatures and the fact that less carbon dioxide must be reduced.
- (5) Flexibility in meeting leakage demand since 32 grams of oxygen can be provided for each 18 grams of makeup water fed into the system up to the limit of carbon dioxide available.

Because of these advantages the open cycle methanization system was evaluated in detail as one of the basic systems in the design analysis section.

2. Closed Cycle

The methanization system, as described, is not a closed cycle and the time-dependent weight penalty is a distinct disadvantage when very long duration missions must be accomplished. Therefore, consideration was given to the possibility of closing this system by recovering the hydrogen from the methane. Several possibilities were considered.



The first reaction, Equation (a), proceeds to the right above 500°F and is essentially complete above 2000°F . Less than 50 watts of heat per man is required to bring the gas from 300 to 2000°F and provide the free energy of formation. This is less power than required for the hydrogen carbonization system and appears to be the simplest method for closing the methanization system.

The additional penalty required to close the methanization system by thermal dissociation will be so close to the difference between the open methanization system and the hydrogen carbonization system that it does not appear to justify showing a difference between the two closed systems. The additional power requirement will be between 60 and 80 watts per man for compression of the methane and thermal cracking compared to 80 to 100 watts per man for the hydrogen carbonization system. This difference is such a small percentage of the total power requirement that it can be considered negligible. The fixed weight penalty is in the same category, since the high temperature cracking chamber will require ceramic construction materials and high temperature insulation offsetting the lightweight methanization reactor. On this basis, therefore, the penalty equations for the hydrogen carbonization system can be used for estimating the performance of the closed cycle methanization system utilizing pyrolysis to recover hydrogen.

Although the second reaction, Equation (b), is slightly exothermic and therefore should require no heating power, it is a repeat of the hydrogen carbonization system using methane as a reducing agent rather than hydrogen. Since methane, as a reducing agent, is not normally as effective as hydrogen, a subsystem more complex than the hydrogen carbonization system will be required to close the methanization system using this reaction. There does not appear to be a significant advantage in utilizing the methanization reactor in a closed cycle system of this type.

The third possibility listed does not appear to be practical since not only is it difficult to achieve the reaction as shown, but to close the system the water must be electrolyzed which will require a 100-per cent increase in the size and power requirements of the electrolysis cell. This penalty is not acceptable if the methanization system is to be competitive with the hydrogen carbonization system.

A water electrolysis cell is required to supply oxygen from the water produced in the reactor. The cell can be fed excess water from the water recovery system to make up as much of the hydrogen balance as is possible for the open cycle. Additional water can also be electrolyzed to provide oxygen leakage makeup. There should be enough excess water available from the water management system to make up the breathing requirements for the closed cycle. The same purity of carbon dioxide supply would be required for this cycle as for the hydrogen carbonization system. Excess hydrogen would be produced in the closed cycle operation and, as in the hydrogen carbonization system, could be useful as a jet reaction fuel, as a means of reactivating the reactor catalyst, as a purge gas for carbon removal or in a hydrogen concentration cell.

Since there is no essential difference from a penalty standpoint between the hydrogen carbonization and closed methanization system, the latter system was not analyzed separately.

VI. COMMON SUBSYSTEMS

A. Carbon Dioxide Collection

Both of the closed systems considered require an almost pure source of carbon dioxide. The open methanization system can accept most inert impurities up to approximately 5 per cent without significantly affecting the reaction. Several systems have been proposed for collection of carbon dioxide from cabin air to be used in a regeneration system. Since one of the principal requirements of this component will be operation in a zero or low gravity field, liquid systems appear to add enough complexity to outweigh their advantages. Some of the more promising proposed systems involve freeze-out, silver oxide, molecular sieves, and electrodialysis.

The freeze-out system would consist of a series of regenerative heat exchangers which would conserve most of the refrigeration necessary to cool the process gas and heat necessary to warm the processed gas. A heat sink is necessary at a temperature below -190°F to absorb the heat of fusion of carbon dioxide at the low partial pressures. For short duration missions metabolic oxygen (stored at cryogenic temperatures) and the collection carbon dioxide sublimating overboard would provide this heat sink. However, when carbon dioxide must be subsequently collected for the regenerative atmospheric control system and cryogenic oxygen is not available in the quantity required, if available at all, this method of operation is not possible. Since the cooling requirements are small, it might be feasible to incorporate a space oriented radiator utilizing a closed gas cycle refrigeration system to provide the cooling for the final freeze-out step. Further energy conservation is available by coupling the high temperature side of the refrigeration system with the heat exchanger which is sublimating CO_2 into the oxygen generation system. This system has the potential of supplying carbon dioxide at any reasonable pressure which is an advantage when used with a regenerative atmospheric system. Reference 18 shows that a similar system is complex and has a high power requirement. The freeze-out carbon dioxide collection system does not look promising unless a cryogenic fluid is available as a heat sink.

Silver oxide has been proposed as a carbon dioxide collector since it does not suffer from water contamination, is regenerable at reasonable temperatures, and has a theoretical collection potential of 0.19 pound of carbon dioxide per pound of silver oxide. A large variation in experimental results has occurred in the investigation of this substance. This is apparently due to variation in methods of preparation, packaging, the purity of the silver oxide, and the number of cycles of the test operation (Reference 17). Although silver oxide might be preferable to molecular sieves in a system where the carbon dioxide is vented to space, the potential hazard of silver oxide decomposing into silver and oxygen when subjected to the temperatures required to release carbon dioxide in a closed system is too great to risk its use until experimental evidence over many cycles conclusively shows that this danger does not exist. This is a two-fold hazard since the loss of the carbon dioxide collection device could be fatal to the crew and the introduction of substantial quantities of oxygen into the hydrogen reduction reactor could initiate an explosion. There is little prospect of utilizing a silver oxide system in a carbon dioxide reduction system until it can be experimentally shown that the silver oxide system will be stable.

Molecular sieves absorb carbon dioxide readily, can be regenerated at moderate temperatures utilizing a small mechanical vacuum pump, and show little degradation over many cycles. There are several disadvantages to a molecular sieve system, however, in that there is a preference for water absorption during the collection cycle and difficulty in complete removal of the carbon dioxide during the regeneration cycle. The process air stream can be dried by passing through a silica gel bed (a molecular sieve could be used, but it is not as adaptable to regeneration as silica gel) before entering the molecular sieve bed. Incomplete regeneration can be compensated for by increasing the molecular sieve bed size. Since the bed size may be dictated by the mass transfer zone and face area requirements, incomplete regeneration may not be a problem. The regenerative molecular sieve system will require at least two beds for continuous operation and a large number of switching valves or a rotating drum arrangement. Since the beds absorb less

than ten pounds of carbon dioxide per one hundred pounds of bed, most of the heat required to regenerate the beds is used for raising the temperature of the beds. None of this heat can be recovered without additional complexity which would compromise the reliability. The heat of regeneration may not be too severe a penalty since it is possible that thermal energy will be available with less penalty than electrical energy. The pressure drop through the molecular sieve is high and the additional pressure loss through the silica gel bed must be added to the penalty of the system. Molecular sieves do not provide a good system, but they do provide the most practical system that can be readily developed at the present time.

Ion exchange electrodialysis has been proposed as a continuous, relatively simple system for removing carbon dioxide and water vapor from the cabin air (Reference 18). Little experimental work is available at present, but preliminary estimates of the power requirements have been made. The power estimates (270 watts per man) are of the same order as required for the electrolysis of water. This power may initially appear to be prohibitive, but when compared to the power requirements of a silica gel-molecular sieve system (50 to 180 watts per man), the difference is slight. If the apparent reliability of the electrodialysis system can be demonstrated, it may be well worth the additional power penalty. Since this system has not been built even on an experimental basis, it cannot be considered to be available for the purposes of this study.

Magnesium oxide has the potential of collecting 1.09 lb CO₂/lb Mg O, but has not received much attention because of its low reaction rate in forming magnesium carbonate. Magnesium oxide does have several attractive characteristics which may justify further investigation. It is one of the most stable compounds known. Although it may form magnesium hydroxide in contact with water, this only enhances the collection of carbon dioxide. The magnesium hydroxide will decompose to magnesium oxide and water during the regeneration cycle restoring the original characteristics of the system. Application of heat will readily decompose magnesium carbonate into carbon dioxide and magnesium oxide. The level of temperature required is dependent on the carbon dioxide pressure required and although the literature does not agree

on the decomposition temperatures, it will apparently begin decomposition as low as 500°F. This property requires further experimental investigation.

The only potential problem which would add to the complexity is the possibility of two-step regeneration. Magnesium carbonate does form hydrates, so it might be necessary to drive off the water before driving off the carbon dioxide. There is a temperature difference greater than 300°F between the two steps, so this should not be difficult. Since it is readily available in large surface area to volume ratio form, both as powder and porous semi-rigid structure, it might be possible to utilize a large percentage of its theoretical potential. An added advantage is the very low material cost. Due to these inherent advantages, it appears that some experimental work would be justified in determining whether the reaction rate of magnesium oxide could be improved to the point where magnesium oxide could be used in a practical carbon dioxide regeneration system.

It was concluded from this study that:

- a. A carbon dioxide collection and concentration subsystem consisting of a silica gel-molecular sieve bed is the only system that has been developed to date which could be adapted for use in a carbon dioxide regeneration system.
- b. Electrodialysis and decomposable carbonates show enough promise to justify further work, since a regenerative molecular sieve system does have significant inherent disadvantages.

B. Water Electrolysis Subsystem

Both carbon dioxide reclamation systems employ water electrolysis for oxygen generation and since it contributes the largest penalty to the system, the electrolysis portion deserves a separate discussion. Some generalities can be applied to the electrolysis components.

- a. The power required decreases with increasing temperature.
- b. The power required decreases with increasing electrode area which is almost directly proportional to weight. This leads to a trade-off between cell weight and power for an optimum combination.

c. Approximately 78 watts of power is theoretically required to produce one pound of oxygen per day by electrolysis of water.

There are three promising basic methods of water electrolysis in a low gravity field. These consist of a rotating cell with a liquid electrolyte, a static vapor cell using a phosphorous pentoxide electrolyte, and a reversed fuel cell using porous metallic or membrane electrodes for phase separation. An excellent discussion of these systems along with many variations may be found in Reference 19 prepared for the USAF Aerospace Medical Division by the Battelle Memorial Institute.

The reversed hydrogen-oxygen fuel cell has been suggested by many fuel cell manufacturers, but there appears to be little, if any, data showing experimental results for this mode of operation. Assuming efficiencies and weights in the same range as reported for power production indicated that power consumption would be between 105 and 130 watts per pound of oxygen produced per day with cell fixed weights of less than 10 lb/lb of O₂ per day. These estimated figures show real promise and work should be initiated to determine whether such a system is feasible.

A rotating cell was built, tested, and reported in Reference 19. This cell required a power input of slightly over 150 watts per pound of oxygen produced per day and had a fixed weight of 71 lb/lb of O₂ produced per day when operating as a two-man system. The report suggested that these values could be reduced to below 125 watts and 50 pounds, respectively, by operating at higher temperatures (165°F) instead of approximately 100°F and suitable redesign. A variation of this method incorporating rotating thin palladium electrodes rather than rotating the body of the cell was also proposed in this reference. The fixed weight was estimated to be 10 lb/lb O₂ per day (which is the same as the reversed fuel cell) and with a power requirement between 112 and 150 watts per pound of oxygen per day. Since the rotating cell utilizes a simple and therefore reliable control system, can be operated over a large load variation without damage, has a good efficiency growth factor (by increasing the operating temperature) and utilizes reliable state-of-the-art components, it must be considered as the leading contender for the electrolysis component of a carbon dioxide regeneration system.

The vapor cell, originally suggested as an outgrowth of a water vapor detector (Reference 20), uses a phosphorous pentoxide porous electrolyte. The phosphorous pentoxide forms hydrogen-phosphorous-oxygen compounds in contact with water vapor. This compound ionizes and is electrolyzed, producing hydrogen, oxygen, and phosphorous pentoxide. The hydrogen remains in the process stream while oxygen is drawn off at the anode which would be separated from the process stream by the electrolyte. The power requirement is dependent upon the cell voltage which was reported to be a minimum of 2.2 volts in Reference 20. Assuming that a system designed for the specific electrolysis function would operate at 2.43 volts, 150 watts would be required to produce one pound of oxygen per day. The fixed weight of this system is difficult to estimate, but it should be less than required for the rotating electrolysis cell. Since this cell might be incorporated directly in the wet stream of either the methanization or hydrogen carbonization system, it could simplify the total operation considerably. A static device normally implies reliability, but the electrolyte may have a short life operating in the described manner. Development work on this system has been initiated at Battelle by the Aerospace Medical Division, but results are not available at this time. If 2.2 volts are the true minimum cell voltage, it is quite likely that higher voltages than the 2.43 volts assumed will be necessary in order to obtain current densities high enough to make the system practical from a volume standpoint. This will raise the power requirements of the system, but this power level would be acceptable if the cell could show a high reliability potential.

The incorporation of an electrolysis cell in the vehicle has the additional advantage of providing voltage regulating characteristics to the power supply. The electrolysis cell acts as a voltage regulator and can be used to smooth out rather large variations in the vehicle power supply. Since the electrolysis power will probably be a substantial percentage of the total power level, the cell power might be programmed in such a manner as to effectively reduce the peak power requirement. The cell power can be reduced during high power demand periods and overloaded during low demand periods. Although the electrolysis efficiency falls off as the power input increases, oxygen production is increased.

If the peak power level of the vehicle can be reduced and at the same time simplify voltage regulation by incorporating the electrolysis cell as a load bank, the net result is a gain to the vehicle since the electrolysis cell size will probably not be affected as long as the $\int Idt$ requirements of the cell are satisfied for oxygen production.

As a result, the following conclusions were reached:

a. The rotating cell electrolysis subsystem is the only electrolysis system that has been developed to the point where it could be considered to be available for use in a carbon dioxide regeneration system. Further work should be directed toward reducing the fixed weight of this system without increasing the power requirements.

b. The hydrogen-oxygen fuel cell, notwithstanding the tremendous development work as a power source, requires experimental verification before it can be considered as an electrolysis cell. It does have the potential of reducing both the fixed weight and power requirement of this component.

c. The vapor cell reliability and operational feasibility must also be proven before it can be evaluated. It will apparently require as much or more power than either of the other systems, but it may reduce the complexity and therefore increase the reliability of carbon dioxide regeneration system.

C. Make-Up Material Supply

A material balance on the vehicle's life support system for realistic design requirements shows that a material make-up supply will be necessary to balance the oxygen supply requirements (breathing plus leakage) of the vehicle.

Some of the make up supply will be available from the water surplus in the water management system. Therefore some oxygen will be provided by the electrolysis of this surplus water.

The surplus water from the water management system will not be enough normally to satisfy the complete oxygen requirements. A stored source of oxygen will be required and it can be provided most conveniently by three

methods - oxygen bottles, water bottles, or hydrogen peroxide bottles. The choice of make-up supply may not be dictated by weight considerations alone. Each system has its particular characteristics which may dictate its use to meet other vehicle requirements.

An oxygen storage bottle system can be used to refill backpacks, pressurize the cabin after decompression and is most adaptable for cabin pressurization control. Long duration storage of cryogenic oxygen may not be practical for low use requirements. High pressure gaseous oxygen storage system weights are prohibitive for any significant quantity of stored oxygen.

The hydrogen peroxide bottle system has both a weight and volume advantage over stored oxygen bottles for any mission duration. It is adaptable to pressurization control and can be used for medium pressure backpack refills. It can be stored indefinitely in lightweight containers. The major disadvantage is the possible complexity involved in developing an operational system. There are two additional steps required to realize the full potential of the hydrogen peroxide. It must first be decomposed into water and oxygen. The water vapor or steam formed must be liquified for electrolysis which can be accomplished with either a condenser or, if the flow requirements are great enough to justify a power extraction system, an expansion engine can be used in series with a condenser separator. The reliability penalty associated with these operations may dictate the choice of a heavier, but less complex system.

The water storage system may be the least complex make-up system since the additional capacity required can be incorporated into the water reserve system for the vehicle. Water make-up can be used for pressurization control only if a compressor or a water pump and high pressure electrolysis cell is used. This tends to cancel the high reliability of a simple water bottle make-up system.

All three methods of storage were considered for the closed systems. Due to the advantage of obtaining 32 gm of oxygen for every 18 gm of make-up water supplied to the methanization system, only water storage was considered for the open methanization system.

VII. VEHICLE LEAKAGE CONTROL

Leakage or, the more appropriate terminology, loss of cabin gases may affect the carbon dioxide regeneration system in the following ways:

- a. The size of the regeneration system.
- b. The mass rate and type of make-up constituent required.
- c. Choice of regeneration system.
- d. If a mixed regeneration system using stored oxygen for make-up is selected, leakage and mission duration will determine whether cryogenic oxygen storage is feasible.
- e. The cross-over point between expendable and regenerative systems is affected.

For these reasons it is necessary to define the range of leakage rates expected for a long mission duration space vehicle.

There are four principal sources of loss of cabin gases: leakage through seals, use of air locks, cabin decompression, and extra-vehicular activity of crew members. Table 3 shows the probable magnitude of these sources.

Table 3. Probable Loss of Vehicle Oxygen.

<u>Source</u>	<u>Loss</u> <u>(lb/man-day)</u>
Seals	0.10
Air lock	0.03
Cabin decompression	0.15
Backpack operation	0.04
	<hr/>
Total	0.32

The construction of numerous large vacuum chambers has shown that static seal leakage can be reduced to insignificant rates. A space vehicle may have dynamic seals and it may not be practical to develop leak-proof

static seals for the vehicle, so an allowance of 0.1 lb/man-day is allotted for this source. The air lock on a long duration space vehicle will no doubt have a mechanical pump for conservation of cabin gases. The air lock will probably be evacuated to about 10 per cent of the cabin pressure. It is doubtful that any attempt will be made to recover the air lock gases much below this pressure level due to the exponentially increasing pump down-time and power requirement coupled with the decreasing recovery of gases. An air lock with 30 ft³ of free volume reduced to 0.5 psia will contain approximately 0.09 pound of gas. For a long duration mission the air lock will probably not be used more than once a day. This averages to 0.03 lb/man-day in a three-man vehicle. It is expected that partially open cycle backpacks will be used for at least some extra-vehicular activities with the carbon dioxide absorbed in lithium hydroxide beds and oxygen supplied from a bottle. Assuming that 2 per cent of the crew time will be spent in this mode of operation, a net loss of oxygen amounting to 0.04 lb/man-day for the vehicle can be shown. Cabin decompression events cannot be readily defined, but the vehicle should be designed well enough to avoid more than one decompression per month. Assuming a loss of 150 ft³ of oxygen at 5 psia for each man-month results in an average loss rate of approximately 0.15 lb/man-day. These figures should be generous, but uncertainty factors of 0.6 and 2.5 were used to obtain a range from 0.2 to 0.8 lb/man-day loss. This range is within the estimates made by several other agencies and will be used in the analysis.

VIII. CONCLUSIONS AND RECOMMENDATIONS

The following principal conclusions and recommendations were reached during the study:

- a. The hydrogen carbonization and methanization systems are the best prospects for a carbon dioxide regeneration system in the near future.
- b. The difference in weight and power requirements between the hydrogen carbonization and closed cycle methanization system is so small as to be within the accuracy limits of the analysis when both systems are operated as closed systems.

c. When the methanization system is operated as an open system, it does have a weight and simplicity advantage for medium duration mission times and high leakage rates. The selection between the open methanization and closed system may depend on leakage rates and whether the by-products can be useful in another vehicle subsystem.

d. Carbon dioxide concentration and recovery subsystems require further development and testing. A system utilizing molecular sieves is the only system that has proven to be reasonably successful, although it suffers from several disadvantages. Electrodialysis and other chemicals such as MgO should be investigated on an experimental basis.

e. Water recovery systems should be developed with higher recovery efficiencies than those tested in order to provide water for oxygen leakage make-up.

f. Electrolysis of water contributes the largest single penalty to the selected carbon dioxide reclamation systems. Further development work should be directed toward reducing the weight and power requirement of this component for low gravity operation.

g. The hydrogen carbonization system development should emphasize higher conversion rates per pass in the reactor in order to reduce the penalty of the recirculation system.

h. A method of reclaiming the hydrogen from methane should be developed for the methanization system. Thermal cracking appears to offer the best prospect.

i. General trade-off comparison studies are only valid for a narrow range based on the particular assumptions made for the study. It will always be necessary to make a penalty comparison study for each vehicle based on the design parameters of that vehicle.

APPENDIX A
NOMENCLATURE

Upper Case

- C** = cooling required by the component (watts per pound of material process per day)
- N_p** = number of personnel
- N₁** = specific power penalty (pounds per watt)
- N₂** = specific cooling penalty (pounds per watt)
- N₃** = specific system weight of water storage system (pounds per pound of useful water)
- N₄** = specific system weight of stored oxygen system (pounds per pound of useful oxygen)
- N₅** = specific system weight of stored hydrogen peroxide system (pounds per pound of useful hydrogen peroxide solution)
- N₆** = decimal concentration of hydrogen peroxide solution by weight
- N₇** = fixed weight of a stored oxygen supply system (pounds per man)
- N₈** = credit given to regeneration system for by-produce use (pounds per man-day)
- P** = power required by the component (watts per pound of material processed per day)
- W_b** = breathing oxygen required (pounds per man-day)
- W_c** = carbon dioxide supply (pounds per man-day)
- W_d** = water demand rate (pounds per man-day)
- W_F** = fixed equivalent weight penalty (pounds)
- W_l** = average oxygen loss from vehicle atmosphere (pounds per man-day)
- W_o** = total oxygen supply required (pounds per man-day)
- W_R** = water recovered (pounds per man-day)

- W_T = total equivalent weight liftoff penalty due to the carbon dioxide regeneration system excluding the collection system (pounds)
 W_t = total water available for processing (pounds per man-day)
 W_w = supply rate of water to be electrolyzed (pounds per man-day)
 W_1 = supply rate of water from reactor (pounds per man-day)
 W_2 = supply rate of surplus water from the water recovery system = $n_w W_t - W_d$ (pounds per man-day)
 W_3 = supply rate of water from a stored source (pounds per man-day)
 W_4 = supply rate of oxygen from a stored source (pounds per man-day)
 W_5 = supply rate of hydrogen peroxide from a stored source (pounds per man-day)

Lower Case

- n_c = decimal ratio of carbon dioxide recovered to carbon dioxide expired
 n_w = decimal ratio of water recovered to total water available for recovery
 w = time dependent weight penalty (pounds)
 w_c = average expired carbon dioxide rate (pounds per man-day)
 t = duration of operation (days)

Subscripts

- r = denotes reactor and components associated with the reactor
 e = denotes electrolysis cell and components associated with the electrolysis cell

APPENDIX B

EXPANSION OF PENALTY EQUATIONS

This appendix shows the expansion of the general penalty equations in terms of design parameters and the method of determination of rank of each parameter.

The penalty equation can be written in its simplest form as

$$W_T = W_F + wt$$

and progressively expanded

$$\frac{W_T}{N_P} = W_c (W_r + P_r N_1 + C_r N_2) + W_w (W_e + P_e N_1 + C_e N_2) + wt$$

$$W_c = n_c w_c$$

$$W_w = W_1 + W_2 + W_3$$

$$W_1 = n_c w_c (36/44)$$

$$W_2 = n_w W_t - W_d$$

$$W_3 = 0 \text{ for stored oxygen supply}$$

$$W_4 = W_o - 16/18 W_w \text{ where } W \geq 0 \quad w = N_4 W_4$$

$$W_o = W_b + W_l$$

For a stored oxygen make-up system using the above substitutions the equation expands to Equation I in terms of design parameters.

$$\text{I. } \frac{W_T}{N_P} = n_c w_c (W_r + P_r N_1 + C_r N_2) + (n_c w_c \frac{36}{44} + n_w W_t - W_d) (W_e + P_e N_1 + C_e N_2) + N_4 t \left[W_b + W_l - \frac{16}{18} (n_c w_c \frac{36}{44} + n_w W_t - W_d) \right]$$

If make-up is supplied from a hydrogen peroxide source,

$$W_4 = \frac{16}{34} W_5 N_6$$

$$W_3 = \left(1 - \frac{16}{34} N_6\right) W_5$$

$$w = N_6 W_5 \geq 0$$

Using these equations in combination with the vehicle oxygen requirements gives Equation II which is to be used for hydrogen peroxide storage.

$$\text{II. } \frac{W_F}{N_P} = n_c w_c (W_r + P_r N_1 + C_r N_2) + \left\{ n_c w_c \frac{36}{44} + n_w W_t - W_d + \left[1 - \frac{16}{34} N_6\right] \right\} \\ \left\{ \left[\frac{W_b + W_\ell - \frac{16}{18} (n_c w_c \frac{36}{44} + n_w W_t - W_d)}{\frac{16}{18} (1 - N_6 \frac{16}{34}) + N_6 \frac{16}{34}} \right] [W_e + P_e N_1 + C_e N_2] \right\} \\ + N_5 t \left[\frac{W_b + W_\ell - \frac{16}{18} (n_c w_c \frac{36}{44} + n_w W_t - W_d)}{\frac{16}{18} (1 - N_6 \frac{16}{34}) + N_6 \frac{16}{34}} \right]$$

It may be more desirable to store water as a make-up than hydrogen peroxide or oxygen. For this case, Equation III can be derived by substituting

$$W_4 = 0$$

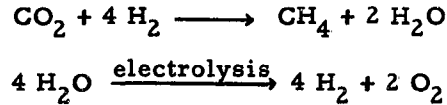
$$N_3 W_3 = w$$

or setting $N_6 = 0$ in Equation II and $N_3 = N_5$.

$$\text{III. } \frac{W}{N_P} = n_c w_c (W_r + P_r N_1 + C_r N_2) + \frac{18}{16} (W_b + W_\ell) (W_e + P_e N_1 + C_e N_2) \\ + N_3 t \left[(W_b + W_\ell) \frac{18}{16} - \frac{36}{44} n_c w_c - n_w W_t + W_d \right]$$

The open cycle methanization is readily adaptable to providing oxygen supply rates in the principle range of interest by using stored water rather than oxygen.

This is due to the fact that one gram-mole of stored water (18 grams) frees one gram-mole of oxygen (32 grams) up to the limit of balancing the carbon dioxide available. Balancing the following equations and substituting gives Equation IV for the open methanization system.



$$\text{IV. } \frac{W}{N_P} = \frac{44}{64} (W_b + W_\ell) (W_r + C_r N_2) + \frac{72}{64} (W_b + W_\ell) (W_e + P_e N_1 + C_e N_2) \\ + \left[\frac{36}{64} (W_b + W_\ell) - (n_w W_t - W_d) \right] N_3 t.$$

subject to the constraint that

$$n_c w_c \geq \frac{44}{64} (W_b + W_\ell)$$

but this equation is satisfied in the range of interest.

These four equations show the penalty of the carbon dioxide system as a function of the design parameters $n_c w_c$, W_r , P_r , N_1 , C_r , N_2 , n_w , W_r , W_d , N_b , t and storage system specific weight. If the by-products are used in another system, an additional term could be added: $N_8 t$ where N_8 is the supply rate weight credit given to the carbon dioxide regeneration system for by-product use rate.

These equations can be used in any specific case to determine the penalties associated with each method of carbon dioxide generation and oxygen supply make-up and can be used for gross comparison with open cycle oxygen supply systems which can be approximated by Equation V.

$$\text{V. } \frac{W}{N_P} = N_7 + (W_b + W_\ell) N_4 t$$

N_7 = fixed weight of oxygen supply system in pounds/man.

It is always of interest to determine the effect of each parameter variation both from the standpoint of knowing which design improvements will benefit the system the most and what parameters should be used in plotting curves.

Table B-1 shows the design range of the various parameters. These values can be used in finite difference equations to determine the net variation of the system weight penalty caused by a variation of each of the parameters. The finite difference equations are formed by approximating the total differential of the penalty equations to finite difference equations and varying each parameter within the range shown in Table B-1. This is not a very satisfactory mathematical analysis, but should be accurate enough to determine the rank of importance and the relative effect of each parameter. When the coefficient of the mission duration time is greater than zero, it is obvious that the time dependent penalty can be made to be a primary factor so time is assumed to be a major influence and will not be investigated in this analysis.

Certain simplifications will be introduced to reduce the analysis somewhat.

$$W_c = 1.2 W_b$$

$$dW_c = 1.2 dW_b$$

$$n_w W_t - W_d = W_2$$

since this term is a function of the water management system, the effect of the water recovery system can be determined from this factor alone. Assuming that all other variables are independent (which is not true in an exact sense) and taking the total derivative of Equation I gives Equation I(a).

Each parameter can be examined in sequence by allowing it to vary within the range shown in Table B-1. Each of the first four equations can be treated in the same manner and both magnitudes relative to the largest variation and order of importance can be approximated.

$$\begin{aligned}
I(a) \Delta \frac{W_T}{N_P} = & \Delta n_c \left[1.2 W_b (W_r + P_r N_1 + C_r N_2) + 1.2 W_b \frac{36}{44} (W_e + P_e N_1 + C_e N_2) \right. \\
& \left. - \frac{16}{18} (1.2 W_b \frac{36}{44} N_r t) \right] + \Delta W_b \left[1.2 n_c (W_r + P_r N_1 + C_r N_2) \right. \\
& \left. + 1.2 n_c \frac{36}{44} (W_e + P_e N_1 + C_e N_2) + N_4 t - \frac{16}{18} (1.2 n_c) \frac{36}{44} N_4 t \right] \\
& + (N_2 \Delta C_r + N_1 \Delta P_r + \Delta W_r) (1.2 n_c W_b) \\
& + \Delta N_1 \left[1.2 n_c W_b P_r + P_e (1.2 n_c W_b \frac{36}{44} + W_2) \right] \\
& + \Delta N_2 \left[1.2 n_c W_b C_r + C_e (1.2 n_c W_b \frac{36}{44} + W_2) \right] \\
& + \Delta W_2 \left[W_e + P_e N_1 + C_e N_2 - N_4 t \right] + \Delta W_\ell \left[N_4 t \right] \\
& + (\Delta W_e + N_1 \Delta P_e + N_2 \Delta C_e) \left[1.2 n_c W_b \frac{36}{44} + W_2 \right] \\
& + \Delta N_4 \left[W_b + W_\ell - \frac{16}{18} (1.2 n_c W_b \frac{36}{44} + W_2) \right] t
\end{aligned}$$

The normalized results are shown in Table B-2. The rank or order of importance are shown along with the comparative effect of each variation. The five most important parameters are the water recovery system, the electrical power system, the leakage rate, the breathing oxygen supply, and mission duration. This result could have been predicted intuitively perhaps but a result based on a reasonable mathematical approximation is a better basis for system study. It is interesting to note that the design of the regeneration system itself has a secondary effect on the total penalty attributed to the system. One result which does not show in the table of normalized values is that the open cycle methanization system is less sensitive to variation than the other systems. This is a two-sided factor since it reflects the ability of the system to respond to unfavorable vehicle design changes without major changes in the penalty associated with the regeneration system, but it also shows that a significant vehicle improvement will not reduce the regeneration system penalty significantly.

Table B-1. Probable Range of Parameter Values.

		<u>Minimum</u>	<u>Maximum</u>
n_c	CO ₂ recovery system efficiency,	0.90	0.96
W_b	Breathing oxygen rate, number/man-day	1.5	3.0
W_r	Reactor specific weight, lb/lb CO ₂ processed per day	15	25
P_r	Reactor specific power, watts/lb CO ₂ processed per day	50	100
C_r	Reactor cooling requirement, watts/lb CO ₂ processed	75	125
N_1	Specific power penalty, lb/watt	0.05	0.55
N_2	Specific cooling penalty, watt/lb	0.02	0.07
W_l	Leakage rate, lb/man-day	0.1	0.8
W_e	Electrolysis cell specific weight, lb/lb H ₂ O processed	15	30
P_e	Electrolysis cell specific power, watts/lb H ₂ O processed	100	150
C_e	Electrolysis cell specific cooling, watts/lb H ₂ O processed	25	75
W_2	Water surplus from water management system, lb/man-day	-0.2	+0.8
N_3	Water system storage weight, lb/lb H ₂ O	1.05	1.10
N_4	O ₂ system storage weight, lb/lb useful O ₂	1.2	2.0
N_5	H ₂ O ₂ system storage weight, lb/lb H ₂ O ₂ mixture	1.1	1.2
N_6	H ₂ O ₂ concentration	0.9	0.98
N_7	Fixed weight of oxygen supply system, lb/man	2.0	10.0
t	Mission duration, days	100	1000

Table B-2. Rank and Relative Magnitude of the Penalty Variation Resulting from Parameter Variation.

	I		II		III		IV	
	Rank	Relative Magnitude						
W ₂	1	1.0	1	1.0	3	0.71	2	0.75
N ₁	2	0.96	2	0.88	2	0.95	3	0.66
W _a	3	0.85	3	0.78	1	1.0	4	0.47
W _b	4	0.82	4	0.78	4	0.68	1	1.0
N ₄	5	0.33		N/A		N/A		N/A
Δ Electrolysis	6	0.26	5	0.24	5	0.24	5	0.31
Δ Reactor	7	0.18	6	0.17	6	0.17	7	0.15
W _e	8	0.14	7	0.14	8	0.13	6	0.18
P _e	9	0.11	8	0.10	8	0.10	8	0.11
P _r	10	0.11	9	0.10	9	0.10		N/A
N ₂	11	0.09	10	0.09	10	0.09	9	0.11
C _e	12	0.02	12	0.02	13	0.02	12	0.02
C _r	13	0.02	13	0.02	14	0.02	10	0.08
n _c	14	0.01	14	0.01	11	0.04		N/A
N ₃		N/A		N/A	12	0.03	11	0.04
N ₅		N/A	11	0.06		N/A		N/A
W _r	15	0.01	15	0.01	15	0.01	13	0.01

REFERENCES

1. "Closed Circuit Respiratory Systems Symposium", WADD Technical Report 60-574, August 1960.
2. Burris, W. L. and J. L. Mason, "Advanced Environmental Systems", IAS-NASA National Meeting on Manned Space Flight, St. Louis, 30 April - 2 May 1962.
3. Shearer, R. E., J. C. King and J. W. Mausteller, "Electrochemical Recovery of Breathing Oxygen for Carbon Dioxide", Paper presented at Aerospace Medical Association Meeting, Chicago, April 1961.
4. Rossini, F. D., D. D. Wagman, W. H. Evans, S. Levine, and I. Jaffee, "Selected Values of Chemical Thermodynamic Properties", U. S. Department of Commerce, N. B. S. Circular 500, July 1961 printing.
5. Del Duca, M. G., R. G. Huebscher, and A. E. Robertson, "Regenerative Environmental Control Systems for Manned Earth-Lunar Spacecraft", Paper presented at the IAS 1962 National Meeting, St. Louis, 30 April - 2 May 1962.
6. Foster, J. F. and J. S. McNulty, "Study of a Carbon Dioxide Reduction System", Aeronautical Systems Division, TR 61-388, August 1961.
7. King, Lowell A., 1/Lt, USAF, "The Mechanism of Some Chemical Reactions Occurring Under the Action of Ionizing Radiation", WADC Technical Note 58-146, February 1959. (Translation from an article of the same title by Dmitriev, M. T. and S. Ya. Pschezhetskii, Uspekhi Khimii, XXVI, 725, 1957.)
8. Chandler, H. W. and W. Oser, "Study of Electrolytic Reduction of Carbon Dioxide", Aerospace Medical Research Laboratories, MRL-TDR-62-16, March 1962.
9. McDowell, M. E., E. M. Nevels and Richard C. Powell, "Algae Feeding in Humans", Journal of Nutrition, 75:61.
10. "The Engineering Biotechnology of Handling Wastes Resulting from a Closed Ecological System", New York University, AFOSR Report No. TR58-148, December 1958.
11. Bass, W. A. and R. W. McJones, "Dynamic Engines Versus Fuel Cells for Space Power Systems", IAS Paper No. 62-119, June 1962.
12. Dole, S. H. and R. A. Tamplin, "The Sebatier Reaction for Inorganic Recovery of Oxygen in Manned Space Capsules", Closed Circuit Respiratory Systems Symposium, WADD TR 60-574, August 1960.

13. Weller, S. M., "Oxygen Recovery from Carbon Dioxide", Closed Circuit Respiratory Symposium, WADD TR 60-574, August 1960.
14. Del Duca, M. G., A. D. Babinsky, and F. D. Miraldi, "Selected Methods for Atmospheric Control in Manned Space Flights", 1961 SAE Aeronautic Meeting, New York, Paper No. 352C, 1961.
15. Foster, J. F. and J. S. McNulty, "Hydrogen Reduction of Carbon Dioxide to Elementary Carbon", Closed Circuit Respiratory Systems Symposium, WADD TR 60-574, August 1960.
16. Bambenek, R. A., R. B. Neveril, G. A. Remus and J. D. Zeff, "Carbon Dioxide Reduction System", Preprint of Aerospace Medical Report, prepared under Contract No. AF33(616)-8223, September 1962.
17. Coe, C. S. and J. Rousseau, personal communication, AiResearch Manufacturing Corporation, October 1962.
18. Coe, C. S., J. Rousseau, and A. Shaffer, "Analytical Methods for Space Vehicle Atmospheric Control Processes", ASD-TR-61-162, Part II, November 1962.
19. Clifford, J., J. Gates, J. McCallum and C. Faust, "Research on the Electrolysis of Water Under Weightless Conditions", MRL-TDR-62-44, May 1962.
20. Czuha, M., J. H. Bochinsky, and K. W. Gardiner, "Process for Concentration and Decomposition of Water", Closed Circuit Respiratory Systems Symposium, WADD TR 60-574, August 1960.

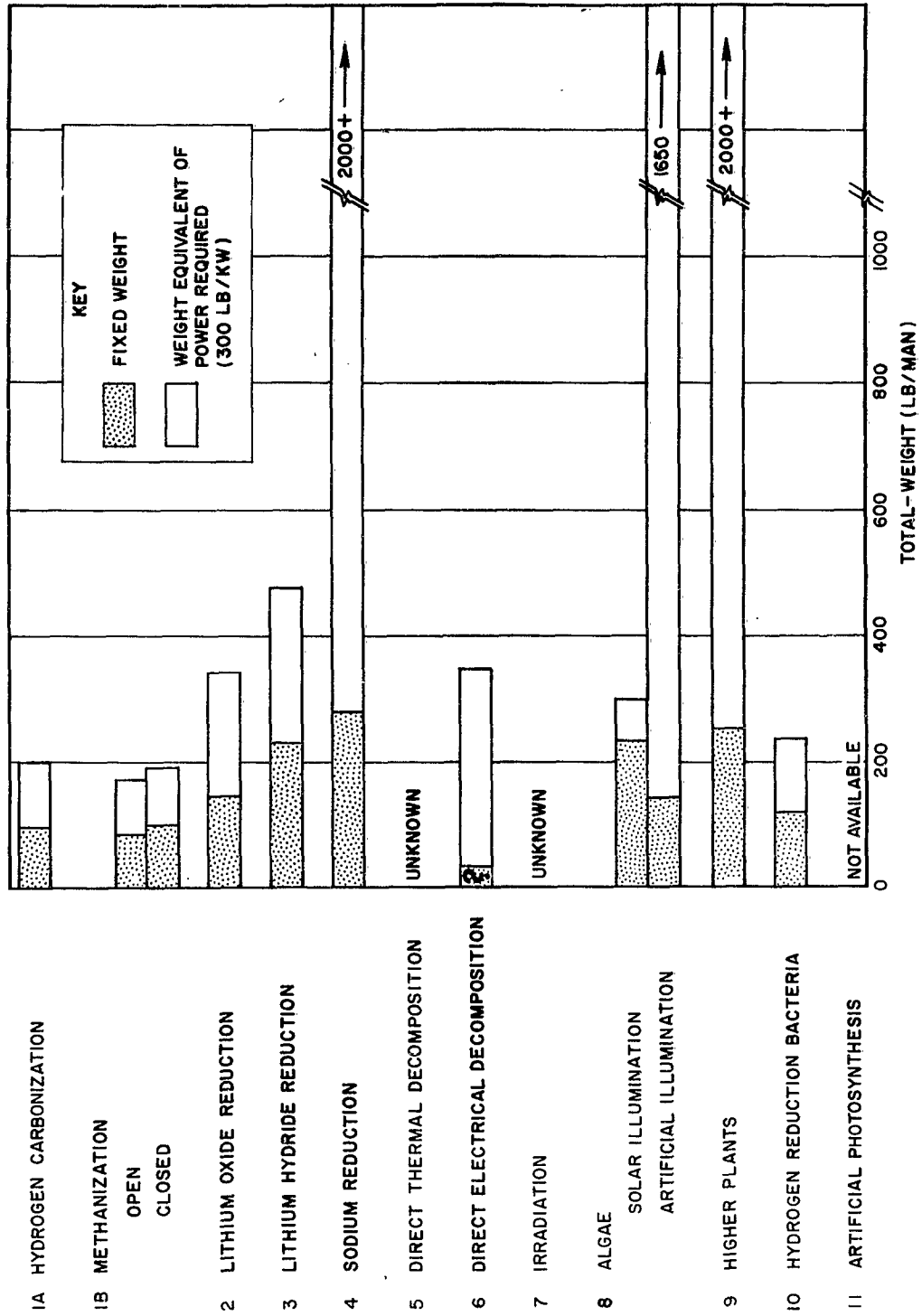


FIGURE I COMPARISON OF REGENERATIVE ATMOSPHERIC CONTROL SYSTEMS

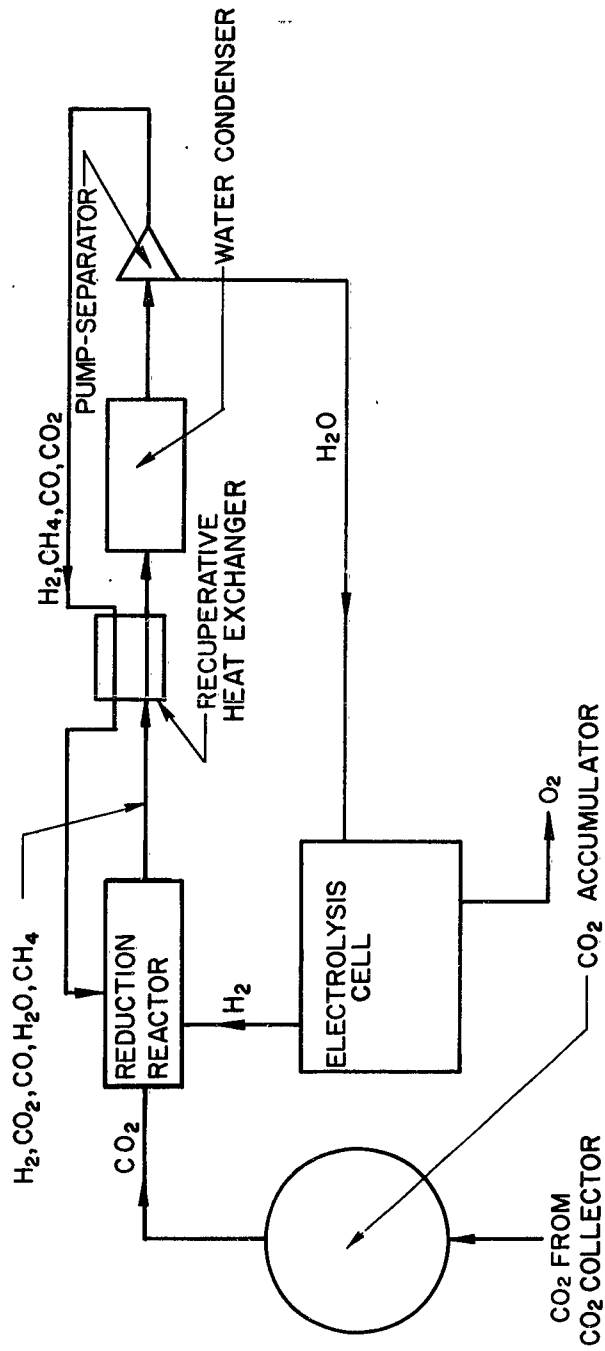


FIGURE 2 HYDROGEN CARBONIZATION ATMOSPHERIC REGENERATION SYSTEM

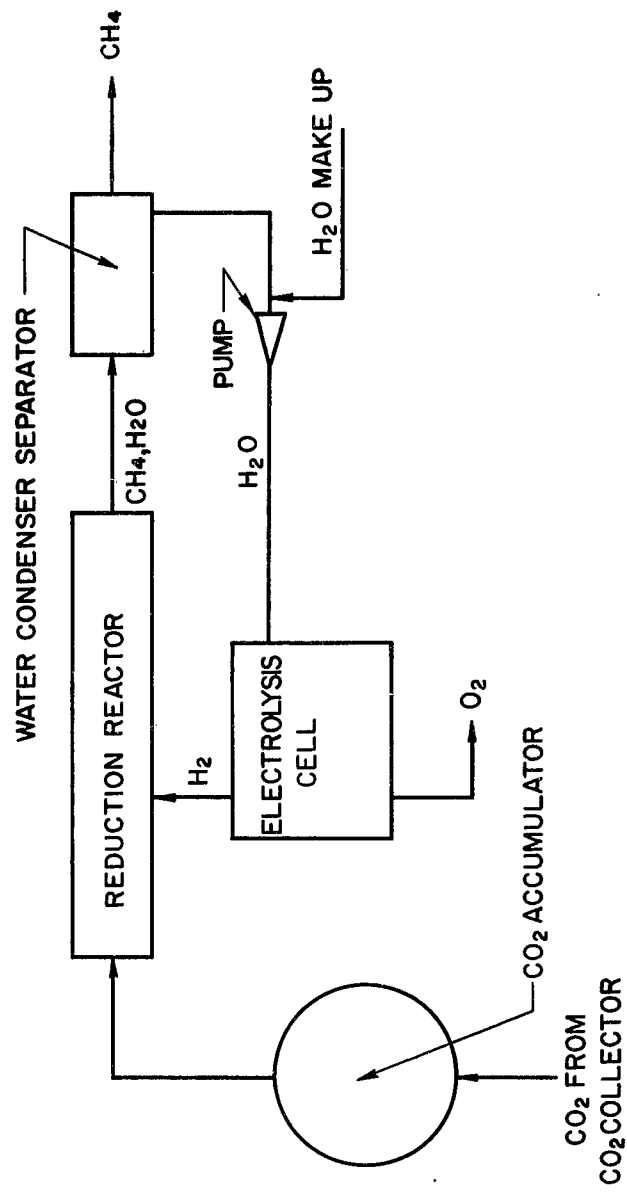


FIGURE 3 METHANIZATION ATMOSPHERIC REGENERATION SYSTEM

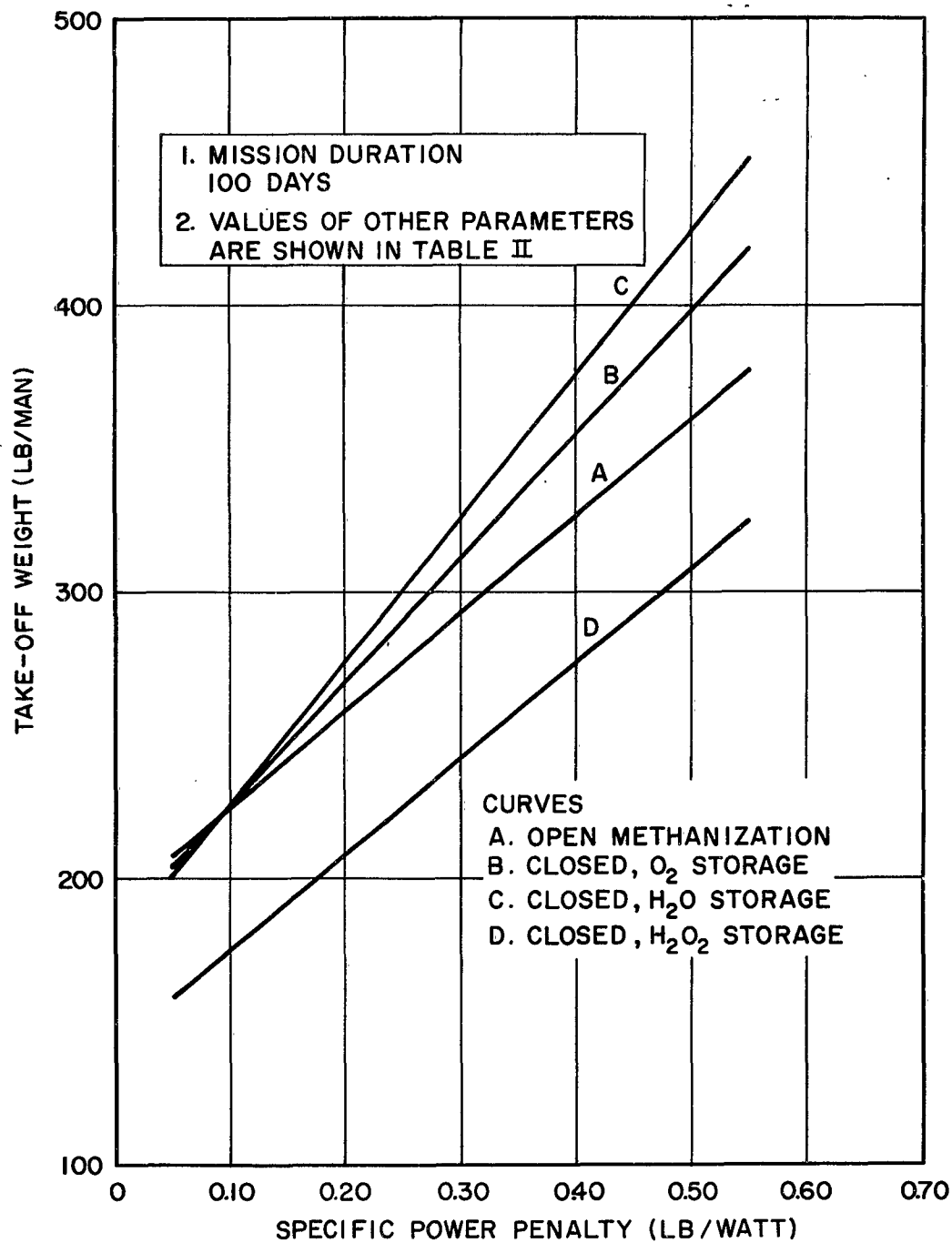


FIGURE 4 ATMOSPHERIC REGENERATION SYSTEMS' PENALTY VS SPECIFIC POWER PENALTY

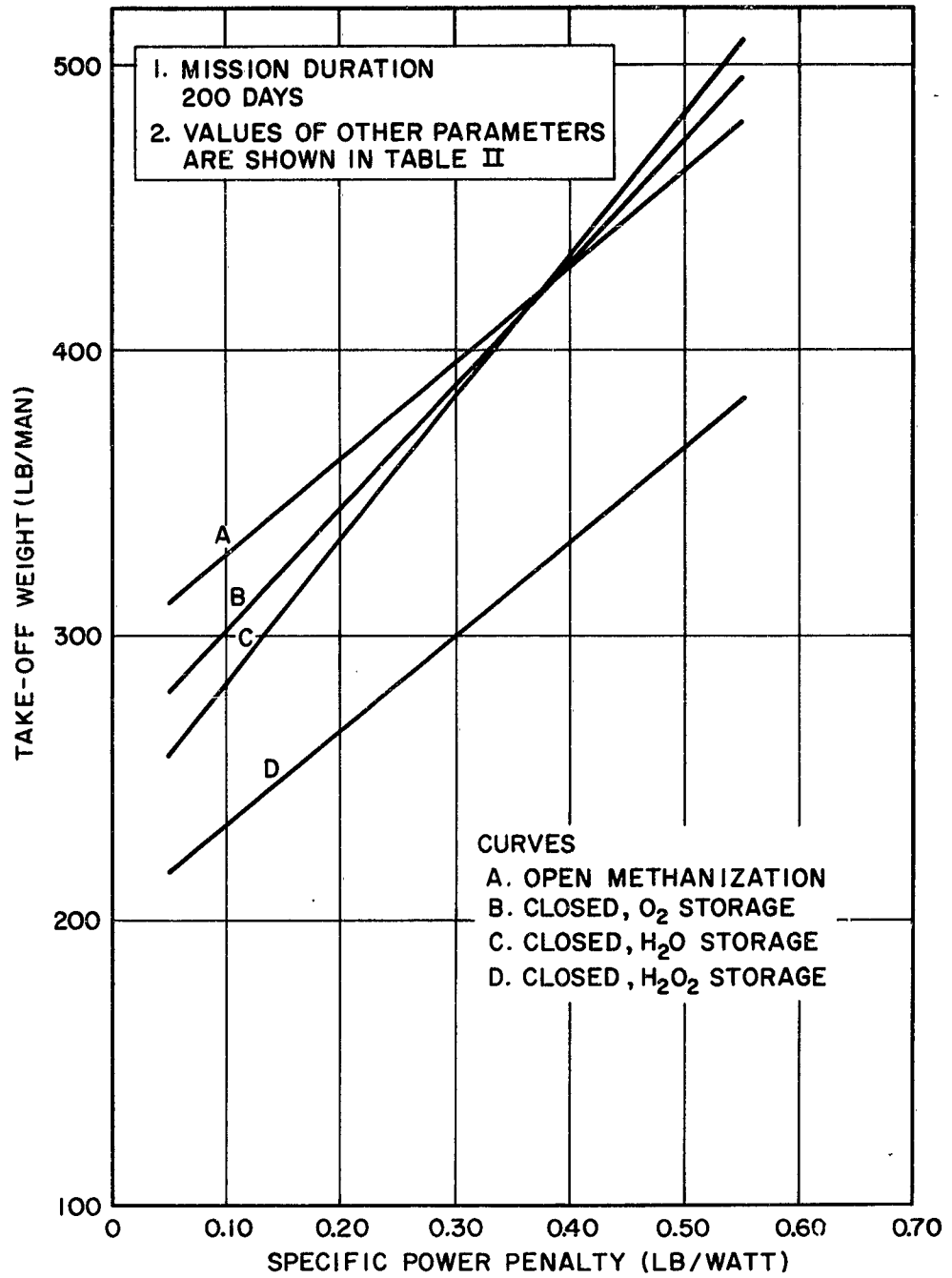


FIGURE 5 ATMOSPHERIC REGENERATION SYSTEMS' PENALTY VS SPECIFIC POWER PENALTY

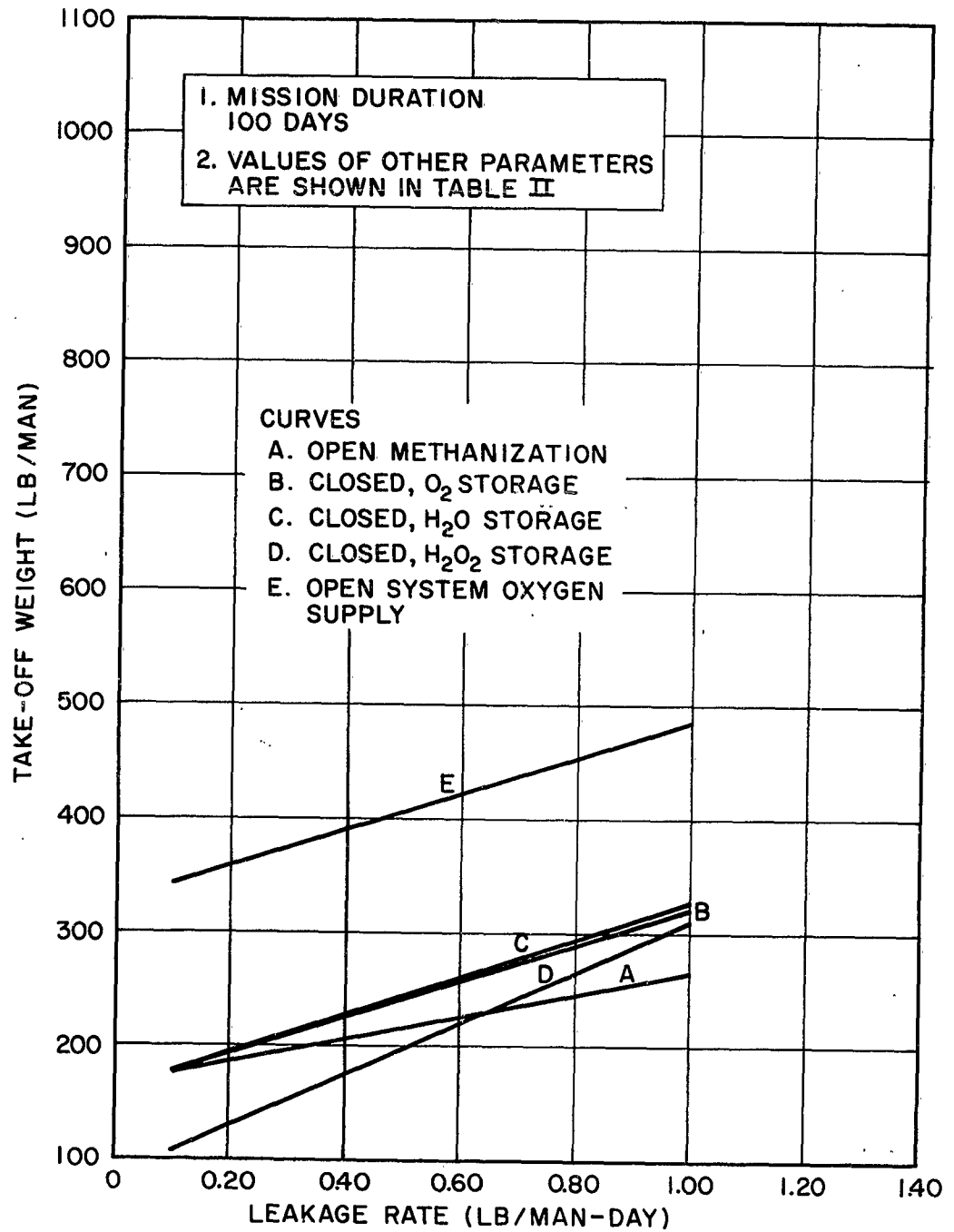


FIGURE 6 ATMOSPHERIC REGENERATION SYSTEMS' PENALTY
VS LEAKAGE RATE

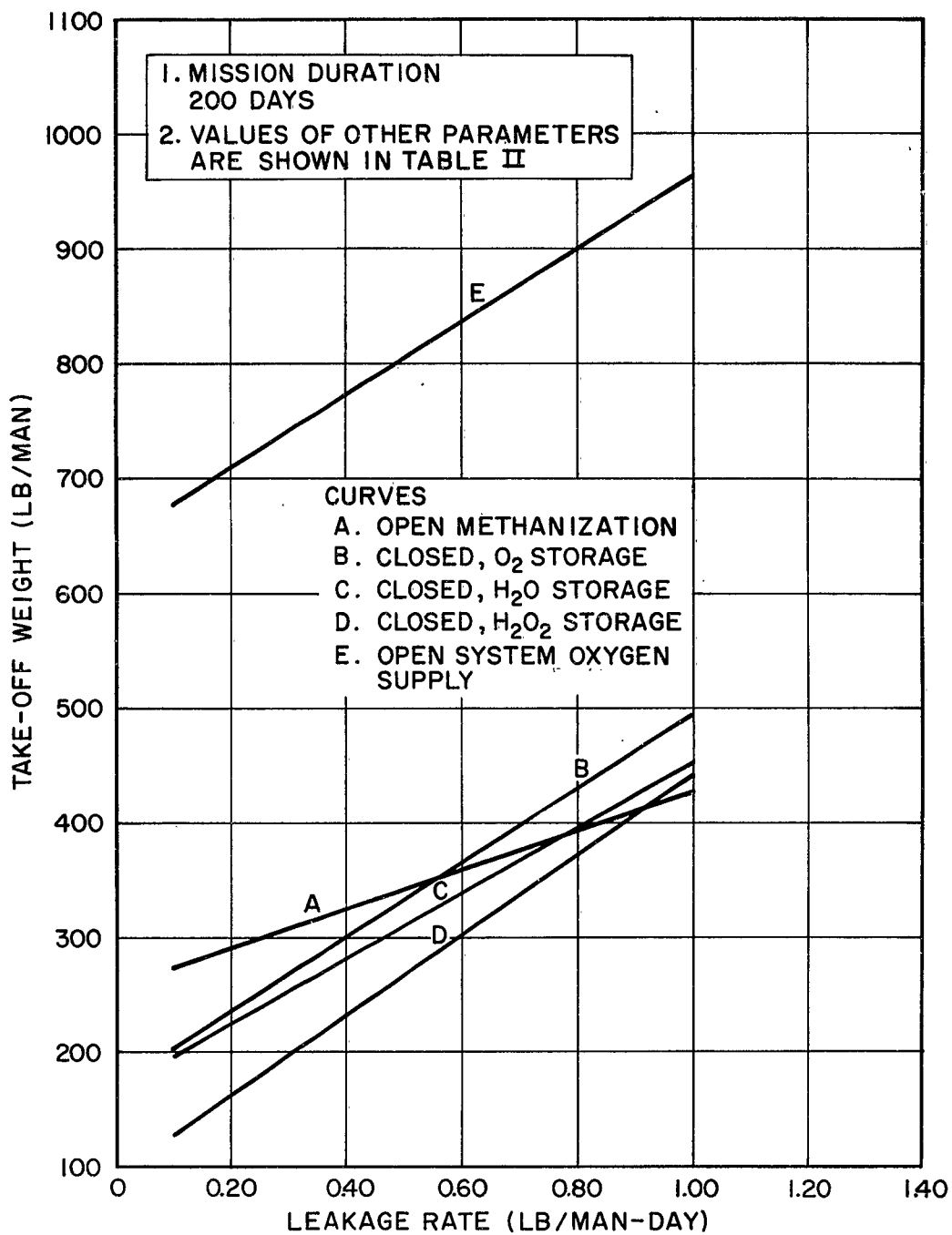


FIGURE 7 ATMOSPHERIC REGENERATION SYSTEMS' PENALTY VS LEAKAGE RATE

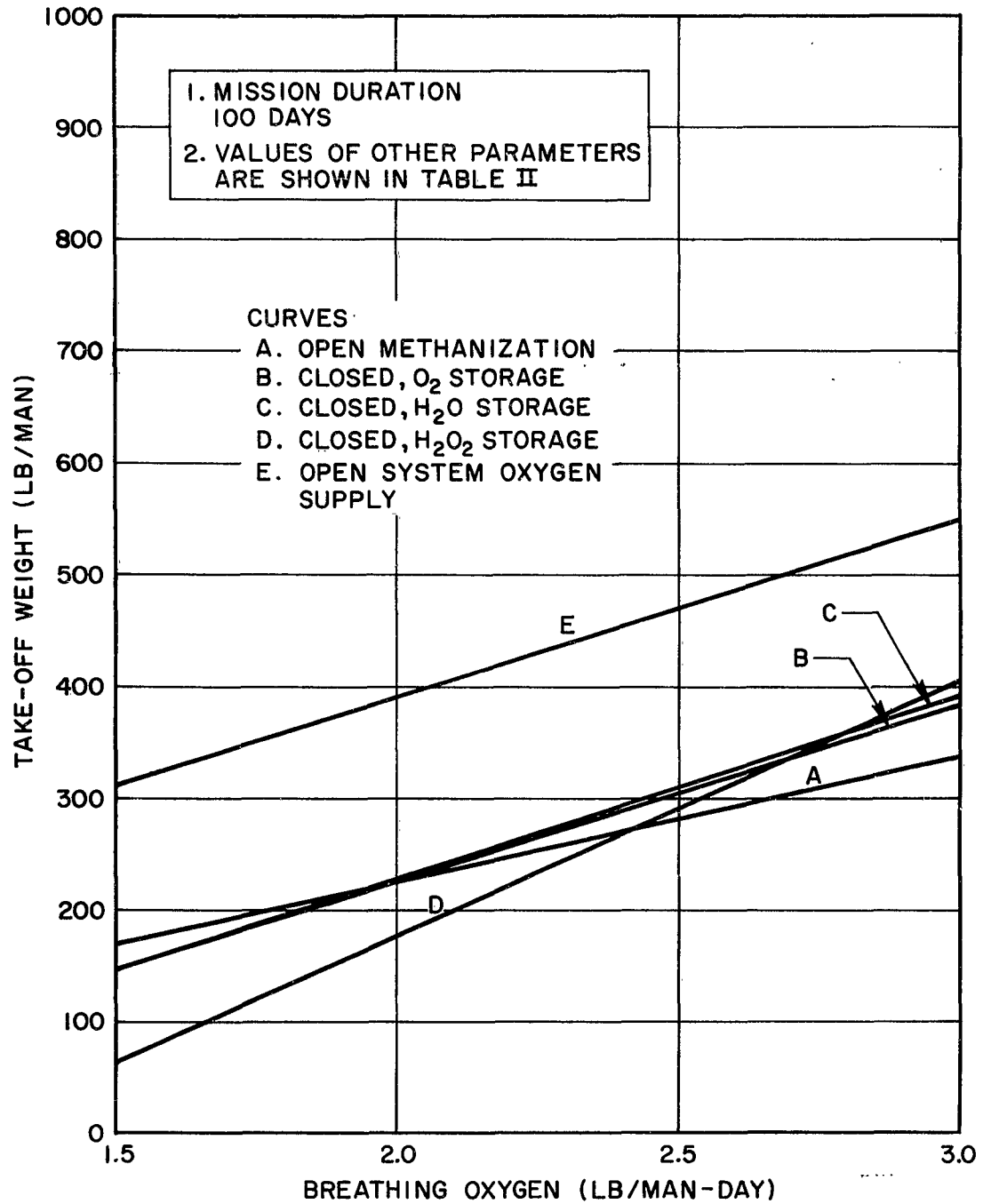
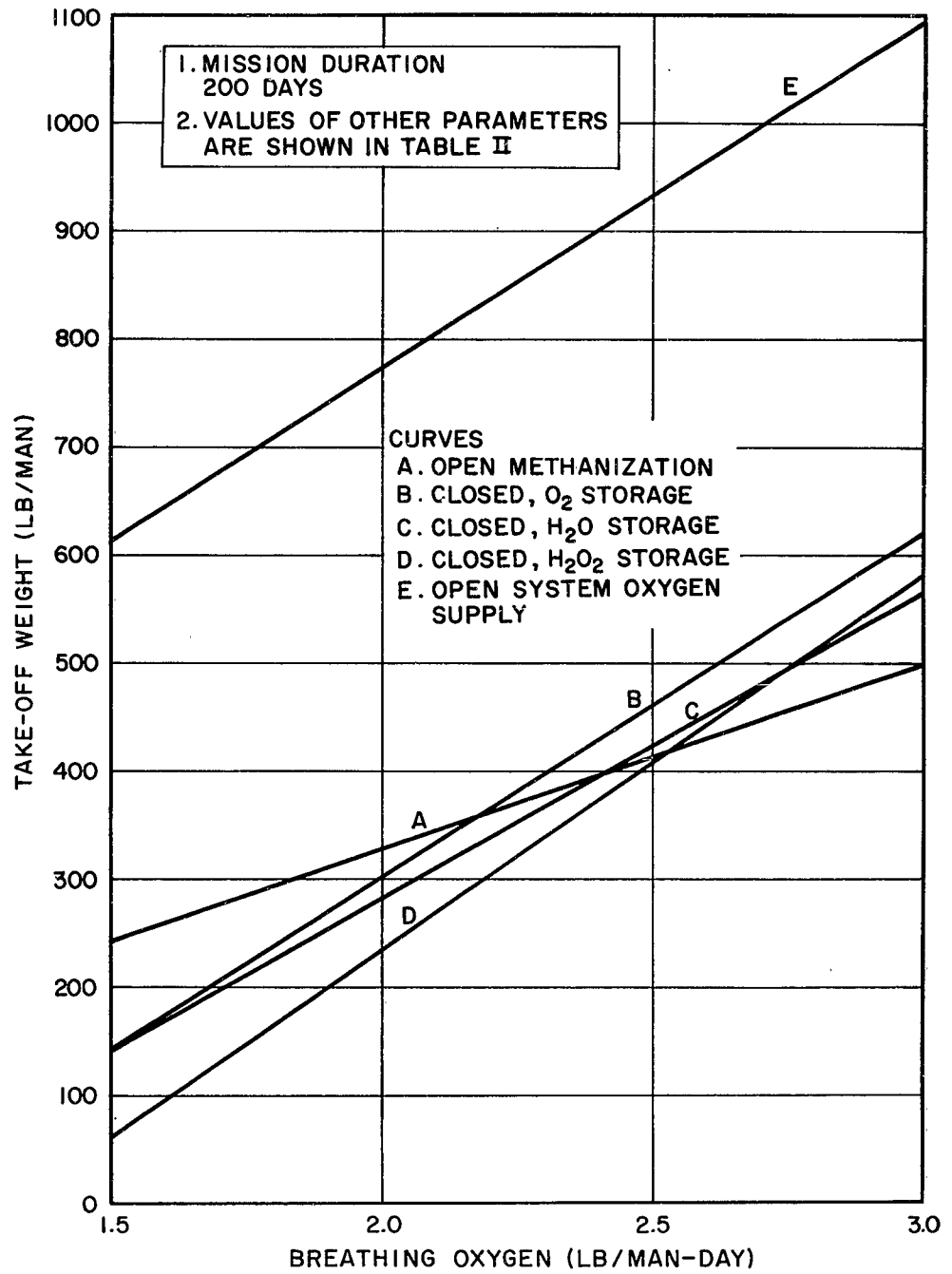


FIGURE 8 ATMOSPHERIC REGENERATION SYSTEMS' PENALTY VS BREATHING RATE



**FIGURE 9 ATMOSPHERIC REGENERATION SYSTEMS' PENALTY
VS BREATHING RATE**

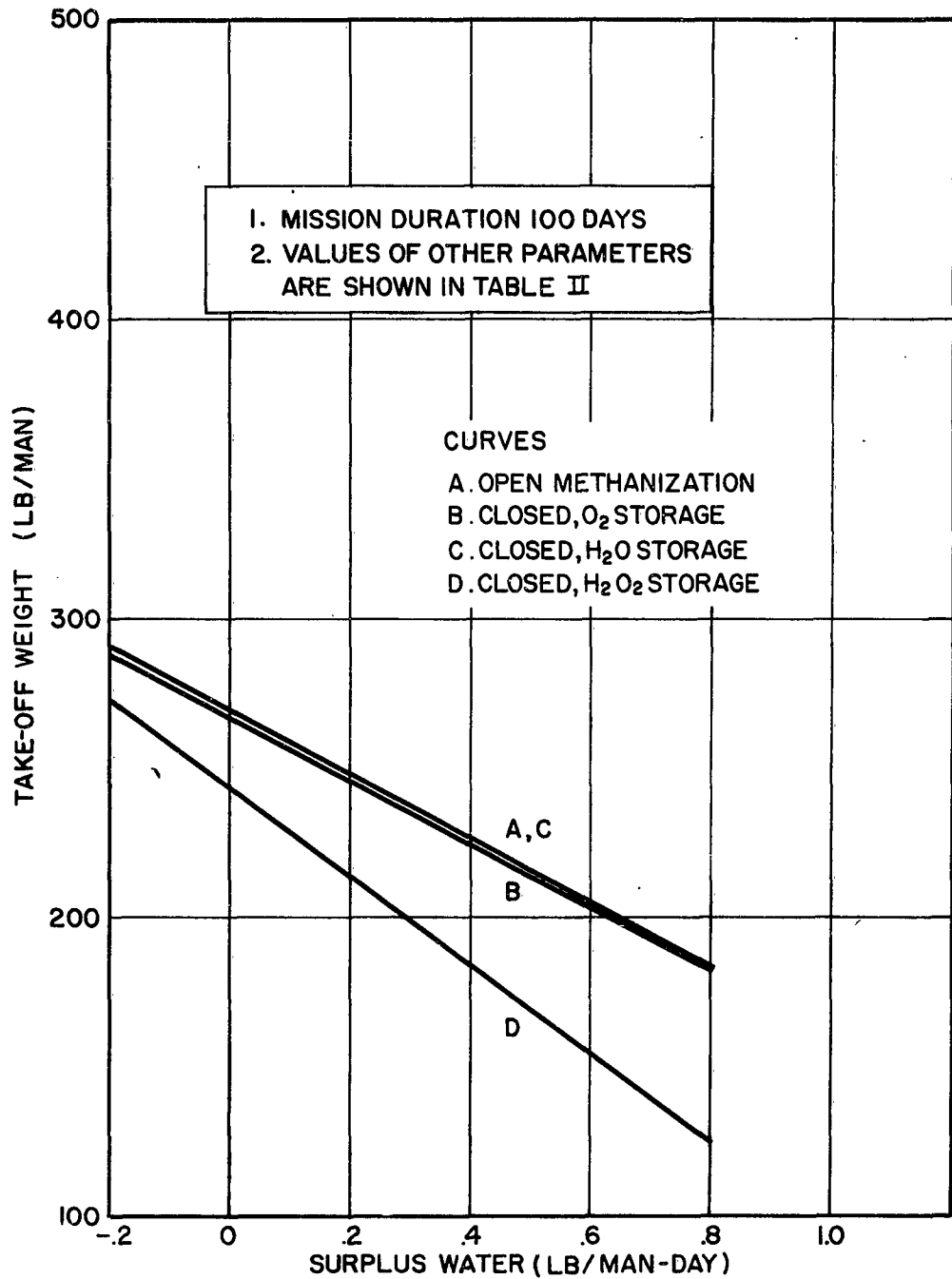


FIGURE 10 ATMOSPHERIC REGENERATION SYSTEMS' PENALTY VS SURPLUS WATER AVAILABILITY

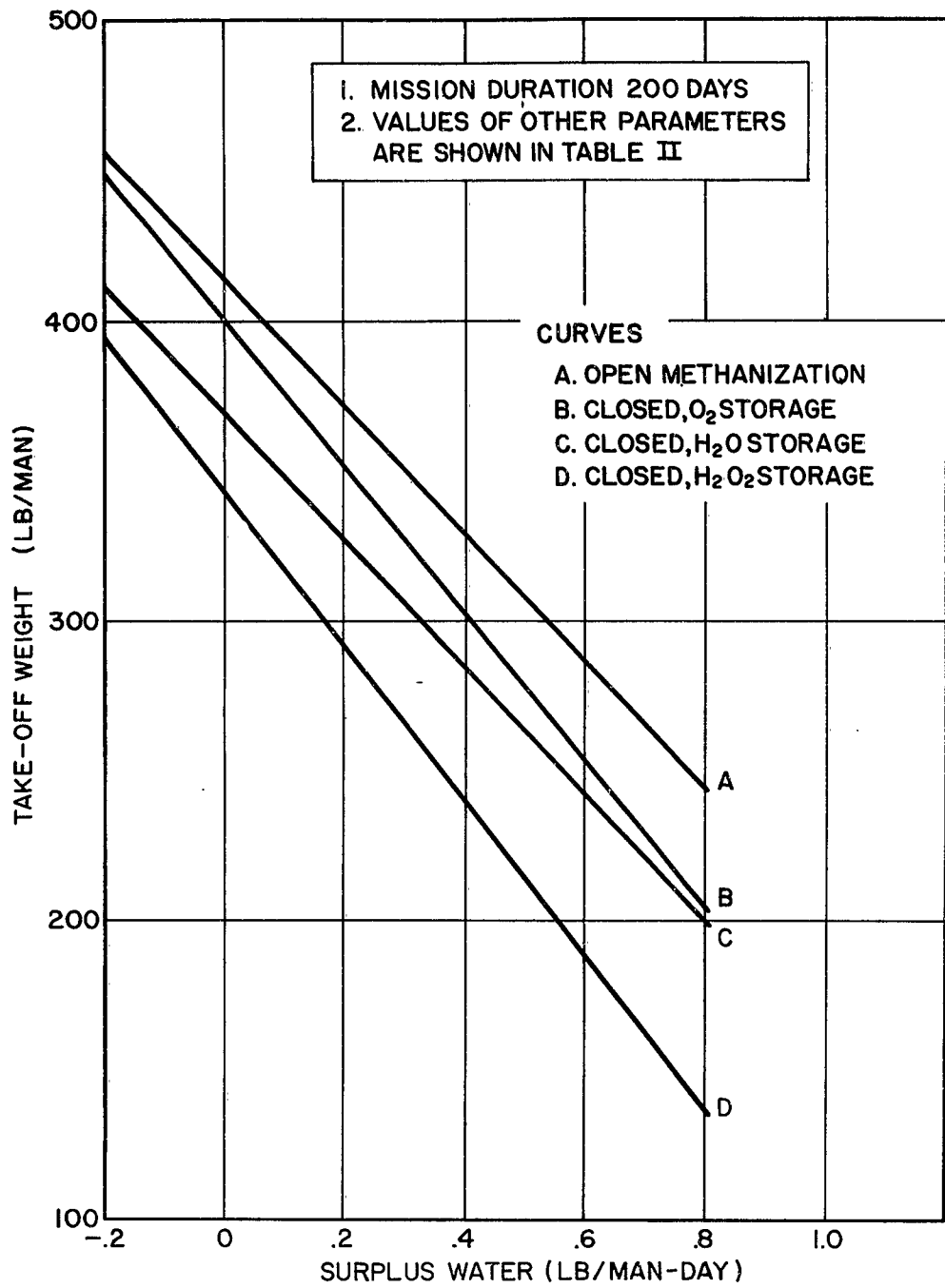


FIGURE II ATMOSPHERIC REGENERATION SYSTEMS' PENALTY VS SURPLUS WATER AVAILABILITY

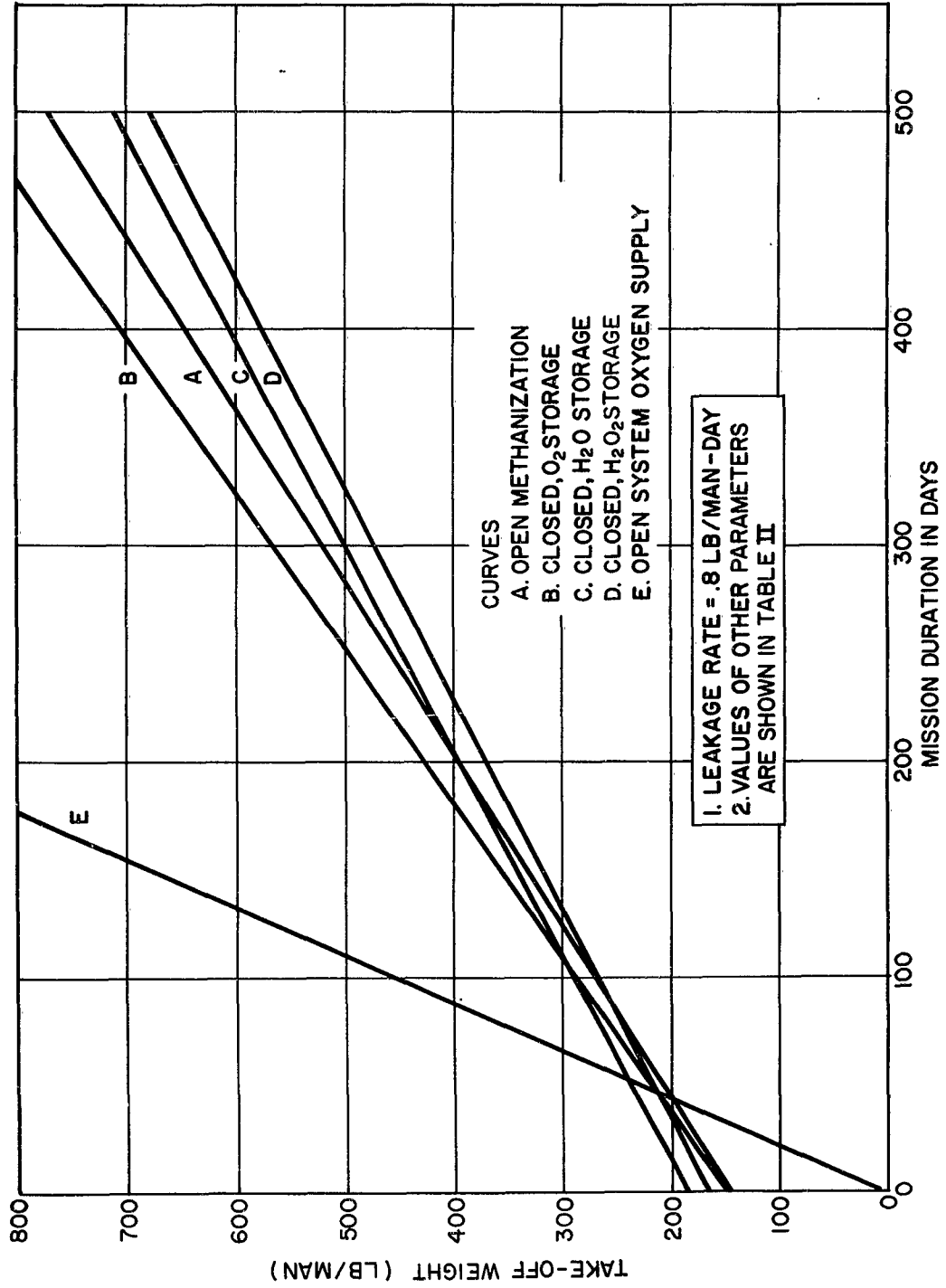


FIGURE 12 ATMOSPHERIC REGENERATION SYSTEMS' PENALTY VS MISSION DURATION

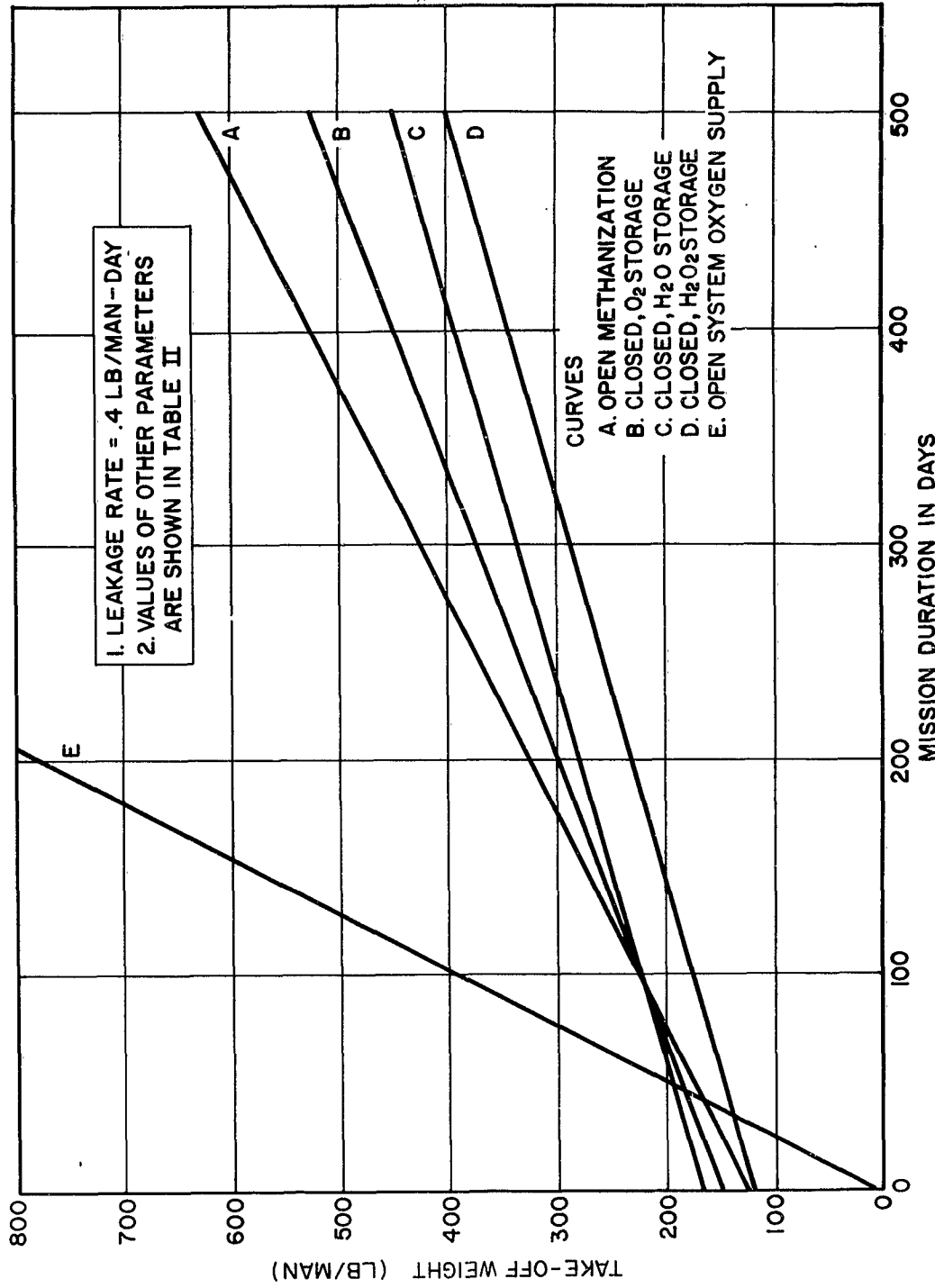


FIGURE 13 ATMOSPHERIC REGENERATION SYSTEMS' PENALTY VS MISSION DURATION

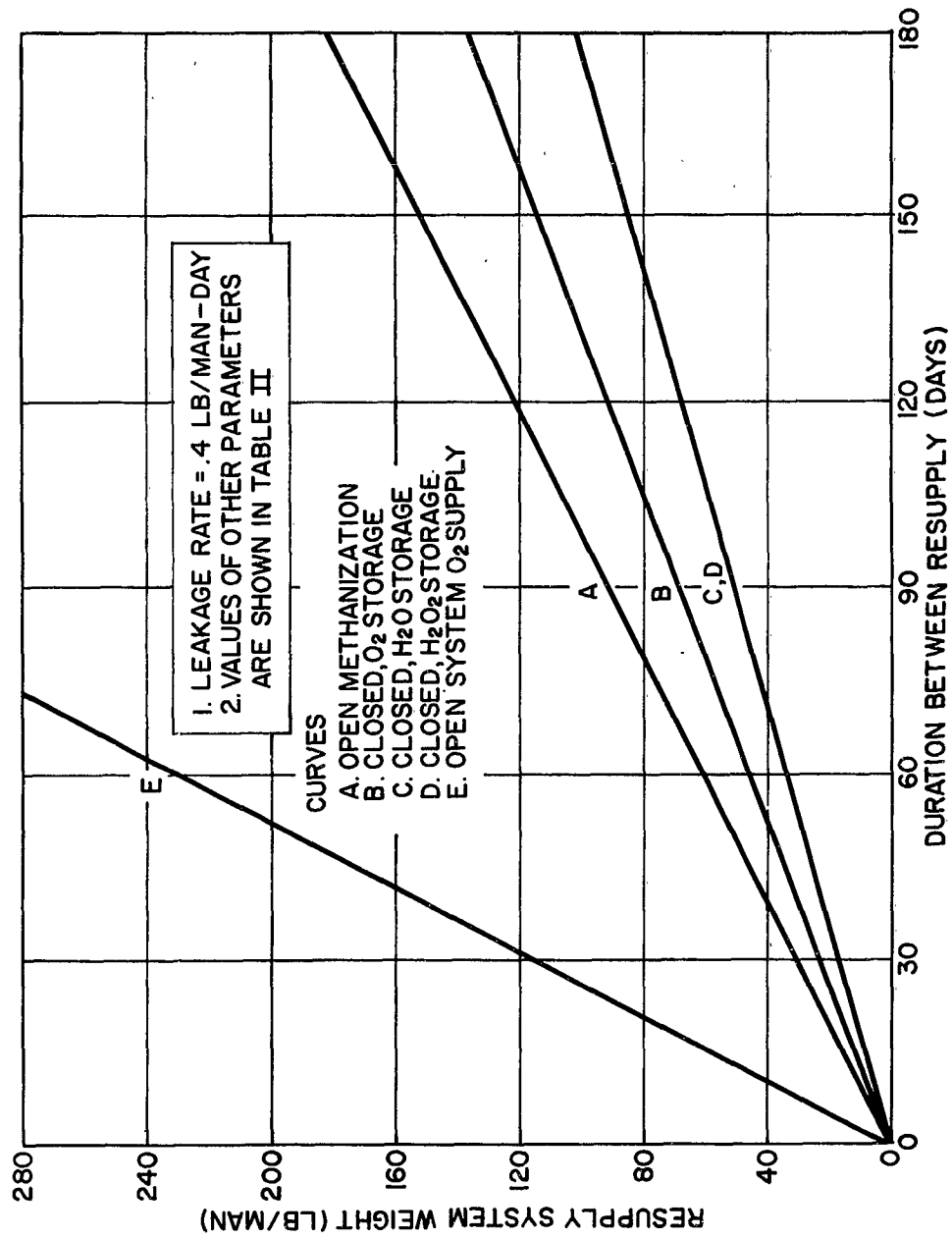


FIGURE 14 RESUPPLY SYSTEM WEIGHT VS DURATION BETWEEN RESUPPLY

Fourth Paper -- "The Application of Chemically Regenerative Atmospheric Control Systems," by J.G. Krisilas & J.W. Smylie, Aerospace Corp. (Presented by J.G. Krisilas)

QUESTION: (McDonnell Aircraft) Please elaborate on the CO₂ collection technique with regard to weight and power penalty.

ANSWER : (Mr. Krisilas) I presume he is referring to a molecular sieve and again I must say that it is dependent upon a number of variables such as total pressures, CO₂ partial pressure, whether waste heat is available, recycle times, and what have you. So you can't be definitive as far as giving specific values. I would suggest that there are numerous references, and we had used in our preliminary designs the conservative values of 40 pounds per man and a hundred watts per man, but this is a little heavy because, as I say, we base this on our recycling time of two or three hours, kept down the power consumption.

QUESTION: (McDonnell Aircraft) Also, what is the effect of introducing impurities, CO₂ et cetera into the system?

ANSWER : (Mr. Krisilas) Mr. Remus answered this very nicely, so it saves me the trouble.

QUESTION: (Mr. Zeff, General American Transportation Co.) Who has been doing work on magnesium oxide, and what are the results that have been attained?

ANSWER : (Mr. Krisilas) No one. We came across this material in the T&A Study I believe that AiResearch put together. We went through the chemistry books and this one seemed very promising--it is a very stable compound. It has the ability to remove 1.09 lb CO₂ per pound of material.

It does react with water but this only enhances the CO₂ capability. It seems that it may be possible to absorb moisture plus CO₂. There is a 300 degree difference in the temperature of getting rid of the water versus CO₂, or even you can condense out the water simultaneously. It seems there is no agreement in the literature as to what is the decomposition temperature. It seems to start at 500 degrees, and we imposed this as a fairly good candidate, and I think that work should be done on this. I was going to ask Mr. Coe if AiResearch was doing any experimental work in whipping these?

(Mr. Coe) We have started some experimental work on magnesium oxide. We find that it looks to us right now that the difficulty is similar to that of silver oxide attaining a rapid efficient reaction at low computation of magnesium oxide or hydroxide with a one per cent concentration. That is quite slow. To me at the present time it seems to be a problem and has to be studied in more detail.

QUESTION: (Mr. Krisilas) Will you be continuing experimental work on magnesium oxide?

ANSWER : (Mr. Coe) Yes.

QUESTION: (Mr. W. Seigler, Research Lab, United Aircraft) Would you expand on the inefficiency of a few salts added to reduction systems?

ANSWER : (Mr. Krisilas) I presume he means sodium reaction, perhaps lithium hydroxide. I think the first step is to look at the energies that are required, and they do come out to be greater than what is required for water electrolysis. There is a four or five step procedure required with sodium, just to go through a few briefly, you start with the sodium, CO₂, and you end up with sodium monoxide plus carbon; sodium monoxide with water you get sodium hydroxide;

water plus oxygen--you have to electrolyze the sodium hydroxide, so it is a rather complicated procedure and there hasn't really been enough work to assess or assign efficiencies, but it seems that because of the exotic materials involved, the high temperatures, the complicated control systems, and the many cycles, et cetera, it seems rather doubtful that this would lend itself to space borne systems.

QUESTION: (Mr. E.G. Koepnick, ASD) In producing your weight penalty curve for open and closed control systems, did you weigh up the systems as to comparable reliability and safety?

ANSWER : (Mr. Krisilas) The answer is yes. What else can you say?

**PHOTOCHEMICAL REACTIONS SIGNIFICANT IN
ATMOSPHERE REGENERATION PROCESSES**

by

Dr. J. P. Allen

**Aeronautical Systems Division
Wright-Patterson Air Force Base, Ohio**

PHOTOCHEMICAL REACTIONS SIGNIFICANT IN ATMOSPHERE
REGENERATION PROCESSES

by

John P. Allen, Ph.D.

Introduction -

Manned spacecraft require a defined atmosphere to provide for man's physical well being in adequately performing his space mission functions. This atmosphere will be altered by man's metabolism and his equipment operation such that replenishment will become necessary. He can replenish his atmosphere from stored supplies. However, he also can use various methods to modify the atmosphere to remove undesirable gases and to generate desirable ones. These methods introduce the concept of regeneration of gaseous constituents and the re-use of on-board materials. The regenerative methods allow attractive tradeoff in weight and volume of on-board supplies when long space missions are planned.

Among the first methods suggested for atmosphere regeneration was that of an algal system for carbon dioxide removal and of oxygen replenishment. This concept is more than adequate as evident by our abundant oxygen supply in the atmosphere. However, when considering a limited volume of gas with an isolated algal culture as the working unit, the problems multiply. The reliability of a single biological unit operating on a time defined demand schedule was affected by many factors. Nature provided countless duplications for our working unit with a virtually unlimited gas working volume. Photosynthetic gas exchangers constituted initial attempts to adapt a natural process for atmosphere control.

In a discussion of the photochemical reactions of significance in atmosphere control processes, we can evaluate in some detail the extent of the effort with algal systems, or more specifically with green-plant photosynthesis. The processes in photosynthetic bacteria are comparable to those in green plants but differ in that free oxygen is not produced. Aside from the pigment catalyzed photosynthetic reactions in living cells, photochemical reactions among and between the constituents of a contained atmosphere are directly applicable in a critical evaluation of control processes and must be considered in atmosphere regeneration concepts.

Photochemical Reaction Characteristics -

In considering what makes photochemical reactions adaptable to the utilization of light energy for atmosphere regenerative techniques, we find that these reactions can be characterized as in the introduction of the symposium on Photochemistry in the Liquid and Solid States (1) as follows: The reaction must be endothermic, reasonably fast, reversible with a large amount of energy stored and active over the visible light range. These characterizations are directly applicable to green plant photosynthesis.

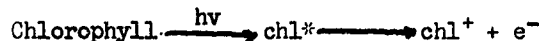
Of the many possible photochemical reactions occurring with light energy activation, the range covers simple inorganic reactions such as the reaction of

hydrogen and chlorine forming hydrogen chloride, the reversible dissociation of iodine to iodine atoms, the breakdown of silver bromide to silver and bromide ions which subsequently re-unite, giving off chemical energy. The breakdown of metallic oxides and of hydrates by light energy also serves to store energy and subsequently to give off the energy in reverting back to their original states.

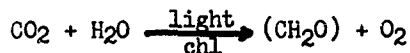
Photoelectric effects as in the photovoltaic cell and the photogalvanic cell are examples of direct conversions of light energy to electric energy. Here in part may also lie the principle effective in the green plant and bacterial photosynthesis and which is significant to the atmosphere control requirements of man in a space vehicle cabin. The photosensitive agent, the pigment chlorophyll (in bacteria, bacterio-chlorophyll) becomes chemically reactive and produces a reducing capacity. This could be ions, electrons, or reactive radicals. The electron production concept is supported by the photoelectric effects described with films of chlorophyll in which electron flow was detected and measured in microamperes (2).

Green Plant Photochemical Systems:

In green plants, chlorophyll becomes light energized and "emits" a working electron which induces a series of reduction-oxidation reactions. The activation can be indicated as follows:



The associated effect is production of a "hole" or electron acceptor which accepts electrons from oxidation-reduction intermediates. Oxygen is evolved in the initial activation process and carbon dioxide is incorporated subsequently in the chain of reactions. The reaction is stated in as general terms as possible so that the many variations of experimental conditions can be given evaluation as to the possible course of action. The general formula for photosynthesis presents the desired end products and indicates a technique for carbon dioxide removal. The reaction can be stated as follows:



A great deal of work on chlorophyll energized photochemical reactions has been done with some species of the alga *Chlorella* and with spinach chloroplasts. Both materials have proven satisfactory for chlorophyll studies that provided information to aid in constructing theories of how these processes occur. The chlorophyll molecule becomes activated in the visible portion of the spectrum, whereas infra red and ultraviolet light showed only slight activation. Accessory pigments such as carotenoids can also become energized in the visible range and may transmit their energized states to chlorophyll.

Another effect is the semi-conductor property of chlorophyll wherein a film of chlorophyll deposited from alcoholic solution shows an induced current flow when irradiated. The opposite effect has not as yet been mentioned where chemical activation of chlorophyll can be induced by passage of an electric

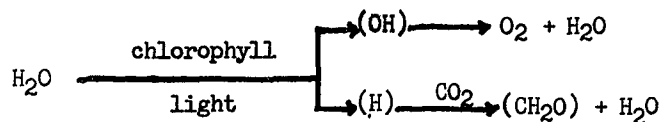
current or the effects of an electric field. The photo-induced chemical activity of chlorophyll is evident by free radical formation and by the detection of electric currents due to electron displacement.

In applying the photosynthesis process for atmosphere regeneration, one must consider the oxygen evolution and the carbon dioxide absorption characteristics as the significant criteria. Photosynthesis accomplishes this gas exchange function at room temperature. Information on oxygen production and evolution, however, is still hypothetical with unknown or rather postulated steps of reaction. X and Y concepts are still used to define the reactive compounds in stepwise reactions. Cytochrome f is hypothesized as the Y factor in oxygen evolution but experimental verification is still lacking. For the X concept, the role of triphosphopyridine nucleotide as the hydrogen acceptor or electron acceptor is receiving experimental support (3). However, an iron containing protein called ferredoxin has recently been postulated as an electron carrier from chlorophyll to triphosphopyridine nucleotide.

The photolysis of water is the core of the chlorophyll role in photosynthesis. If this photolysis does not occur, the associated reaction of oxygen evolution stops. Other photoeffects such as photophosphorylation and photoreduction occur independently of the photolysis of water. These effects are related to the oxygen and the carbon dioxide exchange in that they provide the intermediate reactive compounds upon which the carbon dioxide binding reactions depend. The concept of photosynthesis is that of a metabolic process of inter-related reactions such that the sequence of the entire process could be disrupted at any reaction site. The photolysis of water yields the hydrogen for the carbon dioxide reduction sequence of reactions and the oxygen from the hydroxyl for the free oxygen evolved.

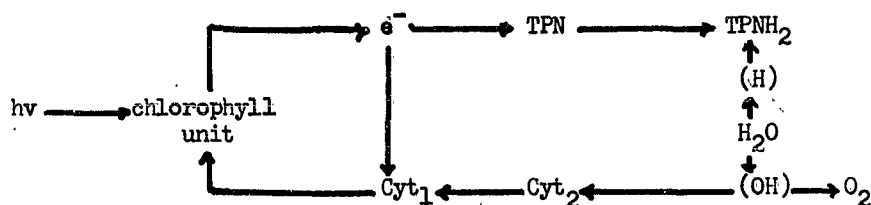
Since the reaction steps of the photolysis of water have not been fully detailed, the true association of chlorophyll and water is unresolved. A hydration effect of chlorophyll on carbons 9 and 10 in Ring V of the molecule has been hypothesized as the site for the further reaction of the photoactivated chlorophyll with the X and Y factors. However, the supporting evidence as yet is lacking.

The energy requirement for oxygen evolution has been given anywhere from 2 to 12 quanta of light energy. This energy is considered adequate for activation of the chlorophyll unit so that an energized state does exist. The initial activation of chlorophyll induces free electrons. In general the initial reaction in accordance with van Neil's concept occurs as follows:



However, this concept doesn't reveal some of the finer steps in the overall reaction.

Arnon presented the following scheme of the light activated processes:

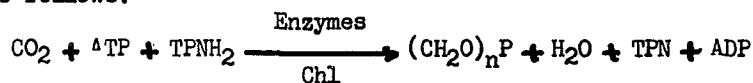


A proposal was presented by Calvin (4) for the formation of an acceptor site and a donor site in a photosynthetic unit having two active pigments. The electrons serve to induce reduction of triphosphopyridine nucleotide with water serving as the source of the hydrogen. The acceptor site serves to accept electrons, probably from a cytochrome pigment associated with the chlorophyll system.

Carbon Dioxide Fixation in Green Plant Photosynthesis -

The carbon dioxide binding portion of photosynthesis though not directly involved in a photochemical reaction depends indirectly upon photochemically activated or produced compounds. The compound that reacts with carbon dioxide has been shown to be ribulose diphosphate. A cycle of the carbon pathway in photosynthesis has been presented by Bassham (5) and shows interactions of enzymes and monosaccharides such that ribulose 1-5 diphosphate is regenerated and the carbon dioxide leaves the cycle as sucrose. The relationship of this carbon dioxide cycle with the photochemistry of chlorophyll is shown to be that of photophosphorylation of adenosine diphosphate and the reduction of triphosphopyridine nucleotide. A rather high phosphorylation rate of 3 adenosine triphosphate molecules per molecule of carbon dioxide reduced is required to support the ribulose diphosphate cycle. This high rate would suggest an alternate carbon path using an activated 2-carbon compound to unite with the carbon dioxide to form the phosphoglyceric acid which is the first product identified upon short time illumination experiments with radio active carbon dioxide. This latter scheme would propose a photoreduction of some precursor to phosphoglyceric acid.

The incorporation of carbon dioxide into the ribulose molecule requires the enzymes carboxydismutase and ribulose diphosphate carboxylase. These are associated in plants with the chloroplasts and tend to disappear when conditions are unfavorable for development of green plastids. The net synthesis of carbohydrate from carbon dioxide occurs in the presence of adenosine triphosphate, reduced triphosphopyridine nucleotide and an array of enzymes (carboxylase, kinase, isomerase, epimerase, dehydrogenase, transketolase, transaldolase and aldolase) which are associated with the chloroplast. This reaction can be visualized as follows:



Photosynthetic Bacteria -

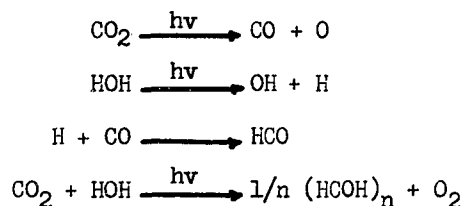
A bacterial photochemical system utilizing the photosensitive pigment bacteriochlorophyll occurs in Rhodospirillum rubrum, in which a photochemically

induced series of oxidation and reduction reactions occur. The photoreactions of the chromatophores of R. rubrum are generally characterized as parallel with those of chloroplasts. The pertinent reaction here is the formation of reduced diphosphopyridine nucleotide which is effective in the carbon dioxide reduction chain of reactions. In this chain of reactions hydrogen and carbon dioxide provide the basic materials for the synthesis of cellular material with light as the energy source. The activation light for the reaction is in the near infra red just beyond the photoactivation range of the green plant chlorophyll. Organic compounds or inorganic hydrogen containing compounds can serve as the hydrogen source. No oxygen production has as yet been demonstrated for bacterial photoreactions but carbon dioxide reduction has been fully substantiated.

Bacterial photosynthesis applies to atmosphere regeneration in that a low concentration carbon dioxide absorber is present and a source of water results from the metabolic process in the bacteria. The disadvantage of using a bacterial system lies primarily in the mass of bacterial cells which accumulate from assimilated carbon dioxide.

Photochemical Reactions of Carbon Dioxide and Water -

The two constituents in an enclosed atmosphere for a manned space cabin system which contain most of the original oxygen after man's metabolic activities are the carbon dioxide and water. These two compounds are subject to a variety of chemical, electrical and electrochemical breakdown processes to recover oxygen for re-use in the respiration demands of man. A photolytic dissociation of a mixture of carbon dioxide and water using ultraviolet irradiation has been accomplished with some degree of success but with a great penalty as to specialized equipment and power (6). This requirement of specialized equipment has limited work on photolytic reactions of carbon dioxide and water for application to atmosphere regeneration. Groth in the Symposium on the Photochemistry in the Liquid and Solid States(1) reported on work on the ultraviolet chemical activation of water and carbon dioxide. He found that carbon dioxide and water are split and the photolytic products interact forming the end reaction products oxygen and a carbohydrate-life compound. The reactions occur as follows:



The interaction of mixtures of carbon dioxide and water is endothermic and stores 112 Kcal/mol or 1800 calories per gram of reactants. This reaction forms a carbohydrate precursor which can be stored, disposed of, or eventually reutilized in a cycled process. This reaction requires very short ultraviolet light which would give the required energy of 112 Kcal/mole. The source of ultraviolet radiation is a limited factor. Use of open carbon arcs or of open ultraviolet

emitters obviously is not satisfactory for this application. The usual ultraviolet sources are limited in output and limited more so in the ultraviolet transmission materials available for the construction of reaction units for this purpose. Xenon resonance lamps emit radiation at 1470 Å and at 1295 Å through a calcium fluoride window in quantities such that the transmitted radiation is effective in the photochemical dissociation of carbon dioxide and water. The stress on power limitation for regenerative techniques shows the desirability of the application of solar radiation for this energy source.

Other photochemical reactions induced by ultraviolet irradiation involve direct photochemical dissociation of methane, ethane and ammonia, in which reactions, hydrogen atoms and the associated free radicals are formed. These reactions apply directly to atmosphere regeneration since these compounds are present in the air stream and constitute a contamination problem. Their photoactivation occurs with ultraviolet irradiation which ordinarily does not occur in a space cabin. A technique for the ultraviolet photolysis of carbon dioxide and water, and for the photoreactions of methane, ethane and ammonia must be given serious consideration in environmental control systems.

Photochemical Effects of Atmospheric Contaminants -

Studies on atmospheric constituents significant in creating undesirable urban air contamination reveal that gaseous contaminants undergo chemical reactions when certain (but usually normal) conditions are present. It can be inferred that these contaminants are the same ones which constitute a problem in space cabin atmosphere regeneration. These space cabin contaminants are variously listed and the sum totals over 300. Of these, sulfur dioxide, nitrogen oxide and some of the aliphatic hydrocarbons are typical of the compounds subject to interaction under visible light conditions.

In an area where atmospheric contamination creates undesirable conditions, such as Los Angeles, investigations revealed a photooxidation of organic compounds present in the air. These have been typically gasoline fumes in the presence of nitrogen dioxide and sulfur dioxide. This mixture eventually produces an organic nitrogen compound such as nitrile, sulfur compounds as sulfate and sulfuric acid aerosol, and carbon dioxide and water.

It may rightly be asked how this smog problem applies to atmosphere control in a space vehicle cabin. For the space cabin contaminant handling problem there are decontamination techniques providing for adsorption on activated carbon, on molecular sieve materials and in lithium hydroxide. For a regenerative system with re-use of gases and materials in closed systems, this concept of photochemical interaction of contaminants and atmospheric constituents must be considered as significant in accounting for new products. This interaction occurs at low concentrations of reactants with the visible light as the energy source, and introduces added problems to decontamination efforts. Direct oxidation of contaminants in catalytic devices makes use of copper and manganese oxides in the oxidation of organic and inorganic compounds. Carbon dioxide and water constitute the greatest part of the products. However, this concept is penalized by the presence of halogens and sulfides which react with the catalysts, forming inert or non-regenerable reactants. Removal of halogen and sulfide can be accomplished

by reaction with an expendable reactor component with some weight and power penalty. The high power penalties for these devices justify a serious consideration of the photooxidizing techniques for contaminant modification and elimination using both ultraviolet and the visible activation energies, as another approach to the contaminant problem in closed environmental control systems.

In a contaminated "smog" atmosphere, the primary light energy absorbing constituents are oxygen, nitrogen dioxide, nitric oxide, sulfur dioxide and various organic aldehydes (7). The interaction of these compounds produce a gaseous atmosphere containing higher aldehydes, peroxyacids and nitrites. Oxygen as an energy absorber forms ozone, with its main reaction subsequently with nitric oxide in the formation of nitrogen dioxide. Nascent oxygen also is formed and reacts with olefins forming aldehyde and ketones, epoxides, and some organic radicals. Ozone in its reactions with olefins forms organic acids, alcohols, ozonides and possibly some organic radicals. Oxygen reacts with sulfur dioxide forming sulfate. These reactions of oxygen with nitrogen dioxide and sulfur dioxide are very significant in smog forming situations and account for the toxic effects to plants, eye irritation and the material discolorations. Some of the major energy absorbers are listed in Table I. These light energy absorbers constitute the basic photoactive agents involved in further reactions of atmosphere contaminants and are directly applicable to the contamination handling problem in atmosphere regeneration.

Table I - Absorbers of light energy 3000-7000Å

oxygen	ozone	nitrogen dioxide
sulfur dioxide	peroxides	nitric acid
nitrites	aldehydes	ketones

Summary -

In summarizing this discussion on photochemical reactions significant in an atmosphere regeneration system, it is evident that light energized reactions provide basic techniques applicable to atmosphere control. Photosynthesis in green plants constitutes a natural time-tested and adequate method for carbon dioxide removal and oxygen generation. However, to provide for the high reliability needed for an aerospace vehicle cabin atmosphere regeneration system, more research is needed to understand and evaluate the many reactions occurring in the photochemical and oxidation-reduction processes in photosynthesis. In the photosynthetic bacteria, the comparable process of carbon dioxide removal requires more research for defining the intermediates in these reactions. Photolytic reactions of carbon dioxide and water mixtures provide for chemical energy storage of light energy as a carbohydrate precursor with release of oxygen, but these reactions involve characteristics difficult to attain and control. Photo-oxidation of atmospheric constituents introduces a concept significant to the contamination build-up processes and in the contaminant monitoring system.

References -

1. Daniels, F. Symposium on Photochemistry in the Liquid and Solid States, 1957, John Wiley & Sons, Inc., N. Y. 1960.
2. Brookhaven National Laboratory, The Photochemical Apparatus, Its Structure and Function, A report of Symposium June 16-18, 1958.
3. Steward, F. C., Editor, Plant Physiology, A Treatise. Vol IB, Photosynthesis and Chemosynthesis, Acad. Press. N. Y. 1960.
4. Calvin, M, and G. M. Androes, Primary Quantum Conversion in Photosynthesis, Science 138:867-873, 1962.
5. Bassham, J. A., The Path of Carbon in Photosynthesis; Scientific American 206:88- , 1962.
6. Ames, R. K., Photochemical Decomposition of Carbon Dioxide, Feasibility Study; Boeing Company Document D2-6428, 1960.
7. Leighton, P. A. Photochemistry of Air Pollution, Academic Press, N. Y., 1961.

Associated References -

1. Clayton, R. K., Symposium on Autotrophy, III Recent Developments in Photosynthesis, Bact Rev. 26:151-164, 1962.
2. Proceedings of an International Symposium Arranged by Stanford Research Institute, San Francisco, Calif., April 18-20 1961, Chemical Reaction in the lower and upper atmosphere. Interscience Publishers, N. Y. 1961.
3. Rabinowitch, E. I. Photosynthesis and Related Processes, Interscience Publishers, Vol I, 1945; Vol II, Part I, 1951; and Part 2, 1956. N. Y.
4. Burton, N., Kirby-Smith, J. S., and Magee, J. L., Comparative Effects of Radiation, Conference at San Juan, Univ. of Puerto Rico, February 15-19, 1960, NAC, NRC. John Wiley and Sons, Inc., N. Y. 1960.

SESSION III
RADIATION AND THERMAL ANALYSIS

CHAIRMAN
DR. A. J. SHINE

SPACE RADIATOR EXPERIMENT

by

C. J. Feldmanis

**Aeronautical Systems Division
Wright-Patterson Air Force Base, Ohio**

311

SPACE RADIATOR EXPERIMENT

by

C. J. Feldmanis

Introduction -

The disposal of waste heat resulting from power generation, equipment operation, or metabolic functions is a problem to all space vehicles. For small unmanned vehicles, outer skin with controlled surface properties can be utilized as a heat radiator. But, as the vehicles grow larger and more complex, radiators containing fluid conduits must be considered. Depending on heat rejection rates and type of vehicle, radiators may be part of the vehicle skin or deployable as separate structure. When the radiator is part of the vehicle skin, only one side of the radiator is effective and will radiate heat to space. For best efficiency, deployable radiators will radiate from both sides. It is also possible to orient a deployable radiator and protect it from solar radiation. This is of special importance for low temperature radiators.

Under actual conditions, when shielding or orientation is not practical or possible, radiators will be exposed to heat inputs from sun and planets, and radiator efficiency under these conditions will be reduced. However, the scope of tests and facilities described in this report did not include solar or planetary heat inputs. Fluid phase change, flow stability and meteoroid protection were also not considered in these tests.

Object of Experiment -

Analysis of extended surface fins for space radiators have been performed (References 1, 2 and 3), including a test (Reference 4). Reference 5 optimizes a tube-fin type radiator. A thermal model test of a lunar spacecraft is described in Reference 6, where performance of a cylindrical tube-fin type radiator is investigated. However, prior to the tests described in this report, none were performed on tube-fin type radiator elements to determine effects upon heat rejection rates when fin length, thickness and materials were varied. Based on these tests, optimum weight configurations (maximum Btu/lb. of radiator element) were determined for radiator elements of two different designs.

To find a heat rejection system of minimum weight, all the components involved must be considered. In an actual radiator system the total weight consists of the radiator, the circulating fluid, pump and the pumping power penalty. Optimization of fin alone would not determine the lightest radiator system or even the lightest radiator. In radiator optimization, liquid and tube weight, (especially when meteoroid protection is considered) cannot be neglected.

It is believed that test results will be helpful in preliminary radiator design, and also for planning of more advanced tests.

Description of Experiment -

1. Test Set-Up

The test set-up is shown on Figures 1 and 2, and consists of the following items:

- a. A bell jar type stainless steel vacuum chamber (17 3/4" dia. x 24" high) equipped with liquid nitrogen cooled enclosure (15 1/4" dia x 23" high). The enclosure is made of two concentric stainless steel cylinders so that when the space between the cylinders is filled with liquid nitrogen, a uniform cold wall temperature is obtained. The inner surface of the enclosure is coated with carbon black pigmented polymethane coating to achieve a surface absorptivity as high as possible (considering availability at the time when these tests were started). The vacuum capability of this chamber with installed specimen is 10^{-6} to 10^{-7} mm Hg.
- b. Constant temperature water bath, accuracy $\pm 0.5^{\circ}\text{C}$.
- c. Circulating pump.
- d. Flow meter, range 0.15 to 2.3 gal/min.
- e. Potentiometer, range $+350^{\circ}\text{F}$ to -350°F .
- f. Potentiometer, range $+525^{\circ}\text{F}$ to -75°F .
- g. Immersion type mercury thermometers.
- h. Liquid nitrogen containers and pumping system.

2. Test Procedure

After the liquid lines and thermocouples were connected to the test specimen, the chamber was sealed and evacuated. When no signs of leaks were present, the water and liquid nitrogen circulating systems were started. Tests were started at a water temperature of approximately 120°F . Then temperature was increased in about 10°F increments up to 180°F or 190°F . Equilibrium condition from one temperature setting to the other was reached in approximately 1/2 hour. The water flow rate was adjusted and maintained at approximately 100 lbs/hr. This flow rate was checked about three (3) times during the test by actually weighing the flow rate through the radiator element.

The cold wall temperature of -320°F (140°R) was maintained at all times during the test. This temperature was checked by a thermocouple attached to the upper portion of the cylinder.

After the cold wall reached a uniform temperature of -320°F and radiator element equilibrium condition (no variation of liquid and fin temperature for about 10 minutes), two basic readings were taken: (1) the quantity of fluid flow through the radiator element, and (2) the temperatures of the liquid entering and leaving the element. Besides these basic readings, temperature drop along the fin was taken.

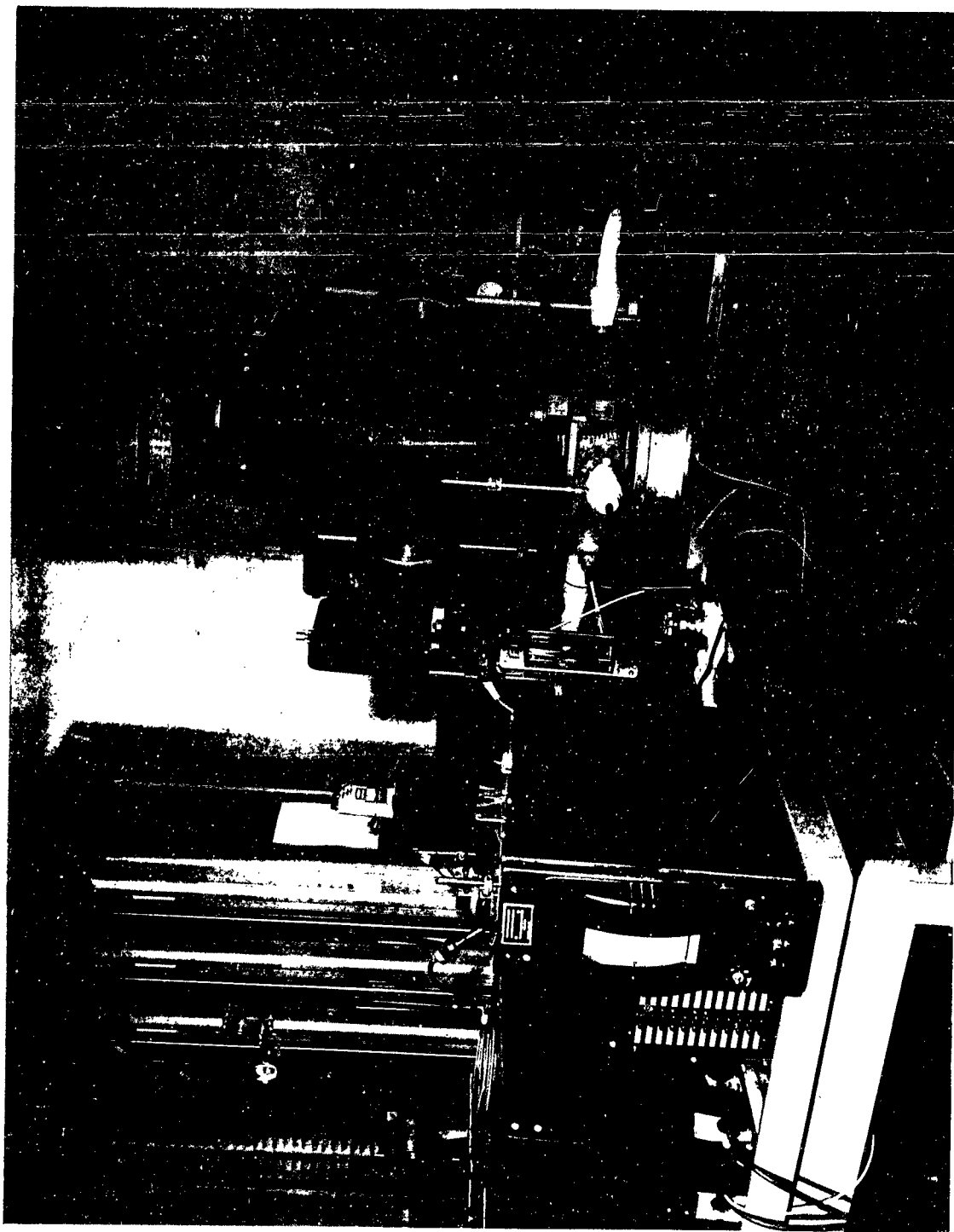


Figure 1. Bell Jar Experimental Apparatus

SPACE RADIATOR TEST SET-UP

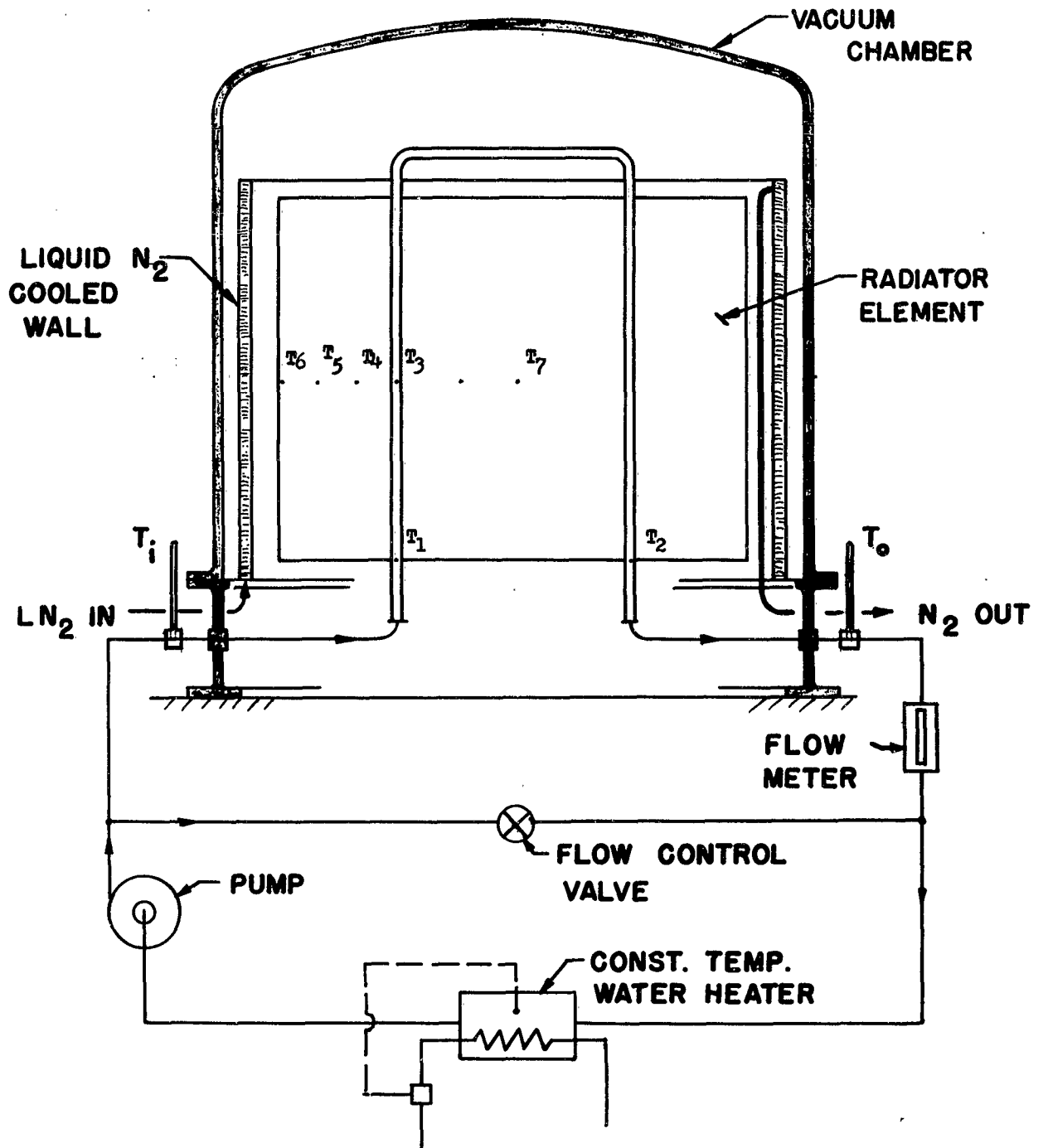


Figure 2. Space Radiator Test Set-up

The heat removed from the liquid per unit time was determined from the following equation:

$$Q_L = WC_p (t_i - t_o) \quad (1)$$

where

Q_L = heat removed from liquid, Btu/hr.

C_p = specific heat of liquid, Btu/lb.°F

W = liquid flow rate, lb./hr.

t_i = liquid inlet temperature, °F

t_o = liquid outlet temperature, °F

As the tests were performed in vacuum, where convection and conduction heat transfer can be neglected, heat removed from the fluid may be set equal to the heat radiated from the radiator surface. Assuming cold wall absorptance equal to 1 ($\alpha = 1$), and neglecting radiant heat exchange between specimen and both ends of vacuum chamber which are not cooled with liquid nitrogen, heat dissipated by radiator element can be determined from the following equation:

$$Q_R = FA \epsilon \eta \sigma (T_T^4 - T_S^4) \quad (2)$$

where

Q_R = heat dissipated by radiation, Btu/hr.

F = view factor

A = radiator area, ft.²

ϵ = total hemispherical emissivity

η = radiator effectiveness, which is defined as the ratio of actual heat dissipated from the radiator element to the net heat flux that would be dissipated if the radiator were at the hot edge temperature.

σ = Stefan-Boltzmann constant

T_S = sink temperature, °R

T_T = tube temperature, °R

As heat removed from fluid equals heat dissipated by radiation:

$$Q_L = Q_R \quad (3)$$

$$FA \epsilon \eta \sigma (T_T^4 - T_S^4) = WC_p (t_i - t_o) \quad (3a)$$

From this equation radiator effectiveness can be determined

$$\eta = \frac{WC_p (t_i - T_o)}{FA \epsilon \sigma (T_T^4 - T_S^4)} \quad (4)$$

3. Test Specimens

All test specimens were of the tube-fin configuration, with fins of rectangular cross-section. Availability of materials "on hand" determined selection, and these materials do not necessarily represent the best selection for an actual radiator.

Depending on operating pressures and meteoroid protection requirements, tubes and fins may be of different materials. As far as fin materials are concerned, selection probably will be based on thermal conductivity and density, unless structural strength sets different requirements.

Physical data of test specimens are presented in data sheet and a typical radiator element is shown on Figures 4 and 5. All coated specimens were coated with white TiO_2 pigmented silicone alkyd coating. Total hemispherical emittance as a function of temperature is shown on Figure 6.

Two methods of attaching thermocouples to the tube and fin surfaces were used: (1) soldering to the steel and copper surfaces, and (2) clamping to the aluminum surfaces by copper screws and/or "c" clamps. Success with the second method depends completely on good thermal contact. Insofar as thermocouple readings could be checked, they were sometimes in close agreement with actual temperature; sometimes different. (See discussion of results.)

Two methods were used to attach fins to the tubes: (1) steel, copper and the thicker aluminum fins were soldered to the steel, copper and aluminum tubes respectively, and (2) the thin aluminum fins were clamped to the aluminum and steel tubes utilizing strips and spotwelding techniques, as shown in Figure 3.

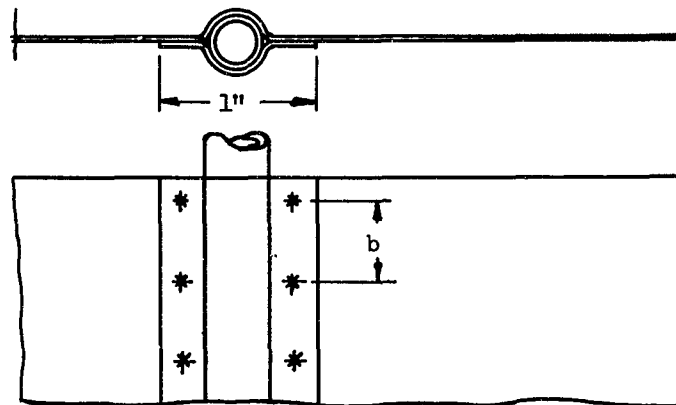
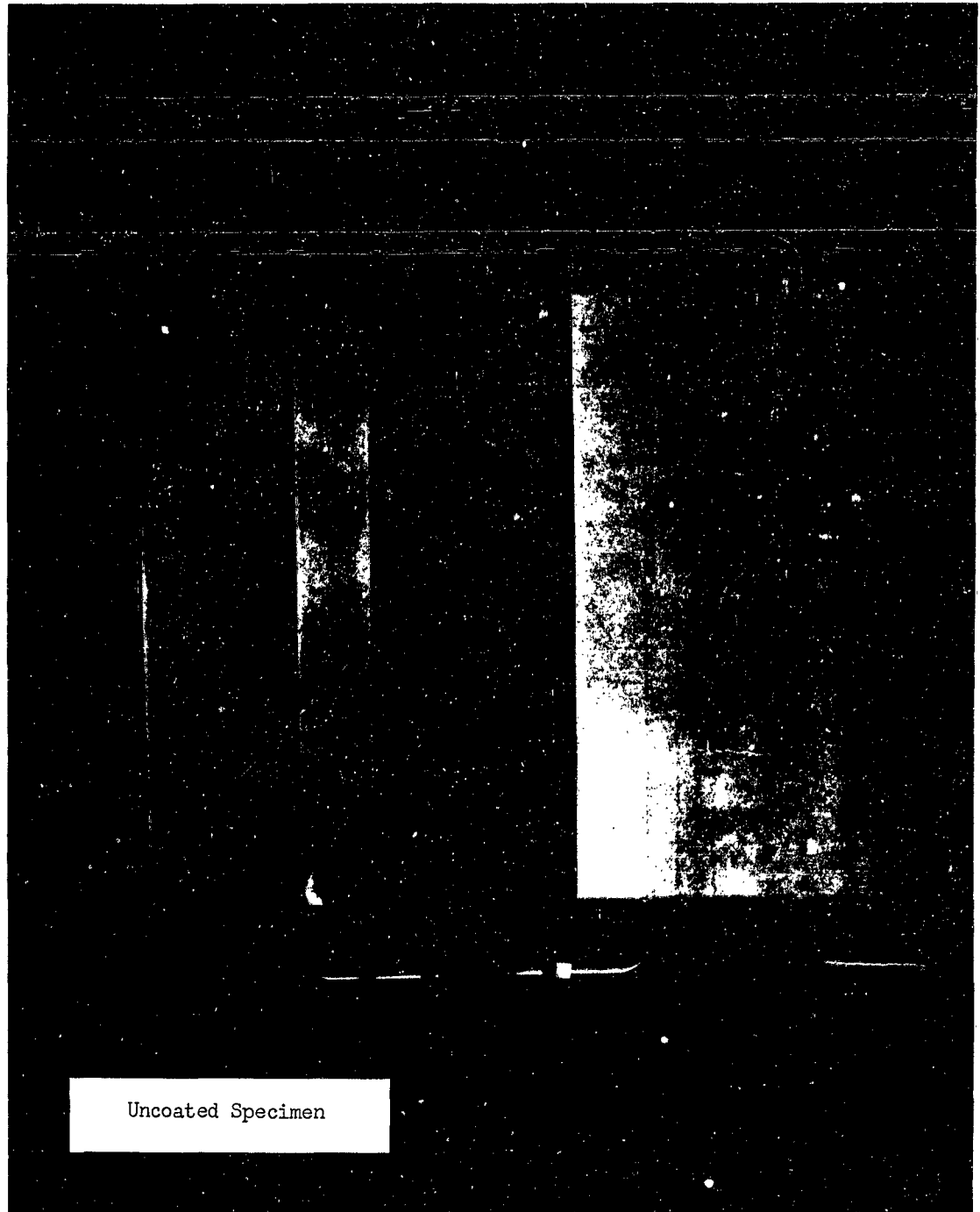


Figure 3. Technique Used to Attach Aluminum Fin to Stainless Steel Tubing



Uncoated Specimen

Figure 4. Radiator Panels

TYPICAL RADIATOR ELEMENT

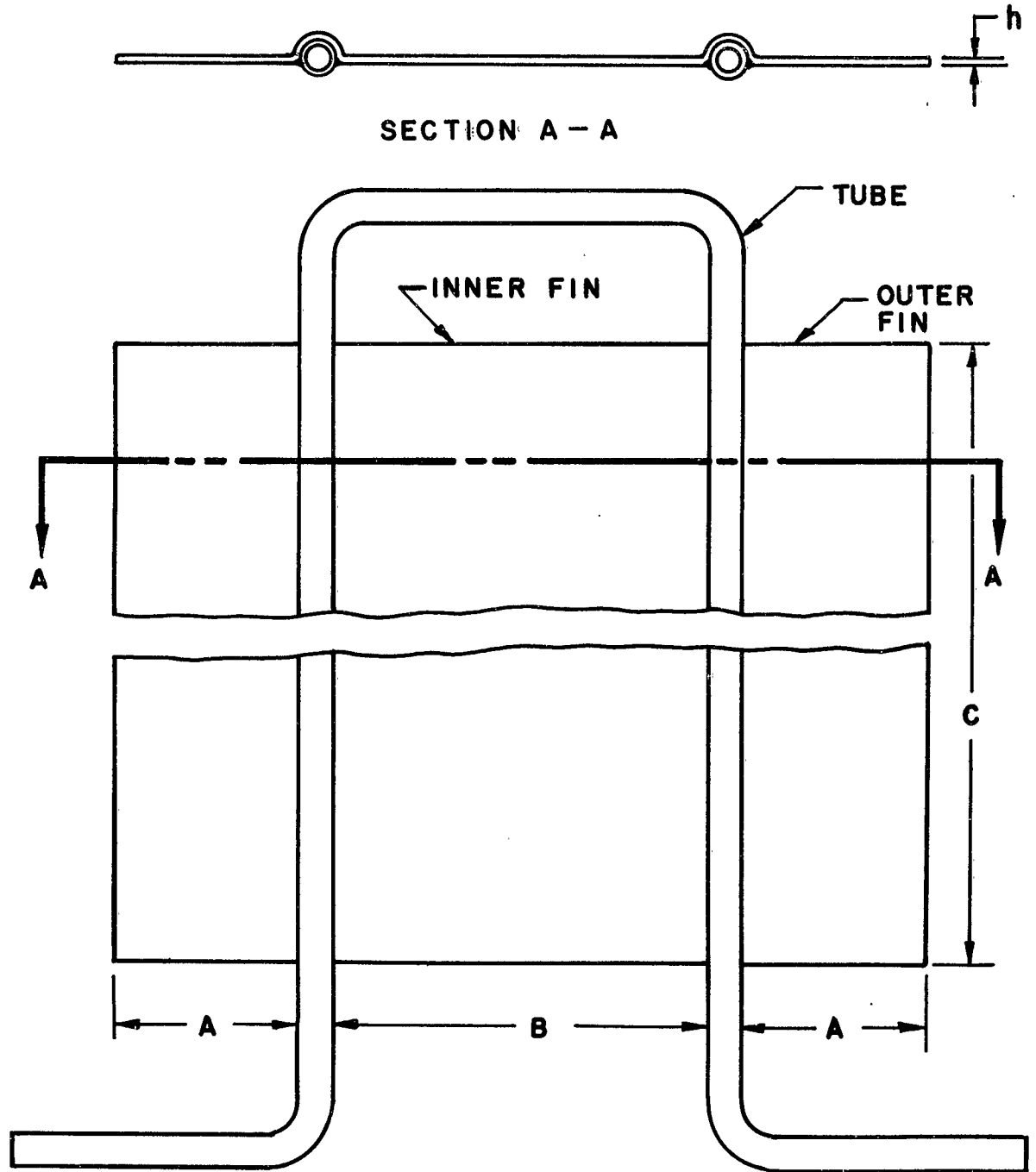


Figure 5. Typical Radiator Element

Figure 6.
TOTAL HEMISPHERICAL EMISSIVITY AS A FUNCTION OF
TEMPERATURE FOR TiO₂ PIGMENTED SILICONE ALKYL COATING

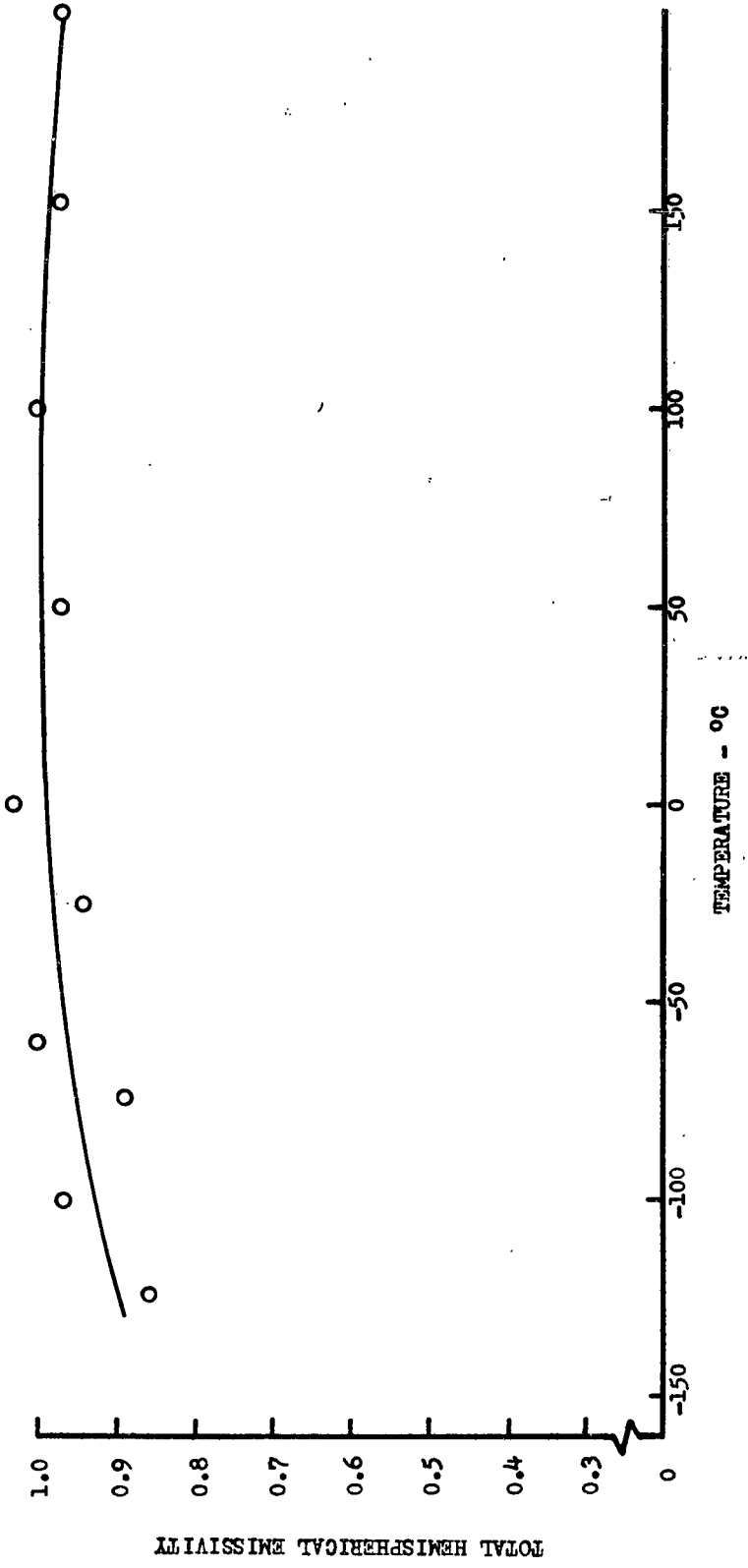


Figure 7.

EMISSIVITY AND ABSORPTIVITY AS A FUNCTION OF TEMPERATURE FOR FLAT BLACK ENAMEL

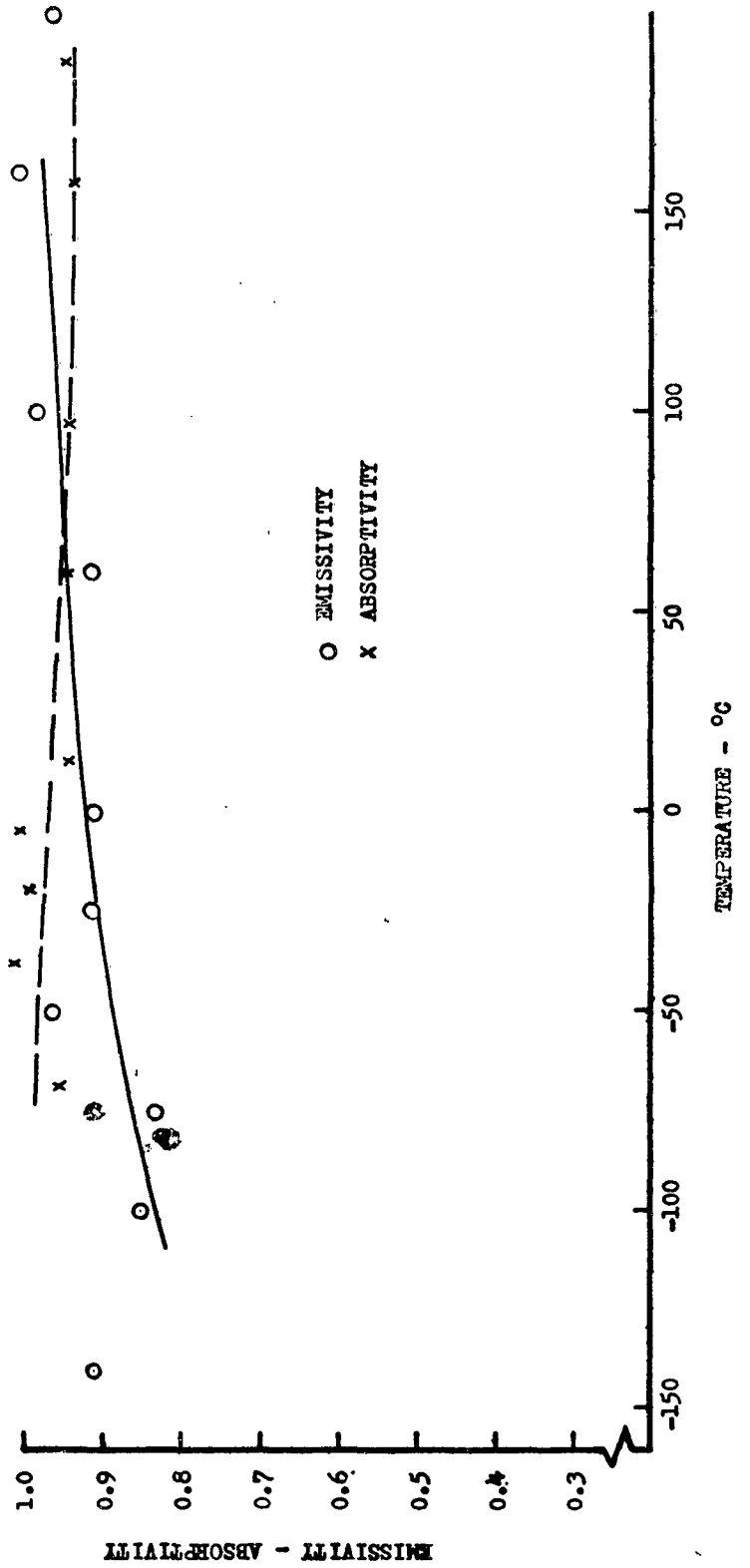


TABLE 1. - DATA OF TEST SPECIMENS

NO.	FIN MATERIAL	FIN DIMENSIONS				TUBE MATERIAL	TUBE DIMENSIONS	COATING	TYPE OF JOINT BETWEEN TUBE AND FIN
		A in.	B in.	C in.	h in.				
1.	Type 321 SS	2 5/8	5 1/4	22	.010	Stainless Steel	1/4"0.D.x.035" wall	None	Soldered
2.	Type 321 SS	2 5/8	5 1/4	22	.010	Stainless Steel	1/4"0.D.x.035" wall	TiO2	"
3.	Type 321 SS	1 3/4	3 1/2	22	.010	Stainless Steel	1/4"0.D.x.035" wall	"	"
4.	Type 321 SS	1	2	22	.010	Stainless Steel	1/4"0.D.x.035" wall	"	"
5.	Type 321 SS	2 5/8	5 1/4	22	.0312	Stainless Steel	1/4"0.D.x.035" wall	"	"
6.	Type 321 SS	2 5/8	5 1/4	22	.0625	Stainless Steel	1/4"0.D.x.035" Wall	"	"
7.	SAE 1018 C.R.S.	2 5/8	5 1/4	22	.050	Stainless Steel	1/4"0.D.x.035" wall	"	"
8.	00-A-561, Al.	1	2	22	.016	Aluminum	1/4"0.D.x.035" wall	"	See Fig. 3 (b = 1 in)
9.	00-A-327, Al.	2 5/8	5 1/4	22	.0625	Aluminum	1/4"0.D.x.035" wall	"	Soldered
10.	00-C-576A, Cu.	2 5/8	5 1/4	22	.0625	Copper	1/4"0.D.x.035" wall	"	"
11.	00-A-362	1 3/8	2 3/4	22	.016	Stainless Steel	1/4"0.D.x.035" wall	"	See Fig. 3 (b = 1/2 in)
12.	00-A-362	2 3/8	4 3/4	22	.016	Stainless Steel	1/4"0.D.x.035" wall	"	"
13.	00-A-362	3 3/8	6 3/4	22	.016	Stainless Steel	1/4"0.D.x.035" wall	"	"
14.	00-A-362	3 3/8	6 3/4	22	.016	Stainless Steel	1/4"0.D.x.035" wall	"	See Fig. 3 (b = 2-3 in)

The same method as shown on Figure 3 was used to attach the 0.016 aluminum fin to aluminum tubing (Specimen No. 8).

Test Results -

All test results are presented in chart form. Heat rejection rates by radiation are plotted as a function of mean liquid temperature, $t_m = (t_i + t_o)/2$, and data in reduced form are presented in Figures 8 through 21. Besides total heat dissipated from radiator element, heat dissipated per unit area and weight are included.

Figures 22 through 34 show temperature distribution along fin. Where data are available, comparison is made between analytical and experimental values. As the outer fin temperatures are in closer agreement with analytically determined values than inner fin temperatures, only outer fin temperatures are presented in charts.

Figure 35 shows comparison of temperature distribution along coated and uncoated aluminum fins. Fins are of the same thickness, material and length.

Figure 36 shows comparison of temperature distribution along coated and uncoated stainless steel fins. Fins are of the same thickness, material and length.

Figures 37 through 40 show difference of temperature distribution between inner fins and outer fins.

Figures 41 through 46 show comparison of heat rejection rates from radiator elements of different emissivities, fin length, fin thickness and materials.

Figure 47 shows effect of contact resistance upon heat rejection rates. Both specimens are of the same size, material and fin thickness. The only difference is in spotweld spacing.

Figure 48 shows heat rejection rates per unit weight of radiator element as a function of fin thickness and mean liquid temperature. All fins are of the same length and material.

Figure 49 shows heat rejection rates per unit area of radiator element as a function of fin thickness and mean liquid temperature. Fins are of the same length and material.

Figures 50 and 51 show heat rejection rates per unit area of radiator element as a function of fin length and mean liquid temperature.

Figures 52 and 53 show effect of fin length and mean liquid temperature upon heat rejection rates per unit weight of radiator element.

Figures 54 and 55 show effect of fin length upon radiator effectiveness. Fins are of the same thickness and material.

Figure 56 shows effect of fin thickness upon radiator effectiveness. Fins are of the same length and material.

Figure 8.

HEAT REJECTION RATES BY RADIATION
VERSUS MEAN LIQUID TEMPERATURE

SPECIMEN NO. 1

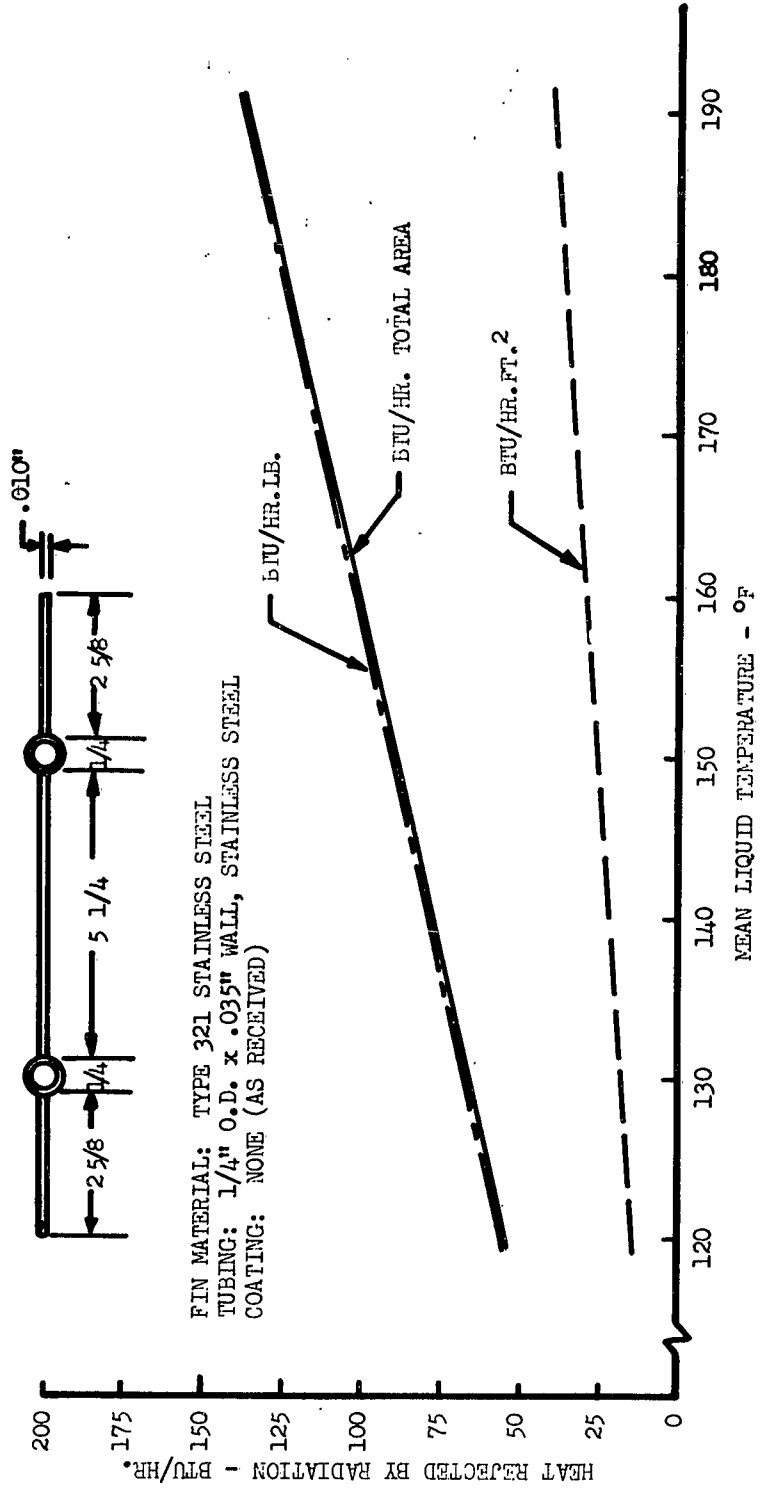


Figure 9.
**HEAT REJECTION RATES BY RADIATION VERSUS
 MEAN LIQUID TEMPERATURE**

SPECIMEN NO. 2

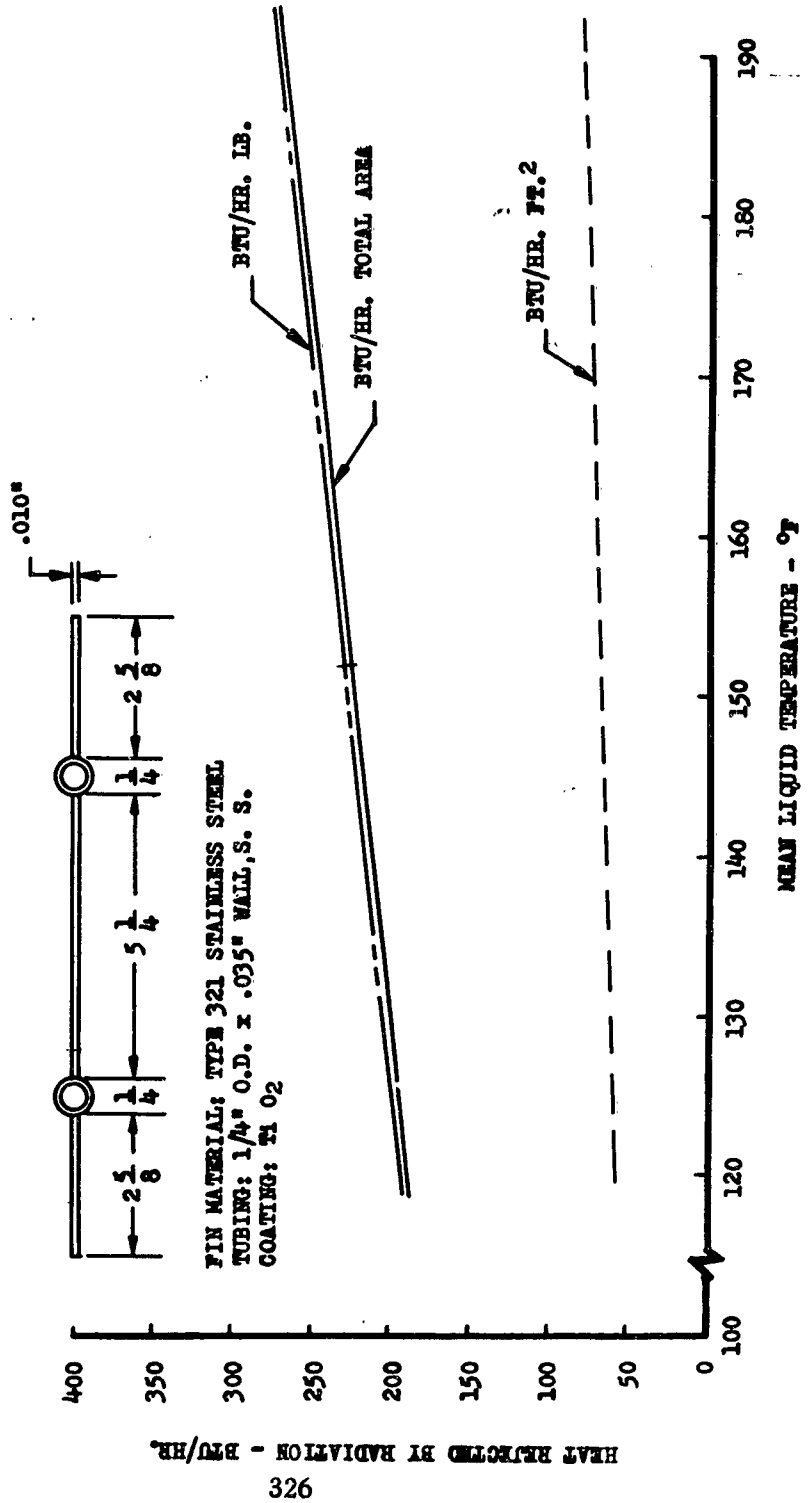


Figure 10.
**HEAT REJECTION RATES BY RADIATION VERSUS
 MEAN LIQUID TEMPERATURE**

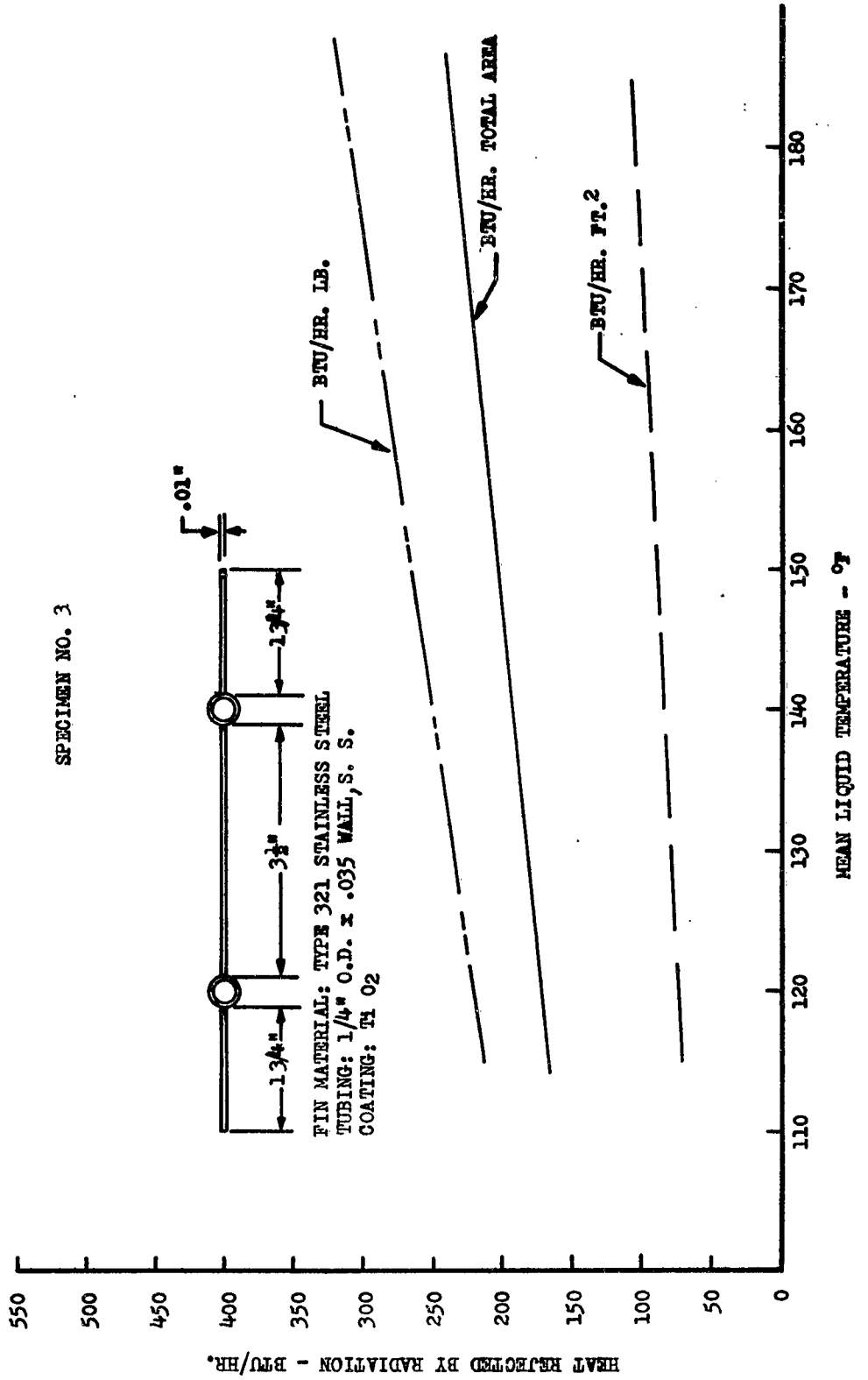


Figure 12.
 HEAT REJECTION RATES BY RADIATION VERSUS
 MEAN LIQUID TEMPERATURE

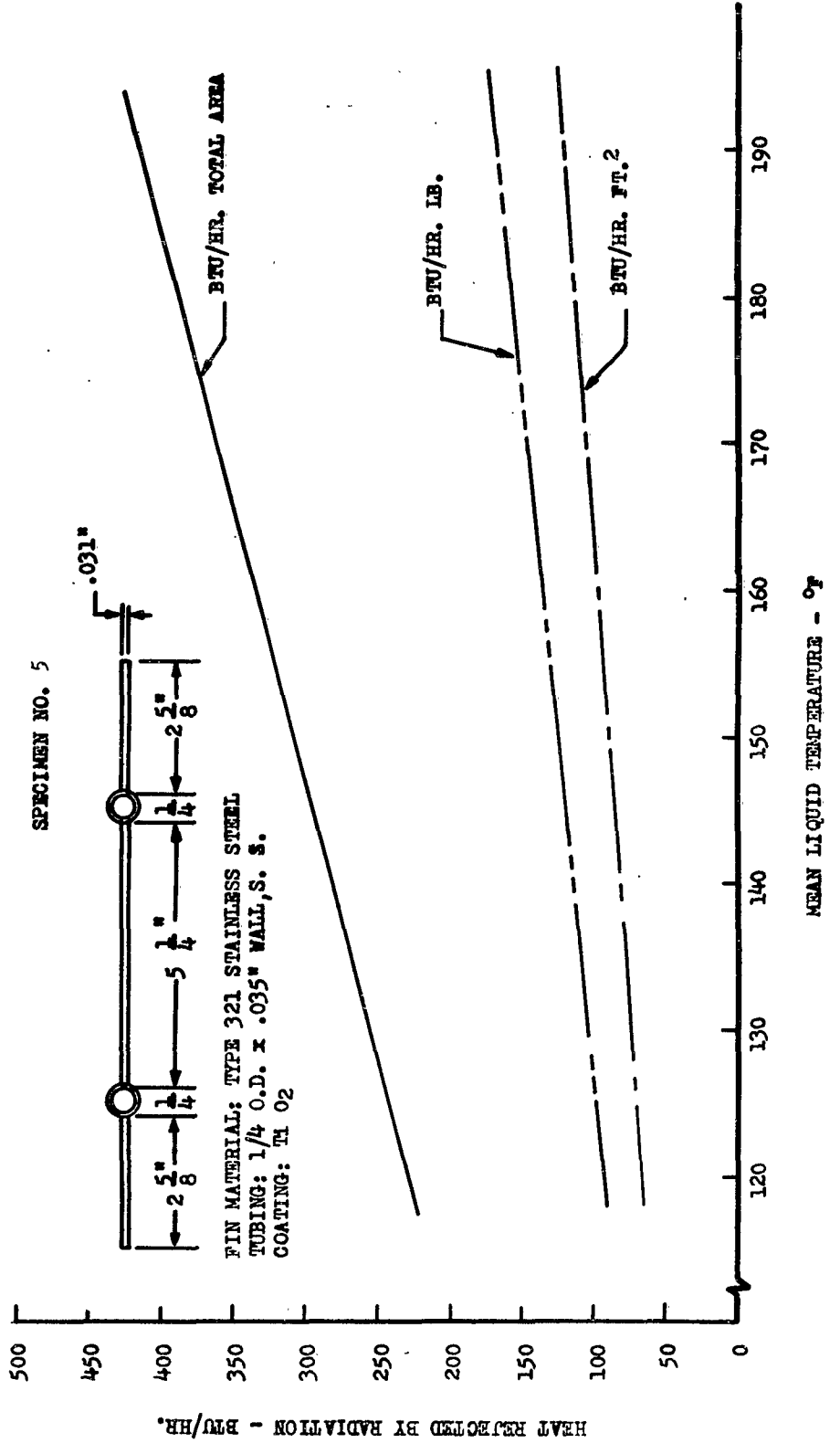


Figure 13.

**HEAT REJECTION RATES BY RADIATION VERSUS
MEAN LIQUID TEMPERATURE**

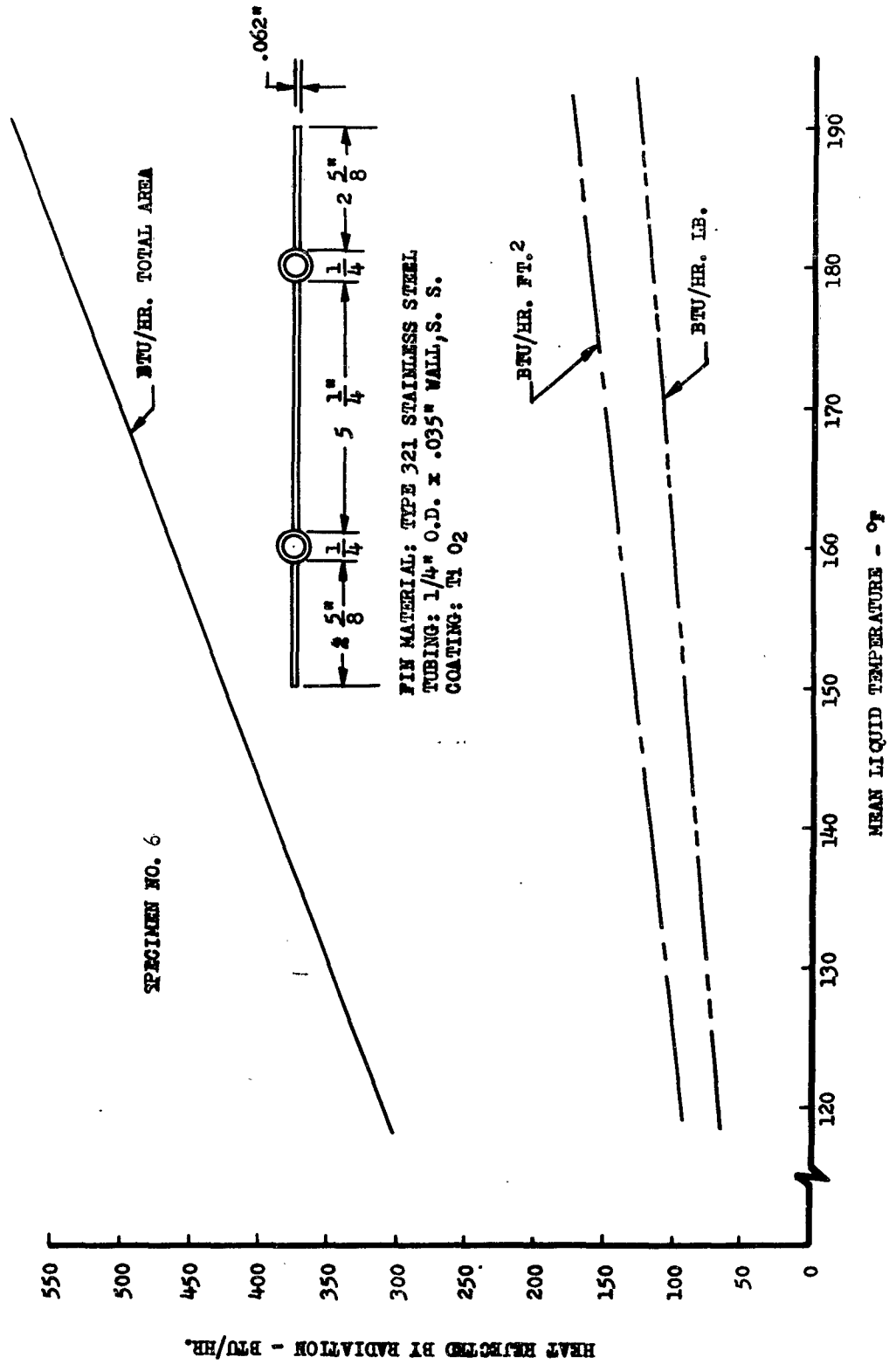


Figure 14.

HEAT REJECTION RATES BY RADIATION
VERSUS MEAN LIQUID TEMPERATURE

SPECIMEN NO. 7

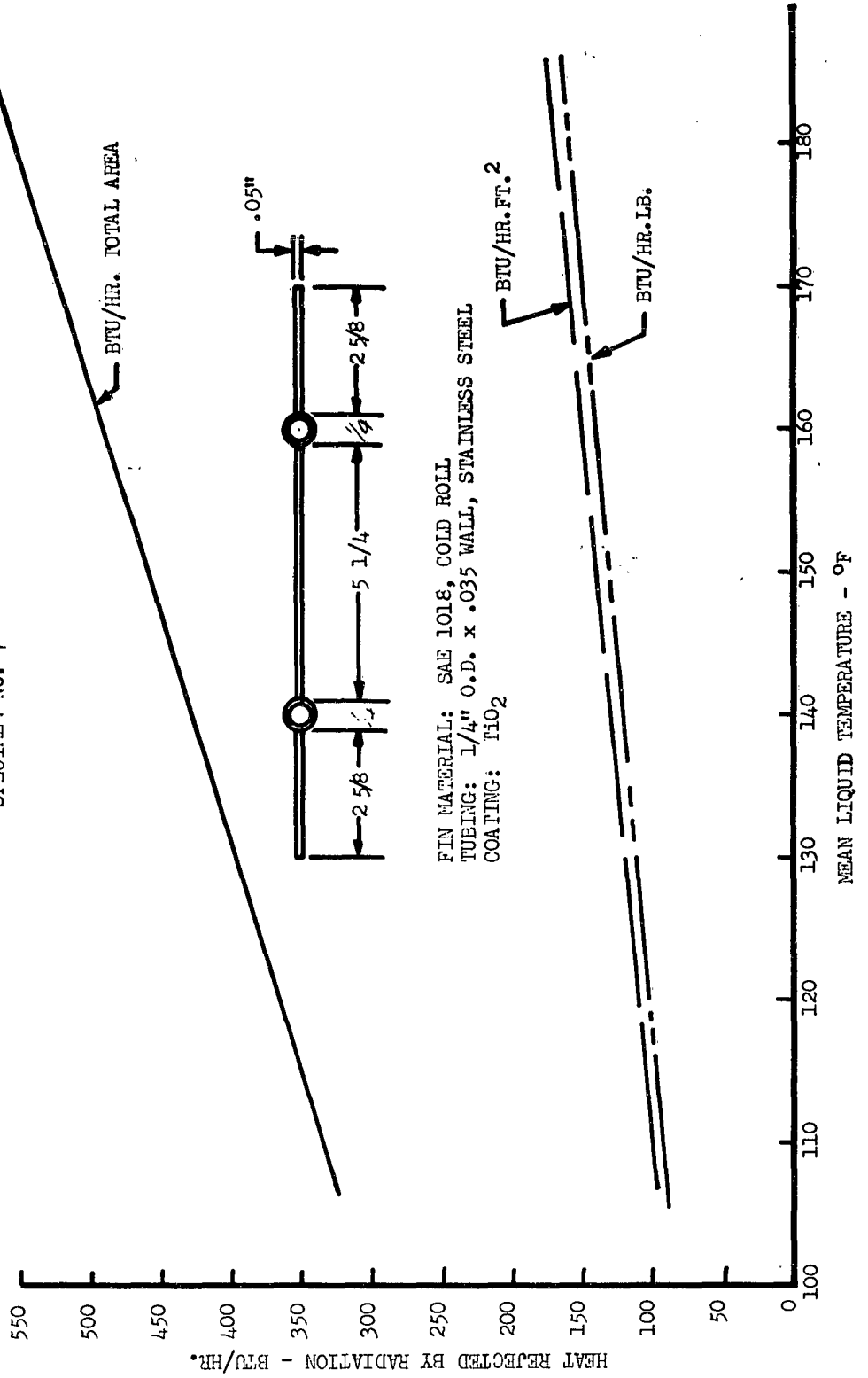


Figure 15.

HEAT REJECTION RATES BY RADIATION
VERSUS MEAN LIQUID TEMPERATURE
SPECIMEN NO. 8

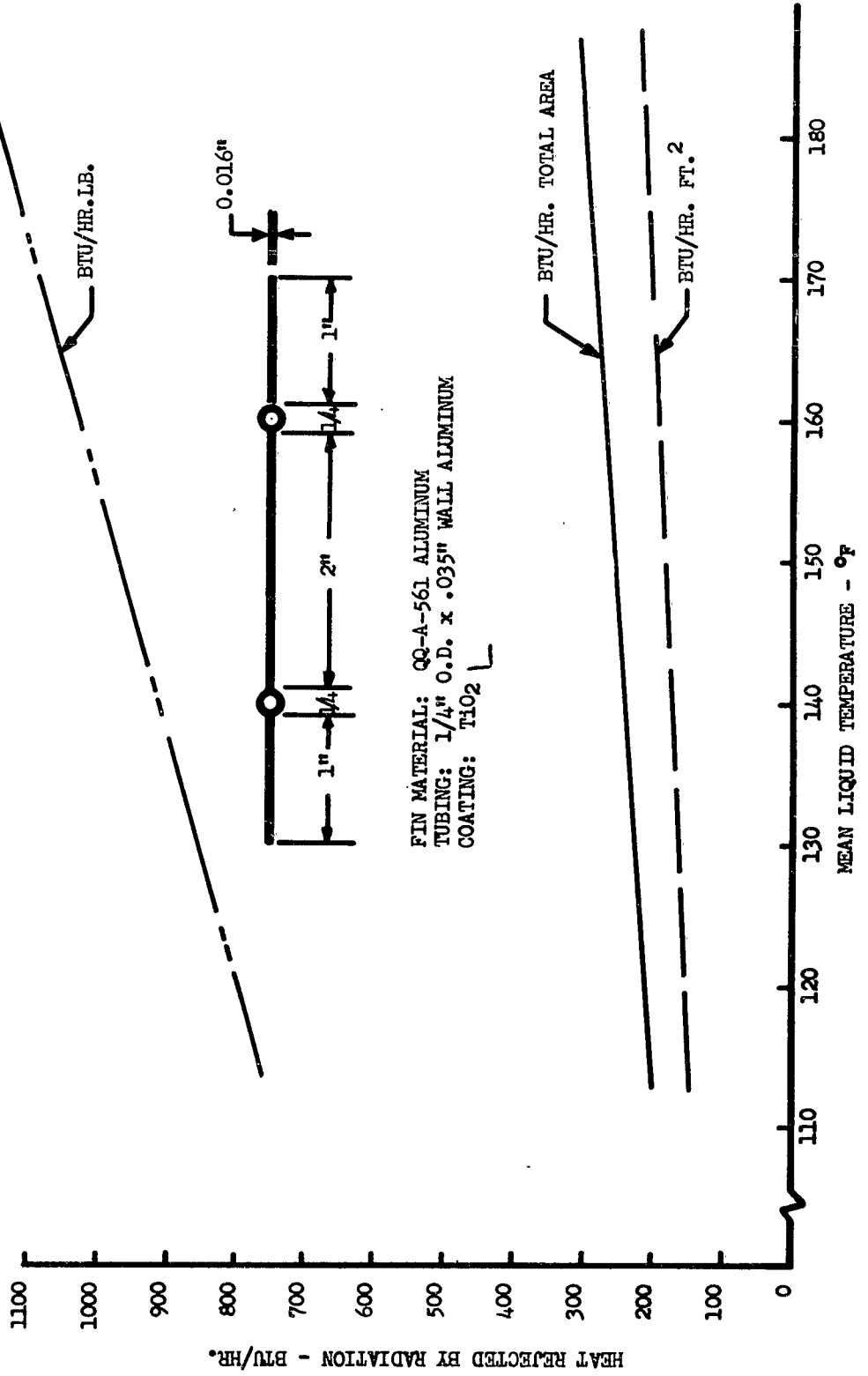


Figure 16.
HEAT REJECTION RATES BY RADIATION VERSUS
MEAN LIQUID TEMPERATURE

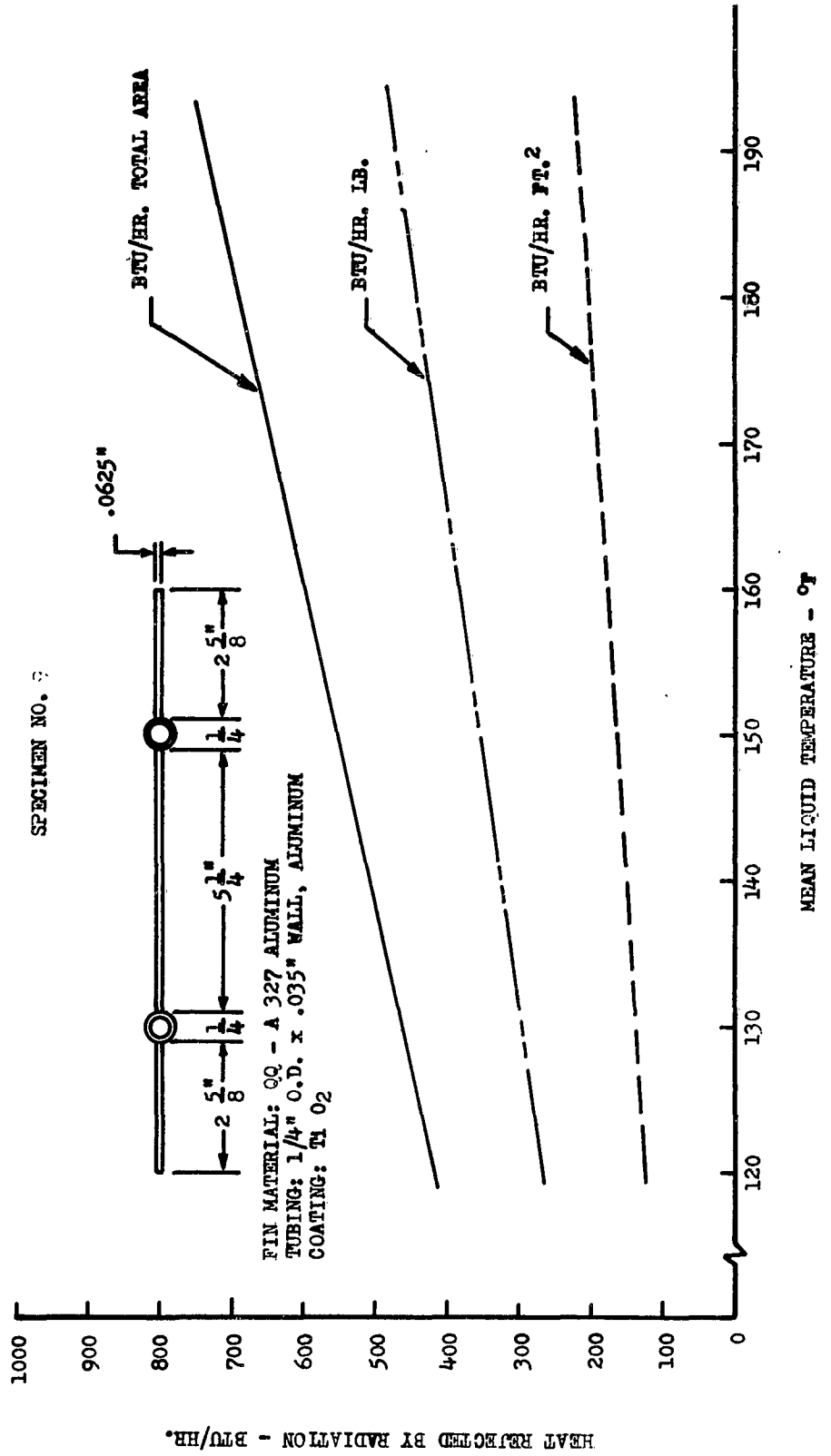


Figure 17.
**HEAT REJECTION RATES BY RADIATION VERSUS
 MEAN LIQUID TEMPERATURE**

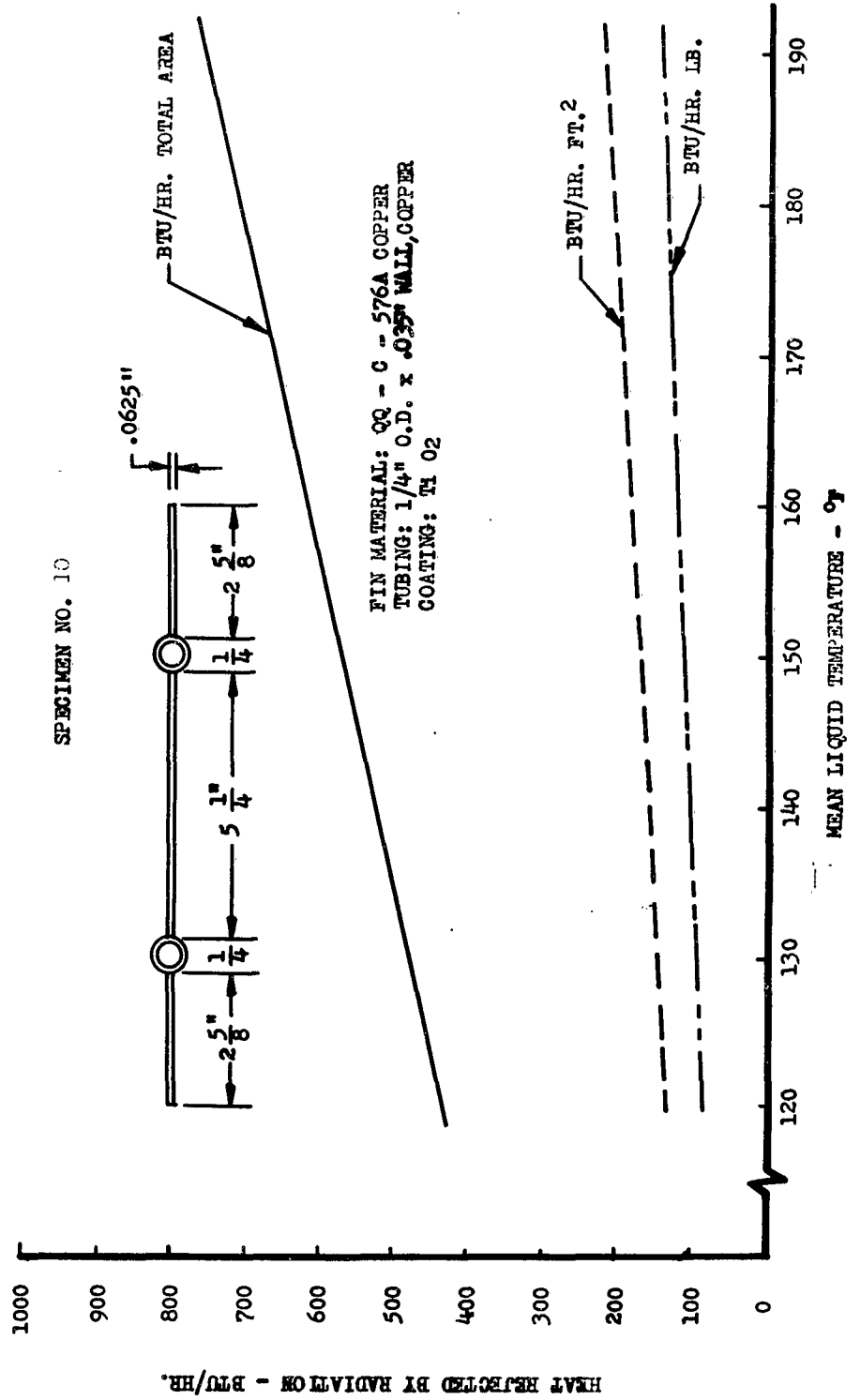


Figure 18.
**HEAT REJECTION RATES BY RADIATION VERSUS
 MEAN LIQUID TEMPERATURE**

SPECIMEN NO. 11

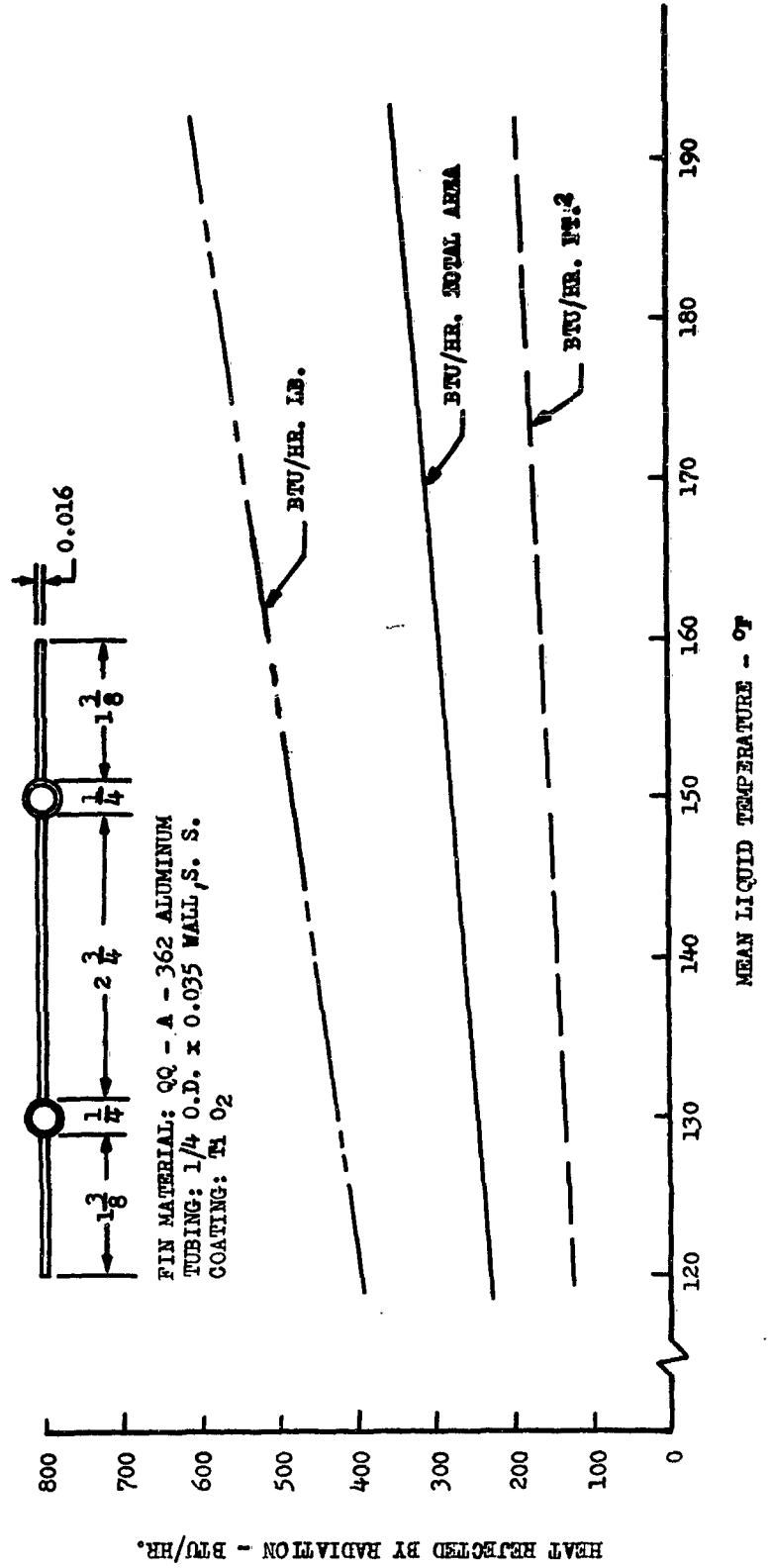


Figure 19.
HEAT REJECTION RATES BY RADIATION VERSUS
MEAN LIQUID TEMPERATURE

SPECIMEN NO. 12

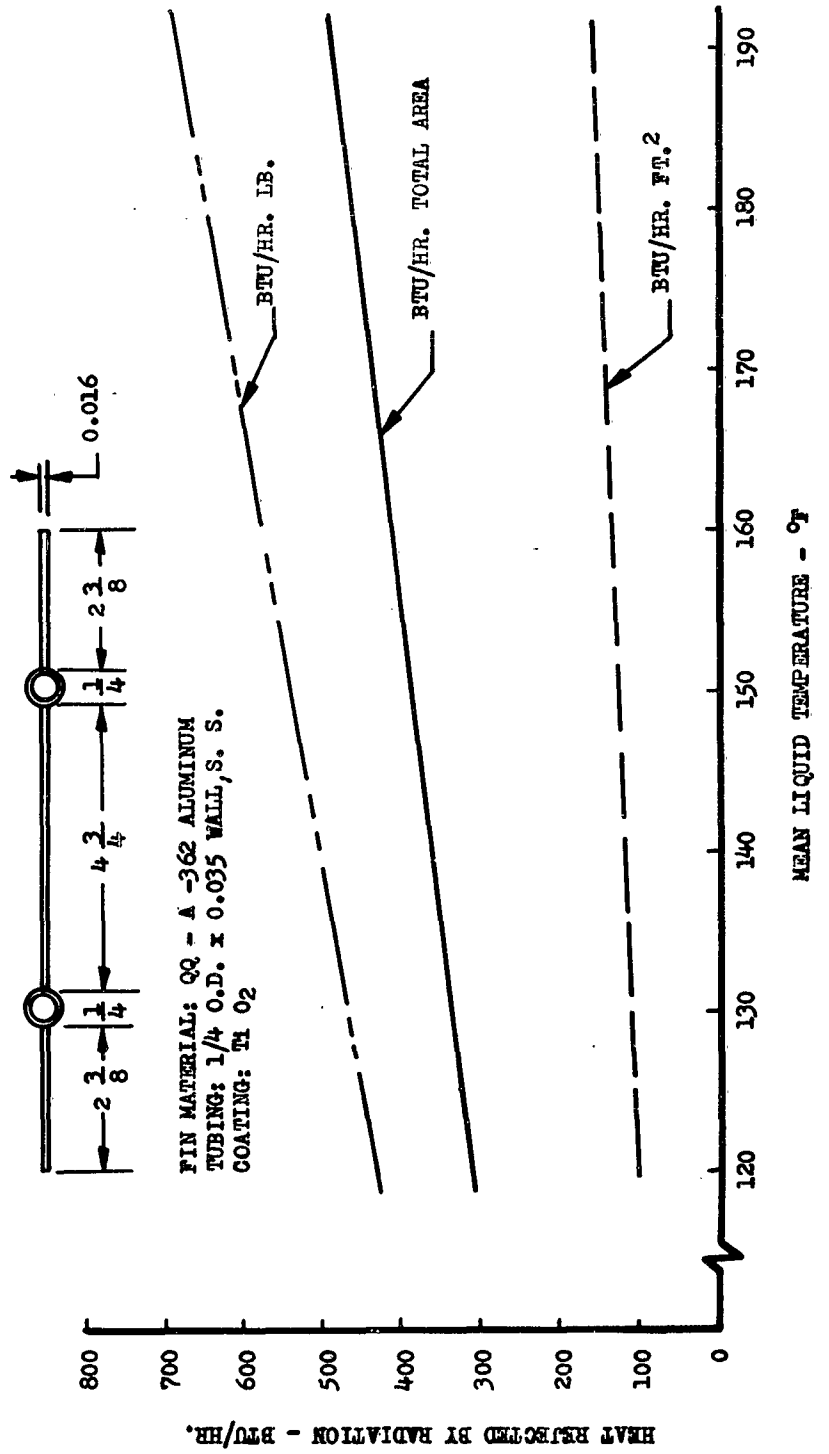


Figure 20.
HEAT REJECTION RATES BY RADIATION VERSUS
MEAN LIQUID TEMPERATURE

SPECIMEN NO. 13

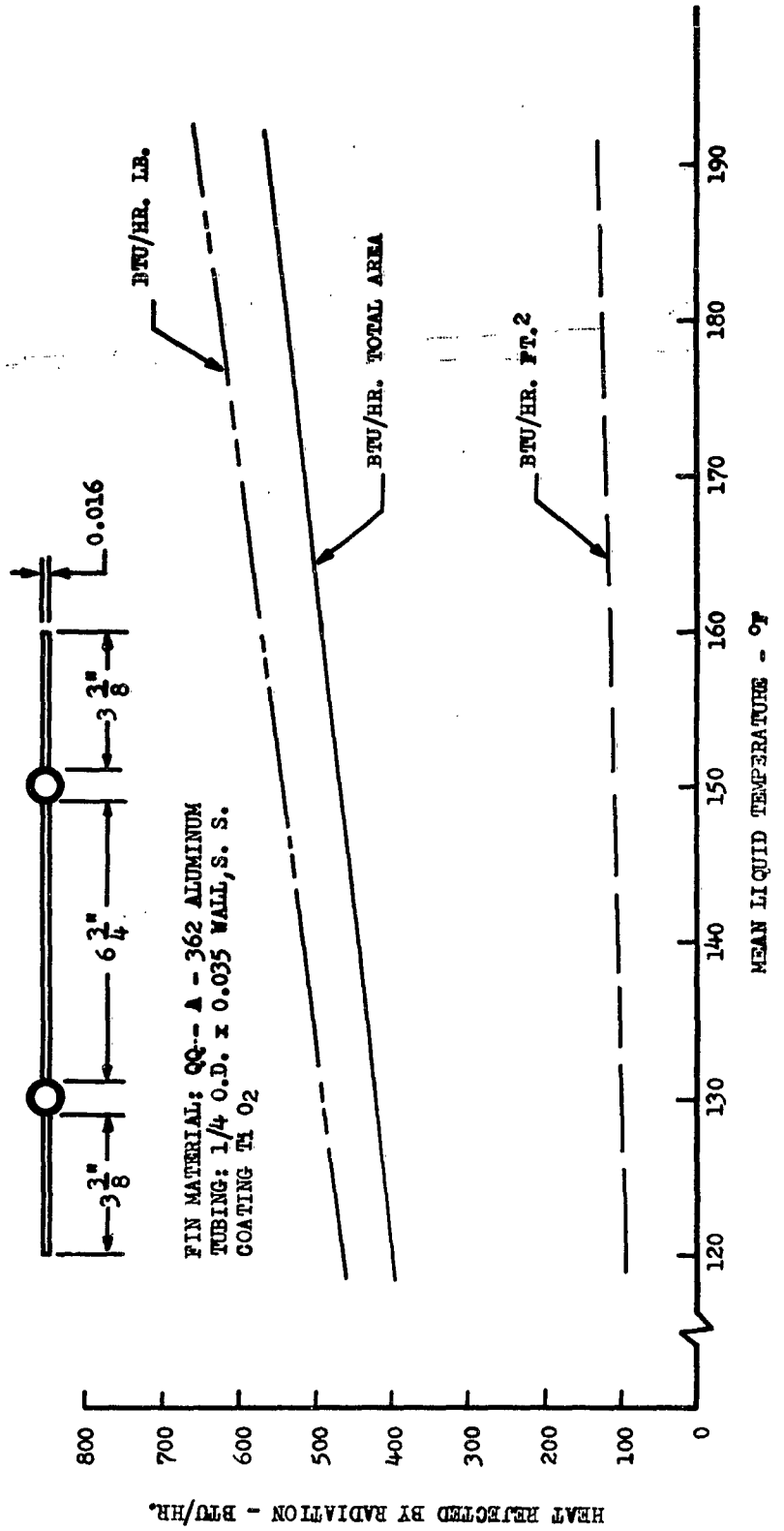


Figure 21.

HEAT REJECTION RATES BY RADIATION
VERSUS MEAN LIQUID TEMPERATURE
SPECIMEN NO. 14

NOTE: SAME AS SPECIMEN NO. 10
EXCEPT DISTANCE BETWEEN
SPOTWELDS 2 TO 3 INCHES

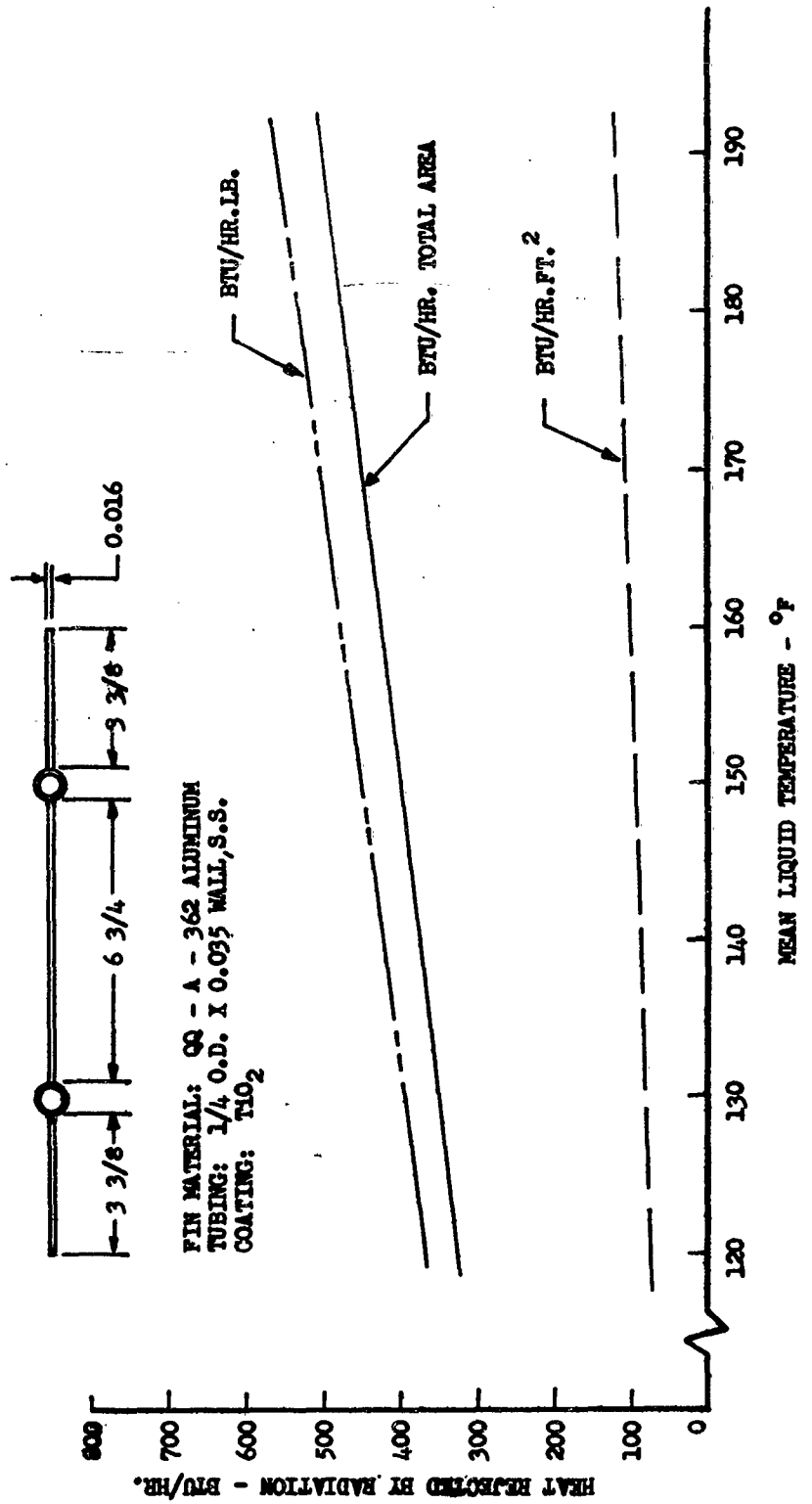


Figure 22.
TEMPERATURE DISTRIBUTION ALONG FIN
SPECIMEN NO. 1

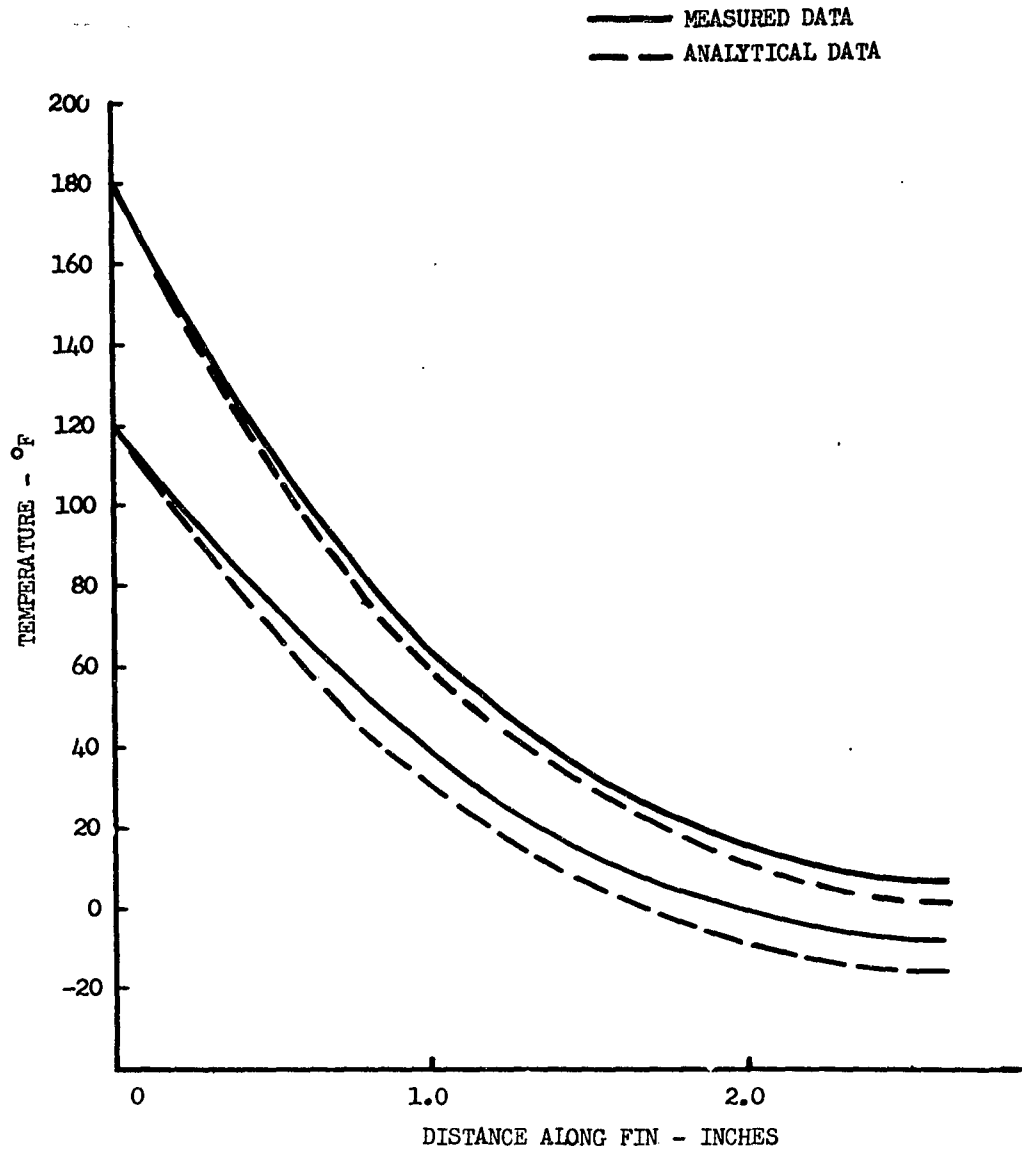


Figure 23.

TEMPERATURE DISTRIBUTION ALONG FIN
SPECIMEN NO. 2

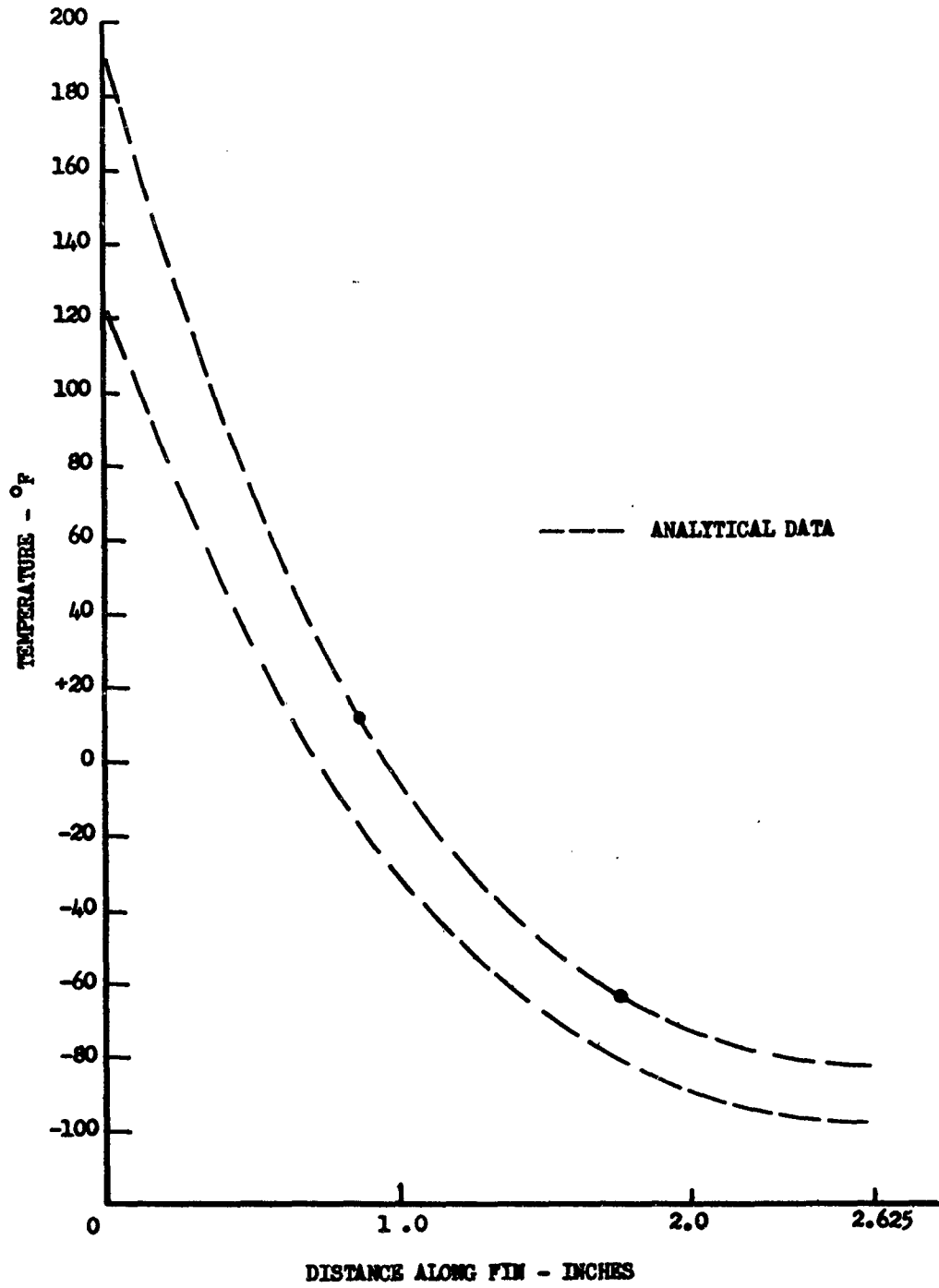


Figure 24.
TEMPERATURE DISTRIBUTION ALONG FIN
SPECIMEN NO. 3

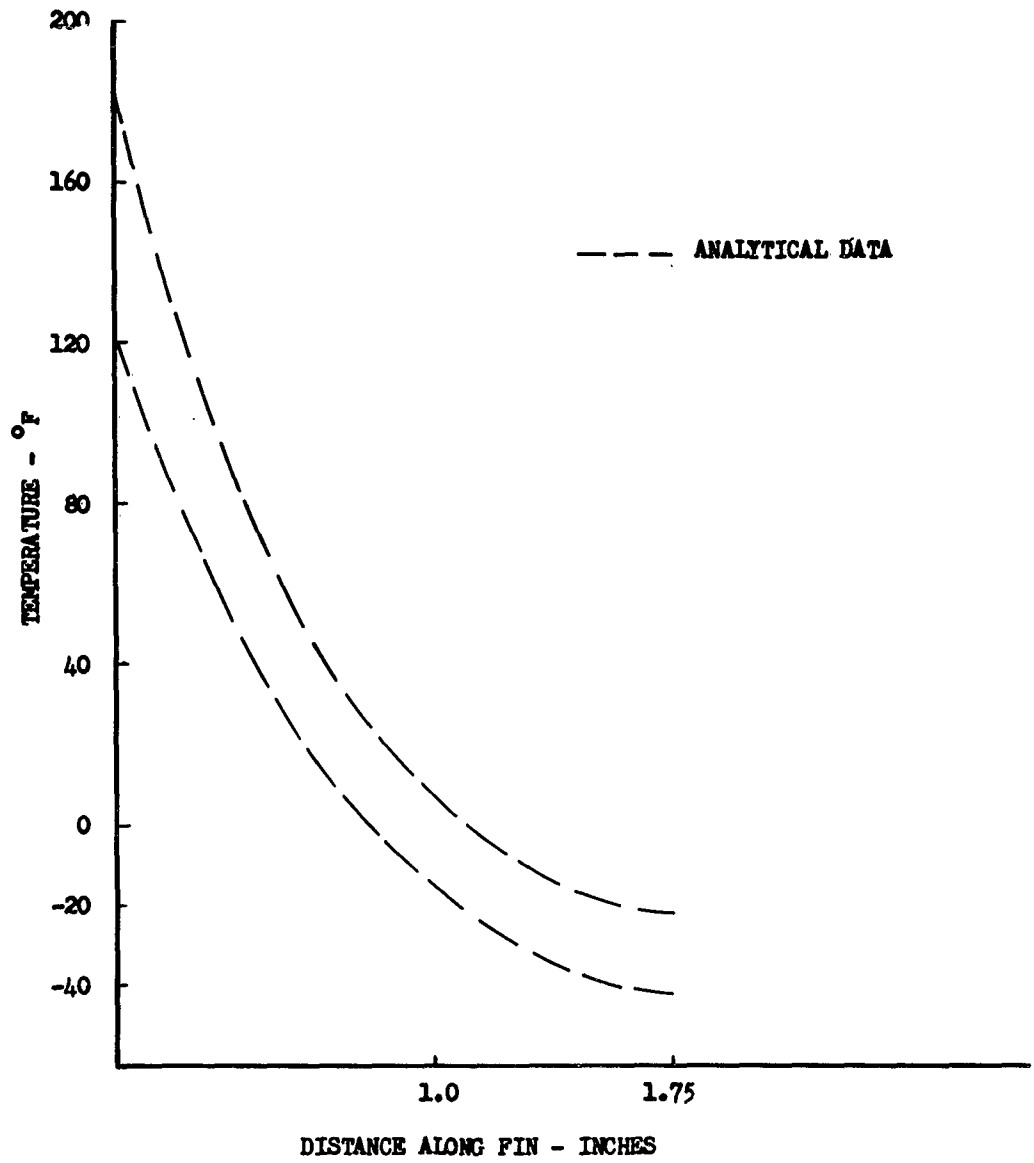


Figure 25.

TEMPERATURE DISTRIBUTION ALONG FIN
SPECIMEN NO. 4

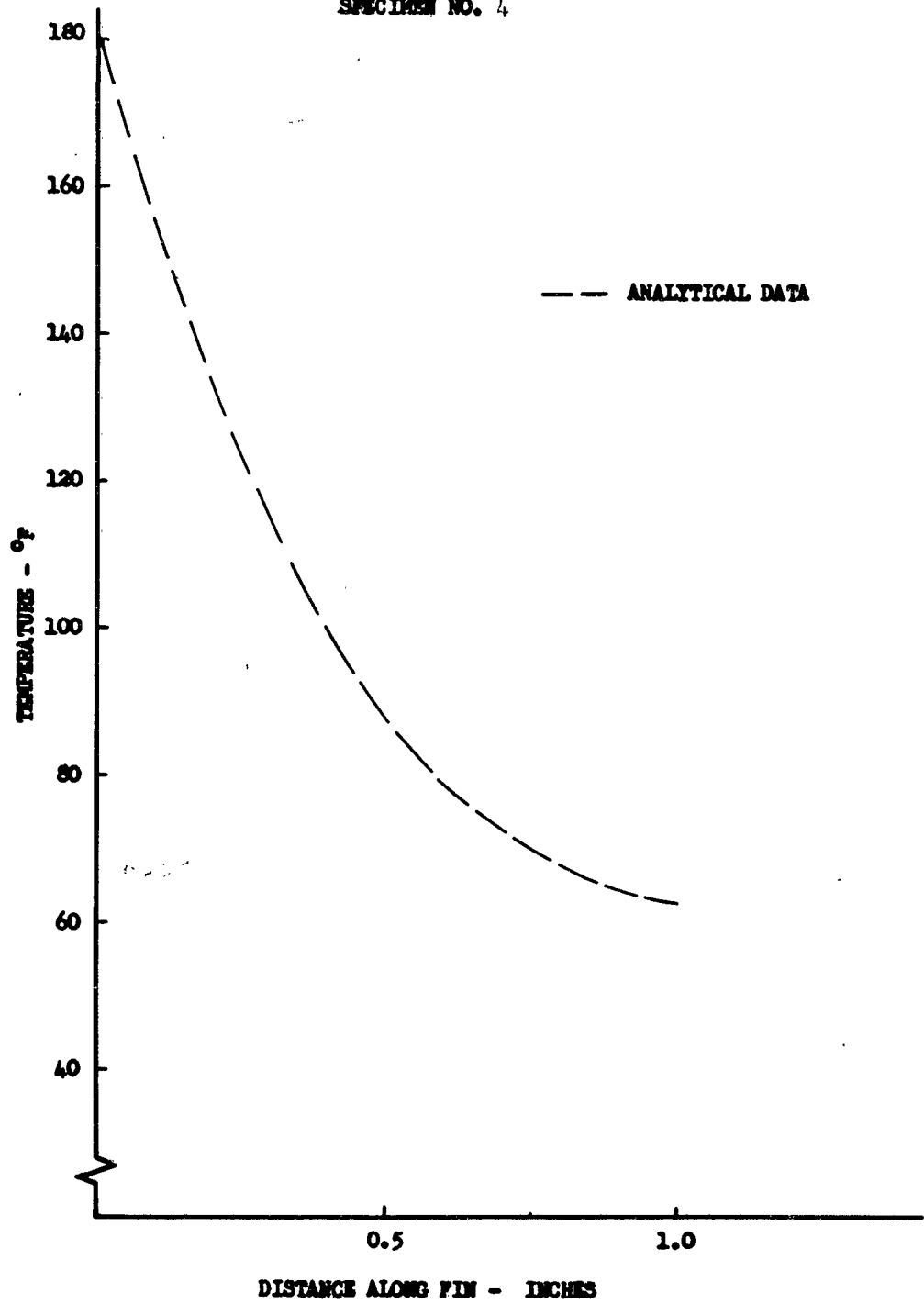


Figure 26.

TEMPERATURE DISTRIBUTION ALONG FIN
SPECIMEN NO. 5

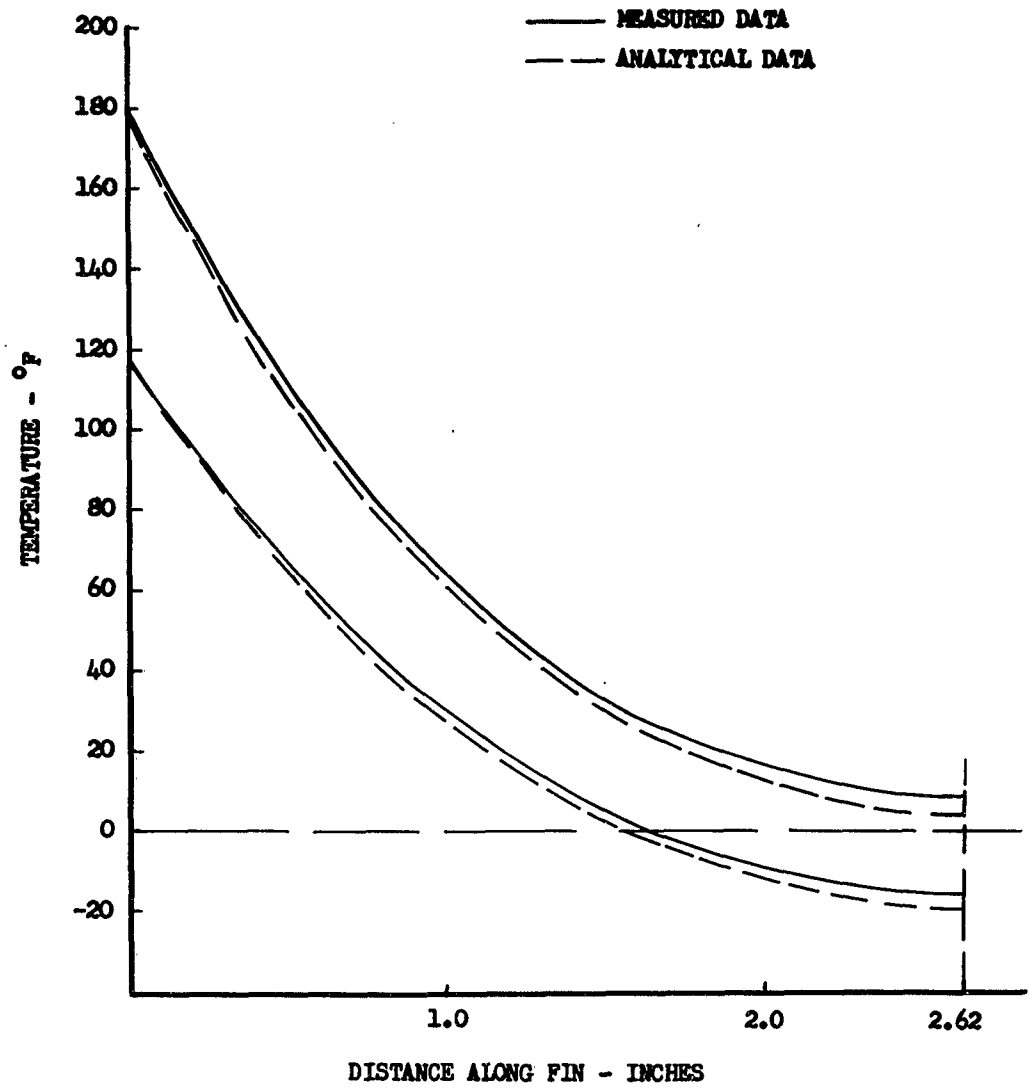


Figure 27.

TEMPERATURE DISTRIBUTION ALONG FIN
SPECIMEN NO. 6

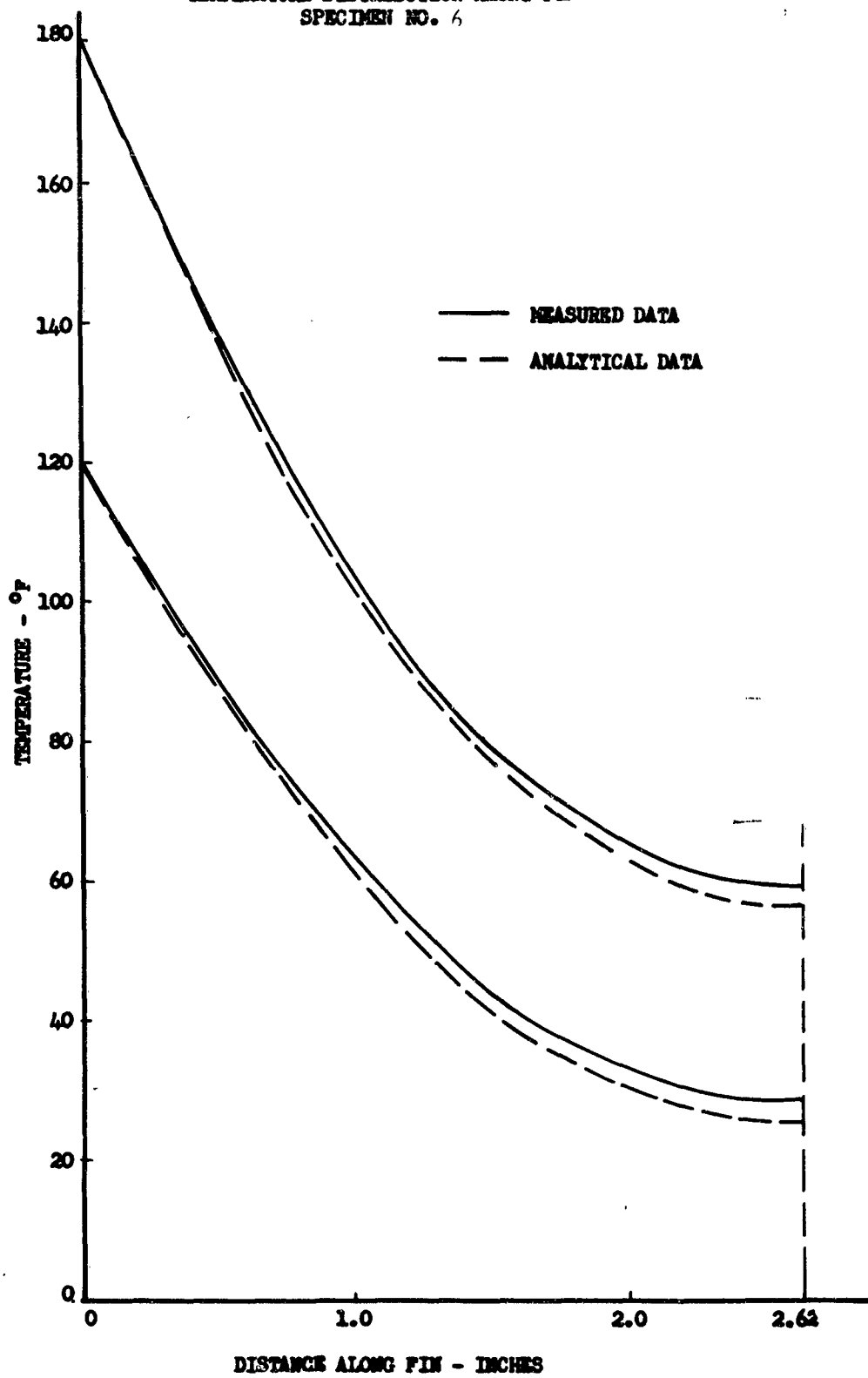


Figure 28.

TEMPERATURE DISTRIBUTION ALONG FIN

SPECIMEN NO. 7

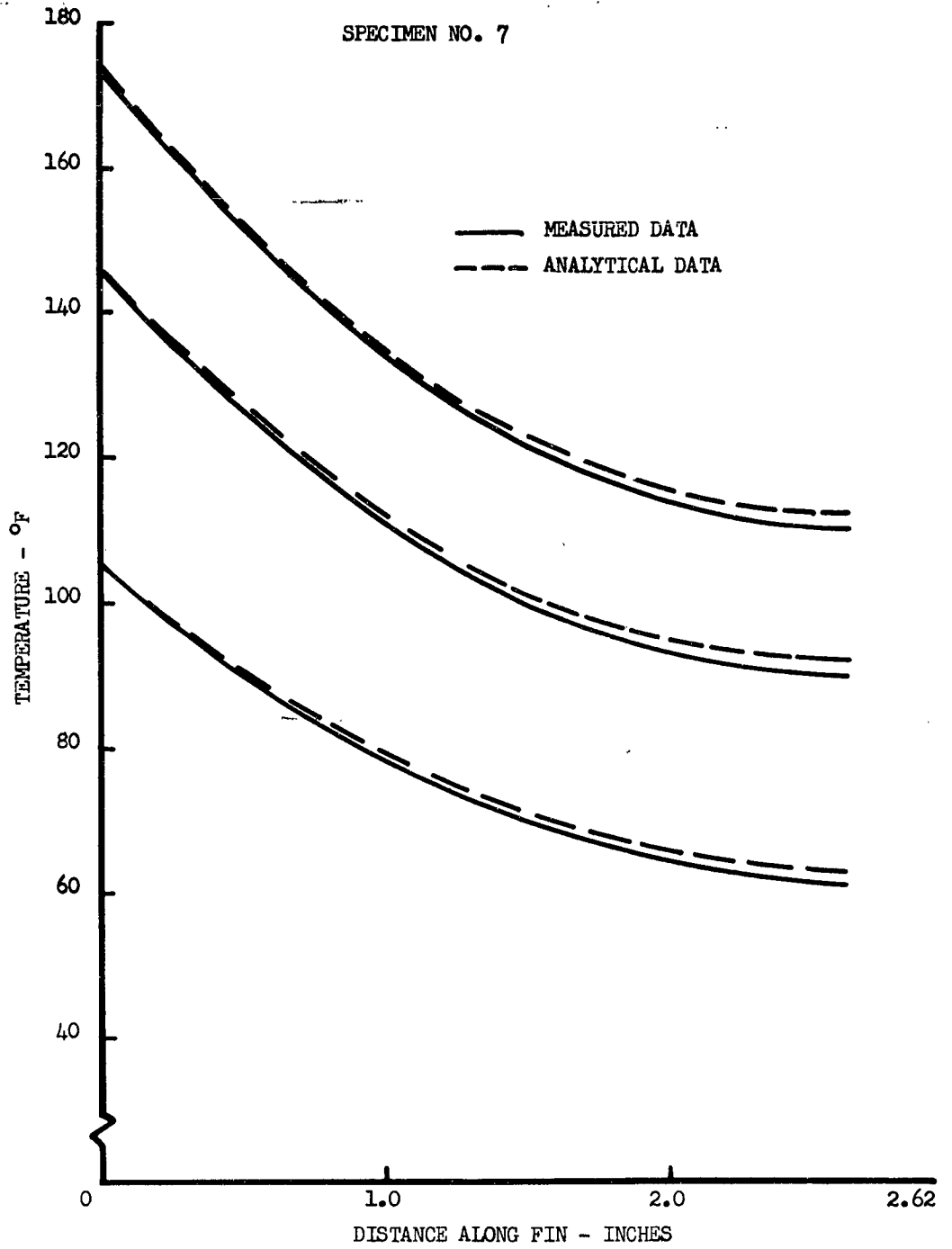


Figure 29.

TEMPERATURE DISTRIBUTION ALONG FIN

SPECIMEN NO. 8

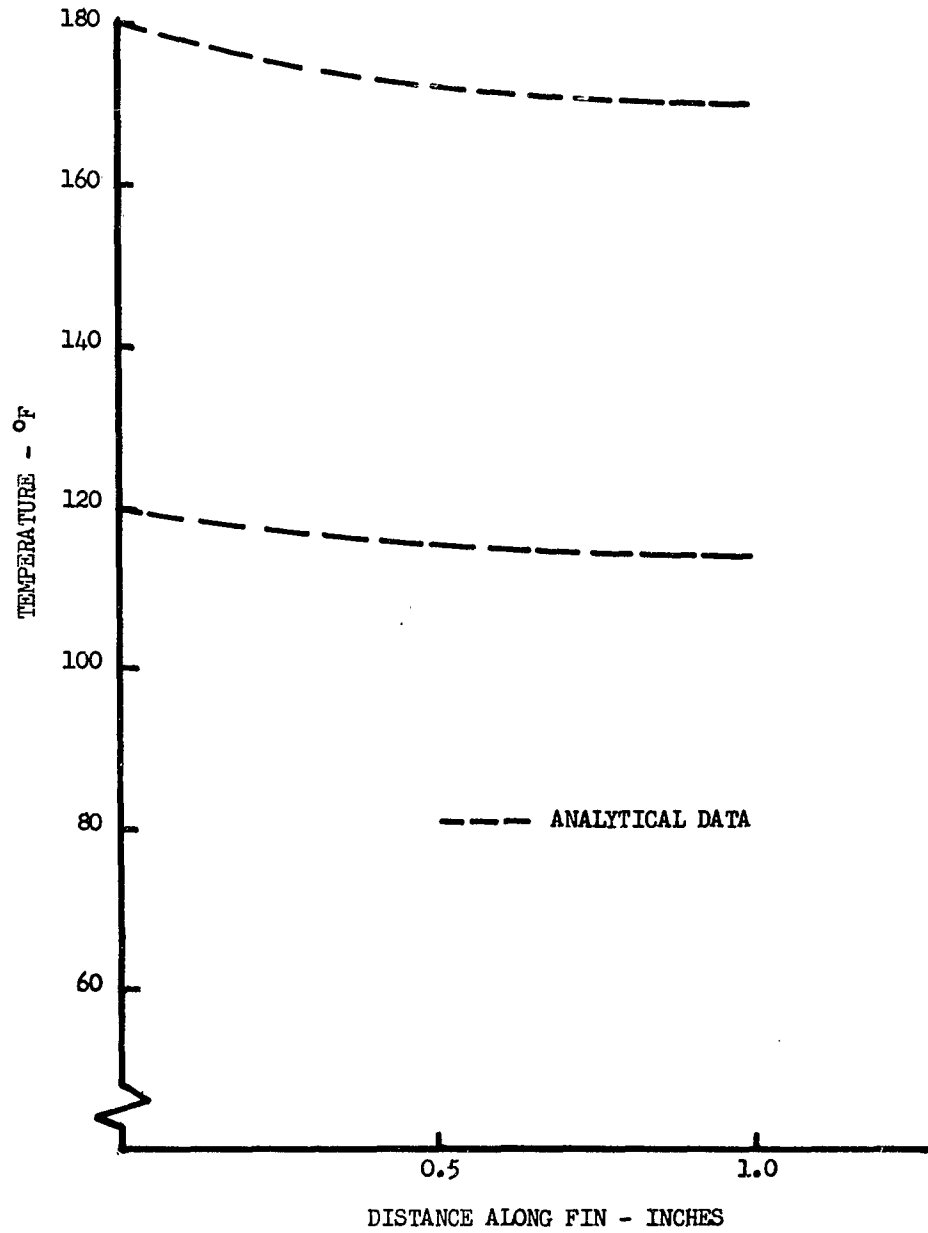


Figure 30.

TEMPERATURE DISTRIBUTION ALONG FIN
SPECIMEN NO. 9

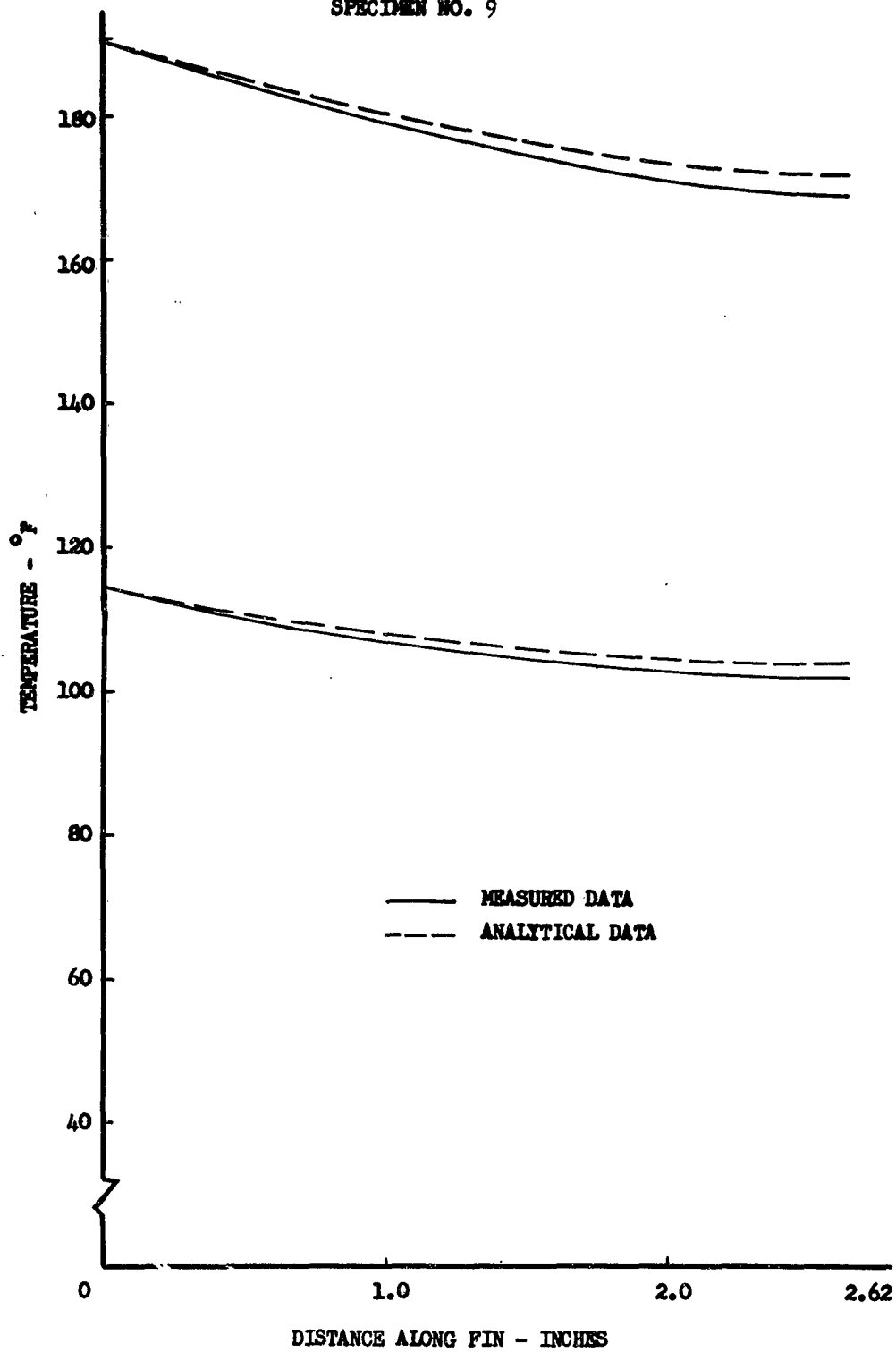


Figure 31.

TEMPERATURE DISTRIBUTION ALONG FIN
SPECIMEN NO. 10

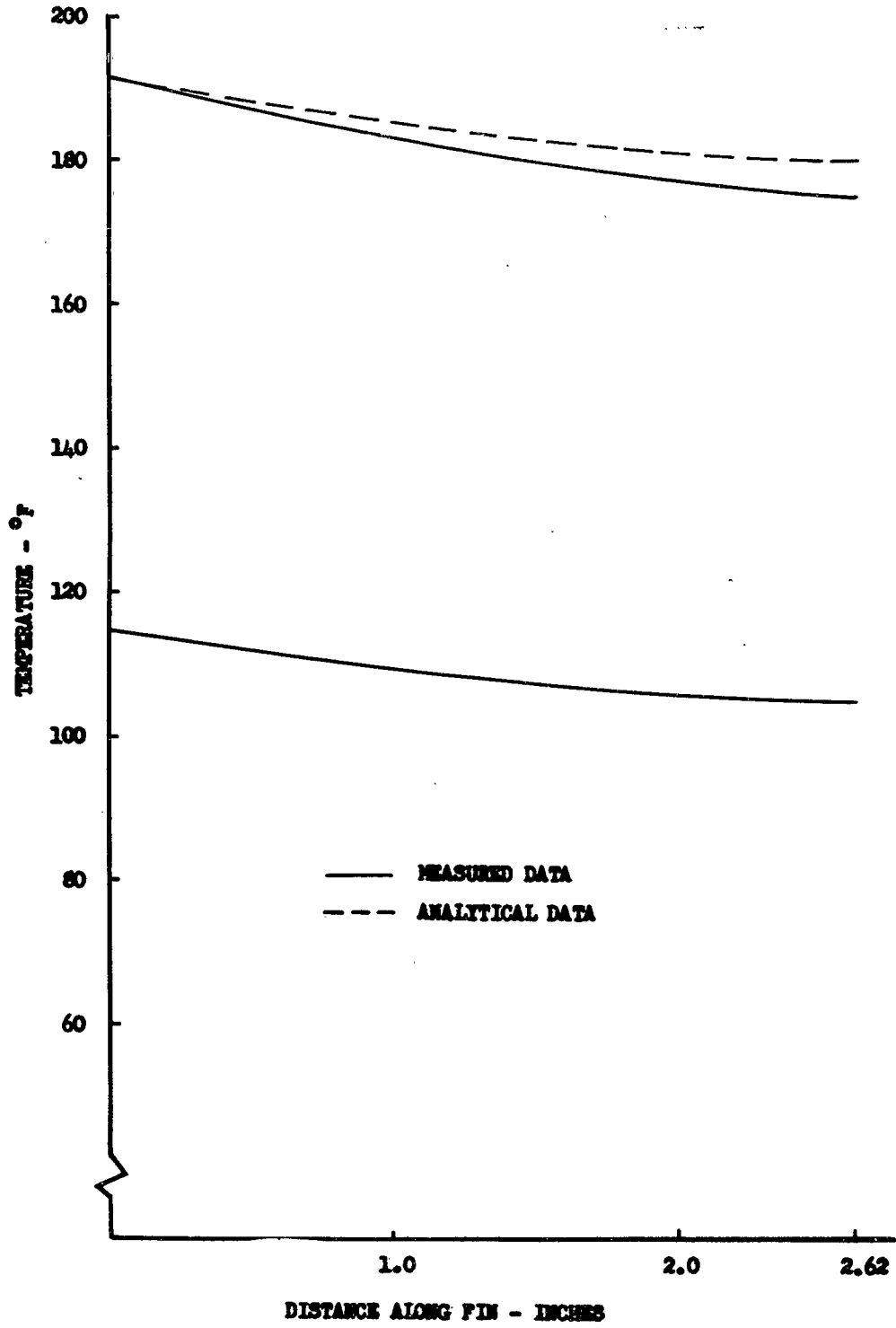


Figure 32.

TEMPERATURE DISTRIBUTION ALONG FIN
SPECIMEN NO. 11

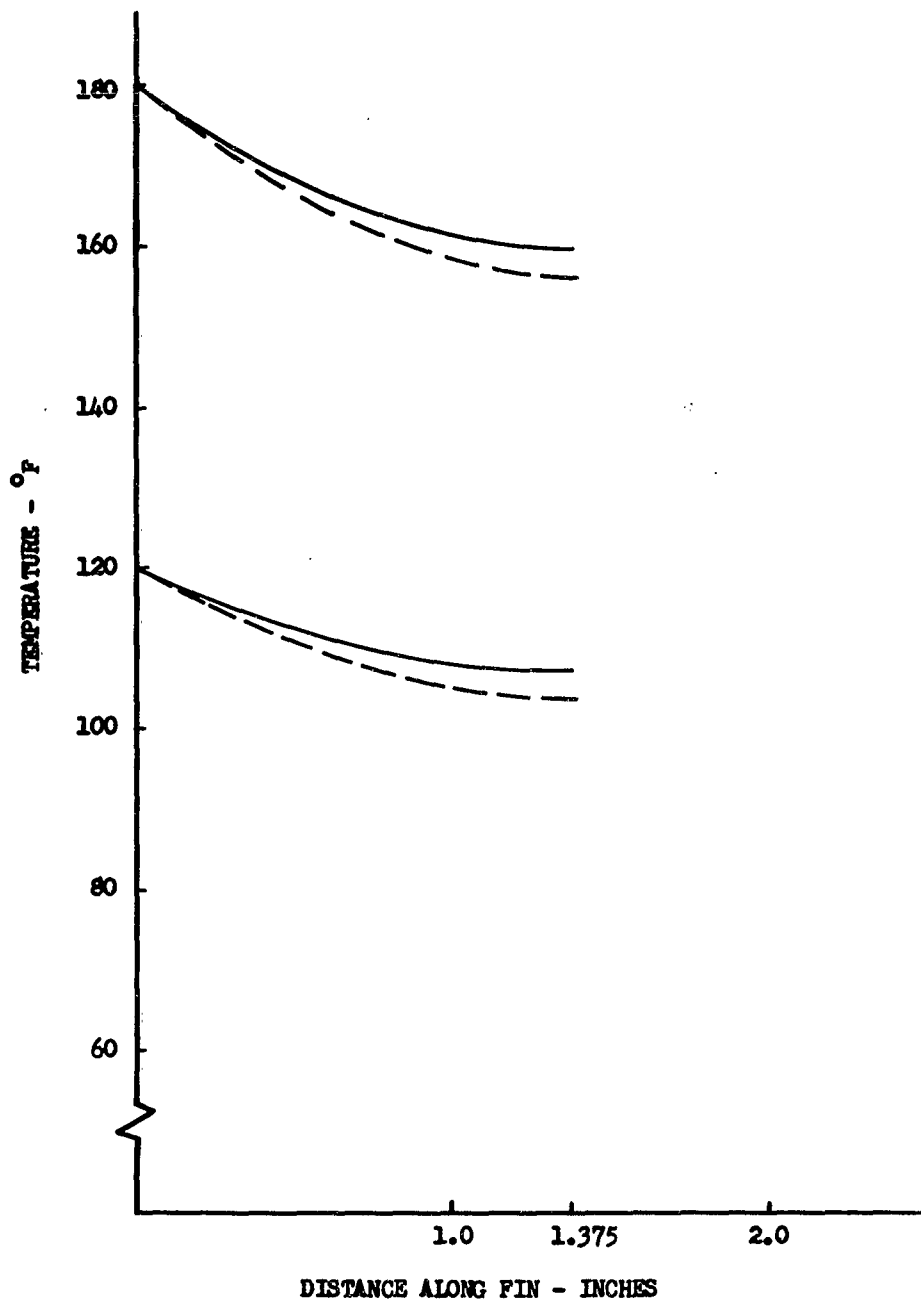


Figure 33.
TEMPERATURE DISTRIBUTION ALONG FIN
SPECIMEN NO. 12

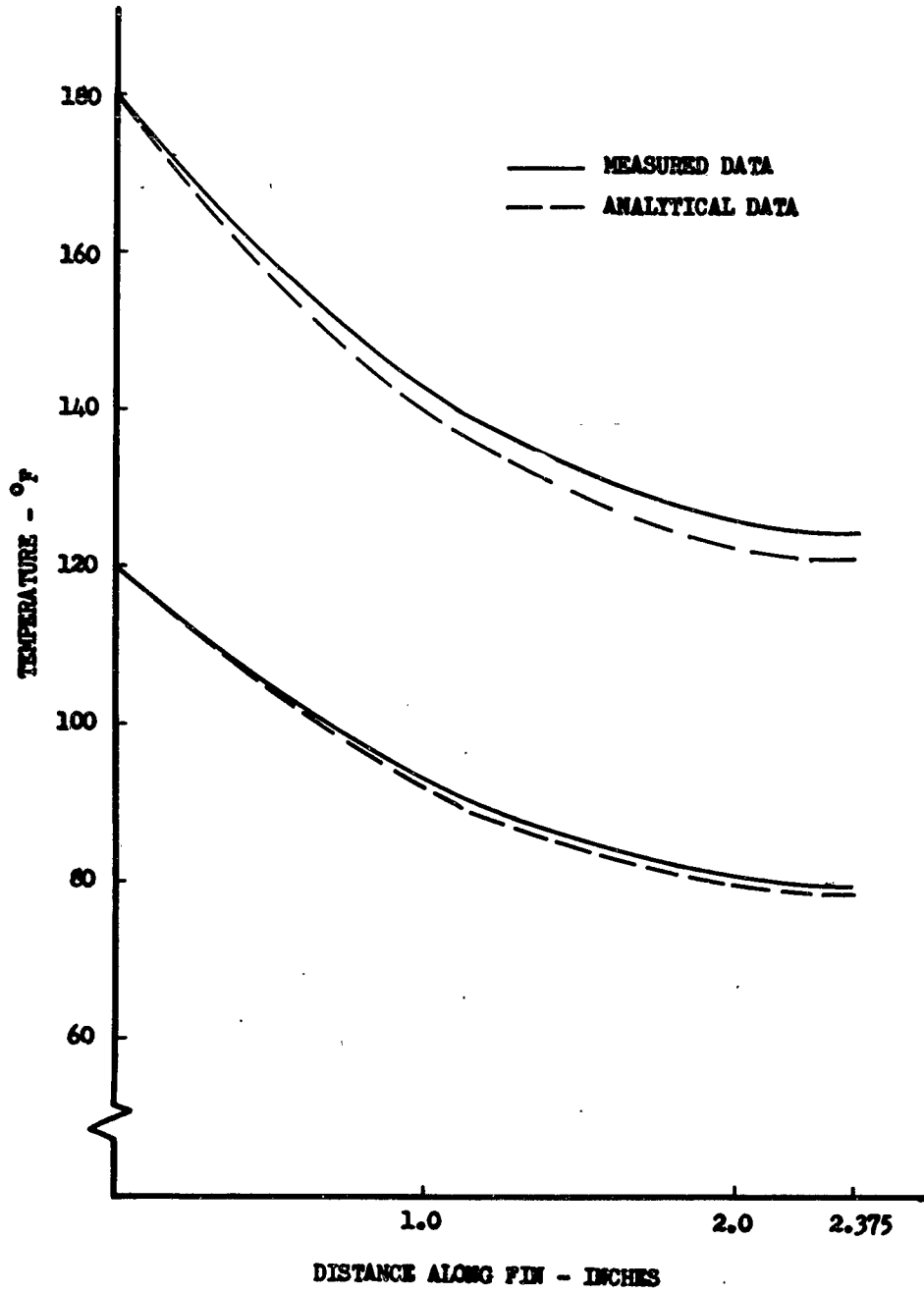


Figure 34.
TEMPERATURE DISTRIBUTION ALONG FIN
SPECIMEN NO. 13

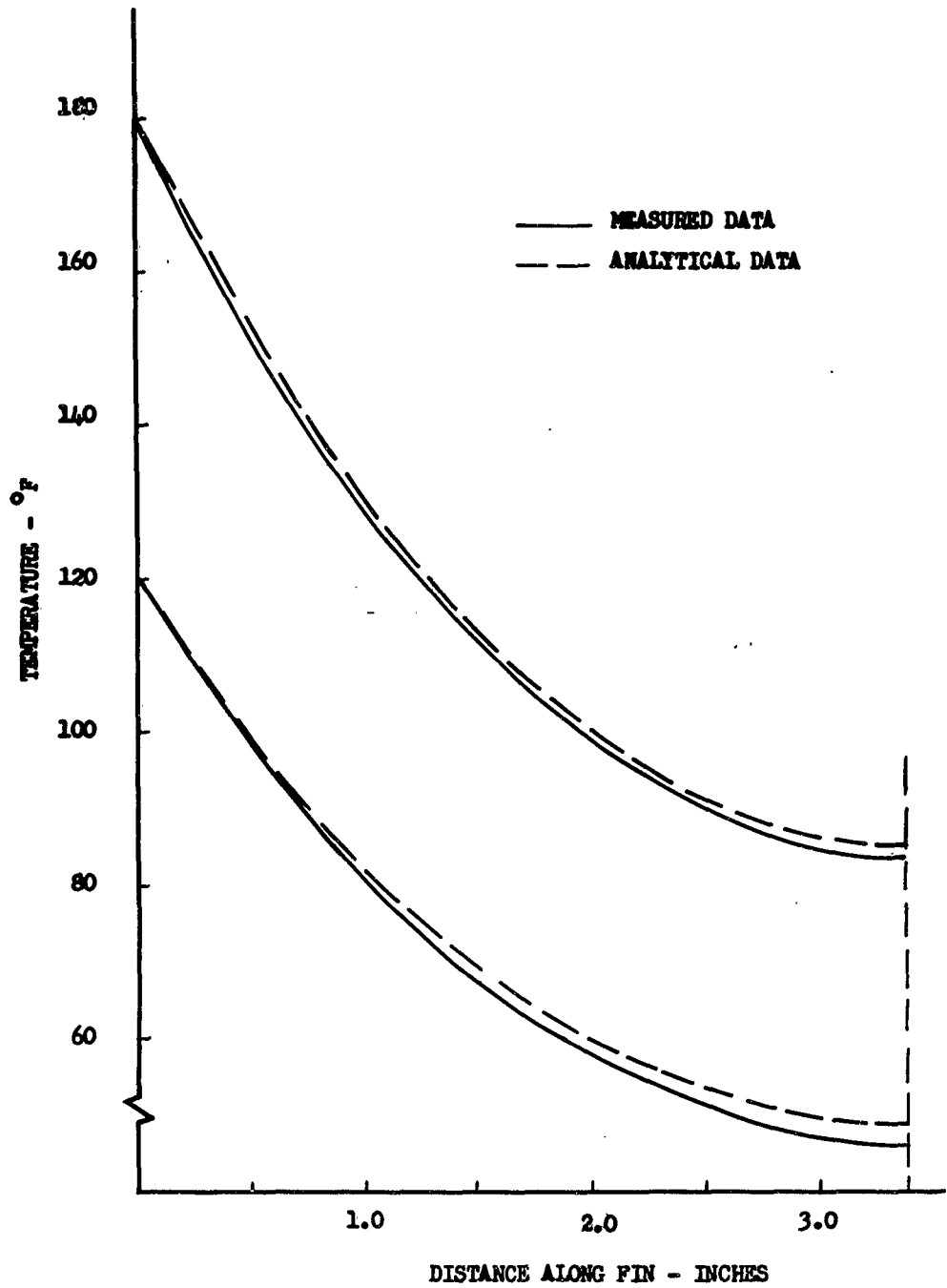


Figure 35.

COMPARISON OF TEMPERATURE
DISTRIBUTION BETWEEN COATED AND UNCOATED
ALUMINUM FINS

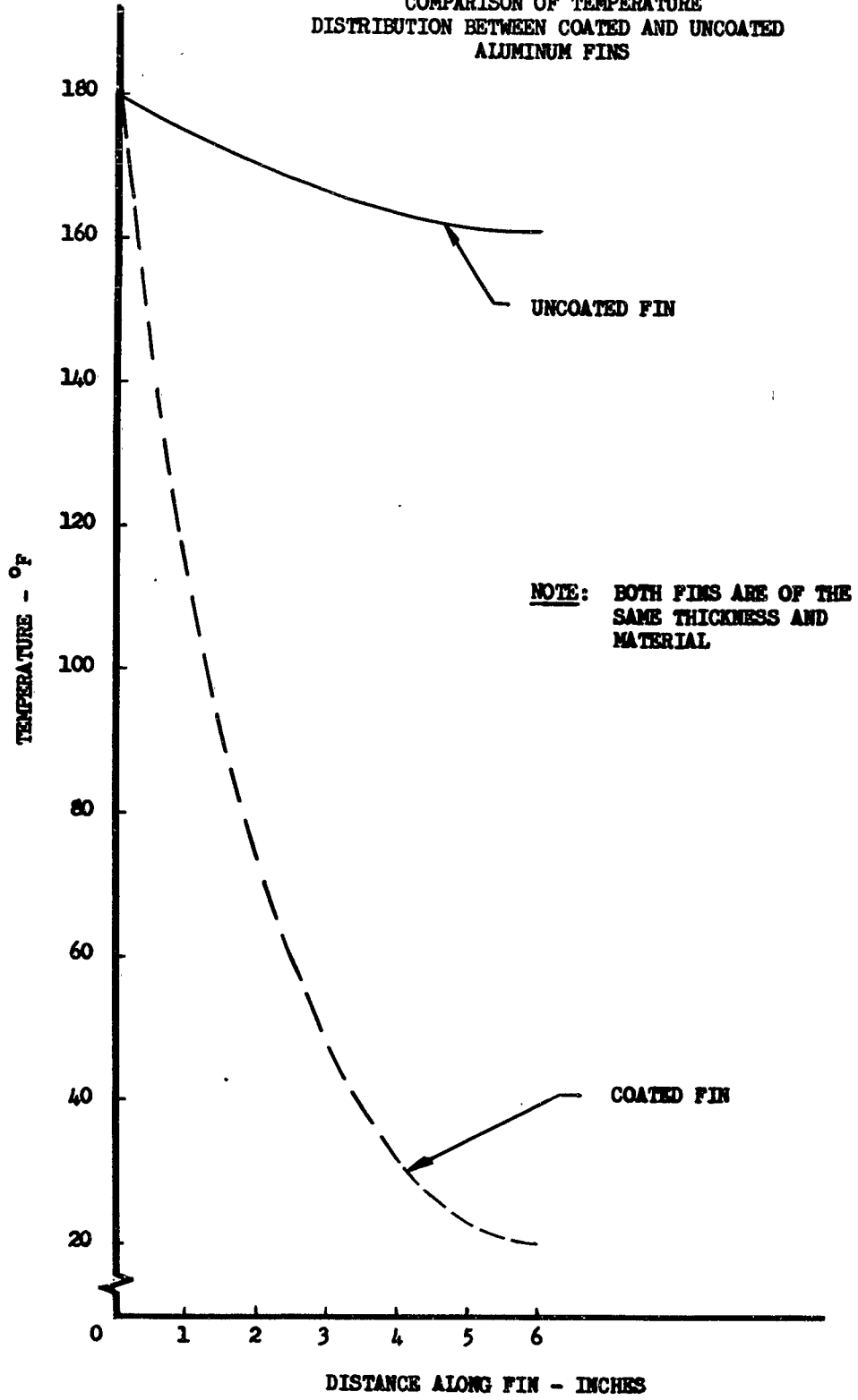


Figure 36.

COMPARISON OF TEMPERATURE DISTRIBUTION
BETWEEN COATED AND UNCOATED STAINLESS
STEEL FINS

NOTE: BOTH FINS ARE OF THE SAME
MATERIAL AND THICKNESS

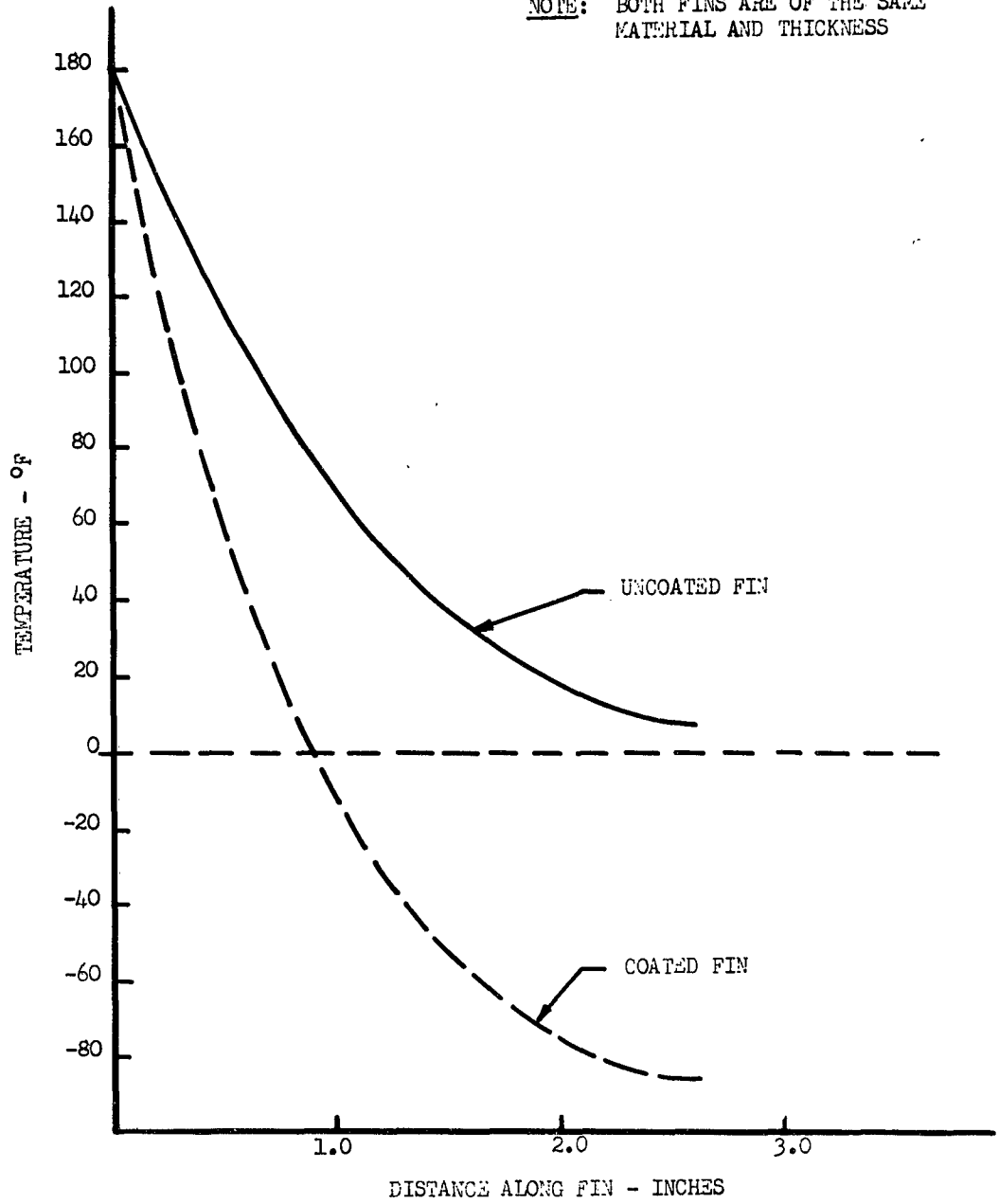


Figure 37.

TEMPERATURE DISTRIBUTION ALONG FIN
COMPARISON BETWEEN OUTSIDE AND INSIDE FINS

SPECIMEN NO. 5

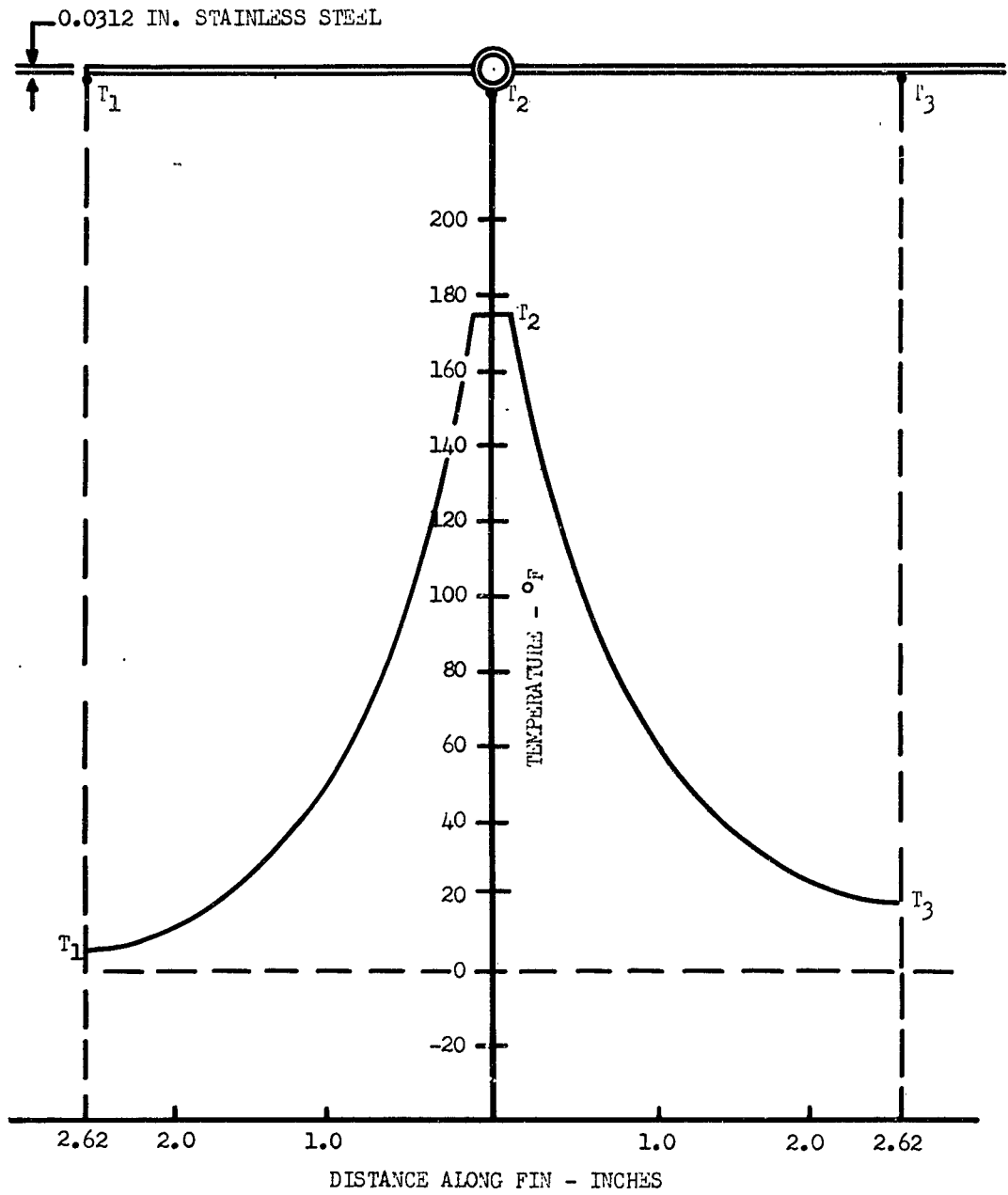


Figure 38.

TEMPERATURE DISTRIBUTION ALONG FIN
COMPARISON BETWEEN OUTSIDE AND INSIDE FINS

SPECIMEN NO. 6

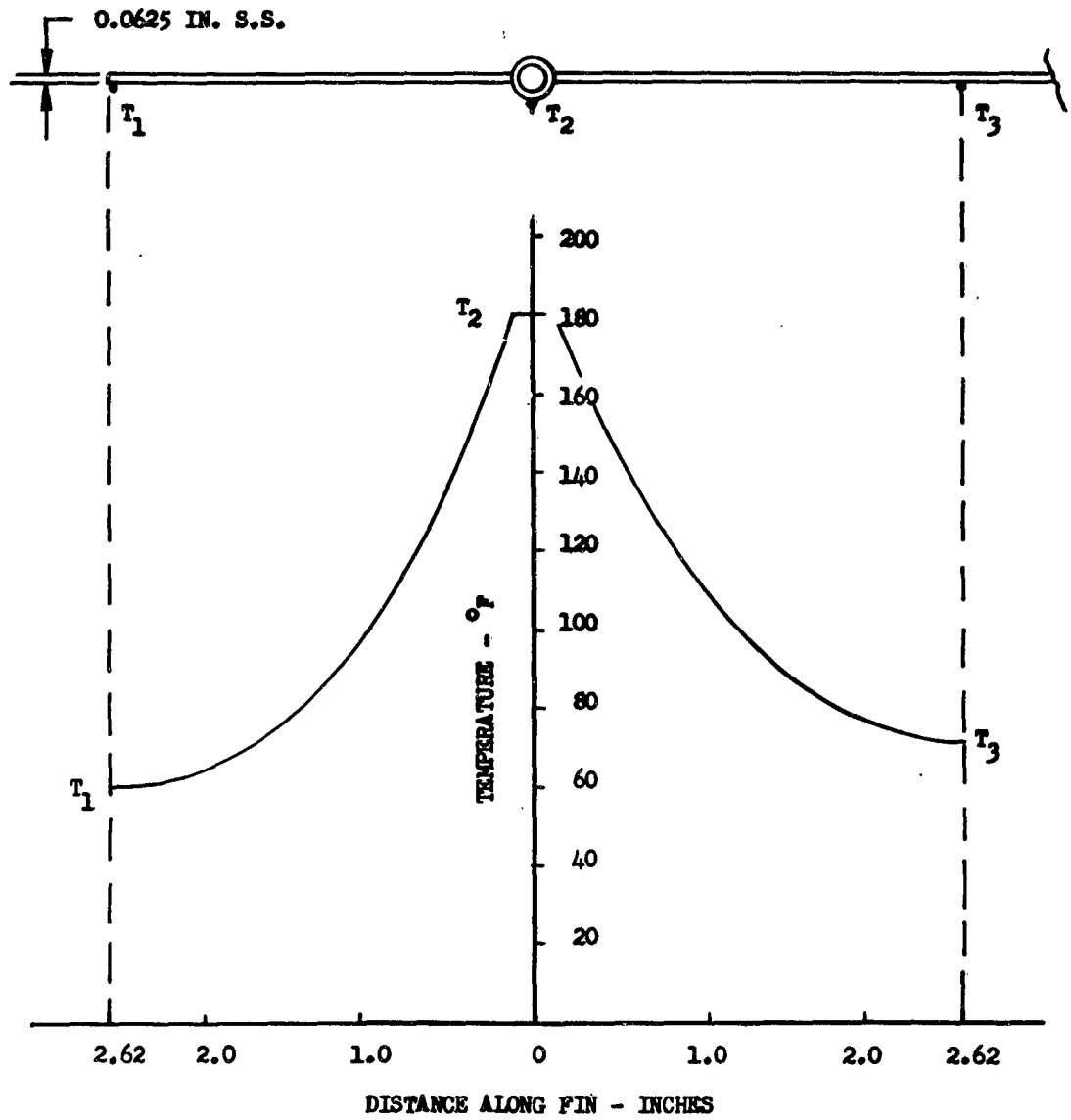


Figure 39.

TEMPERATURE DISTRIBUTION ALONG FIN .

COMPARISON BETWEEN TEMPERATURE AT OUTER
EDGE AND AT MIDDLE POINT BETWEEN TUBES

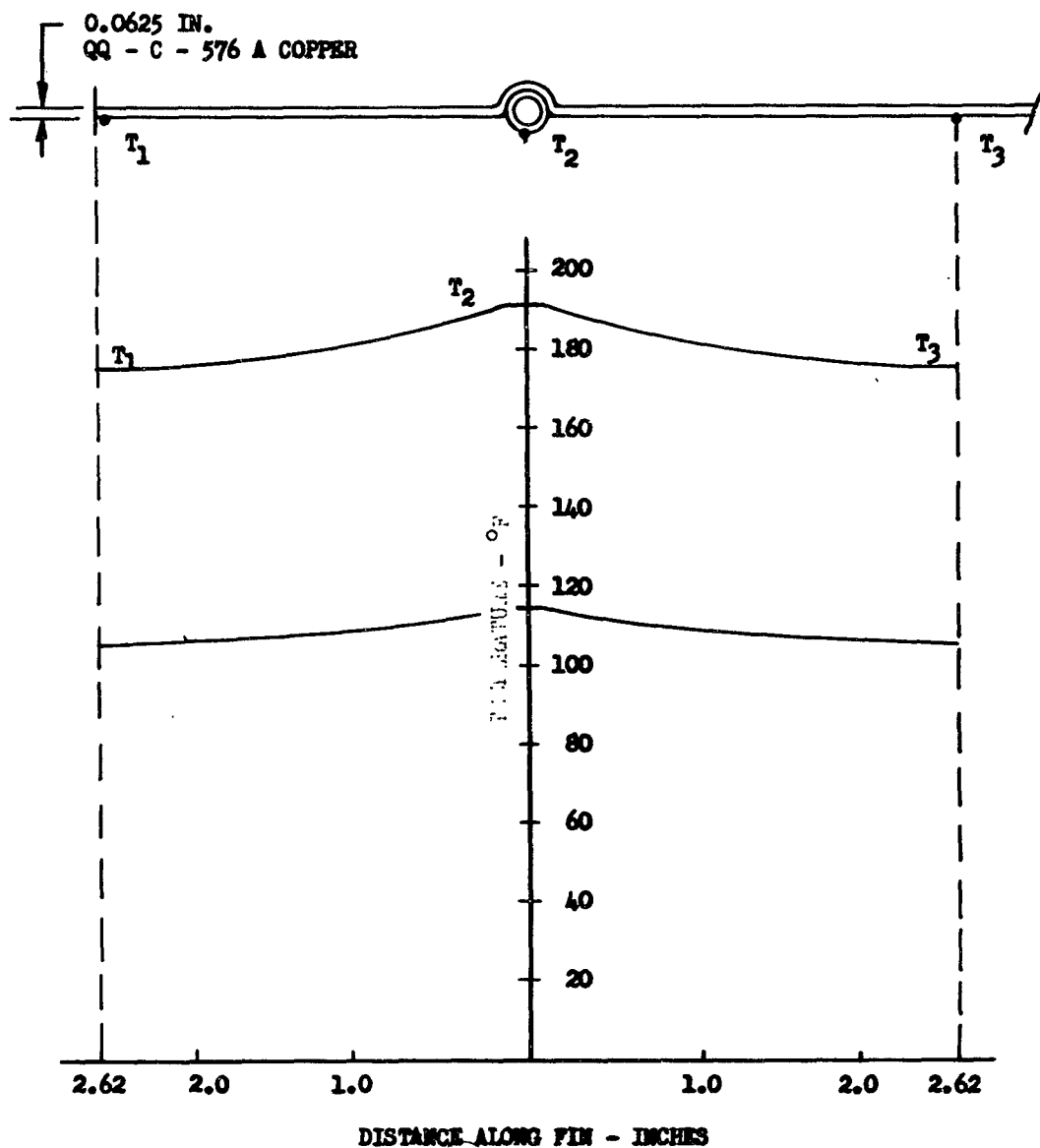


Figure 40.

TEMPERATURE DISTRIBUTION ALONG FIN
COMPARISON BETWEEN OUTSIDE AND INSIDE FIN

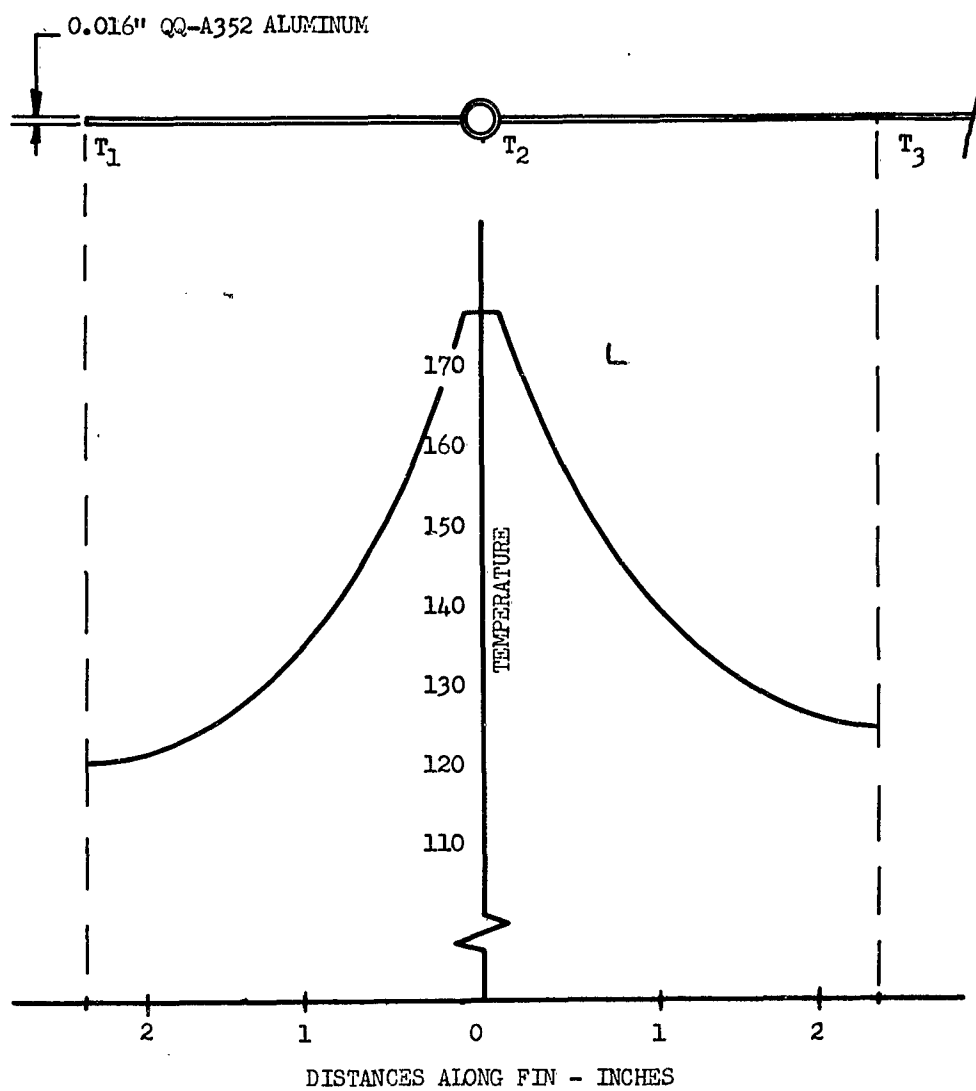


Figure 41.
COMPARISON OF HEAT REJECTION RATES
PER UNIT WEIGHT OF COATED AND
UNCOATED RADIATOR ELEMENTS

NOTE: BOTH SPECIMENS ARE OF THE
 SAME MATERIAL, FIN LENGTH
 AND THICKNESS

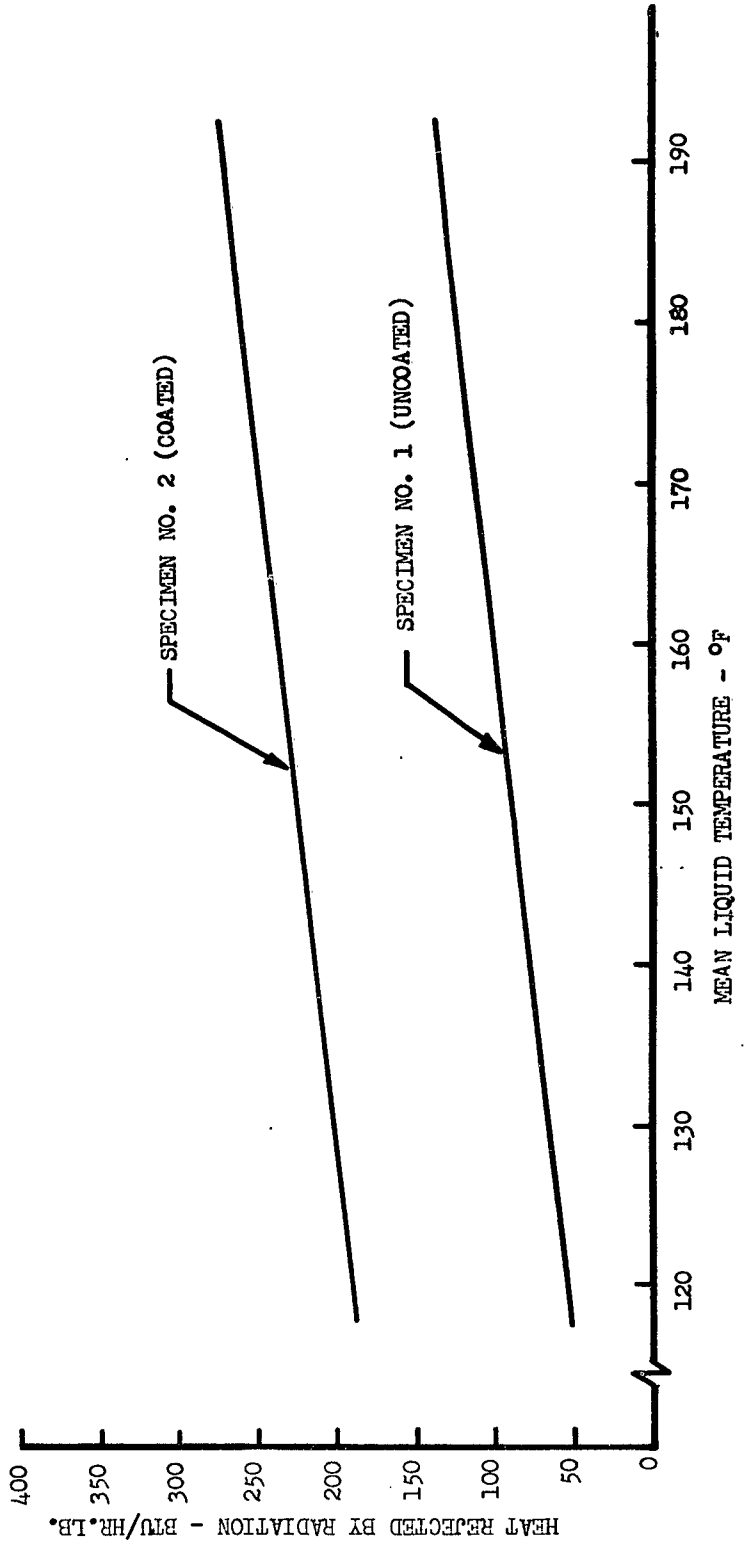


Figure 42.

COMPARISON OF HEAT REJECTION RATES
PER UNIT AREA FOR RADIATOR ELEMENTS
OF DIFFERENT FIN LENGTH

NOTE: ALL SPECIMENS ARE OF THE SAME
MATERIAL, FIN THICKNESS AND
SURFACE COATING

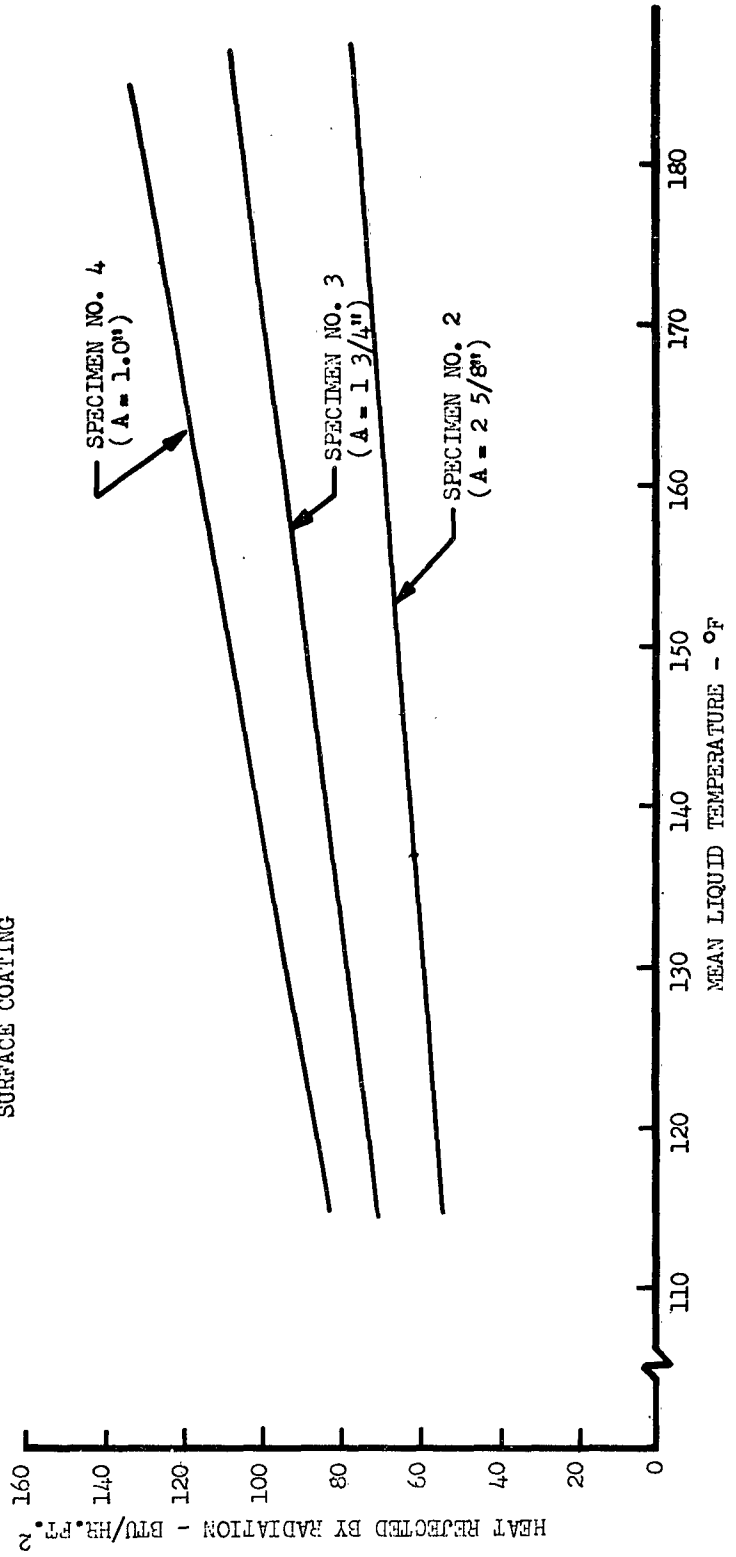


Figure 43.
COMPARISON OF HEAT REJECTION RATES PER UNIT AREA
FROM RADIATOR ELEMENTS OF DIFFERENT FIN THICKNESS

NOTE: ALL SPECIMENS ARE OF THE
 SAME MATERIAL, FIN LENGTH
 AND SURFACE COATING

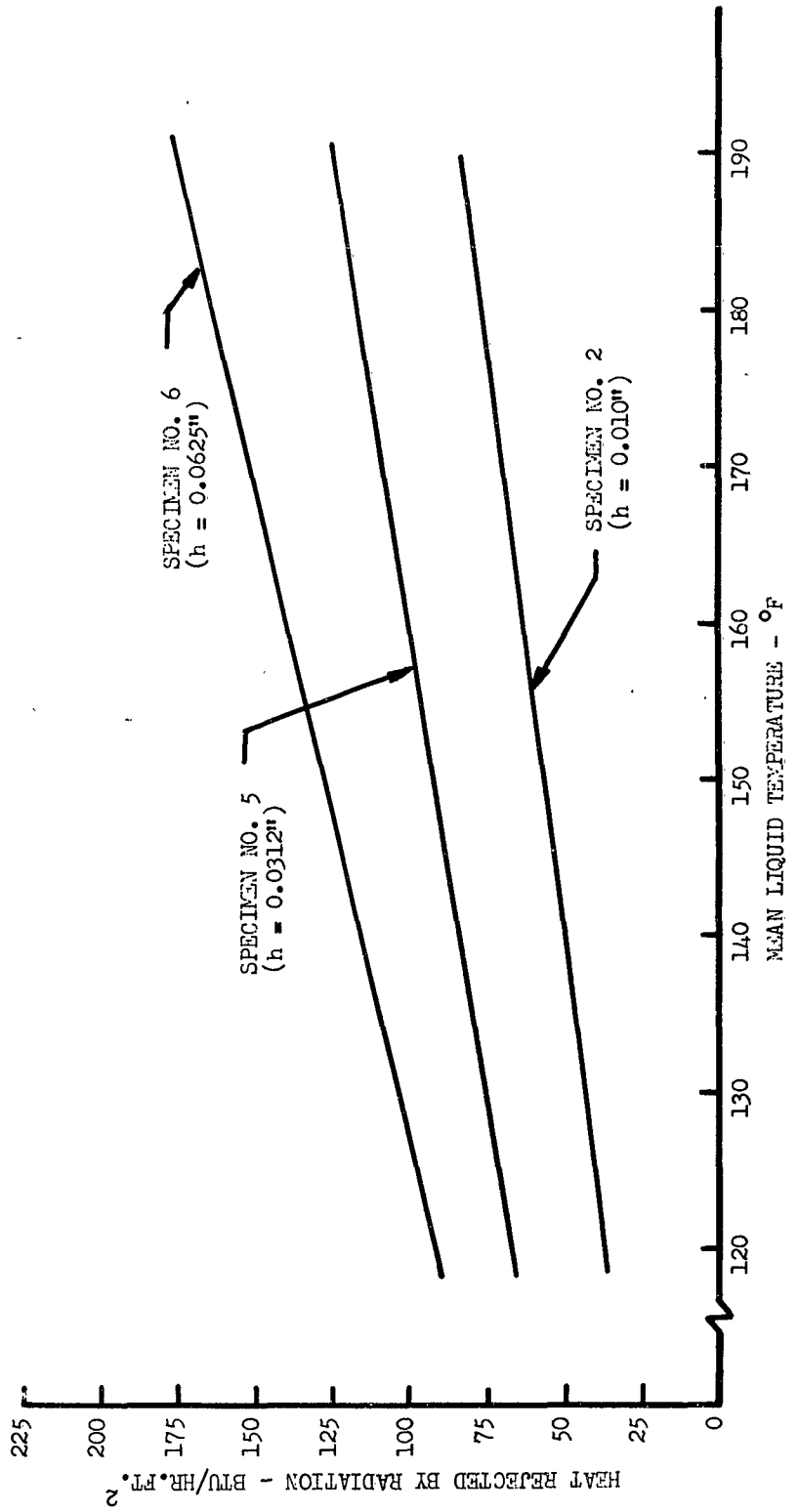


Figure 44.
**COMPARISON OF HEAT REJECTION RATES PER UNIT WEIGHT
 FOR RADIATOR ELEMENTS OF VARIOUS MATERIALS**

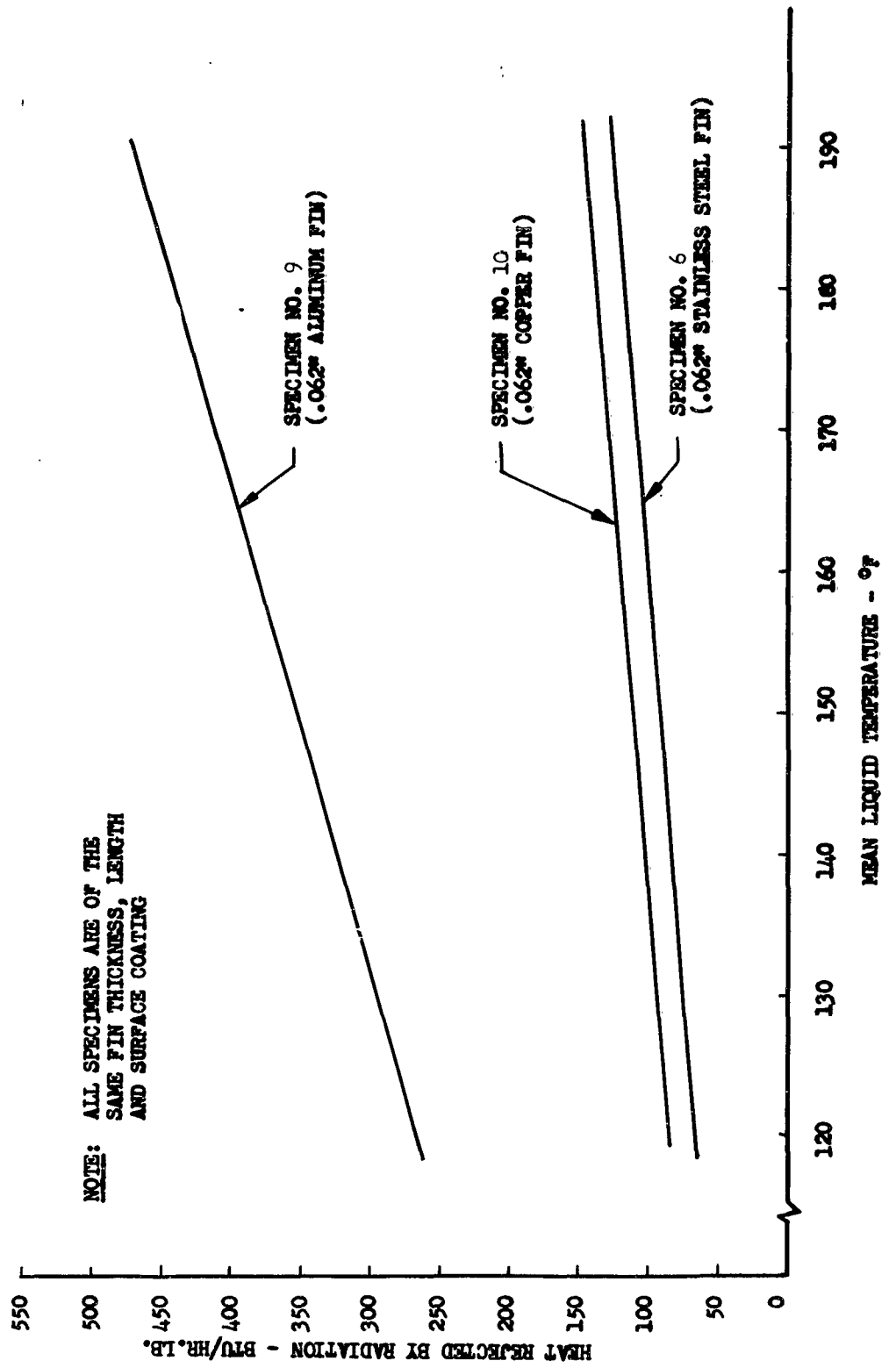


Figure 45.

COMPARISON OF HEAT REJECTION RATES PER UNIT WEIGHT
FOR RADIATOR ELEMENTS OF DIFFERENT FIN THICKNESS

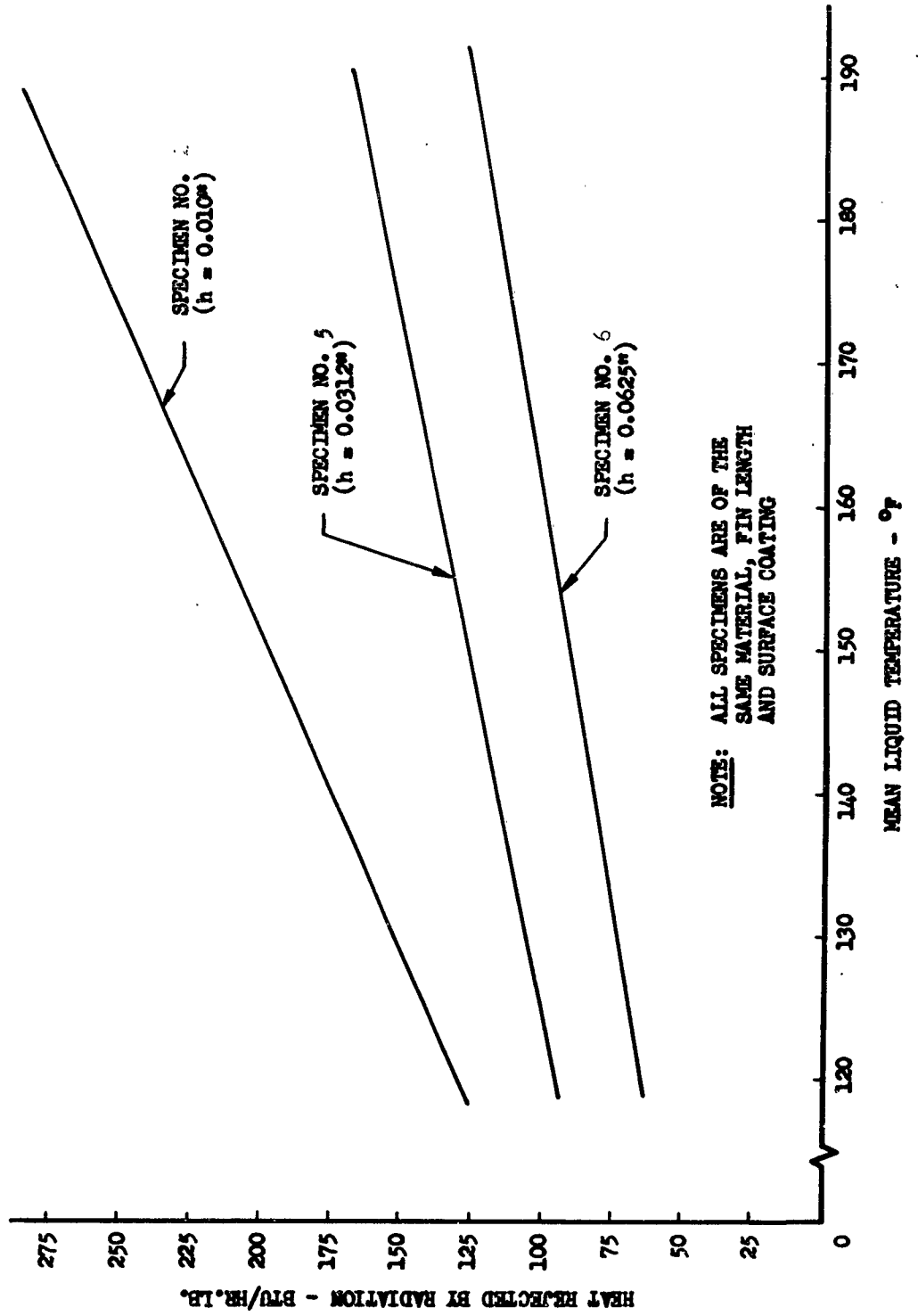


Figure 46.

COMPARISON OF HEAT REJECTION RATES PER UNIT AREA
FOR RADIATOR ELEMENTS OF VARIOUS MATERIALS

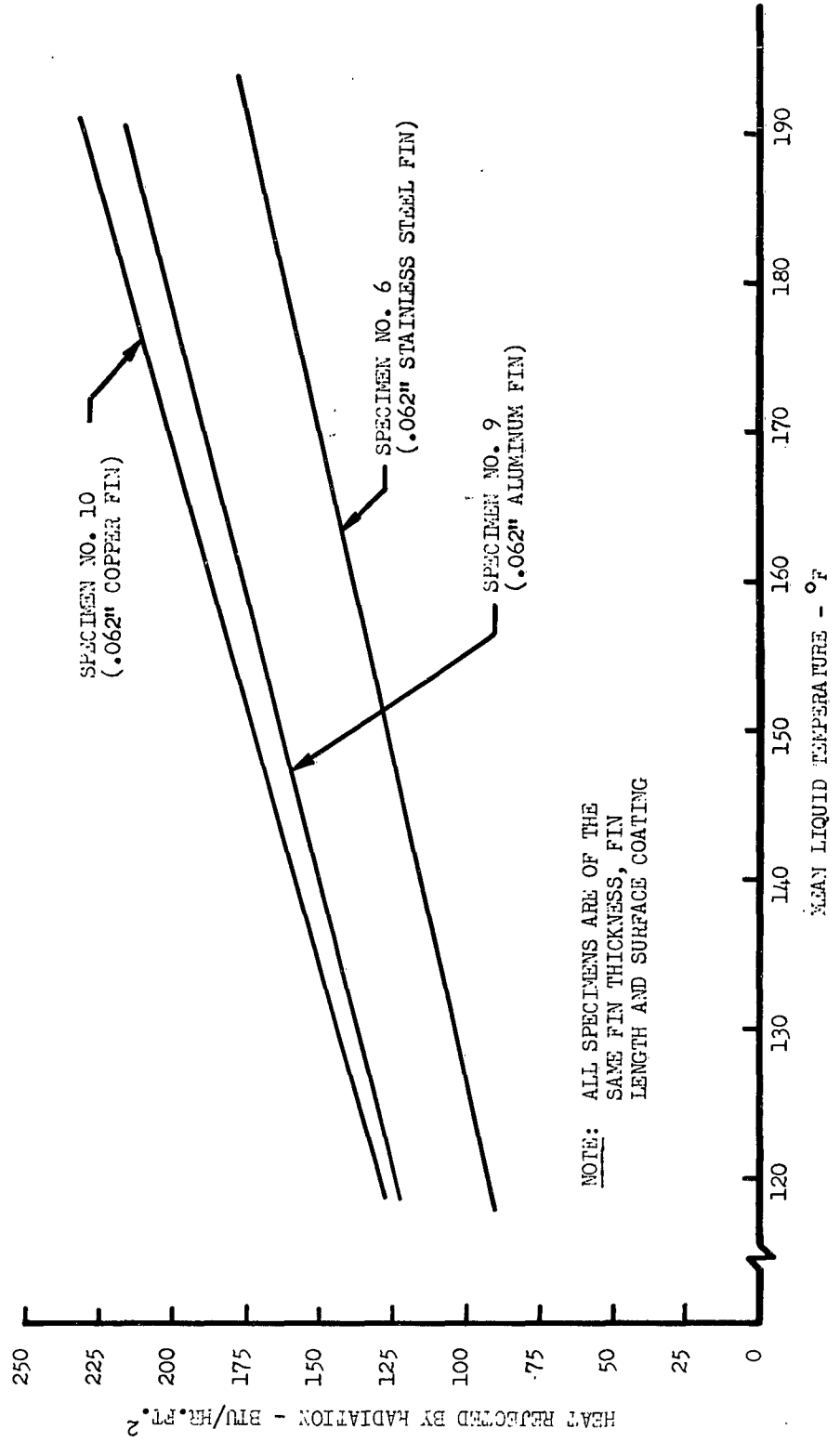


Figure 47.

**EFFECTS OF CONTACT RESISTANCE
UPON HEAT DISSIPATION RATES**

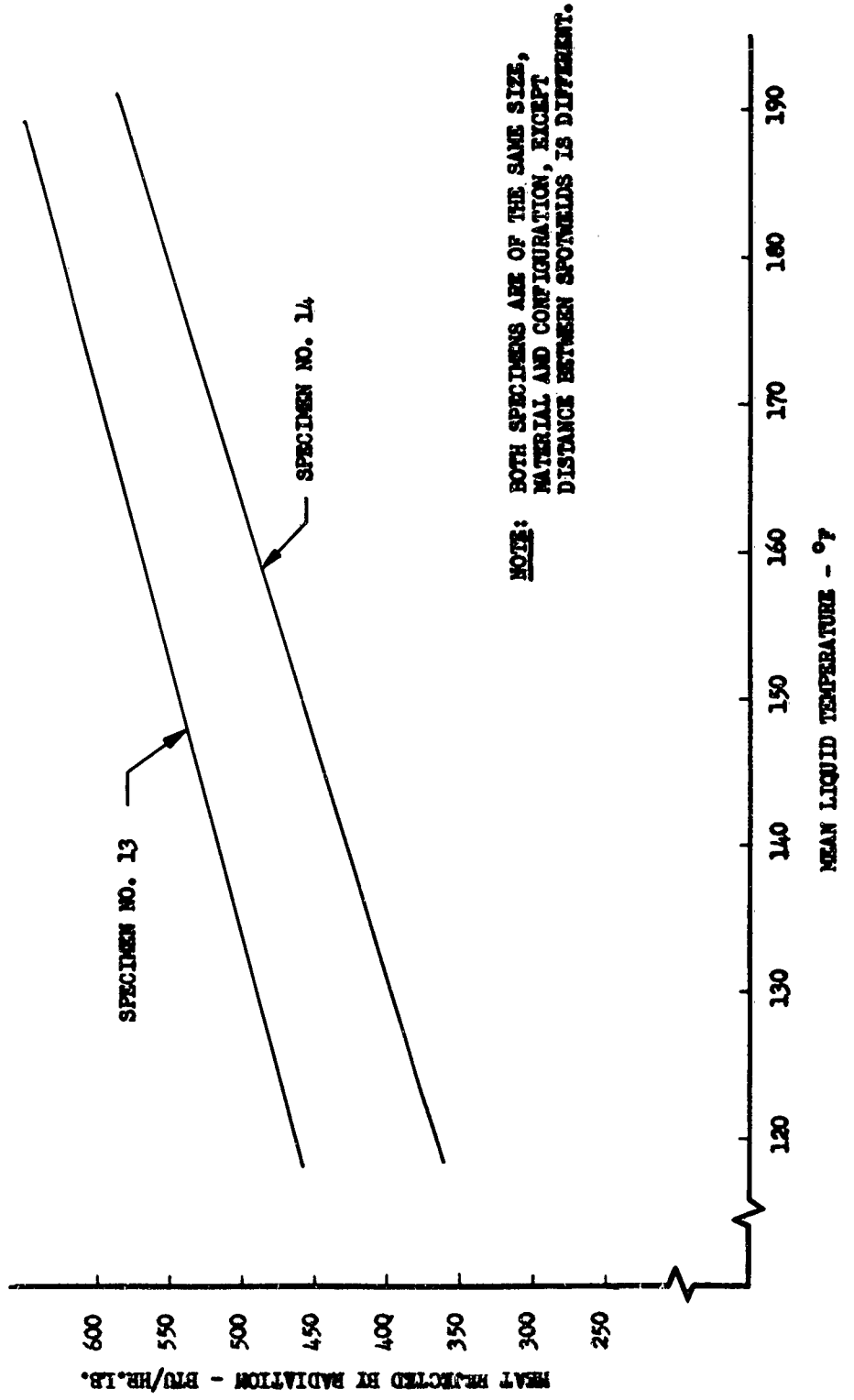


Figure 48.

HEAT REJECTED PER UNIT WEIGHT OF RADIATOR
AS A FUNCTION OF FIN THICKNESS AND MEAN
LIQUID TEMPERATURE

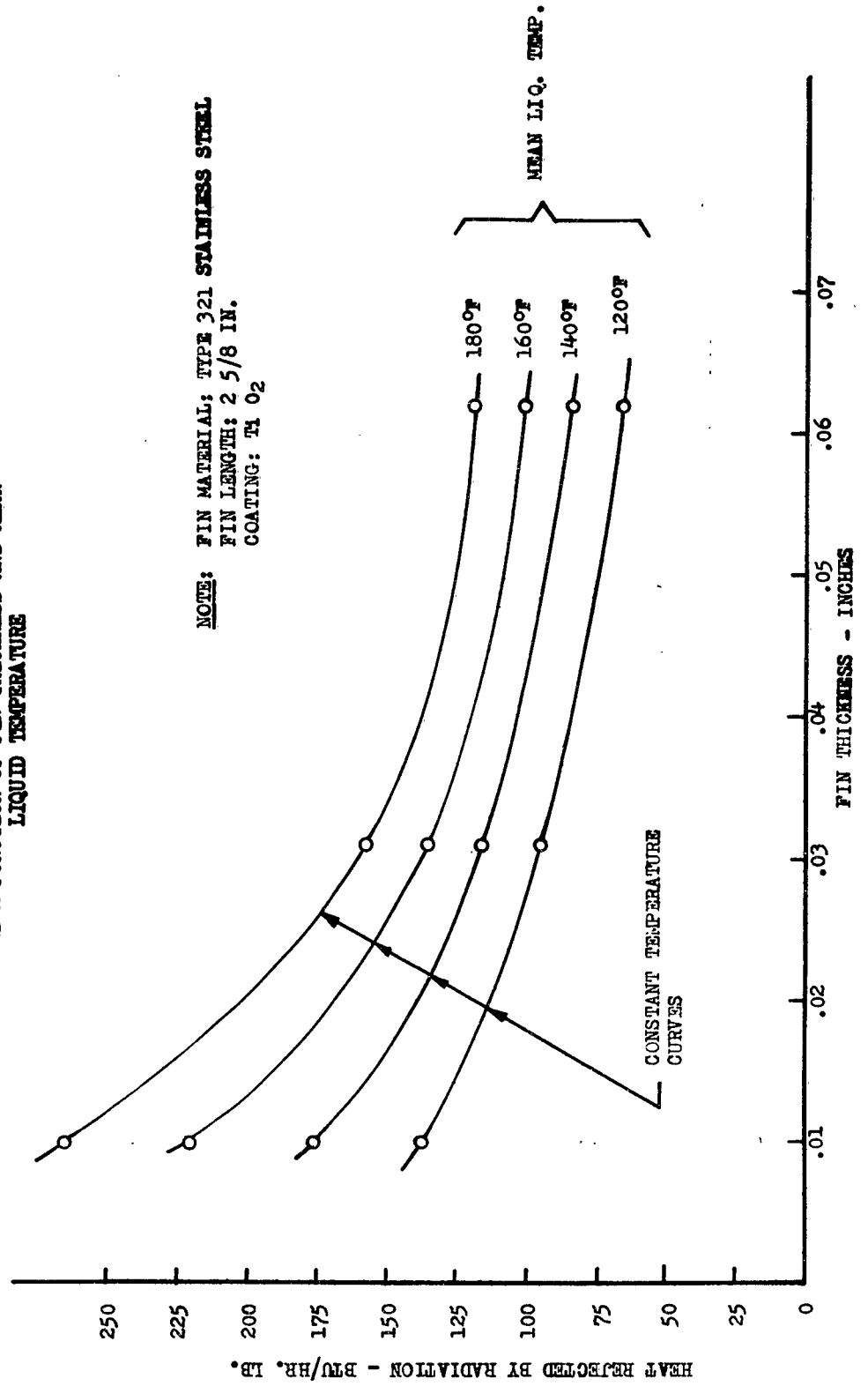


Figure 49.
 HEAT REJECTED PER UNIT AREA OF RADIATOR AS A
 FUNCTION OF FIN THICKNESS AND MEAN LIQUID
 TEMPERATURE

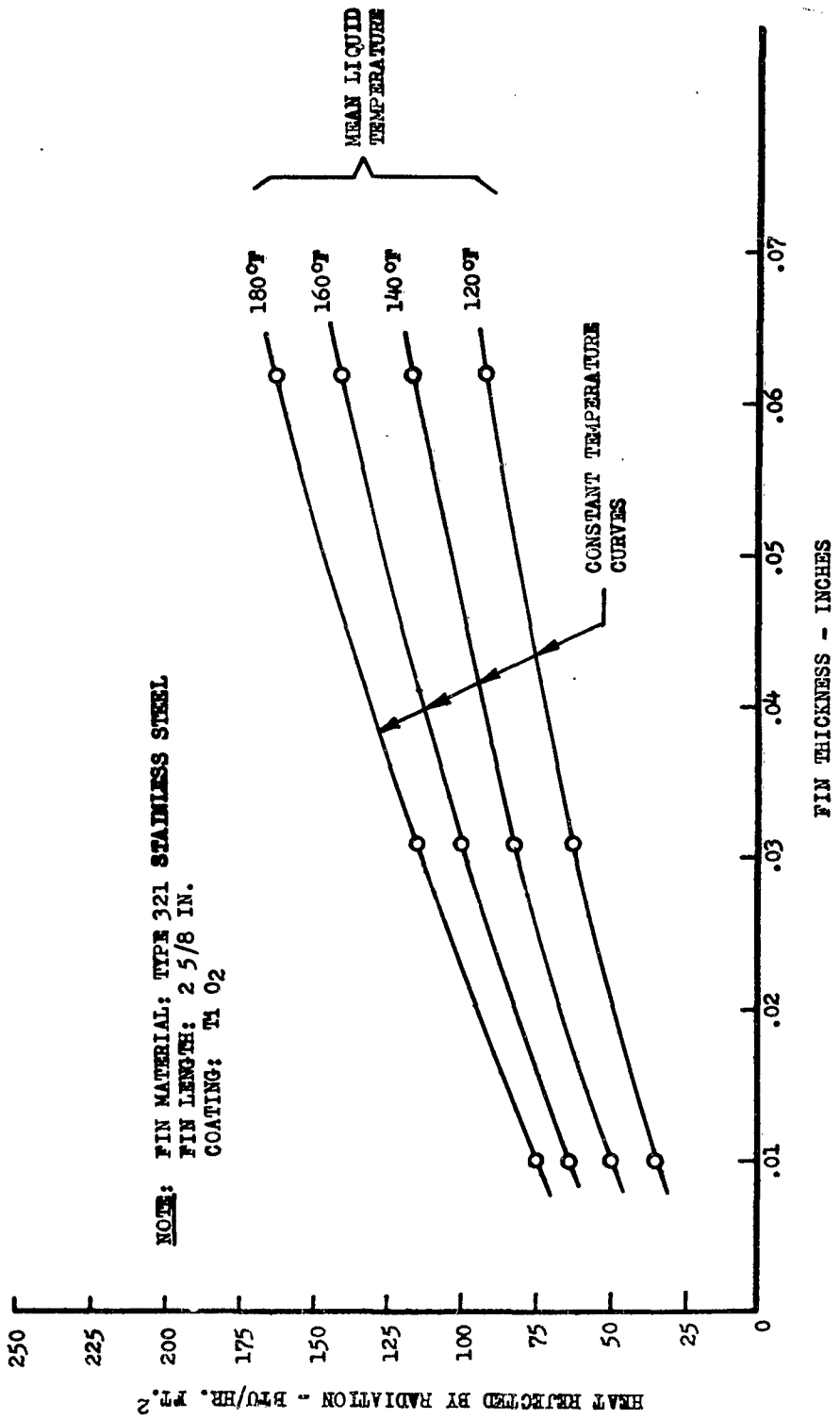


Figure 50.

HEAT REJECTED BY RADIATION PER UNIT AREA OF
RADIATOR ELEMENT AS A FUNCTION OF FIN LENGTH
AND MEAN LIQUID TEMPERATURE

NOTE: DATA ARE TAKEN FROM
SPECIMENS 2, 3 and 4

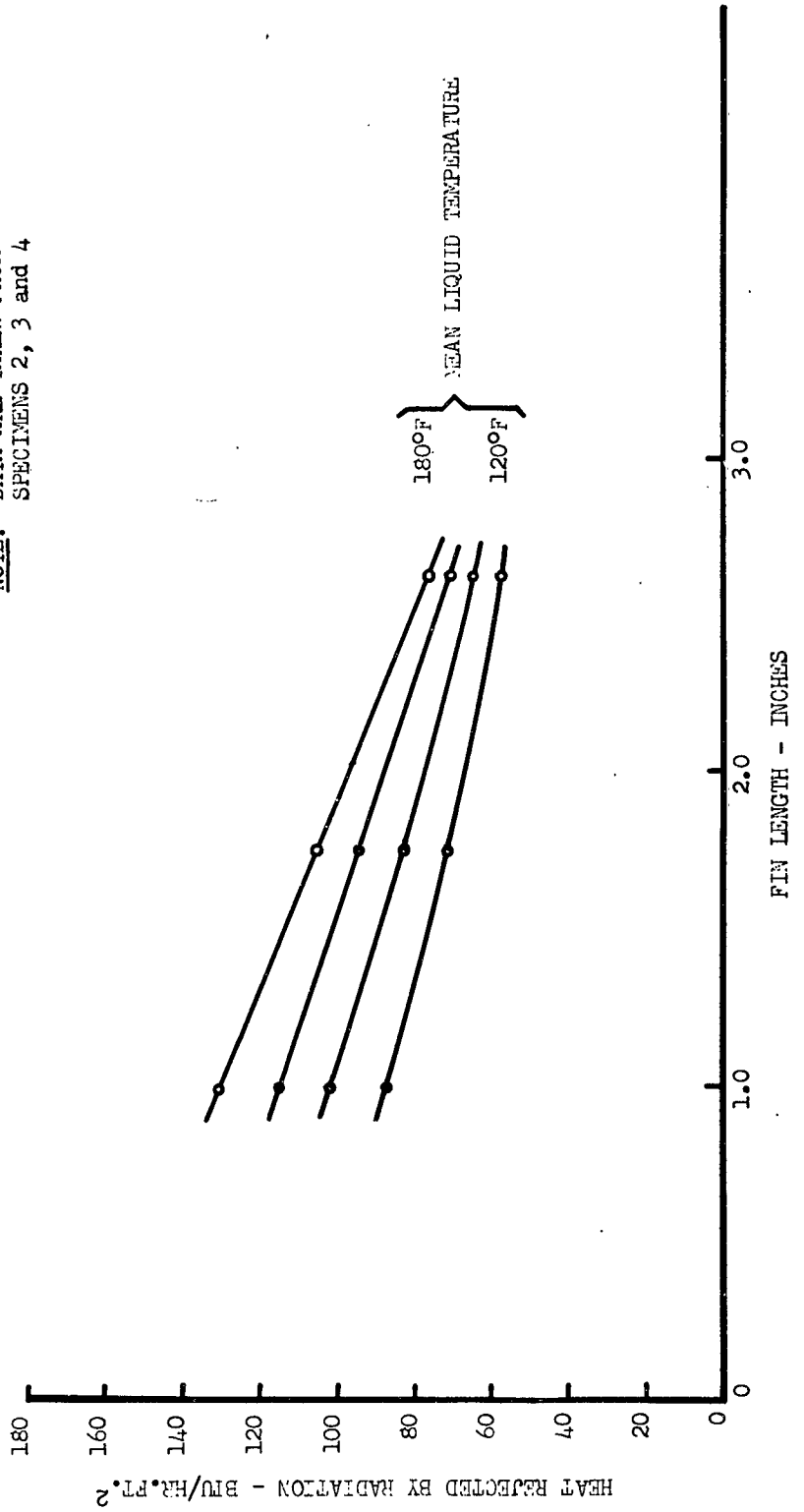
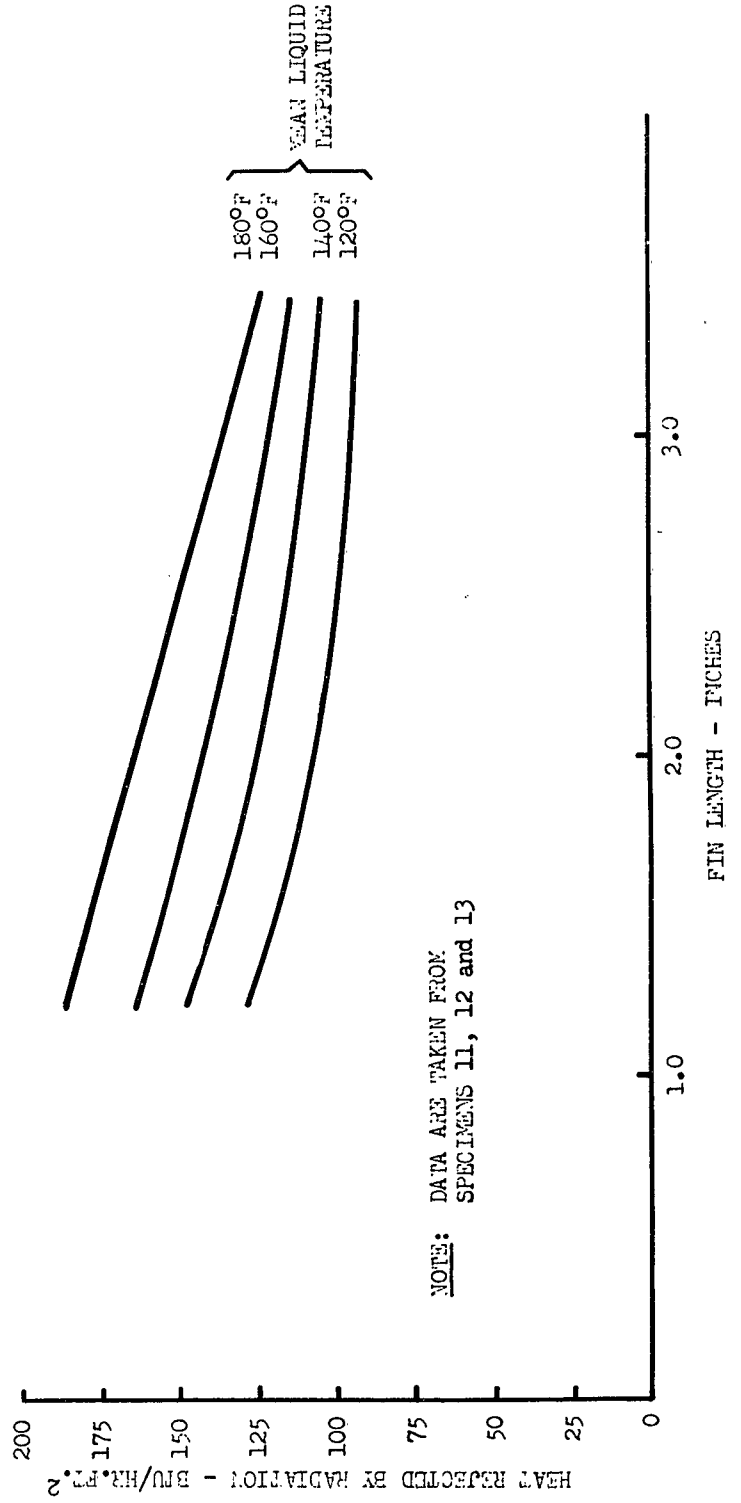


Figure 51.

HEAT REJECTED BY RADIATION PER UNIT AREA
 OF RADIATOR ELEMENT AS A FUNCTION OF FIN LENGTH
 AND MEAN LIQUID TEMPERATURE



NOTE: DATA ARE TAKEN FROM
 SPECIMENS 11, 12 and 13

Figure 52.

DETERMINATION OF FIN LENGTH FOR MINIMUM WEIGHT RADIATOR AS A FUNCTION OF TEMPERATURE

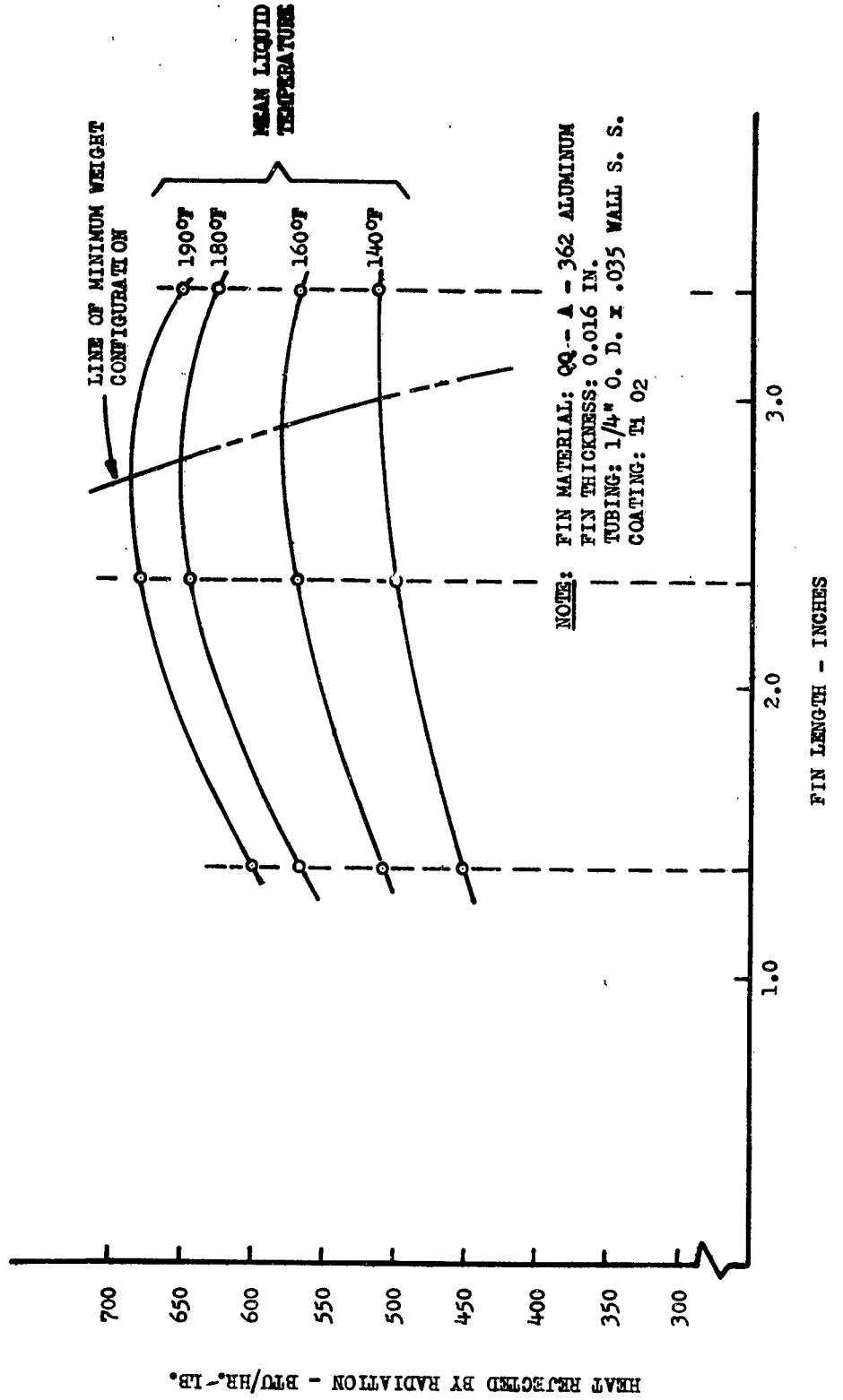


Figure 53.

DETERMINATION OF FIN LENGTH FOR MINIMUM WEIGHT RADIATOR AS A FUNCTION OF TEMPERATURE

NOTE: Fin material: type 321 S.S.
Fin thickness: 0.01 inches
Tubing: 1/4" O.D. x .035" wall S.S.
Coating: T102

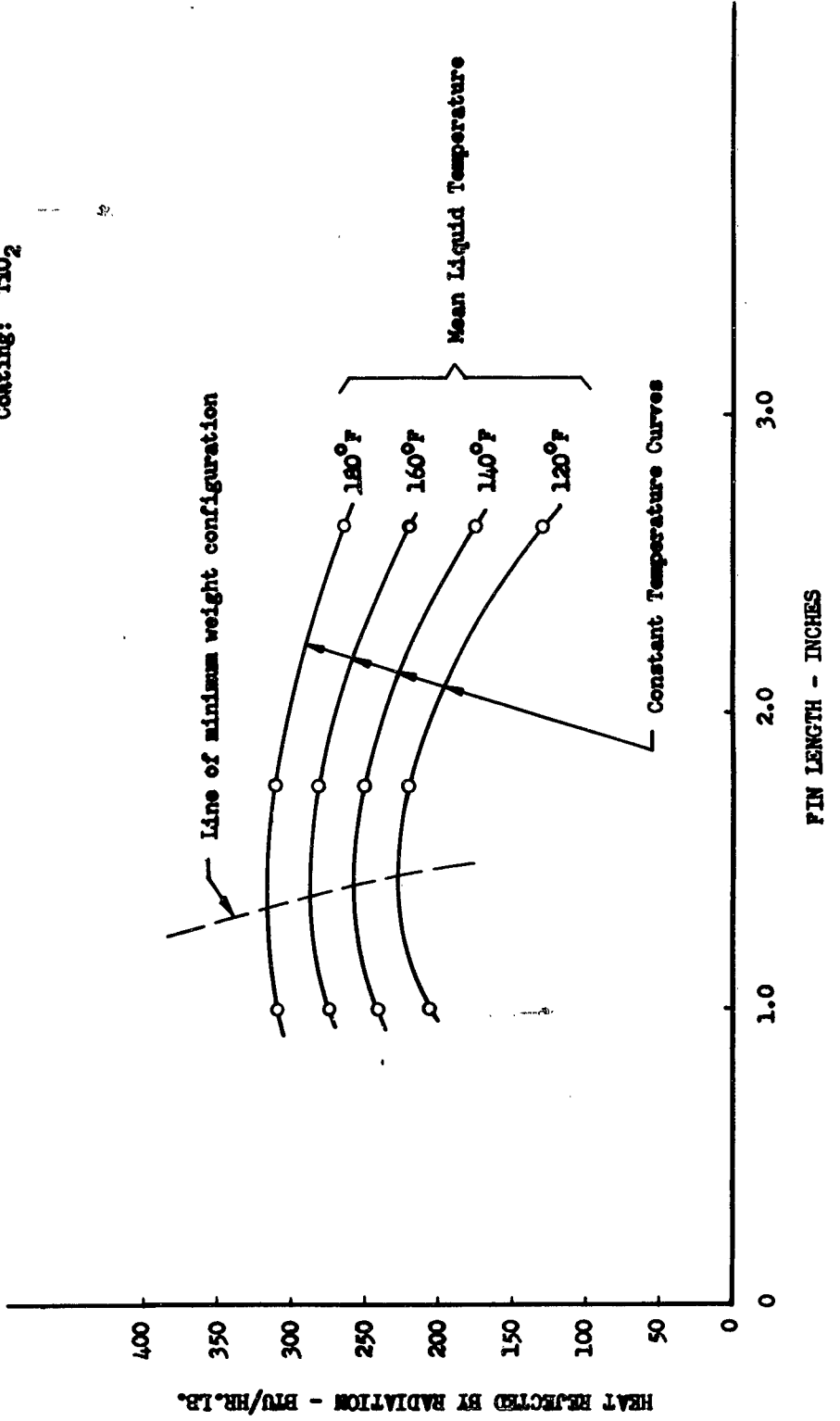


Figure 54.

RADIATOR EFFECTIVENESS AS A FUNCTION
OF FIN LENGTH

NOTE: FIN MATERIAL: TYPE 321 STAINLESS STEEL
FIN THICKNESS: 0.010 INCHES
COATING: TiO₂

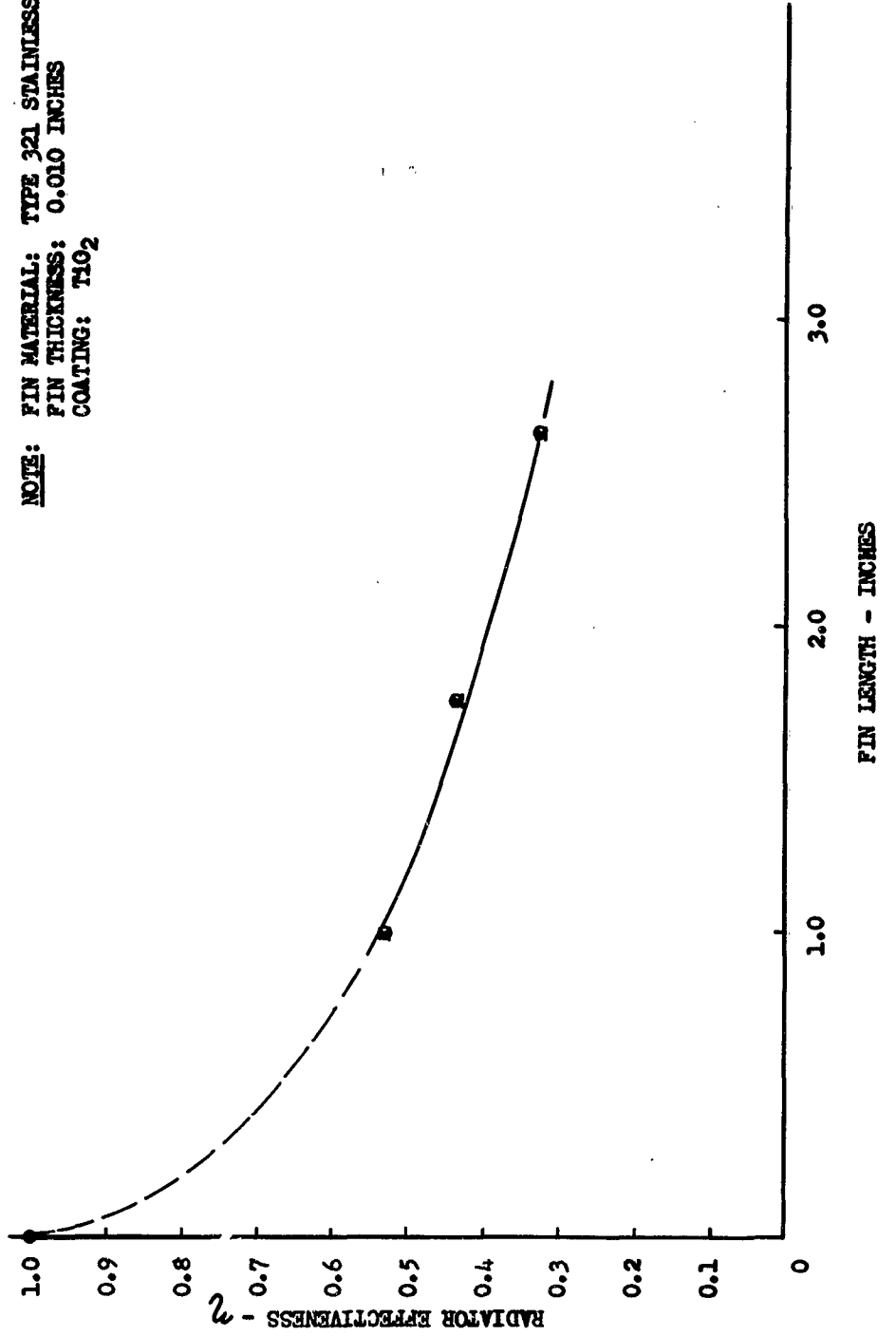


Figure 55.

RADIATOR EFFECTIVENESS AS A FUNCTION
OF FIN LENGTH

NOTE: FIN MATERIAL: QQ - A - 362 ALUMINUM
FIN THICKNESS: 0.016 INCHES
COATING: TiO₂

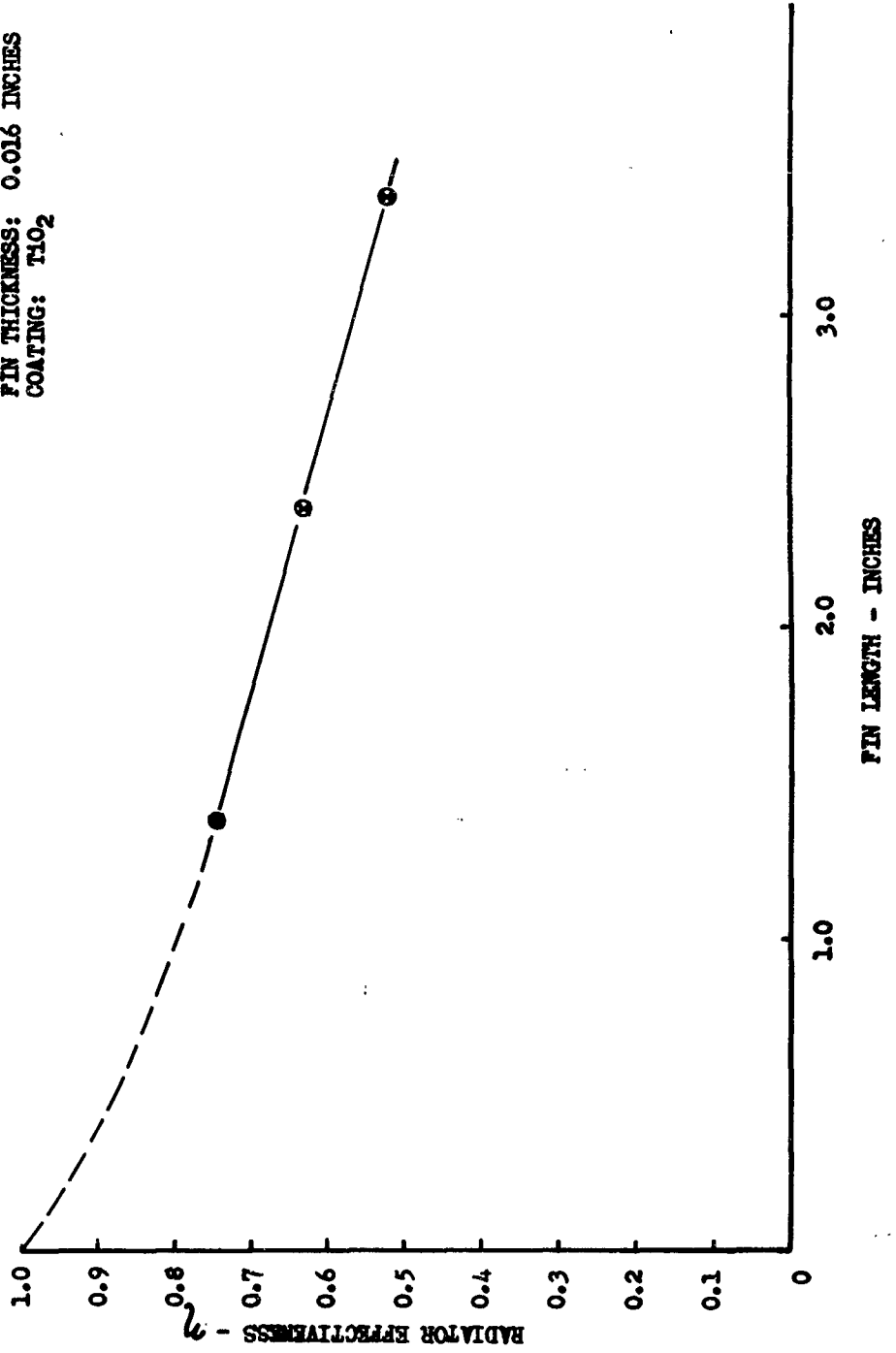
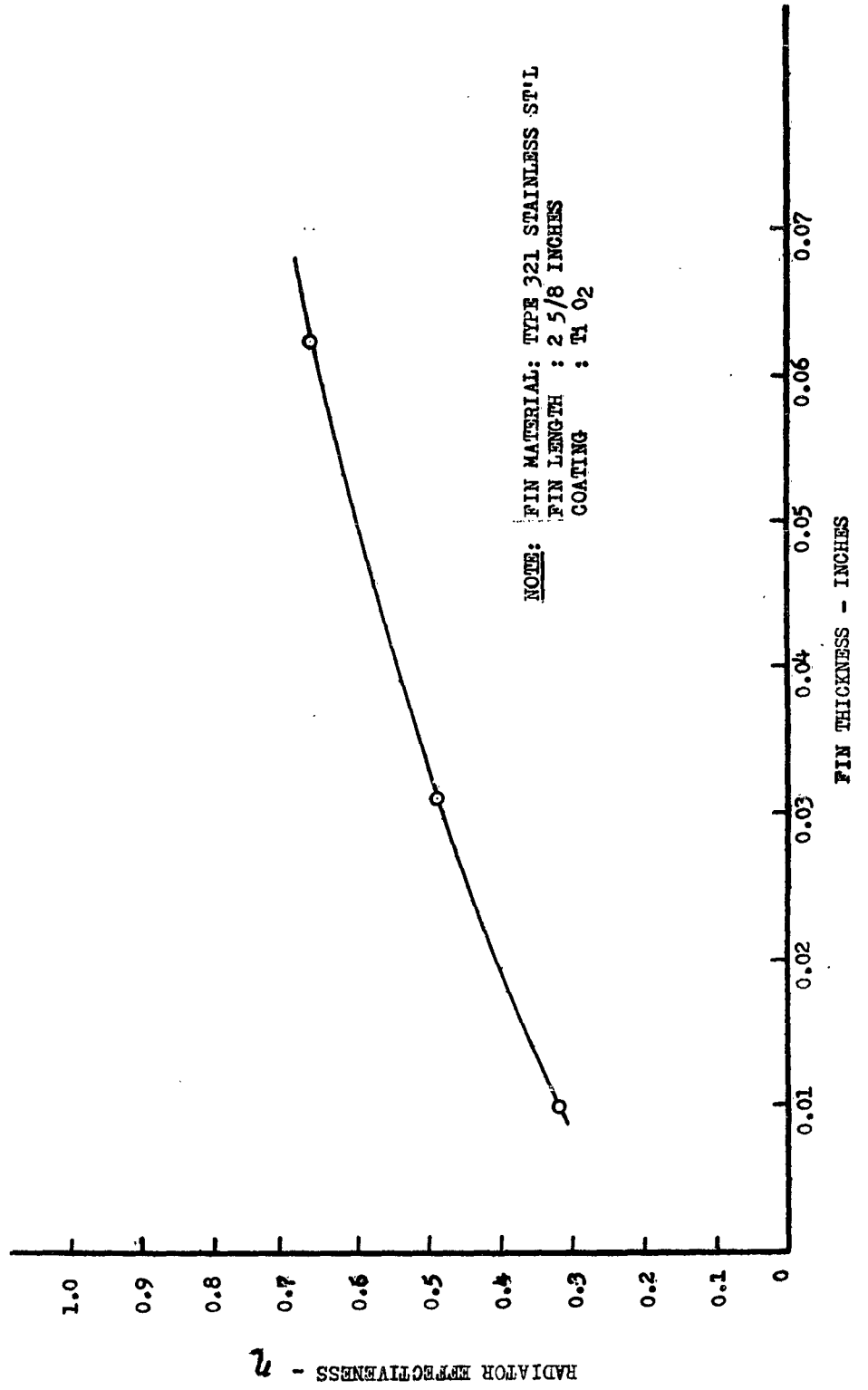


Figure 56.

RADIATOR EFFECTIVENESS AS A FUNCTION
OF FIN THICKNESS



Discussion of Problems and Test Results -

1. Discussion of Problems -

It was realized, because of the rather small specimens, that extreme care should be exercised in determining fluid temperatures and flow rates. It was thought that attaching thermocouples to the outer surface of the liquid conduit would be sufficient to determine heat transport fluid temperature drop across the radiator element. However, when the first test data were analyzed it was discovered that temperature readings were not consistent, especially when the thermocouples were clamped to the aluminum tubes.

To overcome this difficulty, temperature drop across the radiator element was measured outside the test chamber by mercury immersion type thermometers. To account for the heat losses from ducts connecting the radiator element, they were simulated by stainless steel tubing, and heat losses from one outside thermometer to the other determined. To find the net heat loss from the radiator element, heat loss from connecting ducts was subtracted from the total heat loss. Only corrected values are presented in the charts.

Temperature distribution along a fin was determined by attaching the thermocouples directly to the metallic surface, by first removing the surface coating. Thus, these temperature measurements indicate temperature of the metallic surface, but not the radiating surface temperature. For very thin coatings, this assumption is probably justified. However, factors may occur (erosion, etc.) which will dictate relatively thick coatings. In such a case, noticeable temperature drop across the coating will occur and heat transfer rates from the radiator will be reduced. The coating is a thermal insulator, and a certain temperature drop will always take place. Thus, the actual radiating surface temperatures are lower than the temperatures measured. No attempt was made in these tests to determine this temperature drop.

When thermocouples are attached to the fins, some heat is conducted along the leads and dissipated to the surroundings. This condition causes a certain temperature gradient in the vicinity of the point where attachment is made. This error can be reduced by using thin thermocouple wires.

In the first tests, aluminum tubes were used with the aluminum fins, but after ruptures occurred during test, the aluminum tubes were replaced by stainless steel tubes. In some cases very noticeable temperature drop occurred from the stainless steel tubing to the aluminum fin.

2. Discussion of Results -

To calculate heat rejection rates from tube-fin type radiators, it is first necessary to determine the tube and fin temperature. To do this, temperature drop from the fluid to the inside tube wall, and across the tube wall must be determined. Depending on method used to attach fin to tube, the fin root temperature may or may not be the same as the tube temperature.

To determine the actual temperature drop from the fluid to the tube wall, and across this wall, the fluid (water) temperature was measured by mercury immersion type thermometers, and the wall temperature measured with thermocouples attached to the outer surface of the tube. Actually, both measurements were not performed at the same place, but a small distance apart. The temperature difference varied from 1 to 3°F for the stainless steel specimens, and 3 to 5°F for the aluminum and copper specimens. This is in reasonably good agreement with analytically determined results from the following equation:

$$q = UA (\Delta t) \text{ Btu/hr.} \quad (5)$$

where

U = the over-all coefficient, Btu/hr.ft.²°F

A = area of the wall, ft.²

Δt = temperature difference between the fluid and outside surface of wall, °F

For ordinary thin-walled tubes free from scale

$$\frac{1}{U} = \frac{1}{h_i} + \frac{L}{k} \quad (6)$$

For high thermal conductivity materials, or thin-wall tubes, the second term of the right side may be omitted, and

$$\frac{1}{U} = \frac{1}{h_i}; \quad U = h_i \quad (6a)$$

Equation (5) becomes

$$q = h_i A (\Delta t) \quad (7)$$

and

$$\Delta t = \frac{q}{h_i A} \quad (8)$$

where

h_i = film coefficient, Btu/hr.ft.² °F

For fully developed turbulent flow h_i may be determined from equation recommended by McAdams

$$\frac{h_i D}{k} = 0.0225 \left(\frac{DV\rho}{\mu} \right)^{0.8} \left(\frac{C_p \mu}{k} \right)^{0.4} \quad (9)$$

When the clamping method was used to attach an aluminum fin to an aluminum tube (see Figure 3), the temperature drop from tube to fin varied from zero to 4°F. Here again, tube and fin temperatures were not measured at the same location,

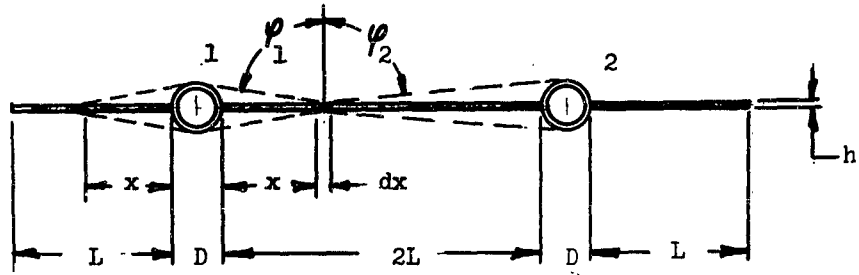
but a small distance apart. When aluminum fins were attached to the stainless steel tubing, temperature drop from 10 to 25°F was observed, depending on distance between spotwelds. This large temperature drop could certainly consist of both poor thermal contact between tube and fin, and between fin and thermocouple. Another reason for large temperature difference could arise from different expansion of the fin and tube material. This means that contact resistance in certain cases can reach significant values and care should be taken to insure good thermal contact between the tube and fin.

To determine temperature distribution along the fin, thermocouples first were attached to the outer fin. When another thermocouple was attached to the inner fin between the tubes (both thermocouples at the same distance from the tube), a temperature difference between these readings was observed. Some of the characteristic cases are presented in Figures 36 through 39. As can be seen from these figures, no temperature difference occurs between the outer and inner copper fins. On the other hand, the stainless steel fins indicate quite a noticeable temperature difference.

This can be explained by radiant heat exchange between the fins and tubes. The outer fin receives radiation from one tube only, while the inner fin receives radiation from two tubes. The small temperature drop along the copper fin causes small temperature difference between fin and tube, and thus small radiant heat exchange. The large temperature drop along the stainless steel fin causes large temperature difference and larger radiant heat exchange between the fin and tube.

In the usual radiation analysis, radiative interaction between tube and fin is neglected. In some cases, when fins of high thermal conductivity are used, this can be justified. However, when fin materials of low thermal conductivity are used, heat exchange between fin and tube will become significant and radiator performance affected.

A brief discussion of irradiation between tube and fin will follow. For more detailed analysis see Reference 7.



Schematic of Radiator Element

Figure 57

Heat rejection of fin surface element, assuming black body radiation

$$dq = \sigma dA T_x^4 \quad (10)$$

or, when both sides are radiating

$$dq = 2 \sigma dA T_x^4 \quad (10a)$$

The left element receives radiant energy emitted by tube 1 only, while the right element receives energy from both tubes.

Radiant energy incident on the left fin element can be expressed as

$$q_L = (\sigma A_1 T_1^4) F_{1-X} \quad (11)$$

Radiant energy incident on the right fin element

$$q_R = (\sigma A_1 T_1^4) F_{1-X} + (\sigma A_2 T_2^4) F_{2-X} \quad (12)$$

Assuming $A_1 = A_2 = A$

and $T_1 = T_2 = T$

$$q_R = \sigma A T^4 (F_{1-X} + F_{2-X}) \quad (13)$$

The right element will receive more radiant energy from the tubes than the left one.

From the reciprocity relationship,

$$A_1 F_{12} = A_2 F_{21} \quad (14)$$

We can conclude that

$$A_1 F_{1-X} = dA F_{X-1} \quad (15)$$

and

$$A_2 F_{2-X} = dA F_{X-2} \quad (16)$$

Substituting these values, the net radiant energy leaving the left fin element

$$dq_L = dA \sigma [T_X^4 - T^4 (F_{X-1})] \quad (17)$$

Similarly, the net radiant energy leaving the right fin element

$$dq_R = dA \sigma [T_X^4 - T^4 (F_{X-1} + F_{X-2})] \quad (18)$$

As equations (17) and (18) indicate, a smaller amount of heat will be rejected from fins connecting two tubes.

Conclusion can be made that temperature profiles and heat rejection rates can be significantly affected by irradiation between tube and fin.

In accordance with the above discussions, an explanation can be given as to why the analytically determined fin temperatures for the stainless steel specimens are below the actually measured values.

Generally, considering certain inaccuracies from thermocouple temperature measurement, difficulties in attaching thermocouples to thin surfaces, and heat conduction away from the surface by the thermocouple wires, a reasonably good agreement between analytical and experimental data was obtained, except for specimens 3 and 4. For these two specimens the actual temperature measurements were noticeably lower, especially for the 1 inch fin, than analytically determined values.

General Discussions of Radiant Heat Exchange and Determination of Temperature Distribution Along Fin, -

1. General Discussions of Radiant Heat Exchange -

When thermal energy is rejected to outer space, it can be assumed that the heat sink has absorptance of unity and temperature of absolute zero. Neglecting planetary heat inputs, heat rejected from an actual body may be calculated from the Stefan-Boltzmann law:

$$q = \sigma e AT^4 \quad (19)$$

However, when radiation heat transfer tests are performed in a space chamber, consideration should be given to other aspects. Depending on configuration of the space chamber, (1) the test item may not be completely enclosed by the cold wall, (2) temperature of the cold wall is not at absolute zero, and (3) the heat sink is not a black body (all incident energy is not absorbed by the sink). Assumption that surfaces may be treated as gray or independent of wave length

also requires careful examination. It has been shown by some investigators that errors up to 30% can be introduced by this assumption.

The Stefan-Boltzmann law is valid only for black and gray bodies. It represents a sufficient approximation for most solid materials, with the exception of metals. The emission of metals increases with higher power than the fourth. For example, in the case of platinum, the emission is proportional to almost the fifth power of absolute temperature.

In accordance with Sieber's experiments, characteristic differences between metals and non-metals were observed. At low temperatures the non-metals absorb nearly all the incident radiation (See Figure 6), while at high temperatures their reflectivity is slightly better than that of polished aluminum (aluminum reflects uniformly well at all source temperatures).

Another assumption generally made is that emission is diffuse. Solids which are good conductors of electricity are generally good reflectors and therefore radiate very little energy. Non-conductors absorb the major part of incident radiation and are also good emitters. In general, non-metallic surfaces are nearly diffuse except at large angles, while metallic surfaces usually deviate from the diffuse at smaller angles.

Also, the intensity of radiation in various directions from actual surfaces do not follow Lambert's law. Usually a polished metallic surface will reflect specularly. The emittance of such a surface is very small when compared to the reflected energy.

To determine radiant heat exchange between actual surfaces, not only the surface properties and temperature, but also their geometrical arrangement should be considered. The net rate at which any surface loses heat to any other surface is equal to the heat emitted by this surface, minus the fraction of heat which is reflected back to this surface, and minus the heat emitted by the second surface which is absorbed by the first surface.

When a test item is placed inside an enclosure consisting of surfaces having different temperatures and surface properties, radiant heat exchange with all these surfaces should be accounted for. In calculating the radiant heat exchange between surfaces it is necessary to know what fraction of the total energy leaving surface 1 arrives at some other surface 2. This fraction is called the angle or view factor. The view factor expressions derived in textbooks apply only for diffuse radiation, and the reciprocity relation is not true for non-diffuse radiation. It does not depend upon the emissivities of the surfaces, or upon presence of other surfaces if they are not between the initial two. If surface 1 sees surfaces 2, 3 and 4, then

$$F = F_{12} + F_{13} + F_{14} \quad (20)$$

If these surfaces form an enclosure

$$F_{12} + F_{13} + F_{14} = 1 \quad (21)$$

The sum of the angle factors from any surface to all of its surroundings is equal to one.

The view factor between two surfaces may be determined from the following equation:

$$F_{1-2} = \frac{1}{A_1} \int_{A_1} \int_{A_2} \frac{\cos \theta_1 \cos \theta_2}{r^2} dA_1 dA_2 \quad (22)$$

In practical situation, determination of the view factors may be relatively simple or complex. However, methods have recently been developed where high speed digital computers can be utilized for determining these factors.

In Reference 8, this computer program was used for determining the view factor between specimen and cold enclosure. The view factor actually varies with size of specimen, but this variation is not significant and a value of 0.85 is used here for calculating radiator effectiveness.

The thermal energy emitted by surface 1 which is incident on surface 2, is

$$q_{1-2} = \epsilon_1 \sigma A_1 F_{1-2} T_1^4 \quad (23)$$

and the amount which is absorbed by surface 2 is

$$q_{1-2} = \alpha_2 \epsilon_1 \sigma A_1 F_{1-2} T_1^4 \quad (24)$$

Since no actual surface is a perfect absorber, the reflected energy must be included in the analysis. As pointed out earlier in this section, polished metallic surfaces do not reflect diffusely and this condition also should be considered in analysis. A method for calculating radiant interchange within an enclosure containing both specularly reflecting and diffusely reflecting surfaces has been described in Reference 9. It is pointed out in this reference that when specular surfaces have a common temperature and emissivity, and diffuse surfaces also have a common temperature and emissivity, deviation from the fully diffuse theory is very small.

To perform a detailed radiant heat transfer analysis, consideration should be given to all the items discussed above. However, as the exact properties of enclosure surfaces in many cases are not known, certain assumptions and simplifications are actually required. For determining the net radiant heat exchange between two isothermal actual surfaces A_1 and A_2 , an approximate equation can be used.

$$q_{\text{net}} = \epsilon_1 \epsilon_2 F_{1-2} A_1 \sigma (T_1^4 - T_2^4) \quad (25)$$

As can be seen from Figure 2, the test chamber actually consists of 3 surfaces which the specimen "sees":

- (a) Liquid nitrogen cooled enclosure
- (b) Top of chamber (approximate temperature 65°F, polished stainless steel)
- (c) Bottom of chamber (approximate temperature 80°F, polished stainless steel)

To determine the net radiant heat exchange between the specimen and its enclosure, consideration should be given to all of these surfaces. Heat rejection to the liquid nitrogen cooled wall will be influenced by the absorption, reflection, and emission of the two polished stainless steel surfaces. However, considering the low emissivities, small view factors and temperature differences between these surfaces and the specimen, the radiant heat exchange equation may be reduced to

$$q = \alpha_2 \epsilon_1 F_{1-2} A_1 \sigma (T_1^4 - T_S^4) \quad (26)$$

As can be seen from Figure 6, for flat black enamel at low temperature, the absorptivity is approaching unity and the above equation may be further reduced to

$$q = \epsilon_1 F_{1-2} A_1 \sigma (T_1^4 - T_S^4) \quad (26a)$$

where

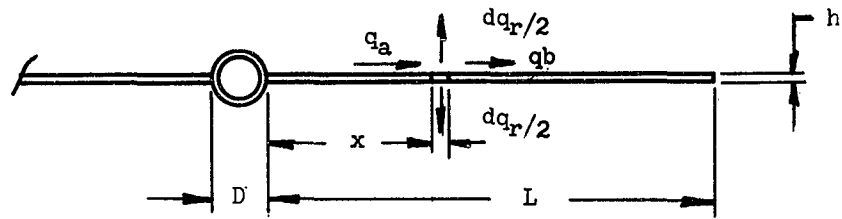
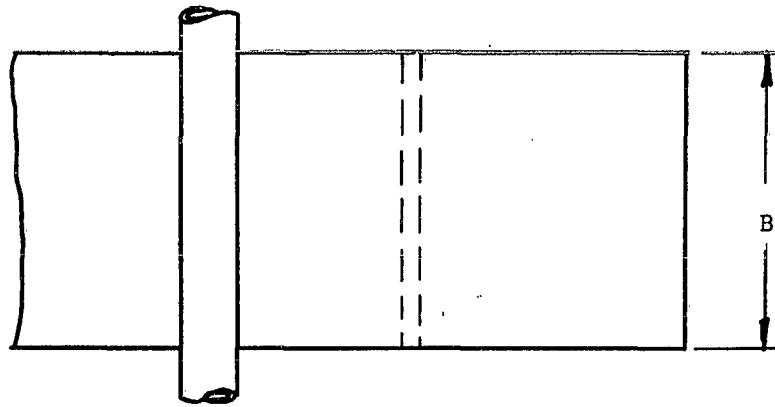
- q = heat rejected from specimen, Btu/hr.
- ϵ_1 = emissivity of specimen
- F_{1-2} = view factor from specimen to liquid nitrogen cooled wall
- A_1 = area of specimen, ft.²
- σ = Stefan-Boltzmann constant
- T_1 = specimen temperature (assumed constant), °R
- T_S = sink temperature, °R

Equation (26a) was used to determine radiator effectiveness.

2. Determination of Temperature Distribution Along Fin

This analysis is based on the following assumptions:

- a. Heat flow is in one direction only (constant temperature along tube axis).
- b. Thermal conductivity does not change with temperature
- c. Emissivity does not change with temperature
- d. Heat is transferred by radiation and conduction only



Radiator Element

Figure 58

Heat flow at steady state conditions

$$q_a = q_b + dq_r \quad (27)$$

From Fourier's conduction equation

$$q = -ka \frac{dT}{dx} \quad (28)$$

Heat entering element

$$q_a = -ka \frac{dT}{dx} \quad (28a)$$

Heat dissipated by radiation

$$dq_r = \epsilon \sigma dAT^4 \quad (29)$$

Let width of fin $B = 1$, then area of element

$$dA = 1 dx = dx$$

and when radiation occurs from both sides, equation (29) can be modified

$$dq_r = 2 \epsilon \sigma T^4 dx \quad (29a)$$

When specimen is not completely enclosed by "cold-wall" and this wall is not at absolute zero temperature, equation (29) becomes

$$dq_r = 2 \epsilon \sigma F (T^4 - T_s^4) dx \quad (29b)$$

Heat leaving element

$$q_b = -kA \left(\frac{dT}{dx} + \frac{d^2T}{dx^2} dx \right) \quad (30)$$

Substituting equations (29a), (29b) and (30) into equation (27)

$$-kA \frac{dT}{dx} = -kA \left(\frac{dT}{dx} + \frac{d^2T}{dx^2} dx \right) + 2 \epsilon \sigma F (T^4 - T_s^4) dx$$

Rearranging and simplifying, the differential equation of temperature distribution along a fin is obtained.

$$d^2T/dx^2 = 2 \epsilon \sigma F/kA (T^4 - T_s^4) \quad (31)$$

For unit width of fin

$$A = l \cdot h = h$$

$$d^2T/dx^2 = 2 \epsilon \sigma F/kh (T^4 - T_s^4) \quad (31a)$$

(This differential equation was solved by analog computer)

where

T = fin temperature, °R

T_s = sink temperature, °R

σ = Stefan-Boltzmann constant

ϵ = emissivity of specimen

F = view factor

k = thermal conductivity

h = fin thickness

Summary -

For all the radiator elements tested, heat rejection rates are presented as a function of temperature, fin thickness, fin length, material and emissivity. Fin effectiveness is determined both from actual heat rejection rates and those determined analytically, (assuming a constant fin temperature the same as tube temperature).

Results show that thermal conductivity and emissivity have the most pronounced effect on heat rejection rates per unit area, while material density has the most effect on heat rejection rates per unit weight.

By increasing fin thickness, heat rejection rates are increased per unit area, but decreased per unit weight. Figure 47 indicates the advantage of thin fins where weight is a limiting factor. For a particular radiator configuration there is a unique fin length that will give a maximum heat rejection rate per unit weight of radiator. As can be seen from Figures 51 and 52, temperature has an effect on optimum fin length, in that fin length will decrease with increased temperature. The limited scope of this test series and limited size of the space chamber did not allow optimum configurations to be experimentally determined for a larger variety of materials, fin thicknesses, length and/or shapes. But, this would not add much to actual radiator design, because for each particular radiator design, fin material, thickness, tube size, tube wall thickness, fluid, and meteoroid protection method will dictate a different "optimum" configuration.

No attempt has yet been made to check these results against contemporary analyses. In actual radiator design probably two main factors will be considered, (1) weight, and (2) area. Depending on these two factors, fin materials, thicknesses and tube spacing will be determined. Consideration must also be given to other factors such as shape and flow stability when fluid phase change occurs in the space radiator.

The large temperature difference (especially for low thermal conductivity materials) between the root and tip of a fin will cause thermal stresses, and should also be considered in actual radiator design.

REFERENCES

1. Lieblein, S., Analysis of Temperature Distribution and Radiant Heat Transfer Along a Rectangular Fin of Constant Thickness, NASA Technical Note D-196, 1959.
2. Mackay, D. B., and Bacha, C. P., Space Radiator Analysis and Design, ASD TR 61-30, Part I, April 1961.
3. Bartas, J. G., and Sellers, W. H., Radiation Fin Effectiveness, ASME Paper 59-HT-17, 1959.
4. Mackay, D. B., and Bacha, C. P., Performance of Extended Surface Space Radiator Model, ASD TDR 62-567, May 1962.
5. Schreiber, L. H., Mitchell, R. F., Gillespie, G. D., and Olcott, T. M., Techniques for Optimization of A Finned-Tube Radiator, ASME Paper 61-SA-44.
6. Knezek, R. A., Thermal Model Tests of Manned Lunar Spacecraft, Report No. 00.11, October 1961, Vought Astronautics.
7. Sparrow, E. M., and Eckert, E. R. G., Radiant Interaction Between Fin and Base Surfaces, ASME Paper 61-AV-30, 1961.
8. Kempton A. Toups, A General Computer Program for the Determination of Radiant-Interchange Configuration Factors, ASD TN 61-101, April 1962.
9. Sparrow, E. M., Eckert, E. R. G., and Jonsson, V. K., An Enclosure Theory of Radiative Exchange Between Specularly and Diffusely Reflecting Surfaces.

QUESTION AND ANSWER PERIOD

SESSION III -- Radiation and Thermal Analysis

First Paper -- "Space Radiator Experiment," by Carl J. Feldmanis, Aeronautical Systems Division. (Presented by Mr. Feldmanis.)

QUESTION: (Mr. Warner, General Dynamics) What is the emissivity of the coating, and what is the UV degradation effect?

ANSWER : (Mr. Feldmanis) The emissivity of the coating varies with the temperature. It is very high. Its range is about .98. Well, the degradation, we could not see any effect at all as far as the vacuum or load was considered because it stayed in the vacuum chamber for about, I would say, 52 hours, something like that. So, nothing could be wrong with the coating.

QUESTION: (Mr. J. Gonzales, Martin) You attribute the temperature difference between the inner and outer fin to the radiation from the tube. What per cent of heat transfer is by conduction and what by radiation?

ANSWER : (Mr. Feldmanis) Now it is hard to say what we have. We have both cases here. We have heat transfer first of all, how is the heat going? You have to utilize this low Q minus $KA \Delta T$ or ΔX and so in the case of high conductivity and high emissivity we will have quite a low heat. However, with low emissivity, if you recall the temperature distribution between the coated and uncoated fin--for the uncoated fin there was almost no temperature. That means at low emissivity, heat is not going out and heat is now flowing along evenly.

QUESTION: (Mr. Gonzales, Martin) What variation in temperature did you experience between top and bottom of fin? Are you talking about the length of the fin?

ANSWER : (Mr. Feldmanis) Actually, this is only the difference between the values in and out of the elements. So this is the point on our heat dissipation rate for the high conductivity and emissivity fins, with very few degrees temperature drop. Where you don't get much heat out there is not much temperature drop.

QUESTION: (Mr. Plamondon, JPL) Have you compared your results against theoretical results which appear in the literature; if so, how do the results compare, assuming that you can subtract out the effect of joint resistance between the fin and the tube?

ANSWER : (Mr. Feldmanis) Well actually, not much comparison was made with the theoretical analysis. For one reason, because most of the analysis is on the tube and fin alone and the tube weight is not included, so, however, this can be done by subtracting the heat dissipation from the tube. However, with the small elements that I have done so far, I'm afraid it will introduce another error and this is the reason it has not been done so far. However, there is another analysis that has lately been published from NASA. This probably will be done in the future.

QUESTION: (Mr. Bailey, Sundstrand Aviation) What was the liquid temperature change during the tests of the radiator segments?

ANSWER : (Mr. Feldmanis) Well as I mentioned already, this liquid temperature change naturally varies, and it depends upon the heat dissipation rate. When we have high heat with dissipation rates the liquid temperature drops, or, you don't have much if it is not much. Actually, there is only a few degrees temperature drop considering those small elements.

QUESTION: (Mr. Gebhardt, Martin) How is "Mean Radiator Temperature" defined?

ANSWER : (Mr. Feldmanis) Well this is the summing up of the in and out temperatures and dividing by two--the mean liquid temperature in and out, divided by two.

QUESTION: (Mr. Wisentaner, Baird-Atomic) Have any of your experiments been done with radiator fins having a tapered thickness?

ANSWER : (Mr. Feldmanis) No, not so far.

QUESTION: (Mr. George Brown, MIT) On your slides were the points shown determined from your experimental data or based on theoretical calculations?

ANSWER : (Mr. Feldmanis) Well those points are mostly based on experimental data, except for fin effectiveness, or rather, radiator effectiveness. How this was calculated considering fin effectiveness. This was calculated actually by assuming the constant temperature and including also the new factor because the specimen was not completely inclosed by cold wall so we had a set view factor and this view factor was determined as Mr. Toups presented in his paper. The same method was used to determine the view factor in this case.

QUESTION: (Mr. Brown, MIT) Were any calculations made to determine the agreement between measured heat transfer rates and temperature and calculated values using appropriate emissivity radiant interchange factors. If so, what was the agreement?

ANSWER : (Mr. Feldmanis) Well as I mentioned already, they were used as consideration factors of emissivity to determine the heat transfer rate.

QUESTION: (Mr. Nordwall, North American) In your schematic you show the cold wall ending at the end of the fin, was this taken into account in your analysis?

ANSWER : (Mr. Feldmanis) Yes, again, North American analogue digital computer program was used to determine the view factor.

QUESTION: (Mr. Nordwall, North American) What was the Epsilon of the radiator coating and cold wall?

ANSWER : (Mr. Feldmanis) As I mentioned, this was a high emissivity coating, .98. The cold wall absorptivity was a black body. Actually you will see a curve in the paper, but really for non metallics at low temperature, nitrogen temperatures, this absorptivity is very close, so this is not the big error that we are assuming.

QUESTION: (Mr. E. Kaplan, Republic Aviation) What were the dimension of the vacuum chamber?

ANSWER : (Mr. Feldmanis) The diameter was approximately 18 inches and the liquid nitrogen cooled wall was about 50½ inches by 23 inches high.

QUESTION: (Mr. Kaplin, Republic Aviation) To what extent could radiation from the fin ends account for discrepancy between inner and outer fin temperatures?

ANSWER : (Mr. Feldmanis) Well, these also were performed on different materials, the chart I showed here was for stainless steel .01 inches thick, one inch long. The tests were performed also on different materials as copper, and in this case the copper fin was about 1/16th of an inch thick. I couldn't notice any difference at all, so they should be very small. What we account for I think is the radiation between the fins and tube and not from the edge.

QUESTION: (Mr. R.M. Byke, Douglas Aircraft) When the variation of the tube wall thickness was investigated, was the internal Reynolds number held constant?

ANSWER : (Mr. Feldmanis) In this case it was held constant.

QUESTION: (Mr. J.E. Hitchcock, AFIT) Have you been successful in theoretically predicting the fin effectiveness?

ANSWER : (Mr. Feldmanis) There are analysis in the literature and published papers, but I have not actually analyzed how close these are, because this was more or less a fin and tube radiator, and I didn't consider it, at the time being at least, as just a fin alone.

QUESTION: (Mr. Erwin Fried, General Electric) Have you computed values for the thermal contact resistance other than in terms of radiator performance?

ANSWER : (Mr. Feldmanis)— No.

QUESTION: (Mr. R.S. Barker, Douglas) Don't you think that the better view factor from the center of the fin to the top of the container influences the higher temperatures at the center of the fin? What was the emissivity of the top of the container?

ANSWER : (Mr. Feldmanis) No, I don't think that there should be a big effect from the fin to this Bell jar type vacuum chamber because the inside first of all is a vacuum. The Bell jar is a standard stainless steel jar and the inside is polished so that means that we have a very long emissivity, and also the temperature difference between the Bell jar and the center of the fin was not very big and in some cases you probably get a little bit of heat in, but I think this can be neglected.

QUESTION: (Mr. R. Campbell, United Aircraft Products) was a theoretical analysis made to predict heat dissipation and compared to actual results? If so, how did it compare?

ANSWER : (Mr. Feldmanis) Well so far no comparison has been made. However I did rough calculations, but including the tube and the fin, so they are not in exact agreement.

QUESTION: (Mr. G. Rennenger, Hamilton Standard) How was aluminum fin fastened to the steel tubing?

ANSWER : (Mr. Feldmanis) Well, I think I mentioned it, maybe you didn't understand me. I used a clamping method where the aluminum fin was wrapped around the tube and then spot-welded along the axis. So actually we had two pieces of aluminum, one is the fin and the other piece is spot-welded along the axis.

QUESTION: (Mr. Truscoe, Hamilton Standard) What was the thickness of coating?

ANSWER : (Mr. Feldmanis) As far as I could measure it was about 2 mil or two thousandths of an inch thick, --the coating.

QUESTION: (Anonymous) What was the flow rates or Delta T's through the radiator?

ANSWER : (Mr. Feldmanis) Well for mostly all of the tests the flow rate was approximately a hundred pounds per hour. This is still considering the small area, small tube and the turbulent flow originally.

**A GENERAL COMPUTER PROGRAM FOR THE DETERMINATION OF
RADIANT-INTERCHANGE GEOMETRIC CONFIGURATION FACTORS**

by

K. A. Toups

**North American Aviation
Downey, California**

NOMENCLATURE

A	Area
F	Configuration factor
h, k, l	Translation components
i, j, k	Unit vectors along the X-, Y-, Z-axis, respectively
O	Center of unit sphere, origin of coordinate system
R	Radius of sphere
S	Distance between two areas
X, Y, Z or x, y, z	Spatial coordinates of a point relative to X, Y, Z axis
α, β, γ	Direction angles of a line relative to X, Y, Z axis respectively
γ	Angle between Z axis and vector normal to plane
θ	Angle between two vectors
π	Numerical constant = 3.14159 +
ω	Solid angle
Subscripts	
A, B, C	Points on an area
s	Sector
ΔA	Finite incremental area
dA	Differential area
dA-A	From a differential area to an area
1, 2,	Areas 1, 2,
12	Area 1 to area 2
ϵ	Elliptical

A GENERAL COMPUTER PROGRAM FOR THE
DETERMINATION OF RADIANT-INTERCHANGE GEOMETRIC CONFIGURATION
FACTORS

by
K. A. Toups

INTRODUCTION

The geometric configuration factor F , otherwise known as view factor, shape factor, form factor, etc., is defined as the fraction of the energy emitted by a black-body radiating surface (A_1) that is intercepted by a receiving surface (A_2). Using known methods of analysis, the determination of this factor in practical situations can be relatively simple or incredibly complex. For instance, consider two parallel, concentric cylinders of infinite length. The factor from the outer cylinder (r_2) to the inner (r_1) is merely

$$F_{21} = \frac{r_1}{r_2}$$

and

$$F_{12} = 1$$

However, one expression for the configuration factor between two skewed plates is (Reference 1)

$$\begin{aligned}
 F_{A_1-A_2} = & \frac{1}{\pi L} \left(-\frac{\sin 2\phi}{4} \left[NL \sin \phi + \left(\frac{\pi}{2} - \phi \right) (N^2 + L^2) + L^2 \tan^{-1} \left(\frac{N - L \cos \phi}{L \sin \phi} \right) + \right. \right. \\
 & N^2 \tan^{-1} \left(\frac{L - N \cos \phi}{N \sin \phi} \right) \left. \left. + \frac{\sin^2 \phi}{4} \log e \left\{ \left[\frac{(1+N^2)(1+L^2)}{1+N^2+L^2-2NL \cos \phi} \right] \right. \right. \right. \\
 & \left. \left. \left. \csc^2 \phi + \cot^2 \phi \left[\frac{L^2(1+N^2+L^2-2NL \cos \phi)}{(1+L^2)(N^2+L^2-2NL \cos \phi)} \right] L^2 \right\} + \right. \right. \\
 & \left. \left. \frac{N^2 \sin^2 \phi}{4} \log e \left[\left(\frac{N^2}{N^2+L^2-2NL \cos \phi} \right) \left(\frac{1+N^2}{1+N^2+L^2-2NL \cos \phi} \right) \cos^2 \phi \right] + \right. \right. \\
 & \left. L \tan^{-1} \left(\frac{1}{L} \right) + N \tan^{-1} \left(\frac{1}{N} \right) - \sqrt{N^2+L^2-2NL \cos \phi} \cot^{-1} \sqrt{N^2+L^2-2NL \cos \phi} + \right. \\
 & \left. \frac{N \sin \phi \sin 2\phi}{2} \sqrt{1+N^2 \sin^2 \phi} \left[\tan^{-1} \left(\frac{N \cos \phi}{\sqrt{1+N^2 \sin^2 \phi}} \right) + \right. \right. \\
 & \left. \left. \tan^{-1} \left(\frac{L - N \cos \phi}{\sqrt{1+N^2 \sin^2 \phi}} \right) \right] + \cos \phi \int_0^L \sqrt{1+z^2 \sin^2 \phi} \left[\tan^{-1} \left(\frac{N-z \cos \phi}{\sqrt{1+z^2 \sin^2 \phi}} \right) + \right. \right. \\
 & \left. \left. \tan^{-1} \left(\frac{z \cos \phi}{\sqrt{1+z^2 \sin^2 \phi}} \right) \right] dz \right)
 \end{aligned}$$

This paper describes a simplified analysis, based upon the Nusselt unit sphere double projection concept, of the configuration factor and a digital computer program utilizing this new approach. The new technique permits the computation of factors to complicated flat or solid surfaces without recourse to complex numerical integration procedures or long, detailed "closed-form" particular solutions. As a consequence, the factor computation is very fast—on the order of a few seconds of IBM 7090 time—for surfaces such as trapezoids.

Much of the labor of data preparation has been eliminated. A description of each surface in terms of the spatial coordinates of its boundaries is given to the computer, and a name is assigned to each surface. Then, the factor between surfaces is asked for by name. The fact that the capability to transform surface coordinates has been provided further simplifies data entry of complex surfaces oriented in difficult, skewed positions. Also, as happens quite often in practice, two surfaces do not completely see each other. The program relieves the analyst of the laborious task of determining whether all, none, or part of each surface is seen by the other. These and other features discussed in more detail later have been provided to promote ease of use and flexibility of application.

ANALYTICAL PROCEDURES

The general equation that must be solved in the determination of the configuration factor is (see Figure 1)

$$F_{12} = \frac{1}{A_1} \iint_{A_1} \iint_{A_2} \frac{\cos \theta_1 \cos \theta_2 dA_2 dA_1}{\pi S^2} \quad (1)$$

The following part of the integrand is the factor from the elemental surface dA_1 to the total surface A_2 , commonly referred to as the plane point factor, $F_{dA_1 - A_2}$.

$$F_{dA_1 - A_2} = \iint_{A_2} \frac{\cos \theta_1 \cos \theta_2}{\pi S^2} dA_2 \quad (2)$$

or

$$F_{12} = \frac{1}{A_1} \iint_{A_1} F_{dA_1 - A_2} dA_1 \quad (3)$$

A very simple geometric interpretation of this integral is given by Nusselt. The principal value of the Nusselt concept is that the computational procedure is simplified and made more accurate by the fact that no mathematical or numerical integration is required to compute the point factor. However, the Nusselt method yields only the factor from the elemental area dA_1 ; one must still integrate all such factors over surface A_1 to yield the area factor F_{12} as given in Equation 3.

The Nusselt concept utilizes a hemisphere of radius R constructed over the incremental plane area dA_1 , as shown in Figure 1. Every point defining the boundary of surface A_2 is projected radially to the hemisphere surface and then vertically downward to the plane of dA_1 , the equatorial plane of the hemisphere. The locus of all points thus projected encloses an area, A''_2 , on the hemisphere base. This area A''_2 , divided by the area of the base, is the plane point factor from dA_1 to A_2 .

The validity of this conclusion can be demonstrated as follows. Note that the elemental area dA_2 is described in surface A_2 by the elemental solid angle $d\omega_1$, or

$$d\omega_1 = \frac{\cos \theta_2 dA_2}{S^2} \quad (4)$$

Similarly, on the sphere having radius R,

$$d\omega_1 = \frac{dA'_2}{R^2} \quad (5)$$

Because dA''_2 is the projection of dA'_2 on the hemisphere base,

$$dA'_2 = \frac{dA''_2}{\cos \theta_1} \quad (6)$$

Inserting Equation 6 in Equation 5,

$$d\omega_1 = \frac{dA''_2}{R^2 \cos \theta_1} \quad (7)$$

The right side of Equation 4 appears explicitly in Equation 1 and, because Equation 7 is identical to Equation 4, Equation 2 becomes

$$F_{dA_1-A_2} = \int \int_{A_2} \frac{\cos \theta_1}{\pi} \left(\frac{dA''_2}{R^2 \cos \theta_1} \right) = \frac{\iint_{A_2} dA''_2}{\pi R^2} = \frac{A''_2}{\pi R^2}$$

For a sphere of unit radius (unit sphere),

$$F_{dA_1-A_2} = \frac{A''_2}{\pi} \quad (8)$$

which completes the proof of Nusselt's method. By inserting Equation 8 in Equation 3, the original equation becomes greatly simplified; only one area integration is now required.

$$F_{12} = \frac{1}{\pi A_1} \iint_{A_1} A''_2 dA_1 \quad (9)$$

The computer program described herein solves Equation 9 numerically by successive algebraic evaluation of A''_2 at preselected points on surface A_1 , with subsequent numerical integration to yield F_{12} , or

$$F_{12} = \frac{1}{\pi A_1} \sum \sum_{A_1} A''_2 \Delta A_1 \quad (10)$$

It should be emphasized that area A''_2 is, in fact, formed by the doubly projected silhouette of surface A_2 as it appears from dA_1 .

The element dA_1 is assumed to be oriented in the XY plane and at the origin of the coordinate system of surface A_2 . The area A''_2 can be found from the line integral where $y_1 = F(x_1)$ is the locus of the boundary of A''_2 ,

$$A''_2 = \frac{1}{2} \int_C (x_1 dy_1 - y_1 dx_1) \quad (11)$$

Let $z = F(x, y)$ be the locus of the silhouette of A_2 , and S the distance from dA_1 to the point (x, y, z) on the silhouette of A_2 .

$$S = \sqrt{x^2 + y^2 + z^2}$$

From similar triangles,

$$x_1 = \frac{x}{S}, \quad dx_1 = \frac{1}{S} dx + x d\left(\frac{1}{S}\right)$$

$$y_1 = \frac{y}{S}, \quad dy_1 = \frac{1}{S} dy + y d\left(\frac{1}{S}\right)$$

Inserting in Equation 11

$$A''_2 = \frac{1}{2} \int_C \frac{xdy - ydx}{S^2} \quad (12)$$

Equation 12 can be transposed to finite difference form by replacing the differentials with increments for numerical evaluation. Because of the problems of increment size control, it appears desirable to solve Equation 12 for a finite line segment in space and to allow the analyst to control accuracy of point-factor computation by suitable selection of line segments describing surface 2. If the surface is actually a polygon or polyhedra, the simulation is perfect; if the surface is curved, like a disk, for example, the validity of the result is a function of the number of line segments used.

However, a much simpler and more easily understood geometric derivation, using the unit sphere, yields the result in superior computational form. Referring to Figure 2, note that the radial projection of line segment AB on the hemisphere surface forms the circular arc A'B'. Projection of A'B' to the base plane produces the elliptical arc A''B'', forming the elliptical sector A''OB'' with the origin.

If all line segments describing surface 2 are similarly projected, the area A''_2 will be formed by a closed series of elliptical arcs. Surface A_2 does not have to be a plane. Actually, the area A''_2 results from the geometry of a silhouette; any surface or object projecting an identical

silhouette in the same spatial position on the hemisphere surface will produce the same area A''_2 and the same point factor.

Inspection reveals that the magnitude of area A''_2 can be determined by computing the area of each elliptical sector, properly signed, followed by an algebraic summation.

In Figure 2, the area of elliptical sector A_c is the projected area of circular sector A_s . If the angle between the plane of the circular sector $A'OB''$ and the XY plane is γ , then

$$\cos \gamma = \frac{A_c}{A_s} \quad (13)$$

The area A_s is computed from the usual polar equation, with θ in radians,

$$A_s = \frac{1}{2} R^2 \theta$$

For our unit radius sphere,

$$A_s = \frac{\theta}{2} \quad (14)$$

Substituting Equations 14 in Equation 13, and solving for A_c ,

$$A_c = \frac{\theta}{2} \cos \gamma \quad (15)$$

For a polygon of N sides, the net area A''_2 is found by algebraic summation of all computed A_c .

$$A''_2 = \frac{1}{2} \left| \sum_{n=1}^N \theta_n \cos \gamma_n \right| \quad (16)$$

Substituting in Equation 8, we have

$$F_{dA_1-A_2} = \frac{1}{2\pi} \left| \sum_{n=1}^N \theta_n \cos \gamma_n \right| \quad (17)$$

The absolute value notation will be explained later. The use of vector algebra greatly facilitates the computation of θ and $\cos \gamma$. Taking, for example, directed line segments \vec{OA} and \vec{OB} , the vector dot product is

$$\vec{OA} \cdot \vec{OB} = x_A x_B + y_A y_B + z_A z_B \quad (18)$$

The cross product $\vec{OA} \times \vec{OB}$ in determinant form is

$$\vec{OA} \times \vec{OB} = \begin{vmatrix} i & j & k \\ x_A & y_A & z_A \\ x_B & y_B & z_B \end{vmatrix}$$

which, upon expansion, becomes the normal vector \vec{V}_N ,

$$\vec{V}_N = \vec{OA} \times \vec{OB} = (y_A z_B - z_A y_B)i + (x_B z_A - z_B x_A)j + (x_A y_B - x_B y_A)k \quad (19)$$

where i , j , and k are mutually orthogonal unit base vectors directed along the principal axes.

\vec{V}_N is equal in magnitude to twice the area of the triangle AOB and is oriented normal to the plane of AOB so that the three vectors form a right-handed system. The magnitude is computed by the Pythagorean theorem,

$$|\vec{V}_N| = \sqrt{(y_A z_B - z_A y_B)^2 + (x_B z_A - x_A z_B)^2 + (x_A y_B - x_B y_A)^2} \quad (20)$$

The angle θ may be evaluated from either the dot or the cross product by use of inverse functions, specifically

$$\theta = \cos^{-1} \left[\frac{\vec{OA} \cdot \vec{OB}}{|\vec{OA}| |\vec{OB}|} \right] \text{ or } \sin^{-1} \left[\frac{|\vec{V}_N|}{|\vec{OA}| |\vec{OB}|} \right]$$

However, an overall economy of computation results from the use of the arctan function,

$$\theta = \tan^{-1} \left[\frac{|\vec{V}_N|}{\vec{OA} \cdot \vec{OB}} \right] \quad (21)$$

As noted earlier, the angle γ is defined as the angle between the plane of AOB and the XY plane. It is also the angle between the vector \vec{V}_N and the

Z axis; $\cos \gamma$ is therefore the direction cosine of \vec{V}_N with respect to the Z axis. Using the Z component in Equation 19,

$$\cos \gamma = \frac{x_{AYB} - x_{BYA}}{|\vec{V}_N|} \quad (22)$$

If the numerator and denominator are both divided by 2,

$$\cos \gamma = \frac{\frac{x_{AYB} - x_{BYA}}{2}}{\left| \frac{\vec{V}_N}{2} \right|}$$

This shows that $\cos \gamma$ is also equal to the ratio of the signed projected area of triangle AOB on the XY plane and the plane area of triangle AOB.

In the right-handed system shown, $\cos \gamma$ is positive when the order of computation of the vectors in the cross product causes the normal vector \vec{V}_N to point in the direction of the +Z axis ($0 < \gamma < 90$). The order in which one proceeds from point to point on the boundary of surface Z will sign each elliptical sector accordingly; however, because the sectors are summed algebraically, the same absolute magnitude will result regardless of order. Because the point factor is always a positive number, the order is computationally unimportant. Nevertheless, the program requires that data be entered in counter-clockwise order for other reasons. This will be discussed in more detail later.

The relative ease with which the point factor can be computed is best illustrated by an example. Using the triangle shown in Figure 2, and starting with line segment \overline{AB} , from Equation 18

$$\vec{OA} \cdot \vec{OB} = 1 + 3 + 9 = 13$$

from Equation 20

$$|\vec{V}_{AB}| = |\vec{OA} \times \vec{OB}| = \sqrt{(-6)^2 + 0 + (2)^2} = \sqrt{40}$$

From Equation 21

$$\theta_{AB} = \tan^{-1} \left\{ \frac{\sqrt{40}}{13} \right\} \cong 0.453$$

From Equation 22

$$\cos \gamma_{AB} = \frac{2}{\sqrt{40}} = 0.316$$

Moving to \overline{BC} ,

$$\overrightarrow{OB} \cdot \overrightarrow{OC} = 3 + 3 + 9 = 15$$

$$|\overrightarrow{BC}| = \sqrt{6^2 + 6^2 + (-8)^2} = \sqrt{136}$$

$$\theta_{BC} = \tan^{-1} \left\{ \frac{\sqrt{136}}{15} \right\} \cong 0.661$$

$$\cos \gamma_{BC} = \frac{-8}{\sqrt{136}} = -0.686$$

Finally, line segment \overline{CA} ,

$$\overrightarrow{OC} \cdot \overrightarrow{OA} = 3 + 1 + 9 = 13$$

$$|\overrightarrow{CA}| = \sqrt{0 + 6^2 + (-2)^2} = \sqrt{40}$$

$$\theta_{CA} = \tan^{-1} \left\{ \frac{\sqrt{40}}{13} \right\} \cong 0.453$$

$$\cos \gamma_{CA} = \frac{2}{\sqrt{40}} = 0.316$$

The point factor is, therefore, from Equation 17,

$$F_{dA_1 - A_2} = \frac{1}{2\pi} |2(0.453)(0.316) + (0.661)(-0.686)|$$

$$= \frac{1}{2\pi} |-0.167|$$

$$F_{dA_1 - A_2} = 0.0266$$

The repetitive nature of the computation should be noted. All surfaces that can be represented by straight line segments in space can be analyzed in the simple, direct manner shown.

COORDINATE TRANSFORMATION

One of the most important features of the computer program is the capability of transformation (translation and/or rotation) of surface coordinates. By this means, data may be entered for each surface from a convenient, local origin. The surfaces may then be linked together by transforming one or both surface coordinates to a convenient third origin common to both surfaces.

The mathematical processing required to perform the transformation of coordinates differs from the usual treatment. One is ordinarily given an "old" set of coordinates along with the necessary transformation information, such as direction cosines and translation terms, Euler angles, etc., from which a second set of coordinates are generated—the "new" position of the surface. However, in the present case, instead of transformation parameters, the program accepts the coordinates of any three points (taken from the "new" origin) and uses this information to derive the transformation criteria. These data are then used to transform the remaining points to the new origin. In most cases, this method requires less computational effort and results in fewer errors in the set-up of surface data.

For example, the factor between two skewed disks arbitrarily located in a particular compartment may be desired. It is assumed that each disk will be simulated by a 32-sided regular polygon. A convenient local origin is selected for each disk. The most obvious is a coordinate system with the origin at the center of the disk, and with the disk in the XY plane. Next, the coordinates of three arbitrarily selected points in each surface are computed to a third origin, which appears relatively convenient to both surfaces. This might be a corner or the center of the compartment. Then the program will transform the remaining 29 points in each surface to the common origin. The data for both surfaces are now in the same coordinate system, as they must be before the factor computation can proceed.

It may be more convenient to transform only one of the surfaces. In the preceding example, the coordinates of one disk may be directly transformed to the origin of the other.

PROGRAM CONTENTS

The computer program is written in Fortran source language for use with the IBM 7090 computer system. The program consists of the main program and subroutines UNIVFC, SELEK, TXFRM, DOICU, MAP, and FACTOR, including an input-output tape compatibility subroutine written in 7090 machine language (FAP). Algebraic NAA library tape routines SQRT and ARCTAN are also used.

MAIN PROGRAM

The main program reads in data, performs the necessary logical and/or arithmetic operations to control processing and flow of data to and from the subroutines, and prints diagnostics and/or program factor output.

SUBROUTINE UNIVFC

This subroutine is used to erect a unit vector normal to the plane formed by the first, second, and last surface data point. This vector is created by taking the cross product of vectors 1-2 and 1-last, erecting the orientation vector so that the three make a right-handed system. Thus, the order in which these points are entered controls the direction of this vector, which indicates the active, or front, side of the surface.

This subroutine also computes the data required for coordinate transformation.

SUBROUTINE SELEK

This subroutine selects, according to the symbol or name assigned to the data given in the run instructions, the position (subscript) of the data bearing the same name in the surface and transformation data originally read in.

SUBROUTINE TXFRM

The first part of this subroutine performs an auxiliary transformation for use in determining the planarity of a surface, computing surface area, and, most important, positioning surface 1 in the XY plane of the coordinate system (required before factor computation).

The second part performs a primary transformation. The surface data as originally entered are transformed to the new position indicated by the three points entered in the transformation data. Both surfaces may be transformed if transformation is desired and so indicated in the run instructions.

SUBROUTINE DOICU

This subroutine, by use of the orientation vector in each surface, determines whether each surface sees none, part of, or all of the other surface. If either or both surfaces bisect the other, the part not seen by the other surface is determined and excluded from the new surface data.

SUBROUTINE MAP

The primary function of this subroutine is to locate the individual positions on surface A_1 from which point factors will be computed. The surface is scribed with a number of horizontal lines equally spaced vertically. Each horizontal line is then divided into equally spaced parts. All horizontal lines are divided into the same number of increments. The vertical and horizontal divisions may be controlled separately through data entry. The sum of the incremental areas represented by each point thus generated is computed as the mapping area. A comparison of the mapping area with the actual surface area yields some indication of the accuracy of the mean factor computation.

SUBROUTINE FACTOR

The actual factor computation is performed in this subroutine. After each horizontal line of factors is computed, the area-weighted factors are integrated by the trapezoidal rule. Upon completion of the horizontal integration, the area-factor products are integrated vertically, also by the trapezoidal rule. The area factor F_{12} is computed from the results.

INPUT DATA

FORMAT

All data may be entered on Fortran fixed 10 digit decimal data sheets or an equivalent. Each line on these data sheets represents 12 card columns with 6 lines per card, or a total of 72 available columns for data entry. The last 8 columns are used for identification (card sequencing).

SPECIFICATIONS

A complete data package consists of a title card, surface data, transformation data (if any), run instructions, and end card. A very brief description will be given of each part of input data. Persons who desire to use the program should study the more complete instructions given in Reference 3. All data must be derived from a right-handed rectangular coordinate system.

SURFACE DATA

Each set of surface data is assembled into a physically separate, independent package. Each package is headed by a name card, uniquely identifying the surface data immediately following. The x, y, and z coordinates of each point defining the boundary of the surface are then given. The points are given in counterclockwise order as they appear facing the active side of the surface.

When entering nonplanar surface data, particular care must be exercised to insure that the data entered do in reality form the silhouette of the nonplanar surface as seen from any point on the other surface. Surface A₁ must always be planar.

TRANSFORMATION DATA

Each set of transformation data is also uniquely identified by a name. The particular position number of each of three surface points, followed by the transformed x, y, z position of the point, is given. Only three cards are required to complete a particular set of transformation data.

RUN INSTRUCTIONS

Immediately following the last surface or transformation data package are instructions that indicate, for each factor computation, the particular data to use, the type of output desired, and the increment size desired.

The format used is best shown by the example problem code sheets. It is important that each name shown in the run instructions be identical to that given in the data.

SAMPLE PROBLEM

A representative sample problem will illustrate the ease of program use in the solution of a difficult factor computation. Figure 3 shows two surfaces located in the same compartment. One surface is a disk and the other a trapezium. The surfaces are positioned so that only part of each surface is seen by the other.

The data sheets giving the necessary data and run instructions are shown in Figure 4. Note that the unit radius disk has been simulated by a 32-sided regular polygon, named DISK. A convenient local origin, indicated by the primed axes, was used for disk data entry. Then, three convenient points, 1, 9, and 17, were chosen for transformation, and the transformation data assigned the name TFDISK. The data describing the trapezium, POLYGN (only six characters may be used for any name), are given in the unprimed system quite easily, since there are only four points to enter.

Two factor computations were requested; the second is merely to demonstrate reciprocity of FA products ($F_1A_1 = F_2A_2$) and the flexibility of surface callout in run instructions. A detailed output was requested by the code letter D in the first factor request and omitted in the second to illustrate the two different outputs available. Both surfaces were transformed to the double-primed system prior to factor computations; these coordinates are given as part of the detailed output, which includes all point factors computed.

Figure 5 shows the computer program results for the sample problem.

Space does not permit more examples to be given at this time. A demonstration of how the program can compute factors to nonplanar surfaces is shown along with other interesting examples in Reference 3.

ACCURACY OF RESULTS

Table 1 compares configuration factors computed by the program to factors given in Reference 1 for various geometries. The P configurations are point factors, and the A configurations are area factors. The point factors are in precise agreement because no approximations are employed to obtain the factors. The effect of increment size on the area factors computed by the program is shown to be negligible when going from 24 to 60 divisions.

Because accuracy to three decimal places is sufficient for most engineering applications, it appears that the results are satisfactory. Furthermore, because of the validity and uniformity of the computational procedure, it may reasonably be inferred that similar accuracy may be expected for configurations other than those given in Table 1.

Table 1. Comparison of Configuration Factors Computed by CONFAC I to Those Given in Reference 1

Configuration	Reference 1	Computer (Trapezoidal Rule)	
		24 x 24 grid	60 x 60 grid
P-1, X = 1, Y = 1	0.13853	0.138532	0.138532
X = 0.1, Y = 0.1	0.00314	0.003141	0.003141
X = 1, Y = 4	0.17527	0.175270	0.175270
X = 0.1, Y = 0.4	0.01147	0.011471	0.011471
X = 1, Y = ∞*	0.17678	0.176777	0.176777
X = 0.1, Y = ∞*	0.02488	0.0248759	0.0248759
P-2, ∅ = 30°, L = 0, N = 1	0.4665	0.466506	0.466506
∅ = 30°, L = 1, N = 1	0.1759	0.175923	0.175923
∅ = 30°, L = 0, N = 4	0.4665	0.466506	0.466506
∅ = 30°, L = 4, N = 4	0.0964	0.096447	0.096447
∅ = 120°, L = 0, N = 1	0.125	0.125000	0.125000
∅ = 120°, L = 1, N = 1	0.0236	0.023554	0.023554
∅ = 120°, L = 0, N = 4	0.125	0.125000	0.125000
∅ = 120°, L = 4, N = 4	0.0077	0.007683	0.007683
A-1, X = 1, Y = 1	0.19982	0.199720	0.199808
X = 0.1, Y = 0.1	0.00316	0.003162	0.003162
X = 1, Y = 4	0.34596	0.345590	0.345902
X = 0.1, Y = 0.4	0.01207	0.012072	0.0120725
X = 1, Y = ∞*	0.41421	0.405493	0.4107468
X = 0.1, Y = ∞*	0.04988	0.048836	0.0494599
A-2, ∅ = 30°, L = 1, N = 1	0.6202+	0.617692	0.6187784
∅ = 30°, L = 4, N = 4	0.3961+	0.394311	0.3944992
∅ = 120°, L = 1, N = 1	0.0870+	0.086649	0.0866228
∅ = 120°, L = 4, N = 4	0.0443+	0.042720	0.0423530

*10⁸ was assumed to approximate ∞ for computer run
+These values were obtained by numerical integration across surface A₁, according to Reference 1.

CURRENT PROGRAM DEVELOPMENTS

A number of important and useful changes to the existing program are being developed. The most significant of these is the silhouette generator. This subroutine determines which points on the boundary of a solid object form the silhouette of that object from any arbitrary viewpoint outside the object. Actually, more than one object may be viewed at once; the silhouette generator will determine the silhouette of all objects taken together. The principal usefulness of the silhouette generator appears in the solution of the so-called "variable shadow" problem. If the factor between two surfaces or objects is desired and an intervening surface is present, the computation of the geometric factor becomes extremely complicated. However, the problem is solved quite easily with the silhouette generator incorporated in the existing program.

For example, suppose that there are two opposed parallel plates in space, and a third plate interposed between them so that the view of one surface from the other varies from point to point on each surface. Using the silhouette generator, the factor from one surface to both of the other surfaces is computed. Then the factor to only one of the other surfaces is computed. Obviously, the factor to the other surface is obtained by simple subtraction.

Besides the current extension of the existing program to solids and occluded surfaces, the capability to internally generate a large variety of commonly encountered shapes, such as cylinders, cones, cubes, etc., is included. Instead of the 17 cards required to simulate a disk, as in the example problem, only one or two are needed.

FUTURE EFFORT

It is clear that the next step in the development of the configuration-factor computer program is to acquire the capability to compute the factor from a curved surface. The basic tools are already developed and need only to be applied to the problem.

REFERENCES

1. Hamilton, D. C. and W. R. Morgan, Radiant-Interchange Configuration Factors, National Advisory Committee for Aeronautics, NACA TN-2836, 1952.
2. Sokolnikoff, I. D. and R. M. Redheffer, Mathematics of Physics and Modern Engineering, McGraw-Hill Book Company, Inc., 1958.
3. Toups, Kempton A., A General Computer Program for the Determination of Radiant-Interchange Configuration Factors, ASD TN 61-101 (Released to ASD for publication April 1962).

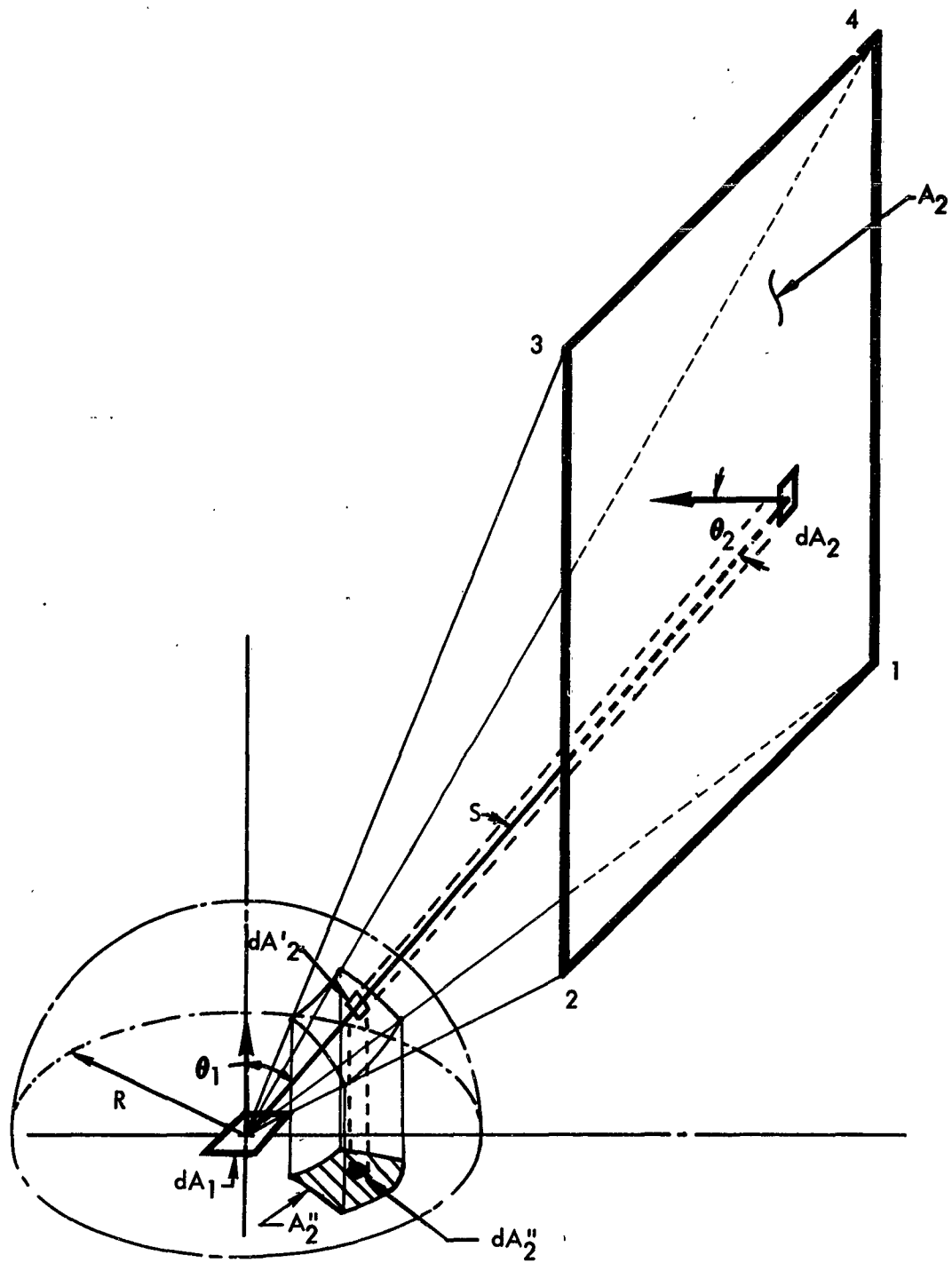


Figure 1. Nusselt Geometrical Relationships

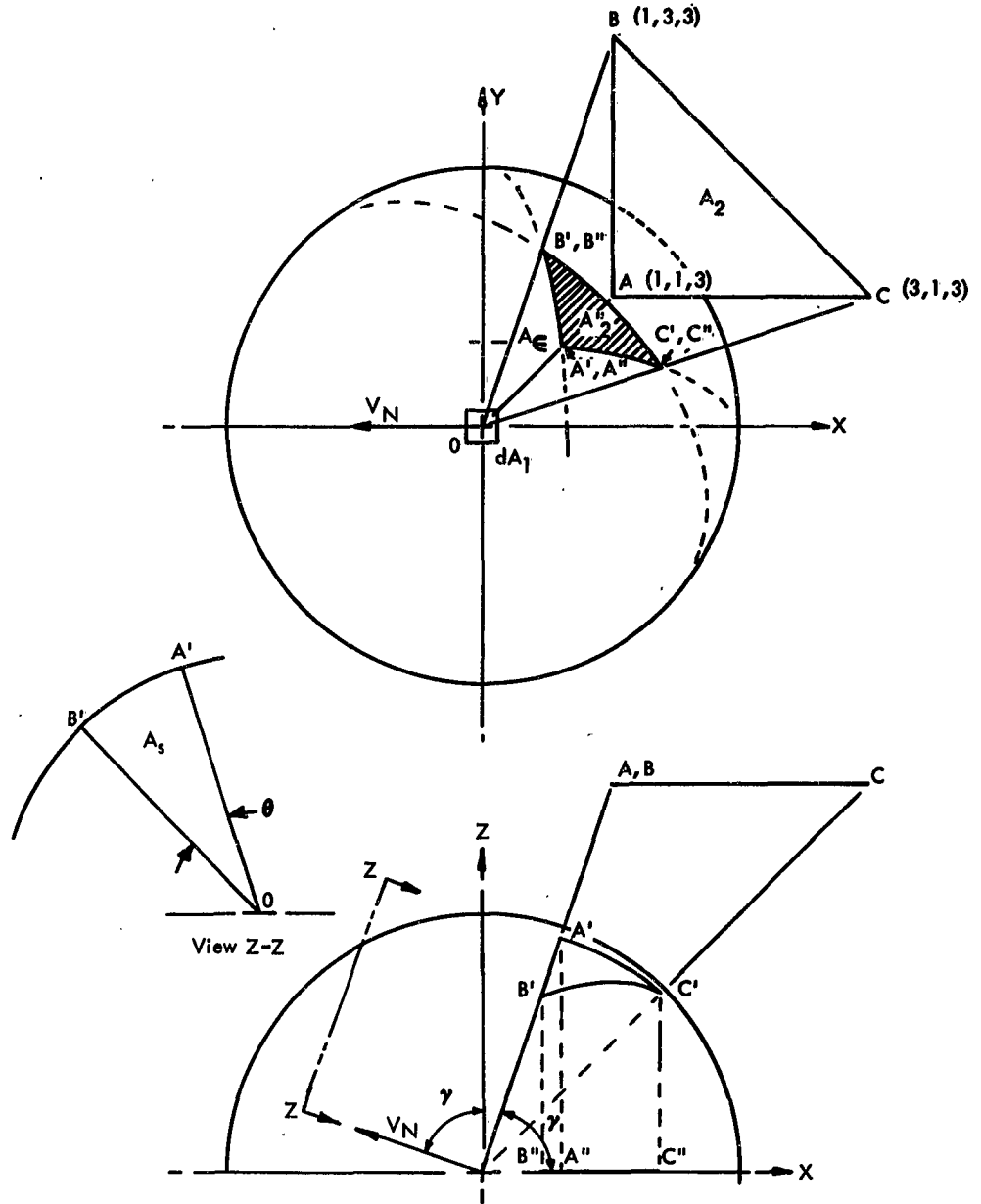


Figure 2. Geometry of New Method

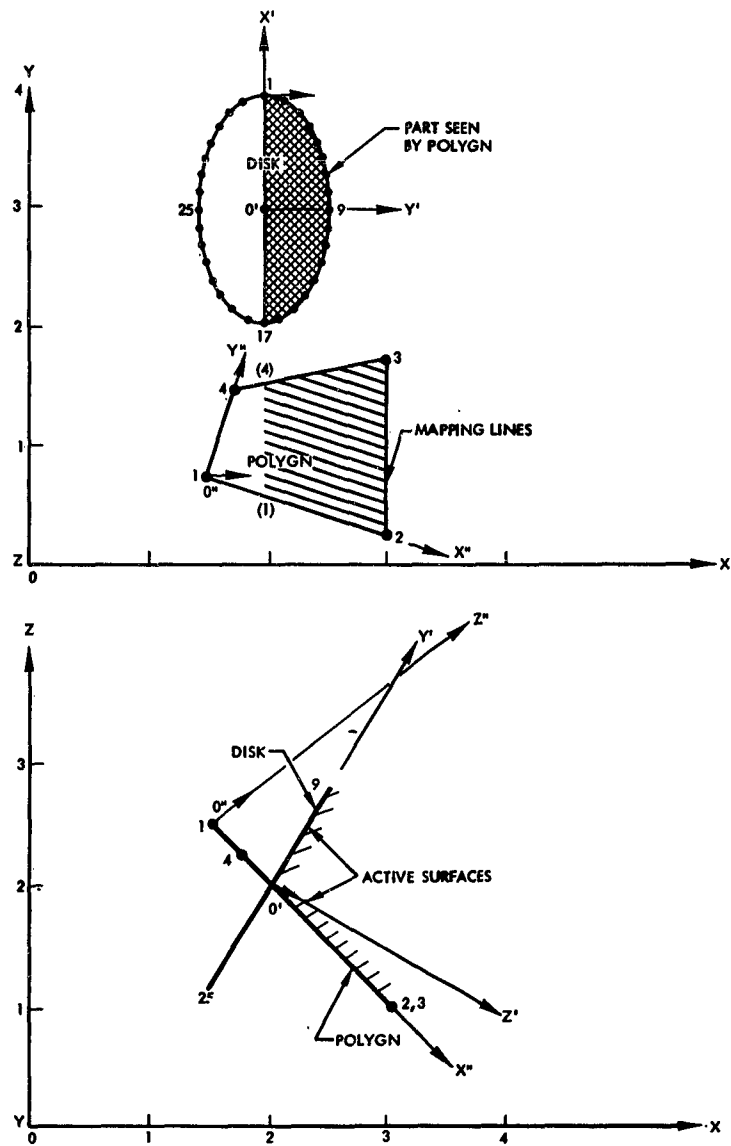


Figure 3. Sample Problem

FORTRAN FIXED 10 DIGIT DECIMAL DATA

DECK NO. _____ PROGRAMMER _____ DATE _____ PAGE _____ of _____ JOB NO. _____ 1.

NUMBER	IDENTIFICATION	DESCRIPTION DO NOT KEY PUNCH
1	A H P L E P R O B L	
13	E M - P L Y G O H T	
25	S K E W E D D I S	
37	K . . . K A T O U P S , 1	
49	/ 3 / 6 3	
61		
1	D I S K	Name assigned to Disk simulated by a 32-sided polygon (Unit Radius)
13		
25		
37		
49		
61		
1	3 2	No. of Points Describing Surface Disk
13	1	
25	0	Coordinates Point 1
37	0	
49	. 9 8 0 . 7 8 5	Point 2
61	. 1 9 5 0 9 0	Etc.
1	0	
13	. 9 2 3 8 8 0	
25	. 3 8 2 6 8 3	
37	0	
49	. 8 3 1 4 7 0	
61	. 5 5 5 5 7 0	

FORM 114-C-111 REV. 1-64

Figure 4. Fortran Fixed 10 Digit Decimal Data (1 of 7)

FORTRAN FIXED 10 DIGIT DECIMAL DATA

DECK NO.	PROGRAMMER	DATE	PAGE	of	JOB NO.
NUMBER		IDENTIFICATION		DESCRIPTION DO NOT KEY PUNCH	
1	0				
19	.7 0 7 1 0 7				
25	.7 0 7 1 0 7				
37	0				
49	.5 5 5 5 7 0				
61	.8 3 1 4 7 0				
1	0				
19	.3 8 2 6 8 3				
25	.9 2 3 8 8 0				
37	0				
49	.1 9 5 0 9 0				
61	.9 8 0 7 8 5				
1	0				
19	0				
25	1				
37	0				
49	.1 9 5 0 0 0				
61	.9 8 0 7 8 5				
1	0				
19	.3 8 2 6 8 3				
25	.9 2 3 8 8 0				
37	0				
49	.5 5 5 5 7 0				
61	.8 3 1 4 7 0				

FORM 114-C-17 REV. 7-68

Figure 4. Fortran Fixed 10 Digit Decimal Data (2 of 7)

FORTRAN FIXED 10 DIGIT DECIMAL DATA

DECK NO.	PROGRAMMER	DATE	PAGE	of	JOB NO.	DESCRIPTION DO NOT KEY PUNCH
	NUMBER	IDENTIFICATION				
1	0					
13	- . 7 0 7 1 0 7					
25	. 7 0 7 1 0 7					
37	0					
49	- . 8 3 1 4 7 0	80				
61	. 5 5 5 7 0	9				
1	0					
13	- . 9 2 3 8 8 0					
25	. 3 8 2 6 8 3					
37	0					
49	- . 9 8 0 7 8 5	80				
61	. 1 9 5 0 9 0	10				
1	0					
13	- . 1					
25	0					
37	0					
49	- . 9 8 0 7 8 5	80				
61	- . 1 9 5 0 9 0	11				
1	0					
13	- . 9 2 3 8 8 0					
25	- . 3 8 2 6 8 3					
37	0					
49	- . 8 3 1 4 7 0	80				
61	- . 5 5 5 7 0	11				

FORM 114-C17 REV. 7-68

Figure 4. Fortran Fixed 10 Digit Decimal Data (3 of 7)

FORTRAN FIXED 10 DIGIT DECIMAL DATA

DECK NO.	PROGRAMMER	DATE	PAGE	of	JOB NO.	DESCRIPTION DO NOT KEY PUNCH
1						
13						
25						
37						
49						
61						
1						
13						
25						
37						
49						
61						
1						
13						
25						
37						
49						
61						
1						
13						
25						
37						
49						
61						

Figure 4. Fortran Fixed 10 Digit Decimal Data (4 of 7)

FORTRAN FIXED 10 DIGIT DECIMAL DATA

DECK NO.	PROGRAMMER	DATE	PAGE	of	JOB NO.	DESCRIPTION DO NOT KEY PUNCH
1						
13						
25						
37						
49						
61						
1						
13						
25						
37						
49						
61						
1						
13						
25						
37						
49						
61						
1						
13						
25						
37						
49						
61						
1						
13						
25						
37						
49						
61						
1						
13						
25						
37						
49						
61						
1						
13						
25						
37						
49						
61						
1						
13						
25						
37						
49						
61						
1						
13						
25						
37						
49						
61						
1						
13						
25						
37						
49						
61						
1						
13						
25						
37						
49						
61						
1						
13						
25						
37						
49						
61						
1						
13						
25						
37						
49						
61						
1						
13						
25						
37						
49						
61						
1						
13						
25						
37						
49						
61						
1						
13						
25						
37						
49						
61						
1						
13						
25						
37						
49						
61						
1						
13						
25						
37						
49						
61						
1						
13						
25						
37						
49						
61						
1						
13						
25						
37						
49						
61						
1						
13						
25						
37						
49						
61						
1						
13						
25						
37						
49						
61						
1						
13						
25						
37						
49						
61						
1						
13						
25						
37						
49						
61						
1						
13						
25						
37						
49						
61						
1						
13						
25						
37						
49						
61						
1						
13						
25						
37						
49						
61						
1						
13						
25						
37						
49						
61						
1						
13						
25						
37						
49						
61						
1						
13						
25						
37						
49						
61						
1						
13						
25						
37						
49						
61						
1						
13						
25						
37						
49						
61						
1						
13						
25						
37						
49						
61						
1						
13						
25						
37						
49						
61						
1						
13						
25						
37						
49						
61						
1						
13						
25						
37						
49						
61						
1						
13						
25						
37						
49						
61						
1						
13						
25						
37						
49						
61						
1						
13						
25						
37						
49						
61						
1						
13						
25						
37						
49						
61						
1						
13						
25						
37						
49						
61						
1						
13						
25						
37						
49						
61						
1						
13						
25						
37						
49						
61						
1						
13						
25						
37						
49						
61						
1						
13						
25						
37						
49						
61						
1						

FORTRAN FIXED 10 DIGIT DECIMAL DATA

DECK NO.	PROGRAMMER	DATE	PAGE	of	JOB NO.	7.	
NUMBER		IDENTIFICATION					DESCRIPTION DO NOT KEY PUNCH
1	1						Point 1 in Disk data
13	2						} New Coordinates of Point 1
23	4						
37	2						} Point 9 in Disk data
49	9						
61	2						} New Coordinates of Point 9
1	3						
13	2						} Point 17 in Disk data
25	1						
37	2						} New Coordinates of Point 17
49	2						
61	2						} Run Instruction 1 with Detailed Printout
1	P						
13	L						} Run Instruction 2, Standard Output
25	F						
37	D						} End card to complete Case Package
49	T						
61	F						
1	E						
13	N						
25	D						
37							
49							
61							

FORM 11-C-113 REV. 7-68

Figure 4. Fortran Fixed 10 Digit Decimal Data (7 of 7)

NAA SPACE AND INFORMATION SYSTEMS DIVISION
T-4 PROJECT CONFIGURATION FACTOR PROGRAM
SAMPLE PROBLEM-POLYGON TO SKEWED DISK. K.A.TOUPS, 1/3/63

I N P U T D A T A

SURFACE AND TRANSFORMATION DATA

THE FIRST DATA SET ARE THE ORIGINAL INPUT DATA.
THE SET IMMEDIATELY FOLLOWING ARE THE ORIGINAL DATA REFERENCED TO THE PLANE FORMED BY THE
1,2 AND LAST DATA POINTS, IF THE ORIGINAL DATA WERE NOT SUBSTANTIALLY IN THE XY PLANE OF ITS CS.

POINT	X	Y	Z	POINT	X	Y	Z
1	0.100000E 01	0.	0.	2	0.9807850E 00	0.1950900E-00	0.
3	0.100000E 01	0.	0.	4	0.8314700E 00	0.555700E 00	0.
5	0.9238800E 00	0.3826830E-00	0.	6	0.555700E 00	0.8314700E 00	0.
7	0.7071070E 00	0.9238800E 00	0.	8	0.1950900E-00	0.9807850E 00	0.
9	0.	0.100000E 01	0.	10	-0.1950900E-00	0.9807850E 00	0.
11	-0.3826830E-00	0.9238800E 00	0.	12	-0.555700E 00	0.8314700E 00	0.
13	-0.7071070E 00	0.7071070E 00	0.	14	-0.8314700E 00	0.555700E 00	0.
15	-0.9238800E 00	0.3826830E-00	0.	16	-0.9807850E 00	0.1950900E-00	0.
17	-0.100000E 01	0.	0.	18	-0.9807850E 00	-0.1950900E-00	0.
19	-0.9238800E 00	-0.3826830E-00	0.	20	-0.8314700E 00	-0.555700E 00	0.
21	-0.7071070E 00	-0.7071070E 00	0.	22	-0.555700E 00	-0.8314700E 00	0.
23	-0.3826830E-00	-0.9238800E 00	0.	24	-0.1950900E-00	-0.9807850E 00	0.
25	0.	-0.100000E 01	0.	26	0.1950900E-00	-0.9807850E 00	0.
27	0.3826830E-00	-0.9238800E 00	0.	28	0.555700E 00	-0.8314700E 00	0.
29	0.7071070E 00	-0.7071070E 00	0.	30	0.8314700E 00	-0.555700E 00	0.
31	0.9238800E 00	-0.3826830E-00	0.	32	0.9807850E 00	-0.1950900E-00	0.
1	0.100000E 01	0.	0.	2	0.9807850E 00	0.1950900E-00	0.
3	0.9238800E 00	0.3826830E-00	0.	4	0.8314700E 00	0.555700E 00	0.
5	0.7071070E 00	0.9238800E 00	0.	6	0.555700E 00	0.8314700E 00	0.
7	0.	0.100000E 01	0.	8	0.1950900E-00	0.9807850E 00	0.
9	-0.3826830E-00	0.9238800E 00	0.	10	-0.1950900E-00	0.9807850E 00	0.
11	-0.7071070E 00	0.7071070E 00	0.	12	-0.555700E 00	0.8314700E 00	0.
13	-0.9238800E 00	0.3826830E-00	0.	14	-0.8314700E 00	0.555700E 00	0.
15	-0.9238800E 00	0.3826830E-00	0.	16	-0.9807850E 00	0.1950900E-00	0.
17	-0.100000E 01	0.	0.	18	-0.9807850E 00	-0.1950900E-00	0.
19	-0.9238800E 00	-0.3826830E-00	0.	20	-0.8314700E 00	-0.555700E 00	0.
21	-0.7071070E 00	-0.7071070E 00	0.	22	-0.555700E 00	-0.8314700E 00	0.

Figure 5. Sample Problems Computer Output (1 of 8)

```

23 -0.3826830E-00 -0.9238800E 00 0. 0.
25 0. 0. 1000000E 01 0.
27 0.3826830E-00 -0.5238800E 00 0.
29 0.7071070E 00 -0.7071070E 00 0.
31 0.9238800E 00 -0.3826830E-00 0.
DATA NAME *POLYGN *
POINT X Y Z
1 0.2207107E 01 0.7500000E 00 0.3207107E 01
3 0.1500000E 01 0.7500000E 00 0.2500000E 01
1 -0.3000000E 01 0.1750000E 01 0.1000000E 01
3 0.1835326E 01 0.1459993E 01 0.
DATA NAME- *TFDISK *
POINT X Y Z
1 0.2010000E 01 0.4000000E 01 0.2000000E 01
17 0.2010000E 01 0.2000000E 01 0.2000000E 01

```

RUN DATA-

```

RUN SURF SURF SURF1 SURF2 HORZ VERT
NO 1 TXFRM TXFRM TXFRM INCR INCR
1 *POLYGN* DISK* *TFDISK*D * *
2 * DISK*POLYGN*TFDISK* * *

```

```

24 -0.1950900E-00 -0.9807850E 00 0.
26 0.1950900E-00 -0.9807850E 00 0.
28 0.5555700E 00 -0.8314700E 00 0.
30 0.8314700E 00 -0.5555700E 00 0.
32 0.9807850E 00 -0.1950900E-00 0.
POINT X Y Z
2 0.3000000E 01 0.2500000E-00 0.1000000E 01
4 0.1750000E 01 0.1500000E 01 0.2250000E 01
2 0.2179449E 01 0.
4 0.1720618E-00 0.8111071E 00 0.
POINT X Y Z
9 0.2510000E 01 0.3000000E 01 0.2866025E 01

```

Figure 5. Sample Problems Computer Output (2 of 8)

SAMPLE PROBLEM-POLYGON TO SKEWED DISK. K.A.TOUPS, 1/3/63

RUN NO. 1 DATA USED FOR THIS RUN- *POLYGN* DISK*
 * * *TFDISK*
 *D * *

THE CONFIGURATION FACTOR FROM SURFACE *POLYGN * TO SURFACE * DISKTFDISK* = 0.00669

THE FA PRODUCT = 0.14789E-01 SQ UNITS

THE MAPPING AREA = 0.1734222E 01 SQ UNITS

ONLY A PART OF SURFACE *POLYGN *, COMPRISING AN AREA OF 0.1735515E 01 SQ UNITS
 SEES SURFACE * DISKTFDISK*

THE AREA OF SURFACE *POLYGN * = 0.2209708E 01 SQ UNITS.

ONLY A PART OF SURFACE * DISKTFDISK*, COMPRISING AN AREA OF 0.1575357E 01 SQ UNITS
 SEES SURFACE *POLYGN *

THE AREA OF SURFACE * DISKTFDISK* = 0.3121445E 01 SQ UNITS.

THE FOLLOWING ARE THE (FINAL) SURFACE COORDINATES USED FOR THE FACTOR COMPUTATION-

POINT	X	Y	Z	POINT	X	Y	Z
1	0.7356945E 00	0.	0.	2	0.1000000E 01	(INTERNALLY GENERATED ORIENTATION VECTOR)	0.
3	0.1835326E 01	0.1459939E 01	0.	4	0.2179449E 01	0.	0.
					0.5131503E 00	0.9441752E 00	0.

DATA NAME * POLYGN *

POINT	X	Y	Z	POINT	X	Y	Z
1	0.8896918E 00	0.3548760E 01	0.2658899E-00	2	0.7071059E-02	(INTERNALLY GENERATED ORIENTATION VECTOR)	0.
3	-0.5047141E-01	0.327161E 01	0.7071059E-02	4	-0.9520940E-01	0.3296874E 01	0.1955135E-00
5	-0.1294121E-00	0.3230349E 01	0.3767143E-00	6	-0.1517648E-00	0.3130138E 01	0.5437103E 00
7	-0.1614085E-00	0.3000094E 01	0.6900837E 00	8	-0.1579255E-00	0.2845214E 01	0.8102091E 00
9	-0.1415890E-00	0.2671452E 01	0.8994704E 00	10	-0.1128875E-00	0.2485483E 01	0.9544363E 00
					-0.7297138E-01	0.2294456E 01	0.9729966E 00
					-0.2337411E-01	0.2105710E 01	0.9544363E 00

Figure 5. Sample Problems Computer Output (3 of 8)

```

11 0.3399792E-01 0.1926499E 01 0.8994703E 00 12 0.9694042E-01 0.1763711E 01 0.8102092E 00
13 0.1630344E-00 0.1623600E 01 0.6900836E 00 14 0.2297397E-00 0.1511551E 01 0.5437103E 00
15 0.2944930E-00 0.1431872E 01 0.3767144E-00 16 0.3548055E-00 0.1387623E 01 0.1955135E-00
17 0.4083599E-00 0.1380505E 01 0.7071096E-02 18 0.4100386E-00 0.1381641E 01 -0.
19 -0.4846185E-01 0.3326894E 01 0.

```

COORDINATES OF POINTS ON BOUNDARY OF SURF *POLYGN * FOR EACH Y INTERVAL

X-LEFT		X-RIGHT		Y		X-LEFT		X-RIGHT		Y	
0.7356945E 00	0.2179449E 01	0.1216661E-00	0.7213560E 00	0.2165111E 01	0.6083303E-01	0.6926790E 00	0.2136434E 01	0.1824991E-00	0.3041652E-00	0.4258312E-00	0.5474973E 00
0.6783406E 00	0.2122095E 01	0.3649982E-00	0.6440021E 00	0.2107757E 01	0.4691634E 00	0.6440021E 00	0.2079080E 01	0.2021726E 01	0.4691634E 00	0.7908294E 00	0.5474973E 00
0.6496636E 00	0.2093419E 01	0.4866643E-00	0.5779712E 00	0.1993049E 01	0.9124955E 00	0.6066643E 00	0.2021726E 01	0.1948372E 01	0.7908294E 00	0.1034162E 01	0.1034162E 01
0.6209866E 00	0.2064742E 01	0.6083303E 00	0.5779712E 00	0.1993049E 01	0.9124955E 00	0.6066643E 00	0.2021726E 01	0.1948372E 01	0.7908294E 00	0.1034162E 01	0.1034162E 01
0.5636327E 00	0.2007388E 01	0.8516624E 00	0.5779712E 00	0.1993049E 01	0.9124955E 00	0.6066643E 00	0.2021726E 01	0.1948372E 01	0.7908294E 00	0.1034162E 01	0.1034162E 01
0.5349557E 00	0.1978711E 01	0.9733285E 00	0.5779712E 00	0.1993049E 01	0.9124955E 00	0.6066643E 00	0.2021726E 01	0.1948372E 01	0.7908294E 00	0.1034162E 01	0.1034162E 01
0.5878778E 00	0.1950034E 01	0.1094995E 01	0.5779712E 00	0.1993049E 01	0.9124955E 00	0.6066643E 00	0.2021726E 01	0.1948372E 01	0.7908294E 00	0.1034162E 01	0.1034162E 01
0.8997397E 00	0.1921357E 01	0.1216661E 01	0.5779712E 00	0.1993049E 01	0.9124955E 00	0.6066643E 00	0.2021726E 01	0.1948372E 01	0.7908294E 00	0.1034162E 01	0.1034162E 01
0.1211602E 01	0.1892680E 01	0.1338327E 01	0.5779712E 00	0.1993049E 01	0.9124955E 00	0.6066643E 00	0.2021726E 01	0.1948372E 01	0.7908294E 00	0.1034162E 01	0.1034162E 01
0.1523464E 01	0.1864003E 01	0.1459993E 01	0.5779712E 00	0.1993049E 01	0.9124955E 00	0.6066643E 00	0.2021726E 01	0.1948372E 01	0.7908294E 00	0.1034162E 01	0.1034162E 01
0.1835326E 01	0.1835326E 01	0.1459993E 01	0.5779712E 00	0.1993049E 01	0.9124955E 00	0.6066643E 00	0.2021726E 01	0.1948372E 01	0.7908294E 00	0.1034162E 01	0.1034162E 01

NO. OF HORIZONTAL INCREMENTS= 24 NO. OF VERTICAL INCREMENTS= 24

THE FOLLOWING ARE PLANE POINT CONFIGURATION FACTORS COMPUTED FOR THIS RUN
LOWEST GRID LINE FIRST, FROM X-LEFT TO X-RIGHT.

0.2007911E-02	0.4116122E-03	0.7934807E-03	0.1144358E-02	0.1463655E-02	0.1751342E-02
0.2963429E-02	0.2234262E-02	0.2431629E-02	0.2601506E-02	0.2745370E-02	0.2865593E-02
0.3185405E-02	0.3040941E-02	0.3099960E-02	0.3142276E-02	0.3169595E-02	0.3183317E-02
0.3020697E-02	0.3177257E-02	0.3159748E-02	0.3134297E-02	0.3101992E-02	0.3063889E-02
0.2234766E-02	0.4624200E-03	0.8899944E-03	0.1281307E-02	0.1635709E-02	0.1953296E-02
0.3254408E-02	0.2481320E-02	0.2694549E-02	0.2876346E-02	0.3028775E-02	0.3154053E-02
0.3453747E-02	0.3332096E-02	0.3382944E-02	0.3428126E-02	0.3450573E-02	0.3458528E-02
0.3238602E-02	0.3437833E-02	0.3412269E-02	0.3378407E-02	0.3337462E-02	0.3290330E-02
0.2494895E-02	0.5215134E-03	0.1002045E-02	0.1439844E-02	0.1834296E-02	0.2185647E-02
	0.2763639E-02	0.2993941E-02	0.3188187E-02	0.3348979E-02	0.3479027E-02

Figure 5. Sample Problems Computer Output (4 of 8)

0.2699804E-01
 0.2231368E-01
 0.1849275E-01
 0.1540458E-01
 0.1291056E-01
 0.2466155E-01
 0.2119856E-01
 0.1830277E-01
 0.1587421E-01
 0.1382960E-01
 0.2196840E-01
 0.1982574E-01
 0.1793812E-01
 0.1627042E-01
 0.1479291E-01
 0.1300011E-01
 0.1143706E-01
 0.1059112E-01
 0.1579647E-01
 0.1683575E-01
 0.1683575E-01
 0.1683575E-01
 0.1683575E-01
 0.1683575E-01
 0.1683575E-01
 0.2615378E-01
 0.2161992E-01
 0.1793106E-01
 0.1495114E-01
 0.2404023E-01
 0.2067945E-01
 0.1766801E-01
 0.1550881E-01
 0.2159189E-01
 0.1949444E-01
 0.1764376E-01
 0.1601165E-01
 0.1913787E-01
 0.1818555E-01
 0.1729281E-01
 0.1645517E-01
 0.1683575E-01
 0.168375E-01
 0.1683575E-01
 0.1683575E-01
 0.1683575E-01
 0.1683575E-01
 0.2533507E-01
 0.2094977E-01
 0.1738905E-01
 0.1451354E-01
 0.2343732E-01
 0.2017557E-01
 0.1744578E-01
 0.1515370E-01
 0.2122342E-01
 0.1917005E-01
 0.1735935E-01
 0.1575811E-01
 0.1897481E-01
 0.1803274E-01
 0.1714949E-01
 0.1632063E-01
 0.1683575E-01
 0.1683575E-01
 0.1683575E-01
 0.1683575E-01
 0.1683575E-01
 0.2454195E-01
 0.2030263E-01
 0.1686065E-01
 0.1409119E-01
 0.2285224E-01
 0.1968642E-01
 0.1703566E-01
 0.1480856E-01
 0.2086275E-01
 0.1885238E-01
 0.1707875E-01
 0.1550956E-01
 0.1881351E-01
 0.1788158E-01
 0.1700768E-01
 0.1618748E-01
 0.1683575E-01
 0.1683575E-01
 0.1683575E-01
 0.1683575E-01
 0.1683575E-01
 0.2377424E-01
 0.1967785E-01
 0.1636141E-01
 0.1388352E-01
 0.2228443E-01
 0.1921154E-01
 0.1643727E-01
 0.1447307E-01
 0.2050971E-01
 0.1854128E-01
 0.1680382E-01
 0.1526592E-01
 0.1865396E-01
 0.1732025E-01
 0.1686736E-01
 0.1605573E-01
 0.1683575E-01
 0.1683575E-01
 0.1683575E-01
 0.1683575E-01
 0.1683575E-01
 0.2303162E-01
 0.1907478E-01
 0.1587446E-01
 0.1328999E-01
 0.2173338E-01
 0.1875047E-01
 0.1625025E-01
 0.1414691E-01
 0.2016410E-01
 0.1823657E-01
 0.1653442E-01
 0.1502707E-01
 0.1849613E-01
 0.1758405E-01
 0.1672852E-01
 0.1592533E-01
 0.1683575E-01
 0.1683575E-01
 0.1683575E-01
 0.1683575E-01
 0.1683575E-01

Figure 5. Sample Problems Computer Output (7 of 8)

SAMPLE PROBLEM-POLYGON TO SKEWED DISK. K.A.TOUPS, 1/3/63

RUN NO. 2 DATA USED FOR THIS RUN- * DISK*POLYGN*
 TFDISK *
 * * *

THE CONFIGURATION FACTOR FROM SURFACE * DISKTFDISK* TO SURFACE *POLYGN * = 0.00475

THE FA PRODUCT = 0.14813E-01 SQ UNITS

THE MAPPING AREA = 0.1566912E 01 SQ UNITS

ONLY A PART OF SURFACE * DISKTFDISK*, COMPRISING AN AREA OF 0.1575357E 01 SQ UNITS
 SEES SURFACE *POLYGN *

THE AREA OF SURFACE * DISKTFDISK* = 0.3121445E 01 SQ UNITS.

ONLY A PART OF SURFACE *POLYGN *, COMPRISING AN AREA OF 0.1735515E 01 SQ UNITS
 SEES SURFACE * DISKTFDISK*

THE AREA OF SURFACE *POLYGN * = 0.2269708E 01 SQ UNITS.

Figure 5. Sample Problems Computer Output (8 of 8)

Second Paper -- "A General Computer Program for the Determination of Radiant-Interchange Geometric Configuration Factors," by K.A. Toups, North American.

QUESTION: (Mr. J.B. Werner, Lockheed) What configuration was used for the comparison with Hamilton & Morgan?

ANSWER : (Mr. Toups) Fortunately, we went into that rather rapidly. Four basic configurations were used with the various dimension ratios in each configuration. The first one was a point factor to a plate; the second was to a point factor to a plate with the plate defined at certain angles relative to the X Y plane where the infinitesimal area was in the X plane. Now the second two were area factors; namely, two parallel opposed plates of various dimensional ratios and then the second one, the second group, this was two plates where one edge touched. One edge of one plate touched the other plate and with various angles and dimensional ratios. Obviously we had to limit ourselves to some of the basic configurations.

QUESTION: (Dr. L.O. Rutz, Douglas Aircraft) Have you determined the view factors for the internal problem of radiant energy transferred through short and long right circular cylindrical paths? What values were obtained for length-diameter ratios of 1 to 100, and, 1 and a hundred?

ANSWER : (Mr. Toups) Well actually, if I understand this properly, I think these factors can be obtained by getting the factor to the disc represented by the exit of the tube, and this can be obtained directly from Hamilton and Morgan. If I am wrong and am misunderstanding, I would like to talk to this gentleman later.

QUESTION: (Mr. J. Gonzalez, Martin) What is the approximate loading time in manhours for the "average" experienced person on a disc-plate problem?

ANSWER : (Mr. Toups) Well, you can reach those real soon because of the fact the disc has to be simulated by multi-side regular paragon, .32 was selected. Now if I can be considered average I would say it takes about an hour to generate the necessary cards which are then punched and put in the machine. However, for the ordinary problem; namely, usually three or four side polygons, this can be done in a matter of five or ten minutes.

QUESTION: (Mr. Gonzales, Martin) What is the approximate running time for 24x24 increments and 60x60 increments?

ANSWER : (Mr. Toups) For the four side, let's say four sided polygon or square, this would take approximately two to three seconds of 7090 time to compute the facts. Now this is a function of how many are loaded together in the program except a large number of factors in one group--a large number of surface data, up to 30 surfaces as a matter of fact, for the basic program, and there is a lot of pre-processing required; what I mean to say is that the time required per factor goes down as you increase the number of factors you request. He then asks, what happens when you go to 60x60? Well, the time would increase as the square of the increase in the number of increments, so that if it took, let's say, three minutes for a 24x24, I presume it would take something like 20--I don't mean three minutes, I mean three seconds--it would take 27 seconds for 60x60. Again, this depends upon the complexity of the surface.

QUESTION: (Mr. Gonzales, Martin) Do you have stability convergence requirements in your program?

ANSWER : (Mr. Toups) No, I don't.

QUESTION: (Mr. K.R. Prentiss, General Precision Aerospace) How does this method compare with the geometric method presented at the joint AICHE-ASME Heat Transfer Conference in August by Sparrow of the University of Minnesota?

ANSWER : (Mr. Toups) Well I have read Dr. Sparrow's paper and I think it is a very very good fundamental exposition of the line integral technique in many factors. I arrived at very similar conclusions and found that computationally, in order to use the work directly, we would have to replace the infinitesimals with finite infinites and then the problem really got difficult because I had problems of internal control. So I developed a direct geometric method which you people saw today. Now it is possible to use the basic line integral equation, which is in the paper, incidently. This particular derivation is shown but it is not as suitable as the derivation you saw for computation factors in a practical sense. Nevertheless, it is a very good paper and very good information.

QUESTION: (Mr. C.V. Dohner, General Electric) What do you consider to be the necessary accuracy for determining FA factors?

ANSWER : (Mr. Toups) Well, since I am not a heat transfer specialist, that shouldn't surprise too many people, I can't answer that question directly but I was informed that more often than not, three places of accuracy is very sufficient. I presume in some cases where temperatures are very, very high, perhaps more accuracy might be required but I wouldn't know whether this is true or not.

QUESTION: (Mr. Dohner, General Electric) Can you program this accuracy at reasonable cost for complicated configurations, such as where there are interfering surfaces between the "source surface" and "sink surface"?

ANSWER : (Mr. Toups) The program in its present state will not compute the factor where there is an intervening surface. I am currently working on an extension of this basic program which will do this and it should be finished in a

couple of months. However, the accuracy will be the same; it will be three or more places, but it will take a lot more time to get these factors.

QUESTION: (Anonymous) How long does it take to run a complicated configuration with your program?

ANSWER : (Mr. Toups) Well, the longest one that I have run is 30 seconds and this was a disc to a disc and this is in the report which will be issued by ASD. It was a 60x60 increment integration and it took about 30 seconds to complete the whole manipulation--3671 factors, point factors, were computed and integrated. It was totally unnecessary but, of course, I just wanted to show that 24 would be sufficient. That is it.

HEAT TRANSFER IN THE PRESENCE OF AN ELECTRIC FIELD

by

Dr. H. Y Choi

Tufts University and Dynatech Corporation
Cambridge, Massachusetts

NOMENCLATURE

A	area
a	acceleration
C	constant
E	electrical field intensity
F	electrical body force
g	gravitational acceleration
g_e	electrical acceleration
h_{fg}	enthalpy difference between vapor and liquid
k	dielectric constant
p	pressure
q	heat transfer rate
r	radius
T	temperature
V	voltage
ϵ_0	permittivity of free space (vacuum)
ρ	density
σ	surface tension

HEAT TRANSFER IN THE PRESENCE OF AN ELECTRIC FIELD

DR. HARRY Y. CHOI

1. INTRODUCTION

The different regimes of boiling have been extensively studied in recent years. Particularly noteworthy are the following experimental works on boiling heat transfer embodying environments other than normal gravitational field. Usiskin and Siegel (1) studied the effects of accelerations less than that of one gravity by means of drop tests. Merte and Clark (2) studied the influence of system acceleration (1 to 21 g's) on free convection and nucleate boiling on a flat surface immersed in saturated water. They found the effect of acceleration on free convection to be large; at moderate nucleate boiling, however, the heat flux at a given temperature difference at high acceleration was actually smaller than that at one gravity. Costello and Adams (3) studied the peak heat fluxes in pool boiling on cylindrical heating elements rotated in a centrifuge assembly (1 to 100 g's), and concluded that at accelerations greater than 10 g's on their system

$$(q/A)_{\text{peak}} \sim (a/g)^{0.25}$$

as predicted in the literature, but at less than 10 g's,

$$(q/A)_{\text{peak}} \sim (a/g)^{0.15}$$

No existing correlations predict this latter behavior. It might be noted here that most of the existing boiling correlations in the literature contain a term for the gravitational acceleration. However, the variation with g's that these equations predict are tentative at best and experimental verification is practically non-existent.

A number of workers have reported their observations of unusual fluid phenomena in strong electric fields. Vettin (4), Avsec and Luntz (5), Sentfleban and Braun (6), and Kronig et al (7), studied single-phase fluid systems. Pohl (8) described many interesting experiments illustrating dielectrophoretic and electrophoretic effects. More recently, Bonjour et al (9) reported their studies on the effect of an electric field on boiling liquids. They used a parallel-wire electrode geometry and investigated several liquids of varying electrical properties. Young (10) studied experimentally the instability of an air-water interface in the presence of an electric field. A similar system was investigated theoretically by Melcher (11), who categorized instabilities in terms of several types of electrohydrodynamic surface waves.

This paper discusses visual as well as quantitative results obtained on the pool boiling of Freon-113 at one atmosphere in the presence of a DC field in the following geometries:

- a. A grounded platinum wire located along the axis of a cylindrical high-voltage electrode.
- b. A grounded flat surface facing down with a paraboloid electrode located below the boiling surface.

The results of this work suggest that many of the effects of the electro-fluid interactions in these systems can be interpreted in terms of the presence of body force fields of electrical origin in these systems.

2. EXPERIMENTAL APPARATUS

Figure 1 shows the overall test set-up, Figure 2 shows the test section for pool boiling on a wire, and Figure 3 shows the test section for pool boiling on a flat surface facing down.

In the first system, a platinum wire 0.0201 inch in diameter served as combination heating element and resistance thermometer. Potential taps of small-diameter platinum wire, 0.01 inch in diameter; were spot-welded to the

heating wire, isolating a central 2 inch portion of the latter as the test section. The high-voltage electrode consisted of a Pyrex tube, 4 inches long and 1.5 inches in diameter, coated on the inner surface with a conducting film. The heating wire was located along the axis of the tube and was at ground potential. The test unit was immersed in the test fluid contained in a rectangular glass jar, which in turn was immersed in a constant temperature water bath. The high-voltage source was provided by a Norelco X-ray unit. All the data reported in this work were taken with chemically-pure Freon-113. Some preliminary tests were run using pentane and benzene, but these were discontinued because of the fire hazard. The properties of Freon-113 are available up to 200 F, adequate for the analysis of data up to and including the peak heat flux. Complete boiling tests were run at several values of the electric field.

In the boiling apparatus shown in Figure 3, the heating surface was the horizontal bottom surface of a copper block, 2 inches in diameter, which formed the lower end of a cylindrical brass pressure chamber. Boiling was regulated by controlling the temperature difference rather than the heat flux, so as to obtain a continuous record of the boiling curve through the peak heat flux into the transition region. Distilled water was boiled by an electric heater inside the pressure chamber. The control of the pressure inside the chamber established the chamber temperature, which in turn fixed the temperature in the copper block. Three thermocouples mounted along the vertical axis of the copper block gave a measure of the heat flux through the block, and by extrapolation, gave the heating surface temperature. The pressure chamber was wrapped with an insulating jacket. The lower end of the jacket was carefully levelled with the test surface to form a non-boiling ring (3/4 inch thick) around the latter. The ring was provided to prevent easy escape of the vapor blanket from the boiling surface. The high-voltage electrode was made from a tea strainer and mounted at an adjustable distance below the boiling surface, as shown in Figure 3. The whole unit was then placed inside a glass jar containing the test fluid (Freon-113), and the assembly was immersed in a constant temperature bath.

3. ELECTRIC FORCES IN DIELECTRIC FLUIDS

The possible interactions between electric fields and fluids are many and complex. We shall examine here only those that are judged to be the most important in explaining some of the phenomena that have been observed in this work.

When a non-uniform electric field is applied to a dielectric fluid and if the free charges and property variation in the medium can be neglected, the fluid experiences a body force given by

$$F = \frac{\epsilon_0}{6} (k - 1) (k + 2) \nabla E^2 \quad (1)$$

where the Clausius-Mossotti law (valid for many non-polar fluids) has been assumed for the equation of state relating the permittivity and fluid density. The following comments might be made regarding this force:

- a. The existence of this force requires a non-uniform electric field and the direction of the force is independent of the field polarity.
- b. Since the force arises from the action of the electric field on individual dipoles, the force on a unit volume of liquid might be expected to be orders of magnitude greater than that on a unit volume of vapor at low pressures (relative to the critical pressure). The term $(k-1)$ in equation (1) reflects this relationship as k for the vapor is of order one. Typically for Freon-113, assuming values of 2.44 for the dielectric constant of the liquid and 1.002 for the vapor,

$$(k - 1)_l / (k - 1)_v = 0.7 \times 10^3$$

The force acting in a multi-fluid or multi-phase system cannot be obtained from equation (1) because the stresses on the interface between the fluids or phases must also be considered in the determination of the net force. If we take the simple case of a small, non-conducting sphere of dielectric constant k in a continuous non-conducting medium of dielectric constant k' , and further assume that the sphere does not distort the field, then the force per

unit volume acting on the sphere in a non-uniform field is given by

$$F = \frac{3k'}{2} \frac{k - k'}{k + 2k'} \nabla E^2 \quad (2)$$

The direction of this force is independent of the field polarity, but changes with the relative magnitude of k and k' . For $k < k'$, the sphere is driven into the region of the highest field strength, and for $k > k'$, it is driven into the region of the lowest field strength.

We shall refer to the forces given by equations (1) and (2) as the dielectrophoretic forces. Since these forces exhibit the characteristics of a gravitational force, we shall find it useful in later discussions to interpret their effects in terms of an equivalent gravitational acceleration defined by

$$g_e \equiv \frac{F}{\rho} \quad (3)$$

This concept could be particularly advantageous when applied to a liquid-vapor system, since the orders of magnitude difference in the body forces in the two phases is roughly balanced by similar orders of magnitude difference in the densities. This means that a single, approximate value of g_e might be used for the interpretation of the behavior of a boiling system, without concern as to the actual distribution of the two phases in space and in time.

In simple geometries, the $\text{grad } E^2$ term in the above equations can be readily expressed in terms of the applied voltage and the system geometry. In the wire-cylinder system, using values from a typical test with liquid Freon-113 in the free convection region ($V = 5.25$ kv, $r_i = 0.010$ inch, $r_o = 0.750$ inch, $k = 2.4$ and $\rho = 93.5$ lbf/cu. ft.), the body force at the wire surface is found from equation (1) to be 1.02×10^4 lbf/cu. ft., a surprisingly large value. Since in this geometry the force varies inversely as the cube of the radius, at a radial distance of $2 r_i$, the force decreases to slightly over 10%

of its value at the surface. In view of the large body forces at the heating surface, we might check whether or not the pressure there was measurably altered by the electric field. For an estimate of the pressure, we might assume hydrostatic equilibrium, $\text{grad } p = F$. Calculations then show that even at the highest applied voltage of 18.5 kv used in the Freon test series, the pressure correction at the heating surface was small enough to be negligible.

4. DISCUSSION OF BOILING ON WIRE

A. Free Convection

In all tests with saturated Freon-113, nucleation occurred at approximately 20°F superheat. Below this temperature, heat was transferred by free convection. The free convection data taken at the normal gravity and at three values of the electric field (48 kv/cm, 95 kv/cm and 168 kv/cm) are shown in Figure 4 to the left of the 20°F line. Figure 5 is a composite graph of the average lines drawn through the data points. The large effect of the electric field on the heat flux is clearly indicated. Typically at $T_w - T_s = 10\text{F}$, the heat flux at the maximum field intensity of 168 kv/cm (corresponding to an applied voltage of 18.5 kv) is almost three times that at the normal gravity.

It is well established both by theoretical solutions for simple systems and by dimensional analysis that the heat transfer coefficient in free convection, as expressed by the Nusselt number, can be correlated in terms of the two similarity parameters, the Grashof and the Prandtl numbers. Further, if the inertia terms in the momentum equation can be neglected, the Nusselt number can be expressed as a function of a single parameter, $(Gr \cdot Pr)$.

Experimental data in the literature for the free convection of air and water from cylinders, plates and spheres have been successfully correlated by equation of the form

$$\text{Nu} = C (Gr \cdot Pr)^n$$

where C and n are empirical constants.

In systems where the centrifugal forces are important, many workers have shown that both laminar and turbulent free convection data can be correlated by the above equation if g in the Grashof number is replaced by the centrifugal acceleration. If we accept the postulate that the electrical field in a fluid dielectric imposes a radial acceleration on the system, then we might expect the electrical free convection data to correlate with the normal gravity data if the gravity in the Grashof number is replaced by the electrical acceleration g_e defined by equation (3). From an operational standpoint, the simplest value of g_e to determine would be right at the wire surface, although argument might be offered for averaging the acceleration over a distance of the order of an average thermal boundary layer thickness. In all tests with the electrical field,

$$|g_e| \gg |g|$$

so that g was conveniently neglected. Otherwise, the two accelerations must be summed vectorially around the wire circumference. The heat transfer coefficient h in the Nusselt number was calculated from the total measured heat flux. No attempt was made to separate the total heat flux into a normal gravity component and an electrical component, since it was not obvious that the two components were simply additive. The final results of the calculations are shown in Figure 6. The normal gravity data are plotted against the conventional Grashof modulus and the electrical data are plotted on the same scale against the equivalent Grashof modulus. The solid line in the figure is the classical Lorentz equation recommended for non-conducting gases and liquids and for tubes as well as plates over the range $10^2 < Gr \cdot Pr < 10^8$

$$Nu = 0.56 (Gr \cdot Pr)^{1/4}$$

This line correlates within $\pm 30\%$ all data taken on electrical convection of Freon-113.

Since the heat transfer in free convection is independent of liquid superheat, the foregoing conclusions should hold also in the case of sub-cooled liquids.

Additional tests were run with approximately 30° F sub-cooling and the results are shown plotted in Figure 6 (some of these tests were run with smaller diameter wires). The confirmation might be considered satisfactory.

As a final point, it might be noted that the normal gravity data are generally higher than the Lorentz line. This might be expected in the low range of $Gr \cdot Pr$, where the 1/4 power slope tends to flatten out to 1/5 or even 1/6 power. It is interesting to note also in Figure 4 that the slopes of the free convection lines increase noticeably with increasing field. A plausible explanation might now be offered; with increasing field, the data move to higher $Gr \cdot Pr$ values with attendant increases in slope.

B. Nucleate Boiling

The high heat transfer rates in nucleate boiling result from agitation of the superheated liquid layer near the wall and heat is transferred primarily from the surface directly to the liquid. The important factors to be considered in nucleate boiling are therefore bubble nucleation and growth, bubble population and dynamics; all of which depend to a varying degree on the liquid superheat, which in turn is not an independent variable but is a sensitive function of the surface nucleating condition.

The nucleation process has been experimentally confirmed to be independent of the fluid dynamic process in the system. In view of the previous discussion regarding the effect of the electric field, it may not be too surprising then to find that the liquid superheat for nucleation is essentially independent of the electric field. One significance of this fact may be noted in Figure 5, where a horizontal line is drawn at $T_w - T_{sat} = 20$ F to mark the free convection zone. At relatively low heat fluxes, say at 6,000 BTU/hr-ft.², nucleate boiling under normal gravity condition can be suppressed by an electric field of the order of 75 kv/cm while the same rate of heat transfer is maintained.

The results of the nucleate boiling tests are summarized in Figure 4. The

distribution of the phases in nucleate boiling is extremely complex. However, the concept of an electrical acceleration can be simply extended to a two-phase system in nucleate boiling, and we need only to evaluate F (or equivalently g_e) in the liquid phase to find the force acting on any bubble.

At heat fluxes up to about 1.5×10^4 BTU/hr-ft.², the effect of the electrical field is still significant. Within this range, the electrical field reduces the temperature difference ($T_w - T_{sat}$) required for a given heat flux. At higher heat fluxes, a reversal of the effect of the electrical field is noted, with the curves corresponding to the higher electrical fields in Figure 4 crossing over to the right of the normal gravity boiling curve. However, the net effect on $T_w - T_{sat}$ is small, as perhaps can be seen more clearly in Figure 5.

In standard gravitational pool boiling, the contribution of non-boiling convection to the total heat flux has been found to be small; however, with the application of an electric field or an electrical acceleration, the contribution of non-boiling convection can be quite appreciable as indicated in the test results. Above about 2×10^4 BTU/hr-ft.² to the point of departure from nucleate boiling, the effect of bubble agitation may be dominant. In this range, the temperature difference ($T_w - T_{sat}$) at a given flux first increases and then decreases slightly with increasing electric field. Visual observation reveals that the bubble sizes at departure become significantly smaller with increasing E , but the bubble frequency is increased. The net effect could be a reduction in agitation effectiveness with increasing E , requiring a higher wall temperature to remove the same flux.

It is interesting to compare these curves with those obtained by Merte and Clark (2) on a heated surface rotated in a centrifuge at accelerations ranging from 1 to 21 g 's. The general trend of the curves is strikingly similar. In particular, the following points in their results may be noted:

- a. The effects in the free convection region are large.

- b. The temperature at which nucleation first occurs does not vary measurably with increasing acceleration.
- c. At moderate heat fluxes, the curves for higher acceleration cross the normal gravity curve.

Figure 9 shows the nucleate boiling sequence at $q/A \approx 17,300 \text{ BTU/hr-ft.}^2$. The "bubble jets" in the electrical nucleate boiling leave the surface in random radial directions, and at $E = 168 \text{ kv/cm}$, the bubbles practically fill the whole tube. The surprising aspect of this sequence is that, despite the large differences in the appearance of the nucleate boiling processes, the surface temperatures differ by no more than 4 or 5 degrees F.

It was not possible to obtain any accurate measurements of the bubble diameters or frequencies from the photographs taken. A rough estimate, however, of the bubble diameters at the surface in normal gravitational boiling, and of the vapor jet diameters in electrical boiling, indicated that the diameter decreased approximately linearly with the electric field intensity at the wire surface or with $(g_e)^{1/2}$. In view of the large uncertainties in this estimate, this result may be entirely fortuitous. The smaller bubbles would be less effective as agitators. Therefore, at any given heat flux, a decrease in agitation due to the smaller bubble sizes must be compensated for in other ways. The frequency of bubble formation may increase (this was observed), the number of active sites may increase (this would probably require a higher surface temperature), or there may be increased contribution by free convection because of the increased area available and because of the electrical acceleration. The problem certainly does not allow a simple conclusion.

C. Peak Heat Flux

Near the peak heat flux in ordinary gravity boiling, the bubble population and frequency are so great that the bubbles coalesce on the surface and form vapor patches. Also, at a given site, the bubbles are emitted at such a high frequency that they coalesce with their predecessor and form a continuous

vapor column. This suggests that the heat flux cannot increase indefinitely. Each new vapor patch or column occupies space formerly occupied by the liquid, and the continuous liquid phase and the discontinuous vapor phase compete for the free volume. Soon, a state of hydrodynamic crisis is attained, corresponding to a critical velocity of the vapor phase, and the heat flux reaches a maximum. Many workers have suggested the peak heat flux as a purely hydrodynamic phenomenon. Zuber (13) derived the following theoretical expression for the peak heat flux by considering the combined effects of the Taylor and the Helmholtz instabilities:

$$\frac{(q/A)_{\max}}{\rho_v h_{fg}} = C \left[\frac{\sigma (\rho_l - \rho_v) g}{\rho_v^2} \right]^{1/4}$$

The constant C in this equation has a value between 0.13 and 0.18. The above equation shows good agreement with available experimental data on flat surfaces at normal gravity. Costello and Adams (3) conducted burnout tests on a cylindrical heater in a centrifuge and concluded that at accelerations greater than 10 g in their system

$$(q/A)_{\max} \sim (a/g)^{0.25}$$

where a is the vector resultant of centripetal and local gravitational accelerations at the heater. However at less than 10 g, they found

$$(q/A)_{\max} \sim (a/g)^{0.15}$$

and the data taken by Usiskin and Siegel (1) in drop tests tended to confirm this.

Figure 7 shows the increase in $(q/A)_{\max}$ with E is approximately linear. At the maximum applied field intensity of 168 kv/cm, the peak heat flux was not attained, but the highest measured point on the nucleate boiling curve is indicated. Each point on the graph represents an average of several measurements.

As a first approximation, we might attempt to explain the increase in $(q/A)_{\max}$ with E in terms of the electrical acceleration g_e at the heating surface. Figure 8 shows our data plotted against the Kutateladse - Zuber moduli, with g replaced by g_e where appropriate. The theoretical line is also shown. Our wire data at $1g$ shows surprisingly close agreement with the theoretical line for flat surfaces. On the other hand, the electrical data deviates markedly from the $1/4$ power slope, although one might argue that at high fields, the slope is indeed $1/4$. In fact, if the plot has any merit, there appears to be a transition point somewhere between $E = 48$ kv/cm and $E = 96$ kv/cm. A number of possible hypothesis were considered, but found to be inadequate to explain the type of transition indicated. Actually, this transition in Figure 8 may be more apparent than real.

The applicability of Zuber's results to our system in the manner indicated may be questioned. Young (10) investigated experimentally and Melcher (11) theoretically the stability of a vapor-liquid interface in the presence of a uniform electric field (the body forces discussed in Section 3 are absent here) normal to the interface, and found that there was a threshold voltage above which an interfacial instability developed. Melcher suggests that the interfacial instability is induced by electrohydrodynamic (EHD) surface waves which are present in addition to the gravity and the capillary waves. He identified several types of EHD waves depending upon the manner in which the interface is stressed by the electric field and the presence or absence of free charges at the interface. These interfacial dynamics would therefore have to be considered in any comprehensive analysis of instability in boiling in the presence of an electric field.

The large destabilizing effect of the electric field is evident in the photo sequence in Figure 10 and also in Figure 5. Both figures show sudden transition from stable film boiling under normal gravity to nucleate boiling in the presence of an electric field, with the heat flux essentially unchanged but with a large decrease in the surface temperature.

D. Film Boiling

The results on film boiling are shown in Figure 4. At these high temperatures, Freon-113 apparently carbonizes as is evident from a slight discoloration of the fluid and a black coating left on the wire surface. At stable film boiling, the surface condition of the heater would not be expected to affect the heat transfer data, but some instantaneous liquid-solid contact does occur and could explain some of the scatter of data points. The lower ΔT limit for film boiling apparently increases with increasing field intensity.

The vapor flow pattern in film boiling at 1 g is characterized by a regular spacing of large bubbles departing at regular intervals, as shown in Figure 11. The vapor flow pattern in the presence of an electric field was not so obvious. Visual observation showed bubble departure from the liquid-vapor interface primarily in the upward direction, but no regularity was discernable. The lower photograph of Figure 11 clearly shows a "vapor sheet"

It might be valid to extend the existing theories on film boiling at 1 g to that in an electric field if the following assumptions can be made:

- a. The electric field primarily acts as an acceleration field.
- b. At any given instant and location on the interface, one bubble departs in any radial direction. This assumption is at best highly debatable in view of the total lack of any visual evidence of this.
- c. A reasonably stable vapor film exists over most of the surface and heat is transferred primarily by conduction through the vapor film.

The Bromley equation fitted well the normal gravity data in Figure 4 if a constant of 0.95 were used in his equation. The foregoing assumptions would then allow a direct extension of the Bromley equation to the electrical data. This was tried with some degree of success, but the results are not reported here in view of the large uncertainties in the physical properties of Freon-113 at these high temperatures.

5. DISCUSSION OF BOILING ON FLAT SURFACE

Tests on this system are still in progress and only a brief discussion of some of the observations to date will be presented. Figure 12 compares the boiling pattern with and without the electric field.

In normal gravity, the pattern was as follows: At low heat fluxes, small bubbles nucleated at random sites on the heating surface and moved around the surface, coalescing and growing in size. As the heat flux was increased, bubbles forming at hundreds of sites coalesced rapidly to form a vapor-film near the center. The film expanded radically in size until it "fragmented" at the center and an irregularly-shaped doughnut travelled radially towards the edge sweeping the surface clean. Meanwhile, another family of bubbles formed, and the cycle was repeated. The frequency of the cycle increased with increasing heat flux. Beyond the peak heat flux, the surface was partially or totally covered with vapor at all times and the escape of vapor at the outer edge took place erratically.

The boiling pattern changed completely when a non-uniform electric field was present in the system (tea strainer electrode). Small bubbles travelled outward towards the edge in a regular radial pattern, with no coalescence observed. As the field was increased, the bubbles became smaller and moved radially outward on the surface at much higher velocities, as shown in Figure 12. This "vapor pumping" action of the electric field from the region of high to the region of low field intensity would have been anticipated on the basis of the dielectrophoretic force, given by equation (2), present in the system. When a uniform field was applied (tea strainer replaced by a plate electrode), the bubbles remained near the center of the heating surface; there was some interfacial perturbation, but the radial motion previously observed in a non-uniform field was completely absent.

Figure 13 shows one typical set of experimental data. The general characteristics of the boiling curve in normal gravity were similar to those observed in boiling on wires or on flat surfaces facing up. The magnitude of the peak heat

flux, however, was less than half of that attained in the wire boiling of Freon-113. The boiling curve obtained with non-uniform electric field shifted appreciably and the peak heat flux, if such a point existed, was not attained. In the nucleate boiling region, there was a marked increase in the heat flux at a given temperature difference.

REFERENCES

1. Usiskin, C.M. and R. Siegel, Trans ASME, Series C, 83, 243, 1961.
2. Merte H. and J. A. Clark, Trans ASME, Series C, 83, 233, 1961.
3. Costello C. P. and J. M. Adams, Int. Dev. in Heat Trans., Part II, 1961, Boulder, Colo., also Dept. of Mech. Eng. Report, University of Washington, 1962.
4. Vettin F., Meteor. Z. 3, 38, 1886.
5. Avsec D. et al, Compt. Rend. 213, 1140, 1936; 204, 470, 1937; 204, 757, 1937.
6. Senftleben H. and W. Braun, Z. Phys. 102, 480, 1936.
7. Kronig R. et al, App. Sci. Res. A1, 35, 1949; A 2, 235, 1950.
8. Pohl H. A., J. App. Phy. 29, 8, 1182, 1958.
9. Bonjour E. et al, Chem. E. Prog. 58, 7, 63, 1962.
10. Young J. A., Thesis, Mech. Eng. Dept. Tufts Univer., June, 1960.
11. Melcher J. R., PhD Thesis, Electrical Engineering Dept., M.I.T., Jan. 1962.
12. Rohsenow W.M. Trans. ASME, 969, August 1952.
13. Zuber N. et al, Int. Dev. in Ht. Trans, Part II, 1961, Boulder, Colo.
14. Choi H. Y. Tufts University Mechanical Engineering Report No. 60-2, 1960; PhD Thesis, Mechanical Engineering Dept., M.I.T. Jan. 1962.
15. Fletcher W.D., Thesis, Mech. Eng. Dept., Tufts Univ., June 1962.
16. Stratten J.A., Electromagnetic Theory, McGraw Hill, 1941.
17. Rohsenow W.M. and H. Y. Choi, Heat Mass and Momentum Transfer, Chap. 9, Prentice-Hall, 1961.

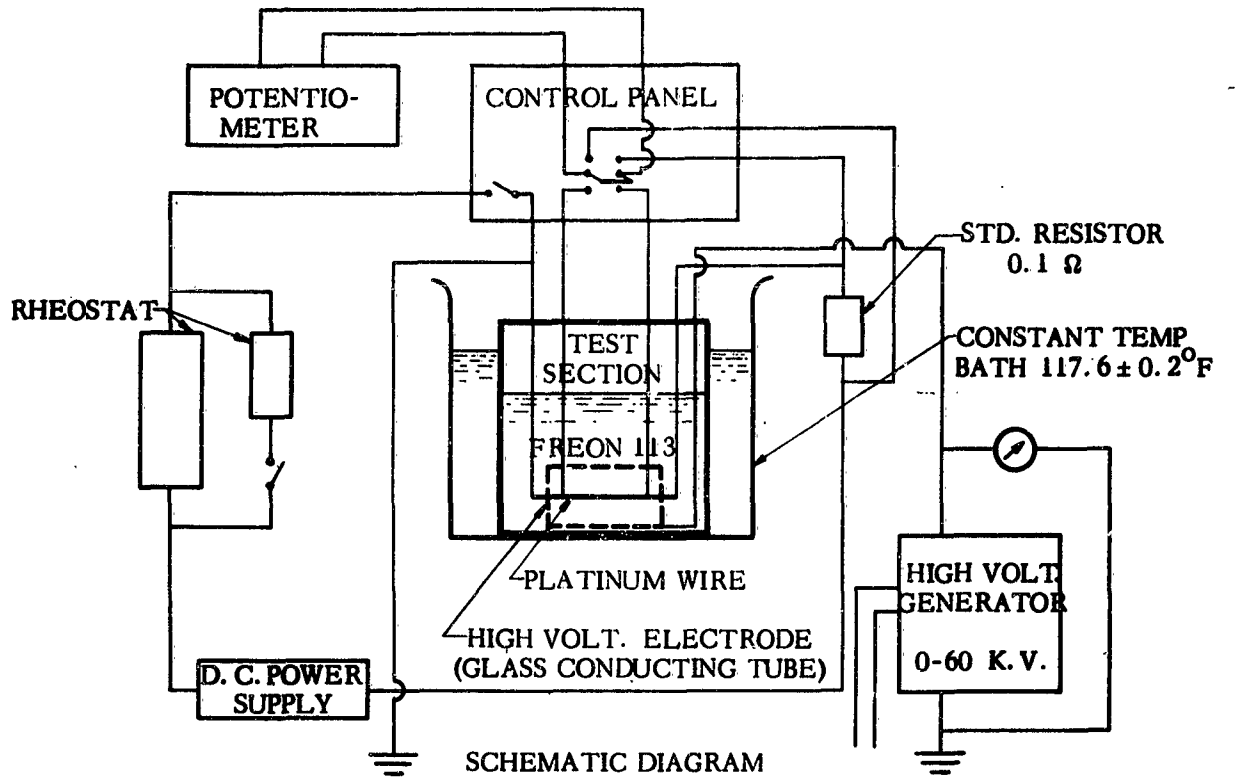


Figure 1. Electrohydrodynamic Boiling Apparatus

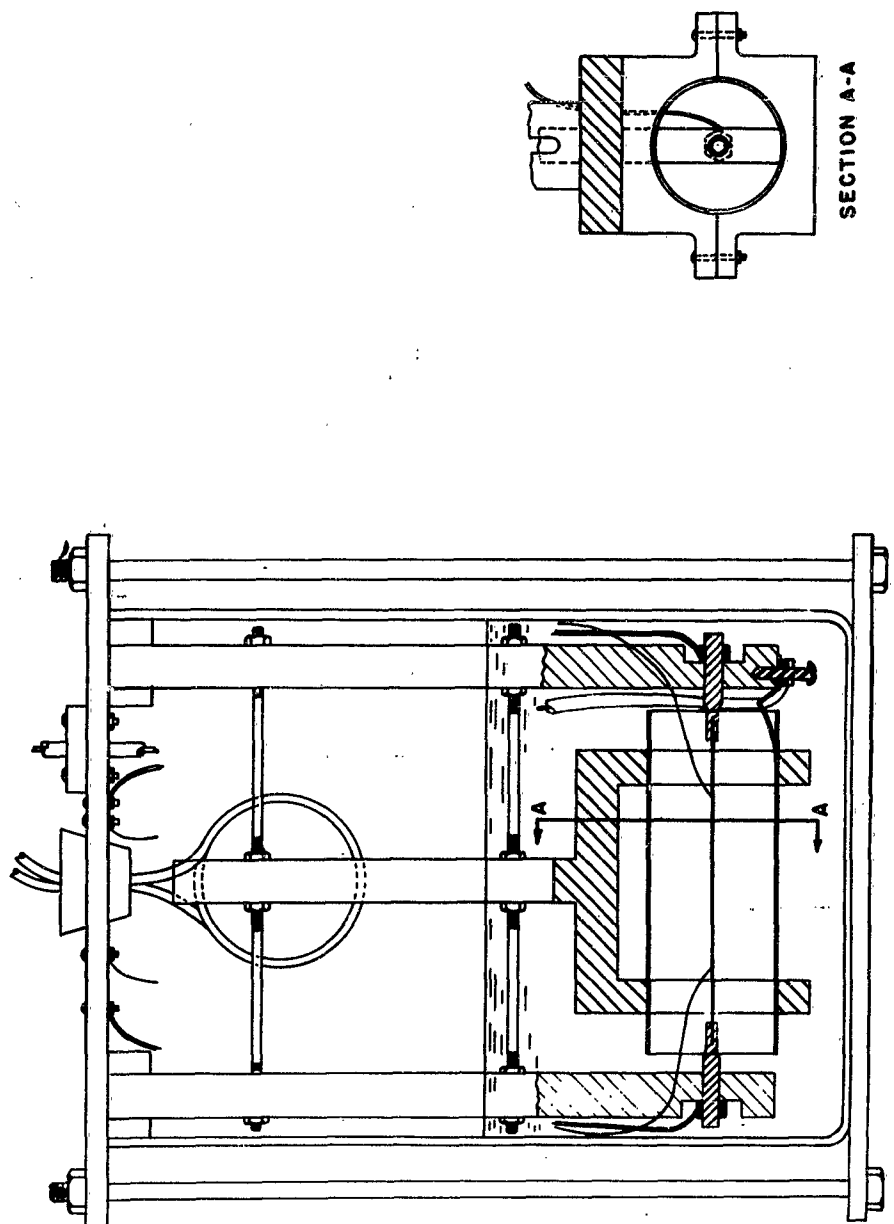


Figure 2. Test Section Assembly - Wire-Cylinder Unit

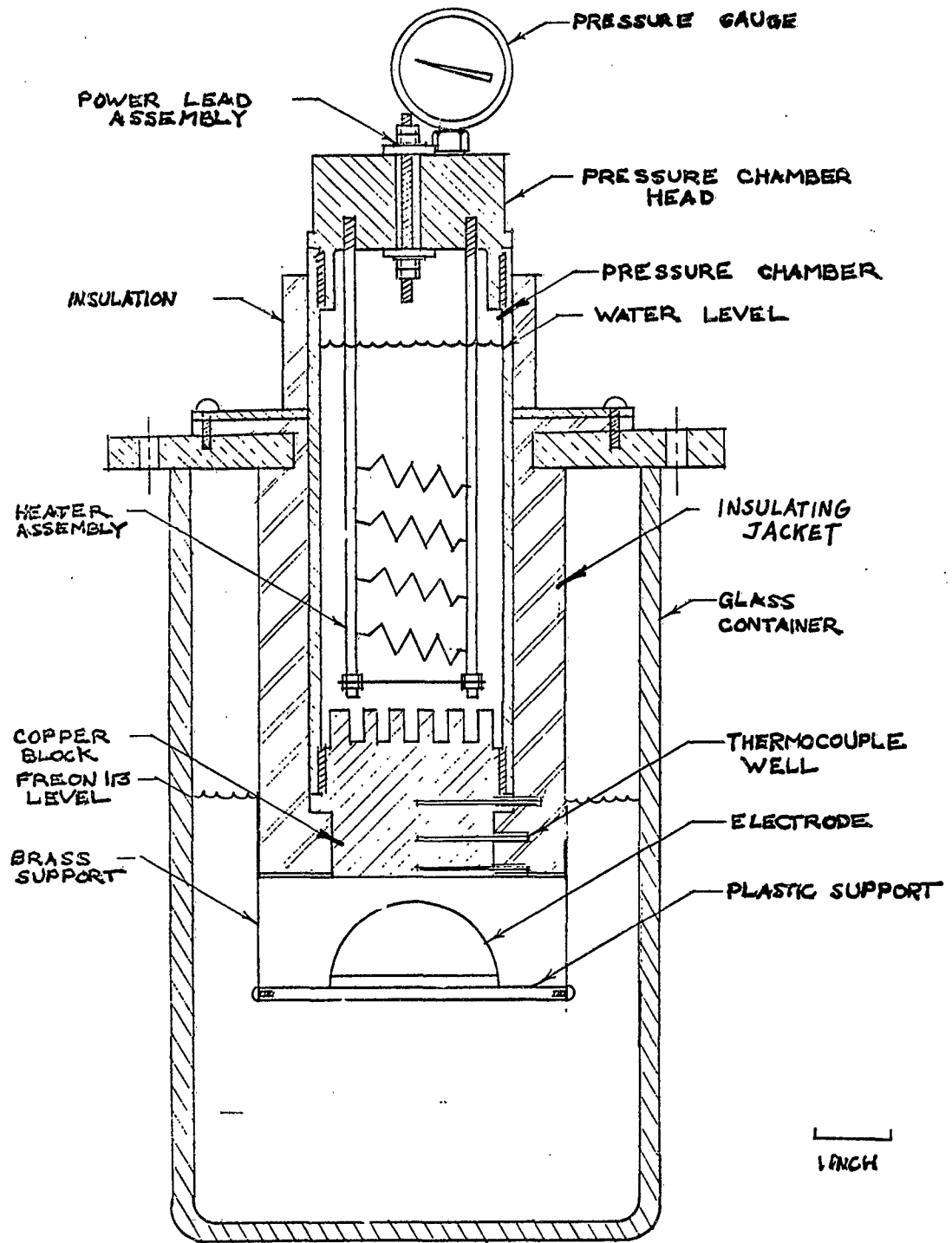
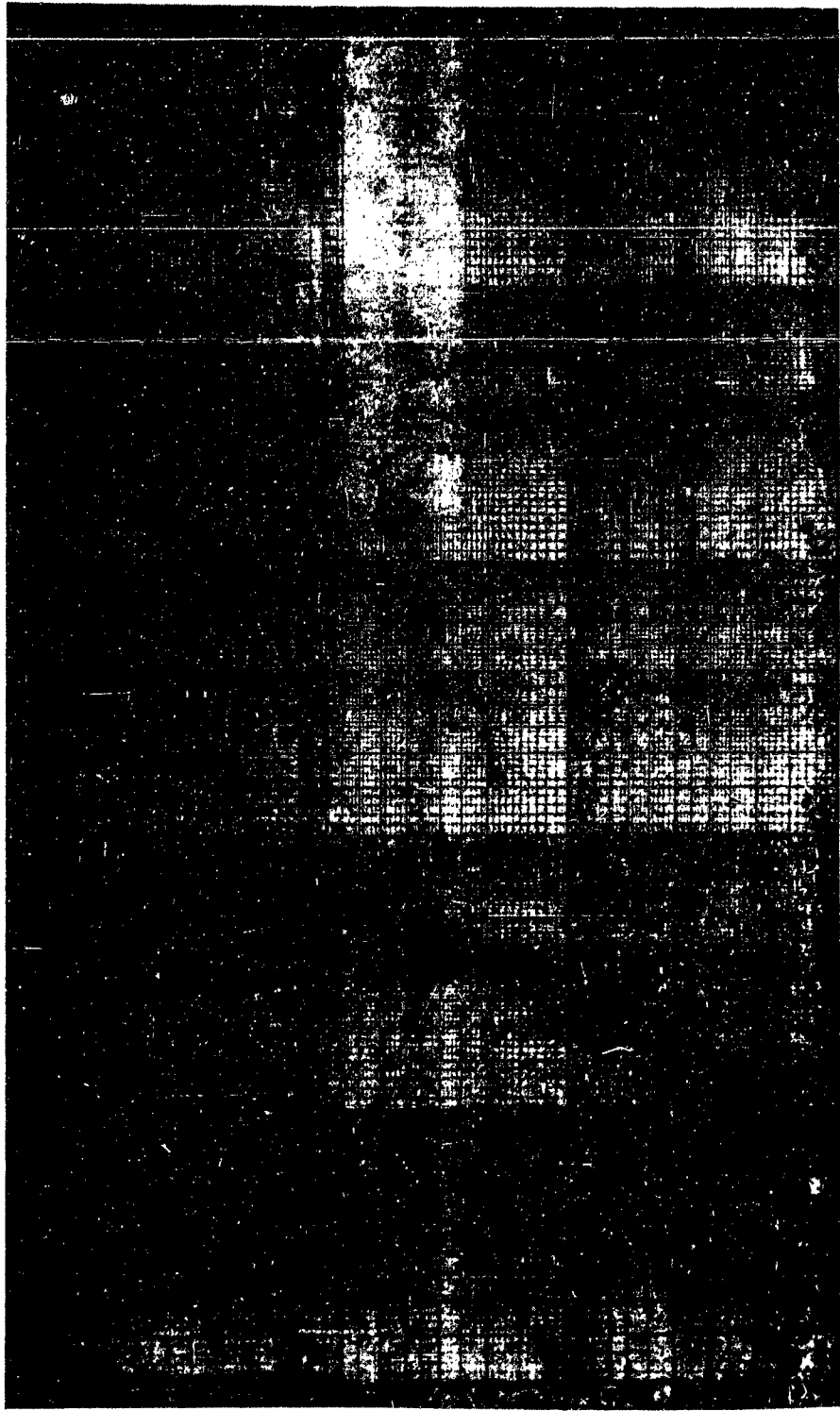


Figure 3. Flat Plate Boiling Unit



q/A Btu/hr ft²

462

$T_w - T_{sat}$ °F

Figure 4. Influence of Electric Field on Convection and Pool Boiling

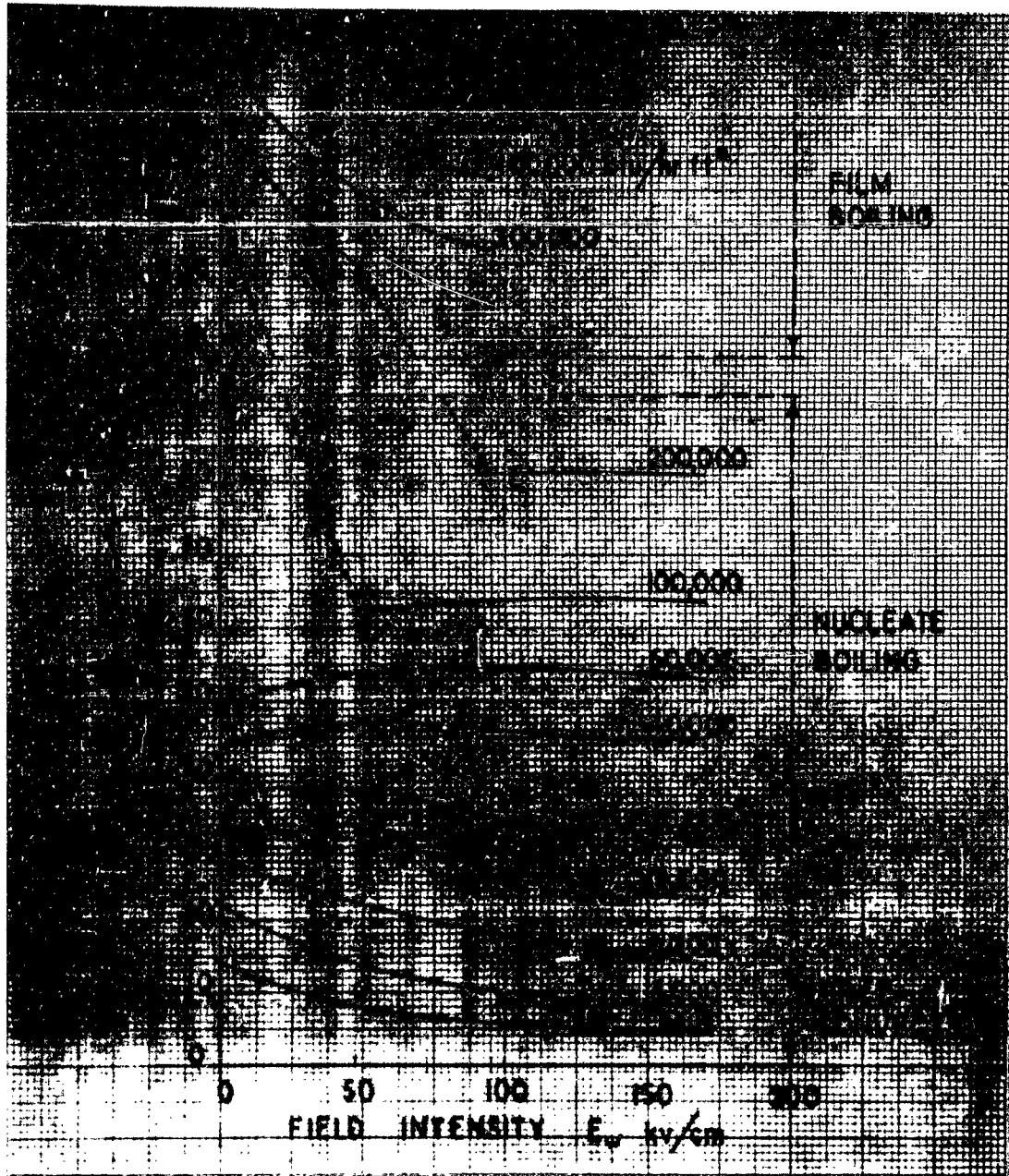
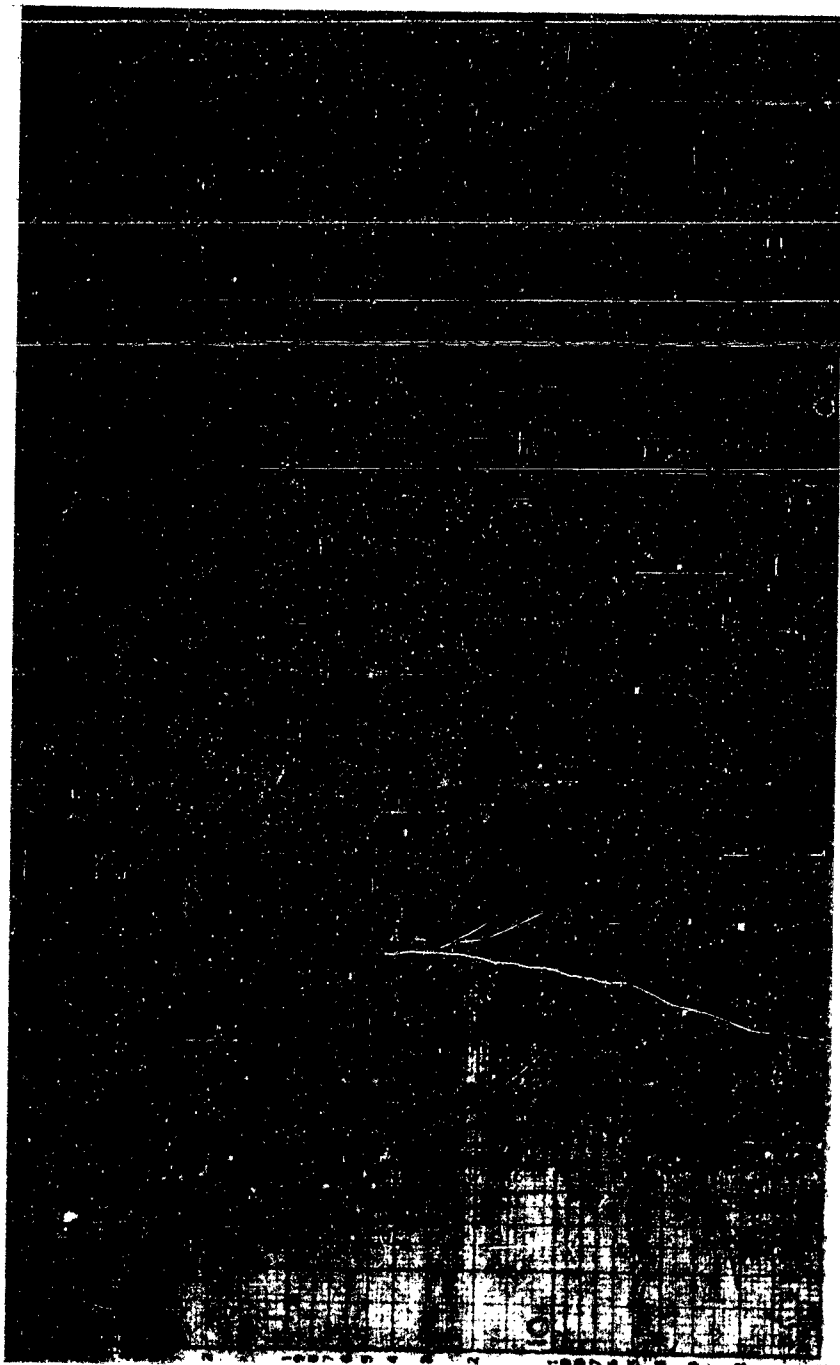


Figure 5. Influence of Electric Field on $T_w - T_{sat}$ with Pool Boiling of Saturated Freon-113.



$(G_r \cdot Pr)$ or $(G_{re} \cdot Pr)$

Figure 6. Correlation of Free Convection Data

Nu_{total}

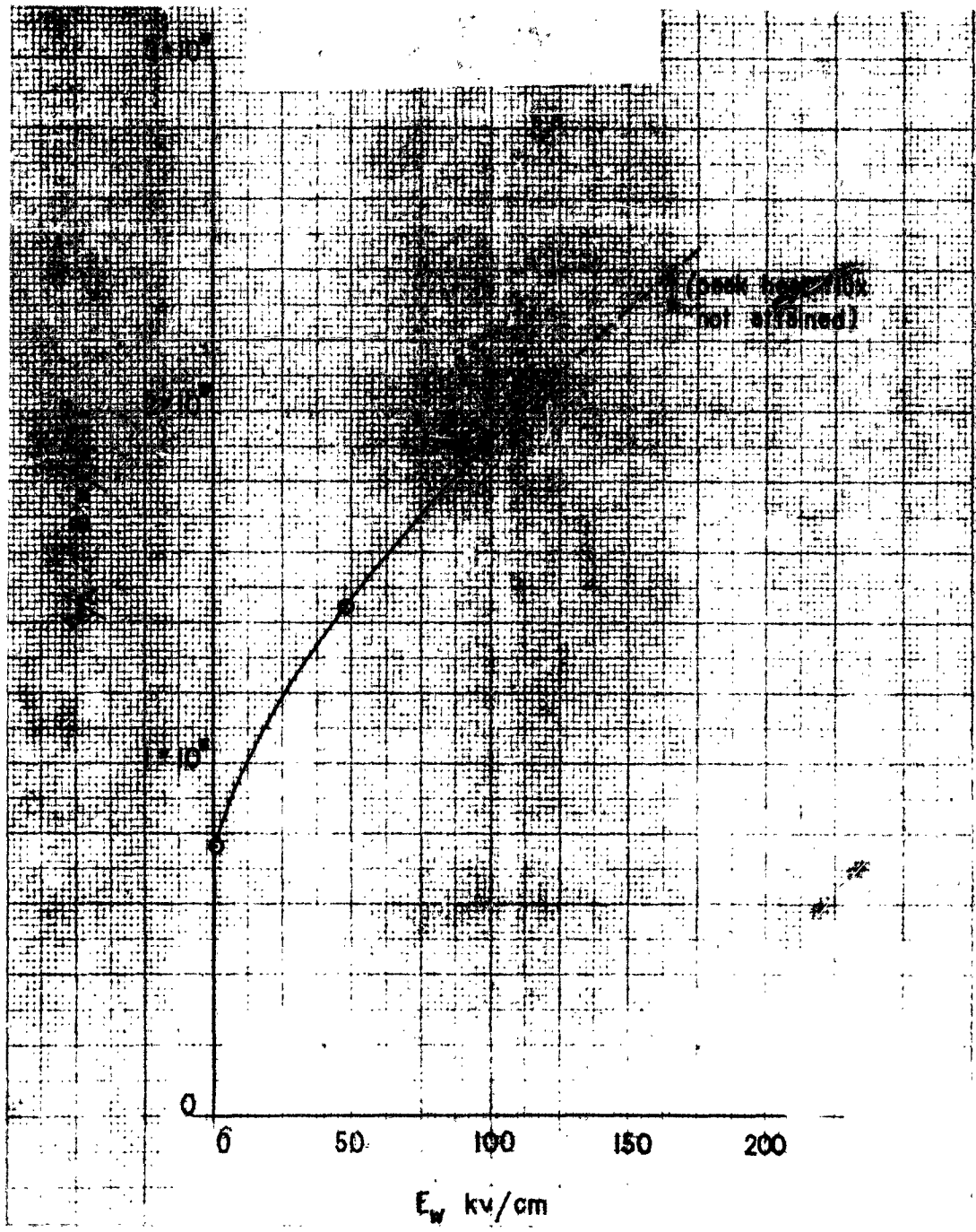
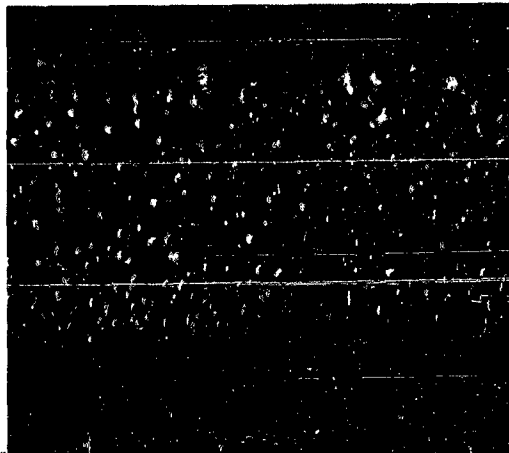


Figure 7. Variation of Peak Heat Flux with Electric Field Intensity at Surface



$$\left[\frac{\sigma g (\rho_L - \rho_v)}{(\rho_v)^2} \right]^{1/4} \left[\frac{\rho_L + \rho_v}{\rho_L} \right]^{1/2} \text{ ft/hr}$$

Figure 8. Comparison of Peak Heat Flux Data with Kutateladse-Zuber Theory



GRAVITY FIELD

$$\Delta T = 33.4 F$$

$$q/A = 17,301 \text{ B/hr ft}^2$$



ELECTRIC FIELD
95 KV/CM

$$\Delta T = 30.6 F$$

$$q/A = 17,311 \text{ B/hr ft}^2$$



ELECTRIC FIELD
168 KV/CM

$$\Delta T = 26.5 F$$

$$q/A = 17,248 \text{ B/hr ft}^2$$

Figure 9. Photo Sequence at Moderate Nucleate Boiling

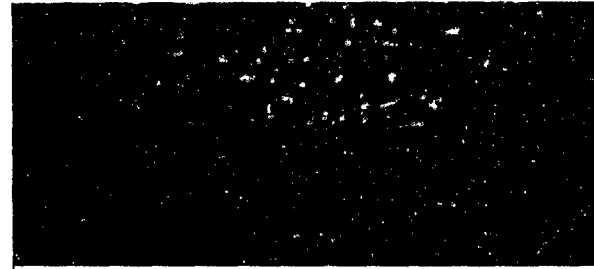
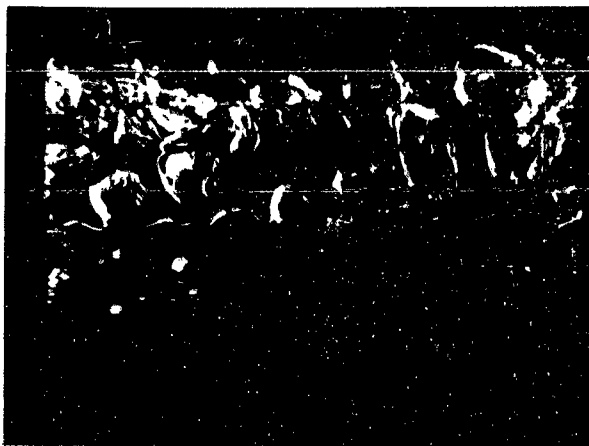


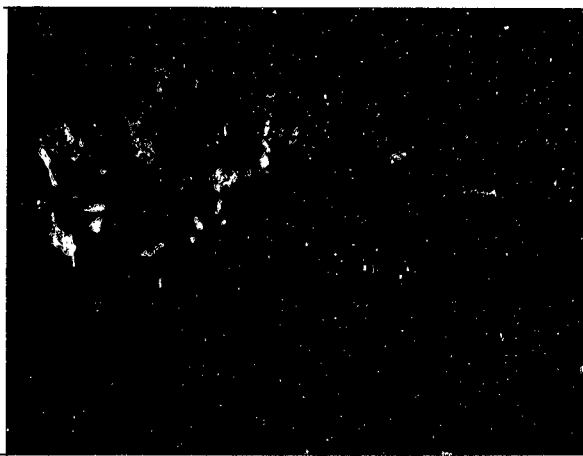
Figure 10. Photo Sequence Showing Transition from Film to Nucleate Boiling when Electric Field is Applied



FILM BOILING IN GRAVITY FIELD

$$\Delta T = 1710 F$$

$$q/A = 1.33 \times 10^5 \text{ B/hrft}^2$$

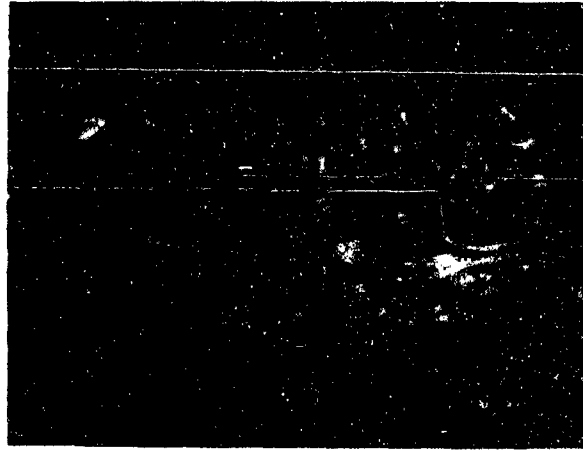


FILM BOILING WITH ELECTRIC FIELD, 95 kV/cm

$$\Delta T = 1244 F$$

$$q/A = 3.35 \times 10^5 \text{ B/hrft}^2$$

Figure 11. Vapor Flow Pattern in Film Boiling



LOW NUCLEATE BOILING IN GRAVITY FIELD



LOW NUCLEATE BOILING WITH ELECTRIC FIELD

Figure 12. Boiling on Flat Surface Facing Down

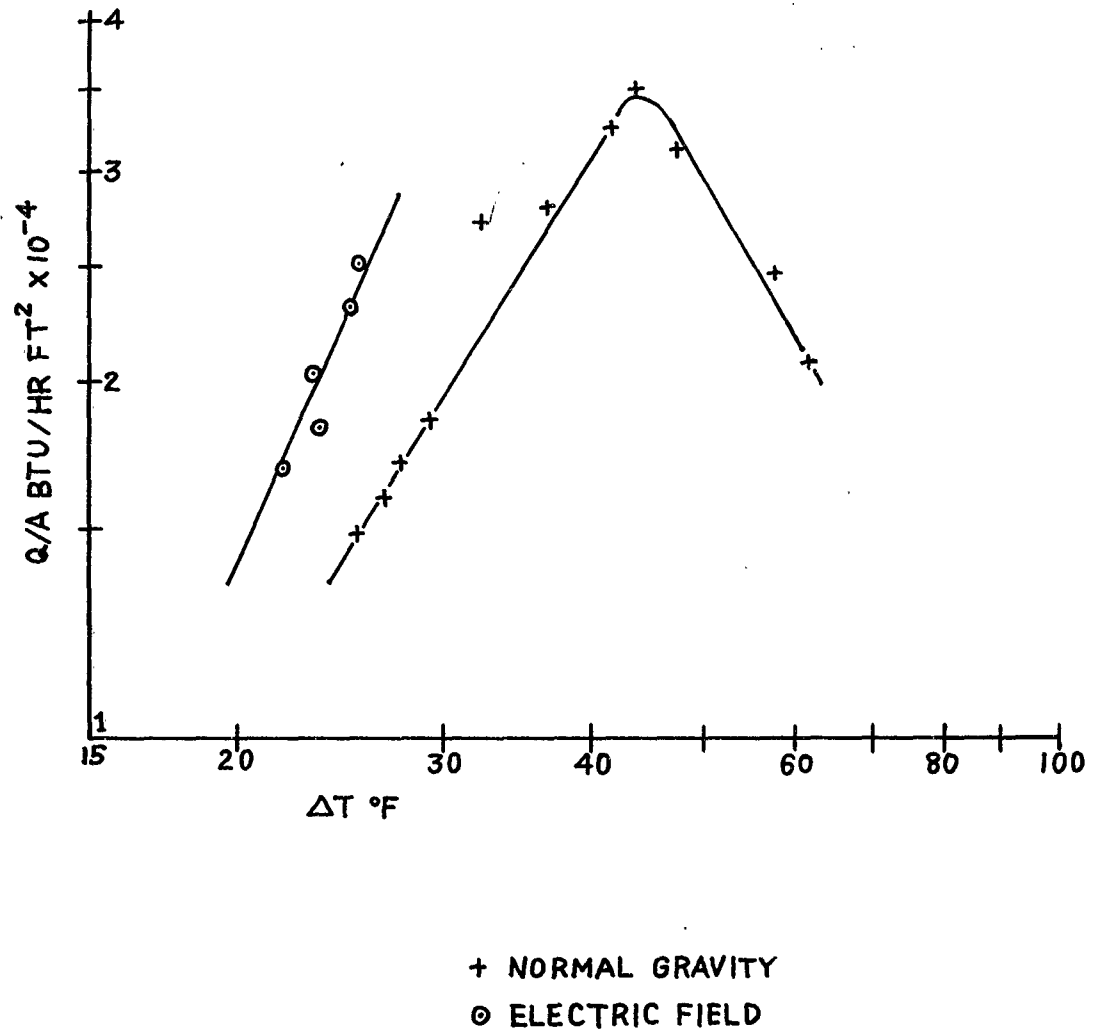


Figure 13. Pool Boiling of Saturated Freon-113 on Flat Surface Facing Down

Third Paper -- "Heat Transfer in the Presence of an Electric Field," by Dr. Harry Y. Choi, Tufts University & Dynatech Corp.

QUESTION: (Mr. Thomas Blatt, Northern Research & Engineering Corp.) The results of Merle & Clark, Costello & Adams and Gambrill suggest the use of one quarter power overestimates the boiling heat flux at high accelerations, particularly at high heat fluxes. Would you state your opinion?

ANSWER : (Dr. Choi) Merle & Clark did not get up heat. Their work was limited to film and nuclear boiling. The general conclusion very closely parallels the characteristics you saw on the boiling curve that was shown here. Costello & Adams obtained or concentrated their studies to peak heat flux and their suggestion is that at high acceleration, above about 10 G, it did follow power evaluation, but at low acceleration the slope flattened out. Gambrill's study was a vortex flow type device but it was difficult to interpret his results in terms of the acceleration in the system. I believe it is difficult to identify the effects that would answer your question there.

QUESTION: (Mr. Blatt, Northern Research) Did you conduct forced convection experiments?

ANSWER : (Dr. Choi) No, we didn't. We did pool boiling and I think this perhaps is about the stage where perhaps we could extend forced convection work.

QUESTION: (Mr. Blatt, Northern Research) Did you conduct tests with different fluids, and if you did, did you find that the relative improved effect of the electrostatic field is greater for fluids having lower boiling heat transfer coefficients under normal conditions?

ANSWER : (Dr. Choi) Initially we conducted several tests

with several different fluids. All the work reported today was performed with Freon 113, which was representative of a large class of dielectric fluids in the hydrocarbon family. I believe there is a talk this afternoon on different fluids and then there is a report from the Atomic Energy establishment in France which discusses the fluids. So I will direct your answer to these references.

QUESTION: (Mr. Rutz, Douglas) To what degree would zero gravity field alter the heat flux with the free convection and nucleate boiling range? Please abstract your contrasting mechanisms of heat transfer?

ANSWER : (Dr. Choi) A suggestion on basing matters of heat transfer would be conduction, except when you get to high film boiling where at high temperature we have radiation, but all the way up to that, the basic mechanism would be conduction with superimposed fluid motion effects of convection. Now these convection effects in boiling systems can be single or two-phase. In zero gravity we would not have any effect, any bouyant type effect; namely, convection in the normal sense, the normal definition of the word; however, the electric field is independent of gravity and, therefore, the electric force is independent of gravity.

**THERMAL ANALYSIS OF STRUCTURES INCLUDING
RADIATION IN AN ENCLOSURE**

by

R. A. Knezek

G. J. French

**Chance Vought Corporation
Dallas, Texas**

LIST OF SYMBOLS

- A - area of a surface
- B - radiosity, all radiant energy per unit area leaving a surface
- H - all radiant energy incident on a surface
- q - radiant heat transfer per unit area
- Q - total radiant heat transfer
- R_r - radiation resistor in thermal analyzer network
- T - absolute temperature
- F_{i-j} - geometrical radiation form factor between surfaces i and j
- \mathcal{G}_{i-k} - combined geometrical and emissivity factor between surfaces i and k
- α - absorptivity of a surface
- β - dimensionless radiosity, $B/\sigma T^4$
- ϵ - emissivity of surface
- ρ - reflectivity of a surface
- σ - Stefan-Boltzmann constant

ASD-TDR-63-260

**THERMAL ANALYSIS OF STRUCTURES INCLUDING
RADIATION IN AN ENCLOSURE**

BY

R. A. Knezek and G. J. French

INTRODUCTION

Thermal analysis of the structure and components in spacecraft compartments is difficult because of the complex geometry and the transient nature of the environment encountered. In this type of analysis, thermal radiation is one of the major modes of heat transfer that must be accounted for. The external temperature of orbital spacecraft, for example, depends on radiation heat exchange with the environment. In the absence of an atmosphere, radiant heat transfer also strongly influences the temperature distributions within the spacecraft. Although boost and reentry usually involve short periods of time, the vehicle surface temperatures are high enough that the radiant heat transfer is significant. Figure 1 depicts some of the areas of a space vehicle which are significantly influenced by thermal radiation during various portions of the mission.

The three basic modes of heat transfer, conduction, convection, and radiation between two surfaces, can be handled readily by digital routines for thermal analysis. Where the structure and components form a compartment or enclosure, however, the analysis becomes much more complicated. The radiant energy reflected and re-reflected from the various surfaces must be accounted for as well as the radiant energy transferred directly from one surface to another. Methods of analyzing radiant heat transfer in an enclosure and a simple means of incorporating the analysis into existing digital thermal analyzer programs are needed. This paper presents such a method.

RADIANT HEAT TRANSFER IN AN ENCLOSURE

Several standard methods have been developed for analysis of radiant heat exchange in enclosed compartments (enclosures). These methods have been attributed to Eckert, Hottel, and Gebhart (Refs. 1, 2, and 3, respectively.) These methods differ principally in the method of accounting for the reflected energies. They employ the same assumptions and yield the same numerical results. The basic assumptions that are made are:

1. Each surface is isothermal. That is, it is at a uniform temperature at any instant of time.
2. The surfaces are gray. This means the surfaces are not selective in their ability to absorb or emit energy at various wavelengths.
3. The reflected energy is uniform at all angles (diffuse) regardless of the angle of incidence of the energy.
4. The energy is emitted equally well at all angles from the surface (again, the surface is diffuse).
5. The reflected energy is uniformly distributed over a surface.

Although these assumptions limit the general applicability of the analyses, specular reflecting and non-gray surfaces may be included as special cases (Refs. 4 and 5).

Eckert's analysis utilizes the concept of radiosity. With this concept the total energy leaving a surface is termed the radiosity without distinguishing between energy emitted by the surface and reflected energy. Similarly all of the energy incident on the surface from all sources is considered as a whole and includes all emitted and reflected energy. Since the energy incident on a surface can be expressed in terms of the energy leaving each of the other surfaces, a set of linear equations can be developed from which the radiosity at each surface can be found. Once the radiosity is found it is a simple matter to calculate the net heat transferred by the surface. Hottel's approach was to determine the net rate of heat transfer between a typical pair of surfaces in the enclosure. This considered only the net energy transferred from surface 1 to 2 which is due to the energy emitted by surfaces 1 and 2. The rest of the enclosure merely aided in reflecting these two energies. Once the net rate of heat transfer is found between all pairs of surfaces, the net energy transferred from a single surface is found by summing the interchange between that surface and all others.

The starting point of Gebhart's method is a definition of the net rate of heat transfer between a single surface and all other surfaces in the enclosure. Only Eckert's radiosity method will be discussed in detail since Hottel's method and Gebhart's method yield similar results. The latter methods are discussed in more detail in Ref. 6.

The concept of radiosity considers the total energy incident on and leaving each surface without distinguishing between emitted and reflected energy. Consider the enclosure of n surfaces represented in Figure 2. The total energy per unit area leaving a surface, both emitted by and reflected from the surface, is termed the radiosity, B . (A list of symbols is included on page 13.) All energy incident on the surface, both emitted by and reflected from the other surfaces, is denoted by the symbol, H . The radiosity may be expressed in terms of the incident energy and the temperature of the surface as follows:

$$B_1 = \epsilon_1 \sigma T_1^4 + (1 - \epsilon_1) H_1 \quad (1)$$

The term $(1 - \epsilon_1) H_1$ is the incident energy which is reflected by surface 1. Also the incident energy can be expressed in terms of the radiosity of each of the other surfaces of an enclosure having n surfaces.

$$A_1 H_1 = A_1 F_{1-1} B_1 + A_2 F_{2-1} B_2 + \dots + A_n F_{n-1} B_n \quad (2)$$

The factor F_{2-1} is a geometrical radiation form factor which represents the fraction of energy per unit area leaving surface 2 and impinging on surface 1. If surface 1 does not "see" itself, F_{1-1} is zero. Since there can be no net interchange of energy between surfaces 1 and 2 when $T_1 = T_2$, the reciprocity relation yields

$$\begin{aligned} A_2 F_{2-1} &= A_1 F_{1-2} \\ A_3 F_{3-1} &= A_1 F_{1-3} \\ A_n F_{n-1} &= A_1 F_{1-n} \end{aligned} \quad (3)$$

Combining Equations (2) and (3) yields

$$H_1 = F_{1-2} B_2 + F_{1-3} B_3 + \dots + F_{1-n} B_n \quad (4)$$

Substituting Equation (4) into Equation (1) yields a linear equation involving n unknown radiosities. Similarly, equations

$$B_i = \epsilon_i \sigma T_i^4 + (1 - \epsilon_i) (F_{i-2} B_2 + F_{i-3} B_3 + \dots + F_{i-n} B_n) \quad (5)$$

may be written for the radiosity at each of the other surfaces so that there result n linear equations with n unknowns. These equations may be solved by a suitable technique, analytical or digital, for the radiosity at each surface.

The heat transferred from surface 1 may be determined from an energy balance.

$$q_1 = \epsilon \sigma T_1^4 - \alpha_1 H_1 \quad (6)$$

Since $\alpha_1 = \epsilon_1$, Equations (1) and (6) may be combined to give

$$q_1 = \frac{\epsilon_1}{1 - \epsilon_1} (\sigma T_1^4 - B_1) \quad (7)$$

Once the radiosities have been found, it is a simple matter to determine the heat transferred to or from each surface.

In applying the radiosity method of analysis to an enclosure of fixed geometry but with various boundary conditions, it is sometimes more convenient to utilize a variation of the previously described technique. This variation separates the temperature dependent parameters from the parameters involving geometrical and radiation properties. In developing the desired equations, it is useful to consider an enclosure in which one surface has a temperature T_1 , and all the other surfaces are at absolute zero temperature. A dimensionless radiosity term β can be defined as

$$\beta_i^{(1)} = B_i / \sigma T_1^4 \quad (8)$$

The superscript (1) indicates that the $\beta_i^{(1)}$ were derived considering T_1 the only non-zero temperature. Then remembering that all surfaces except surface 1 are at absolute zero temperature, Equation (5) becomes

$$\begin{aligned} \beta_1^{(1)} &= \epsilon_1 + (1 - \epsilon_1) \sum_{k=1}^n \beta_k^{(1)} F_{1-k} \\ \beta_2^{(1)} &= (1 - \epsilon_2) \sum_{k=1}^n \beta_k^{(1)} F_{2-k} \\ \beta_n^{(1)} &= (1 - \epsilon_n) \sum_{k=1}^n \beta_k^{(1)} F_{n-k} \end{aligned} \quad (9)$$

Again a set of n equations involving n unknown β 's are formulated so that each β can be calculated. The β terms are completely independent of the surface temperatures in the enclosure, being functions only of the geometry and radiative properties of the surfaces. Similarly values for $\beta_i^{(2)}, \beta_i^{(3)}, \dots, \beta_i^{(n)}$ can be calculated considering each time T_2, T_3, \dots, T_n , respectively, to be zero.

Because of the linearity of the equations, the radiosity in an enclosure with surfaces at arbitrary temperatures T_1, T_2, \dots, T_n can be determined by adding the solutions where each surface was considered non-zero *separately*. (Ref. 2) The radiosity B , then may be calculated by

$$\begin{aligned} B_1 &= \beta_1^{(1)} \sigma T_1^4 + \beta_1^{(2)} \sigma T_2^4 + \dots + \beta_1^{(n)} \sigma T_n^4 \\ B_2 &= \beta_2^{(1)} \sigma T_1^4 + \beta_2^{(2)} \sigma T_2^4 + \dots + \beta_2^{(n)} \sigma T_n^4 \\ B_n &= \beta_n^{(1)} \sigma T_1^4 + \beta_n^{(2)} \sigma T_2^4 + \dots + \beta_n^{(n)} \sigma T_n^4 \end{aligned} \quad (10)$$

The B terms were calculated for the situation where all surfaces except one were considered at absolute zero temperature.

Equation (10) can be further simplified by utilizing a reciprocity relation between the various $\beta_i^{(j)}$. This reciprocity relation may be derived by once again considering the condition where all surfaces except one are at absolute zero temperature. For this condition, the energy incident on surface 2 is $H_2^{(1)} A_2$ where the superscript (1) indicates that surface 1 is considered to be the only emitting surface (only surface at a non-zero temperature). Since $\alpha_2 = \epsilon_2$ for gray surfaces, the energy absorbed by surface 2 is

$$\alpha_2 H_2^{(1)} A_2 = \epsilon_2 H_2^{(1)} A_2 \quad (11)$$

Remembering that T_2 is considered zero, $B_2^{(1)}$ may be expressed as

$$B_2^{(1)} = \rho_2 H_2^{(1)} = (1 - \epsilon_2) H_2^{(1)} \quad (12)$$

or

$$H_2^{(1)} = \frac{B_2^{(1)}}{1 - \epsilon_2} \quad (13)$$

With the aid of Equation (8), the energy absorbed by surface 2 may then be written

$$\frac{\epsilon_2}{1-\epsilon_2} B_2^{(1)} A_2 = \frac{\epsilon_2}{1-\epsilon_2} \beta_2^{(1)} \sigma T_1^4 A_2 \quad (14)$$

A similar expression may be developed for surface 1 when all temperatures except T_2 are zero. The energy absorbed by surface 1 is then

$$\frac{\epsilon_1}{1-\epsilon_1} \beta_1^{(2)} \sigma T_2^4 A_2 \quad (15)$$

However, there can be no net interchange between surfaces 1 and 2 when the temperatures are equal. Therefore

$$\frac{\epsilon_2}{1-\epsilon_2} A_2 \beta_2^{(1)} = \frac{\epsilon_1}{1-\epsilon_1} A_1 \beta_1^{(2)} \quad (16)$$

Introducing the general relationship of Equation (16) into Equation (10), the equation may be written

$$B_i = \frac{1-\epsilon_i}{\epsilon_i A_i} \left[\frac{\epsilon_1 A_1}{1-\epsilon_1} \beta_1^{(i)} \sigma T_1^4 + \frac{\epsilon_2 A_2}{1-\epsilon_2} \beta_2^{(i)} \sigma T_2^4 + \dots + \frac{\epsilon_n A_n}{1-\epsilon_n} \beta_n^{(i)} \sigma T_n^4 \right] \quad (17)$$

or, in general

$$B_i = \frac{1-\epsilon_i}{\epsilon_i A_i} \sum_{k=1}^n \frac{\epsilon_k A_k}{1-\epsilon_k} \beta_k^{(i)} \sigma T_k^4 \quad (18)$$

One other useful relation must be developed before arriving at the desired form of the equation for calculating radiant interchange in the enclosure. Considering all the surface temperatures except T_i to be zero, Equations (7) and (8) yield

$$Q_i = \frac{\epsilon_i}{1-\epsilon_i} A_i (1 - \beta_i^{(i)}) \sigma T_i^4 \quad (19)$$

$$Q_k = -\frac{\epsilon_k}{1-\epsilon_k} A_k \beta_k^{(i)} \sigma T_i^4 \quad k \neq i$$

From the conservation of energy, the energy lost by surface i must equal the energy absorbed by all of the other surfaces, $Q_i = \sum Q_k$. Therefore from Equation (19)

$$\frac{\epsilon_i A_i}{1 - \epsilon_i} = \sum_{k=1}^n \frac{\epsilon_k}{1 - \epsilon_k} \beta_k^{(i)} A_k \quad (20)$$

Finally, the desired form of the equation may be obtained by considering Equations (7) and (18).

$$Q_i = \frac{\epsilon_i A_i}{1 - \epsilon_i} \sigma T_i^4 - \sum_{k=1}^n \frac{\epsilon_k A_k}{1 - \epsilon_k} \beta_k^{(i)} \sigma T_k^4 \quad (21)$$

Introducing Equation (20) into the first term on the right side of the equal sign yields

$$Q_i = \sum_{k=1}^n \frac{\epsilon_k A_k}{1 - \epsilon_k} \beta_k^{(i)} \sigma (T_i^4 - T_k^4) \quad (22)$$

A combined geometry and radiation property factor, \mathcal{F}_{i-k} , may be defined as

$$\mathcal{F}_{i-k} = \frac{\epsilon_k A_k}{1 - \epsilon_k} \beta_k^{(i)} \quad (23)$$

Then Equation (22) becomes

$$Q_i = \sum_{k=1}^n \mathcal{F}_{i-k} \sigma (T_i^4 - T_k^4) \quad (24)$$

It may be noted that the factors \mathcal{F}_{i-k} are completely independent of temperatures of the surfaces in the enclosure and depend only on geometry and surface emissivity. Once the \mathcal{F}_{i-k} terms have been found for an enclosure of fixed geometry and constant radiation properties of the surfaces, then Q_i , the net energy transferred from any surface i , may be readily found for any combination of surface temperatures.

DIGITAL ANALYSIS

The solution of a complex thermal enclosure problem may be approached by two methods: (1) the development of a new computer routine or (2) the utilization of an existing thermal analyzer program. If a new routine is to be developed, the most convenient method of accounting for the radiation equations may be included. If an existing

routine is to be used a method must be found to include radiation in an enclosure.

The development of a new computer routine could include provisions for solving the series of linear equations developed from one of the methods for analyzing radiating enclosures; i.e., Eckert's method, Hottel's method, or Gebhart's method. The extent to which the routine can formulate equations, calculate geometrical radiation form factors, etc. depends on the generality of the routine. As the generality increases, the complexity of the input data also increases. This is shown graphically in Figure 3. Routines for specific applications can be developed that require minimum input information and are easily applied. General type thermal analyzer routines require more complex and more extensive input data.

Since general thermal analyzer programs are readily available and are currently being used for thermal analysis of structures and components, it is often desirable to use these existing programs for radiating enclosure analysis. It was found that Oppenheim's electrical analog network method of representing radiosity could readily be used with existing thermal analyzer programs.

The thermal analyzer program used in this analysis is a general routine which can be used for a wide variety of thermal problems. The program solves an equivalent electrical analog network consisting of resistances and capacitances which represent the thermal system to be analyzed. This routine is capable of combining conduction, convection, and radiation into a single problem. (Ref. 7)

The thermal analyzer program solves the equivalent electrical circuit by linear or non-linear equations depending on the modes of heat transfer; i.e., conduction, convection, or radiation. Conduction, being the most linear of the modes is represented as a conductance. It is represented in the network as a resistance (the reciprocal of conductance). The resistance can be made a function of time and one other parameter such as temperature. Convection is handled by a similar treatment. Radiation is not linear and is represented by an equation of the form

$$q_r = \frac{1}{R_r} (T_1^4 - T_2^4) \quad (25)$$

where T_1, T_2 = temperatures of surfaces 1 and 2, respectively

q_r = heat transferred due to radiation

R_r = "Radiation resistor"

This equation is represented in an analog network by the radiation resistor connecting surfaces 1 and 2. For radiation between two surfaces, the radiation resistor takes the form

$$R_r = \frac{1}{A F_e F_a \sigma} \quad (26)$$

where

- A = area of surface
- F_e = surface emissivity factor
- F_A = geometrical form factor
- σ = Stefan-Boltzmann constant

Since the radiation resistor term is included in the input data, it may be made to satisfy various conditions of radiant heat transfer.

The problem of including reflected energies in the equivalent analog network is that of representing the radiant exchange in terms of radiation resistors. According to Oppenheim (Ref. 8) the radiant interchange in an enclosure may be represented by an electrical network as shown in Figure 4. The four nodes 1, 2, 3, and 4 represent the four surfaces considered. Although only four surfaces are considered in this example, the method is general and may be used for any number of surfaces. The assumptions are made, however, that each surface is at a uniform temperature (at any instant of time although the temperatures may vary with time), the surfaces are diffuse, and that they are irradiated uniformly. Large areas which are not closely approximated by these assumptions may be handled by breaking the large surfaces into several smaller ones.

The nodes in the electrical analog representing the surfaces have potentials corresponding to the black body emissive power (σT^4) of each surface. A second set of nodes, 1', 2', 3', and 4' are separated from each of the surfaces by a resistor which is a function of the area and radiative properties of the surface. The value of this resistor is shown in Figure 4 to be $\frac{1-\epsilon_1}{A_1 \epsilon_1}$

In the analysis leading to the development of the electrical analog network, the potentials at the nodes 1' through 4' correspond to the radiosities at surfaces 1 through 4, respectively. The radiosity node at each surface is connected to the radiosity node at each other's surface that it can "see". If the surface cannot "see" another surface, then no radiation leaving the first surface can strike the other directly; hence there is no radiant heat transfer path (resistor) between them. The resistance values between the radiosity nodes are seen to depend solely on the geometry of the enclosure. Although

these resistances are shown in terms of the area of the surface with the lower number as a subscript, either area the resistor connects may be used. The resistance between node 1' and 2', for example, is $1/(A_1 F_{1-2})$. Since

$$A_1 F_{1-2} = A_2 F_{2-1} \quad (27)$$

by the reciprocity law, the resistance might just as well have been written $1/(A_2 F_{2-1})$.

When a surface is completely reradiating (a no flux surface), the potential E is replaced by a "floating" node in the network. In other words, the node is not connected to any potential and is free to assume the same potential as the corresponding radiosity node. Figure 5 shows a network with two radiating surfaces and one reradiating surface. In an actual enclosure, an example of a reradiating surface is one that is well insulated from its surroundings and its heat capacity has negligible effect on the transient thermal response.

By recognizing the meaning of configuration factors and the significance of the assumptions of diffuse surfaces, uniform temperature, and evenly irradiated surfaces, this analysis can be extended to configurations and boundary conditions not covered by the general case. For example, a specularly reflecting surface can often be included in a diffuse enclosure by geometrically accounting for the energy paths (Ref. 4).

In order to incorporate the radiant interchange analog with the thermal analyzer routine, the analog network must be represented so as to be compatible with the calculation technique of the routine. The routine calculates radiation by an equation of the form

$$q_r = \frac{1}{R_r} (T_1^4 - T_2^4) \quad (28)$$

where R_r is input data. If the potential corresponding to the radiosity at the radiosity node in the network is represented by σT_B^4 then the heat flow between the radiosity node and the surface node can be expressed as

$$q_1 = \frac{\epsilon_1 A_1}{1 - \epsilon_1} (\sigma T_{B1}^4 - \sigma T_1^4) \quad (29)$$

$$q_1 = \frac{\epsilon_1 A_1 \sigma}{1 - \epsilon_1} (T_{B1}^4 - T_1^4)$$

Therefore, T_B is a fictitious temperature used solely to define the radiosity at the radiosity node. An equivalent network representing the radiosity as σT_B^4 is shown in Figure 6.

Comparing the thermal analyzer network in Figure 6 to Oppenheim's network in Figure 4, it is readily seen that the resistor values differ only by the term σ . Since σ is a constant, the networks are seen to be equivalent.

This method of analysis has been used by the Chance Vought Corp. for some time in analysis of spacecraft structures and components. The ability to use a single routine for many thermal problems, with combinations of conduction, convection, and radiation in an enclosure has proved very valuable.

Other people are also using this technique. North American Aviation (Ref. 9) has also considered the technique described in this paper. Rather than employing Oppenheim's analog, however, they reduced the radiant interchange equations to a form similar to Equation (24). The radiant interchange between a pair of surfaces is then expressed as

$$Q_{1-2} = A F_{1-2} \sigma (T_1^4 - T_2^4) \quad (30)$$

The radiant interchange between each pair of surfaces is then expressed by a single radiation resistor. This was done to eliminate the possibility of divergence in the method of calculation due to zero capacitance at the radiosity nodes. This requires additional calculation, by a digital program if the problem is complex, before the data can be used in the thermal analyzer. No problems have been encountered, however, with convergence using Oppenheim's analog as long as the calculating increments of time are kept small. For problems that do not involve extensive computing time it is more economical to use a small increment in calculation although for long problems, it is conceivable that reduction of the equations to a form of Equation (24) might be advisable.

CONCLUSIONS

1. If a new digital program is to be developed for thermal analysis including radiant interchange in an enclosure, several methods of incorporating the radiant analysis should be investigated. Radiosity, Hottel's method, and Gebhart's method of analysis, and Oppenheim's analog representation of radiant heat transfer are applicable to digital computer methods.

2. Oppenheim's analog method of representing radiant interchange in an enclosure is readily adaptable to existing thermal analyzer digital programs. This method provides a simple means of including radiant heat transfer in digital thermal analysis of enclosed spacecraft compartments.

3. In special cases, such as extensive study of an enclosure with fixed geometry and radiative surface properties, it may be desirable to incorporate variations of the equivalent analog network into thermal analyzer digital programs.

REFERENCES

1. Eckert, E. R. G. and Drake, Robert M., Jr., Heat and Mass Transfer, McGraw-Hill Book Company, New York, 1959, pp. 407-418.
2. Hottel, H. C., "Radiant Heat Transmission," Chapter 3 of Heat Transmission by McAdams, W. H., Third Edition, McGraw-Hill Book Company, Inc., New York, 1954.
3. Gebhart, B., "Unified Treatment for Thermal Radiation Transfer Processes - Gray-Diffuse Radiators and Absorbers," A.S.M.E. Paper No. 57-A-34, 1957.
4. Sparrow, E. M., Eckert, E. R. G., and Jonsson, V. K., "An Enclosure Theory for Radiative Exchange Between Specularly and Diffusely Reflecting Surfaces," Heat Transfer Laboratory, University of Minnesota, Minneapolis.
5. Eckert, E. R. G. and Sparrow, E. M., "Radiative Heat Exchange Between Surfaces with Specular Reflection," International Journal of Heat and Mass Transfer, Vol. 3, 1961.
6. Sparrow, E. M., "On the Calculation of Radiant Interchange Between Surfaces," Heat Transfer Laboratory, University of Minnesota, Minneapolis, 1961.
7. Abrahams, R. S., "Thermal Network Analyzer Program," Lockheed Aircraft Corp., Missile and Space Div., Sunnyvale, California, Technical Memorandum No. TM 59-24-1, April 28, 1961.
8. Oppenheim, A. K., "Radiation Analysis by the Network Method," Trans. A.S.M.E., Vol. 78, 1956, pp. 725-735.
9. Grafton, J. C. and Nordwall, H. L., "Radiation Heat Transfer Analysis for Space Vehicles," A.S.D. Technical Report No. ASD-TR-61-119, Part II, 1962.

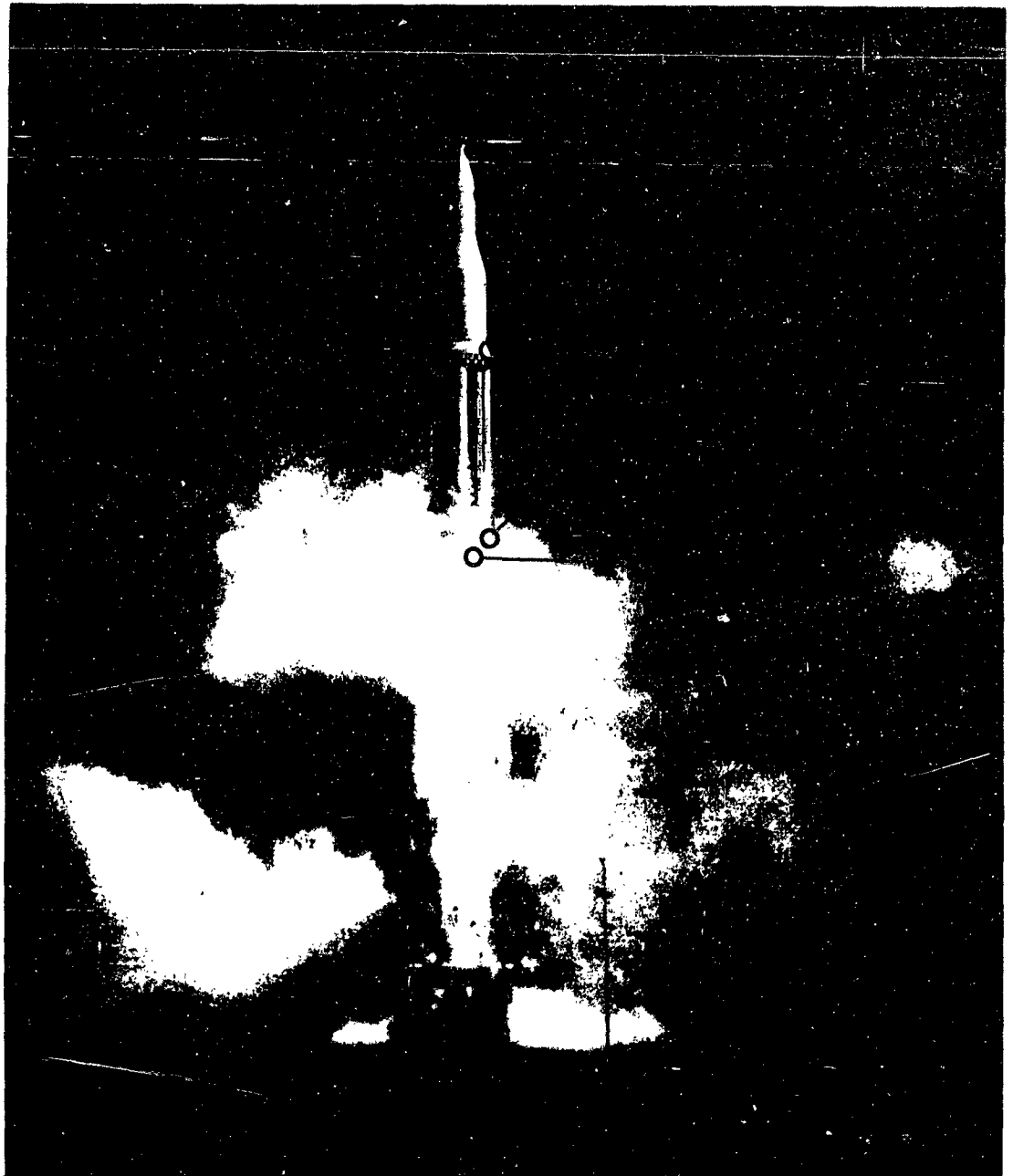


FIGURE 1 SPACECRAFT AFFECTED BY RADIATION IN AN ENCLOSURE

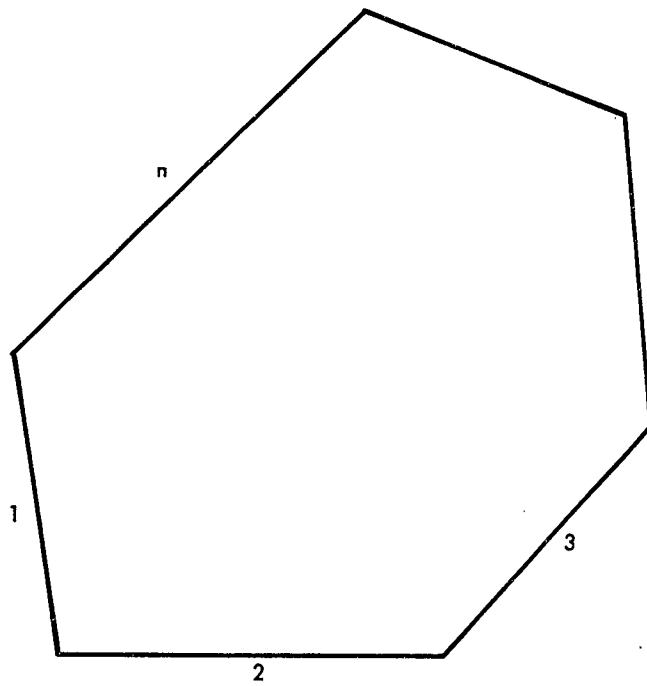


FIGURE 2 TYPICAL RADIATING ENCLOSURE WITH n SURFACES

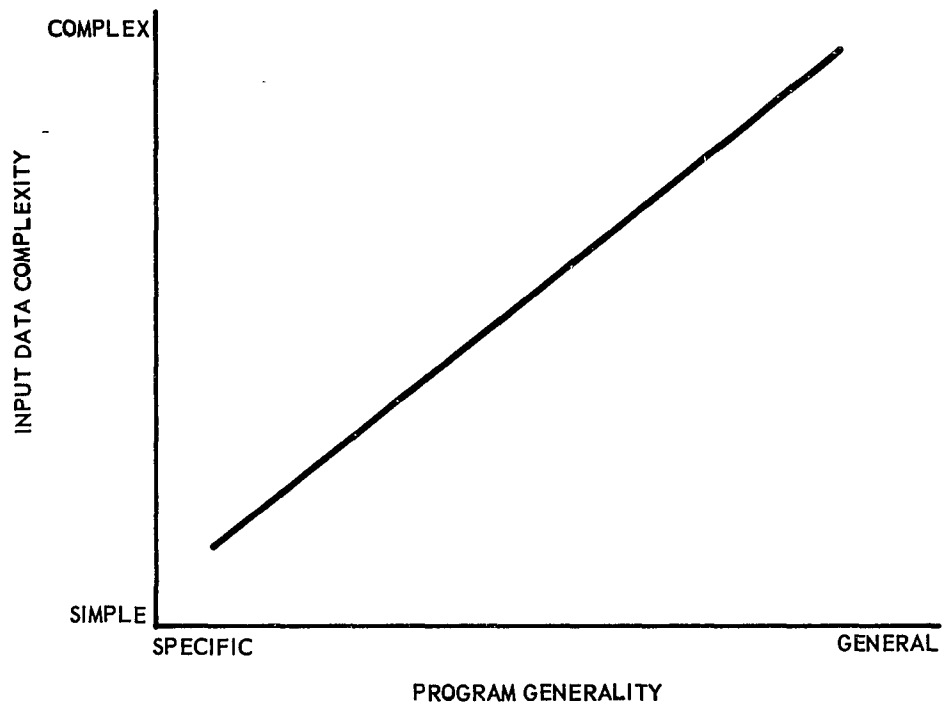
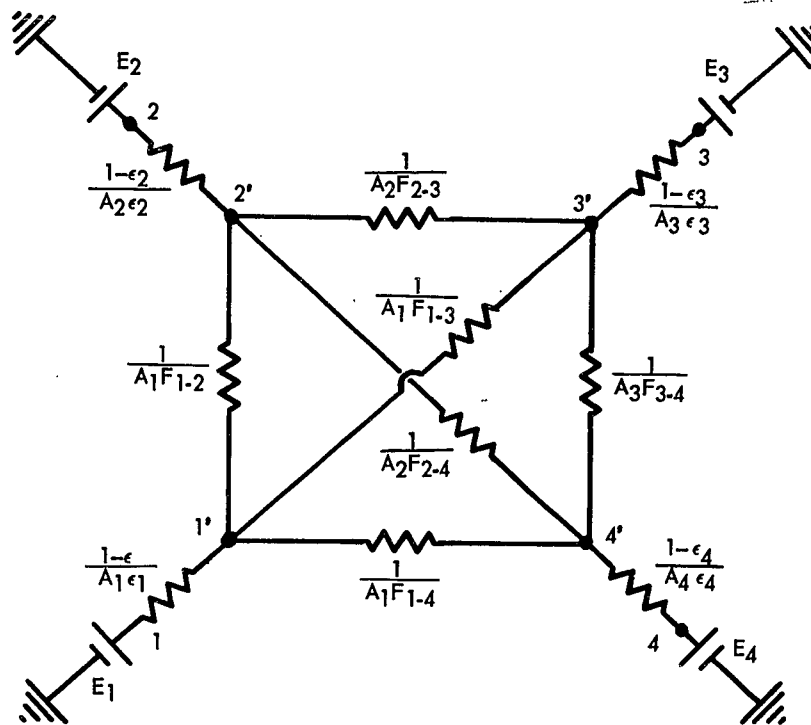
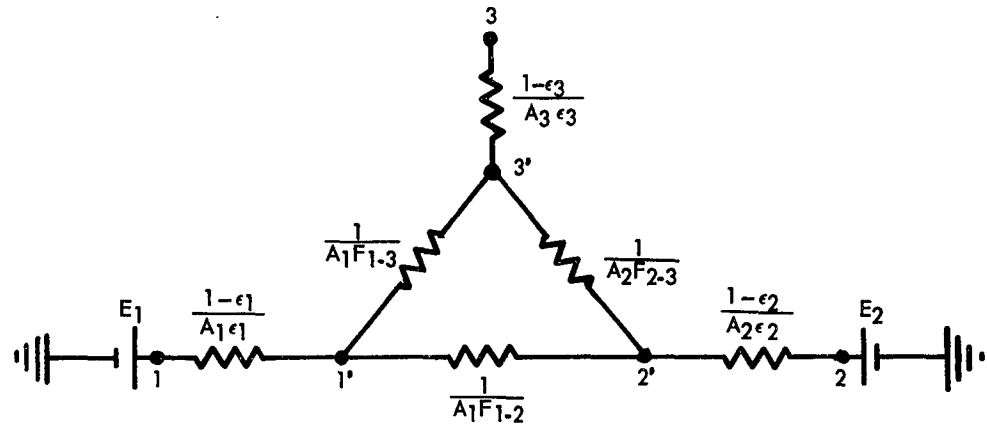


FIGURE 3 COMPLEXITY OF INPUT DATA



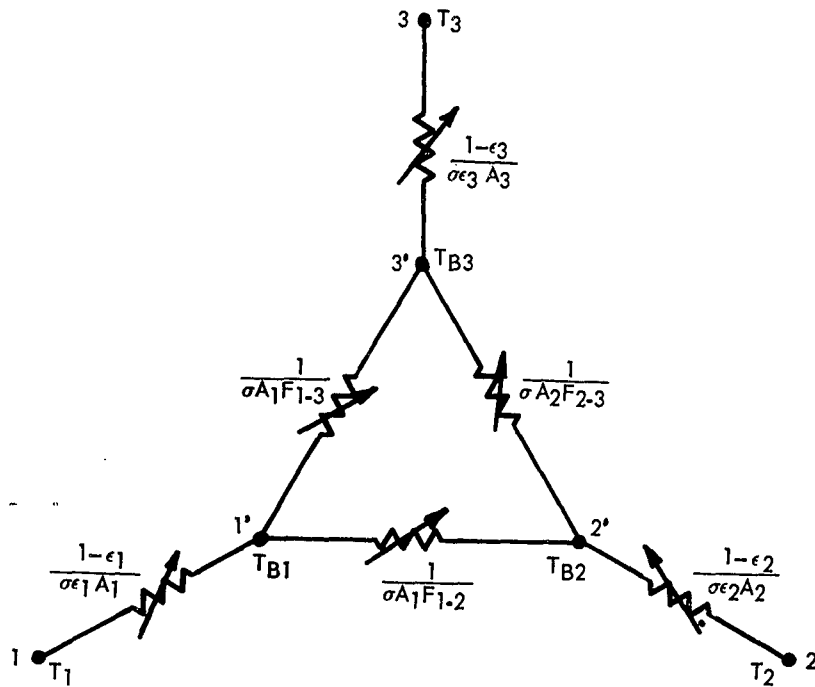
- NOTES: 1. $E_i = \sigma T_i^4$ (BTU/HR-FT²)
 2. ϵ_i = EMISSIVITY OF SURFACE i
 3. A_i = SURFACE AREA OF SURFACE i (FT²)
 4. F_{ij} = GEOMETRICAL CONFIGURATION FACTOR BETWEEN SURFACE i AND SURFACE j

FIGURE 4 OPPENHEIM'S ELECTRICAL ANALOG



- NOTES: 1. SURFACE 3 IS A RERADIATING SURFACE
 2. NODE 3 IS A "FLOATING" NODE

FIGURE 5 EQUIVALENT NETWORK WITH A RERADIATING SURFACE



NOTE: THE SYMBOL  DENOTES A "RADIATION RESISTOR"
 SO THAT $q_{B1} - q_{B2} = \frac{1}{R_{B1-B2}} (T_{B1}^4 - T_{B2}^4)$

FIGURE 6 THERMAL ANALYZER NETWORK

Fourth Paper -- "Thermal Analysis of Structures Including Radiation in an Enclosure," by R.A. Knezek & G.J. French, Chance Vought.—(Presented by Mr. Knezek)

QUESTION: (Mr. Barker, Douglas) How would you propose to solve problems with temperature dependent radiant properties?

ANSWER : (Mr. Knezek) I could think of three situations where you would have radiation with radiant properties; one if the temperature of all the surfaces in the enclosure are not too different from one another but the whole enclosure is changing, well then, you can still consider a great many surfaces, and simply change the radiant properties of these surfaces from time to time as you go along. Sometimes this can be built into the routine. It is primarily a problem of the routine technique. Another problem would be where one or more of the sources is at a more vastly affected temperature than the rest of the surfaces in the enclosure. Now an example of this might be the sun shining in through an open space. Now here you would have to, I think, solve the problem in essentially two steps. For the solar energy for example, you could consider where the energy is absorbed. Now you can set up radiosity equations as we did in the enclosure, except that the surfaces wouldn't be emitting energy and the radiosity would simply be the reflected energy, except for the source. Now once you set up these equations, they can be solved for the heat absorbed by each surface and this can be added as an input to the overall problem. The third problem is the in between situation and I don't know of a good technique of handling this. I suspect that what you have to do would be to consider where the energy is absorbed that is emitted by each separately and this gets pretty hairy.

QUESTION: (Mr. Cannizzaro, ASD) What is the maximum number of nodes the computer program can handle?

ANSWER : (Mr. Knezek) The program that is referenced in the paper is a fortran program and is somewhat limited. I believe the conversion with which I am most familiar is limited to 700 nodes. Now we also used a 704 version, sheer routine, which I believe was also originated by Lockheed. This program is limited only by the total capacity of the machine. For example, it may be limited by the total number of nodes or temperatures, resistors, capacitors and so forth. I don't know that the maximum number would be, but it would be quite large.

QUESTION: (Mr. Cannizzaro, ASD) How many dimensions can be used, one, two, or three?

ANSWER : (Mr. Knezek) The method is not limited to any number of dimensions. You can use three-dimension analysis just as well as two, as long as you can set up an electric network of resistance and capacitance for the problem; the program will handle it.

QUESTION: (Mr. Cannizzaro, ASD) What is the form of the input needed?

ANSWER : (Mr. Knezek) Certainly the initial temperatures for the entire enclosure are required. For the surfaces that can have a heat capacitance there is a capacitance value required for each surface, for each node. In some cases you also have to put in specified zero capacitance, surfaces or nodes which do not have any mass to them. The radiosity nodes and then all the resistors which will present heat paths will have to be specified. Conduction--it is simply a number, a constant, or, well, let me back up just a second. I believe the temperatures for resistors and capacitors can be programmed also as a function of time and one other variable, so that they aren't necessarily constants.

TABLE 1

TYPICAL SATELLITE HEATING ENVIRONMENTS

Insolation	443 BTU/hr-ft ²
Albedo Radiation	168 BTU/hr-ft ² (reflectivity 38%)
Earth Emission	68.7 BTU/hr-ft ²
Internal Generation	Function of Skin Temperatures

III. THE MATHEMATICS OF THE THERMAL ANALYSIS

For purposes of analysis a structure may be represented by a set of spatially distributed points or nodes. The temperature of each node is determined by solving the generalized heat balance equation in finite difference form:

$$T'_j - T_j = \frac{\Delta \tau}{\rho V C_p} [\dot{Q}_j''' + \dot{Q}_j'' - \sum_{i=1}^n U_{ij} (T'_j - T_i)] \quad (1)$$

T'_j and T_j represent the temperatures at the end and beginning of the time step, respectively. The parameters \dot{Q}_j''' and \dot{Q}_j'' represent volumetric heating and incident surface flux, respectively. U_{ij} is the thermal conductance between node i and node j. The analysis consists of an iteration for T'_j and re-evaluates temperature dependent functions on the mean temperature of T'_j and T_j . The iteration for T'_j is then repeated. This is the so-called implicit or backward time step method.

The analysis may also use the explicit or forward time step method, in which T'_j and T_j are the same as the implicit method. There is no necessity of iteration for T'_j in this case, since the heat balance equation then becomes explicit in T. Once T'_j is evaluated, the temperature dependent functions are re-evaluated for the mean of T' and T, and T' is re-evaluated.

$$T'_j - T_j = \frac{\Delta \tau}{\rho V C_p} [\dot{Q}_j''' + \dot{Q}_j'' - \sum_{i=1}^n U_{ij} (T_j - T_i)] \quad (2)$$

There is now a limit on the length of time step $\Delta \tau$ which the program calculates and is given by $\Delta \tau = \rho V C_p / U_{ij}$ and taken so that this expression is a minimum for the entire nodal system. The expression used to evaluate zero-volume nodes (surface) and steady-state calculations is

$$\sum_{i=1}^n U_{ij} (T_j - T_i) - \dot{Q}_j''' - \dot{Q}_j'' = 0 \quad (3)$$

The parameters \dot{Q}_j''' and \dot{Q}_j'' are the same as defined previously.

The thermal conductance term, U_{ij} , is used in three basic forms: (1) solid to solid conduction, with contact coefficient; (2) solid to solid radiation, with radiation coefficient; and (3) solid to fluid, with conduction and film coefficient. Details of the mathematical analysis appear in Appendix A.

IV. COMPUTER PROGRAM

A. General Description

The mathematical analysis presented in Section III has been programmed for the IBM 7090 installation at Aeronautical Systems Division, WPAFB. The program is coded, for the most part, in Fortran coding language. There are four FAP subroutines.

The program possesses the following features:

1. Systems may be one-, two-, or three-dimensional in nature.
2. Material properties are temperature-dependent (they are inputted in tabular form) and may have discontinuities such as, latent heat of transformation, and irreversible property transformations.
3. Thermal connections between systems nodal volumes may include any or all of the following: conduction (with or without interface contact resistance), convection in channels totally enclosed by the system or bounding the system, and radiation between nodes of the system or with time-dependent boundary-temperature tables.
4. Boundary conditions that may be utilized include: (a) volumetric-heating rates as arbitrary functions of time; (b) surface heat flux rates as arbitrary functions of time; (c) time-dependent fluid flows with convection coefficients either as functions of time; or (d) time dependent fluid flow rates and Nusselt numbers, and compute the film coefficients.
5. In one subroutine, the program will compute one dimensional surface ablation for ablative material. The analysis accounts for all energy available from radiation, surface flux, and/or mass heating during an interval of time by means of a quasi-steady-state analysis. The ablative material may be either charring or non-charring. The remaining sections of the system being analyzed, however, are still three-dimensional and the analysis transient in nature.
6. Problems may be terminated in the event that the temperature of one or more nodes exceeds the specified material limits.
7. In addition to print-out of any or all nodal temperatures at the end of each time step, the program can print out data which will permit heat fluxes along given thermal connections to be calculated.
8. The program can proceed to a steady-state temperature distribution for the system at any time without further transient calculations.

9. The number of nodes for a given problem is not fixed since data storage is allocated at execution time based on the input actually received by the program. Generally, if the number of material property tables and boundary conditions is reasonable, over 500 nodes can be accommodated in a single problem.

B. PROGRAM CAPACITY

Due to the large amounts of machine logic required for this type of problem, a stacked storage technique is used. With this approach, specific areas are not reserved for node data storage, materials, tables, etc. As each block of data is read in, it is stored in the next available cell. The program logic keeps track of the next available cell and continually checks to see that incoming data will not overrun the program logic.

Another device used to save data storage is the use of packed words for connection information. This technique involves the packing of several pieces of data into one 36 binary bit word.

Consequently, the size of problem that can be run depends on the particular problem under consideration. In general, it is feasible to handle 500 nodes. It should be possible to handle up to 1000 nodes if the boundary conditions and materials tables do not require large amounts of data storage.

C. PROGRAM STRUCTURE

The program is divided into five (5) chains in order to maintain adequate data storage. The data is inputted in a form which is convenient in that the user requires little or no knowledge of computer programming or techniques to prepare the problem for the program. As the data is accepted, the program stacks the data and continually checks for the possibility of logic storage overrun. If this occurs the program is stopped with an error comment. Chain 2 processes the data from Chain 1 into a form which can be efficiently used by the program logic. This is accomplished in the following manner: The input data as originally prepared refers to various nodes, materials, and boundary conditions by arbitrarily assigned I.D. numbers. Chain 2 replaces these I.D. numbers with the location numbers in core storage of these various tables. It also processes the inputted node connection data. This is accomplished more efficiently at this point since all the previously mentioned data processing must be complete beforehand. This is a requirement of the program logic.

Chain 3 is the mathematical computation chain. It takes the processed input data and computes the heat balance. Subroutines in this chain calculate current volumetric heat rates, heat flux rates, and fluid node flow rates as well as the thermal capacitance of each node. The conductance matrix is formulated and the heat balance performed. This sequence of events is repeated until the computed time step data is exhausted. The temperature for each node is printed out as the temperature balance for each time step is completed.

Chain 4 is an output editing chain which prints out the following: (1) time, temperature history for a given set of nodes, (2) time, heat-flux history for a given set of nodes, and is capable of (3) punching on decimal cards the final temperature distribution. Item 3 is in a format acceptable for input to the program and is valuable in restarting the problem.

Chain 5 can be used for setting up change cases.

Figure 2 gives in flow chart form the basic structure of the program with the main operations of each chain. A simple example problem is given in Appendix B.

D. DISCUSSION

The program is designed so that there are relatively few restrictions on shapes, sizes, boundary conditions and materials. While rectangular and parallelepipeds are used most often, the shapes are not restricted to those configurations. Nodes could be cylindrical, spherical, polyhedrons, or even combinations of these. The only restriction on node shape is the number of thermal connections. A maximum of 8 thermal connections per node is allowed.

Boundary conditions may exist in a variety of ways. Such things as volumetric heating rates and surface flux rates can be given for each node as a function of time.

Material property tables contain the following data: (1) thermal conductivity, (2) specific heat, (3) emissivity, (4) enthalpy, and (5) viscosity all as a function of temperature. In addition, there are provisions for heat of transformation, transformation temperature, and density above and below transformation temperature. Both reversible and irreversible phase changes may be treated in materials.

The time step data can be handled by the program in various ways. The length of time steps can be varied. The program can accept any combination of transient, steady-state conditions. Thus it is possible to have a period of transient conditions followed by a period of steady-state conditions and then again transient conditions.

Figure 3 illustrates the manner in which a section of a typical re-entry vehicle could be divided into a node network. The vehicle section considered is a honeycomb sandwich structure with a composite thermal protection system. The number of nodes is approximately 800, the number of material property tables approximately 4, and the number of boundary conditions tables is approximately 13. While the boundary conditions do not appear in the Figure, they would be equally distributed over the surface of the body in such a manner as to represent the actual thermal environment of the vehicle.

CONCLUSION

A three-dimensional transient thermal analysis computer program has been developed by Aeronca Manufacturing Corporation personnel. It was the result of the need for an efficient thorough analysis of the composite thermantic shield of reinforced ceramic and insulation as applied to re-entry vehicles. However, the generality of the program allows it to analyze any simple or composite structure, constructed of any number of different materials and for any size and shape vehicle.

The basis for the thermal analysis is the generalized lumped approximation wherein a system is approximated by a set of small, nodal volumes, each of which is assumed to have a uniform temperature within it. The method of solution is either by the explicit (forward time-step) or implicit (backward time-step) method.

The data necessary to run a problem included such things as: (1) time, boundary temperature tables; (2) time, rate tables; (3) Nusselt number correlation tables; (4) material property tables as a function of temperature; (5) node description data; and (6) connection data for each node.

This computer program presents a means of greatly facilitating the preliminary and final design of both space and re-entry vehicles in that it offers a means of making a detailed and economically efficient transient analysis for the environments encountered by these vehicles.

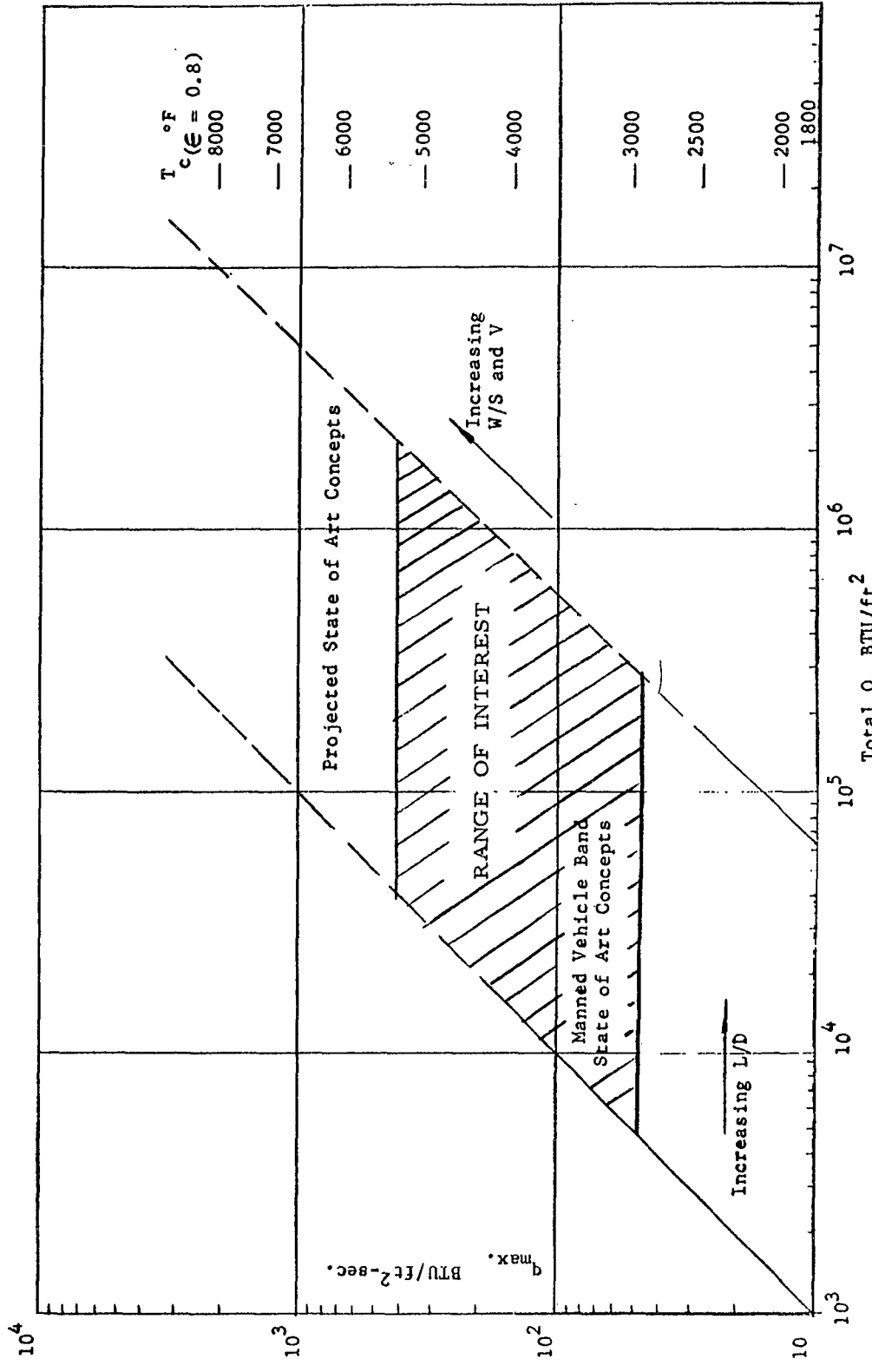


Figure 1 Re-Entry Vehicle Band

NOTE: CHAIN #5 USED
FOR CHG CASE ONLY

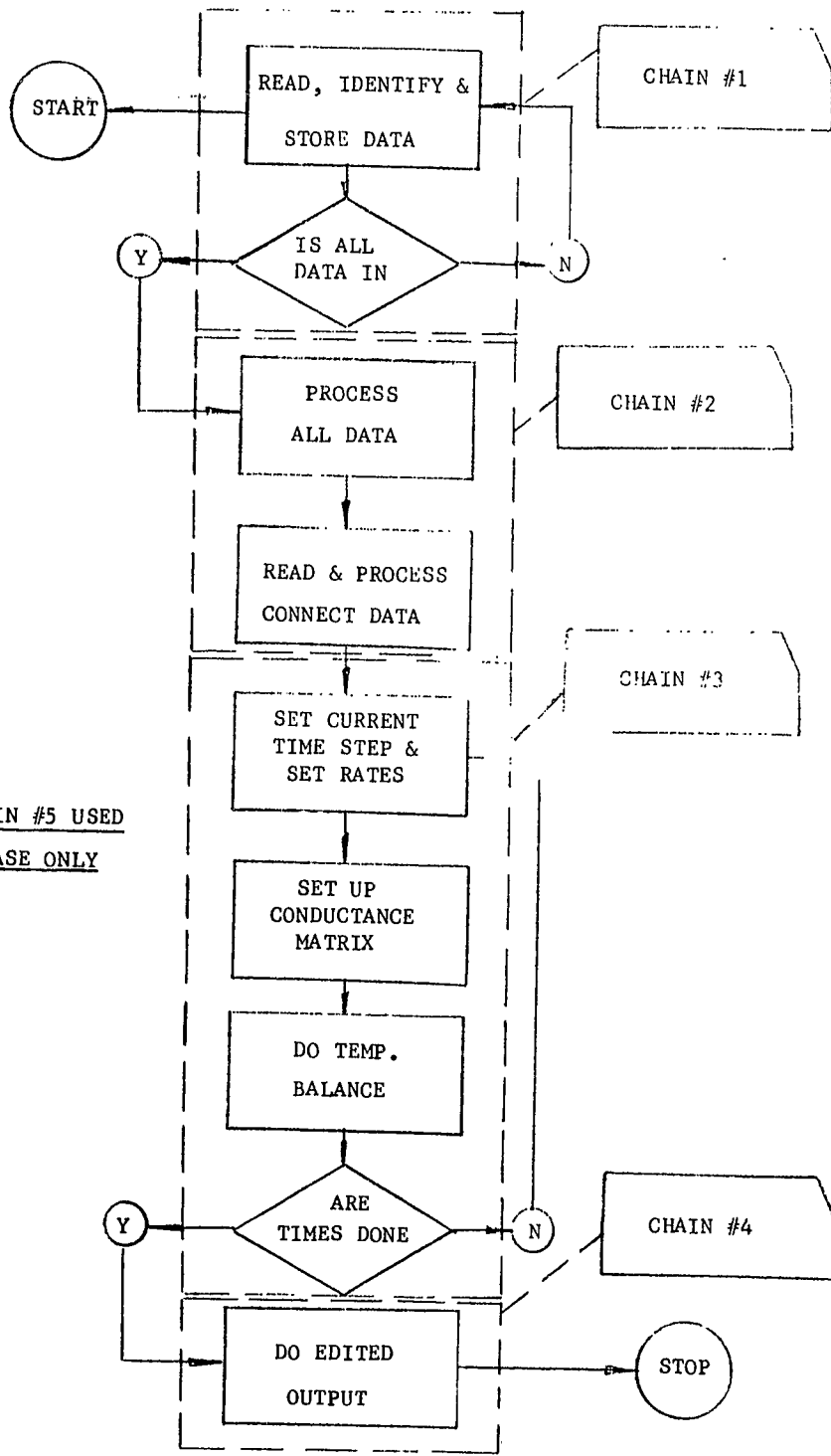


Figure 2 Flow Chart of Five Program Chains

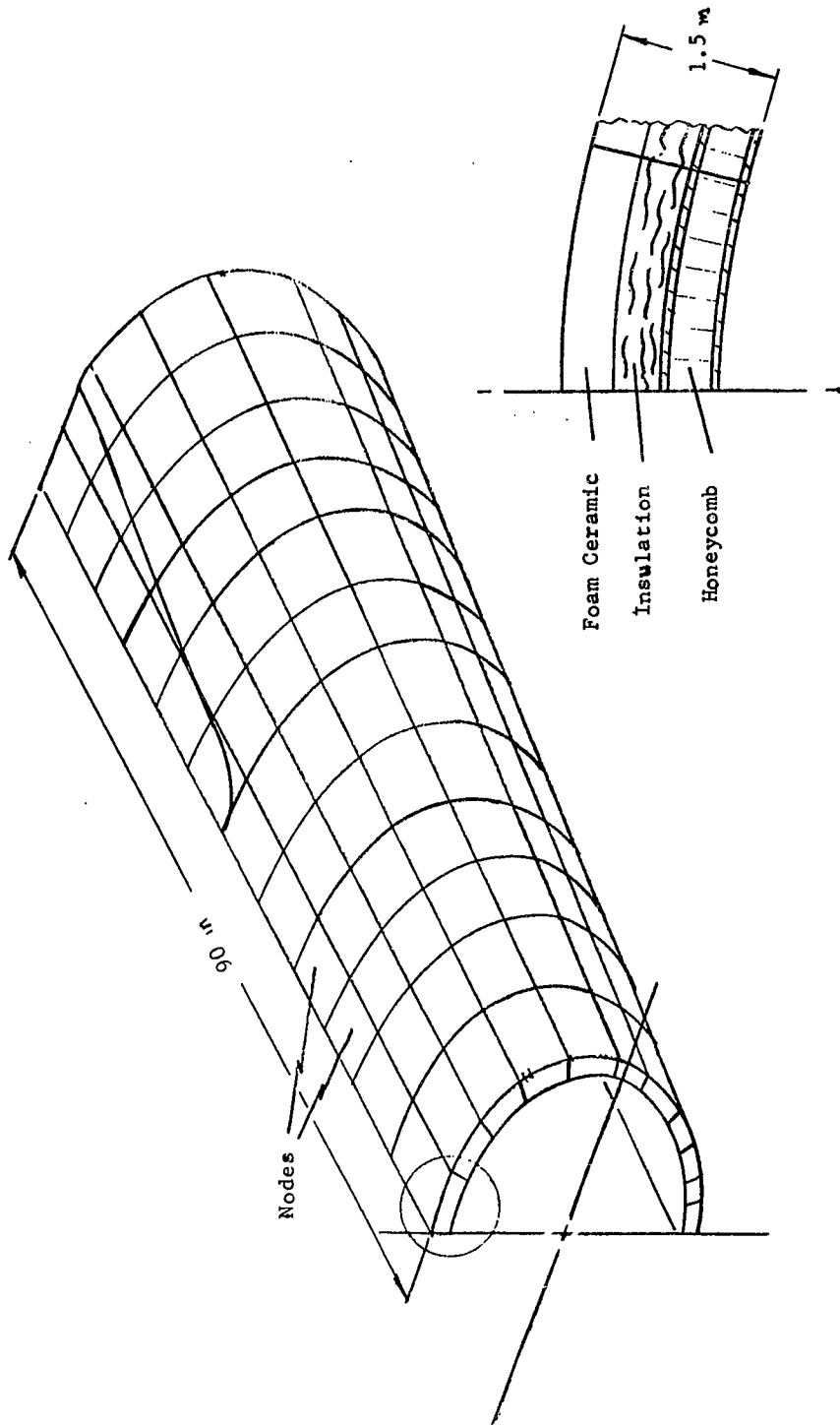


Figure 3 Feasible Node Network for Re-Entry Type Vehicle

APPENDIX A

A1. GENERAL TRANSIENT HEAT BALANCE

The few methods available for the solution of the completely general transient thermal problem all employ what is alternatively known as the "lumped parameter approximation" or "nodal approximation". (This approach is sometimes referred to as the "finite-difference method", but finite difference is actually a method of solution rather than a method of problem formulation). In this general approach, the actual continuous spatial distribution of temperatures and associated thermal property values is approximated by a spatially distributed set of discrete points. The approximation is better as the number of points is increased, but there is a corresponding increase in the computational labor associated with obtaining solutions.

Each of the discrete points used to approximate the actual system has associated with it a small volume of space and the term "node" is rather interchangeably associated either with the discrete point itself or with the small spatial volume. The temperature and the thermal properties are assumed to be constant throughout the small (nodal) volume.

The general heat balance can be formulated simply by virtue of the fact that the algebraic imbalance in all of the heat flows entering or appearing in the nodal volume is proportional to the rate of temperature rise within the nodal volume. This can be expressed mathematically for a system containing n nodes by the following equation written for the j -th node:

$$\dot{Q}_j''' + \dot{Q}_j'' + \sum_{i=1}^n \frac{T_i - T_j}{R_{ij}} = C_j \frac{dT_j}{dt} \quad (1A)$$

where $\dot{Q}_j''' =$ the rate of heat generation in the j -th nodal volume.

$\dot{Q}_j'' =$ the rate at which surface flux enters the j -th nodal volume.

$T_i =$ the temperatures of the nodes with which the j -th node exchanges thermal energy.

$T_j =$ the temperature of the j -th node for which the heat balance is being written.

$R_{ij} =$ the thermal resistance which expresses the amount of heat which flows from the i -th node to the j -th node by virtue of the $(T_i - T_j)$ temperature difference.

$C_j =$ the total heat capacity of the j -th nodal volume.

$t =$ time

If the conventional single over-dot is adopted to indicate first derivative with time and use thermal conductance, Y , instead of thermal admittance, where

$$Y_{ij} = \frac{1}{R_{ij}} \quad (2A)$$

Equation (2) can be rewritten as

$$-\sum_{i=1}^n Y_{ij} T_i + T_j \sum_{i=1}^n Y_{ij} + C_j \dot{T}_j = \dot{Q}_j''' + \dot{Q}_j'' \quad (3A)$$

The set of equations for all n j -th nodes can now be written in matrix form as

$$[Y][T] + [B][T] = [Q] \quad (4A)$$

where the individual matrix elements are

$$Y_{ji} = \sum_{i=1}^n Y_{ij}, \quad Y_{ij} \leq 0 \quad (5A)$$

$$B_{jj} = C_j \quad (6A)$$

and

$$Q_j = \dot{Q}_j''' + \dot{Q}_j'' \quad (7A)$$

For the general problem where the thermal properties are temperature dependent, the elements of the conductance matrix, $[Y]$, and the thermal capacitance matrix, $[B]$, are temperature dependent. The heat input matrix, $[Q]$, is generally time-dependent and may, under some circumstances to be described, even contain temperature dependent terms.

Each of the boundary conditions and types of thermal resistances will now be discussed.

Volumetric Heating is being included since it is simple and will permit the simulation of structures operating near nuclear devices such as propulsion systems or auxiliary power systems. In terms of a base volumetric heating rate, \dot{q}_j''' , which might be in BTU/hr-ft³, the volume heating would be simply

$$\dot{Q}_j''' = \dot{q}_j''' V_j \quad (8A)$$

where V_j is the j -th nodal volume

Surface Heat Flux can be expressed in terms of the basic surface rate, \dot{q}_j'' , which might be given in BTU/hr-ft², simply as

$$\dot{Q}_j'' = \dot{q}_j'' A_{sf,j} \quad (9A)$$

where $A_{sf,j}$ is the surface area of the j-th volume upon which the surface flux is incident. For purposes of experimental verification, it is desirable that the analysis also be able to accommodate imposed, arbitrary surface temperatures, T_x . This can be done in the guise of surface flux by an expression of the form

$$\dot{Q}_j'' = \frac{T_x - T_j}{R_{xj}} \quad (10A)$$

where R_{xj} is the conductive type of thermal resistance associated with the path from the surface to the centroid of the j-th nodal volume. The appearance of the T_j and the R_{xj} in the "surface flux" \dot{Q}_j'' will result in the presence of temperature dependent terms in the heat input matrix, $[Q]$.

Conductance between two nodes of Different Materials with Interfacial Contact Thermal Resistance can be expressed as

$$Y_{ij} = \frac{A_{ij}}{\frac{l_i}{k_i} + \frac{1}{h_{ct}} + \frac{l_j}{k_j}} \quad (11A)$$

where

l = the length of the conduction path in a node from surface to centroid

k = the thermal conductivity

h_{ct} = the thermal contact resistance at the node's interface

A_{ij} = the cross sectional area of the conduction path between the i-th and j-th nodes

The subscripts, of course, refer to the i-th and j-th nodes, as appropriate.

Conductance Between Two Radiating Nodes can be expressed as

$$Y_{ij} = \frac{1}{\frac{l_i}{A_{ix} k_i} + \frac{1}{A_{rad,ij} h_{rad,ij}} + \frac{l_j}{A_{ix} k_j}} \quad (12A)$$

where

A_{-x} = the area to associated with the conductive part of the part in the ___-th node

$A_{rad,ij}$ = an area to be in agreement with the configuration factor used to evaluate $h_{rad,ij}$

$h_{rad,ij}$ = the radiation heat transfer coefficient defined by

$$h_{rad,ij} = F_{ij} \sigma \frac{(T_i^4 - T_j^4)}{(T_i - T_j)} \quad (13A)$$

where

σ = the Stefan-Boltzmann constant, = 1.73×10^{-9} BTU/hr-ft²-R⁴

F_{ij} = the configuration factor for radiative interchange from the i-th to the j-th node

Conductance Between a Convective Fluid Temperature and A Solid Node can be expressed as

$$Y_{ij} = \frac{1}{\frac{1}{A_{cv,ij} h_{cv,ij}} + \frac{l_j}{A_{cn,ij} k_j}} \quad (14A)$$

where

$A_{cv,ij}$ = the area for convective heat transfer between the i-th fluid node and the j-th solid node

$h_{cv,ij}$ = the convective heat transfer coefficient between the i-th and j-th nodes

$A_{cn,ij}$ = the cross section area of the conduction path within the j-th solid node for heat transfer with the i-th fluid node

When the bounding surfaces are close together, the heat transferred is more commonly characterized by a free convective heat transfer coefficient based on the temperature difference between the bounding walls rather than the fluid temperature. This results in an expression for the thermal conductance between the bounding surfaces of the form

$$Y_{ij} = \frac{1}{\frac{l_i}{A_{cv,ij} k_i} + \frac{1}{A_{cv,ij} h_{fcv,ij}} + \frac{l_j}{A_{cv,ij} k_j}} \quad (15A)$$

where the symbols have a similar meanings to those in Equation 14A except that

$h_{fcv,ij}$ = the free convective heat transfer coefficient based on bounding wall temperature difference

It should be noted that by suitable deletions from Equations (11A), (12A), (13A), or (15A), virtually any heat transfer node can be simulated, including the pseudo-surface-flux of Equation (10A). Distinct cross sectional areas have been identified for many of the heat flows where in practice the same area would be used as characteristic of the entire path length.

A2. Solution by Explicit Finite Difference Method

The basis of the finite difference methods is the representation of the temperature derivatives by the finite-difference approximation

$$T_j \equiv \frac{dT_j}{dT} \approx \frac{T_j' - T_j}{\Delta T} \quad (16A)$$

where the prime indicates that it is the temperature of the j-th node at the end of the time step. We can rewrite Equation (3A), solving for the temperature change of the j-th node as

$$T_j' - T_j = \frac{\Delta T}{C_j} \left\{ \dot{Q}_j''' + \dot{Q}_j'' + \sum_{i=1}^n Y_{ij} T_i - T_j \sum_{i=1}^n Y_{ij} \right\} \quad (17A)$$

Equation 17A is the basic equation for the finite difference methods.

As stated, with all temperatures on the right those existing at the beginning of the time step, Equation (17A) represents one of n independent equations for a system of n nodes. Computation of the temperatures at the end of the time step can be carried out directly, node by node. There is, however, a restriction on the length of time step, ΔT , for which stability of the transient solutions is assured. The maximum length of time step which can be used with the assurance of stable solutions is given by

$$\Delta T \leq \frac{C_j}{Y_{ij}} \quad (18A)$$

for the node which has the smallest value of this ratio. C_j is the thermal capacity of the limiting node and will be small for small volumes and/or low specific heat. Obviously, a system with any physically small nodes or very large conductance is going to have a very short limiting time step.

A3. Solution by Implicit Finite Difference Method

The basis for the implicit method of solution is again Equation (17A). However, all temperatures on the right are considered to be primed

temperatures; that is, those existing at the end of the time step. This formulation leads to a system of n simultaneous equations for a system of n nodes.

The approximation of Equation (16A) can be incorporated into the matrix Equation (4A) and rearranged to yield

$$(\Delta\tau [Y] + [B]) [T'] = \Delta\tau [Q] + [E] [T] \quad (19A)$$

When n is reasonably small, as would be the case for the present application, Equation (19A) can be solved directly to yield

$$[T'] = (\Delta\tau [Y] + [B])^{-1} (\Delta\tau [Q] + [E] [T]) \quad (20A)$$

When n is large, iterative methods are used to calculate the temperature field at the end of the time step. Typical is the Gauss-Seidel matrix sweeping technique wherein improved values of the individual node temperatures are generated with the modified Equation (17A) and immediately substituted in the temperature vector. Convergence is recognized when no temperature is changed more than a prescribed amount during a complete sweep thru the temperature vector. In a problem which is converging slowly, slowness of convergence can be mistaken for actual convergence. The solution is stable for any length time step, however.

Chart 1 compares the explicit and implicit finite difference methods.

A4. Radiation Interchange Factors

Radiation configuration factors for thermal radiation between two surfaces are defined as the fraction of the thermal radiation leaving one surface which is incident on the other surface. For black bodies, the configuration factors are purely geometry dependent. However, for gray bodies the reflections must be considered and, hence, the interchange factor is defined as the net fraction of the total energy which is delivered to the receiver surface after all reflections and re-radiations have been accounted for.

Virtually all standard textbooks on heat transfer give differential forms for the configuration or interchange factors plus a few closed-form analytical values for simple configurations.

Chart 1 - Comparison of the Explicit and Implicit Methods
of Solving the Transient Heat Balance Equations

Method	Advantages	Disadvantages
Explicit	<ol style="list-style-type: none"> 1. Independent equations which can be directly solved. 2. Probable time savings for short transients, especially with rapidly varying boundary conditions. 3. Mathematically more simple. 	<ol style="list-style-type: none"> 1. Must run through entire transient to calculate steady state. 2. Very short time steps required to assure stable solution for system with very small nodes can lead to excessive computer time.
Implicit	<ol style="list-style-type: none"> 1. Solution is stable for any steps. 2. Presence of small nodes is no more demanding of computer time than requirements for actual number of nodes present. 3. Can proceed directly to steady state solution. 	<ol style="list-style-type: none"> 1. Mathematically more demanding. 2. Requires user judgement in recognition of solution convergence.

APPENDIX B
EXAMPLE PROBLEM

To illustrate the basic features of the computer program, the following example problem is shown. The problem consists of a rectangular solid insulated on all but one surface. The remaining surface is bounded by an incident heat flux and radiates to a space environment of -460°F . The problem is to determine the temperature distribution in the solid 60 seconds after the solid, which is initially at a uniform temperature of 100°F , is subjected to the above boundary condition. The node network is chosen as in Figure 4 to give a temperature at both end surfaces, as well as at selected points along its length.

The node dimensions, connections, material properties, boundary temperature, incident heat flux rates, and resulting temperatures are given in Tables (B1) to (B6).

Figure 4. Example Problem Node Network

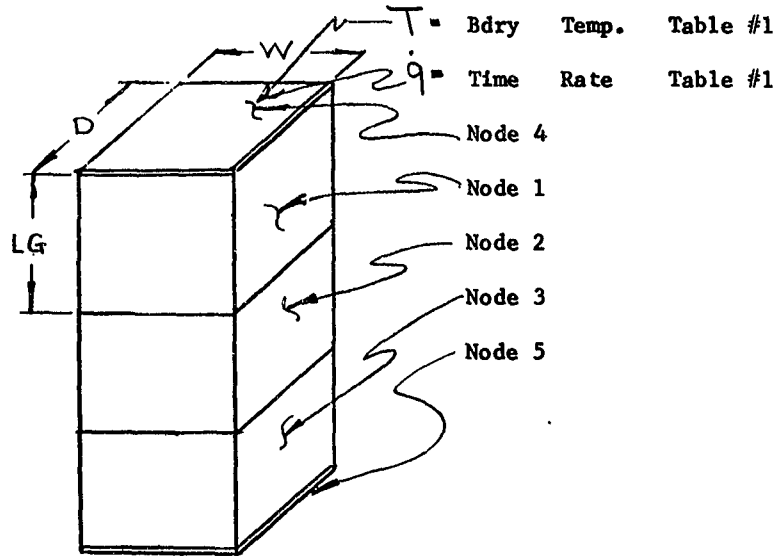


TABLE B1 NODES:

GEOMETRY							
<u>No.</u>	<u>Temp.</u>	<u>Mat'l</u> <u>Code</u>	<u>Width</u> <u>Ft.</u>	<u>Lg</u> <u>Ft.</u>	<u>Depth</u> <u>Ft.</u>	<u>Sur. Flux</u> <u>BTU/hr-ft</u>	<u>Rate</u>
1	100°F	1	1.0	1.0	1.0	0.0	0
2	100°F	2	1.0	1.0	1.0	0.0	0
3	100°F	3	1.0	1.0	1.0	0.0	0
4	100°F	1	1.0	0.0	1.0	7.2 x 10 ⁴	1
5	100°F	2	1.0	0.0	1.0	0.0	0

TABLE B2 MATERIALS PROPERTIES:

<u>No.</u>	<u>ρ</u> <u>lb/ft</u>	<u>T</u> <u>°F</u>	<u>k</u> <u>BTU/hr-ft°F</u>	<u>C_P</u> <u>BTU/lb-°F</u>	<u>ε</u>
1	2.0	-460 to 10 ⁴	20.0	0.25	0.6
2	1.0	-460 to 10 ⁴	10.0	0.5	0.8
3	0.5	-460 to 10 ⁴	5.0	1.0	0.0

TABLE B3 BOUNDARY TEMPERATURES:

<u>Table No. 1</u>	<u>Times</u>	<u>Temps.</u>
	0.0	-460.0
	10 ⁴ sec.	-460.0

TABLE B 4 TIME RATE TABLES:

<u>Table No.</u> 1	<u>Times</u>	<u>Rates</u>
	0	0
	120 sec.	1.0
	6000 sec.	1.0

TABLE B5 CONNECTIONS FOR NODE 1:

<u>Node</u>	<u>To Node</u>	<u>By Type</u>
1	2	Conduction
1	3	Radiation
1	4	Conduction
2	3	Conduction
3	5	Conduction
4	-460°F	Radiation
5	-460°F	Radiation

TABLE B6 RESULTS OF PROGRAM ANALYSIS:

TEMPERATURES AT 60 SEC.

<u>Node</u>	<u>Temperatures °F</u>
1	739.6
2	275.9
3	139.7
4	1379.6
5	139.7

REFERENCES

1. "Program to Develop and Correlate a Method for Investigating The Effects of an Arbitrarily Imposed External Aerodynamic Heating Rate on the Temperature Distribution Through Composite Structures". Aeronca Mfg. Corp. Proposal BCN 2388 to ASD, WPAFB, Ohio, Feb. 1962.
2. Clauss, Francis, J., "First Symposium - Surface Effects on Spacecraft Materials", held at Palo Alto, California, May 1959 sponsored by Air Research & Development Command, U. S. A. F., and Missiles and Space Div., Lockheed Aircraft Corp.
3. LeGalley, Conald P., "Re-Entry and Vehicle Design", Vol. IV of Ballistic Missile and Space Technology, Space Technology Laboratories, Inc., Los Angeles, California, 1960.

Fifth Paper -- "A Transient Thermal Analysis Digital Computer Program," by R. Cannizzaro, Aeronautical Systems Division.

QUESTION: (Mr. Don Glaspie, Boeing) What is the machine running time for a 500 node problem with a structure similar to the one described in your paper.

ANSWER : (Mr. Cannizzaro) The best way to answer this is to refer to a problem which I recently ran and am still running at ASD. It is a rectangular piece of glass from the window of the X-15. It has approximately 385 nodes with 77 boundary temperatures inputted with a Delta T of two seconds for eight seconds and was one material property. This ran for a running time of about five minutes actual machine time. This 800 node problem which I described in the paper on the random vehicle ran for approximately twelve minutes.

QUESTION: (Mr. Herb Johnson, Pratt & Whitney) Is the running time strongly dependent upon the extent and amount of material properties, boundary and other input conditions used? Or, is running time mostly just a function of a number of iterations?

ANSWER : (Mr. Cannizzaro) The best way to answer this is that it is a function of both. I mentioned a thousand node problem, it seemed sort of astounding to mention that many nodes but it can be run if the material properties and the boundary temperature tables are relatively small. So it does depend on the material property table and the amount that is used.

QUESTION: (Mr. D. J. Roberts, General Dynamics) Is there a stability problem with this computer program?

ANSWER : (Mr. Cannizzaro) This is a sort of a controversial question, specially when talking about explicit and

implicit methods, I would say that there is a stability problem but it is not of great consequence. You can get more details on this from the paper itself. It will explain why it is not a real large problem in this program.

QUESTION: (Mr. Donald Ting, Republic Aviation) Who decides the method of computation, explicit or implicit?

ANSWER : (Mr. Cannizzaro) This is up to the user, whichever method he wants to use. The rest of the questions on this card can be answered in the paper.

QUESTION: (Mr. Cannizzaro) One question I was asked during the intermission: Is this program available to industry?

ANSWER : (Mr. Cannizzaro) This program was not directly under contract and we are presently in the process of writing a users manual with a source listing. Hopefully this will come out some time this summer, say, June or July. It will be in the form of a users manual and will include many great details as far as mathematical analysis. We consider that this is what you want. You want to know how to use it and a listing of the programs itself. These other questions can be answered by the paper itself, so I won't go into them and take up any more time.

SESSION IV
THERMAL CONTROL SUBSYSTEMS

CHAIRMAN
E. G. KOEPNICK

THE EFFECT OF ELECTRICAL POTENTIAL ON
BOILING HEAT TRANSFER

by

Michael Markels, Jr., and Robert L. Durfee

Atlantic Research Corporation
Alexandria, Virginia

THE EFFECT OF ELECTRICAL POTENTIAL ON BOILING HEAT TRANSFER

M. Markels, Jr., and R. L. Durfee

I. INTRODUCTION

Early in 1960 a group of French scientists⁽³⁾ found that application of voltage between a liquid and a hot surface during boiling resulted in a significant increase in the boiling heat transfer coefficient. The hot surface used in these experiments was an electrically heated platinum wire of small diameter. In that same year the authors independently demonstrated a similar large effect of applied voltage on boiling heat transfer in experiments using isopropyl alcohol with a steam-heated copper tube as the hot surface. The increase in boiling heat transfer is many times the electrical power required. This gives the effect of a heat transfer amplifier which should have many interesting applications to space vehicle thermal and atmospheric control.

II. APPARATUS AND EXPERIMENTAL

In our experiments, steam heating was used instead of electrical heating so that the effects of voltage on the normal transition and film boiling modes could be easily observed. The over-all temperature difference between the condensing steam and the boiling liquid was substantially the same as the temperature difference between the surface and the liquid boiling point. In fact, steamside coefficients as high as 20,000 B.t.u./hr.-sq.ft.-°F. were probable because of promotion with oleic acid and a high steam velocity which was obtained by allowing up to half the steam supply to blow through the system past the test section. In Figure 1, the assembled apparatus is shown less the steam bleed, which was added later.

Both A. C. power and D. C. power were effective in improving boiling heat transfer (the set-up shown in Figure 1 was for tests with A. C.), but D. C. was somewhat more effective when isopropyl alcohol was used as the boiling liquid. The voltage was applied between the aluminum tank (high potential) and the steam line (ground). Teflon spacers were used to insulate the tank from the 3/8-inch copper tube and to eliminate end effects. The effective length of the heat transfer surface was three inches.

Vaporized liquid was condensed and fed back into the tank through a rotameter. Since the liquid in the tank was maintained at its boiling point by auxiliary heaters, this rotameter reading served as a measure of the heat transfer rate.

The procedure used in operating the apparatus consisted of measuring the amount of liquid vaporized at constant steam pressure for various impressed voltages. Besides the amount of liquid vaporized, the quantities measured included steam pressure, voltage, and amperage.

III. RESULTS AND DISCUSSION

Preliminary heat flux and ΔT measurements at zero voltage were made for comparison with published values. The maximum in the Q/A versus ΔT curve for isopropanol occurred at a ΔT of 60°F., corresponding to a measured Q/A of 87,000 B.t.u./hr.-sq.ft. and a heat transfer coefficient of 1,450 B.t.u./hr.-sq.ft.-°F. These values compare quite well with the measurements reported by Kaulakis and Sherman⁽⁶⁾ of a maximum coefficient of about 1,500 B.t.u./hr.-sq.ft.-°F. at a ΔT of 60°F. for pool boiling isopropanol on a chrome-plated copper tube. For isopropanol boiling on an uncoated copper tube, Dunskus and Westwater⁽⁵⁾ measured a peak Q/A of 90,000 B.t.u./hr.-sq.ft. at a ΔT of 40-50°F. The peak heat flux and the corresponding temperature were found to vary somewhat with the purity of the alcohol and with the surface condition. Similar variations have been observed by many investigators.^(5,9)

The effects of applied voltage on the heat flux versus temperature difference curve is shown on Figure 2. At low voltage only the normal film boiling region was affected, while at the higher voltages the peak heat flux was increased and the corresponding temperature difference shifted until the maximum in the curve was no longer observed.

The data shown on Figure 2 was taken using D. C. voltage with the aluminum tank charged positively and the heating tube at ground potential. Reversing the polarity did not affect the heat transfer rate at a given voltage. The power consumption at the heat fluxes plotted on Figure 2 ranged from 0.0068 watts at 100 volts to 1.95 watts at 1,500 volts in the normal film boiling region. The power consumption in this region was constant for each voltage. At 3,000 volts for a ΔT of 79°F., the electrical

power used was 8.1 watts at a total heat transfer rate of 1,930 watts and an increase in heat transfer over film boiling of 1,830 watts. The electrical power dissipation includes both the power dissipated in the region of vapor formation and the power dissipated in the bulk alcohol. Typically, the electric power dissipated in these two regions were roughly equal in the geometry of our tests.

Alternating current voltage was also used in another test series. Comparison of heat flux measurements at equal values of D. C. and A. C. (rms.) voltage (negligible phase angle for 60 cycle A. C.) showed that the heat flux with D. C. was 10 to 50 per cent higher than with A. C., and that the D. C. dissipated approximately one-third the power required to maintain the A. C. voltage. Frequency traverses from 50 to 5,000 cycles per second were made with A. C. current at various voltages. No resonance frequencies were observed, and there was very little variation of heat flux with frequency in the range covered. At the lowest and highest frequencies, the heat flux tended to decrease slightly with frequency.

At a constant temperature difference of 128°F., which is in the normal film boiling region, the heat flux increased almost linearly with increasing voltage up to 7,000 volts as shown in Figure 3. The electrical resistance of the bulk liquid can be assumed constant at 0.4×10^6 ohms, and the total resistance was approximately twice this value. Therefore, approximately one-half the total voltage of Figure 3 occurred across the region of vapor formation and was effective in increasing heat transfer. At the maximum impressed voltage, the electrical power dissipated in the region of vapor formation was 25 watts which produced an increase in heat transfer of 3,820 watts. This is an "amplification factor" of 154 which

is not often found in heat transfer processes.

Results of tests with isopropanol at somewhat higher voltages and temperature differences are shown on Figure 4. The characteristic maximum and minimum of the zero voltage curve appear at all voltages, although the corresponding temperature differences increased with voltage. These curves indicate that increases in heat transfer obtainable from voltage application are limited by neither voltage nor temperature difference.

Photographs of the boiling process with and without applied voltage are shown on Figures 5, 6, 7, 8, and 9. Figures 5, 6, and 7 show the normal boiling modes for isopropanol, and Figures 8 and 9 show the effect of applied voltage on normal film boiling. The boiling with a fully destabilized vapor film (Figure 9) closely resembled normal nucleate boiling (Figure 5) except that, with the voltage applied, more vapor was visible between the tube and the surface of the liquid and the individual bubbles forming on the heat transfer surface appeared slightly smaller than with no voltage. The partial destabilization of the film shown in Figure 8 occurred both at low voltages and during each buildup to high voltage, as shown by high speed motion pictures. The mode of boiling during partial destabilization closely resembled the normal transition boiling of Figure 6.

Distilled water was also used as the boiling liquid. Direct current voltage was not effective in increasing the boiling heat transfer rate above the normal nucleate peak, but with 60 cycle A. C. results were obtained which were similar to those with alcohol. Data from the water tests are plotted on Figure 10. The voltage which could be applied was limited to about 2,500 volts by sparking. Although the water entering the

system was very pure (2 to 4 megohm/cm. resistivity) its resistivity decreased rapidly to about 0.15 megohm/cm. There is little doubt that heat transfer rates greater than those indicated on Figure 10 could be obtained with more resistive water. One such test in the normal film region reached 4,000 volts without sparking with a measured heat transfer rate of approximately 1.8 times the normal peak.

The results as presented here corroborate the findings of other researchers using fine wires^(3,4) in that a large general effect was observed and film boiling could be completely eliminated by applied voltage. On the other hand the heat transfer rates obtained at high ΔT with alcohol were a factor of two or more higher than the highest obtained on wires, and the voltages used in these tests were orders of magnitude smaller than those used by other researchers. Another point of difference is that much greater increases in heat flux were observed near the nucleate peak on tubes than on wires. These differences may be attributed to the large difference between the wire diameter and the tube diameter.

Thus far no mathematical expression relating heat flux, applied voltage, and system geometry is available; neither does there appear to be a simple mechanistic effect of voltage on the boiling process. Velkoff⁽¹⁰⁾ describes qualitatively two effects which may enter into the phenomenon: (1) Coulomb attraction, and (2) Dielectrophoresis.

Coulomb attraction, or the condenser effect, involves the force of attraction between two plates of a condenser. In stable film boiling, the plates are the solid surface and the liquid-vapor interface. When voltage is applied, a perturbation at the liquid-vapor interface will be

accelerated toward the hot surface, thereby destabilizing the vapor film. It is believed that the breakup of stable film boiling by voltage can only be initiated by the condenser effect.

Dielectrophoresis denotes motion of a dielectric fluid placed in a non-uniform electrical field, caused by induced polarization. When liquid and vapor are present, as in boiling, the liquid tends to move toward the region of greater field strength (normally the heat transfer surface). Vapor bubbles would thus be ejected from the region around a heated fine wire. Dielectrophoresis also occurs in single-phase systems, and can be used to explain increases in convective heat transfer under the influence of voltage whereas the condenser effect cannot.

IV. APPLICATION TO SPACE VEHICLE PROBLEMS

We have discussed a generally applicable means for controlling fluid orientation using electric fields. Depending on the voltage and geometry involved, the orienting force may be described by electrostatic (coulomb) attraction or dielectrophoresis. The results presented illustrate one way in which these forces may be utilized, namely, boiling heat transfer.

The large increase in heat flux, which has been demonstrated, should be useful in many aspects of aero-space vehicle heat transfer problems, specifically in high capacity refrigeration and heating systems, as well as auxiliary power systems. It is especially noteworthy that the electrical forces are not gravity dependent. Therefore, under reduced gravity conditions, the relative effectiveness of these electrical forces in improving heat transfer must increase. The importance of this attribute in space vehicle applications is obvious.

We have extended our work to cover conductive liquids and find that, as one would expect, the improvement in heat transfer depends upon the potential difference available across the vaporization zone. Where highly conductive liquids, such as liquid metals, are involved, it may be necessary to insulate the heat transfer surface electrically in order to maintain the potential differences required. We hope to further investigate this problem during the coming year.

Condensation of vapors is another process which must be carried out at high efficiency under reduced gravity in space vehicles. The problem here is to remove the condensate from the heat transfer surface in order to promote high heat transfer coefficients and to prevent such low

fluid temperature that solid formation becomes a problem. This may be done by positioning an electrode within the condenser tube. Dielectrophoresis can then draw the liquid formed to the central electrode leaving the heat transfer surface relatively liquid free and available for maximum heat transfer. It should be noted that this effect, while predictable from our present knowledge of the boiling process, is yet to be demonstrated in the laboratory.

Electrical forces can also be used to orient fluids under zero gravity conditions without the added complication of significant heat fluxes. In this application it competes with surface tension as an orienting force. It would appear from the success reported by NASA with the surface tension approach that the added complexity of the electrode processes could not compete for most applications. (7)

The solution of new problems involving fluid orientation and heat transfer are implicit in space vehicle thermal and atmospheric control. New approaches, such as those outlined here should prove useful in the development of suitable apparatus and methods.

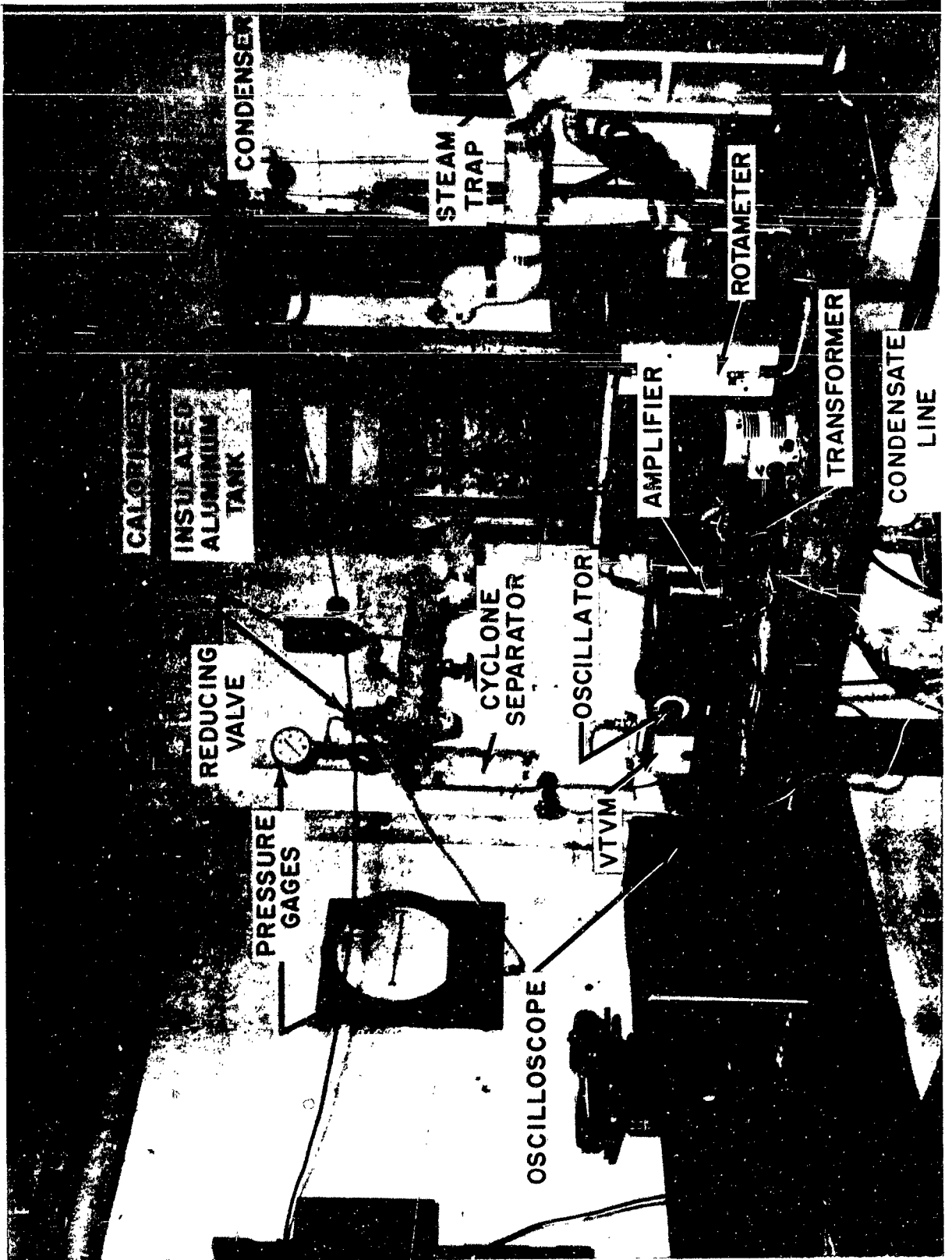


Figure 1. Assembled Apparatus for Boiling Heat Transfer Experiments

V. BIBLIOGRAPHY

1. Bankoff, S. G., A.I.Ch.E. Journal, 8, No. 1, pp. 63-65, (1962).
2. Bankoff, S. G., and U. S. Mehra, "A Quenching Theory for Transition Boiling," Personal Communication, March, 1962, (Chem. Engr. Dept., Northwestern Univ., Evanston, Ill.)
3. Bochirol, L., E. Bonjour, and L. Weil, Compte Rendus, 4 Jan., 1960, pp. 76-78.
4. Choi, H. Y., Personal Communication, Boston, Mass., April 5, 1962 (Ph.D. thesis, Dept. of Mech. Engr., Tufts Univ.).
5. Dunskus, T., and J. W. Westwater, "The Effect of Trace Additives on the Heat Transfer to Boiling Isopropanol," Fourth Heat Transfer Conf. (A.I.Ch.E. - A.S.M.E.), Buffalo, N. Y., August 14-17, 1960.
6. Kaulakis, A. F., and L. M. Sherman, S. B. thesis in Chemical Engineering, Massachusetts Institute of Technology, 1951.
7. Petrash, Donald A., Robert F. Zappa, and Edward W. Otto, Technical Note D-1197, National Aeronautics and Space Administration, Washington, April, 1962.
8. Pohl, H. A., J. Appl. Phys., 29, pp. 1182-8 (1958).
9. Stock, B. J., "Observations on Transition Boiling Heat Transfer Phenomena," Argonne National Laboratory Report No. 6175 (1960).
10. Velkoff, H. R., "Electrofluidmechanics: A Study of Electrokinetic Actions in Fluids," ASD-TR-61-642, ASD, Wright-Patterson Air Force Base, Ohio (1961).

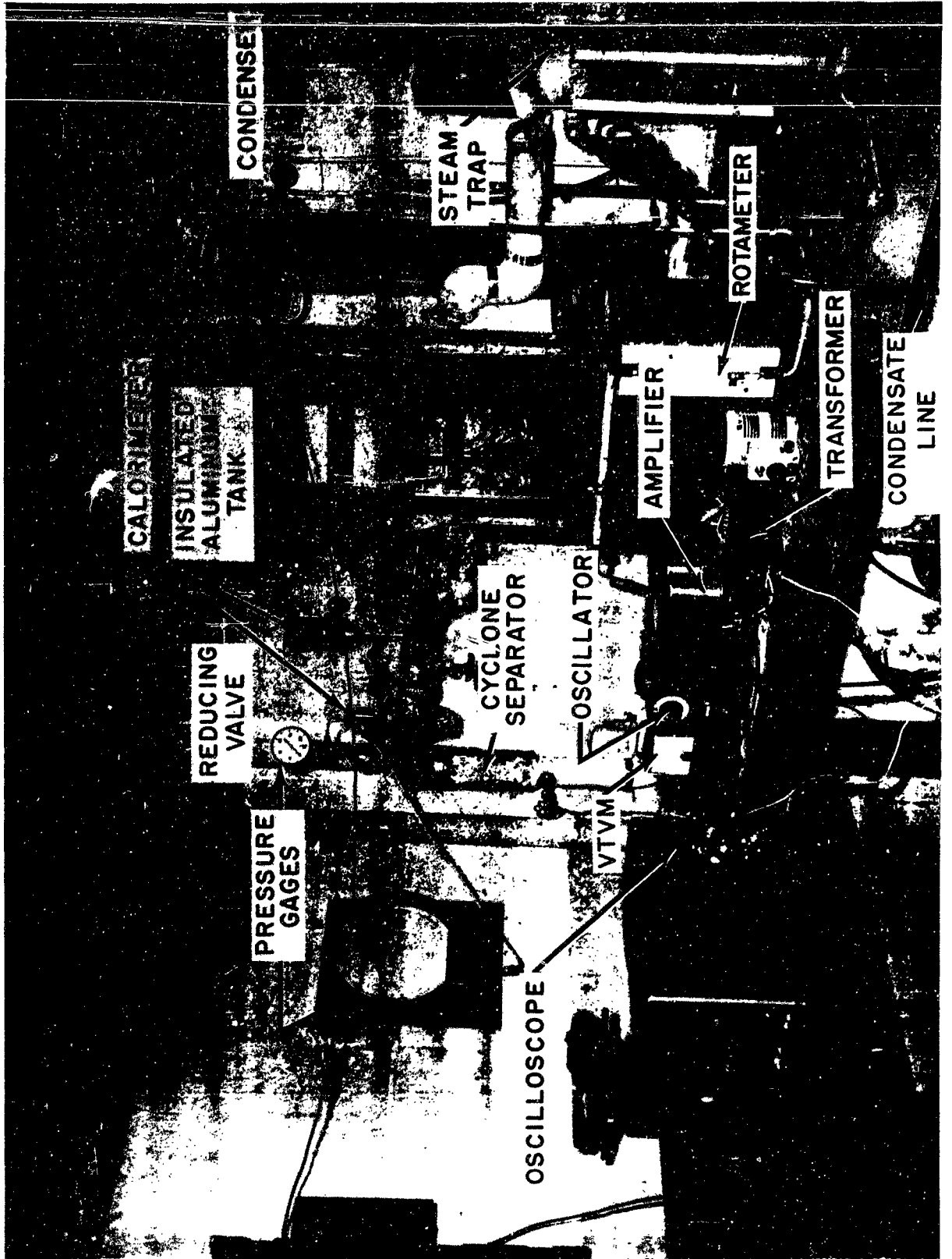
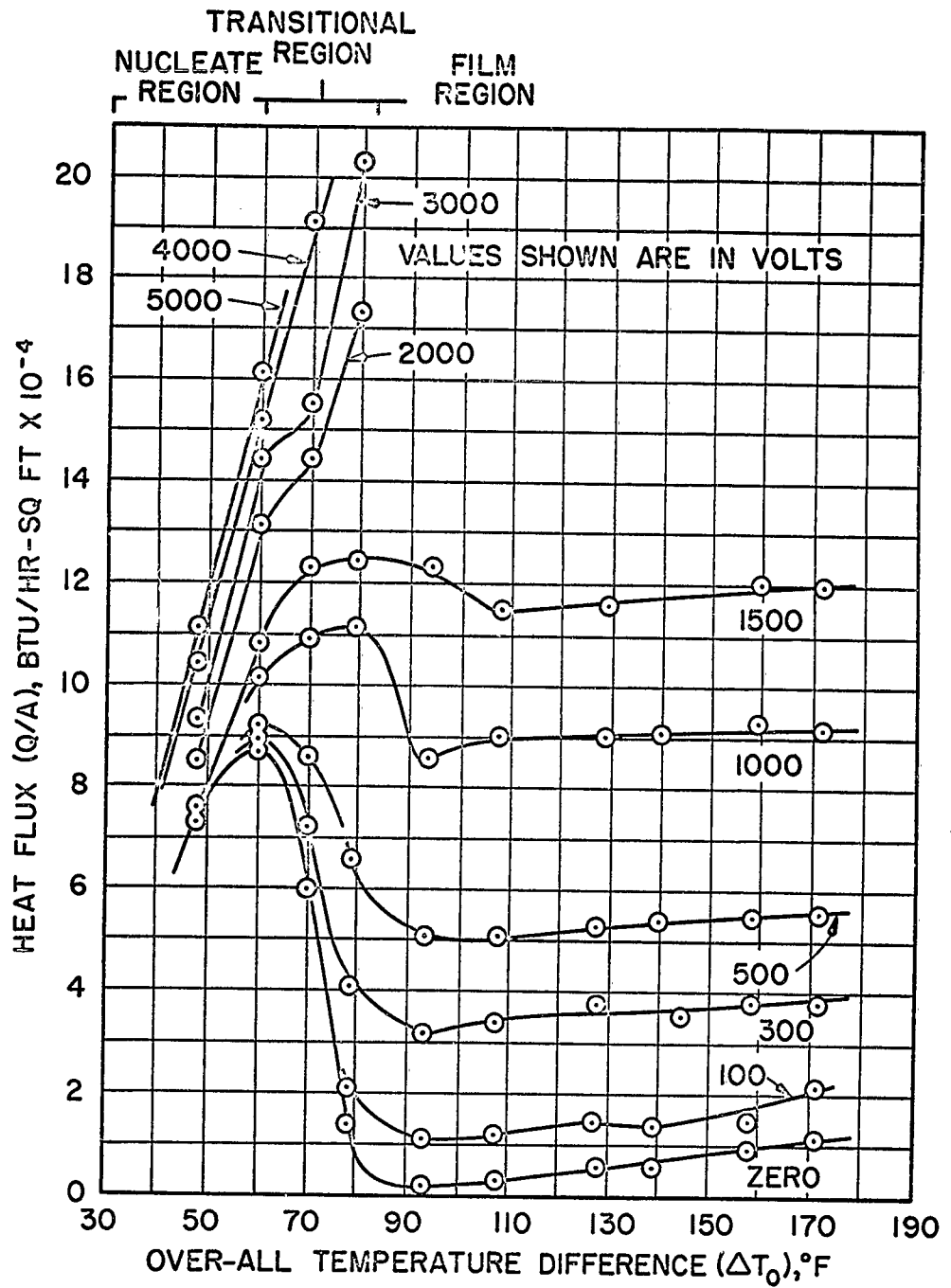
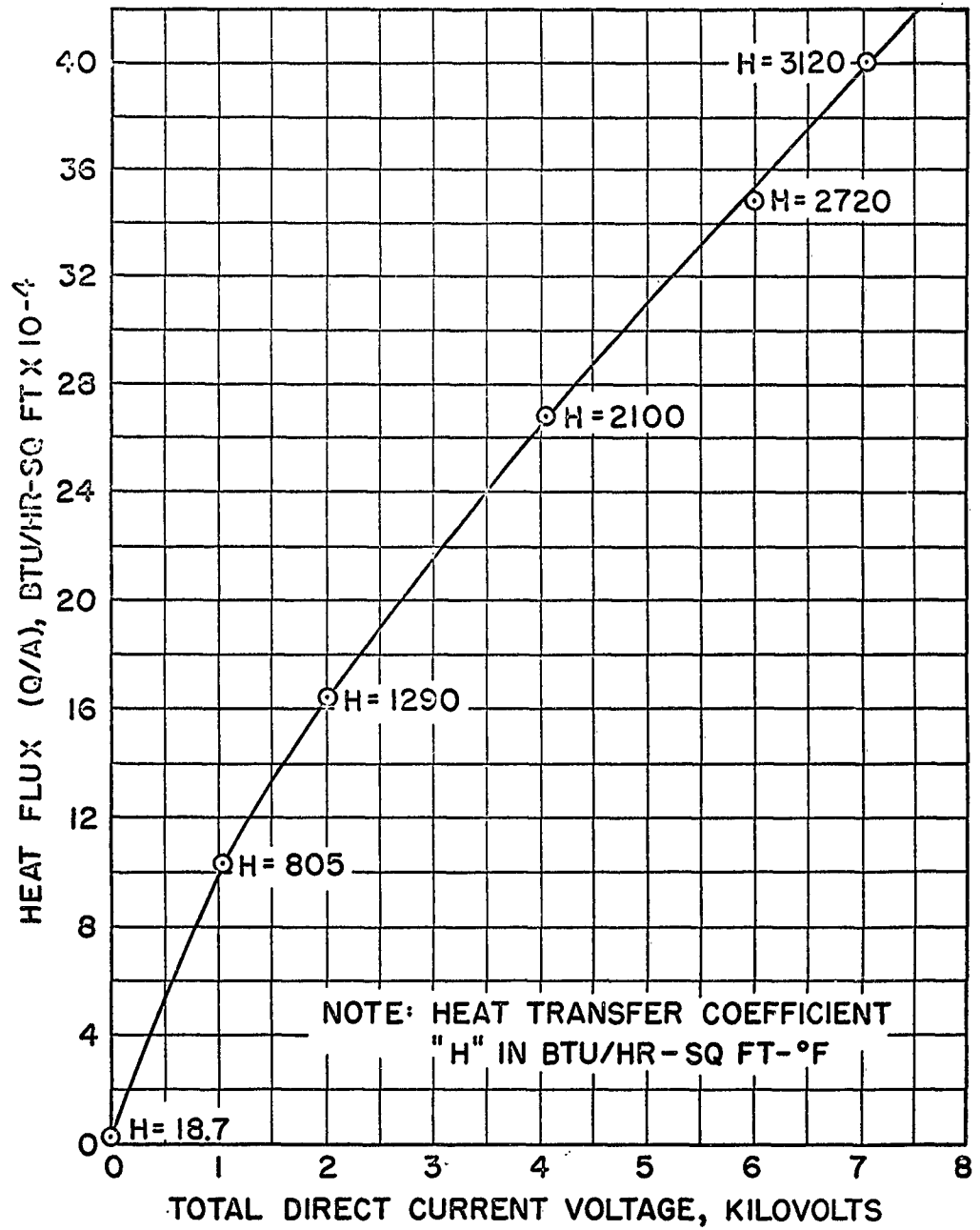


Figure 1. Assembled Apparatus for Boiling Heat Transfer Experiments



Isopropanol at One Atmosphere

Figure 2. Effect of D. C. Voltage on Pool Boiling Heat Transfer



Pool Boiling Isopropanol at One Atmosphere

Figure 3. Effect of D. C. Voltage on Heat Transfer in the Normal Film Boiling Region ($\Delta T_0=1280^\circ\text{F}$)

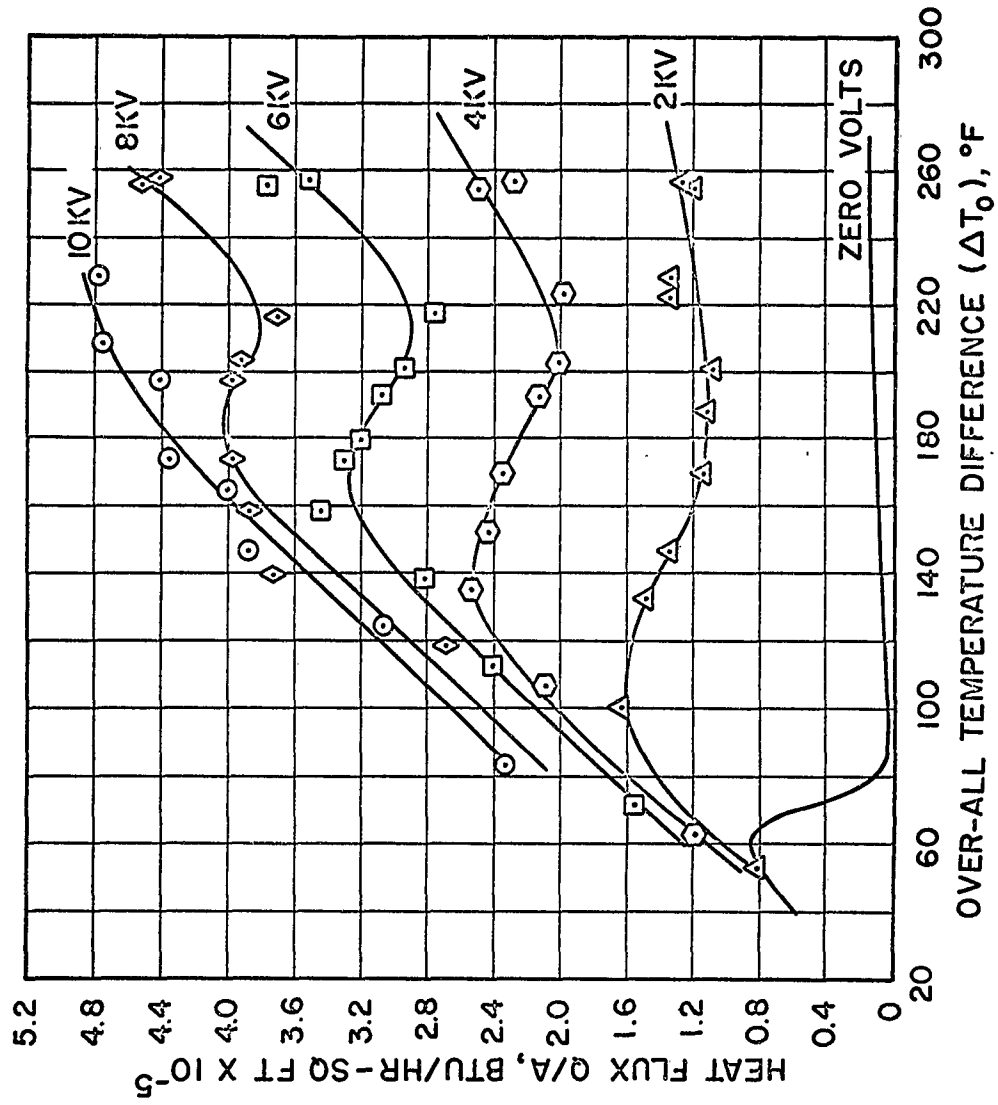


Figure 4. Effect of D. C. Voltage on Heat Transfer to Isopropanol at Over-all Temperature Differences up to 260° F

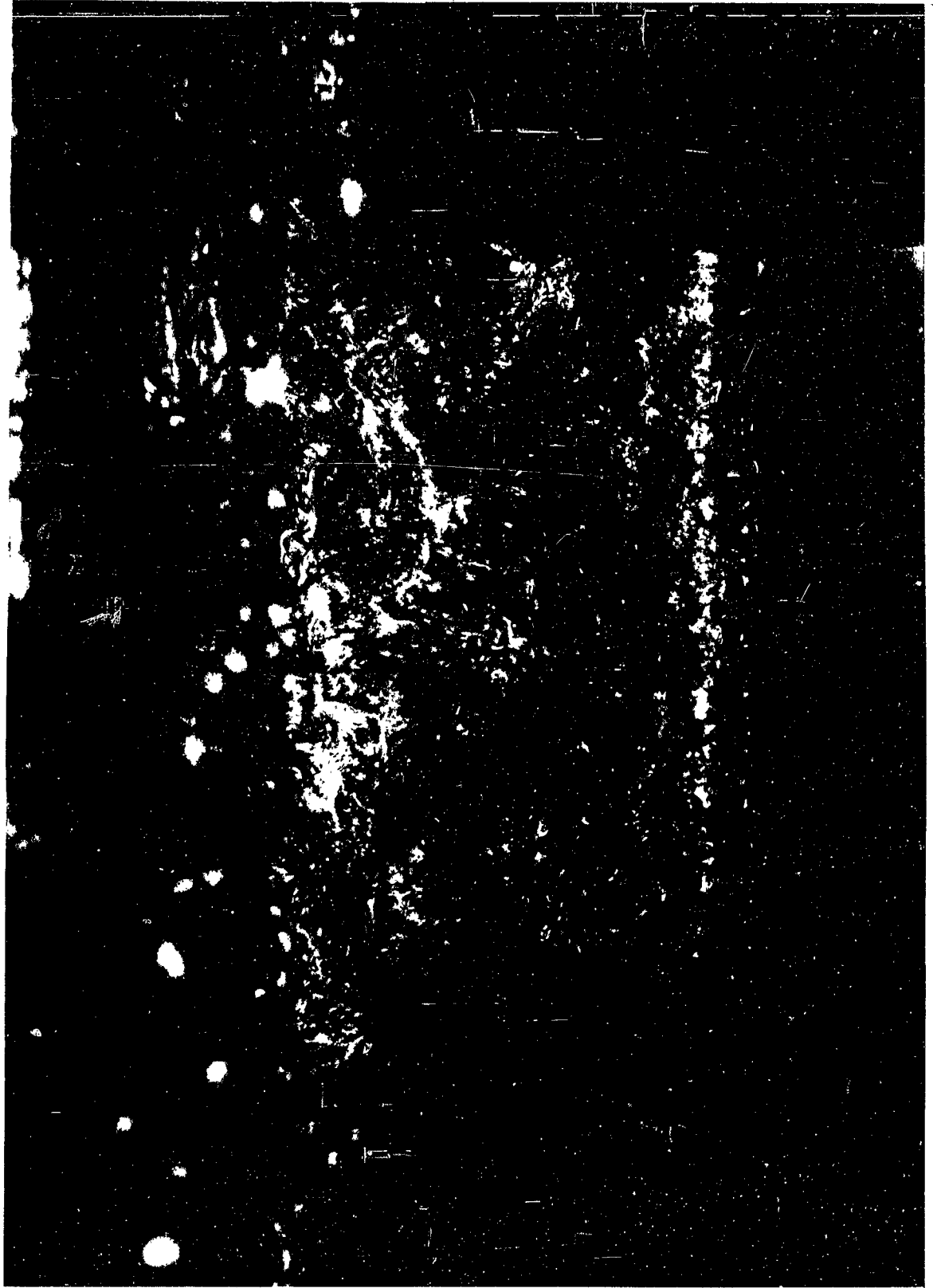


Figure 5. Normal Nucleate Boiling of Isopropanol ($\Delta T_o = 60^\circ\text{F.}$)

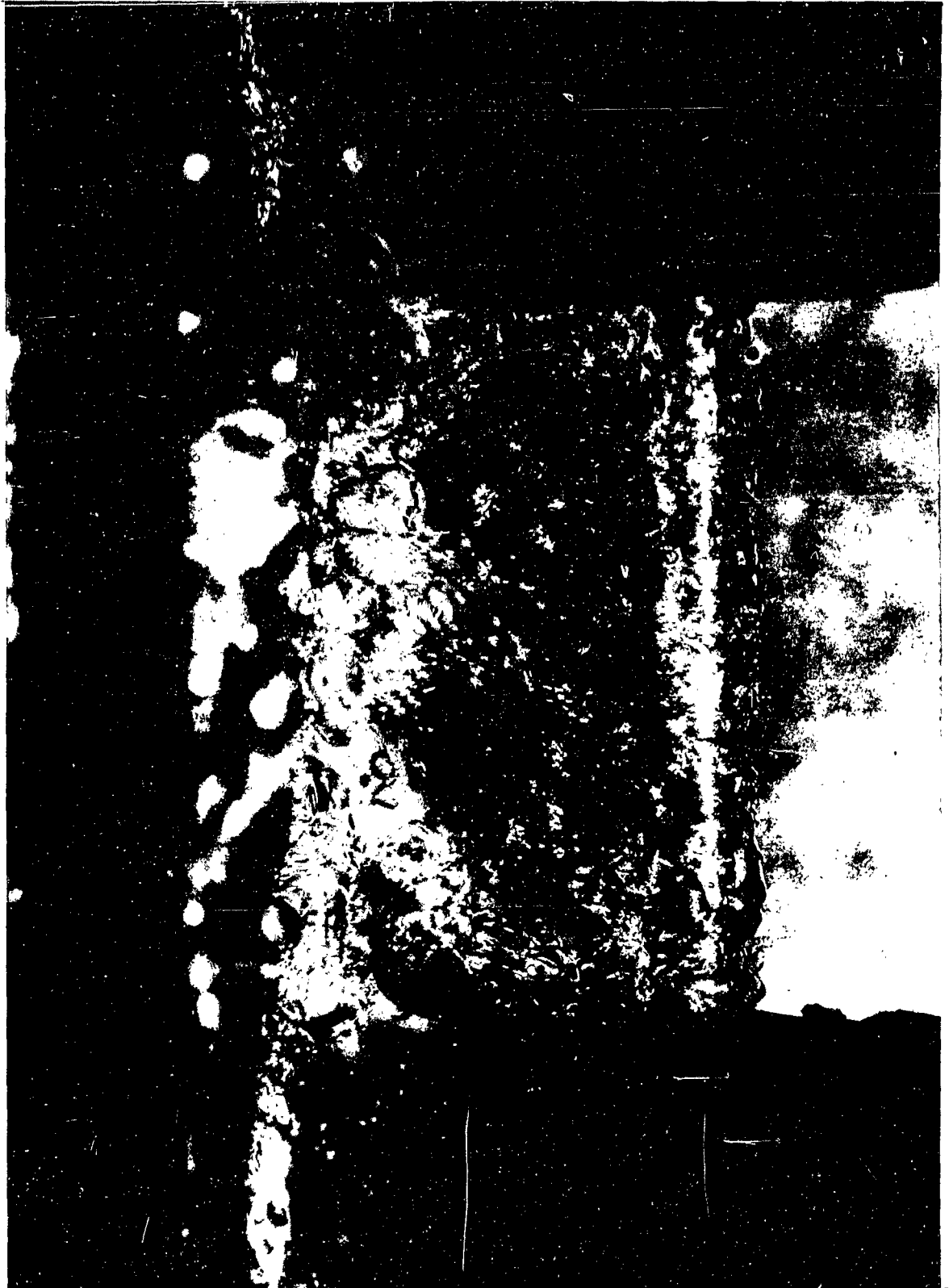


Figure 6. Normal Transitional Boiling of Isopropanol ($\Delta T_0 = 75^\circ\text{F.}$)

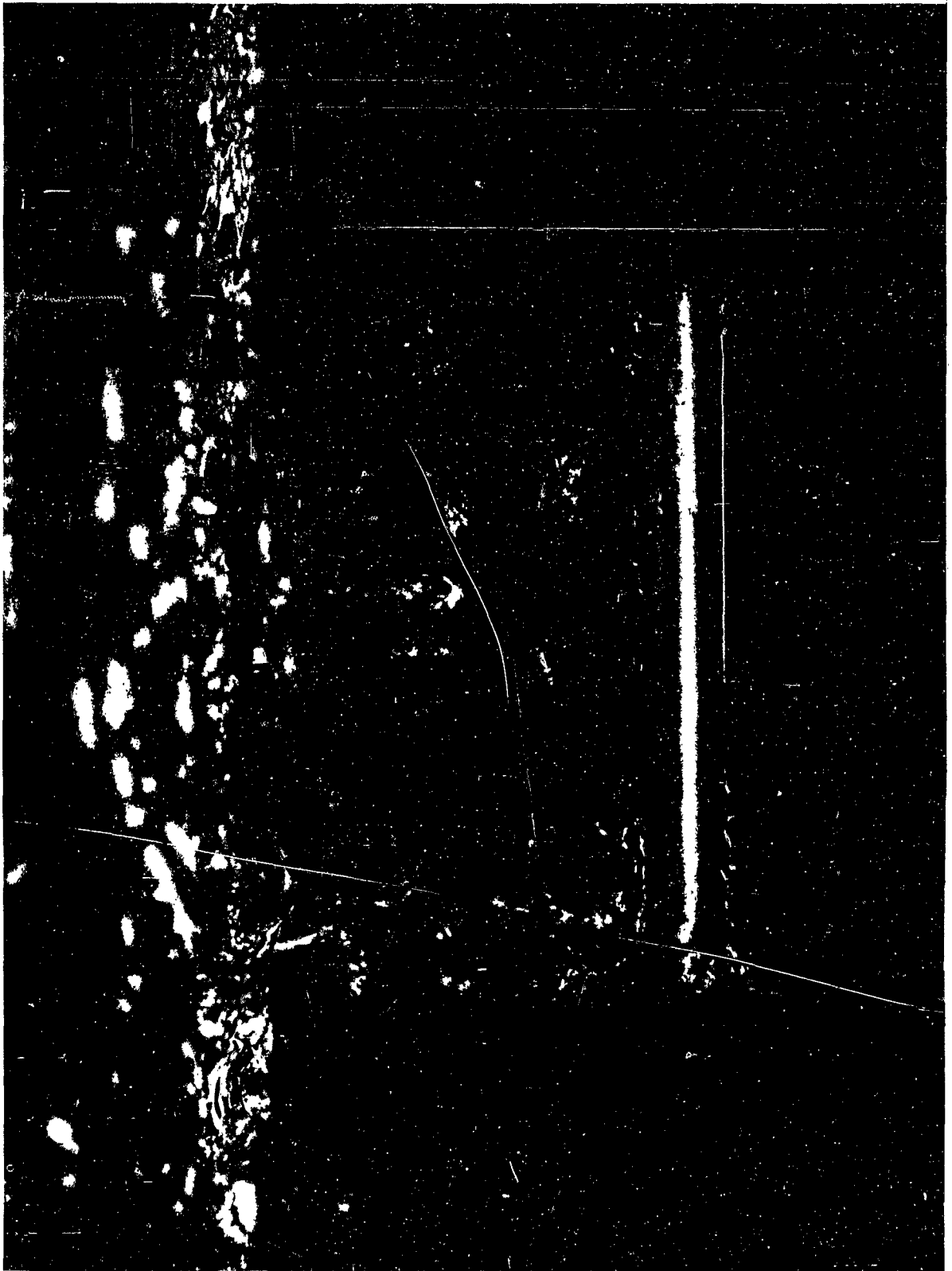


Figure 7. Normal Film Boiling of Isopropanol ($\Delta T_0 = 115^\circ\text{F.}$)



Figure 8. Electrostatic Effect: Film Partially Broken
During Voltage Build-Up ($\Delta T_0 = 87^\circ\text{F.}$)



Figure 9. Electrostatic Effect: Film Fully Broken by
1000 Volts D. C. for Isopropanol ($\Delta T_0 = 87^\circ\text{F}.$)

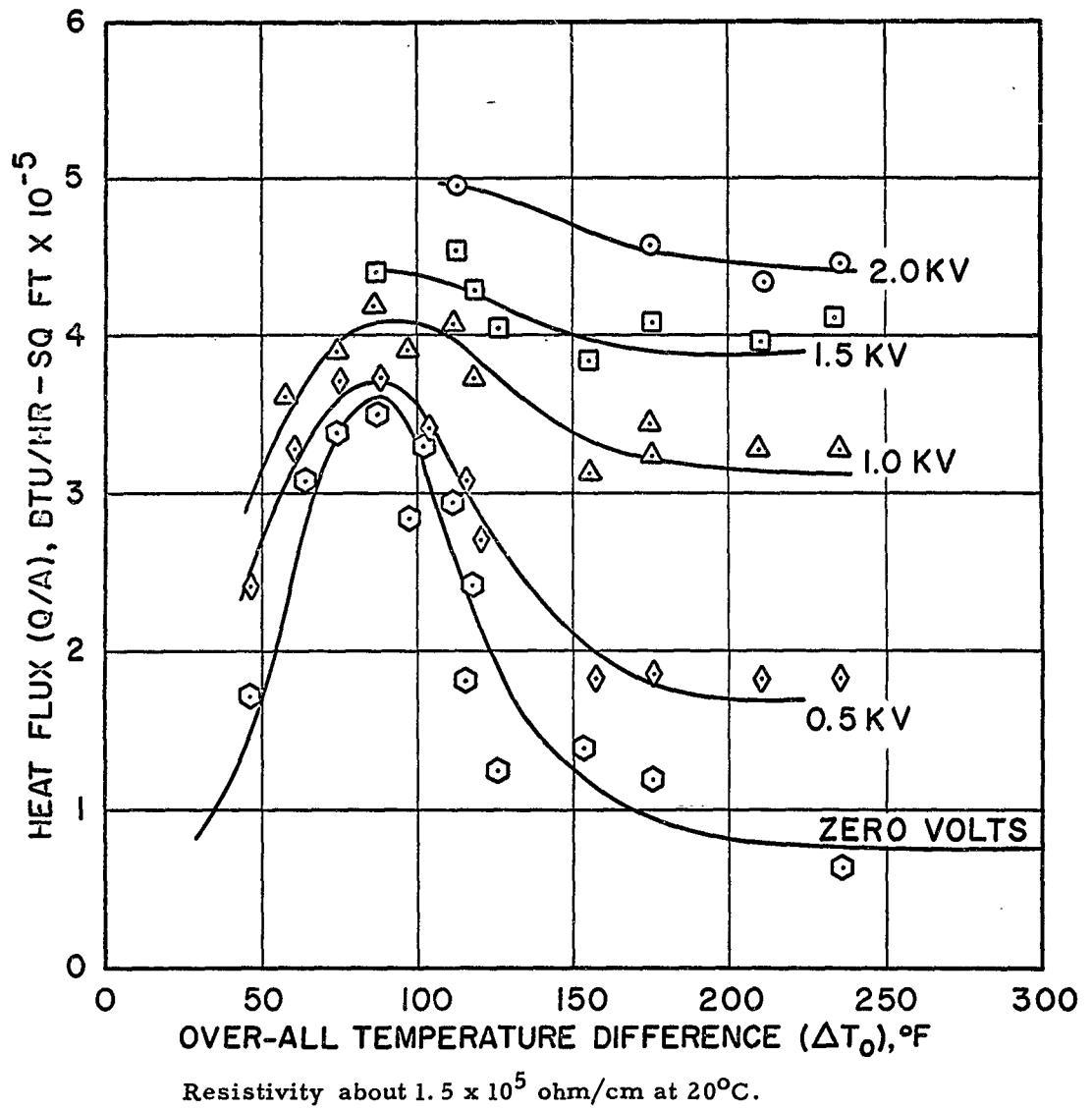


Figure 10. Effect of Applied A.C. Voltage on Boiling Heat Transfer to Distilled Water

QUESTION & ANSWER PERIOD

SESSION IV -- Thermal Control Subsystems

First Paper -- "Effect of Electrical Potential on Boiling Heat Transfer," by Dr. Markels, Atlantic Research.

QUESTION: (Mr. Rayburn, Raytheon) This method of increasing heat transfer would seem especially promising for certain electrical equipment; namely, high power microwave tubes. I am interested in your opinions regarding such an application?

ANSWER : (Dr. Markels) I have only seen an electron tube of this kind once and I am not personally familiar with the problems involved there, although I understand that high speed fluxes are required in the small channels that are available in the geometry of the tube. I would think that this would be an excellent place for it to utilize a phenomena such as we have discussed today. Actually the kind of application that one might look for as far as heat transfer improvement, is one in which you are looking for a very high performance device where space is limited, where weight is limited. It is not the kind of a thing you want for your home furnace or something of that kind.

QUESTION: (Mr. Byke, Douglas) Can you speculate on the effects of zero G on this phenomena?

ANSWER : (Dr. Markels) Yes, we have thought about this considerably. Actually what we would expect here is that as one goes to lower and lower G forces, the maximum from the Q/A, versus Delta T curve would continually decrease. The effect when one is using the electrical energy amounts to a pseudo G force around a heat transfer surface, and of course, would not be gravity dependent; therefore we would expect that the relative improvement that one might get as the

ordinary gravity is reduced by the addition of electric power would considerably increase.

QUESTION: (Mr. E. Zara, ASD) In your converted dynamic system, do you intend to take measurements of the reported increase in apparent viscosity which can cause a larger pressure drop?

ANSWER : (Dr. Markels) Yes, in our closed system we have inlet and outlet pressures recorded. We, of course, expect that increased pressure drop will occur. Just the increase in total velocity of the emitted fluid due to the much lower density as you increase heat transfer will give you an acceleration term by itself which will increase pressure drop. These are the results that we have seen so far which just occurred late last week and early this week, so all I can tell you is that by walking by and looking at the pressure gauges, the increase pressure drop was no more than might be accounted for by ordinary dynamic pressures of the ones I just mentioned.

QUESTION: (Mr. Fried, General Electric) Have you observed the effects of heat transfer surface property variations as a result of the electric field application?

ANSWER : (Dr. Markels) Now there are two kinds of properties that one might look for here. One is just plain deterioration, for instance, of the heat transfer surface and with this chrome plated copper tube the only thing that we get is some junk, you might call it, coming out of the tube and fouling up the surface. The usual thing that one might expect from a slight impurity is very rapid deterioration of the processes we had here. Now as far as thing like that are concerned, from what we can tell in looking at the pictures, the active site considerations pretty much leave you as far as limitations on the heat transfer process when you get in the vicinity of the original peak heat flux. What happens is that as you increase Delta T you activate more and more sites until

essentially when you are near the peak the entire tube or the entire heat transfer surface is essentially activated.

QUESTION: (Mr. Fried, General Electric) Have you been able to reproduce good reproducibility of results?

ANSWER : (Dr. Markels) I think the answer is in the context of heat transfer experiments of this kind. The answer is yes. As you know, surface phenomena, slight changes in the fluid that you are using can always make a difference in the results and you usually consider that plus or minus ten per cent is quite adequate for research of this kind. Our results are that good and better, and so we are quite pleased with the reproducibility involved.

QUESTION: (Mr. Koplow, Vitro Laboratories) Would you explain the reason for the apparent difference between the effects of an electric field on the boiling mechanism? In Dr. Choi's pictures we saw a return to nucleate boiling, while in your pictures we saw very clearly a destabilization of the film, but no return to nucleate boiling?

ANSWER : (Dr. Markels) I think here, well, here are two things: First of all, in the films that I showed the current was not taken off. There were just two modes. The first one, the film boiling mode and the second one the mode with the electric field. Had we also flipped the switch and cut the power off, we would have immediately returned to the film boiling mode. Now we think there is a difference in the relative importance of these two phenomena, that being due to the geometric difference in Dr. Choi's work and ours, and this I think, is the reason that you see these spurts of vapor coming from Dr. Choi's experiments, whereas in our case what you see is this great bed of unstable bubbles which then radiate from the heat transfer surface.

QUESTION: (Mr. Koplou, Vitro Laboratories) Would you expect film destabilization or nucleate boiling to be the effect of an increased gravitational field?

ANSWER : (Dr. Markels) Well what we expect here is essentially this: If there is no destabilizing force, such as a gravitational field for instance, tending to move liquid to the heat transfer surface in the limit one would expect, that very low heat fluxes will immediately provide a film boiling situation. Gravity, itself, then is destabilizing since the bouyancy forces provide a mechanism for moving the vapor and for destabilizing the situation as we go to higher and higher gravity fields. It has now been amply demonstrated that what happens is when one continues up along the Q over Delta T curve to higher and higher peaks, one stays in a nucleate boiling regime; whereas, when one adds the electrical field, this is a different type of destabilizing mechanism, then one gets a somewnat different phenomena, but certainly looking at it just grossly, you have similarities in that you have very large vapor generations.

THERMOELECTRIC TEMPERATURE CONTROL
IN
SATELLITES

By
C. W. Usiskin

RADIO CORPORATION OF AMERICA
Princeton, N. J.

ASD-TDR-63-260

THERMOELECTRIC TEMPERATURE CONTROL IN SATELLITES

by C. W. Usiskin

ABSTRACT

The art of spacecraft temperature control involves a number of different types of thermal problems. Thermoelectric devices, due to their versatility and simplicity, can be useful in solving many of these problems.

To date, the limited power capability of the spacecraft power supply has prevented the use of thermoelectric devices. However, with the advent of large spacecraft and improved thermoelectric modules, the use of these devices is becoming feasible.

This paper analyzes several common satellite component control problems and establishes the usefulness of thermoelectric control. In addition, the experiments carried out to demonstrate the feasibility of using thermoelectric modules as a thermal switch are discussed in detail. This application is very interesting since it requires no power.

1. INTRODUCTION

The trend in satellite thermal control is toward the increasing use of active thermal controllers. This is due to problems associated with the increasing complexity of new spacecraft systems, and to the larger powers now dissipated in the payload and in some individual components. A complex system requires that the reliability of each of its components be higher than a simple system if the overall reliability is to remain the same. In order to achieve higher component reliability, it is necessary to maintain the component at near its optimum operating temperature. Higher payload power usually means a more uneven power profile. In order to maintain the payload at a constant temperature, heat must be rejected from the payload at a greater rate during the periods of high-power use, and must be conserved during periods of low-power use.

Thermoelectric temperature control devices are, in many respects, ideally suited for use in satellites. They are light, very small, simple in construction, and require very simple control electronics. One of the main drawbacks to the use of devices of this nature has been that all satellites thus far have had extremely limited power capabilities. All previous thermal controllers have required no

electrical energy for operation. When larger satellite power supplies become available, thermoelectric devices will probably be used in a number of rather specialized ways.

Thermoelectric devices are now used on the ground to cool individual electronic components. It is likely that the first use of thermoelectric devices in satellites will also be to control the temperature of individual components. Many of the studies done to optimize various aspects of thermoelectric heat pumps are not applicable due to the wide change in thermal conditions that occurs in satellites. For many cases a few simple fundamental concepts will be quite adequate to size a thermoelectric module. Further refinements will probably best be done by tests on specific thermal models.

An interesting application of thermoelectric modules, which requires no power is investigated in this paper. The basic principle is the change of thermal conductivity between a short circuited and open circuited thermoelectric module. This change comes from the increased thermal conductivity due to the energy transport of charged carriers in the short circuited device. The change of thermal conductivity is shown to be proportional to the figure of merit of the semiconductor material. The change of the thermal conductivity of a module is used to control the heat flow to either the bulk of the payload in the case of component control, or to outer space when the payload temperature as a whole is controlled.

2. FUNDAMENTALS OF THERMOELECTRIC HEAT PUMPS

A frequent problem in satellite design is maintaining a component within a narrow temperature range while the main payload varies between much wide temperature limits. To further complicate the problem, the internal heat generation of the component will frequently vary. For complex control problems of this type, thermoelectric modules are very well suited. The direction of the thermoelectric pumping action can be changed by simply changing the direction of the current, making it possible to use the same module to heat up a component and to cool it down.

For components which are small compared to the rest of the payload, the payload can be considered a heat sink. Figure 1 shows the model which will be used to analyze the component temperature control problem.

The basic equations for steady-state heat balance and power requirements for the model illustrated in Figure 1 are

$$Q = \alpha T_1 I - \frac{1}{2} I^2 R - K(T_0 - T_1) \quad (1)$$

and

$$P = I \left[\alpha (T_0 - T_1) + I(R+r) \right], \quad (2)$$

where

- Q is electrical heat dissipation in the sinks,
- $T_0 T_1$ is temperature of the payload (sink) and component,
- α is the Seebeck coefficient,
- R is resistance of T/E module,
- r is external resistance of T/E module,
- I is the current through the module, and
- K is total effective conductive coupling.

The most standard treatment of these equations is to find the value of I which makes the quantity Q/P a maximum for a given temperature difference (see Reference 1). In most satellite applications, conditions change too much to use such a simple approach. Solving for P in terms of Q results in the following useful relation.

$$P/Q_{\max} = C_0 + C_1 \beta^2 - (C_0 + C_1) \beta \quad (3)$$

where

$$Q_{\max} = (\alpha T_1)^2 / R$$

$$C_0 = T_0 / T_1 + r/R$$

$$C_1 = 1 + r/R$$

$$\beta = \left[1 - \frac{2(Q + K(T_0 - T_1))}{Q_{\max}} \right]^{1/2}$$

The quantity $\frac{Q_{\max}}{2}$ is the maximum amount of heat a thermoelectric device can pump across a zero temperature gradient. It is a useful quantity to get a feel for the size of heat load a given module can handle.

From Equation 3 certain relations become immediately obvious. For Q positive, the maximum amount of heat which can be pumped occurs when $\beta = 0$.

Hence

$$Q \leq \frac{Q_{\max}}{2} + K(T_1 - T_0)$$

$$P \leq \frac{T_0}{T_1} Q_{\max}$$

$$(T_0 - T_1)_{\max} = \frac{Q_{\max}}{2K} = \frac{ZT_1^2}{2}$$

where

$$\bar{Z} = \text{effective figure of merit.}$$

If the quantity $|Q + K(T_0 - T_1)|$ is small compared to $\frac{Q_{\max}}{2}$, then a useful approximation can be made to reduce Equation 3 to the following form.

$$\frac{P}{Q + K(T_0 - T_1)} = \frac{T_0}{T_1} - 1 + \frac{Q + K(T_0 - T_1)}{Q_{\max}} \left(\frac{1 + T_0/T_1}{2} \right) + \dots \quad (4)$$

The first term in this expression represents the maximum Carnot pumping efficiency. The second and higher order terms represent a device degradation due to material effects. The higher the figure of merit, the greater the value of Q_{\max} and hence the smaller the device degradation.

Thermoelectric cooling modules are available from many manufacturers. Many of these modules contain 10 or more couples in a single stage. These modules have, in general, required high d-c currents in the range of 10 to 30 amperes. Recently, the design trend has been to produce as small an element as possible to reduce the required current. The current which produces maximum temperature gradients and maximum pumping has been reduced in some modules to as low as one ampere.

The quantity Q_{\max} can be calculated from data supplied by the manufacturer in the following manner. Most manufacturers give a series of temperature-difference-amounts of heat pumped. For a constant current, the difference in the temperature differences, Δ (ΔT), for two values of Q will determine the thermal conductivity, K , directly from Equation 1. The maximum temperature difference with no load determines the figure of merit, Z . Once K and Z are known Q_{\max} is easily calculated. For most modules, the total Q_{\max} is between 5 and 10 watts. Figure 2

shows the actual Q_{\max} for several modules computed on a per couple basis. An attempt was made to compare this data with what might be expected from elements with $Z = 2.2 \cdot 10^{-3} \text{ }^\circ\text{K}^{-1}$, and $K = 0.02$ watts per degree K (reasonable values for Bi_2Te_3 , see Reference 2). Since the data on element size was poor for most modules, the comparison is only qualitative in nature.

In order to better understand the type of problems that a satellite thermoelectric heat pump system would be required to solve, consider a satellite which has a sun time which varies between 60 and 100 percent of the total orbit time. Due to this variation, the temperature of the payload goes down to -10 degrees C for low-sun-time orbits at night, while in the daytime the temperature of the payload rises to 25 degrees C. The batteries in this hypothetical satellite must have long life and hence should be kept within the temperature range of 5 to 25 degrees C. In addition to the payload temperature change, the internal heat dissipation of the battery changes due to the variation in the state of charge. The variation in power is assumed to be from 5 to 20 watts. A first approximation for the design of the control module would be to size the module so that when the payload is at the minimum temperature (-10 degrees C) and the power dissipation in the battery is an average 15 watts, the battery temperature would be the minimum 5 degrees C without any applied power to the module. This sizes the module thermal conductivity as 1 watt per degree C. For most practical modules, the effective figure of merit is conservatively about $1 \times 10^{-3} \text{ }^\circ\text{K}^{-1}$. This immediately sizes Q_{\max} as 45 watts for $T_1 = 300^\circ\text{K}$. Since Q is appreciably smaller than 45 watts, Equation 4 can be used.

The maximum amount of power required to keep the batteries warm occurs when the payload is at -10 degrees C and the batteries dissipate only 5 watts. Figure 3 shows the curve of power required to warm the batteries as a function of the payload temperature. On the other hand, when Q is above 15 watts, power is never required to warm the batteries. The shaded area shown to the right on Figure 3 is the envelope of curves for Q between 5 and 15 watts. The maximum amount of power required to keep the batteries cool occurs when the batteries dissipate 20 watts and the payload is at 25 degrees C. The curve of power required to cool the batteries when 20 watts are dissipated as a function of payload temperature is also shown in Figure 3. From this curve and a prediction of the time history of payload temperature and battery power, a good estimate can be made of the average power required. By changing the value of K and Q_{\max} an optimum design for a given satellite can be achieved.

3. THERMOELECTRIC THERMAL SWITCH

In order to actively control the temperature of a satellite payload, it is necessary to alter the amount of thermal radiation from the payload to space. This is done in many satellites by mechanically moving a shutter which changes the radiation coupling between the payload and space. Quite often there are complicated mechanical and reliability problems associated with these heat controllers. A simpler

method of altering the thermal radiation from a satellite would be to change the conduction path from the payload to outside radiation surfaces. High-contact resistances in vacuum prevent this from being done by making or breaking a conduction path mechanically. A thermoelectric module can be used for this type of controller by attaching a radiator to one face of the module and a structural member of the payload to the other face. Thus heat must pass through the module before it is radiated to space. The conduction path can be increased or decreased by shorting or opening of the module circuit by means of a thermostat.

a. Effective Thermal Conductivity

The effective thermal conductivity for thermoelectric modules is defined here as the total heat transported divided by the temperature difference across the module. This can be found in terms of thermodynamic properties by setting up the energy balances for open circuited and short circuited devices. When the module is open circuited the heat transfer is simply

$$q_{oc} = K (T_1 - T_2) \quad (5)$$

The heat transfer when the module is short circuited is

$$q_{sc} = K (T_1 - T_2) - \frac{I_{sc}^2 R}{2} + I_{sc} T_2 \quad (6)$$

where

$$I_{sc} = \frac{(T_1 - T_2)}{R}$$

This expression for q can be reduced to

$$q_{sc} = K(T_1 - T_2) (1 + Z\bar{T}) = K_{eff}(T_1 - T_2) \quad (7)$$

where

$$Z = \frac{\alpha^2}{KR} = \text{figure of merit}$$

and

$$\bar{T} = \frac{T_1 + T_2}{2}$$

The effective conductivity of the short circuited module is just $1 + Z\bar{T}$ times the conductivity of the open circuited module. Theoretically $Z\bar{T}$ can be as

large as 0.8 for room temperature devices. However, for the standard commercial devices which were tested,* the effective change in thermal conductivity indicated a $Z\bar{T}$ of about 0.3. With modules designed without regard to power input requirements, the effective $Z\bar{T}$ could easily be increased.

b. Experimental Verification

In order to test the concept of a thermoelectric thermal switch, an experiment was set up to simulate a satellite component. The component heat input was duplicated by twelve, 10,000 ohm resistors mounted on one face of a Sanyo 1025 module. Power was supplied to the resistors from a standard variarc. The resistors were insulated from the air by one inch of Min K insulation. The experimental setup is shown in Figure 4.

The quantity that we were most interested in measuring in these tests was the control temperature. The control temperature is defined as the difference between the component temperature with the module open circuited and the component temperature with the module short circuited. The control temperature can be expressed in terms of \bar{Z} by use of Equations 5 and 7.

$$\begin{aligned} T_1 - T'_1 &= T_1 - T_0 - (T'_1 - T_0) \\ &= (T_1 - T_0) \frac{Z\bar{T}}{1 + Z\bar{T}} = \frac{q}{K} \frac{Z\bar{T}}{1 + Z\bar{T}} \end{aligned} \quad (8)$$

where

$$T = \frac{T'_1 + T_0}{2}$$

and T'_1 is the short-circuited component temperature.

The results of the experiment with no power used by the thermoelectric module are shown in Figure 5. The resistor temperature rose linearly with power for both the module open circuited and the module short circuited; however, the slope was different in each case. The data was reasonably good and proves that the concept of effective thermal conductivity is valid for short-circuited thermoelectric modules. From these results and Equation 8, the effective figure of merit was computed to be $1 \times 10^{-3} \text{ } ^\circ\text{K}^{-1}$. If a small amount of power (1/2 watt) is used to pump heat from the component and then reversed, the temperature difference can be thought of as a control temperature difference. Figure 6 shows the control that can be achieved with 1/2 watt as well as zero power. For small temperature differences between

* Sanyo TEM - 1025

the component and sink temperature, the control temperature with power is fairly constant while for larger differences the control temperature increases in the same manner as the zero power case.

c. Temperature Control of the Entire Payload

Thermoelectric modules can be used to change the temperature level of the entire satellite by altering the amount of heat radiated from the payload to outer space. This is done by connecting radiators to the back of a thermoelectric module which is in turn connected through a good conduction path to the satellite payload. In order to illustrate this application consider the following simplified satellite model. The satellite shown in Figure 7 is a sun-oriented cylindrical satellite with the payload mounted on a baseplate that is pointing away from the sun. For simplicity, assume that the satellite is at a high enough altitude so that the heat inputs other than solar can be neglected. For this example, the internal generation is assumed negligible although it would not alter the results to take it into account. A thermostatic switch short circuits the modules when the satellite payload temperature rises about 16 degrees C and open circuits the modules when the payload drops below 14 degrees C. This will solve the problem of keeping the temperature of the payload constant while the percent of sun time varies. The energy balance equations are:

$$q = s\psi\alpha_1 - \epsilon_1\sigma T_1^4$$

$$q = F(\sigma T_1^4 - \sigma T_2^4)$$

$$q = \epsilon_3\sigma T_3^4$$

$$q = \frac{K_{eff}}{A} (T_2 - T_3)$$

where

ψ is percent of sun time,

S is solar flux,

F is black body interchange factor,

α_1 is solar absorptivity, and

ϵ is thermal emissivity.

$$K_{\text{eff}} = K(1+ZT) \text{ when short circuited}$$

and

$$K_{\text{eff}} = K \text{ when open circuited}$$

These equations can be solved in terms of T_2 . The result is

$$\sigma T_2^4 = \frac{S\psi\alpha_1 F}{F\epsilon_1 + \epsilon_3(F+\epsilon_1)(1-\phi)^4}$$

where

$$\phi = \frac{AF(S\psi\alpha_1 - \sigma T_2^4 \epsilon_1)}{K_{\text{eff}} T_2 (F + \epsilon_1)}$$

Subscripts 1, 2, and 3 refer to front surface, payload, and radiator, respectively.

In order to keep the temperature of the payload constant, it is necessary that ϕ be increased when ψ decreases. The only way that this can be done is to decrease K_{eff} when ψ is decreasing. For maximum effectiveness, ϕ_{max} should be about one when ψ is minimum.

Figure 8 shows the solution to the energy balance equations as a function of percent of dark time. No attempt to optimize parameters to achieve maximum temperature change was made. The following values of the parameters represent a reasonable estimate for most cylindrically-shaped satellites with base plates.

$$\alpha_1 = 0.75$$

$$\epsilon_1 = 0.9$$

$$\epsilon_3 = 0.9$$

$$F = 0.2$$

$$K_{\text{eff}_1} = 0.160 \text{ (open circuited)}$$

$$K_{\text{eff}_2} = 0.214 \text{ (short circuited)}$$

From Figure 8 it can be seen that the active thermal controller cuts the temperature range down by about 10 degrees C over a passive satellite. Hence for a satellite in a 1200-mile circular orbit, the temperature range with the controller

working would be 6 to 25 degrees C instead of -5 to 25 degrees C or 6 to 35 degrees C. This change in range, although not large, is usually important due to the narrow range of maximum battery performance.

SUMMARY

The energy balance equation and the power requirement for thermoelectric heat pumping were combined to form an equation relating the heat pumped to the power required. An important parameter which results is $Q_{\max} = (\alpha T)^2/R$, which determines the heat pumping capacity of a thermoelectric module. It was shown that for Q small compared to $Q_{\max}/2$ the pumping efficiency approached the carnot pumping efficiency.

Thermoelectric modules can be used as a thermal switch by changing the effective conductivity of the modules. This can be accomplished by short circuiting the module. It is possible with modules now commercially available to achieve a 10 to 20 degree C component temperature control with no use of power provided the temperature of the component is 50 degree C higher than that of the payload. If a small amount of power (15 percent of the component dissipation) can be used for temperature control, the component temperature can be lowered and the control possible is increased by a factor of two or more. These results were shown by theory as well as experiment. For calculation, the experiments showed that an effective figure of merit of 1×10^{-3} is a realistic number for thermal heat switching application.

The capability of controlling the temperature level of the entire payload without power was investigated. The amount of heat radiated by the satellite was controlled by controlling the radiator temperature by means of a thermoelectric thermal switch. For a realistic example calculated in this paper, it was shown that a 10 degree C reduction in the temperature extremes due to changes in the percent of dark time was possible. Although small, it would not take a great advance in thermoelectric-module performance to increase the temperature reduction to a more significant number.

REFERENCE

1. A. Joffe, "Semiconductor Thermoelements and Thermoelectric Cooling", Infosearch, London, 1957.
2. Radoff and Miller, "Thermoelectric Materials and Devices", Reinhold, N. Y., 1960.

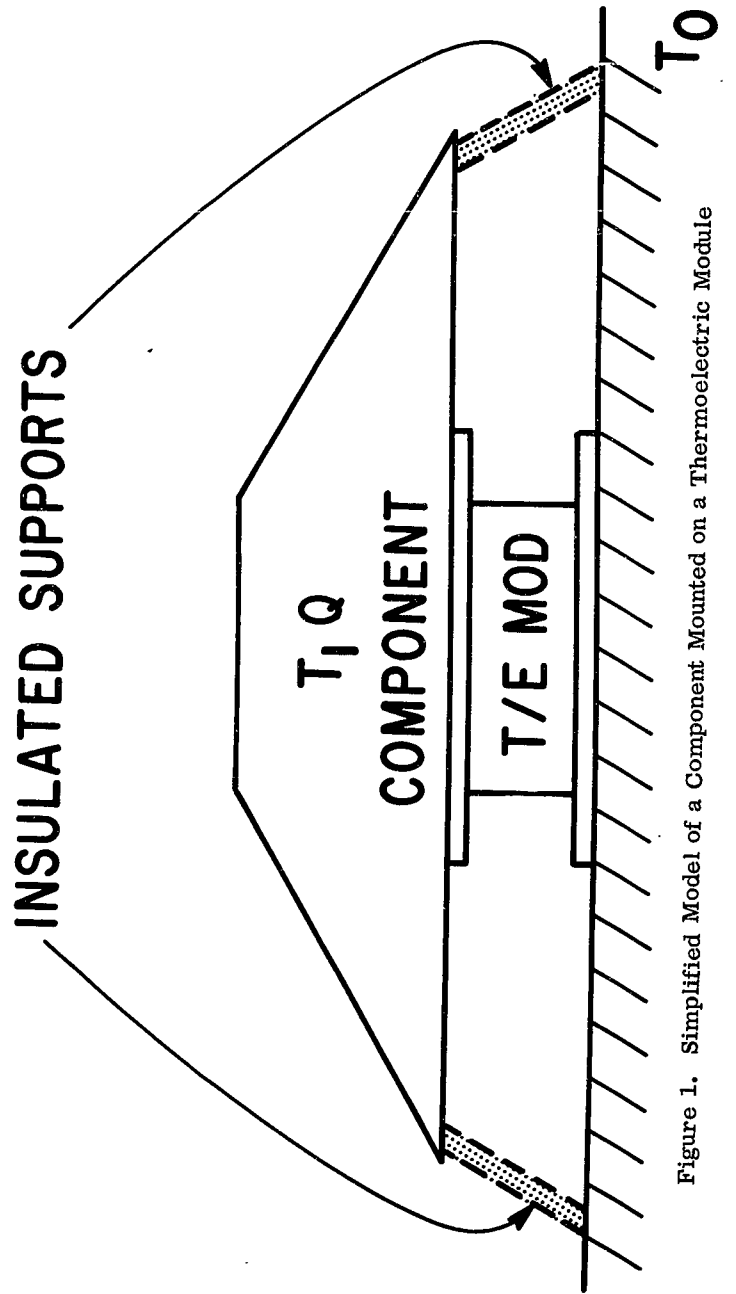
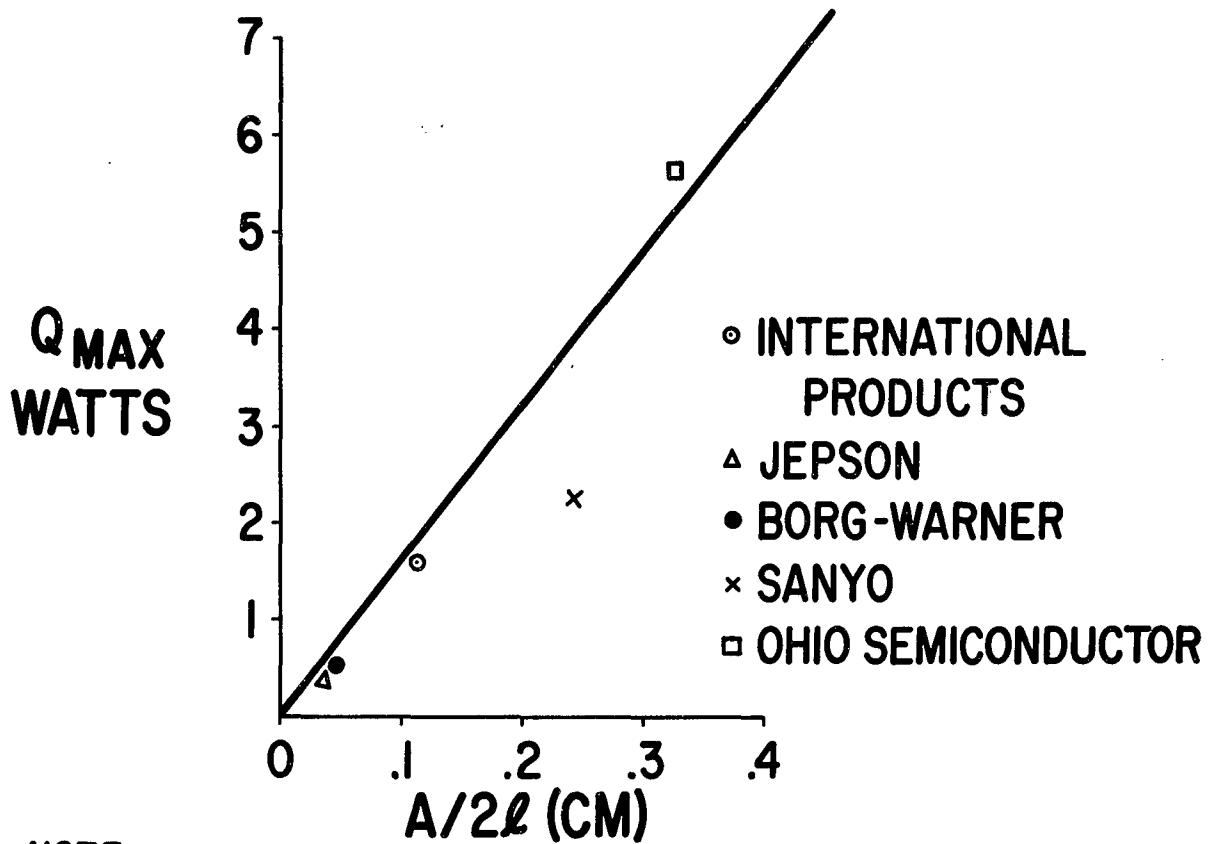


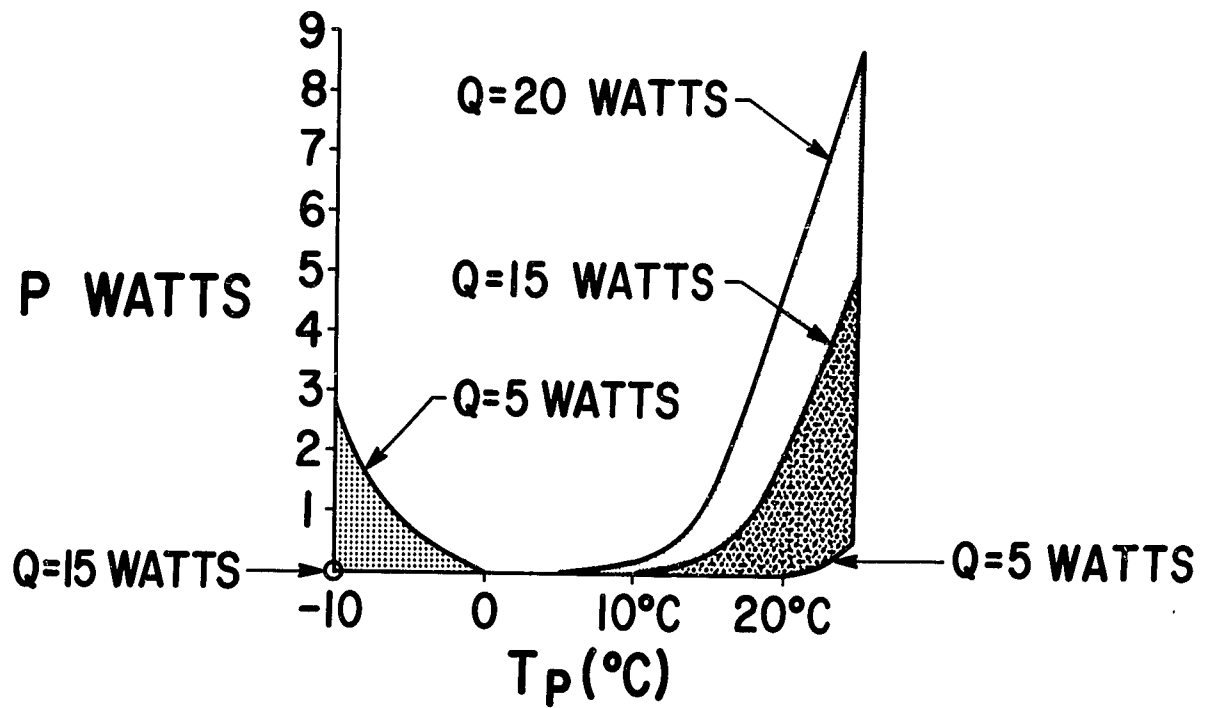
Figure 1. Simplified Model of a Component Mounted on a Thermoelectric Module



NOTE:

THE STRAIGHT LINE REPRESENTS A COUPLE WITH
 $Z = 2.2 \cdot 10^{-3} (\text{°K})^{-1}$ AND $\mathcal{L} = .02$ WATTS/°K.

Figure 2. Q_{max} per Couple for Thermoelectric Modules of Several Manufacturers



NOTE:

THERMOELECTRIC MODULE
Q_{MAX} = 45 WATTS. K=1 WATT/°C

Figure 3. Power Required to Keep Satellite Batteries Between 5 and 25°C

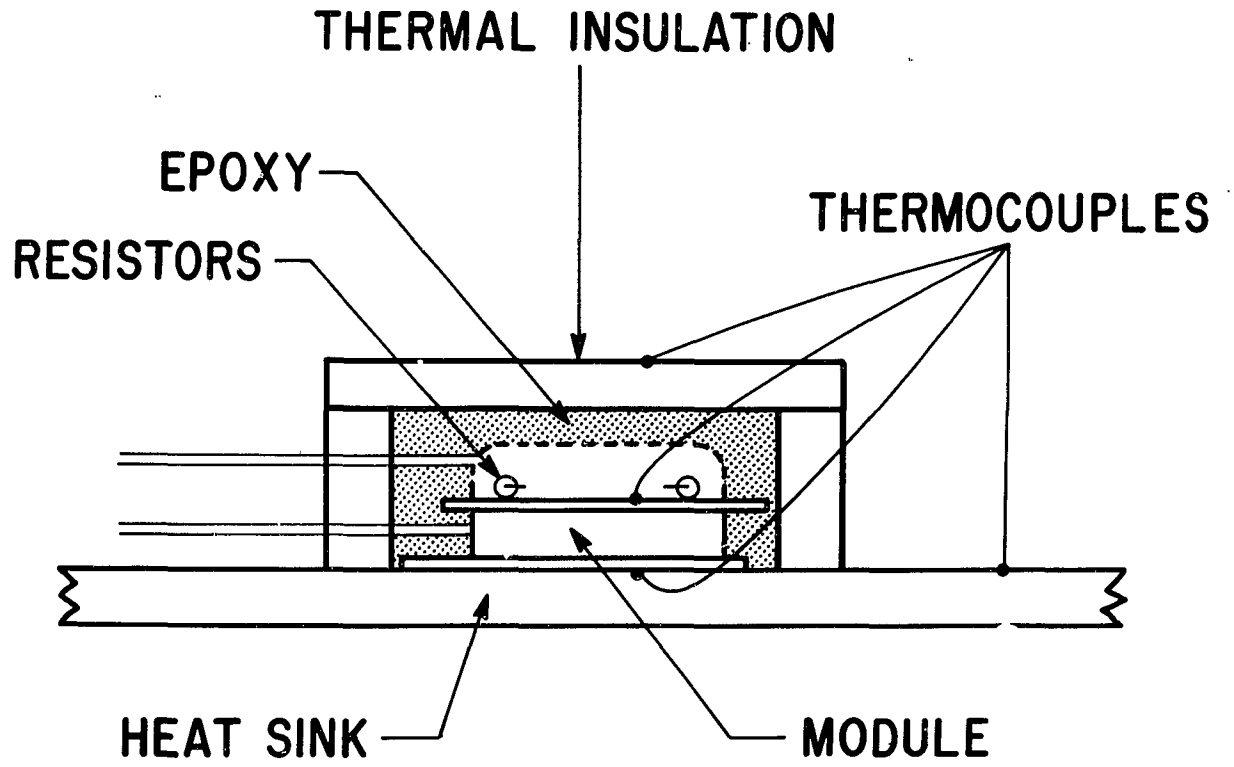


Figure 4. Experimental Test Setup Using Sanyo Thermoelectric Modules

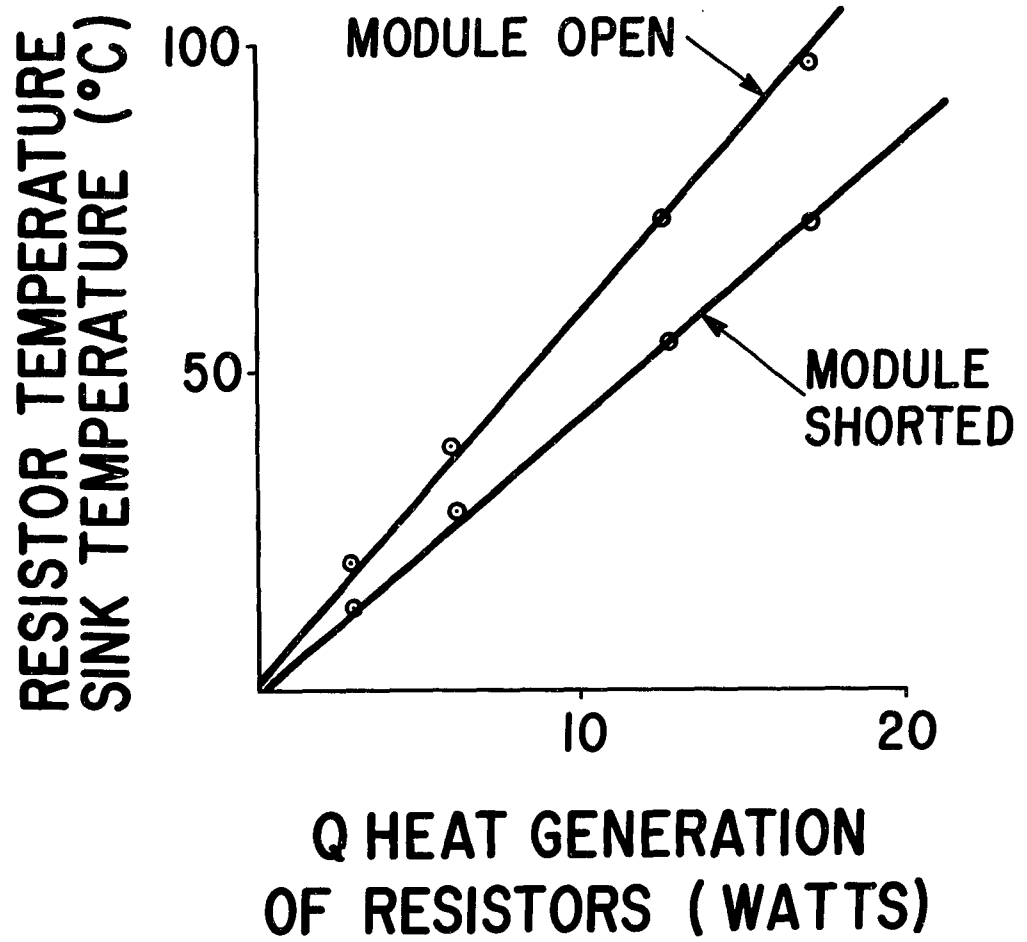


Figure 5. Change in Temperature of the Resistors Shown in Figure 2 Due to Short Circuiting of Thermoelectric Module

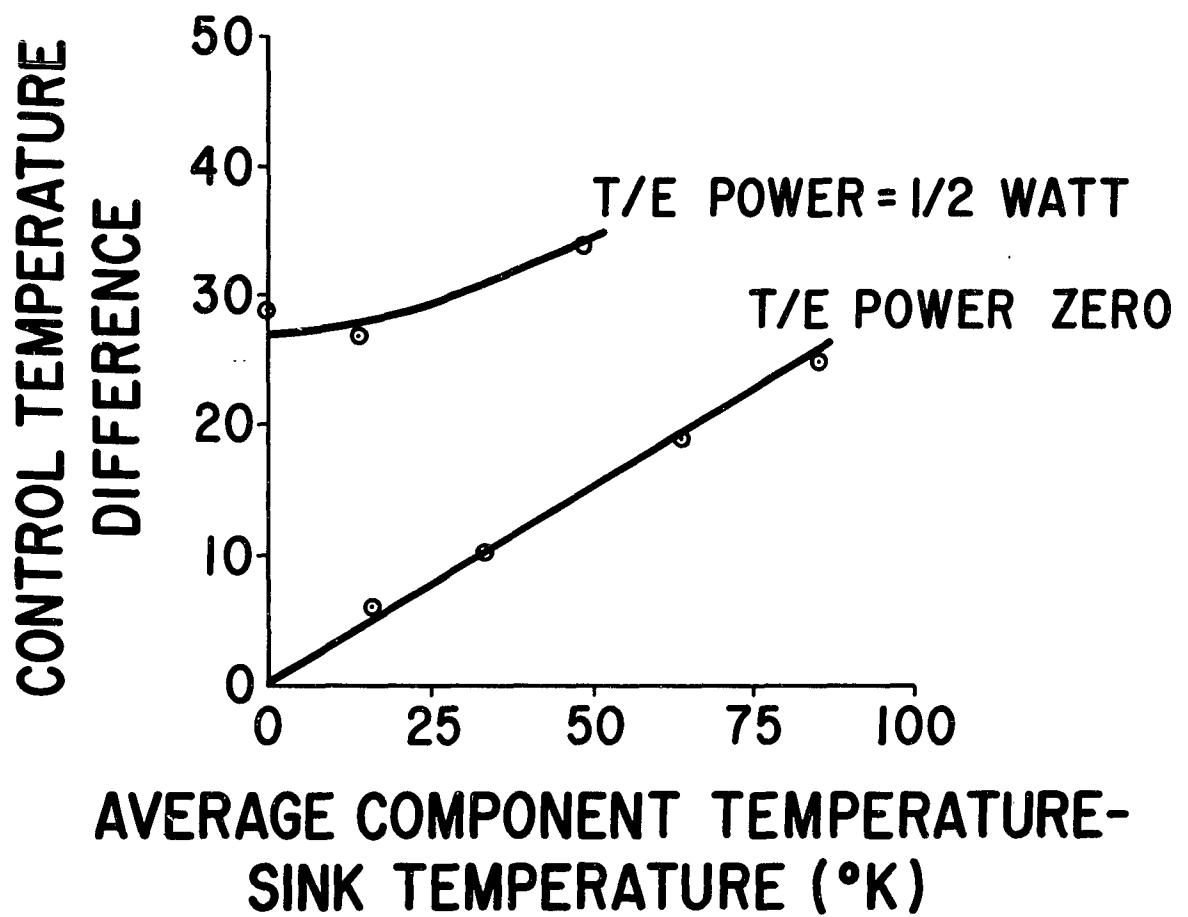
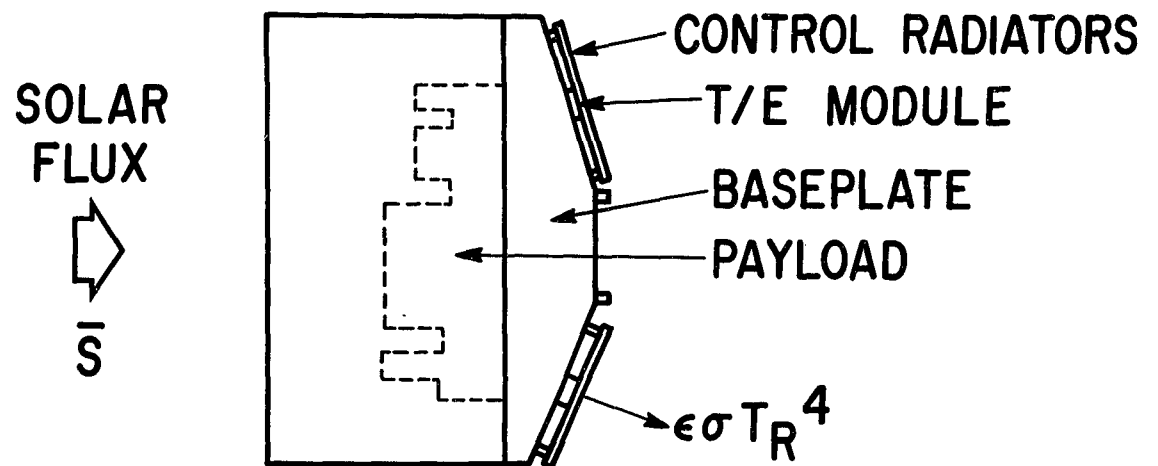


Figure 6. Control Temperature Difference Experimentally Determined with a Sanyo 1025 Thermoelectric Module



NOTE:

THE WEIGHT REQUIRED FOR A CONTROL UNIT IS ABOUT 1.1 LB/FT². FOR THE RELAY SATELLITE 3 FT² OF CONTROL AREA WOULD EQUAL THE PRESENT CONTROLLER.

Figure 7. Sun-Oriented Satellite with Thermoelectric Temperature Control Units

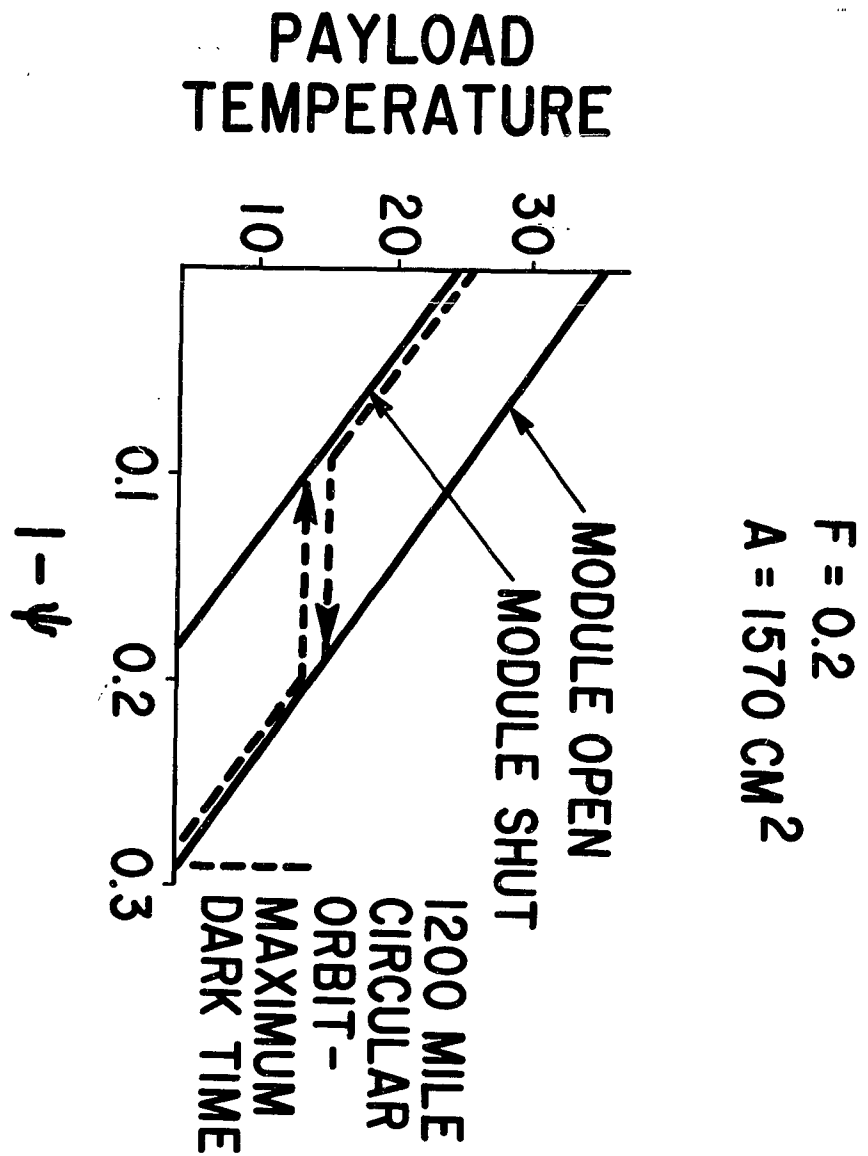


Figure 8. Calculated Satellite Temperature vs Function of Dark Time

Second Paper -- "Thermoelectric Temperature Control in Satellites," by C. Usiskin, RCA.

QUESTION: (Mr. Cohan, Lockheed) For the battery case illustrated, have you compared the total integrated power for a thermoelectric device against a system using conductance to prevent overheating and thermostatically controlled electric heating to maintain minimum temperature?

ANSWER : (Mr. Usiskin) The answer is simply, "No." But in defense of myself I might point out that you really can't do it, because with the requirements that you have, in order to maintain the high temperatures you would have to heat sink, you would have to conduct batteries completely into the payload to maintain zero temperatures with gradients of 21. You would have to cut completely oonnected into the payload, essentially a very very hard conductance, but then on the low temperature side you wouldn't be able to supply enough heat to keep it warm because of this high conductance, you conduct all the heat away and so you would have to heat up the whole payload. Now actually any time you are using a thermoelectric device for a heater you gain a factor of two or three in the temperature, at least a factor of three in the temperature ranges we are talking about because the coefficient of performance in these small temperature ratings.

QUESTION : (Anonymous) Have you ever considered just an isotope that you can pull in and out of the satellite without any electrical device?

ANSWER : (Mr. Usiskin) It is possible. Of course there are a lot of mechanical difficulties.

QUESTION: (Anonymous) In other words, instead of having an electrical generator, use an isotope?

ANSWER : (Mr. Usiskin) Well, this was considered with the radio isotope package between the capsule and the shield in the case there wasn't just the isotope package.

SELECTION OF A TEMPERATURE CONTROL SYSTEM
FOR A MARS PROBE

by

Clark V. Dohner

General Electric
Philadelphia, Pennsylvania

NOMENCLATURE

A_P	= projected area of vehicle (a function of view angle) - ft. ²
A_T	= total surface area of vehicle - ft. ²
α	= solar absorptivity - dimensionless
α_e	= effective solar absorptivity (between capsule and sink) - dimensionless
C_p	= specific heat of vehicle - $\frac{\text{BTU}}{\text{lbm} \cdot ^\circ\text{F}}$
ϵ	= emissivity - dimensionless
ϵ_e	= effective emissivity (between capsule and sink) - dimensionless
\mathcal{F}	= radiation configuration factor - dimensionless
k	= thermal conductivity - BTU/hr-ft- ^o F
Q_g	= internal heat generation - watts; BTU/hr.
σ	= Stefan-Boltzmann constant = $.1713 \times 10^{-8}$ BTU/ft ² -hr- ^o R ⁴
S	= solar flux per unit area - BTU/hr-ft. ²
t	= shield liner thickness - ft.
T	= temperature - ^o R; ^o F
w	= weight of vehicle - lbm.
θ	= time - hr.; or view angle - degrees

SUBSCRIPTS

B	= battery; back (aft) end of vehicle
C	= capsule
e	= effective
H	= holes in insulation or attachment points to vehicle
i	= initial, interior
MIN.	= minimum

SUBSCRIPTS (Cont'd)

MAX. = maximum

P = projected

S = shield

S_i = inside of shield

S_o = outside of shield

T = total

W = sink (environment)

ASD-TDR-63-260

SELECTION OF A TEMPERATURE CONTROL SYSTEM FOR A MARS PROBE

By

C. V. Dohner

INTRODUCTION:

This paper presents the thermal design study for a Mars-probe entry vehicle. Four types of temperature control systems are considered:

- 1) α/ϵ coating with solar cells
- 2) α/ϵ control
- 3) superinsulation with solar cells
- 4) radioisotope heat generation

The purpose of this paper is to show how the selection of a system should be approached by considering the analyses of several systems. Then, on the basis of a comparison of these systems, the ones which appear to be the most desirable are selected for further consideration.

DISCUSSION:

I. General System Requirements

Certain problem areas exist with any of the systems to be considered. The capsule must be held within a certain temperature range so that the electronic components will operate satisfactorily. Shield temperature must be maintained above a certain minimum; and the gradient around the shield must be prevented from exceeding a certain value, or else excessive thermal stresses will be encountered. Since the vehicle's battery is adversely affected by temperature extremes, it, too, must be maintained within specified temperature limits. During entry into the Martian atmosphere the capsule must be maintained within temperature limits until impact with the surface of Mars. All these problem areas must be considered when analyzing the various temperature control systems.

The general Mars-probe entry vehicle configuration is presented in Figure 1. This probe vehicle is attached to the "space bus", whose mission it is to fly-by Mars while the probe enters the Martian atmosphere. The probe remains attached to and in the shade of the space bus until separation of the two occurs. Separation may occur anywhere from 18 hours to 180 days prior to entry at Mars. However, the case for which the probe "sees" the greatest variation in environmental temperature (i. e., solar flux) occurs for separation at 180 days prior to entry (i. e., 180 day free-flight duration). The solar flux, for this case, varies from 406 BTU/hr-ft² (at separation) to 184 BTU/hr-ft² (at Mars).

During the transit phase of flight, the following temperature restrictions are imposed upon the probe:

$$14^{\circ}\text{F} \leq T_C \leq 160^{\circ}\text{F}$$

$$50^{\circ}\text{F} \leq T_B \leq 100^{\circ}\text{F} \text{ (battery activated)}$$

$$-20^{\circ}\text{F} \leq T_B \leq 100^{\circ}\text{F} \text{ (battery unactivated)}$$

$$T_{S_{\text{MIN.}}} \geq -150^{\circ}\text{F} \text{ (310}^{\circ}\text{R)}$$

$$T_{S_{\text{MAX.}}} - T_{S_{\text{MIN.}}} \leq 300^{\circ}\text{F} \text{ (gradient around shield)}$$

where:

subscript C refers to capsule

subscript B refers to battery

subscript S refers to ablation re-entry heat shield

II. α/ϵ Coating System

This is a system of temperature control which makes use of coatings on the shield and capsule to limit the change in temperature of the capsule as the solar flux varies during the journey from earth to Mars. The basic system concept employed here is to allow the capsule to first heat up and then cool down as free flight time elapses (vehicle separated from space bus); but in so doing, to maintain the capsule temperature in the range 14°F to 160°F and the battery temperature in the range 50°F to 100°F .

A. Capsule Temperature

Required capsule coating values of α and ϵ are determined essentially by the free-flight phase of the vehicle's journey between earth and Mars (i. e., period between separation from bus and entry to Mars). Consider the transient temperature of the capsule as described by:

$$wC_p \frac{dT_C}{d\theta} = \alpha_e A_p S - \epsilon_e A_T \sigma T_C^4 + Q_g \quad (1)$$

and

$$\alpha_e = \frac{\alpha}{\epsilon} \epsilon_e \quad (2)$$

where

- w = vehicle weight
- C_p = specific heat capacity of vehicle
- T_C = capsule temperature
- α_e = effective value of solar absorptivity (based on capsule and sink temperatures)
- A_P = projected area of vehicle
- S = solar flux per unit area
- ϵ_e = effective emissivity
- A_T = total vehicle surface area
- σ = Stefan-Boltzmann constant
- Q_g = internal heat generation
- α = solar absorptivity of exterior of vehicle
- ϵ = emissivity of exterior of vehicle

The General Electric Matrix Heat Transfer Program was run on the IBM-7090 computer for obtaining solutions to the above equations. From the results of this run, Figure 2 was drawn.

Stable emissivities below approximately .02 are obtainable by the use of superinsulation. However, since the design concept presented here makes use of coatings rather than superinsulation, an effective emissivity of approximately .03-.04 will be used as a practical lower limit. For these values of effective emissivity, it may be seen from Figure 2 that the capsule temperature follows the sink temperature closely. $\left[\text{Sink temperature is defined by equation (1) when } \frac{dT_C}{d\theta} = 0. \right]$

Since orientation of the vehicle with respect to the sun may be arbitrary and since A_P is a function of orientation, it is necessary to achieve a fairly constant value of $\alpha_e A_P$ by the use of different coatings on different body parts (or nodes). This would then mean that the variation in the term $\alpha_e A_P S$ of equation (1) would be due principally to the variation in S. It may be found that the three nodes (or zones) of the vehicle can be coated to give the following values:

$$\left(\frac{\alpha}{\epsilon}\right)_1 = 2.46$$

$$\left(\frac{\alpha}{\epsilon}\right)_2 = 1.86$$

$$\left(\frac{\alpha}{\epsilon}\right)_3 = 2.32$$

With a tolerance of $\pm 5\%$ for these coatings, the capsule temperature can vary from 14°F at separation from the space bus to 160°F at entry to Mars. The α/ϵ values for these coatings can be obtained by using a platinum, rhodium, or tantalum coating on the outside of the vehicle along with patches of black paint over some portions of the coating.

B. Shield Temperature

1. Shield Gradient

Since the maximum allowable shield temperature gradient is 300°F , a magnesium liner is required to maintain the gradient at this value or below since the shield ablation material has a low thermal conductivity.

Figure 3 is derived from the analysis of Reference 1 and presents the maximum and minimum shield temperatures occurring when the solar flux equals $406 \text{ BTU/hr.} \cdot \text{ft.}^2$ (at time of separation of vehicle from space bus). These curves neglect internal radiation and are, therefore, conservative.

For $\alpha/\epsilon = 2.5$ and $T_{\text{S MAX.}} - T_{\text{S MIN.}} = 300^\circ\text{R}$, it may be seen from Figure 3 that $(kt)/\epsilon = 1$. This means that a .02 inch thick magnesium liner may be used to limit the maximum thermal gradient to 300°R .

2. Minimum Shield Temperature

The case for which the shield temperature reaches a minimum may be evidenced when the vehicle is in the shade of the space bus. For a capsule emissivity of .03 to .04 and a shield inner emissivity of .9, the outer shield emissivity (outside of vehicle) may be equal to .1. This will prevent the shield temperature from falling below -150°F .

C. Battery Configuration

The allowable temperature range for the battery is 50°F to 100°F for an activated battery, or -20°F to 100°F for an unactivated battery which is to be

chemically activated at a predetermined time after separation of the vehicle from the space bus. Since the latter case would require heating the battery up to 50°F after activation, it would impose as much of a problem as would the former case. Battery temperature, therefore, could be maintained between 50°F and 100°F. Figure 4 shows a typical thermal configuration for the battery.

To maintain the battery temperature under 100°F, thermal isolation of the battery from the capsule would be employed. This is accomplished by the use of nylon strands to support the battery from its corners along with the use of a low effective emissivity insulation (superinsulation) around the battery. A heat of fusion material (eicosane) is necessary to accept the heat which would otherwise be absorbed by the battery when the capsule temperature exceeds 100°F. The weight of eicosane (melts at 100°F and absorbs approximately 100 BTU/lb. of system) required would be 6.5 lb. This weight could be reduced if a water vaporization system similar to the one used on the bio-medical packages of the Discoverer were used instead of the eicosane. The water vaporization system would have a heat absorbing capacity of 500 BTU/lb. of system. Hence, it would weigh only one-fifth as much as the eicosane - namely 1.3 lb.

To maintain the battery temperature above 50°F, thermostatically-controlled heaters could be used, with a control point of approximately 80°F. Heater power would be generated by solar cells attached to the outside of the vehicle.

A frangible disc, set to break at 5 psi pressure difference, can be used in the shell around the battery to keep the system free from contamination prior to launch.

D. Heater Power Supply

Due to the long time duration for which heater power will be required to maintain battery temperature, solar power appears to be best. The low power dissipation (≈ 1 watt) indicates that photovoltaic cells are ideally suited for the mission.

Random orientation of the vehicle during transit dictates that patches of cells must be placed over the vehicle so that some cells can always supply sufficient power to operate the heaters. Since the output of each patch, or grouping of cells, is limited to approximately the output of the least exposed cell in the patch, the patches must be connected in parallel, rather than in series, so an unilluminated patch does not act as a load for an illuminated patch.

Figure 5 shows the logical locations for solar cell patches. A power system optimization with respect to patch sizes and number of patches indicates that the 4-patch circumferential arrangement shown in Figure 5 is best for this case; it keeps the number of heaters and thermostats to a minimum and yet is adequate to maintain the one watt power required for maintaining the battery temperature. A five-patch system would provide redundancy in case of the failure of one patch, if the patches themselves cannot be made redundant.

Power output of the entire solar cell system as a function of view angle (θ) is shown in Figure 6. For this figure, the angle ϕ was chosen to minimize the output.

E. Heating Requirements while on Space Bus

In order to maintain the capsule minimum temperature of 14°F and the battery minimum temperature of 50°F while the vehicle is attached to and in the shade of the space bus, it may be calculated that 26 watts are required for heating the capsule and 1 watt is necessary for heating the battery.

F. Capsule Temperature during Entry at Mars

During entry at Mars, the capsule may become too cold unless a one inch thick layer of fiberglass insulation is used. This fiberglass insulation blanket would be placed on the inside of the capsule and would weigh approximately 3 lbs.

III. α/ϵ Control System

This type of system would require the placement of a magnesium "clam-shell" around the outside of the vehicle. Copper tubing filled with a liquid Freon or Propane then would be wound around the outside of this clam-shell and in intimate thermal contact with it. Contraction or expansion of the liquid due to temperature changes would actuate open-closed type shutters (no intermediate positions, only full-open or full-closed) to increase or decrease the α/ϵ value so that an average vehicle temperature of approximately 80°F would be maintained.

Open-closed type shutters are necessary for this system rather than proportional control type of shutters because of varying solar flux received by the vehicle during free flight. Varying flux means that the value of α/ϵ necessary to maintain an average temperature of 80°F at the beginning of free flight will be different from the value needed to maintain the same temperature at Mars. The lowest value of α/ϵ which is needed to maintain an average temperature of 80°F is approximately equal to 1.39 and occurs at the beginning of free flight (with maximum projected area). The highest value of α/ϵ needed to maintain the same average temperature is approximately 3.44 and occurs at Mars (with minimum projected area).

Solar cells and heat of fusion material would not be needed for temperature control if this system were used, since the temperature of the entire vehicle would be maintained around 80°F , which is well within the temperature limitations imposed upon the battery.

The clam-shell and shutters must be ejected from around the vehicle prior to parachute deployment at Mars. This is a disadvantage in the respect that an ejection system would be required; however, it is an advantage in the respect that the weight of the clam-shell, shutters, and tubing will not add to the entry weight of the vehicle.

The reliability of such a system must be considered. This system uses mechanical control to vary α/ϵ and to eject the clam-shell and shutters. Reliabilities of these mechanical systems must be compared with the thermal reliabilities of the other types of systems considered.

IV. Superinsulation System with Solar Cells

This system consists of superinsulation wrapped around the outside of the vehicle with solar cells affixed to it. The superinsulation would minimize the effects due to the variation in solar flux and also maintain the shield temperature at that of the capsule (hence reducing shield thermal gradients). Solar cells would maintain the capsule temperature above the required minimum.

A. Variation in Effective Emissivity

The effective emissivity of a superinsulation (i. e., multiple-radiation-barrier type insulation) may vary by a factor of 10:1 from one end of the vehicle to another. This is due to one or more of the following reasons:

- 1) Method of attachment to vehicle
- 2) Local variation in foil emissivity
- 3) Random contact between foils

The approach to this problem may be made in terms of $\left(\frac{A_P}{A_T}\right)_e$, where:

$$\left(\frac{A_P}{A_T}\right)_e = \frac{A_{S,P} + \frac{\mathcal{F}_B}{\mathcal{F}_S} A_{B,P} + \frac{\mathcal{F}_H}{\mathcal{F}_S} A_{H,P}}{A_S + \frac{\mathcal{F}_B}{\mathcal{F}_S} A_B + \frac{\mathcal{F}_H}{\mathcal{F}_S} A_H}$$

Subscripts:

P - refers to projected value of area

T - refers to total value of area

S - refers to shield

B - refers to back end (domed end) of vehicle

H - refers to holes in the insulation or attachment points to the vehicle

Figure 7 is then constructed with $\frac{\mathcal{F}_B}{\mathcal{F}_S} = \frac{\epsilon_B}{\epsilon_S} = 10$ or .1 for various cases of

$\frac{\mathcal{F}_H}{\mathcal{F}_S} = \frac{\epsilon_H}{\epsilon_S}$. Thus, it may be seen that $\frac{A_P}{A_{T_e}}$ can vary from .04 to .8.

B. Design Selection

The design selection for this system may be made by considering the sink temperature, T_W :

$$\sigma_{T_{W_{MAX.}}}^4 = \left(\frac{\alpha}{\epsilon}\right) \left(\frac{A_P}{A_T}\right) e_{MAX.} S_{MAX.} + \frac{Q_g \text{ (watts) } 3.413}{\epsilon_{e_{MAX.}} A_T} \quad (3)$$

$$\sigma_{T_{W_{MIN.}}}^4 = \left(\frac{\alpha}{\epsilon}\right) \left(\frac{A_P}{A_T}\right) e_{MIN.} S_{MIN.} + \frac{Q_g \text{ (watts) } 3.413}{\epsilon_{e_{MAX.}} A_T} \quad (4)$$

where

$$\left(\frac{A_P}{A_T}\right)_{e_{MAX.}} = .8 ; \quad \left(\frac{A_P}{A_T}\right)_{e_{MIN.}} = .04$$

$$S_{MAX.} = 406 \frac{BTU}{hr-ft^2} ; \quad S_{MIN.} = 184 \frac{BTU}{hr-ft^2}$$

$$\epsilon_{e_{MAX.}} = .00308 ; \quad \epsilon_{e_{MIN.}} = .000308 \text{ for one inch of superinsulation}$$

$$A_T = 25 \text{ ft}^2$$

From these values it can be shown that by selecting $\alpha/\epsilon = .5$:

$$T_{W_{MAX.}} = 95^{\circ} \text{ F using } Q_g = 0 \text{ watts}$$

$$T_{W_{MIN.}} = 50^{\circ} \text{ F using } Q_g = 2.54 \text{ watts}$$

The required solar cells to produce 2.54 watts would weigh 1.62 lb. and would be attached in the locations shown by Figure 5. The one inch thickness of superinsulation would weigh 9.8 lb.

In order to prevent the shield temperature from falling below -150°F , it is necessary to insulate it. A fiberglass or a glass wool insulation could be used to accomplish this, but it is more advantageous, weightwise, to use a layer of foil around the outside of the shield. A nylon net would be used to prevent the foil from coming into contact with the shield in order to minimize the thermal conductance from the shield to space.

2. Capsule and RTG Temperatures

Figure 9 shows a cross-section through the vehicle. From a steady-state heat balance on the vehicle in the shade (assuming $\epsilon_f = .04$ and $\epsilon_{c_o} = .05$), it may be seen that:

Q_g (WATTS) (THERMAL PLUS ELECTRICAL)	TEMPERATURES WITH VEHICLE IN SHADE (i. e., $S=0$)			
	T_{C_o} ($^{\circ}\text{F}$)	T_{C_i} ($^{\circ}\text{F}$)	T_{RTG} ($^{\circ}\text{F}$)	T_S ($^{\circ}\text{F}$)
55	215	270	350	23
30	120	150	243	-43
25	93	118	190	-63
20	65	85	155	-85
18	52	70	140	-95
15	27	42	93	-110
10	-20	-12	50	-147

The capsule temperature (T_{C_i}) given above is for the case where the vehicle is in the shade of the bus with no solar flux incident upon it. The maximum and minimum capsule temperatures in the sun may be found from the following:

$$\sigma T_{C_i}^4 \text{ MAX.} = \left(\frac{\alpha}{\epsilon}\right) \left(\frac{A_P}{A_T}\right)_{\text{MAX.}} S_{\text{MAX.}} + \sigma T_{C_i}^4 \text{ (in shade)} \quad (6)$$

$$\sigma T_{C_i}^4 \text{ MIN.} = \left(\frac{\alpha}{\epsilon}\right) \left(\frac{A_P}{A_T}\right)_{\text{MIN.}} S_{\text{MIN.}} + \sigma T_{C_i}^4 \text{ (in shade)} \quad (7)$$

where

$$\alpha = .2$$

$$\epsilon = .9$$

$$\left(\frac{A_P}{A_T}\right)_{\text{MAX.}} = .26 ; \left(\frac{A_P}{A_T}\right)_{\text{MIN.}} = .23$$

V. Radioisotope Heat Generation System

Capsule temperature may be controlled through the use of a radioisotope thermoelectric generator (RTG) unit which could be mounted either inside the capsule or outside the vehicle. The RTG unit would be desirable in the respect that it would provide a source of electrical power for recharging the vehicle's battery.

The underlying ideas in using an RTG for temperature control are:

- 1) Minimization of the effect that the variation in solar flux has on capsule temperature.
- 2) Provision of a source of heat to maintain capsule temperature requirements when vehicle is in shade of bus.

Due to the scalability of the RTG unit (i. e., 2.7 to 25 electrical watts), all sizes can be considered. However, because of the relatively low efficiency of the thermoelectric elements (5%), the thermal dissipation is twenty times the electrical power output. For this reason, the larger units need to be used in conjunction with a liquid transfer system when they are mounted inside the capsule.

Capsule sink temperature may be used in approaching the problem of temperature control for this case.

Considering sink temperature

$$\sigma T_w^4 = \left(\frac{\alpha}{\epsilon}\right) \left(\frac{A_P}{A_T}\right) S + \frac{Q_g}{\epsilon_e A_T} \quad (5)$$

it is evident that using a low value of $\frac{\alpha}{\epsilon}$ will minimize the effect of S upon T_w . Using a coating with a low value of α/ϵ (i. e., white paint with $\alpha = .2$ and $\epsilon = .9$) allows Q_g/ϵ_e to be "sized" to obtain the required T_w .

A. RTG Mounted Inside Capsule

1. Shield Temperature

Figure 8, derived from the analysis presented in Reference 1, shows that for $\alpha/\epsilon = .2$, T_S approaches 470°R as (kt/ϵ) approaches zero MAX.

(i. e., as t approaches zero). Since the minimum shield temperature would be allowed to go no lower than -150°F (310°R), this means that with no shield liner the maximum gradient which could exist is $470 - 310 = 160^\circ\text{R}$. Hence, no shield liner is required.

In order to prevent the shield temperature from falling below -150°F , it is necessary to insulate it. A fiberglass or a glass wool insulation could be used to accomplish this, but it is more advantageous, weightwise, to use a layer of foil around the outside of the shield. A nylon net would be used to prevent the foil from coming into contact with the shield in order to minimize the thermal conductance from the shield to space.

2. Capsule and RTG Temperatures

Figure 9 shows a cross-section through the vehicle. From a steady-state heat balance on the vehicle in the shade (assuming $\epsilon_f = .04$ and $\epsilon_{c_o} = .05$), it may be seen that:

Q_g (WATTS) (THERMAL PLUS ELECTRICAL)	TEMPERATURES WITH VEHICLE IN SHADE (i. e., $S=0$)			
	T_{C_o} ($^{\circ}\text{F}$)	T_{C_i} ($^{\circ}\text{F}$)	T_{RTG} ($^{\circ}\text{F}$)	T_S ($^{\circ}\text{F}$)
55	215	270	350	23
30	120	150	243	-43
25	93	118	190	-63
20	65	85	155	-85
18	52	70	140	-95
15	27	42	93	-110
10	-20	-12	50	-147

The capsule temperature (T_{C_i}) given above is for the case where the vehicle is in the shade of the bus with no solar flux incident upon it. The maximum and minimum capsule temperatures in the sun may be found from the following:

$$\sigma T_{C_i}^4 \text{ MAX.} = \left(\frac{\alpha}{\epsilon}\right) \left(\frac{A_P}{A_T}\right)_{\text{MAX.}} S_{\text{MAX.}} + \sigma T_{C_i}^4 \text{ (in shade)} \quad (6)$$

$$\sigma T_{C_i}^4 \text{ MIN.} = \left(\frac{\alpha}{\epsilon}\right) \left(\frac{A_P}{A_T}\right)_{\text{MIN.}} S_{\text{MIN.}} + \sigma T_{C_i}^4 \text{ (in shade)} \quad (7)$$

where

$$\alpha = .2$$

$$\epsilon = .9$$

$$\left(\frac{A_P}{A_T}\right)_{\text{MAX.}} = .26 ; \left(\frac{A_P}{A_T}\right)_{\text{MIN.}} = .23$$

$$S_{\text{MAX.}} = 406 \text{ BTU/hr-ft}^2; S_{\text{MIN.}} = 184 \text{ BTU/hr-ft}^2$$

It may be found from this and the previous heat balance analysis that:

Q_g (WATTS) (THERMAL PLUS ELECTRICAL)	T_{C_i} ($^{\circ}\text{F}$) (IN SHADE)	$T_{C_i\text{MAX.}}$ ($^{\circ}\text{F}$) (IN SUN)	$T_{C_i\text{MIN.}}$ ($^{\circ}\text{F}$) (IN SUN)	T_{RTG} ($^{\circ}\text{F}$) (IN SHADE)	T_s ($^{\circ}\text{F}$) (IN SHADE)
20	85	100	87	155	-85
19	78	98	85	147	-90
18	70	93	77	140	-95
17	60	83	67	125	-100
16	50	74	58	115	-105
15	42	67	50	93	-110

Hence, if between 15 and 20 watts are employed for temperature control, the capsule will change in temperature from a minimum of 42°F in the shade to 100°F in the sun at time of separation from the space bus. If the battery remains unactivated until after separation of the vehicle from the space bus occurs, then these temperature limits are acceptable; if the battery is activated before this, then between 16 and 20 watts will be required.

B. RTG Mounted Outside Vehicle

This type of temperature control system would employ an RTG unit mounted outside the vehicle. The electrical output from this RTG would be dissipated in heaters inside the capsule which, in turn, would maintain the capsule temperature. If the electrical output were used for communication, a great percent of it would be dissipated directly in the electronic equipment, thereby maintaining its temperature. Separation of the RTG from the vehicle prior to entry at Mars would be necessary and could be attained by the use of an explosive bolt type of device.

A. Shield Temperature

The analysis made for the case of the internally mounted RTG applies here also. Hence, no shield liner is required for minimizing the thermal gradient around the shield.

B. Capsule and RTG Temperatures

Again, as in the case of the internally mounted RTG, a steady-state heat balance may be investigated. This will result in the following possible design points:

Q_g (WATTS) (THERMAL PLUS ELECTRICAL)	T_{C_1} ($^{\circ}$ F) (IN SHADE)	$T_{C_1\text{MAX.}}$ ($^{\circ}$ F) (IN SUN)	$T_{C_1\text{MIN.}}$ ($^{\circ}$ F) (IN SUN)	T_s ($^{\circ}$ F) (IN SHADE)
20	85	100	87	-85
19	78	98	85	-90
18	70	93	77	-95
17	60	83	67	-100
16	50	74	58	-105
15	42	67	50	-110
14	30	56	40	-118
13	17	43	27	-125
12	8	38	20	-132

As before, it is evident that between 15 and 20 watts may be used for temperature control.

It should be noted that in the analysis of steady-state heat balance employed for the cases of RTG mounted inside the capsule and outside the vehicle, no variation (with view angle) in the emissivity across the foil was assumed. At present, a single foil has not been tested to see if such a variation does indeed exist as it does for multiple foils (i. e., superinsulation). Since the amount of heat necessary to control the capsule temperature is quite dependent upon effective (or overall) emissivity, a modulated form of heat generation would be more desirable than a constant heat output. Such a modulated device could be obtained by using the RTG mounted outside the vehicle as described above.

VI. Temperature Control System Weights

Figure 10 presents the summary of weights for the various temperature control systems. It is assumed that scaling down the RTG unit to 19 thermal watts scales the electrical output down to .95 watts.

It may be seen that the system utilizing the RTG unit mounted internal to the capsule is the lowest in weight. While the system employing the externally mounted RTG unit weighs more than any other system, it produces a quantity of electrical power equal to 15 watts. This weight must, then, be considered in conjunction with the weight required for the power supply of the vehicle and also the reliability of same.

CONCLUSIONS:

The principal conclusion to be made in this paper is that in order to select a temperature control system for a Mars probe, several systems should be considered and compared.

The analyses presented here for the four types of temperature control system should not be considered to be all-inclusive. These analyses are preliminary and could be subject to change. However, based on this preliminary investigation, the RTG type of system appears to be quite desirable. Tests have shown the RTG units to be very rugged and reliable. In addition, the electrical power output from these units is affected only slightly by a variation of solar flux incident upon them (as is the case of the externally mounted unit).

REFERENCES

1. Tatom, John W.; Shell Radiation; A.S.M.E., Paper number 60-WA-234
2. Eckert and Drake; Heat and Mass Transfer; Second Edition; McGraw-Hill Book Co., Inc.
3. Baker, Joel K.; Temperature Control Techniques for Solar Energy Converters; ASD Technical Report 61-689; Dec. 1961

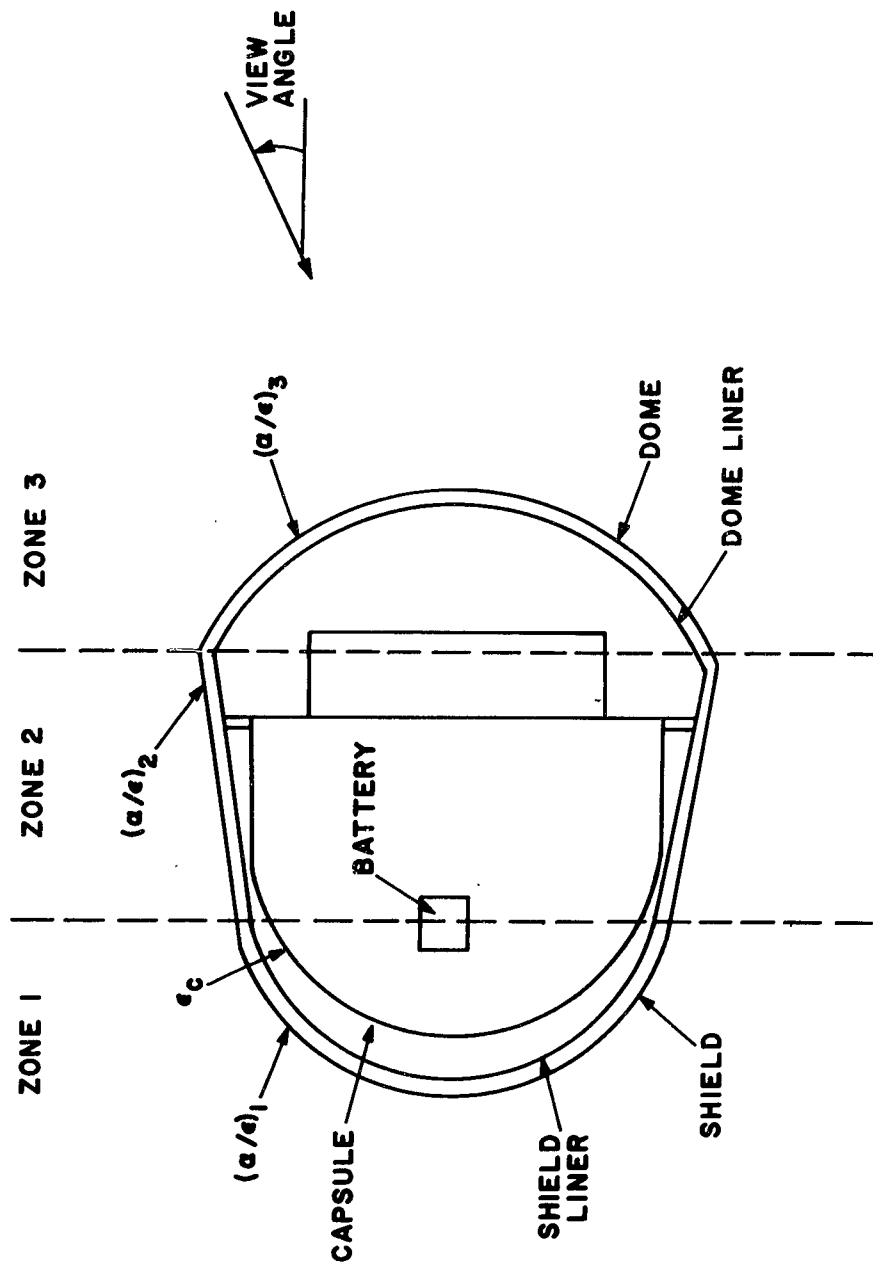
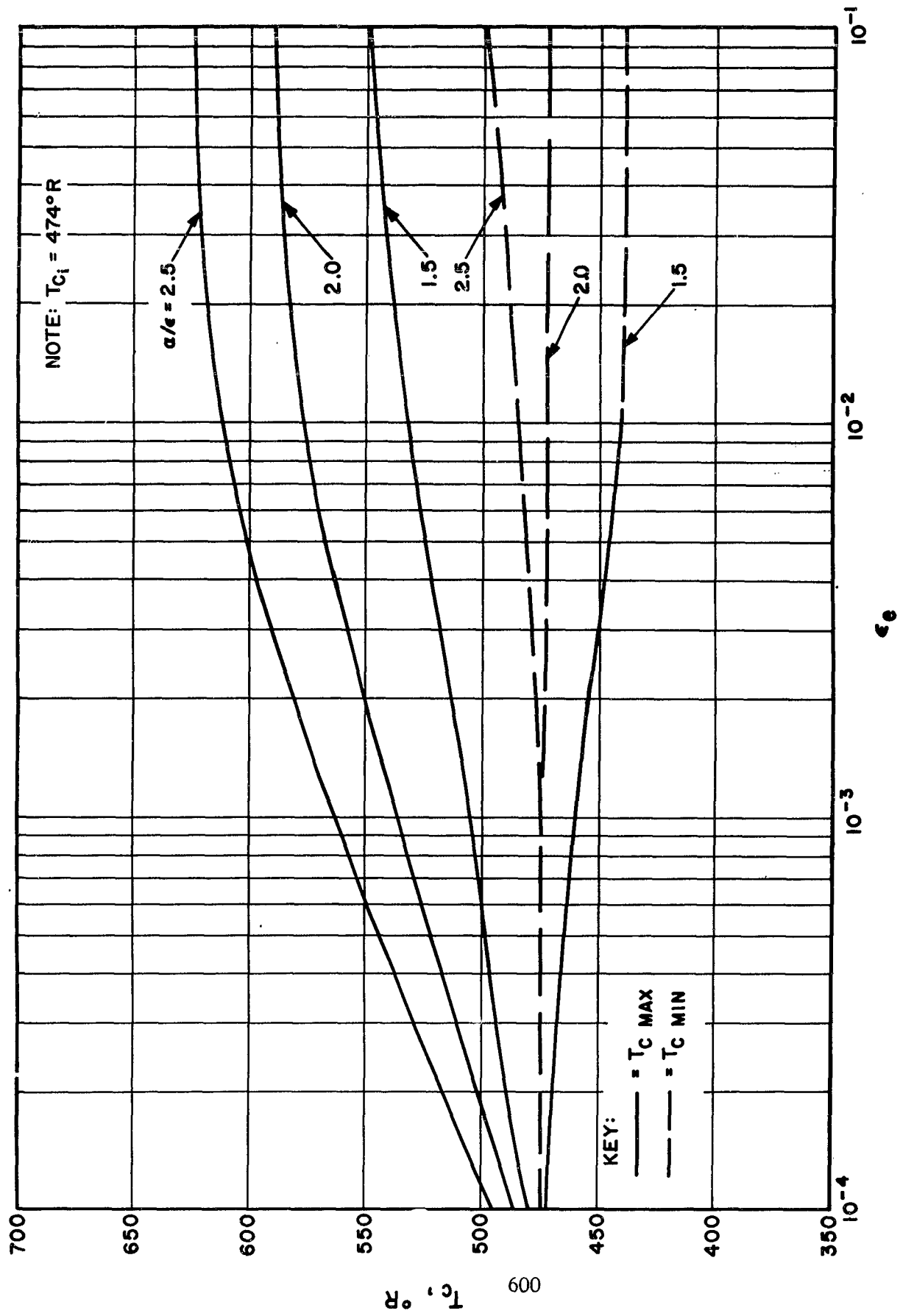


Figure 1. Vehicle Configuration



700

650

600

550

500

450

400

350

α_0

600

10^{-4}

10^{-3}

10^{-2}

10^{-1}

ϵ

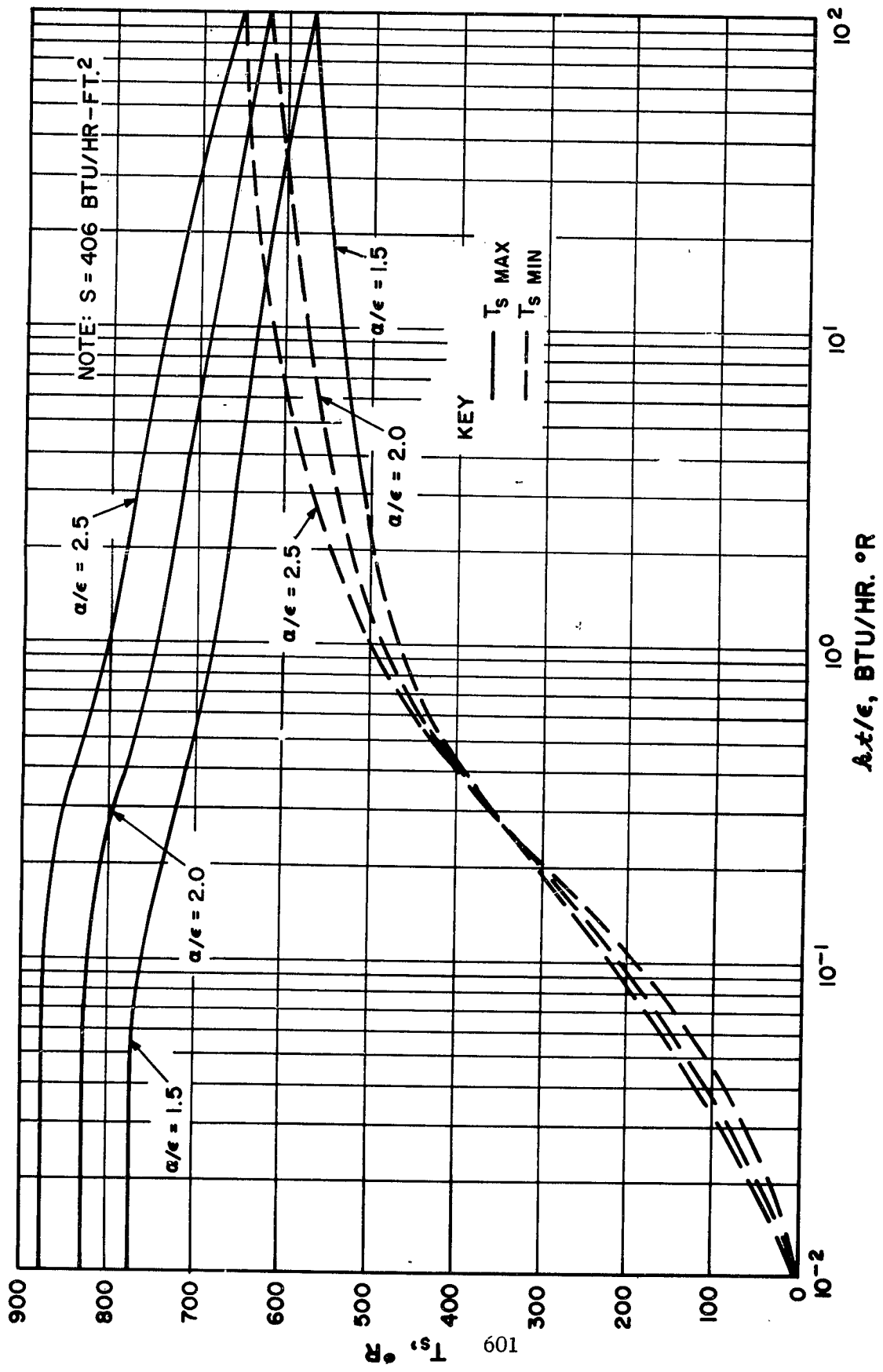


Figure 3. Shield Temperature Versus (kt/ϵ)

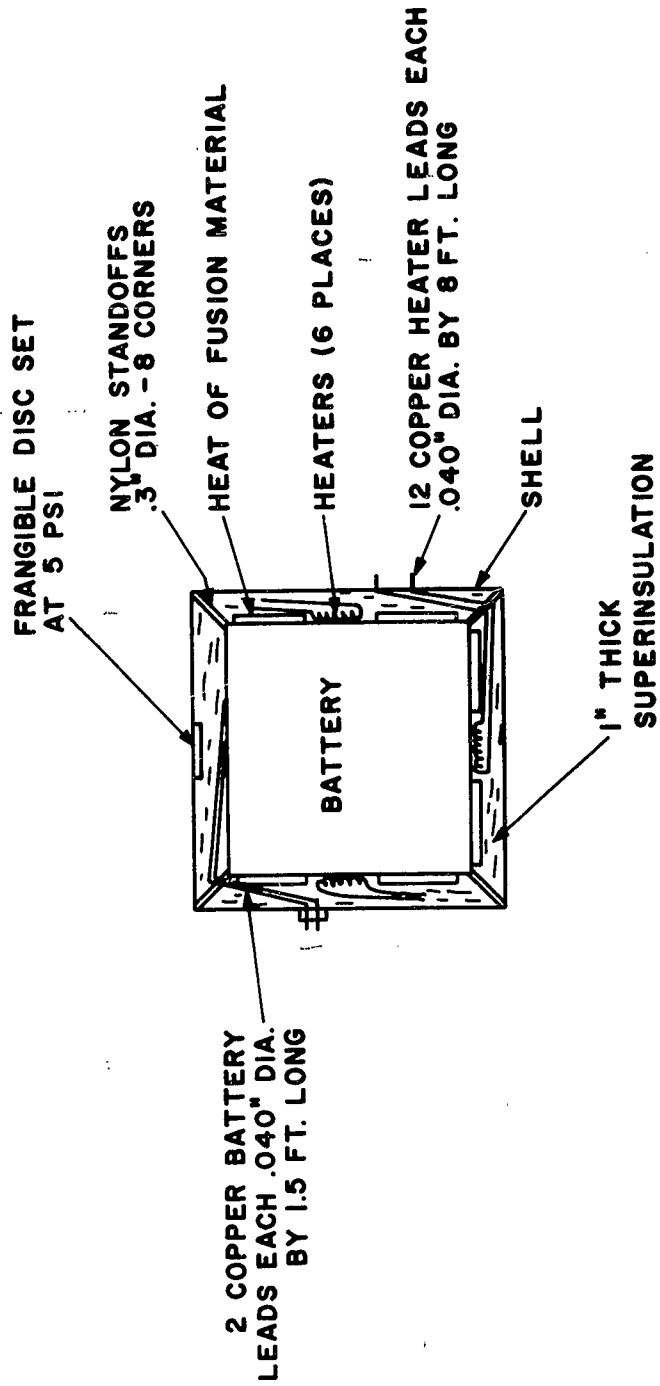
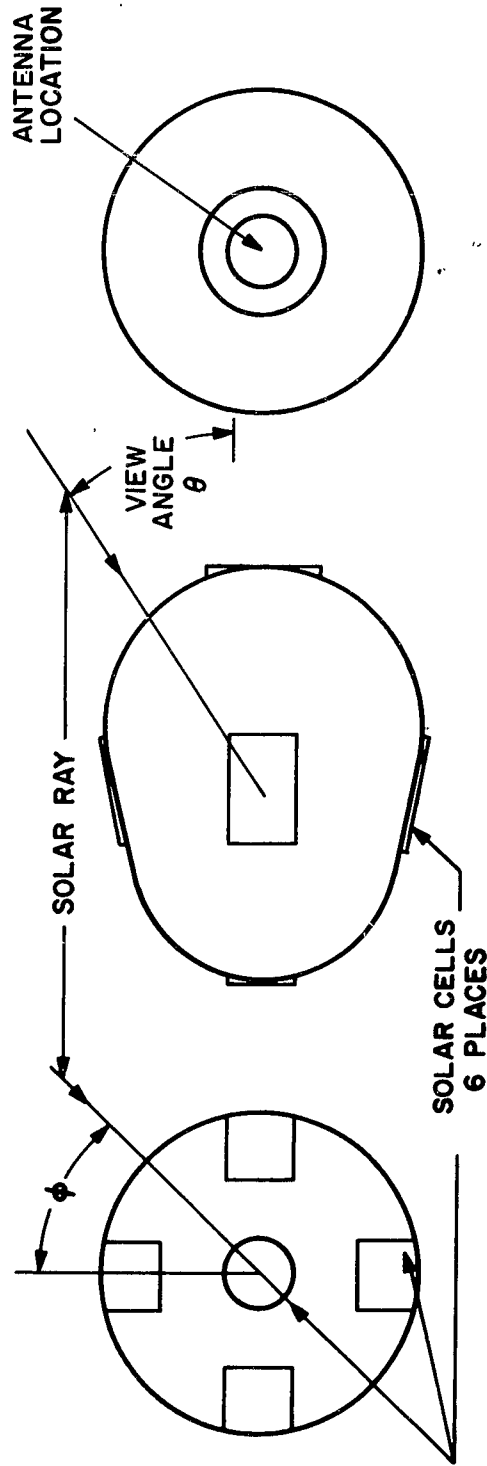


Figure 4. Battery Configuration



603

Figure 5. Solar Cell Configuration

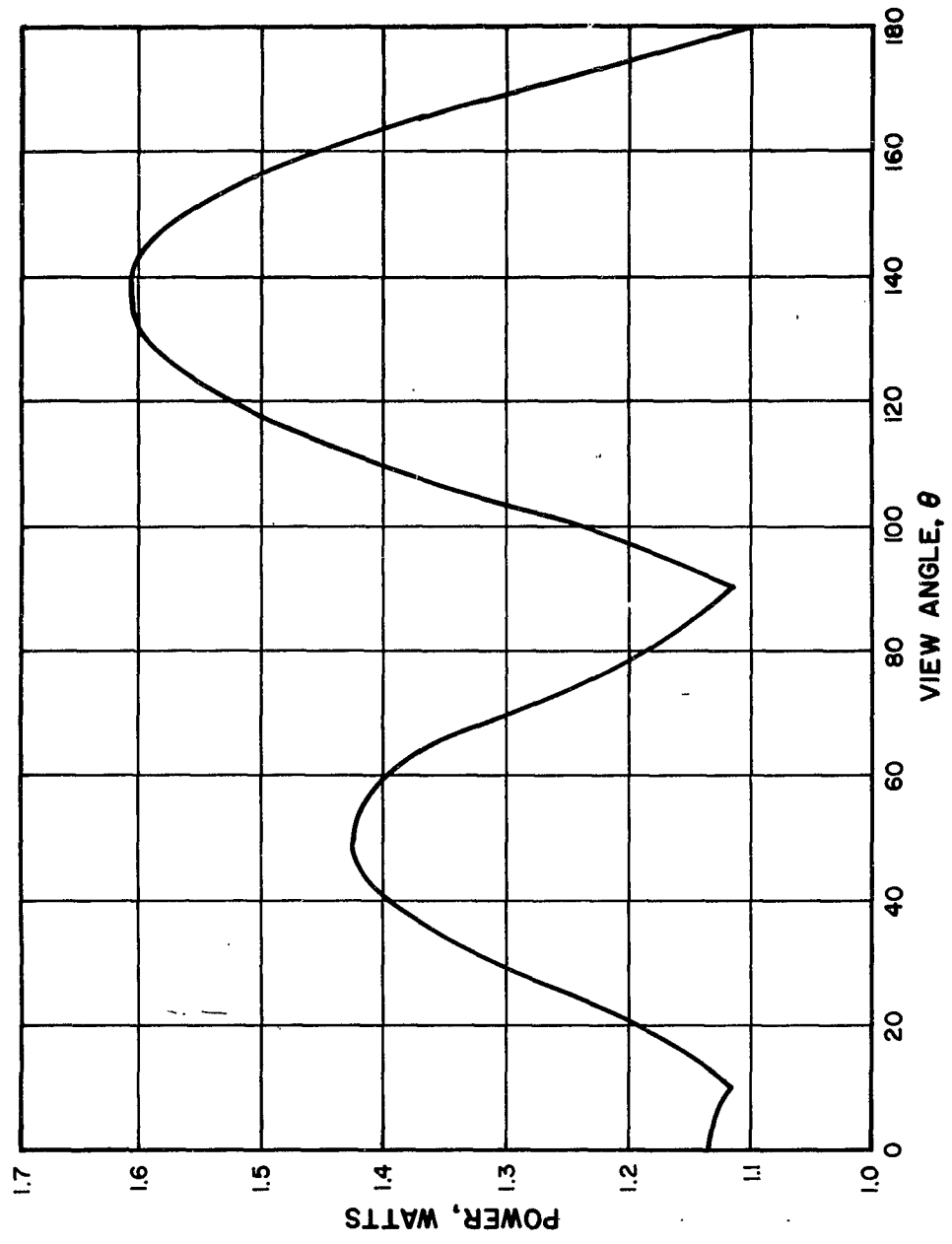


Figure 6. Solar Cell Power Output At Mars

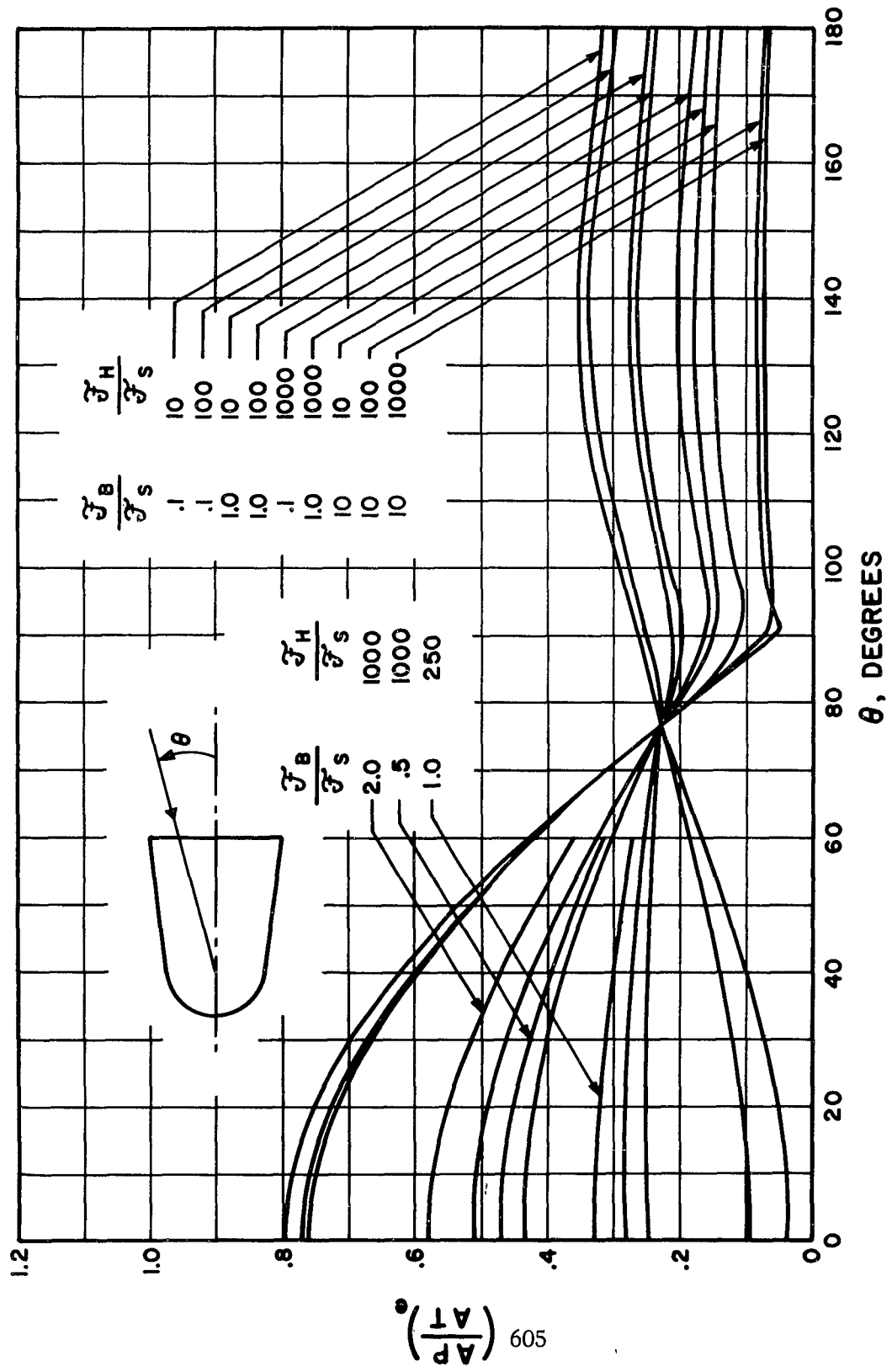


Figure 7. Variation of $\left(\frac{A_P}{A_T}\right)^0$ With View Angle

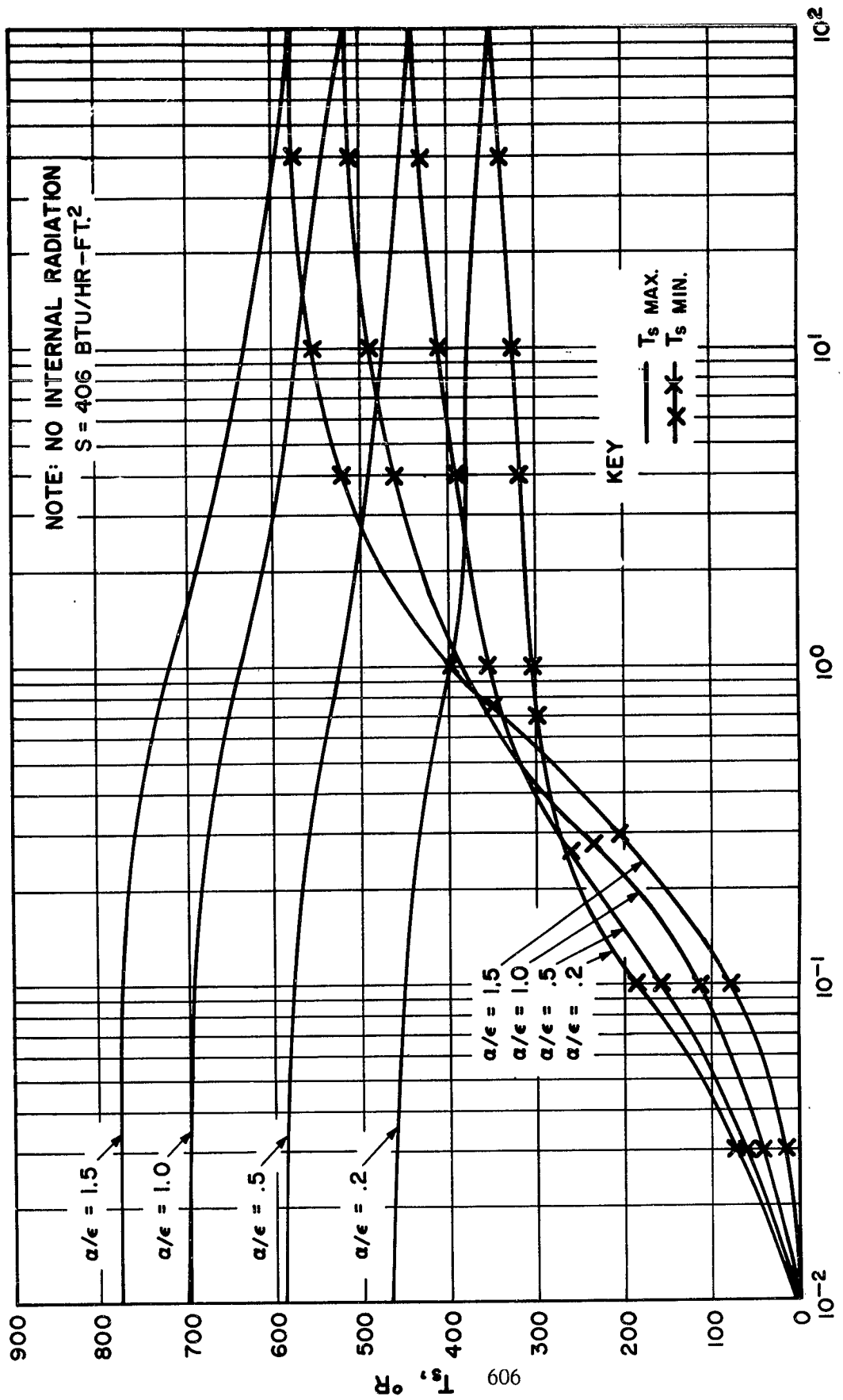


Figure 8. Shield Temperature Versus (kt/ϵ)

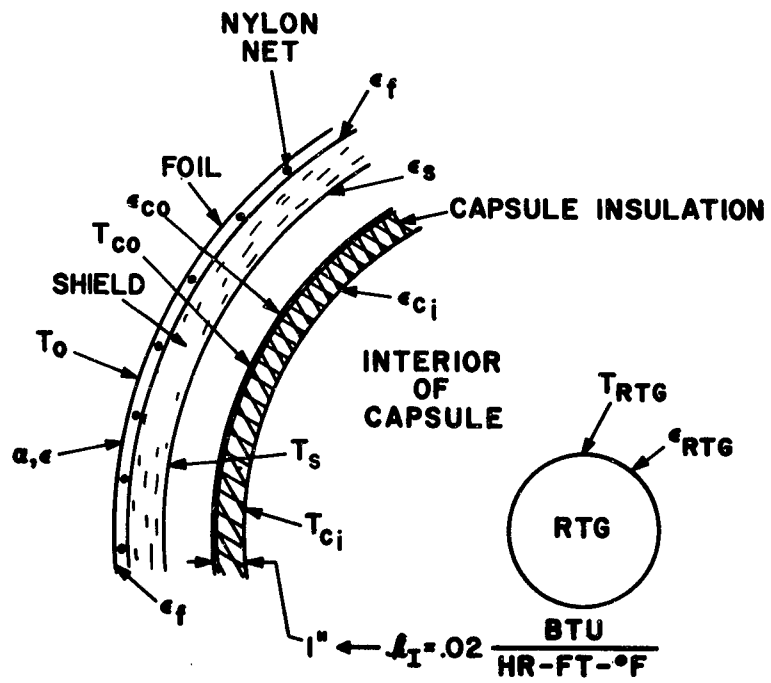


Figure 9. Section Through Vehicle

COMPONENT	SYSTEM WEIGHT				RADIOISOTOPE SYSTEMS	
	α/ϵ COATING SYSTEM	α/ϵ CONTROL SYSTEM	SUPER-INSULATION SYSTEM	RTG INSIDE CAPSULE (.95 ELECTRICAL WATTS)	RTG OUTSIDE VEHICLE (15 ELECTRICAL WATTS)	
Magnesium Liner or Shell	4.7 lb.	5.0 lb.	-	-	-	-
Solar Cells	.7	-	1.6 lb.	-	-	-
α/ϵ Shutters and Tubing	-	8.0	-	-	-	-
Battery Insulation	.7	.7	.7	.7 lb.	.7 lb.	
Heat of Fusion Material	6.5	-	-	-	-	-
Superinsulation Shell	-	-	9.8	-	-	-
RTG Unit	-	-	-	4.5	20.6	
Foil and Nylon Net	-	-	-	3.0	3.0	
Capsule Insulation	3.0	3.0	3.0	3.0	3.0	
RTG Separation Device	-	-	-	-	5.0	
Superinsulation or Clam-Shell Removal Device	-	5.0	5.0	-	-	
Total	15.6	21.7	20.1	11.2	*32.3	

*Assumes no heaters necessary (heat is dissipated in electronic equipment).

Figure 10. Thermal Control System Weights

DYNAMIC RESPONSE
ANALYSIS OF TEMPERATURE
CONTROL SYSTEMS BY USE
OF DIGITAL COMPUTER

by

F. I. Honea

North American Aviation Inc.
Downey, California

NOMENCLATURE

A	Area, ft
c_p	Specific heat, Btu/(lb _m) (°F)
C()	Constant (AESOP)
D	Diameter, ft
DCALC	Calculation time interval (AESOP, same as $\Delta\tau$), hr
f	Fluid flow friction factor, non-dimensional
Ξ	Radiation configuration factor, non-dimensional
g_c	Gravitational constant, 32.2 (lb _m) (ft)/(lb _f) (sec) ²
G	Controller gain, (°F) (hr)/lb _m
h	Heat transfer film coefficient, Btu/(hr)(°F)(sq ft)
k	Thermal conductivity, Btu/(hr)(°F)(ft)
K	Equation Parameter (see Equation 3)
L	Length, ft
m	Mass, lb _m
\dot{m}	Mass flow rate, lb _m /hr
p	Pressure, psf (lb _f /sq ft)
P	Flow perimeter, ft
q	Heat transfer rate (or load), Btu/hr
T	Temperature, °F (or °R for T ⁴)
T'	Temperature at present time interval, °F (or °R for T ⁴)

\dot{T}	Temperature rate of change with time $\left(\dot{T} = \frac{\partial T}{\partial \tau} \approx \frac{T' - T}{\Delta \tau}\right), \text{ } ^\circ\text{F/hr}$
TB()	Table value (AESOP)
U	Overall heat transfer coefficient, Btu/(hr)($^\circ\text{F}$)(sq ft)
V	Velocity, ft/sec
V()	Variable with time (AESOP) at last calculation time (such as T at τ_0)
VP()	Variable with time (AESOP) at present calculation time (such as T' at $\tau_0 + \Delta\tau$)
Δ	Increment
ρ	Density, lb _m /cu ft
σ	Stefan-Boltzman constant, 0.1713×10^{-8} Btu/(sq ft)(hr)($^\circ\text{R}$) ⁴
τ	Time; hr

Subscripts

1, in	fluid inlet
2, out	fluid outlet
cp	cold plate
f	fluid
hx	heat exchanger
p	pump
r	radiator
s	sensor
v	valve
w	wall

Dynamic Response of Temperature Control Systems by the Use of Digital Computer

F. I. Honea

INTRODUCTION

Often temperature control systems designed for space vehicle or aircraft applications have not performed as well as desired. As a result, several major redesign efforts are usually required after vehicle assembly in order to develop an acceptable system. This inferior system performance can generally be traced to the improper choice of location and types of sensors, controllers, and regulating devices, and to the neglect of dynamic response analysis for prediction of system performance. From a consideration of the analysis approach used for most designs, the heat transfer and thermodynamic analyses appear satisfactory, but the control and flow rate choices are usually based on maximum and minimum temperature and heat load considerations. Obviously, this procedure does not lead to an optimum, well controlled system, since neither consideration for the heat storage of the equipment, coolant, and components nor prediction of control system response is included.

The real importance of dynamic response analysis for space vehicle temperature control systems is not apparent unless a detailed breakdown of the system heat loads is considered. The basic heat loads can be listed as:

Solar, reflected, and planetary radiant heat (variable with vehicle spin, orientation, distance from sun and orbit conditions)

Equipment and personnel heat load to heat exchangers and cold plates (variable with time and function)

As the heat load for most vehicles obviously must vary with time, there should be no doubt that such factors as speed of response, damping factor, phase lag and dead band, stability, control band, and prediction of temperature versus time for individual components are necessary outputs to any analysis. Apparently, the main cause of the neglect of dynamic response analysis is that most texts on dynamic response systems are directed toward hydraulic, pneumatic, and electrical systems with little or no mention of temperature control applications.

Another cause is the need for three or four courses in linear and non-linear system analysis for basic understanding of the block diagram, Laplace transform analysis method. Also, it may be noted that a block diagram, Laplace transform solution becomes extremely complex for a system with fluctuating heat loads which controls temperature by fluid flow modulation. To alleviate the deficiency of reference material and background, the differential equation method of analysis has been developed and uses the basic differential equations for temperatures, heat transfer, and fluid flow in a

form that can be solved by the existing AESOP computer program, or by an analog network. This method has advantages over the block diagram, Laplace transform method for estimating variations of the temperature of individual control system components with time for any type of variable heat input and for calculating temperature control band and response. This method may also be more accurate, since more types of equations are possible without the Laplace transform restrictions.

The method of analysis and the example system presented herein were developed for inclusion in Reference 1 (ASD TDR 62-493, Part II) from the current Space Vehicle Thermal and Atmospheric Control Systems study program ASD contract with the Space and Information Systems Division of North American Aviation, Inc.

FLUID ELEMENT HEAT TRANSFER TO WALL

To develop the differential equations for temperature control components in circulating, variable-flow fluid systems, the heat transfer between the fluid element and the component wall should be described. Considering a fluid element of length dx , as shown in Figure 1, the following heat transfer balance can be obtained:

$$hP(T_W - T) = \dot{m}c_p \frac{\partial T}{\partial X} + \rho Ac_p \frac{\partial T}{\partial \tau} \quad (1)$$

For a finite length ΔX as shown in Figure 2, this equation can be rewritten as

$$hP \left[T_W - \left(\frac{T_1 + T_2}{2} \right) \right] = \frac{\dot{m}c_p}{\Delta X} (T_2 - T_1) + \frac{\rho Ac_p}{2\Delta\tau} [(T_1' + T_2') - (T_1 + T_2)] \quad (2)$$

where the prime temperatures are at the present time interval, $\tau_0 + \Delta\tau$, and the non-prime values are at the previous calculation time interval. A rearrangement of this equation yields

$$T_2' = K(\Delta\tau) T_1 + (1 - K)(\Delta\tau) T_2 + \left(\frac{2hP\Delta\tau}{\rho Ac_p} \right) T_W + (T_1 - T_1') \quad (3)$$

where

$$K = \frac{2\dot{m}c_p - hP\Delta x}{\rho Ac_p}$$

This equation is similar to one derived by Dusingberre¹, except for the inclusion of T_1' . It may be noted that T_W , T_1' , and T_2' are neglected in this case for the convection and flow terms, since these terms have a negligible effect on the initial slope of the temperature change of the fluid with time. The overall heat transfer coefficient, U , could also be used to more accurately describe the transfer from fluid element to wall.

To describe the temperature change of the wall, the heat transfer balance is

$$(\dot{m}c_p)_W \left(\frac{T_W' - T_W}{\Delta\tau} \right) = hP\Delta x \left[\frac{(T_1 + T_2)}{2} - T_W \right] + q \quad (4)$$

for average temperature difference and for external heat load q .

¹Reference 1

Rearranging,

$$T_W' = hP\Delta x \left[\frac{(T_1 + T_2)}{2} - T_W \right] \frac{\Delta\tau}{(mc_p)_W} + \frac{q\Delta\tau}{(mc_p)_W} + T_W \quad (5)$$

Thus, Equations 3 and 5 can be used to define the heat transfer to a wall from a fluid element with negligible pressure drop. The equations derived have physical limitations due to the use of finite length Δx and the calculation interval $\Delta\tau$. These limitations can be shown to be

$$\Delta\tau \leq \frac{\rho\Delta c_p}{hP + \frac{\dot{m}c_p}{\Delta x}} \quad (6)$$

and

$$\Delta x \leq \frac{2\dot{m}c_p}{hP} \quad (7)$$

These limitations are important in choosing calculation time intervals and increment lengths for computer analysis.

An alternative set of equations can be obtained by assuming an exponential temperature change in the fluid element instead of the average used previously. The equations for an increment Δx with negligible heat storage in the fluid then become

$$T_2 = (T_W - T_1)e^{-\frac{hP\Delta x}{\dot{m}c_p}} + T_1 \quad (8)$$

and

$$T_W' = \frac{hP\Delta x}{(\dot{m}c_p)_W} \left[\frac{(T_2 - T_1)}{\ln\left(\frac{T_2 - T_W}{T_1 - T_W}\right)} \right] \Delta\tau + \frac{q\Delta\tau}{(mc_p)_W} + T_W \quad (9)$$

In Equation 8, $T_2 \rightarrow T_W$ for $\dot{m} \rightarrow 0$ and $T_2 \rightarrow T_1$ for $\dot{m} \rightarrow \infty$, which is to be expected. Thus, these equations can be used without the restriction of Δx (Equation 7).

If a pressure drop equation is desired, an equation such as

$$\Delta p = f\rho\left(\frac{L}{D}\right)\left(\frac{V^2}{2g_c}\right) \quad (10)$$

can be added to equation groups 3 and 5 or 8 and 9. Other equations for heat transfer coefficient, h , and for thermal properties can be used. Terms can also be added to the equations for heat transfer to adjacent node points or elements.

TEMPERATURE CONTROL SYSTEMS

For simple temperature control systems with small pressure drops, the Equations 3 and 5, or 8 and 9, or similar equations with terms added can be used to completely define the system. In the simplest case, for example, a cold plate could be represented as a wall element or "lumped mass" with fluid cooling. T_1 would be the inlet fluid temperature, T_2 would be the outlet fluid temperature, and T_w would be the cold plate temperature. This cold plate could be coupled to the next fluid cooled component by using T_2 of the cold plate as the fluid inlet temperature to that component. Similarly, a whole system could be defined. Table I shows some of these simple lumped-mass components for temperature control systems.

For control purposes, some form of flow rate variation to control temperature naturally will be desired. This variation can be assumed as linear with different slopes (or gain) for proportional control, or as on-off for solenoid valve or thermo-switch actuation. If more exact controller characteristics are available, they also can be used.

Table 1 includes some of these equations for proportional and on-off valves and for sensors and thermostats. The use of equations to compare parameters in determining whether a given parameter is greater or less than a desired value, may be noted. This type of comparison with equations is easily set up with the AESOP program. The use of these equations makes possible the definition of the actuation of the on-off valve that switches from open to closed position, and the thermostat that switches on at one temperature and off at another.

Table 1. Differential Equations for Dynamic Response

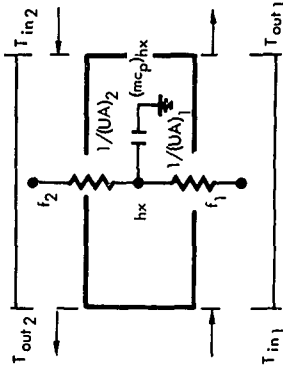
COMPONENT AND SKETCH	EQ. NO.	EQUATION	REMARKS
<p>HEAT EXCHANGER (A) FLUID-FLUID FLOW:</p> 	1	$T_{hx} = \frac{(UA)_{1-hx}}{(mc_p)_{hx}} \left[\frac{T_{in1} - T_{out1}}{T_{in1} - T_{hx}} \right] \ln \left(\frac{T_{out2} - T_{hx}}{T_{in2} - T_{hx}} \right) + \frac{(UA)_{2-hx}}{(mc_p)_{hx}} \left[\frac{T_{in2} - T_{out2}}{T_{in2} - T_{hx}} \right] \ln \left(\frac{T_{out2} - T_{hx}}{T_{in2} - T_{hx}} \right)$	TEMPERATURE OF HEAT EXCHANGER LUMPED MASS
	2	$T_{out2} = (T_{in2} - T_{hx}) e^{-\frac{(UA)_{2-hx}}{(mc_p)_{2-hx}} (T_{in2} - T_{hx})} + T_{hx}$	OUTLET TEMPERATURE OF COOLANT FLUID #2
	3	$T_{out1} = (T_{in1} - T_{hx}) e^{-\frac{(UA)_{1-hx}}{(mc_p)_{1-hx}} (T_{in1} - T_{hx})} + T_{hx}$	OUTLET TEMPERATURE OF COOLANT FLUID #1
	4	$h_2 = F \left(\frac{T_{in2} + T_{out2}}{2} - T_{in1} \right), \dot{m}_2$	HEAT TRANSFER FILM COEFFICIENT FOR FLUID #2 $U_2 = f[h_2, (k/x)_{hx}, A_{hx}]$

Table 1. Differential Equations for Dynamic Response (Cont.)

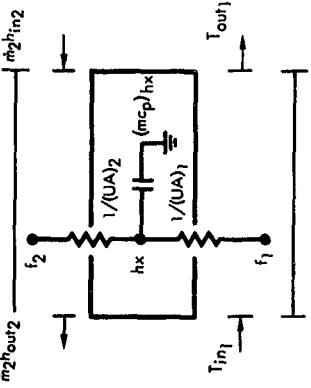
COMPONENT AND SKETCH	EQ. NO.	EQUATION	REMARKS
<p>HEAT EXCHANGER (A) FLUID-FLUID FLOW:</p> <p>(B) FLUID-VAPORIZING (OR CONDENSING) LIQUID FLOW:</p> 	5	$h_1 = f \left(\frac{T_{in1} + T_{out1}}{2}, m_1 \right)$	<p>HEAT TRANSFER FILM COEFFICIENT FOR FLUID #1</p> $U_1 = f [h_1, (k/x)_{hx}, A_{hx}]$
	6	$T_{hx} = \frac{(hA)_{2-hx}}{(mcp)_{hx}} (T_2 - T_{hx}) + \frac{(UA)_{1-hx}}{(mcp)_{hx}} \ln \left[\frac{T_{in1} - T_{out1}}{T_{in1} - T_{hx}} \right]$	<p>TEMPERATURE OF HEAT EXCHANGER LUMPED MASS ASSUMES VAPORIZING LIQUID IS AT CONSTANT TEMPERATURE</p>
	7	$T_{out1} = \text{(SAME AS EQUATION #3)}$	<p>OUTLET TEMPERATURE OF FLUID</p>
	8	$\dot{m}_2 (\bar{h}_{in2} - \bar{h}_{out2}) = (hA)_{2-hx} (T_2 - T_{hx})$	<p>\bar{h} = ENTHALPY ENERGY BALANCE FOR VAPORIZING LIQUID</p>
	9	$h_2 = f(T_2, T_{hx}, x, \dot{m}_2)$	<p>BOILING OR CONDENSING FILM COEFFICIENT</p>

Table 1. Differential Equations for Dynamic Response (Cont)

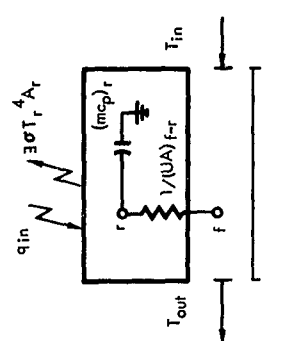
COMPONENT AND SKETCH	EQ. NO.	EQUATION	REMARKS
	10	$h_1 = \text{(SAME AS EQUATION #5)}$	
<p>SPACE RADIATOR</p> <p>(A) FORCED CONVECTION</p> 	11	$\dot{T}_r = \frac{(UA) f - r}{(mcp)_r} \left[\frac{T_{in} - T_{out}}{\ln \left(\frac{T_{in} - T_r}{T_{out} - T_r} \right)} \right] + \frac{q_{in}}{(mcp)_r} - \frac{3A_r (T_r)^4}{(mcp)_r}$	TEMPERATURE OF RADIATOR LUMPED MASS. A_r IS EFFECTIVE RADIATOR AREA
	12	$T_{out} = (T_{in} - T_r) e^{-\frac{(UA) f - r}{(mcp)_r} t} + T_r$	OUTLET TEMPERATURE OF FLUID
	13	$q_{in} = f(q_{pr}, q_r, q_s, s, E_r, t)$	RADIATOR HEAT INPUT (TABLE VALUE AS FUNCTION OF TIME)
	14	$h = f\left(\frac{T_{in} + T_{out}}{2}, m, t\right)$	HEAT TRANSFER FILM COEFFICIENT FOR FLUID $U = f(h, A, k/x)$

Table 1. Differential Equations for Dynamic Response (Cont)

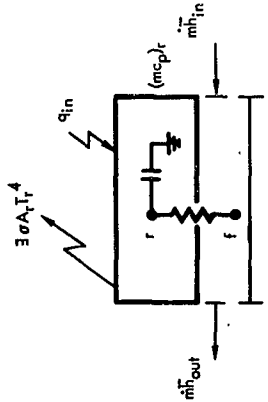
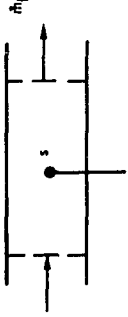
COMPONENT AND SKETCH	EQ. NO.	EQUATION	REMARKS
<p>(B) CONDENSING (OR VAPORIZING) LIQUID:</p> 	15	$\dot{T}_f = \frac{(hA)_f - r}{(mcp)_f} (T_f - T_f) + \frac{q_{in}}{(mcp)_f} r$ $- \frac{\exists \sigma A_f T_f^4}{(mcp)_f} r$	TEMPERATURE OF RADIATOR LUMPED MASS. TEMPERATURE OF CONDENSING VAPOR ASSUMED CONSTANT
	16	$\dot{m}_f (\bar{T}_{in} - \bar{T}_{out}) = (hA)_f - r (T_f - T_f)$	ENERGY BALANCE FOR CONDENSING LIQUID
	17	$q_{in} = \text{(SAME AS EQUATION #13)}$	
	18	$h - f (T_{fr} T_r x, \dot{m}_f)$	CONDENSING (OR BOILING) FILM COEFFICIENT
<p>PROPORTIONAL TEMPERATURE SENSOR</p> <p>(A) FLUID TEMPERATURE</p> 	19	$\dot{T}_s = \frac{(hA)_s - f}{(mcp)_s} (T_f - T_s)$	SENSOR TEMPERATURE
	20	$h = f (T_{fr} T_s, \dot{m}_f)$	FLUID HEAT TRANSFER COEFFICIENT
	21	$R_s = f(T_s)$	RESISTANCE FOR RESISTANCE TYPE SENSOR

Table 1. Differential Equations for Dynamic Response (Cont)

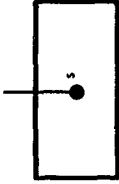
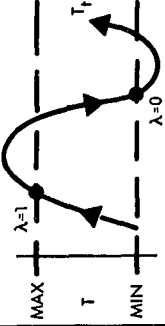
COMPONENT AND SKETCH	EQ. NO.	EQUATION	REMARKS
<p>PROPORTIONAL TEMPERATURE SENSOR</p> <p>(B) SOLID TEMPERATURE:</p>  <p>SOLID EQUIPMENT (e)</p>	22	$\dot{T}_s = \left(\frac{kA}{x}\right)_{s-e} \frac{1}{(mc_p)_s} (T_e - T_s)$	SENSOR TEMPERATURE
	23	$k = f(T_s, T_e)$	THERMAL CONDUCTIVITY (AVERAGE) TO SENSOR
	24	$R_s = f(T_s)$	RESISTANCE FOR RESISTANCE TYPE SENSOR
THERMOSTAT	25	$\dot{T}_t = \frac{(UA)}{(mc_p)_t} (T_f - T_t), (U = h \text{ or } k/x)$	TEMPERATURE OF THERMOSTAT
	26	<p>TEST 1: TEST FOR $\lambda = 1$ OR 0</p> <p>TEST 2: FOR $\lambda = 1$</p> <p>if $T_t > T_{MIN}$ SET $\lambda = 1$</p> <p>if $T_t = T_{MIN}$ SET $\lambda = 0$</p> <p>if $T_t < T_{MIN}$ SET $\lambda = 0$</p>	<p>$\lambda =$ SWITCH FUNCTION (1 OR 0)</p> <p>T_{MAX} - UPPER SWITCH LIMIT</p> <p>T_{MIN} - LOWER SWITCH LIMIT</p>

Table 1. Differential Equations for Dynamic Response (Cont)

COMPONENT AND SKETCH	EQ. NO.	EQUATION	REMARKS
	26 (CONT)	TEST 3: FOR $\lambda = 0$ IF $T_1 > T_{MAX SETA} = 1$ IF $T_1 = T_{MAX SETA} = 0$ IF $T_1 < T_{MAX SETA} = 0$	
	27	$h = f(\dot{m}, T_f, T_p)$	FLUID FILM COEFFICIENT IF FLUID TEMPERATURE SENSED
	28	$k = f(T_s, T_g)$	AVERAGE THERMAL CONDUCTIVITY IF SOLID TEMPERATURE SENSED
VALVES	29	$\delta = f(T_v)$	δ = VALVE POSITION, (δ_{MAX} = CLOSED POSITION)
(A) PROPORTIONAL	30	$\dot{m}_v = f(\delta, T_p)$ (SEE EQUATION #34)	FLUID FLOW RATE
	31	$T_v = \frac{(UA)_{f-v}}{(m c_p)_v} \left[\frac{T_{in} - T_{out}}{T_{in} - T_v} \right] + \frac{q_v}{(m c_p)_v}$	VALVE TEMPERATURE

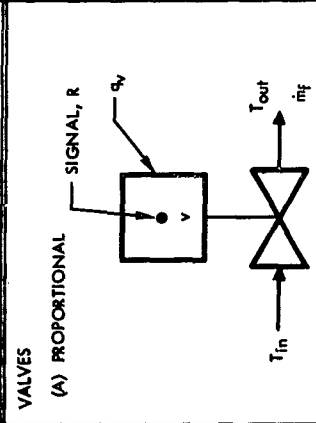


Table 1. Differential Equations for Dynamic Response (Cont)

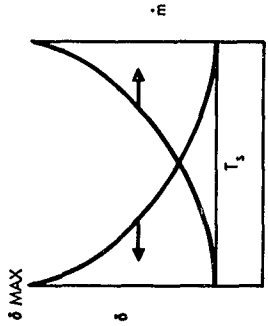
COMPONENT AND SKETCH	EQ. NO.	EQUATION	REMARKS
	32	$T_{out} \approx T_{in}$ <p>FOR $q_v, m, \text{ SMALL}$</p> $(\bar{T}_{in} = \bar{T}_{out} \text{ FOR THROTTLING AND } \bar{h} = c_p T.)$	FLUID OUTLET TEMPERATURE WITH SIGNIFICANT POWER TO OPERATE VALVE
	33	$T_{out} = (T_{in} - T_v) e^{-\frac{(UA) f_{-v}}{(m c_p) f}} + T_v$	FLUID OUTLET TEMPERATURE WITH SIGNIFICANT POWER TO OPERATE VALVE
	34	$\dot{m} f = \left(\frac{A \dot{m}}{A T_s} (T_s - T_o) \right) = K_1 (T_s - T_o)$ <p>$T_o = \text{REFERENCE, } K_1 = \text{SLOPE}$</p>	FLUID FLOW RATE FOR LINEAR FLOW CONTROL AS FUNCTION OF SENSOR TEMPERATURE
<p>VALVES</p> <p>(B) ON-OFF (SOLENOID):</p>	35	<p>TEST 1: COMPARE T_s TO T_{SET}</p> <p>TEST 2: FOR $T_s > T_{SET}$</p> <p>$\delta = \delta_{MIN}$ OR $\dot{m} = \dot{m}_{MAX}$</p> <p>TEST 3: FOR $T_s < T_{SET}$</p> <p>$\delta = \delta_{MAX}$ OR $\dot{m} = 0$ (OR $\dot{m} < \dot{m}_{MAX}$)</p>	<p>THE FLUID FLOW SYSTEM WITH $\dot{m} = 0$ WOULD REQUIRE A COMPLETELY DIFFERENT SET OF EQUATIONS FROM THE FLOW EQUATIONS. THE USE OF A SMALL LEAKAGE VALUE $\dot{m} < \dot{m}_{MAX}$ WILL ALLEVIATE THIS PROBLEM</p>

Table 1. Differential Equations for Dynamic Response (Cont)

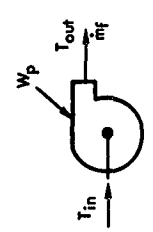
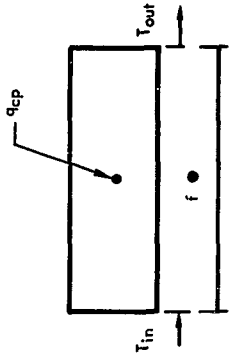
COMPONENT AND SKETCH	EQ. NO.	EQUATION	REMARKS
	36	$\dot{T}_v = \text{SAME AS EQUATION \#35 FOR VALVE OPEN OR } \dot{m} \ll \dot{m}_{MAX}$	VALVE TEMPERATURE WITH FLOW
	37	$T_{out} = \text{SAME AS EQUATION \#35 FOR VALVE OPEN OR } \dot{m} \ll \dot{m}_{MAX}$	FLUID OUTLET TEMPERATURE WITH FLOW
	38	$T_{out} \approx T_{in} \approx T_f \text{ FOR } \dot{m} = 0$	SYSTEM FLUID LUMPED - MASS TEMPERATURE WITH NO FLOW
	39	$(mcp)_f (T_{f1} - T_{f2}) = \sum_{i=0}^n (hA)_f (T_f - T_i) \Delta t$ <p style="text-align: center;">$(mcp)_f = \text{LUMPED THERMAL CAPACITY OF FLUID}$</p>	$\dot{m} = 0, i = \text{ANY COMPONENT, } h = \text{FREE CONVECTION } (= (k/\lambda)_f, i \text{ FOR ZERO "g"})$
<p>PUMP (OR FAN)</p> 	40	$\dot{T}_p = \frac{(UA)_p - f}{(mcp)_p} \left[\frac{T_{in} - T_{out}}{\ln \left(\frac{T_{in} - T_p}{T_{out} - T_p} \right)} \right] + \frac{(1 - \eta)}{(mcp)_p} W_p$	PUMP TEMPERATURE

Table 1. Differential Equations for Dynamic Response (Cont)

COMPONENT AND SKETCH	EQ. NO.	EQUATION	REMARKS
	41	$T_{out} = (T_{in} - T_p)e^{-X} + T_p$ $X = \frac{(UA)_{p-f}}{(m c_p) f} \left[1 - \frac{7 \gamma V_p}{m c_p (T_{in} - T_{out})} \right]$	FLUID OUTLET TEMPERATURE FOR INCOMPRESSIBLE FLOW
	42	$h_{p-f} = f \left(\dot{m}, \frac{T_{in} + T_{out}}{2}, T_p \right)$	HEAT TRANSFER FILM COEFFICIENT $U = f(h, k/x, A)$
COLD PLATE (OR ANY MASS WITH HEAT GENERATION AND FLUID FLOW)	43	$T_{cp} = \frac{(hA)_{cp-f}}{(m c_p)_{cp}} \left[\frac{T_{in} - T_{out}}{\ln \left(\frac{T_{in} - T_{cp}}{T_{out} - T_{cp}} \right)} \right] + \frac{q_{cp}}{(m c_p)_{cp}}$	COLD PLATE TEMPERATURE
	44	$T_{out} = (T_{in} - T_{cp})e^{-\frac{(hA)_{cp-f}}{(m c_p) f}} + T_{cp}$	FLUID OUTLET TEMPERATURE
	45	$h_{cp-f} = f \left(\dot{m}, \frac{T_{in} + T_{out}}{2}, T_{cp} \right)$	HEAT TRANSFER FILM COEFFICIENT. U_{cp-f} CAN BE USED INSTEAD IF $(k/x)_{cp-f}$ IS SIGNIFICANT

THE AESOP COMPUTER PROGRAM

The equations presented for the fluid element and wall have been relatively easy to formulate. However, even these simple equations would be difficult to solve by hand calculation methods. Fortunately, a program—AESOP—that can be used with these types of equations has been developed¹.

The AESOP computer program was developed first by G. Edward Eversole for use in solving the differential equations for transient heat transfer temperature of the X-15 skin, structure, and insulation. The method has been improved and modified since then to the present program, which allows the use of actual equations as input data for IBM 7090 computer solution. Recently this program has been made available to ASD in conjunction with the Space Vehicle Thermal and Atmospheric Control Study Program Contract with S&ID.

This computer program is ideally suited for solving equations such as (3), (5), (8), (9), and (10). Input can be in the form of differential or auxiliary equations with constants, initial values, and tables of functions that vary with time. The program can also include interrelated values of the equations for the present calculation interval and the previous interval, as used in Equation (3). The output from this program includes a print-out of the original equations, constants, initial values, and tables, and a listing of the calculated value of each equation for which recording is desired for each time interval. A typical input equation print-out is shown for the following example temperature control system solution. (See Figure 6).

¹Reference 2.

TEMPERATURE CONTROL SYSTEM RESPONSE ANALYSIS EXAMPLE

DESCRIPTION OF EXAMPLE SYSTEM

To illustrate the method of analysis of temperature control systems, the system shown in Figure 3 will be used as an example. The vehicle orbit and the heat input to the radiator from solar radiation and planetary radiation (Figure 4) are based on an orbital heat load analysis using a computer program that has been released to ASD¹. The vehicle is assumed to be cylindrical, rotating about its axis, and in orbit about the earth. The radiator surrounding the vehicle is assumed to be cylindrical. To make the system more realistic, a variable heat load to the cold plate with time has also been included (Figure 5). This variable heat load is represented here as a variation due to warming-up electronic equipment and broadcasting messages or control functions to a station on earth.

The desired function of the temperature control system for this vehicle is to maintain the electronic equipment mounted on the cold plate at operating temperature with band limits set at 0 and 150 F. The coolant fluid for the vehicle was chosen as 60 percent ethylene glycol-water. The characteristics for the components of the system are based on actual components and are shown in Table 2.

OBJECTIVES OF ANALYSIS

Since the example system as introduced is a completely designed system, questions arise pertaining to the usefulness of the response analysis. The desired objectives however, show the importance of such an analysis, and they are listed as follows:

- (1) To find the controlled temperature (and other component temperatures) versus time for a proportional sensor and proportional valve
- (2) To find the controlled temperature (and others) versus time for a proportional sensor and on-off valve
- (3) To compare the results of (2) and (3)
- (4) To determine the minimum flow rate for the valve-on position required for on-off control within the desired temperature limits

¹Reference 4.

Table 2. Component Properties for Example System

Component	Mass m	Specific Heat, C_p	mc_p	Area	Miscellaneous
	lb _m	Btu/ (lb _m)(°F)	Btu/°F	Sq Ft	
Sensor (or thermostat)	0.1	0.2	0.02	0.01	U = 480 Btu/ (sq ft)(°F)(hr) Contact resistance (Fig. 2, Part I)
Valve	0.5	0.2	0.10	0.02	
Cold plate	4.0	0.2	0.80	1.50	
Pump	1.0	0.2	0.20	0.03	W = 80 Btu/hr $\eta_p = 0.9$
Radiator	20.0	0.2	4.00	20.00 (Space) 7.33 (Coolant)	$\alpha_s = 0.2$ $\epsilon_v = 0.9$ $\eta_r = 0.8$
Tubing and fittings	Lumped with components, can vary dependent on line lengths and fittings				
Coolant: (EGW, 60% Ethylene glycol- water)	Properties at 70 F: Density, $\rho = 67.2$ lb _m /cu ft Specific heat, $C_p = 0.78$ Btu/(°F)(lb _m) Viscosity, $\mu = 15.8$ lb _m /(ft)(hr) Conductivity, $k = 0.226$ Btu/(ft)(°F)(hr)				

SETUP OF EQUATIONS FOR EXAMPLE SYSTEM ANALYSIS

The setup of differential equations for the example system is based on those presented in Table I, and they are based on assumptions of negligible heat storage in the fluid element, and of an exponential type fluid temperature change in a segment or component. Obviously, these assumptions can be expected to impair the accuracy of the analysis. However, the equations used should be sufficient for initial predictions of the temperature response of the system. This conclusion is borne out by the actual results to be presented.

Assumptions for this first quick analysis included the use of a small flow leakage at the valve-off position to eliminate no-flow heat transfer problems, and the use of a linear variation of mass-flow rate with sensor temperature for the proportional valve with a slope gain of two and valve-off set point of 40 F,

$$T_s - T_{s0} = G (\dot{m} - \dot{m}_0) \quad (11)$$

or

$$T_s - 40 = 2 (\dot{m} - 0.001).$$

Also the set point temperature for on-off control was set at 40 F.

The following set of equations was used for the analysis:

(1) Sensor: (Table I, Equation 22)

$$\dot{T}_s = \left(\frac{kA}{x} \right)_{s-e} \frac{1}{(mc_p)_s} (T_{cp} - T_s)$$

(2) Fluid flow rate at valve:

(a) Proportional (gain = 2): (Table I, Equation 34)

$$\text{if } (T_s - T_0) \geq 0: \quad (\text{Case 1})$$

$$(\dot{m}c_p)_f = K_1 (T_s - T_0) = 0.94 (T_s - 500)$$

$$\text{if } (T_s - T_0) < 0:$$

$$(\dot{m}c_p)_f \rightarrow 0 \text{ (or small value) (} \dot{m} = 0.01 \text{ lb/hr used)}$$

(b) On-off: (Table I, Equation 34)

if $T_s - T_{so} \leq 0$,

$(\dot{m}c_p)_f = 0$ (or small value) [$(\dot{m}c_p)_f = 0.01$ used]

if $T_s - T_{so} > 0$,

$$(\dot{m}c_p)_f = (\dot{m}c_p)_f \text{ max} \quad (\text{Case 2})$$

$$= 117.0 \text{ Btu}/(\text{hr}) (^\circ\text{F}) \quad (\text{Case 2a})$$

$$= 99 \text{ Btu}/(\text{hr}) (^\circ\text{F}) \quad (\text{Case 2b})$$

$$= 70.2 \text{ Btu}/(\text{hr}) (^\circ\text{F}) \quad (\text{Case 2c})$$

(3) Fluid convective heat transfer coefficient:

Assume: (1) $h \neq f(T)$

(2) $D = 0.375$ in. average ID

(3) $h_{cp-f} = h_{p-f} = h_{r-f} = h_{v-f}$

(4) Average $L \approx 2$ ft

$$Re = \frac{\dot{m}D}{\mu A} = 2100 \text{ for transition}$$

or

$$\dot{m} = 2100 \left(\frac{\mu A}{D} \right) = 815 \text{ lb m/hr}$$

$$(c_p \dot{m})_f = (0.78 \times 815) = 636 \text{ Btu}/(\text{hr}) (^\circ\text{F}) \text{ (For EGW at } 70 \text{ F)}$$

(a) Laminar flow:

$$(c_p \dot{m})_f \leq 636$$

$$\begin{aligned} \Phi &= \frac{4}{\pi} \left(\frac{c_p \dot{m}}{kL} \right) = \frac{4}{\pi} \left(\frac{0.78}{0.226 \times 2} \right) \dot{m} = 2.19 \dot{m} \\ &= 2.80 (c_p \dot{m}) \end{aligned}$$

From the Nusselt-Graetz equation:

$$\text{Nu} = 3.65 + \frac{0.0668\Phi}{1 + 0.04(\Phi)^{2/3}} \quad (12)$$

or

$$h_{\text{avg}} = 3.65 \frac{k}{D} + \frac{0.0668\Phi (k/D)}{1 + 0.04(\Phi)^{2/3}}$$

$$h_{\text{avg}} = 26.3 + \frac{1.346 (c_p \dot{m})}{1 + 0.0794(c_p \dot{m})^{2/3}}$$

(b) Turbulent flow:

$$(c_p \dot{m})_f > 636$$

$$h \approx 0.055 \frac{(V)^{0.8}}{(D)^{0.2}} \quad \text{For EGW at 70 F} \quad (13)$$

(Based on Colburn "j" factor)

Rearranging:

$$h = \frac{0.055}{c_p} \left(\frac{\dot{m} c_p}{A} \right)^{0.8} \frac{1}{(D)^{0.2}} = 1.60 (\dot{m} c_p)^{0.8}$$

(4) Valve temperature: (Table I, Equation 31)

(assume $q_v \approx 0$)

$$\dot{T}_v = \frac{(hA)_{f-v}}{(mc_p)_v} \left[\frac{T_4 - T_1}{\ln \frac{T_4 - T_v}{T_1 - T_v}} \right]$$

(5) Fluid outlet from valve: (Table I, Equation 33)

$$T_1 = (T_4 - T_v) e^{-\frac{(hA)_{v-f}}{(mc_p)_f}} + T_v$$

(6) Cold plate: (Table I, Equation 43)

$$\dot{T}_{cp} = \frac{(hA)_{cp-f}}{(mc_p)_{cp}} \left[\frac{T_1 - T_2}{\ln\left(\frac{T_1 - T_{cp}}{T_2 - T_{cp}}\right)} \right] + \frac{q_{out}}{(mc_p)_{cp}}$$

(7) Fluid outlet from cold plate: (Table I, Equation 44)

$$T_2 = (T_1 - T_{cp})e^{-\frac{(hA)_{cp-f}}{(mc_p)_f}} + T_{cp}$$

(8) Pump: (Table I, Equation 40)

$$\dot{T}_p = \frac{(hA)_{p-f}}{(mc_p)_p} \left[\frac{T_2 - T_3}{\ln\left(\frac{T_2 - T_p}{T_3 - T_p}\right)} \right] + \frac{(1 - \eta)W_p}{(mc_p)_p}$$

where

W_p = pump power = 80 Btu/hr

η = pump efficiency = 0.9

(9) Fluid outlet from pump: (Table I, Equation 41)

$$T_3 = (T_2 - T_p)e^{-\frac{(hA)_{p-f}}{(mc_p)_f} \left(\frac{1}{1 - \frac{\eta W_p}{mc_p(T_3 - T_2)}} \right)} + T_p$$

(10) Radiator: (Table I, Equation 11)

$$\dot{T}_r = \frac{(hA)_{r-f}}{(mc_p)_r} \left[\frac{T_3 - T_4}{\ln\left(\frac{T_3 - T_r}{T_4 - T_r}\right)} \right] + \frac{q_m}{(mc_p)_r} - \frac{3A_r \sigma (T_r)^4}{(mc_p)_r}$$

(11) Fluid outlet from radiator: (Table I, Equation 12)

$$T_4 = (T_3 - T_r)e^{-\frac{(hA)_{r-f}}{(mc_p)_f}} + T_r$$

For solution by use of the AESOP program these equations were set up on an IBM 7090. $\dot{T} \approx (T' - T)/\Delta\tau$ was used for the program setup with $VP(\) = T'$ at present time and $V(\) = T$ at previous time interval. The equations as set up for computer solution are shown in Figure 6. Figure 7 lists the constants and initial values for these equations. The time interval for the computer solution was based on the smallest constant for a system component, as calculated previously. This time constant was $\tau = 0.00417$ hours for the sensor. The actual calculation time interval was set at 0.001 hours, which is well below the smallest time constant. The run time for the problem for three orbits was approximately two minutes.

RESULTS OF EXAMPLE SYSTEM ANALYSIS

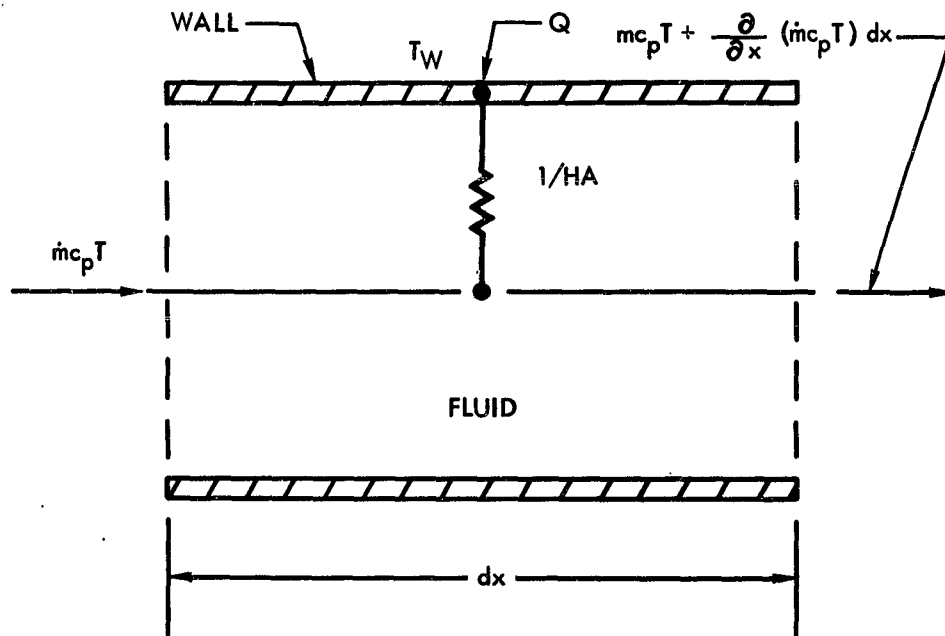
The results of the analysis are shown in Figures 8, 9, and 10. Figure 8 shows the results for a proportional valve, Figure 9 for an on-off valve, and Figure 10 for the temperature control ranges as a function of maximum flow rate for the on-off and proportional valves. Thus, the results accomplish the objectives listed for temperature versus time for proportional and on-off control. The indicated minimum flow rate for valve-on position required for on-off control within the 75 ± 75 F desired limits is 104 lb/hr (Figure 10).

CONCLUSION

The use of differential equations with the AESOP computer program to analyze the response of a temperature control system has been illustrated. The simplified system shown does not represent the ultimate capacity of this analysis method, since the use of much more complex characteristic differential equations for components is possible, and components such as space radiators can be segmented into smaller lumped-mass nodes. Also, temperature control systems with two-phase flow, or with other control methods besides fluid circulation can be analyzed. The system equations can be as complex or as simplified as the analysis demands, as long as the maximum storage capacity of the IBM 7090 in use is not exceeded.

REFERENCES

1. Dusinberre, G. M. Calculation of Transient Temperatures in Pipes and Heat Exchangers by Numerical Methods. American Society of Mechanical Engineering, Transactions of the ASME (April 1954).
2. Eversole, G. Edward An Easy System of Programming (AESOP). Los Angeles Division of North American Aviation, Inc., company report (released to ASD) NA 60-1368 (21 November 1960).
3. Honea, F. I. Temperature Control Systems for Space Vehicles, Part II. Space and Information Systems Division of North American Aviation, Inc., ASD Technical Documentary Report TDR 62-493 Part II (20 December 1962).
4. McCue, G. A. Program for Determining the Thermal Environment and Temperature History of Orbiting Space Vehicles. Space and Information Systems Division of North American Aviation, Inc., Air Force Report ASD TN61-83 (7 March 1962).



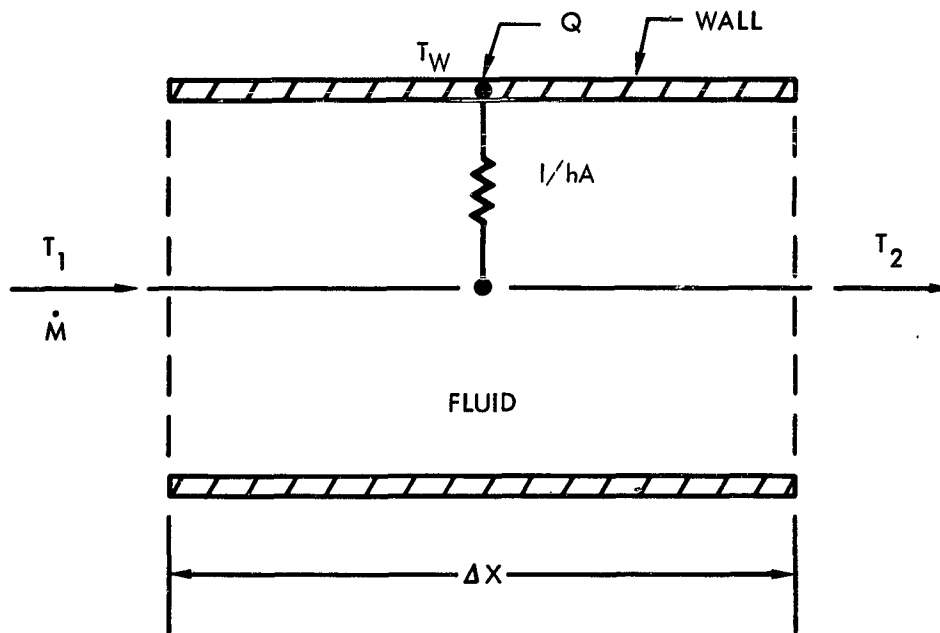
HEAT BALANCE TO FLUID:

$$hP(T_W - T) = \dot{m}c_p \frac{\partial T}{\partial x} + A c_p \rho \frac{\partial T}{\partial T} \quad (1)$$

HEAT BALANCE TO WALL:

$$(mc_p)_W \frac{\partial T_W}{\partial T} = hP(T - T_W) + q$$

Figure 1. Incremental Fluid Element and Wall



HEAT BALANCE TO FLUID:

$$hP \left[T_W - \frac{T_1 + T_2}{2} \right] = \frac{\dot{m}c_p}{\Delta X} (T_2 - T_1) + \frac{\rho A c_p}{2 \Delta \tau} \left[(T'_1 + T'_2) - (T_1 + T_2) \right] \quad (2)$$

HEAT BALANCE TO WALL:

$$(mc_p)_W \frac{(T'_W - T_W)}{\Delta \tau} = hP \left[\frac{(T_1 + T_2)}{2} - T_W \right] + q$$

Figure 2. Finite Fluid Element and Wall

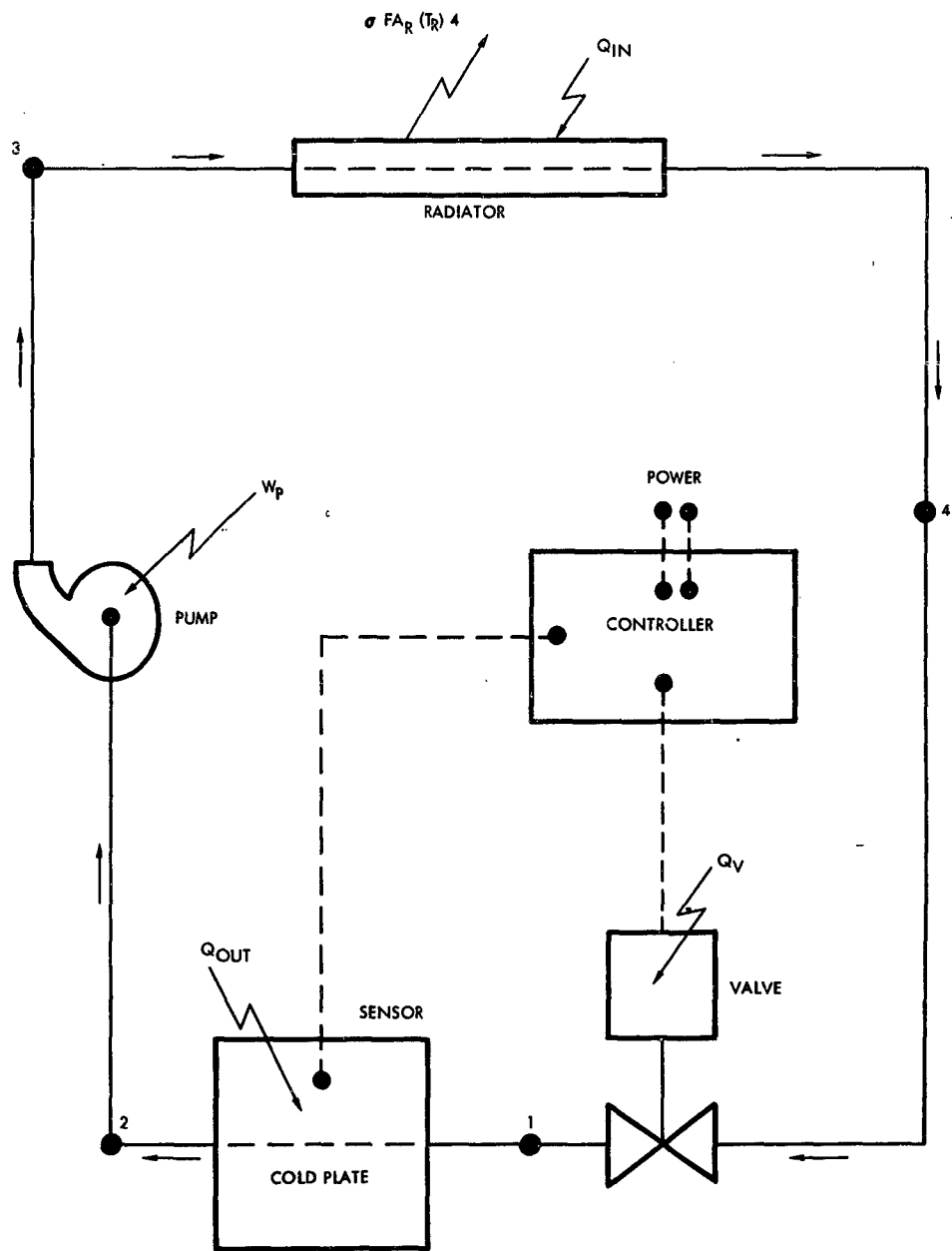


Figure 3. Example Semipassive Fluid Temperature Control System

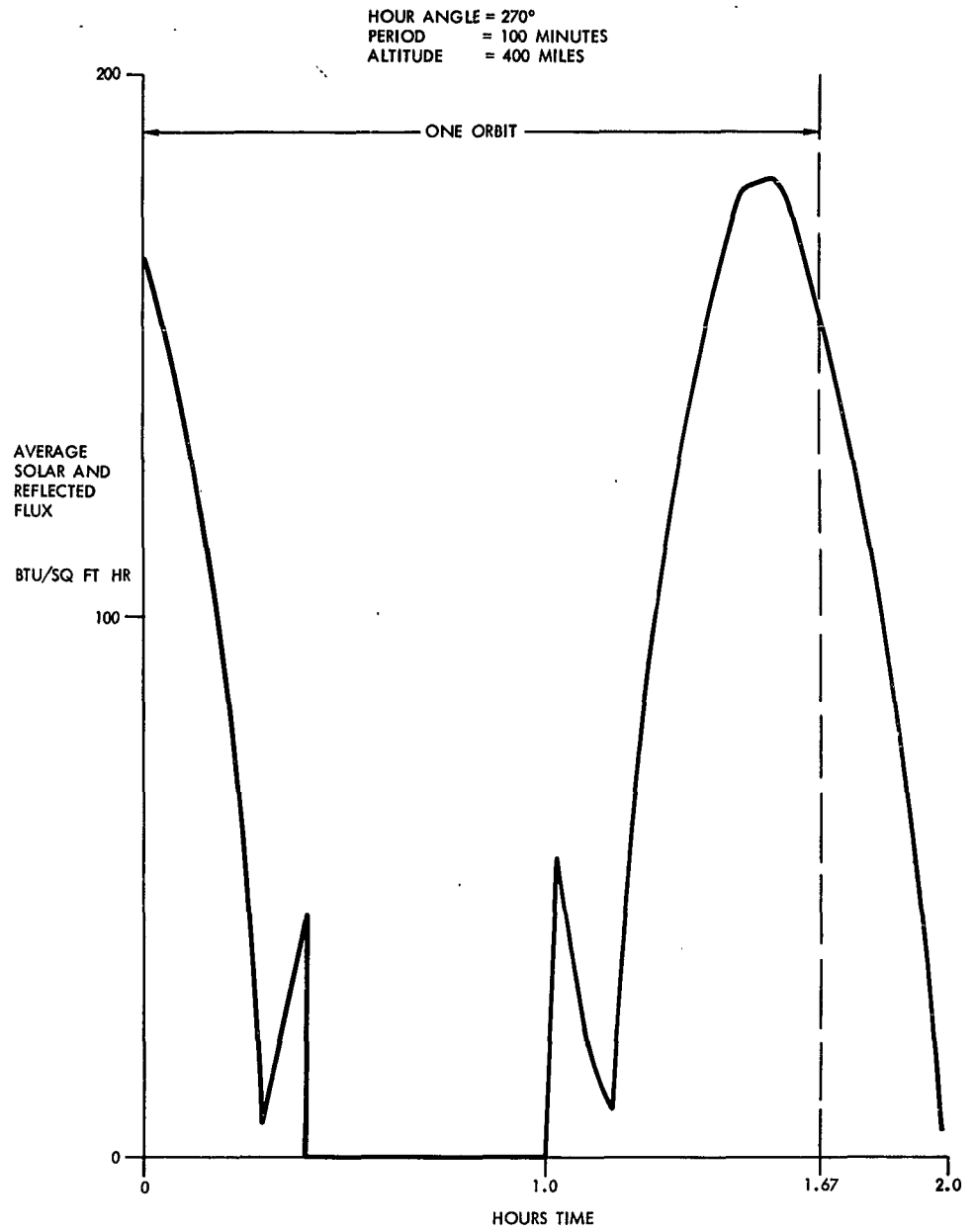


Figure 4. Typical Solar and Reflected Flux for Example Problem

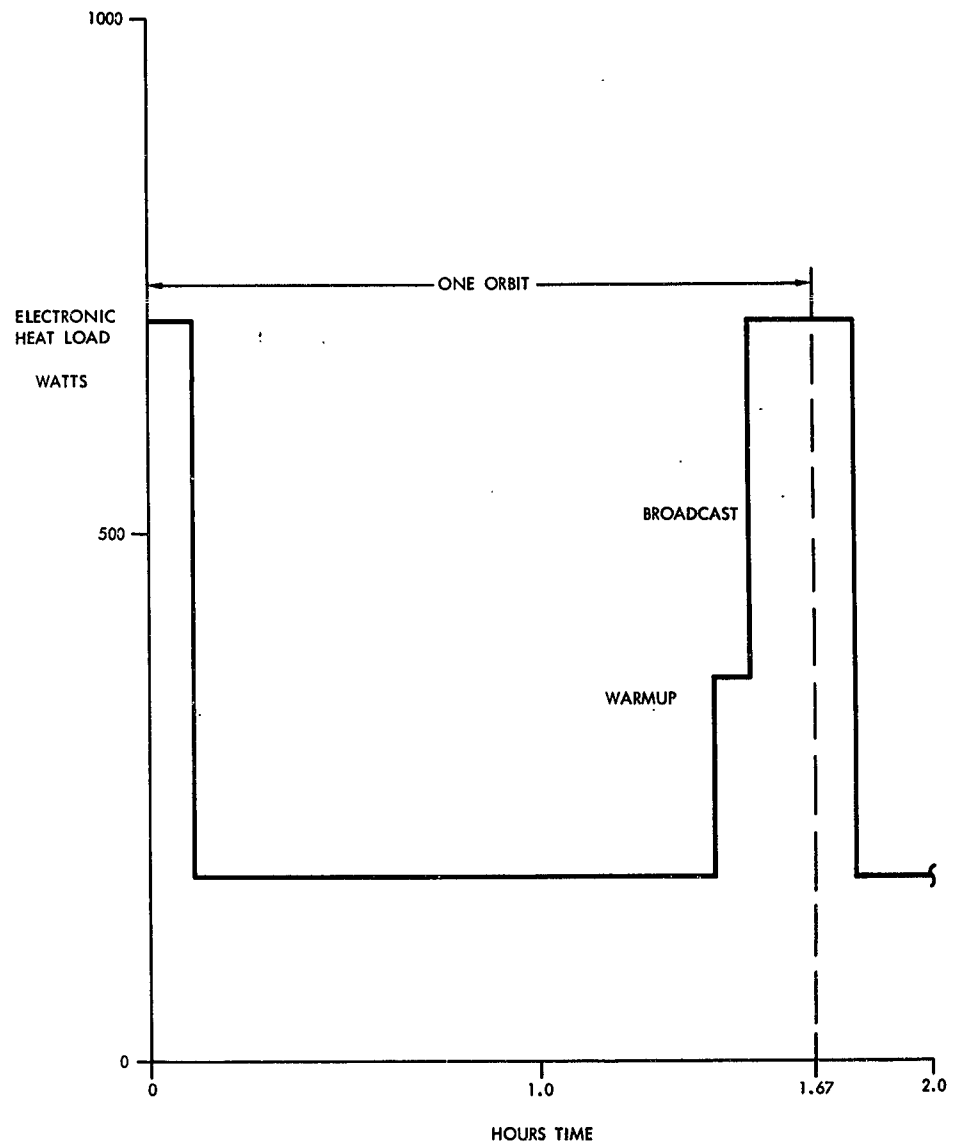


Figure 5. Typical Electronic Heat Load for Example Problem

Case 1 Proportional Valve

1	VP(1) = V(1) + DCALC /C(2) * C(1) * (V(6) - V(1))	00000010
2	IF (V(1) - C(3)) 5,5,3	00000020
3	VP(2) = 0.94 * (V(1) - C(3))	00000030
4	GO TO 6	00000040
5	VP(2) = 0.01	00000050
6	IF (V(2) - C(5)) 7,7,9	00000060
7	VP(3) = 26.3 + 1.346 * V(2) / (1.0 + 0.0794 * V(2)**0.67)	00000070
8	GO TO 13	80
9	VP(3) = 1.60 * V(2)**0.8	00000090
13	A1 = 1.0	00000130
14	IF (V(5) - V(4)) 15,17,15	00000140
15	VP(4) = V(4) + DCALC /C(6) * C(7) * V(3) * A1 * (V(11) - V(5)) / 1LOGEF (ABSF ((V(11) - V(4)) / (V(5) - V(4))) + 0.001)	00000150 160
16	GO TO 18	00000170
17	VP(4) = V(4)	00000180
18	VP(5) = (V(11) - V(4)) * EXPF(-V(3) * C(7) / V(2)) + V(4)	00000190
22	A2 = +1.0	00000230
23	IF (V(7) - V(6)) 25,27,25	00000240
25	VP(6) = V(6) + DCALC /C(8) * (V(3) * C(9) * A2 * (V(5) - V(7)) / 1LOGEF (ABSF ((V(5) - V(6)) / (V(7) - V(6))) + 0.001) + TB(2))	00000250 260
26	GO TO 28	00000270
27	VP(6) = V(6) + DCALC /C(8) * TB(2)	280
28	VP(7) = (V(5) - V(6)) * EXPF(-V(3) * C(9) / V(2)) + V(6)	00000290
32	A3 = +1.0	00000330
35	IF (V(9) - V(8)) 34,36,34	00000340
34	VP(8) = V(8) + DCALC /C(10) * (V(3) * C(11) * A3 * (V(7) - V(9)) / 1LOGEF (ABSF ((V(7) - V(8)) / (V(9) - V(8))) + 0.001) + C(12))	00000350 360
35	GO TO 37	00000370
36	VP(8) = V(8) + DCALC /C(10) * C(12)	380
37	IF (V(9) - V(7)) 38,40,38	00000390
38	D1 = 1.0 - C(13) / (V(2) * (V(9) - V(7)))	00000400
39	GO TO 41	00000410
40	D1 = -1.E10	00000420
41	VP(9) = (V(7) - V(8)) * EXPF(-V(3) * C(11) / V(2) / D1) + V(8)	00000430
45	A4 = 1.0	00000470
46	IF (V(11) - V(10)) 47,49,47	00000480
47	VP(10) = V(10) + DCALC /C(14) * (V(3) * C(16) * A4 * (V(9) - V(11)) / 1LOGEF (ABSF ((V(9) - V(10)) / (V(11) - V(10))) + 0.001) + C(17))	00000490 500
48	GO TO 50	510
49	VP(10) = V(10) + DCALC /C(14) * (C(17) * TB(3) - C(15) * V(10)**4.0 * 1 1.E-08)	00000520 530
50	VP(11) = (V(9) - V(10)) * EXPF(-V(3) / V(2) * C(16)) + V(10)	535 00000540
	RETURN	00000550
	END(1,0,0,0,0,0,1,0,0,1,0,0,0,0,0)	

Case 2 On-Off Valve (Additional Equations)

3	VP(2) = 117.0	30
3	VP(2) = 99.0	30
3	VP(2) = 70.2	30

Figure 6. Equations for Dynamic Response Example System

DYNAMIC RESPONSE CASE NO. 1A

00001000

SHEET A									
DCALC	0.0010	DPRINT	0.0100	TINIT	0.	TMAX	4.9000	CGGI	0.
EGNUM	11.	CNUM	22.	PHV	0.	DMP	0.	PDI	2.
VPHX1	C.	VPHX2	0.						
RKI	C.								
VP	PRINT VALUES	VP VALUES	WORK VALUES	INITIAL VALUES	UPPER LIMITS	LOWER LIMITS			
1	0.	0.	0.	5.300000E 02	1.000000E 04	-1.000000E 04			
2	0.	0.	0.	3.000000E 01	1.000000E 04	-1.000000E 04			
3	0.	0.	0.	5.200000E 01	1.000000E 04	-1.000000E 04			
4	0.	0.	0.	5.310000E 02	1.000000E 04	-1.000000E 04			
5	0.	0.	0.	5.290000E 02	1.000000E 04	-1.000000E 04			
6	0.	0.	0.	5.310000E 02	1.000000E 04	-1.000000E 04			
7	0.	0.	0.	5.300000E 02	1.000000E 04	-1.000000E 04			
8	0.	0.	0.	5.310000E 02	1.000000E 04	-1.000000E 04			
9	0.	0.	0.	5.290000E 02	1.000000E 04	-1.000000E 04			
10	0.	0.	0.	5.310000E 02	1.000000E 04	-1.000000E 04			
11	0.	0.	0.	5.300000E 02	1.000000E 04	-1.000000E 04			
SHEET F									
SEL	2.	PARN	3.	PTPAR	55.	DEI	0.	ACCTB	0.
INPUT CONSTANTS									
C 1	4.79999995E -00			1.99999997E -02		5.00000000E 02	0.		6.35999995E 02
C 6	9.99999988E -02			1.99999997E -02		7.99999994E -01	1.50000000E 00		1.99999999E -01
C 11	2.99999997E -02			8.00000000E 00		7.99999999E 01	4.00000000E 00		2.48999998E 00
C 14	7.32999998E 00			4.00000000E 00		0.	0.		0.
C 21	9.99999988E -03			1.99999997E -02		0.	0.		0.

Figure 7. Initial Values and Constants for Example System

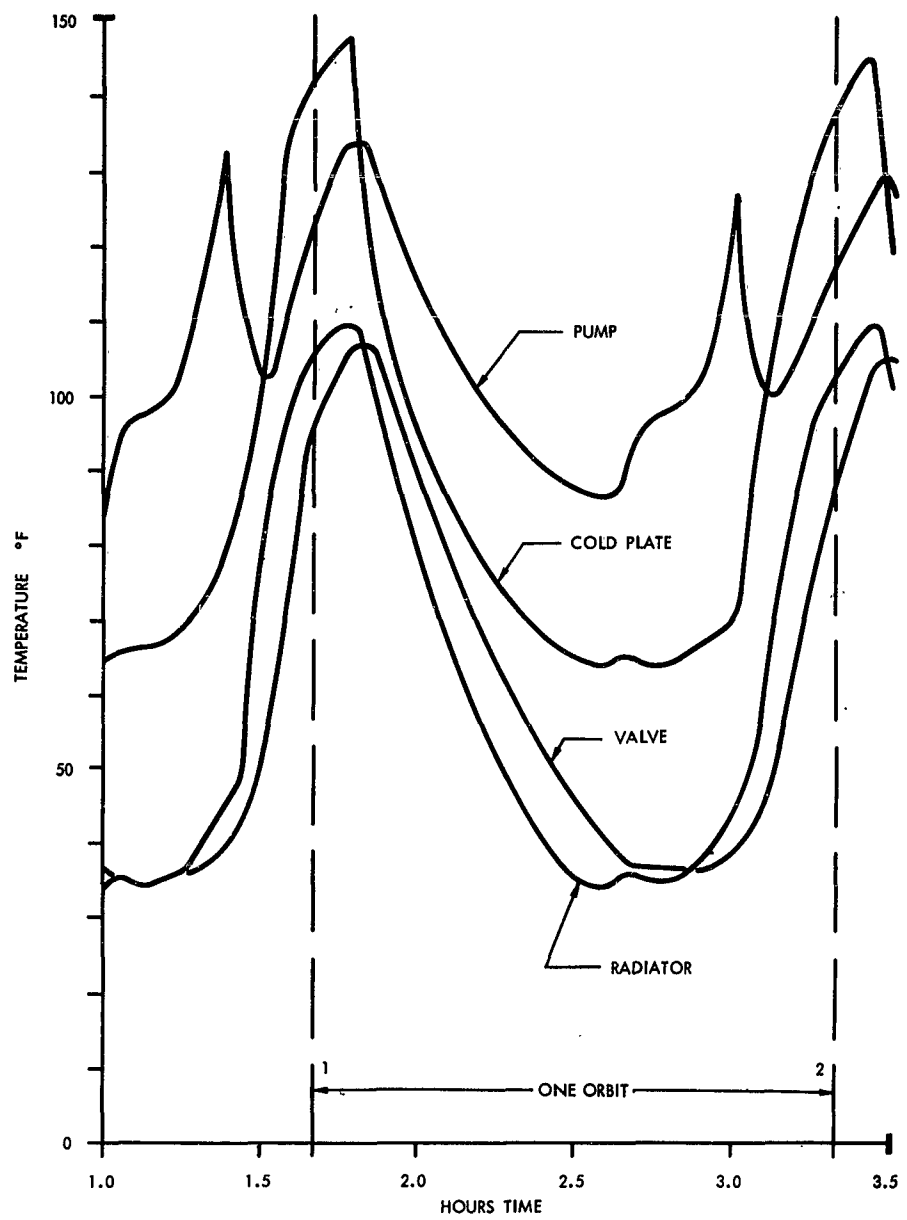


Figure 8. Example System Component Temperatures Versus Time
 —Proportional Valve

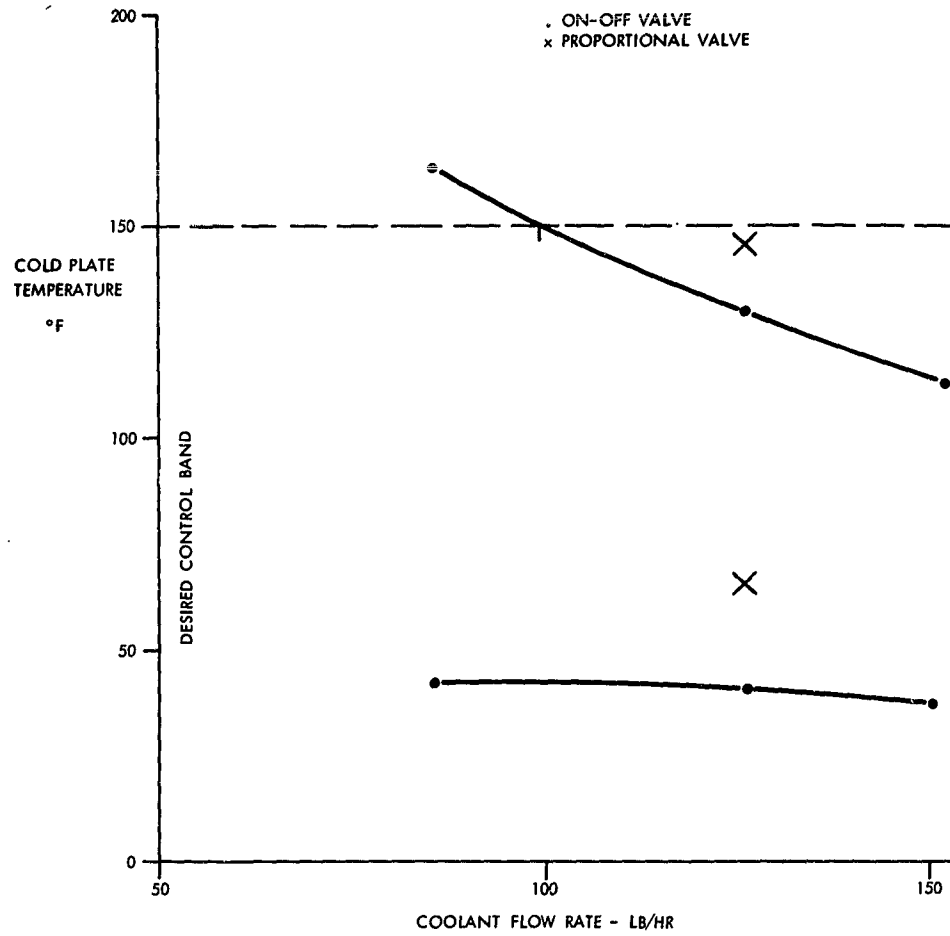


Figure 10. Example System Temperature Control Band as a Function of Coolant Flow Rate

SECTION II
ASSOCIATED TECHNICAL PAPERS

TRANSIENT HEAT TRANSFER ANALYSIS OF
SYSTEMS INVOLVING FLUID FLOW

by

John C. Grafton

North American Aviation, Inc.,
Downey, California

651

NOMENCLATURE

t	temperature, degrees F
q	heat flow, Btu/hr
R	Thermal resistance, (hr) (F)/Btu
L	length, ft
A	area, ft ²
k	thermal conductivity, Btu/(hr) (ft ²) (F/ft)
h _c	heat transfer coefficient for convection, Btu/(hr) (ft ²) (F)
h _r	heat transfer coefficient for radiation, Btu/(hr) (ft ²) (F)
T	temperature, degrees R
σ	Stefan-Boltzmann constant, 0.1713 x 10 ⁻⁸ Btu/(hr) (ft ²) (R ⁴)
f	radiation interchange factor
W	mass, lb
c _p	specific heat capacity at constant pressure, Btu/(lb) (F)
c _v	specific heat capacity at constant volume, Btu/(lb) (F)
θ	time, hr
ε	emissivity
F	geometric configuration factor
ρ	density, lb/ft ³
w	mass flow rate, lb/hr
P	perimeter of tube
A _c	cross-sectional area of tube
x	distance down tube, ft

ASD-TDR-63-260

TRANSIENT HEAT TRANSFER ANALYSIS OF SYSTEMS
INVOLVING FLUID FLOW

by

J. C. Grafton

INTRODUCTION

It has become increasingly evident in the past few years that the majority of heat transfer problems cannot properly be solved by purely analytical methods, but must be solved by use of analog networks. This is especially true with regard to transient problems. Even relatively simple temperature prediction problems usually involve transient three-dimensional heat transfer with radiation, conduction, and convection. Directly solving the differential equations associated with such a problem almost inevitably becomes a mathematical nightmare. The process usually involves so many simplifying assumptions that the results are questionable in the few cases where answers can be obtained at all. Fortunately, with the advent of the high-speed digital computer, practical application of analog network theory becomes possible, and heat transfer problems formerly considered impossible to solve are now solved as a matter of routine.

A number of existing IBM 7090 general heat transfer programs are under development by the aerospace industry in which thermal analog networks are digitally solved by means of finite differences. The types of problems usually solved by these programs do not ordinarily involve heat and mass transfer simultaneously. The intent of this paper is to present methods which achieve analog network simulation of space radiators, heat exchangers, or any system involving heat transfer with fluid flow. These methods can be directly utilized on most of the general heat transfer programs now in existence.

BASIC PRINCIPLES

The basic principles of analog networks—as applied to thermal problems—are well known. However, it is pertinent that a brief review be given. In any case involving the transfer of heat between two points at temperatures t_1 and t_2 , the heat flow is given by an equation analogous to Ohm's electrical law:

$$q = \frac{t_1 - t_2}{R} \quad (1)$$

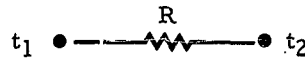
The thermal resistance R is evaluated with respect to the mode of heat transfer:

$$R = \frac{L}{kA} \quad \text{for conduction}$$

$$R = \frac{1}{h_c A} \quad \text{for convection}$$

$$R = \frac{1}{h_r A} = \frac{1}{\sigma f (T_1^2 + T_2^2) (T_1 + T_2) A} \quad \text{for radiation}$$

The analogous thermal circuit for Equation 1 is



It is often required to analyze heat transfer problems on a transient basis, i.e., temperature versus time. In this case, the effect of heat capacity must be included in the analysis of the problem. The heat stored in a material undergoing a heating or cooling process can be written:

$$(Wc_p)_i \frac{dt_i}{d\theta} = \sum q = \sum \frac{1}{R} (t_j - t_i) \quad (2)$$

where

t_i = temperature of material

t_j = ambient temperatures

If the above equation is integrated for the case of a single ambient temperature, we obtain

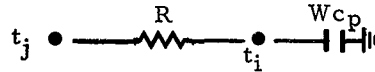
$$\frac{t_i' - t_j}{t_{i_0} - t_j} = e^{-\frac{1}{R} \frac{\Delta\theta}{(Wc_p)_i}} \quad (3)$$

where

t_{i_0} = initial temperature

t_i' = temperature at end of time increment $\Delta\theta$.

Equation 3 is analogous to the charging or discharging of a capacitor. The thermal analog of electrical capacitance is Wc_p . The analogous network is:



The basic premise of analog network theory is that any object which is to be thermally analyzed must be broken up, or sectioned, into a number of relatively small increments which are assumed to be isothermal. Each section is represented by a node such as the above figure. The thermal resistors attached to each node are based on the conduction, radiation, or convection paths between nodes. The mass of any given section is assumed to be "lumped" at the node representing that section. The total network representing the heat transfer problem at hand is usually composed of many such systems, all interconnected to form a single unified network consisting of as many as several hundred nodes, capacitors, and resistors.

RADIATION NETWORKS

In order to properly account for the complex interreflections encountered in radiation heat transfer, it is often necessary to use special "radiosity" networks as described in Reference 1. These networks differ from ordinary thermal networks in that the driving potential is $\Delta(\sigma T^4)$, not Δt . Radiosity networks are often combined with the overall network of a thermal problem so that the entire analysis may be solved as one problem. This is a necessary procedure for transient conditions. A typical radiosity network for a four-sided enclosure is shown in Figure 1.

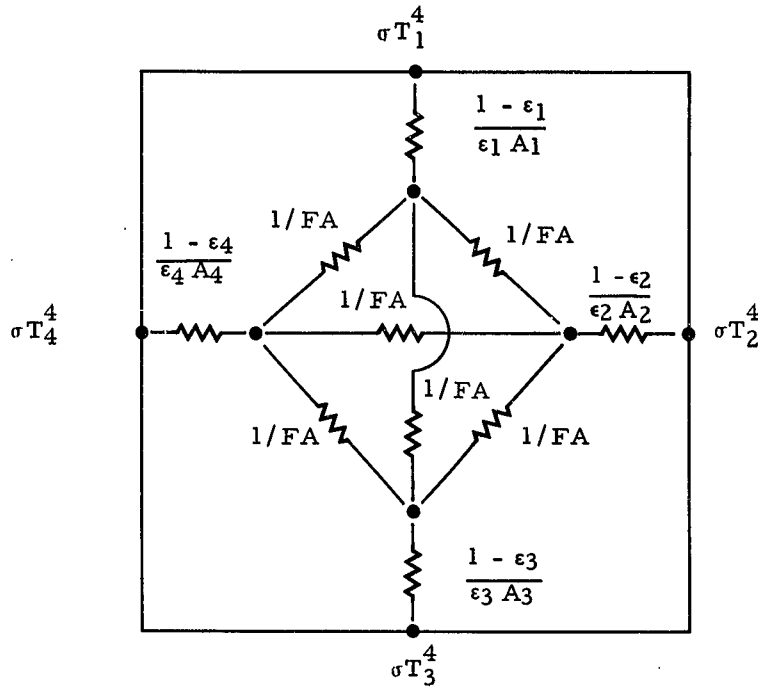


Figure 1. Four-Sided Enclosure

Digital Method of Solution

Once the analog networks are completed and combined into one overall network, the final step is problem solution on the IBM 7090. All of the general heat transfer programs now in existence use the same basic approach, i.e., for each node i the following heat balance is solved:

$$(Wc_p)_i \frac{dt_i}{d\theta} = \sum_{j=1}^n \left[\frac{1}{R_{ij}} (t_j - t_i) \right] + q_i \quad (4)$$

The numerical solution to the above equation is achieved by converting it to finite difference form. There are three basic approaches to the finite difference solution. The method most commonly used at the present time is called the "explicit" or "forward-difference" method. This method solves the temperature at each node i as follows:

$$t_{i, \theta + \Delta\theta} = t_{i, \theta} + \frac{\Delta\theta}{(Wc_p)_i} \left\{ \sum_{j=1}^n \left[\frac{1}{R_{ij}} (t_{j, \theta} - t_{i, \theta}) \right] + q_i \right\} \quad (5)$$

where

θ = time at beginning of interval

$\theta + \Delta\theta$ = time at end of interval $\Delta\theta$

The explicit method is quite straightforward and requires only one basic equation to calculate the temperature of each node at the end of the time interval $\Delta\theta$. However, the time interval $\Delta\theta$ is related to the physical parameters of the network, and must not exceed the minimum RC product of the network. Exceeding the minimum RC product would result in an unstable solution for those nodes whose RC product is smaller than the time interval. (In thermal terms, the RC product is equivalent to $Wc_p/\sum \frac{1}{R}$.) This stability requirement places definite limits on the magnitude of the time intervals which can be used in the solution. This requirement becomes a problem when small nodes or large conductors are present in the system.

The stability requirement and the limitation on size of time interval can be avoided by solving for the node temperatures at the end of the time interval, rather than at the start. This method is known as the "implicit" or "backward-difference" solution. In this case the basic nodal equation becomes:

$$t_{i, \theta + \Delta\theta} = t_{i, \theta} + \frac{\Delta\theta}{(Wc_p)_i} \left\{ \sum_{j=1}^n \left[\frac{1}{R_{ij}} (t_{j, \theta + \Delta\theta} - t_{i, \theta + \Delta\theta}) \right] + q_i \right\} \quad (6)$$

Equation 6, when applied to a system of N nodes, generates N equations with N unknowns, and from this system of equations, all node temperatures must be determined simultaneously for a given time interval. There is no stability requirement when using the implicit solution. However, care must be taken in selecting a time interval to reduce any truncation error in time.

The third method, known as the "mid-difference" method, is similar to the backward-difference method except that the driving temperatures used in the nodal equation are taken at the mid-point of the calculation interval. Thus:

$$t_{i, \theta + \Delta\theta} = t_{i, \theta} + \frac{\Delta\theta}{(Wc_p)_i} \left\{ \sum_{j=1}^n \left[\frac{1}{R_{ij}} (t_{j, \theta + \Delta\theta/2} - t_{i, \theta + \Delta\theta/2}) \right] + q_i \right\} \quad (7)$$

The solution to the mid-difference method is similar to the backward-difference method in that all node temperatures must be determined simultaneously for a given time interval. It is possible for the solution to become unstable if too large a time interval is used, but the instability is not nearly as critical as with the forward-difference method.

Reference 2 summarizes some of the features of the three methods. At the present time, it appears there is some controversy as to which method is best for heat transfer problems.

FLUID FLOW NETWORKS

The approximate heat transfer equation (References 3 and 4) for fluid flowing in a duct is:

$$\rho c_v A_c \frac{\partial t}{\partial \theta} + \dot{w} c_p \frac{\partial t}{\partial x} + hP (t - t_w) = 0 \quad (8)$$

where

t = temperature of fluid

t_w = tube wall temperature

Equation 8 ignores friction losses, kinetic energy changes, and fluid conduction in the x -direction. It is assumed that flow is in one direction and that fluid density is constant.

If the assumption is made that fluid temperature varies linearly with distance in a given section of tubing, then:

$$\frac{\partial t}{\partial x} \approx \frac{t_{OUT} - t_{IN}}{\Delta x} \quad (9)$$

Thus, the following equation can be written for incompressible flow in a section of tubing of length Δx :

$$W c_p \frac{dt}{d\theta} = \dot{w} c_p (t_{IN} - t_{OUT}) + hP \Delta x (t_w - t) \quad (10)$$

where

W = mass of fluid in section of tube

If analog networks are to be used to solve a problem that includes fluid flow effects, it is necessary to convert Equation 10 to network form. One method of network representation is shown in Figure 2. To prove the validity of this network, a heat balance is performed around t_{OUT} . Thus,

$$W c_p \frac{dt_{OUT}}{d\theta} = \dot{w} c_p (t_{IN} - t_{OUT}) + hA (t_{WALL} - t_{OUT}) \quad (11)$$

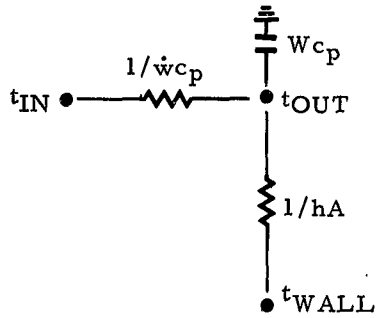


Figure 2. Fluid Flow Network

Equation 11 demonstrates that the network of Figure 2 satisfies the requirement of Equation 10 with the assumption that heat is transferred to or from the outlet fluid temperature instead of the average temperature of the fluid.

A better approximation is shown in Figure 3. This is the network representation of the equation derived by Dusinberre (References 5 and 6). A nodal analysis of this network follows:

$$\begin{aligned}
 Wc_p \frac{dt_{OUT}}{d\theta} &= \left(\dot{w}c_p - \frac{hA}{2} \right) (t_{IN} - t_{OUT}) + hA (t_{WALL} - t_{OUT}) \\
 &= \dot{w}c_p t_{IN} - \frac{hA}{2} t_{IN} - \dot{w}c_p t_{OUT} + \frac{hA}{2} t_{OUT} \\
 &\quad + hA t_{WALL} - hA t_{OUT} \\
 &= \dot{w}c_p t_{IN} - \dot{w}c_p t_{OUT} + hA t_{WALL} - hA \left(\frac{t_{IN} + t_{OUT}}{2} \right) \\
 &= \dot{w}c_p (t_{IN} - t_{OUT}) + hA \left[t_{WALL} - \frac{(t_{IN} + t_{OUT})}{2} \right] \quad (12)
 \end{aligned}$$

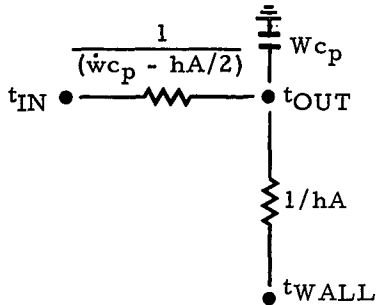


Figure 3. Network Representation of Dusinberre's Equation

It can be seen that heat is transferred to or from the average fluid temperature of the section, with the approximation that the fluid capacitance effect is a function of t_{OUT} .

Both of the above networks are capable of analyzing temperature-time (transient) effects in the fluid, due to the capacitance term, $Wc_p (dt/d\theta)$. Thus, system warm-up or cool-down effects can be considered. For systems involving gaseous (compressible) flow, it is seldom necessary to include the fluid capacitance term, due to the small heat capacity of gases. (Rizika, Reference 3, neglects fluid capacitance for compressible flow based upon the assumption that fluid pressure at any point in the system is independent of time.) Even for liquid (incompressible) flow, the fluid capacitance term is often found to be negligible, i.e., transient effects are caused mainly by the thermal capacity of the tube wall and connected structure. For these cases, it is possible to equate the term $Wc_p (dt/d\theta)$ to zero with a resultant simplification of the network.

For those cases where fluid capacitance can be ignored, a third network representation can be used. This is shown in Figure 4.

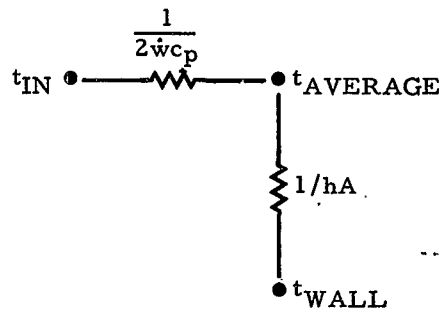


Figure 4. Fluid Flow Network

A nodal analysis of this network follows:

$$2\dot{w}c_p (t_{IN} - t_{AVE}) + hA (t_{WALL} - t_{AVE}) = 0$$

$$2\dot{w}c_p \left[t_{IN} - \frac{(t_{IN} + t_{OUT})}{2} \right] + hA \left[t_{WALL} - \frac{(t_{IN} + t_{OUT})}{2} \right] = 0$$

$$\dot{w}c_p (2t_{IN} - t_{IN} - t_{OUT}) + hA \left[t_{WALL} - \frac{(t_{IN} + t_{OUT})}{2} \right] = 0$$

$$\dot{w}c_p (t_{OUT} - t_{IN}) = hA \left[t_{WALL} - \frac{(t_{IN} + t_{OUT})}{2} \right] \quad (13)$$

This solution works quite well for systems that do not include the fluid capacitance terms, $Wc_p(dt/d\theta)$. If fluid capacitance is included, however, the explicit type of numerical analysis used by most IBM heat transfer programs will cause oscillation of temperatures down the tube.

In general, the basic method of utilizing the above special networks involving fluid flow is to divide all tubes or components carrying fluid into small sections, and apply the special network to each section. Fortunately, presently existing IBM general heat transfer programs in use at NAA, Lockheed, Boeing, and elsewhere, have the capability to take the outlet temperature from a given section and apply it as the inlet temperature of the next section downstream. This is often called the "cathode follower" function after the analog computer device of the same name.

As an example of network set-up, consider the tube of Figure 5, which is subdivided into three sections whose wall temperatures are t_A , t_B , and t_C .

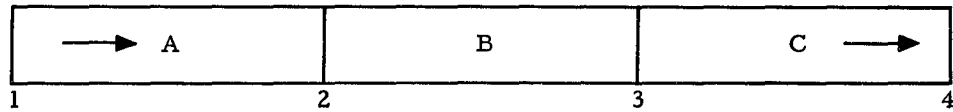


Figure 5. Fluid Flow in a Tube

The analog network based upon Equation 11 is shown in Figure 6, noting that the dashed lines indicate cathode followers. This method has been used for several years at Lockheed and NAA.

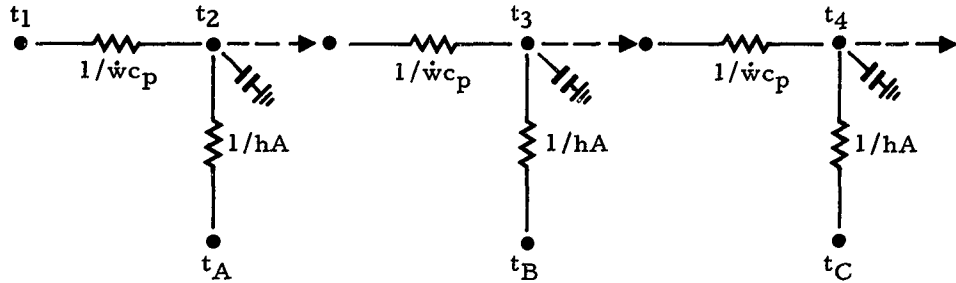


Figure 6. Network for Fluid Flow in a Tube

The network based upon Equation 12 is shown in Figure 7. It is to be noted that a number of additional cathode followers are indicated. This is necessary for IBM programs that have not been developed to handle fluid flow specifically. Program modification could eliminate most of this complication.

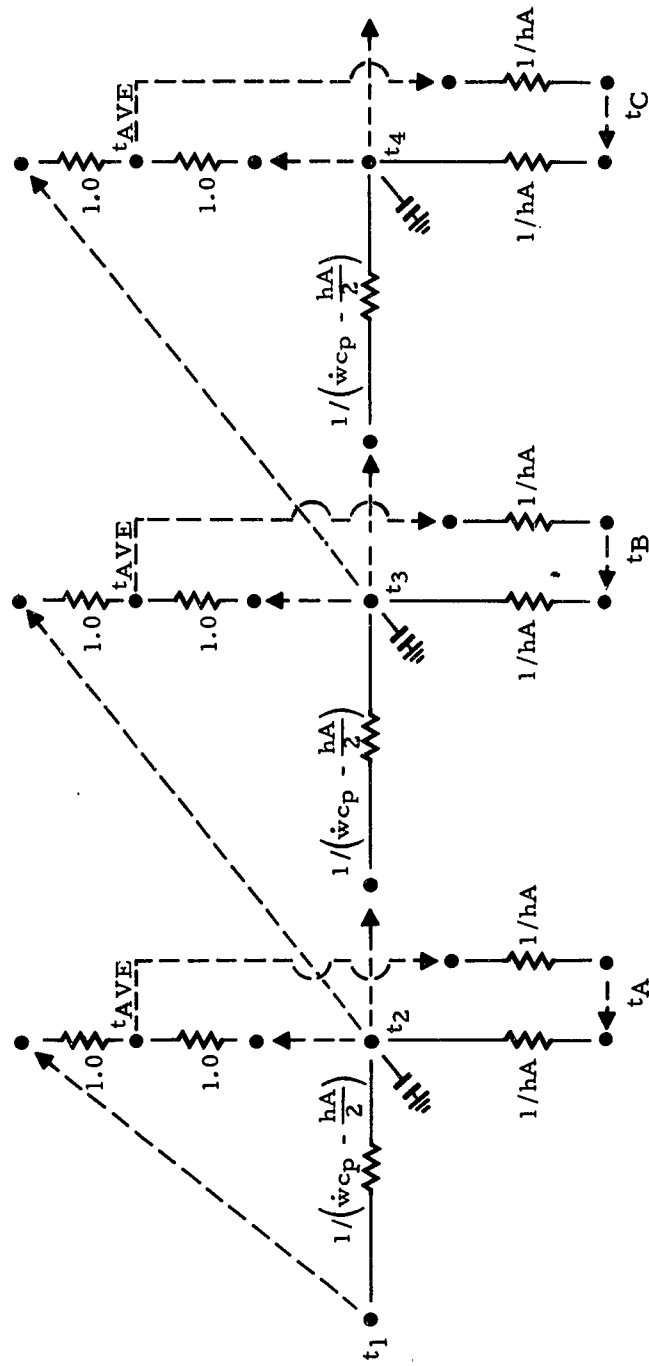


Figure 7. Network for Fluid Flow in a Tube

The network based upon Equation 13 is shown in Figure 8. Here again appears a certain amount of complication that could be eliminated by appropriate program modification. It is to be noted that the networks of Figures 7 and 8 will give identical results if the capacitors in Figure 7 are eliminated.

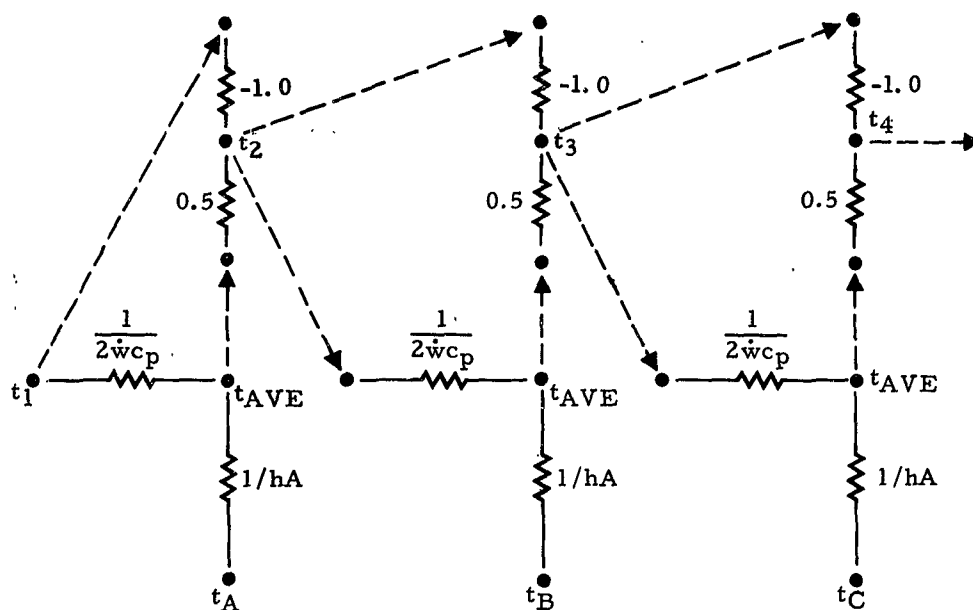


Figure 8. Network for Fluid Flow in a Tube

It is a simple matter to integrate the fluid flow network into the overall problem network. For instance, if the tube of Figure 5 represented an insulated pipe, the network of Figure 6 would be expanded to that shown in Figure 9. This type of expansion could be extended to any degree of complexity required by the problem at hand.

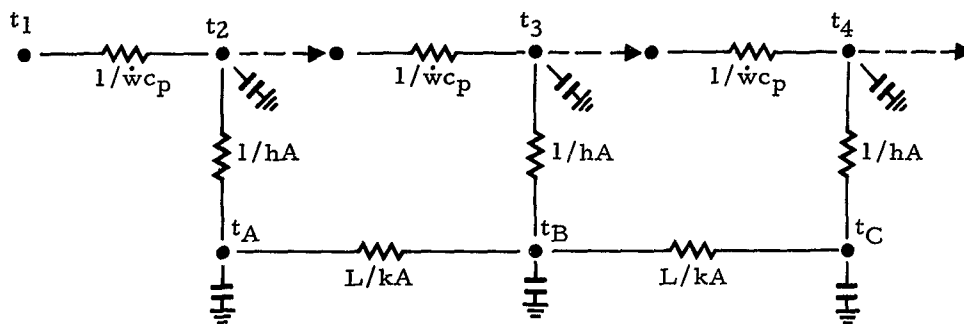


Figure 9. Network for Insulated Tube

A simple comparison can be made to demonstrate the validity of analog network application to fluid flow. Consider the 12-inch length of tubing shown in Figure 10, which is sectioned as indicated. It is assumed that

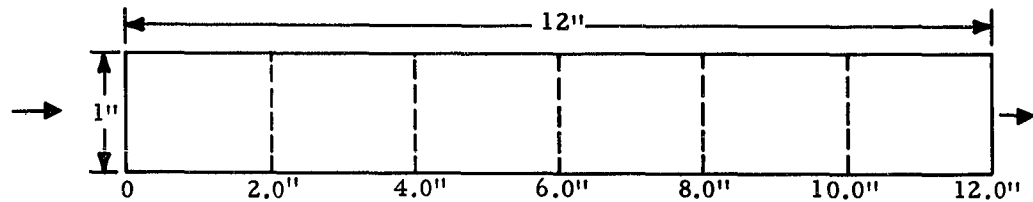


Figure 10. Fluid Flow in a Tube

initially the entire system (tubing and liquid) is at a temperature of 0 F, with a flow velocity of 1.0 ft/min. It is also stipulated that the film heat transfer coefficient is 50 Btu/hr-ft²-F, liquid specific heat is 1.0 Btu/lb-F, and the inlet temperature remains at all times at 0 F. If the tube wall is assumed to be stepped to 150 F and held constant, a transient situation will develop which can be solved analytically by following a slug of liquid down the tube:

$$t_{x_2} = t_{WALL} + (t_{x_1} - t_{WALL}) e^{-\frac{hP \Delta x}{\dot{w}c_p}} \quad (14)$$

A comparison of results is shown in Table 1 for fluid temperatures down the tube. (Temperatures in brackets indicate results obtained with 12 sections instead of six.) A comparison of equilibrium fluid temperature is plotted in Figure 11. Although the problem chosen for comparison admittedly could have been better, it can be seen that there is a close correlation between analytical and IBM results.

Table 1. Comparison of Results

Time, Sec	Fluid Temperature at 2.0 Inches			Fluid Temperature at 4.0 Inches		
	Eq. 14	IBM, Eq. 11	IBM, Eq. 12	Eq. 14	IBM, Eq. 11	IBM, Eq. 12
0	0 F	0 F	0 F	0 F	0 F	0 F
4	6.3	5.2	5.2 (5.9)	6.3	6.2	6.2 (6.4)
10	15.2	9.7	9.9 (11.4)	15.2	13.7	13.9 (14.9)
20	15.2	12.9	13.4 (14.5)	28.9	21.4	21.9 (24.0)
30	15.2	14.0	14.6 (15.1)	28.9	25.0	25.9 (27.5)
40	15.2	14.3	15.0 (15.2)	28.9	26.6	27.6 (28.5)
50	15.2	14.4	15.1 (15.2)	28.9	27.2	28.4 (28.8)
60	15.2	14.5	15.2 (15.2)	28.9	27.4	28.7 (28.9)
				Fluid Temperature at 8.0 Inches		
0	0 F	0 F	0 F	0 F	0 F	0 F
4	6.3	6.3	6.3 (6.4)	6.3	6.4	6.3 (6.4)
10	15.2	15.0	15.0 (15.5)	15.2	15.3	15.3 (15.6)
20	28.9	26.0	26.3 (28.1)	28.9	28.1	28.2 (29.2)
30	41.2	32.7	33.4 (35.8)	41.2	37.3	37.8 (39.9)

Table 1. Comparison of Results (Cont.)

<u>Time, Sec</u>	<u>Eq. 14</u>	<u>IBM, Eq. 11</u>	<u>IBM, Eq. 12</u>	<u>Eq. 14</u>	<u>IBM, Eq. 11</u>	<u>IBM, Eq. 12</u>
40	41.2	36.3	37.4 (39.3)	52.2	43.2	44.2 (46.7)
50	41.2	38.0	39.4 (40.6)	52.2	46.6	48.0 (50.1)
60	41.2	38.8	40.4 (41.0)	52.2	48.4	50.1 (51.5)
<u>Fluid Temperature at 10.0 Inches</u>						
0	0 F	0 F	0 F	0 F	0 F	0 F
4	6.3	6.4	6.3 (6.4)	6.3	6.4	6.3 (6.4)
10	15.2	15.4	15.4 (15.6)	15.2	15.4	15.4 (15.6)
20	28.9	28.8	28.9 (29.5)	28.2	29.1	29.1 (29.5)
30	41.2	39.8	40.0 (41.5)	41.2	40.9	41.0 (41.9)
40	52.2	47.7	48.4 (50.7)	52.2	50.3	50.7 (52.4)
50	62.1	52.9	54.1 (56.6)	62.1	57.2	58.0 (60.4)
60	62.1	56.1	57.6 (59.8)	71.1	61.9	63.1 (65.7)
<u>Fluid Temperature at 12.0 Inches</u>						
0	0 F	0 F	0 F	0 F	0 F	0 F
4	6.3	6.4	6.3 (6.4)	6.3	6.4	6.3 (6.4)
10	15.2	15.4	15.4 (15.6)	15.2	15.4	15.4 (15.6)
20	28.9	28.8	28.9 (29.5)	28.2	29.1	29.1 (29.5)
30	41.2	39.8	40.0 (41.5)	41.2	40.9	41.0 (41.9)
40	52.2	47.7	48.4 (50.7)	52.2	50.3	50.7 (52.4)
50	62.1	52.9	54.1 (56.6)	62.1	57.2	58.0 (60.4)
60	62.1	56.1	57.6 (59.8)	71.1	61.9	63.1 (65.7)

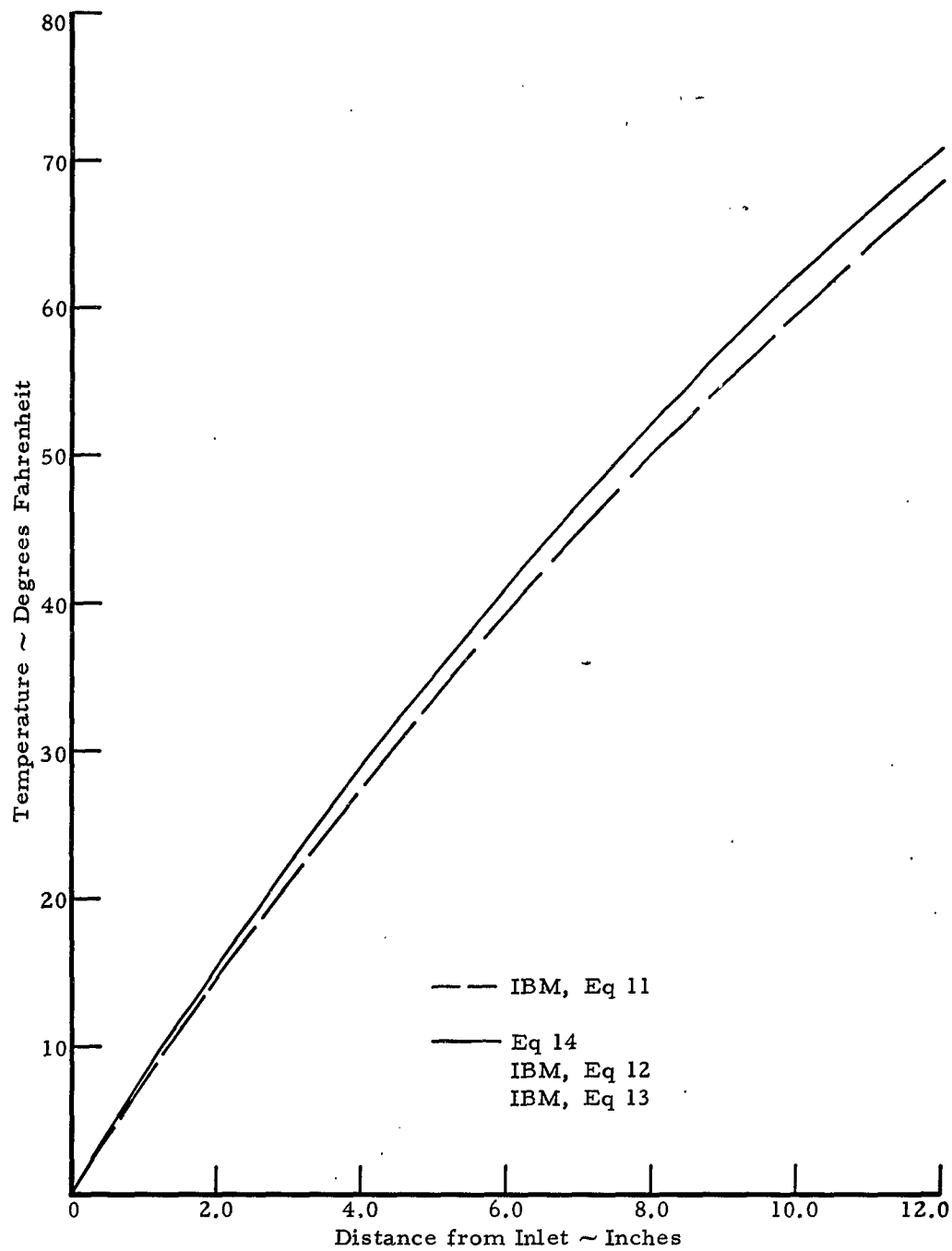


Figure 11. Equilibrium Fluid Temperature

DISCUSSION

Using the basic methods described in this paper, it is possible to simulate by analog network, any thermal problem which involves fluid flow, such as space radiators, heat exchangers, or even entire systems. Presently available IBM general heat transfer programs can be used for problem solution.

A possible source of error with respect to the network analysis of flow systems should be mentioned. Sudden changes in inlet temperature will usually be reflected downstream almost instantaneously, due to the type of numerical analysis used with digital computers. In reality, of course, a finite time is required for the effect of a change in inlet temperature to appear at a point downstream. This inaccuracy is most pronounced when the capacitors representing the rate of change of fluid temperature with time are equated to zero. It is possible, however, to eliminate most of the error by a controlled choice of the calculation interval used in the numerical solution.

Concurrent with the thermal analysis of a system, it is possible to set up an analog of steady-state incompressible flow to determine pressures and flow rates for any system configuration. A "flow" network is set up, for the flow part of the problem, in which voltages are analogous to pressures, and the flow conductors are a function of pressure difference, fluid density, viscosity, pipe diameter, length, and roughness. Generally speaking, however, the usual type of IBM heat transfer program would need modification to fully utilize this type of network.

REFERENCES

1. Oppenheim, A.K., "Radiation Analysis by Network Method," Trans. ASME, Vol. 78, p. 725, 1956.
2. Gaumer, G.R., "Stability of Three Finite Difference Methods of Solving for Transient Temperatures," ARS Journal, Oct. 1962, p. 1595-1597.
3. Rizika, J. W., "Thermal Lags in Flowing Systems Containing Heat Capacitors," Trans. ASME, Vol. 76, No. 3, p. 411, 1954.
4. Rizika, J. W., "Thermal Lags in Flowing Incompressible Fluid Systems Containing Heat Capacitors," Trans. ASME, Vol. 78, No. 7, p. 1407, 1956.
5. Dusinberre, G. M., "Calculation of Transient Temperatures in Pipes and Heat Exchangers by Numerical Methods," Trans. ASME, Vol. 76, No. 3, p. 421, 1954.
6. Dusinberre, G. M., Heat-Transfer Calculations by Finite Differences, International Textbook Company, Scranton, Pennsylvania, 1961.

**THE CONDENSING - EJECTOR REFRIGERATION
SYSTEM FOR SPACE VEHICLES**

by

C. A. Kemper

G. A. Brown

**Joseph Kaye & Company, Inc.,
Cambridge, Massachusetts**

NOMENCLATURE

A	cross-section area
C.O.P.	coefficient of performance, Eq. (14)
g_0	acceleration given to unit mass by unit force
h	enthalpy per unit mass
J	mechanical equivalent of heat
p	pressure
P	power input to pump or compressor
Q_r	heat rejected from radiator per unit heat input to system, $(Q_s + W_s)/Q_s$
Q_s	heat input to system per pound of fluid passing through evaporator
s	entropy per unit mass
Δs	total entropy increase through ejector per unit total flow rate through ejector, Eq. (2) or (2a)
Δs_M	minimum value of Δs which satisfies all system and condensing ejector laws
$\Delta \bar{T}$	difference between arithmetic mean radiator temperature and radiation mean effective temperature, Fig. 4
ΔT_r	temperature change of fluid in radiator, Eq. (16)
T	absolute temperature (Fahrenheit temperature where indicated)
\bar{T}_e	radiation mean effective radiator temperature, Eq. (15)
V	velocity
W	work input to pump or compressor per pound of fluid passing through evaporator
W_s	total work input to system per pound of fluid passing through evaporator, Eq. (6)
W_s'	total work input to system per unit heat input to system, W_s/Q_s
w	mass flow rate
η_c	compressor efficiency
η_p	pump efficiency
ρ	density
ω	ratio of liquid inlet flow rate to vapor inlet flow rate, w''/w

Subscripts

c	refers to compressor
ce	denotes condition at exit of evaporator
ci	denotes condition at inlet of evaporator
f	denotes saturated liquid state
g	denotes saturated vapor state
o	denotes a stagnation state
oy	refers to condensing ejector stagnation state
p	refers to pump
re	denotes condition at exit of radiator
ri	denotes condition at inlet of radiator
sc	refers to isentropic compressor operation
sp	refers to isentropic pump operation
x	refers to conditions just upstream of condensation shock
y	refers to conditions just downstream of condensation shock. Also States y and 3 are equivalent.
1	denotes conditions at the exit plane of the ejector nozzles
2	denotes conditions at the exit plane of the contracting mixing section
3	denotes conditions at exit of constant-area section

Superscripts

'	denotes vapor inlet flow at condensing ejector or vapor stream
"	denotes liquid inlet flow at condensing ejector or liquid stream

THE CONDENSING-EJECTOR REFRIGERATION SYSTEM FOR SPACE VEHICLES

by

C. A. Kemper* and G. A. Brown**

INTRODUCTION

The problems attendant to the rejection of heat from space vehicles are of great concern to those involved in the tasks of providing power supplies and of maintaining a suitable environment for men and equipment for two main reasons. First, every system placed on board the vehicle must be very reliable, and secondly, every system must be as light as possible and desirably, should be compact.

The final heat-rejection process from a heat engine, a refrigeration cycle, or any cooling system on board a space vehicle must occur by radiation unless the mission time is sufficiently short to permit the waste heat to be rejected from the vehicle via an expendable material or absorbed by a suitable heat reservoir. Since the radiative process is governed by the Stefan-Boltzmann law, the area of the radiator per unit of cooling rate becomes very large if low radiator temperatures are used. Thus, it is necessary to investigate whether the weight of a cooling system can be reduced if active or refrigerative cooling is used rather than passive cooling. If the required radiator area for a passive cooling system greatly exceeds the available surface area of the vehicle, the use of the vehicle skin for the radiative surface is precluded, and it may be profitable on an overall weight basis to employ a refrigeration device to increase the radiator temperature.

Except for condensing the working fluid, conventional vapor-compression refrigeration machines would be practical in the temperature range in which a cooling system optimized for space vehicle use would be expected to lie; that is, roughly between 32°F and 300°F. The condensation process in the cooling cycle is normally dependent on the existence of a gravitational field for removal of the condensate from the condenser surfaces. If a surface condenser is expected to function in a zero-gravity field such as a satellite trajectory, an alternate method will be required for supplying vapor to the surfaces and of removing condensate from the surfaces. Several methods have been suggested for supplying force fields to surface condensers in space vehicles; these include curved-tube condensers, rotating condensers, high velocity condensers, and spray condensers. Most of these systems have undetermined reliability for operation in a zero-gravity environment, and each of them has advantages and disadvantages relative to the others.

*President, Joseph Kaye and Company, Inc., 737 Concord Avenue, Cambridge 38, Massachusetts.

**Consultant to Joseph Kaye and Company. Also Associate Professor of Mechanical Engineering, Massachusetts Institute of Technology, Cambridge 39, Massachusetts.

This publication describes a different solution to the problem; one which involves the use of a condensing ejector to accomplish the condensing task. The proposed system has the advantages of simplicity, small size, and a minimum number of moving parts. The inertial and pressure forces induced in the device are much larger than those exerted by gravity, so that the device will function, if desired, in a field several times as large as that of the earth's gravity, regardless of the direction of the field. In particular, because of its relative independence of gravity, the condensing ejector will function quite satisfactorily at zero-gravity conditions. There has been excellent agreement between the theory and experimental data for the condensing ejector so that system studies for applications involving this device can be performed with engineering certainty. The space-vehicle cooling system is one example of such an application.

DESCRIPTION OF CONDENSING EJECTOR

The condensing ejector is a form of the jet pump in which a condensable vapor stream is mixed with a liquid stream in such a way that a completely condensed liquid state is obtained at the exit of the device. In addition the condensation process is utilized in such a manner that favorable pumping characteristics for the condensing ejector are produced. Although similar to a spray condenser on the basis of the above description, the condensing ejector differs in that the key to its operation is in the rapid exchanges of momentum and energy that occur in the device due to the dynamic nature of the mixing process. The spray condenser relies upon fine dispersions of liquid droplets in the vapor coupled with long residence times to enable the condensation process to occur. Instead of using several small spray nozzles which usually lead to large losses in liquid stagnation pressure, the liquid enters the condensing ejector through a single nozzle so that most of

the stagnation pressure of the liquid stream is converted into useful momentum. Thus, the stagnation pressure of the exit stream of a condensing ejector can be made greater than that achievable with a spray condenser.

A sketch of the condensing ejector is shown in Fig. 1. The condensable vapor enters the ejector at the stagnation state, $()_0$, and is expanded through its nozzle to Section 1. The liquid, flowing from a secondary loop, enters the ejector at the stagnation state, $()_0''$, and is expanded through its nozzle to Section 1. The velocities of the streams at Section 1 ordinarily will be high with the vapor velocity being higher than the liquid velocity. The streams enter the convergent portion of the mixing section which exists between Sections 1 and 2. Due to the velocity difference between the streams some of the liquid stream will be thrown into the vapor stream. Some condensation of the vapor stream will occur before the streams reach Section 2 and this may be a sizeable fraction of the vapor stream. At Section 2 the streams enter a constant-area portion of the mixing section. At an arbitrary distance along this section (Section x) two distinct streams still exist. In a very short axial distance, the vapor stream is completely condensed due to interaction of the vapor and liquid streams with each other and with the liquid in the mixing section. At some arbitrary Section y, the condensation process is essentially complete and a liquid state exists. The process which occurs between Sections x and y has been called a condensation shock since it appears almost as a discontinuity in the flow path. The rapid condensation process produces a momentum change such that an increase in pressure occurs between Sections x and y. (In some cases the increase is primarily an increase in static pressure while in other cases the increase is primarily an increase in dynamic pressure. Based on these extreme cases, the increase can be described as an increase in stagnation pressure at Section y relative to the static pressure at Section x.) The location of Sections x and y have been described as arbitrary since the position of the condensation shock can be controlled by the pressure at the exit of the condensing ejector.

The flow between Sections y and 3 is the flow of a liquid in a constant area duct. If the dynamic head at Section 3 is appreciable, a diffuser section

is added between Sections 3 and 4. The stagnation pressure at the exit of the condensing ejector may be greater than either of the inlet stagnation pressures under certain operating conditions and geometric constraints. Other relations between these three stagnation pressures may also be produced.

CONDENSING-EJECTOR REFRIGERATION SYSTEMS

The flow diagram of a general configuration for a space environmental control system employing a condensing ejector is shown in Fig. 2. A corresponding temperature-entropy diagram for this configuration is given in Fig. 3. The general configuration contains both a liquid pump and a vapor compressor. A second configuration would contain only the liquid pump, while a third configuration would contain only the vapor compressor. It will be shown in the next section that, for any given conditions of temperatures and cooling rates, the total amount of ideal work required to operate a condensing-ejector refrigeration system is the same regardless of the relative amounts of work introduced through the liquid pump and the vapor compressor. Thus, the second and third configurations are only special cases of the general configuration.

In all cases it is assumed that the liquid which leaves the radiator is divided into two streams. The stream which is returned to the primary cooling loop is flashed to the evaporator temperature through a Joule-Thomson expansion valve. The other stream is returned to the condensing ejector either through a liquid pump (general and second configurations), or directly (third configuration). It is assumed that the fluid leaving the evaporator is saturated vapor. This vapor may be returned to the condensing ejector either through a vapor compressor (general and third configurations), or directly (second configuration).

In all cases the system is designed such that the fluid leaving the condensing ejector is saturated liquid. Except for cases where the liquid flow rate is considerably greater than the vapor flow rate, the liquid at the condensing ejector exit will be at a higher temperature than either the

entering liquid or the entering vapor. This is a direct result of the simultaneous solution of the First and Second Laws of Thermodynamics, and the equation of state. Thus it is possible to obtain any reasonable value of radiation mean effective temperature for the radiator. Preliminary analyses indicate that any radiation mean effective temperature which is possible with a given conventional vapor-compressor refrigeration system may also be obtained with a condensing-ejector refrigeration system under the same conditions of cooling temperature and cooling rate and using the same working fluid.

Although it would be possible to separate a portion of the liquid stream leaving the condensing ejector before cooling it in the radiator for direct introduction to the Joule-Thomson valve, performance of the system in every respect examined is greatly improved by cooling the entire liquid stream before separation.

THERMODYNAMIC ANALYSIS FOR CONDENSING-EJECTOR REFRIGERATION SYSTEM

A thermodynamic analysis of the condensing-ejector refrigeration system can be performed which will yield the heat-absorption, work input and coefficient of performance characteristics of the system with the need for only a specification of the entropy increase across the condensing ejector. This analysis and the results will be presented in this section. The relationship between these system results and the requirements they place on the condensing ejector will be examined in the next section.

The specification of thermodynamic states are shown in Figs. 2 and 3. The following assumptions will be made:

1. The working fluid is a pure substance.
2. Pressure drops in the radiator and the evaporator are negligible.
3. All thermodynamic properties are evaluated at stagnation conditions.
4. The fluid leaving the evaporator is saturated vapor, and

the fluid leaving the condensing ejector is saturated liquid.

5. The expansion through the Joule-Thomson valve is a constant-enthalpy process.

6. For the basic analysis the compression in the vapor compressor and in the liquid pump are assumed to be isentropic processes. Actual work inputs may then be calculated by dividing the ideal work inputs by the efficiency of the component doing the work.

7. The condensing ejector has no heat loss from its external surfaces.

8. There are no changes in the stagnation thermodynamic properties through the piping connecting various system components.

For a control volume around the condensing ejector the First Law of Thermodynamics requires the following:

$$h_{oy} = \frac{\omega}{\omega + 1} h_o'' + \frac{1}{\omega + 1} h_o' \quad (1)$$

The Second Law of Thermodynamics requires that the entropy of the mixture leaving the ejector must equal or exceed the total entropy of the two entering streams. This condition is expressed by the following definition and requirement for Δs :

$$\Delta s \equiv s_{oy} - \left[\frac{\omega}{\omega + 1} s_o'' + \frac{1}{\omega + 1} s_o' \right] \quad (2)$$

$$\Delta s \geq 0 \quad (3)$$

The entropy at the exit of the ejector, s_{oy} , is determined from the enthalpy at the same state, h_{oy} , and by the requirements that this state must correspond to saturated liquid conditions (Assumption 4).

The power delivered to the fluid flowing through the liquid pump is:

$$P_{sp} = w'' (h_o'' - h_{re}) \quad (4)$$

The power delivered to the fluid flowing through the vapor compressor is:

$$P_{sc} = w' (h_o' - h_{ce}) \quad (5)$$

Therefore, the total work input to the fluid in the system per pound of fluid flowing through the evaporator is:

$$(P_{sp} + P_{sc})/w' \equiv W_s = \omega (h_o'' - h_{re}) + h_o' - h_{ce} \quad (6)$$

Solving for h_o'' in Eq. (1) yields the following:

$$h_o'' = \frac{1}{\omega} \left[(\omega + 1) h_{oy} - h_o' \right] \quad (7)$$

Substituting this value of h_o'' into Eq. (6) yields the following:

$$W_s = \omega (h_{oy} - h_{re}) + h_{oy} - h_{ce} \quad (8)$$

Solving for ω from Eq. (2) yields the following:

$$\omega = \frac{s_o' - s_{oy} + \Delta s}{s_{oy} - s_o'' - \Delta s} \quad (9)$$

Since it is assumed that the compression in the liquid pump and the vapor compressor are isentropic processes, the following is true:

$$s_o' = s_{ce} \quad (10)$$

and

$$s_o'' = s_{re} \quad (11)$$

Substituting Eqs. (9), (10) and (11) into Eq. (8) yields the following expression for system work:

$$W_s = \left[\frac{s_{ce} - s_{oy} + \Delta s}{s_{oy} - s_{re} - \Delta s} \right] (h_{oy} - h_{re}) + h_{oy} - h_{ce} \quad (12)$$

Assuming that the expansion through the Joule-Thomson valve is a constant-enthalpy process, the heat absorbed by the system per pound of fluid flowing through the evaporator may be written as follows:

$$Q_s = h_{ce} - h_{re} \quad (13)$$

From the definition of coefficient of performance, the following may be written:

$$\text{C.O.P.} \equiv Q_s / W_s = \frac{h_{ce} - h_{re}}{\left[\frac{s_{ce} - s_{oy} + \Delta s}{s_{oy} - s_{re} - \Delta s} \right] (h_{oy} - h_{re}) + h_{oy} - h_{ce}} \quad (14)$$

Since none of the properties of the states at the exits of the liquid pump or the vapor compressor appear in the final expression for system work, Eq. (12), or in the expression for system heat absorption, Eq. (13), it is obvious that the total work required for a given cooling load is independent of the relative amounts of work done by the pump or compressor.

In order to complete the system analysis it is useful to employ the radiation mean effective radiator temperature and the temperature change of the fluid in the radiator as independent parameters. The radiation mean effective temperature of a radiator in which a fluid enters at a certain temperature, T_{ri} , and leaves at a different value of temperature, T_{re} , is defined as follows:

$$\bar{T}_e^4 \equiv \frac{3 T_{ri}^3 T_{re}^3}{T_{ri}^2 + T_{ri} T_{re} + T_{re}^2} \quad (15)$$

The temperature change of the fluid flowing through the radiator is defined as follows:

$$\Delta T_r \equiv T_{ri} - T_{re} \quad (16)$$

The characteristics of the system can be calculated from Eqs. (12) through (16) using the following procedure:

1. Select values for \bar{T}_e and ΔT_r and solve Eqs. (15) and (16) for T_{ri} and T_{re} . Since simultaneous solution of Eqs. (15) and (16) is to be avoided, an alternate method has been developed using Fig. 4 in which the difference between the arithmetic mean temperature and radiation mean effective temperature, $\Delta \bar{T}$, is shown as a function of ΔT_r and \bar{T}_e . Using this quantity there follows:

$$T_{ri} = \Delta\bar{T} + \bar{T}_e + (\Delta T_r/2) \quad (17)$$

$$T_{re} = T_{ri} - \Delta T_r \quad (18)$$

2. Since the states $()_{ri}$ and $()_{oy}$ are identical, and since the state $()_{oy}$ is assumed to be a saturated liquid state, knowledge of T_{ri} will define values for the following quantities: s_{oy} , h_{oy} .

3. Since the state $()_{re}$ is assumed to be a saturated liquid state, knowledge of T_{re} will define values for the following quantities: s_{re} , h_{re} . (It is also possible to include a radiator pressure drop in the system analysis. For such cases values of p_{re} and T_{re} will define state $()_{re}$.)

4. Select a value for the cooling coil temperature, $T_{ci} = T_{ce}$. Since state $()_{ce}$ is assumed to be a saturated vapor state, values for the following quantities will be defined: s_{ce} , h_{ce} .

5. Select a value for the entropy change through the condensing-ejector, Δs .

6. Values are now known for all quantities in Eqs. (12), (13) and (14).

The above procedure was used to determine the characteristics of a condensing-ejector refrigeration system for the conditions given in Table I.

TABLE I

CONDITIONS FOR CALCULATION OF SYSTEM PERFORMANCE

Radiation Mean Effective Temperature, $\bar{T}_e = 150$ F

Cooling Coil Temperature, $T_{ci} = T_{ce} = 50$ F

Refrigerant is Freon - 11*

The results are shown in Figs. 5, 6 and 7

*Thermodynamic properties were obtained from, "Thermodynamic Properties of Freon-11" by E. I. du Pont de Nemours and Company, 1938

The heat absorption characteristics of the system are shown in Fig. 5 as a function of the temperature change in the radiator. Between 0 and 80 Btu/lbm can be absorbed by the evaporator over the temperature range considered. Higher capacities result as the radiator temperature change is increased since the temperature (and enthalpy) at the evaporator inlet are decreased.

The ideal work inputs are shown in Fig. 6. Although the heat absorption capacity is independent of the entropy change across the condensing ejector, Eq. (13), the ideal work input depends on this entropy change, Eq. (12). Thus, various curves for work input are obtained as a function of the entropy change. The lowest work inputs, about 15 Btu/lbm, are obtained when Δs is zero, or a reversible-adiabatic condensing ejector is used. This particular mode of operation for the condensing ejector might be approached if the two streams which enter the ejector were expanded to a common pressure in the two-phase region. This would insure equality of pressure and temperature for the two streams at Section 1 (see Fig. 1). The inlet states would also have to be adjusted such that equal velocities existed at Section 1, thus removing the irreversible effects arising from viscous stresses. The condensation process could then occur in a reversible manner. For irreversible condensing ejectors ($\Delta s > 0$) the ideal work inputs are two to three times higher than those for reversible operation at the lower values of radiator temperature change. For radiator temperature changes of about 200 F, the work inputs are only 10 percent higher.

The coefficients of performance for the system are shown in Fig. 7. A C.O.P. of about 4.5 is obtained for the reversible case. The percentage changes in C.O.P. due to variation in Δs are identical to those mentioned for the work inputs, since the heat absorption capacities are independent of Δs . The values for Δs were based on estimates obtained from previous analyses of condensing-ejector performance. In Fig. 6 it will be noted that the shapes of the curves for reversible and irreversible condensing ejectors diverge at low values of ΔT_r . This is explained by the results for C.O.P. in Fig. 7 where the values of C.O.P. for the reversible case can have a finite limit

as ΔT_r approaches zero whereas the values of C.O.P. for the irreversible cases approach zero as ΔT_r approaches zero.

MOMENTUM ANALYSIS OF CONDENSING EJECTOR

The system study of the previous section required only a knowledge of the entropy increase across the condensing ejector. In order to determine what entropy change will actually be produced it is necessary to analyze the condensing ejector in detail. Table II summarizes the information which is available at this point in the analysis. The quantities in the last column are of particular interest since they pertain directly to the condensing ejector. It will be seen that the exit state for the condensing ejector is completely defined. Also the inlet entropies and flow rate ratio are known. The following procedure has been selected for purposes of studying the condensing ejector.

A maximum allowable liquid pressure at the inlet of the condensing ejector, p_o'' , is selected. The enthalpy change across the pump then becomes:

$$h_o'' - h_{re} = \frac{p_o'' - p_{re}}{\rho_{re}} \quad (19)$$

Equation (19) actually determines a value for h_o'' and hence the state $()_o''$ is now completely defined. The isentropic pump work per pound of fluid flowing through the evaporator is:

$$W_{sp} = \omega (h_o'' - h_{re}) \quad (20)$$

The isentropic compressor work per pound of fluid flowing through the evaporator is:

$$W_{sc} = W_s - W_{sp} \quad (21)$$

It is possible that the maximum value of p_o'' will yield an isentropic pump work which is greater than the total ideal work input. In such a case the value of p_o'' can be reduced until $W_{sp} = W_s$ and the compressor can be eliminated. It is advisable to put as much as possible of the ideal work input

TABLE II
 INFORMATION DETERMINED BY THERMODYNAMIC ANALYSIS

ASSUMED PARAMETERS	SYSTEM PARAMETERS DETERMINED	CONDENSING EJECTOR PARAMETERS DETERMINED
\bar{T}_e	$T_{ri}, P_{ri}, h_{ri}, s_{ri}$	$T_{oy}, P_{oy}, h_{oy}, s_{oy}$
ΔT_r	$T_{re}, P_{re} = P_{ri}, h_{re}, s_{re}$	$s_o'' = s_{re}$
$T_{ci} = T_{ce}$	$P_{ce}, h_{ce}, s_{ce}, \rho_{ce}$	$s_o' = s_{ce}$
Δs	$Q_g, W_g, C.O.P.$	ω

into the liquid pump so as to obtain high values of h_o'' . High values of h_o'' make it possible to approach "reversible-adiabatic" or isentropic ($\Delta s = 0$) operation of the condensing ejector. That this is true follows from the fact that isentropic operation requires velocity equality of the two streams at Section 1, or

$$V_1' = V_1'' \quad (22)$$

or from the steady flow energy equation

$$(h_o' - h_1') = (h_o'' - h_1'') \quad (23)$$

In general, the enthalpy change for the vapor stream will be higher than that for the liquid stream since a unit pressure difference will cause a higher velocity for the lower density vapor than for the higher density liquid. Thus, for the equality of Eq. (23) to hold and, hence isentropic operation of the ejector to be obtained, large values of h_o'' or p_o'' must be used.

Assume for the present that $W_{sp} < W_s$ and hence that both a pump and a compressor will be required. The isentropic compressor work can be used to calculate a value of h_o' since:

$$W_{sc} = h_o' - h_{ce} \quad (24)$$

This value of h_o' and the previously known value of s_o' fix the inlet state of the vapor stream at the condensing ejector.

At this point the inlet states and the exit state for the condensing ejector are fixed. The First and Second Laws of Thermodynamics and the Law of Conservation of Mass have been satisfied. It is still necessary to satisfy the Momentum Equation. Also there is one quantity which can be varied for the condensing ejector; namely, the pressure to which the streams expand at Section 1, p_1 . The problem is to determine if there is a value of p_1 which can be used with the data for the inlet states and the momentum equation which will match the known exit state.

The momentum analysis for the condensing ejector employs four assumptions which are usually valid.

1. The acceleration processes in the inlet nozzles are isentropic, and the flow leaving each nozzle is one-dimensional.
2. The pressure is uniform across the entrance of the mixing section, although the velocity and temperature of the two entering streams may be different.
3. The flow entering the diffuser is one-dimensional, and the deceleration process in the diffuser is isentropic.
4. Wall shear stresses on the fluid are negligible.

In addition to these assumptions it is necessary to have a knowledge of the shape of the mixing section. Normally, three possible shapes are considered:

1. Constant-Area Mixing Section

The mixing section between Sections 1 and 3 is a constant-area tube and the mixing and condensation processes are complete at Section 3.

2. Constant-Pressure Mixing Section

The mixing section is contoured between Sections 1 and 3 in such a manner that the static pressure is constant between these sections. The mixing and condensation processes are complete at Section 3.

3. Convergent/Constant-Area Mixing Section

The mixing section is converged between Sections 1 and 2 and has a constant area between Sections 2 and 3. The static pressure may remain constant or decrease in the convergent section and the flow leaving the convergent section need not be uniform. However, the mixing and condensation processes are complete at Section 3.

The best performance for the condensing ejector is obtained with the convergent/constant-area mixing section. The poorest performance is obtained with a constant-area mixing section. The performance for the constant-pressure mixing section is between these extremes. For this system study the constant-pressure mixing section has been employed since the results will be conservative and a simplification of analysis results.

The momentum equation for a control volume between Sections 1 and 3 (for the constant-pressure mixing section) can be written as follows.

$$w_y V_y - (w' V_1' + w'' V_1'') = 0 \quad (25)$$

The continuity equation yields:

$$w' + w'' = w_y \quad (26)$$

Combining Eqs. (25) and (26) and the definition of the flow rate ratio, ω :

$$(1 + \omega) V_y = V_1' + \omega V_1'' \quad (27)$$

The Steady Flow Energy Equation for the two nozzles and the diffuser yields:

$$(V_1')^2 = 2 g_o J (h_o' - h_1') \quad (28)$$

$$(V_1'')^2 = 2 g_o J (h_o'' - h_1'') \quad (29)$$

$$V_y^2 = 2 g_o J (h_{oy} - h_y) \quad (30)$$

The following procedure can be used with the above analysis to calculate the performance of the condensing ejector.

1. Select a value of p_1 which is less than p_o and p_o'' . This value of p_1 and the values of $s_1' = s_o'$ and $s_1'' = s_o''$ define the states $()_1'$ and $()_1''$.
2. Calculate V_1' and V_1'' from Eqs. (28) and (29).
3. Calculate V_y from Eq. (27) since ω is known. (See Table I).
4. Calculate h_y from Eq. (30) since h_{oy} is known. (See Table I).
5. For constant-pressure mixing section, $p_y = p_1$.
6. Evaluate s_y from values of h_y and p_y using tables of thermodynamic properties. From Assumption 11, $s_y = s_{oy}$.
7. Calculate Δs from its definition, Eq. (2).
8. Return to Step 1 and vary p_1 in order to determine the variation of Δs with p_1 . Usually a minimum value of Δs will be found. If this minimum value of Δs does not correspond to the value in the thermodynamic analysis, repeat the entire analysis (including thermodynamic analysis) until the

minimum value of Δs from Step 7 matches the assumed value of Δs in the thermodynamic analyses. Rapid convergence will be obtained by this iterative procedure if the minimum value of Δs from Step 8 is used in thermodynamic analysis. The resulting set of values for the system and condensing ejector performance satisfy all the controlling physical laws for the system.

Calculations were made using the above procedure using the conditions in Table I. In addition, the pressure of the liquid at the condensing ejector, p_o'' , was limited to 500 psia. The results are shown in Fig. 8, where the calculated entropy change from the momentum analysis is shown as a function of p_1 for constant values of ΔT_r . The value of Δs in the thermodynamic analysis for each value of ΔT_r was taken as the minimum value of Δs on the particular curve for ΔT_r given in Fig. 8. Thus, for each curve the minimum point is a valid solution for all physical laws. Points on the curves above the minimum do not satisfy all physical laws since values of Δs from the momentum analyses are greater than that used for the thermodynamic analysis. For a value of ΔT_r of 200 F, Δs is about 0.002 Btu/lbm R while for values of ΔT_r less than about 80F, Δs is about zero so that isentropic operation of the condensing ejector has been approached.

In order to make the results somewhat more realistic an entropy change of 0.0001 Btu/lbm R has been added to account for the effects of wall shear stress in the actual operation of the condensing ejector. This is equivalent to modifying Eq. (2) as follows:

$$\Delta s \equiv s_{oy} - \left[\frac{\omega s_o'' + s_o'}{1 + \omega} \right] + 0.0001 \quad (2a)$$

The thermodynamic and momentum analyses were repeated using Eq. (2a) in place of Eq. (2). The results are presented in Figs. 9 through 13.

Figure 9 shows the minimum entropy change for the condensing ejector as a function of ΔT_r . The minimum value of Δs is used since the results of Figs. 5, 6 and 7 indicate that the best system performance is obtained when Δs is a minimum. It will be seen that the values of Δs in Fig. 9 are greater than the minimum values of Δs from Fig. 8 by about 0.0001 Btu/lbm R as is to be expected from Eq. (2a).

For reference purposes the flow rate ratio is shown in Fig. 10 for two limiting values of Δs . At lower values of ΔT_r the values of ω are about 20 to 30 while at the higher values of ΔT_r , the values of ω have dropped to about unity. The high values of Δs_M in Fig. 9 are related to the low values of ω in Fig. 10. The limitation on maximum liquid pressure reduces the fraction of the total work input to the liquid stream when ω is low, Eq. (20). Consequently, the isentropic operation of the condensing ejector cannot be approached for reasons given following Eq. (23).

The distribution of the total ideal work input between the liquid pump and the vapor compressor is shown in Fig. 11. At high values of ΔT_r most of the work input goes into the compressor for the reason just mentioned. As ΔT_r is reduced, an increasing amount of work goes into the pump until when ΔT_r is about 20 F, the total work input goes into the pump and the vapor compressor can be eliminated. The dashed extension of the pump work line for values of ΔT_r less than about 20 F is based on the assumption that the maximum liquid pressure of 500 psia is used. Comparison of this dashed line with the total work line indicates that the pump work will be greater than the total work actually required. Consequently the pump work line follows the total work lines for values of ΔT_r less than 20 F and the required values of p_o'' will be less than 500 psia. The value of ΔT_r , at which the compressor can be eliminated will shift as the maximum allowable liquid pressure is varied.

The coefficients of performance for the condensing-ejector system and for a pure vapor compressor system are shown in Fig. 12. For systems using a reversible pump and compressor the C.O.P. is about 4.3. For values of ΔT_r between 50 and 110 F the C.O.P. for the condensing ejector system is slightly higher than that for the pure vapor compressor system. For values of ΔT_r outside this range in the worst case, the C.O.P. for the condensing ejector system is about 15% lower. For systems using real pumps and compressors, the C.O.P. decreases to about 3.0. In the important region of ΔT_r where the compressor can be eliminated from the condensing ejector system the C.O.P. of this system is about 7 percent higher.

Finally, Fig. 13 shows the heat rejected from the radiator and the work input for the system based on unit cooling load. Both quantities are just about independent of ΔT_r and have values of about 1.35 Btu/Btu and 0.35 Btu/Btu, respectively. These values were obtained for the conditions of a real pump and compressor shown in Fig. 12.

CONCLUSIONS

1. Active cooling systems will replace passive systems in space vehicles as cooling loads increase and weight penalties of auxiliary power decrease.

2. The condensing-ejector refrigeration system for space vehicles will perform satisfactorily in a zero-gravity environment since all processes which might be affected by the zero-gravity condition are performed at relatively high velocities.

3. The condensing-ejector system can have a greater coefficient of performance than a conventional vapor compression system, and for equal cooling loads and mean effective radiator temperatures the condensing-ejector system will have a smaller and lighter radiator.

4. System conditions are possible such that the condensing-ejector system will require only a liquid pump for satisfactory operation. (See Fig. 2).

5. The performance characteristics of the condensing ejector system calculated assuming a constant pressure mixing section for the ejector are conservative, since available data indicate that a convergent/constant-area mixing section will yield better ejector performance than that obtained with a constant-pressure mixing section.

6. The method of analysis of the condensing-ejector system is unique in its use of the Second Law of Thermodynamics and represents a valuable concept in the field of systems analysis.

7. The results indicate that additional analytical studies should be made involving variations on the refrigerant used, temperature levels, maximum liquid pressure, etc. The analyses for the convergent/constant-area

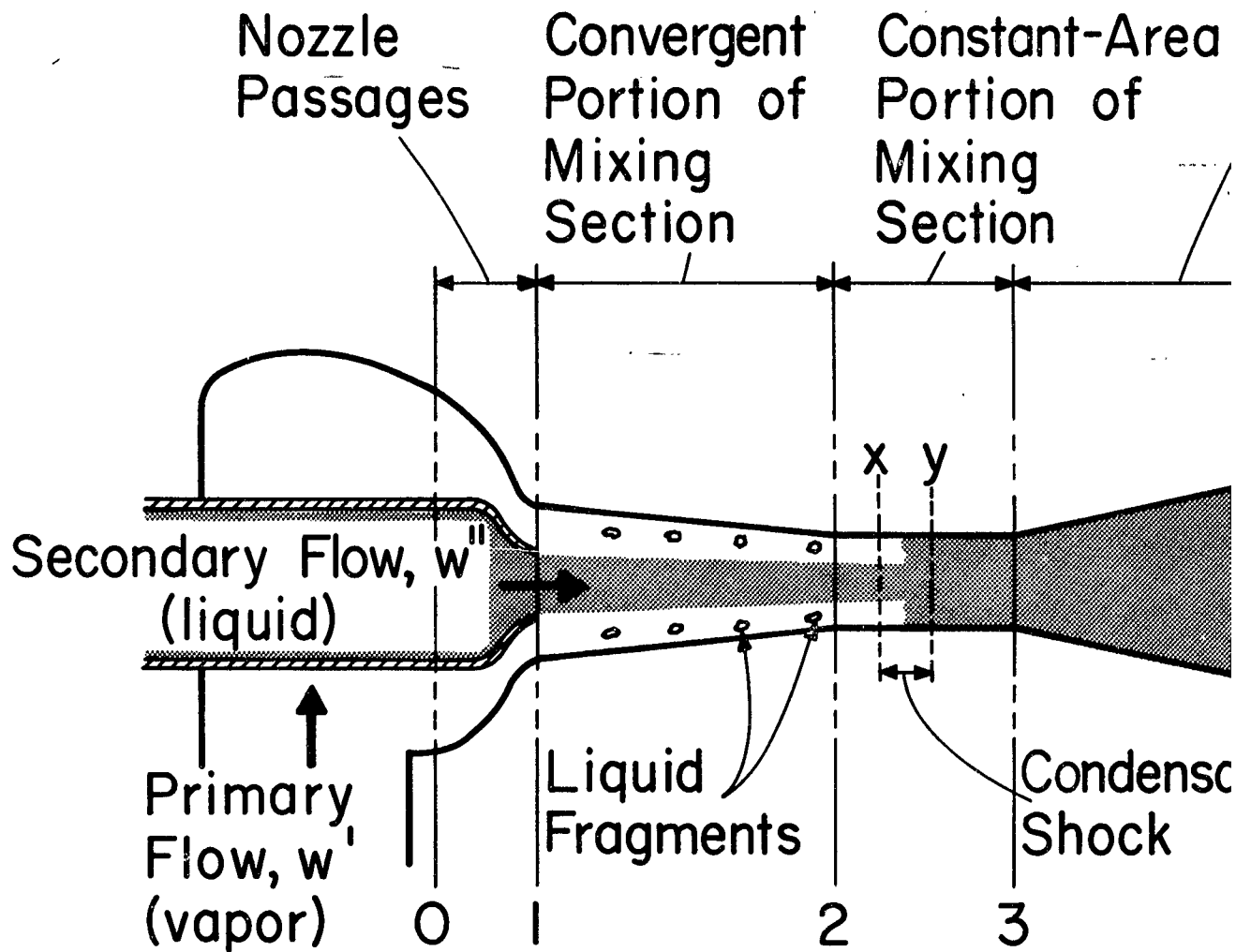
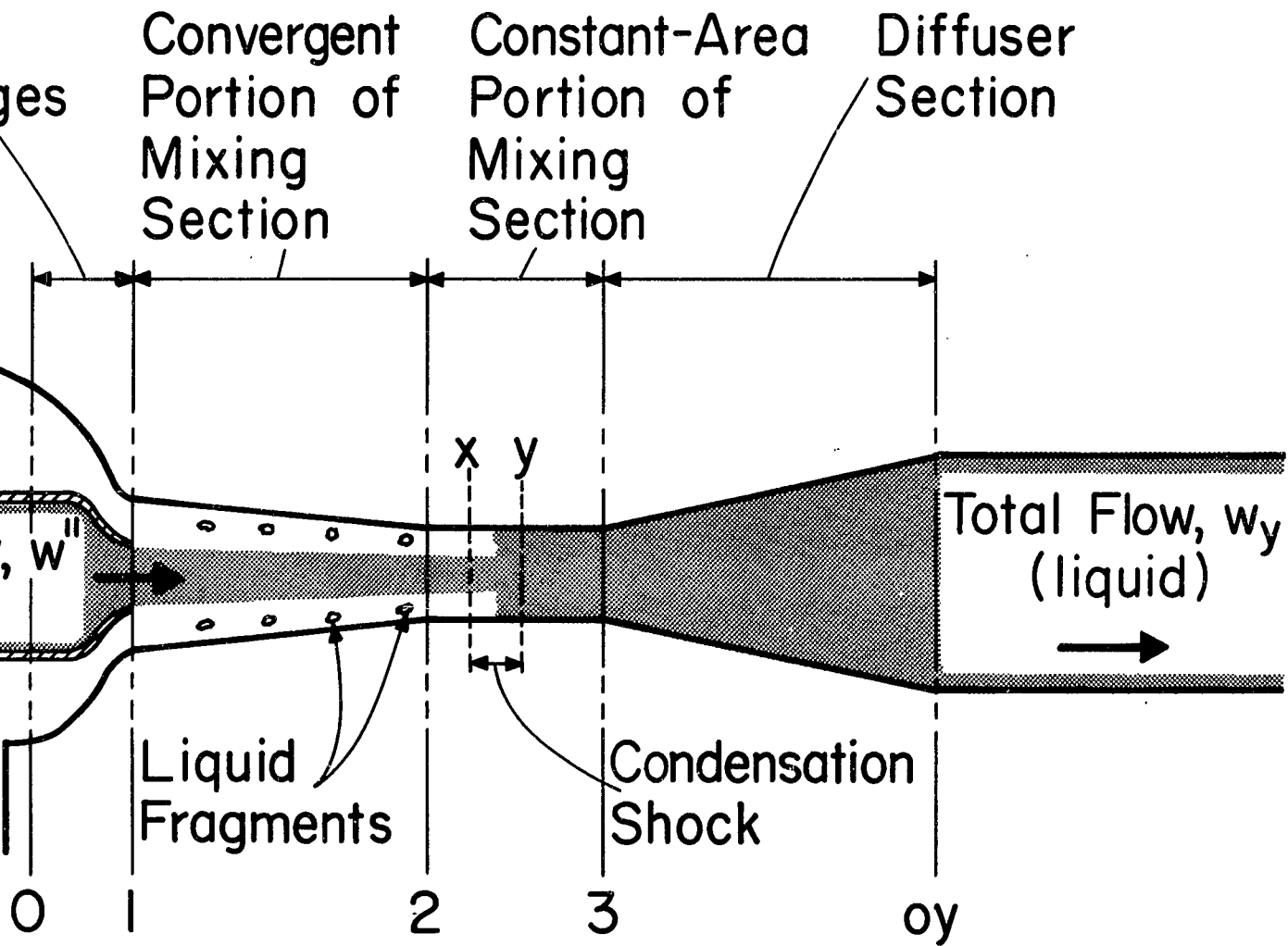


FIGURE 1 SCHEMATIC DRAWING OF CONDE

1



SCHEMATIC DRAWING OF CONDENSING EJECTOR

2

mixing section should be used to calculate the ejector performance. Actual system features should also be considered such as pressure drops, sub-cooling requirements, radiator and system weights for a range of cooling capacity, etc.

8. An experimental study should be made of the operation of the condensing ejector when two-phase states exist in the liquid and vapor nozzles and when a saturated or slightly-subcooled exit state is required, as little experimental data exist for these modes of operation.

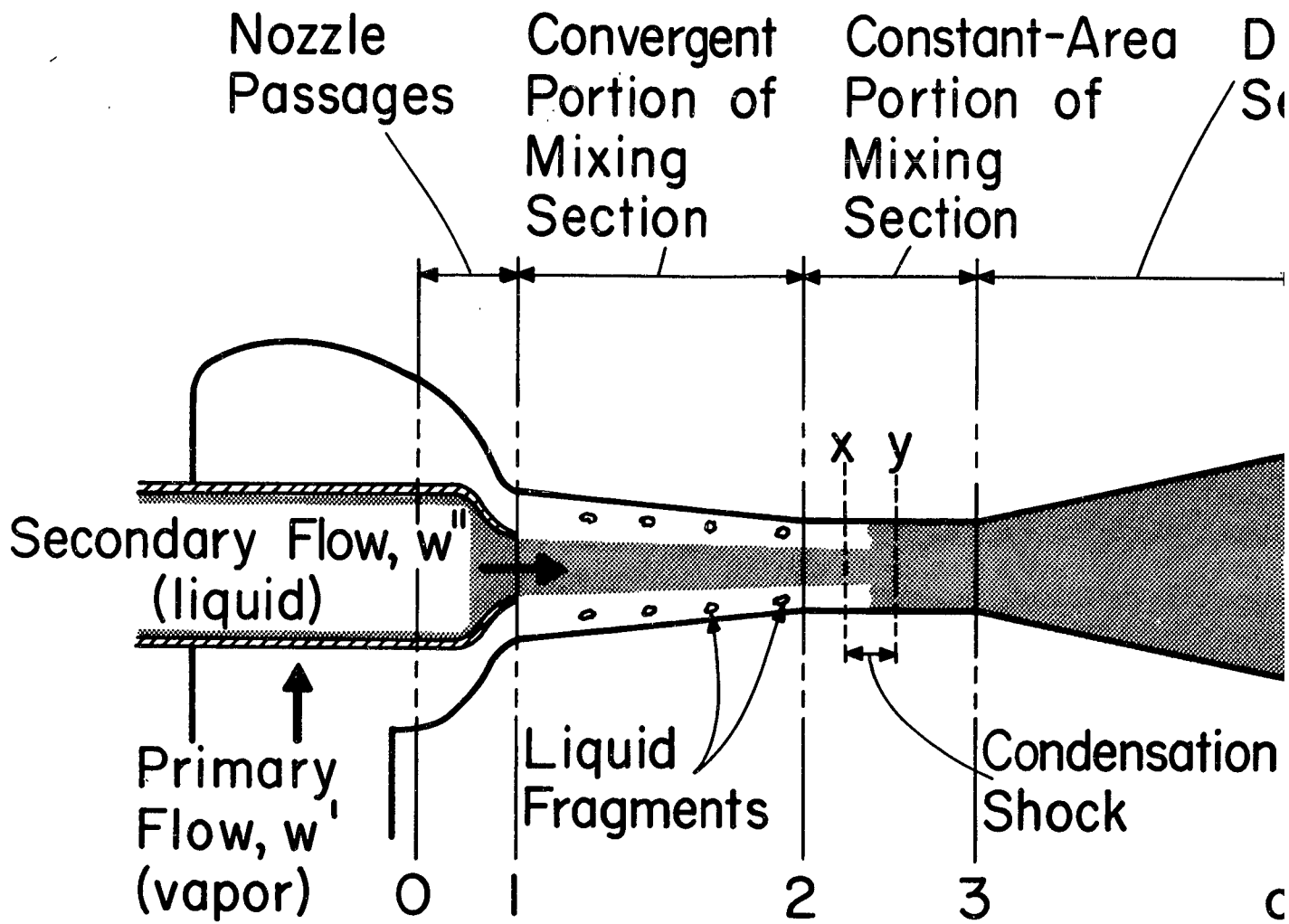
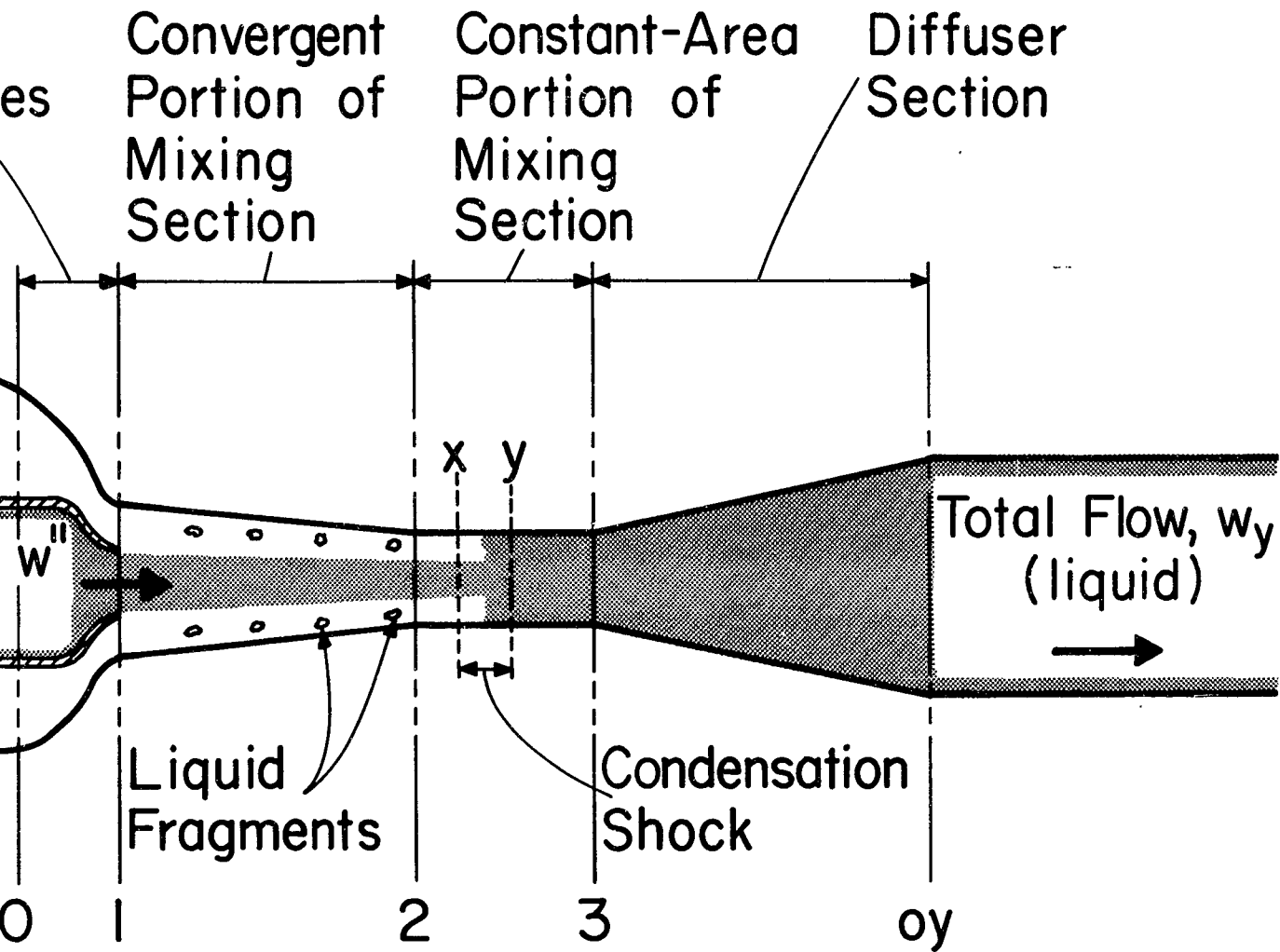


FIGURE 1 SCHEMATIC DRAWING OF CONDENSATION

1



SCHEMATIC DRAWING OF CONDENSING EJECTOR

2

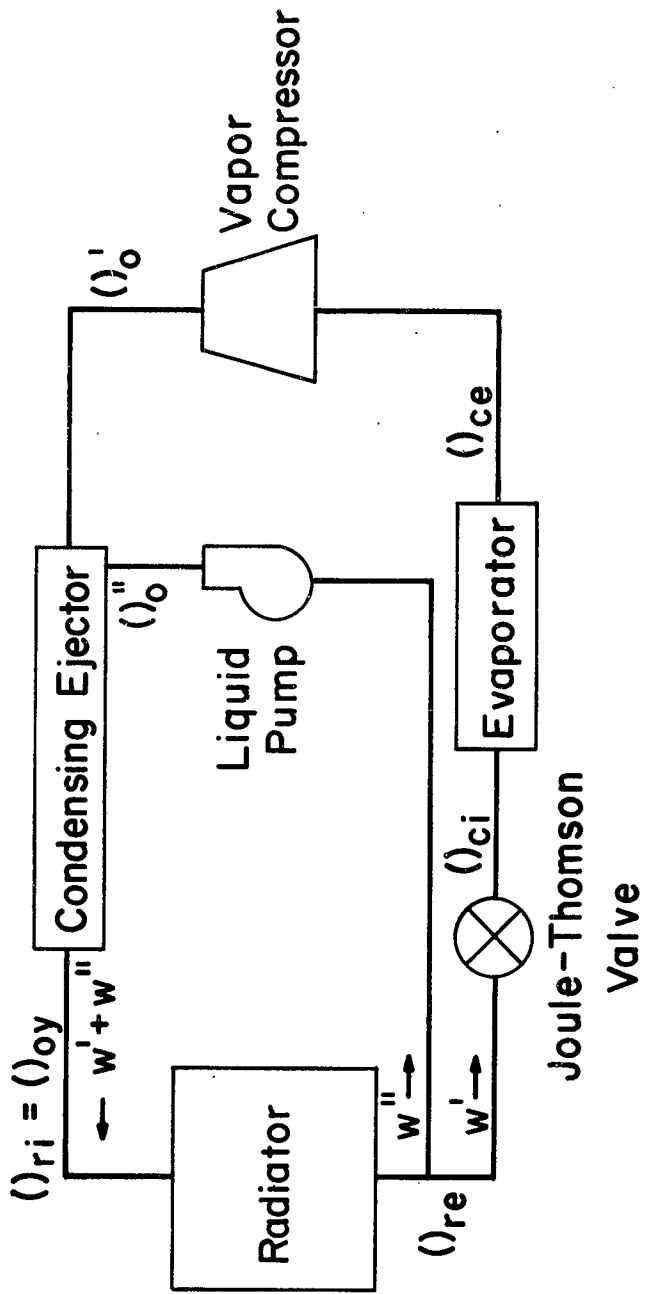


FIGURE 2 GENERAL CONFIGURATION OF CONDENSING-EJECTOR REFRIGERATION SYSTEM

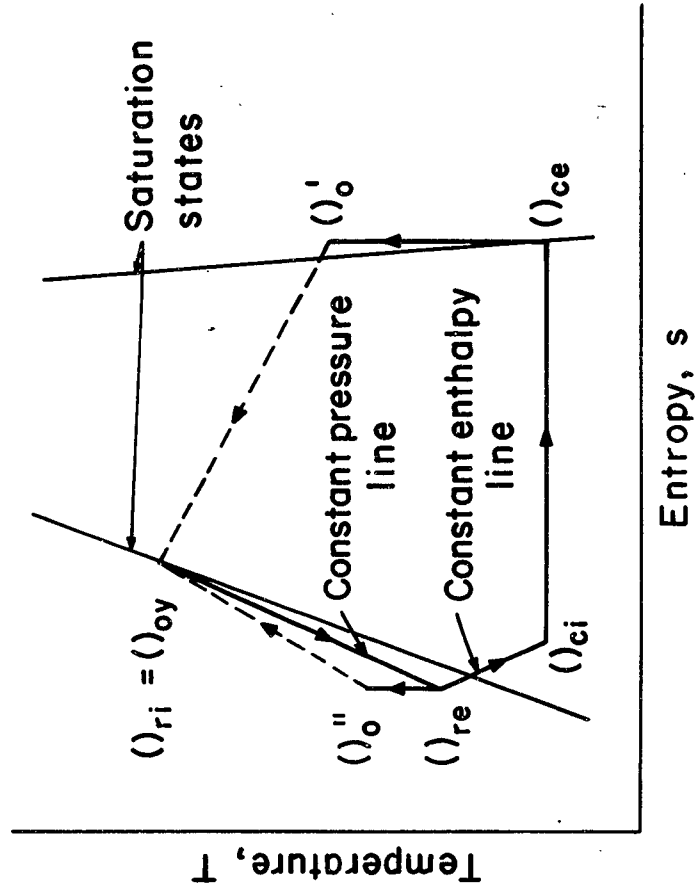


FIGURE 3 TEMPERATURE-ENTROPY
DIAGRAM OF GENERAL
CONFIGURATION

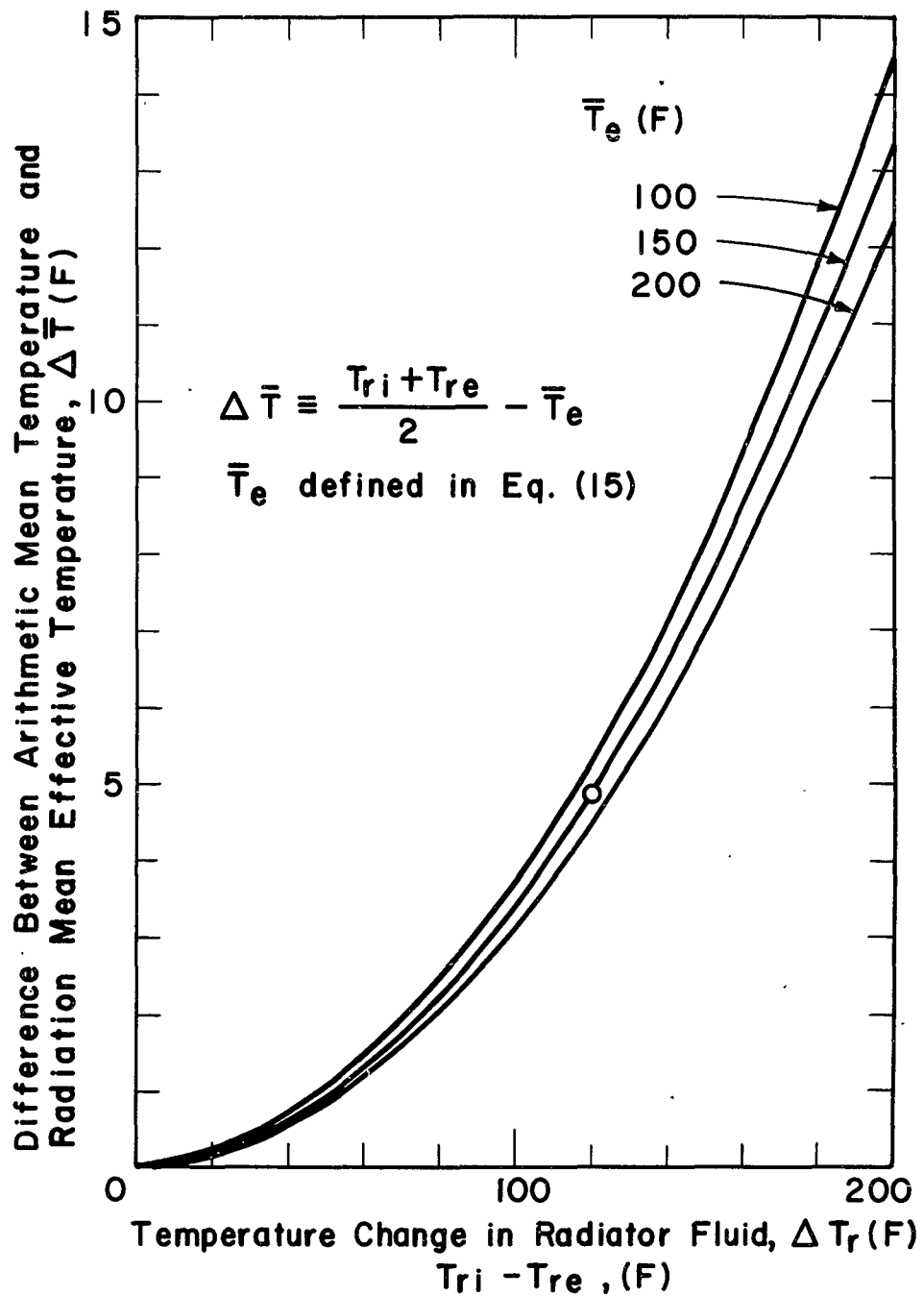


FIGURE 4 DIFFERENCE BETWEEN ARITHMETIC MEAN TEMPERATURE AND RADIATION MEAN EFFECTIVE TEMPERATURE

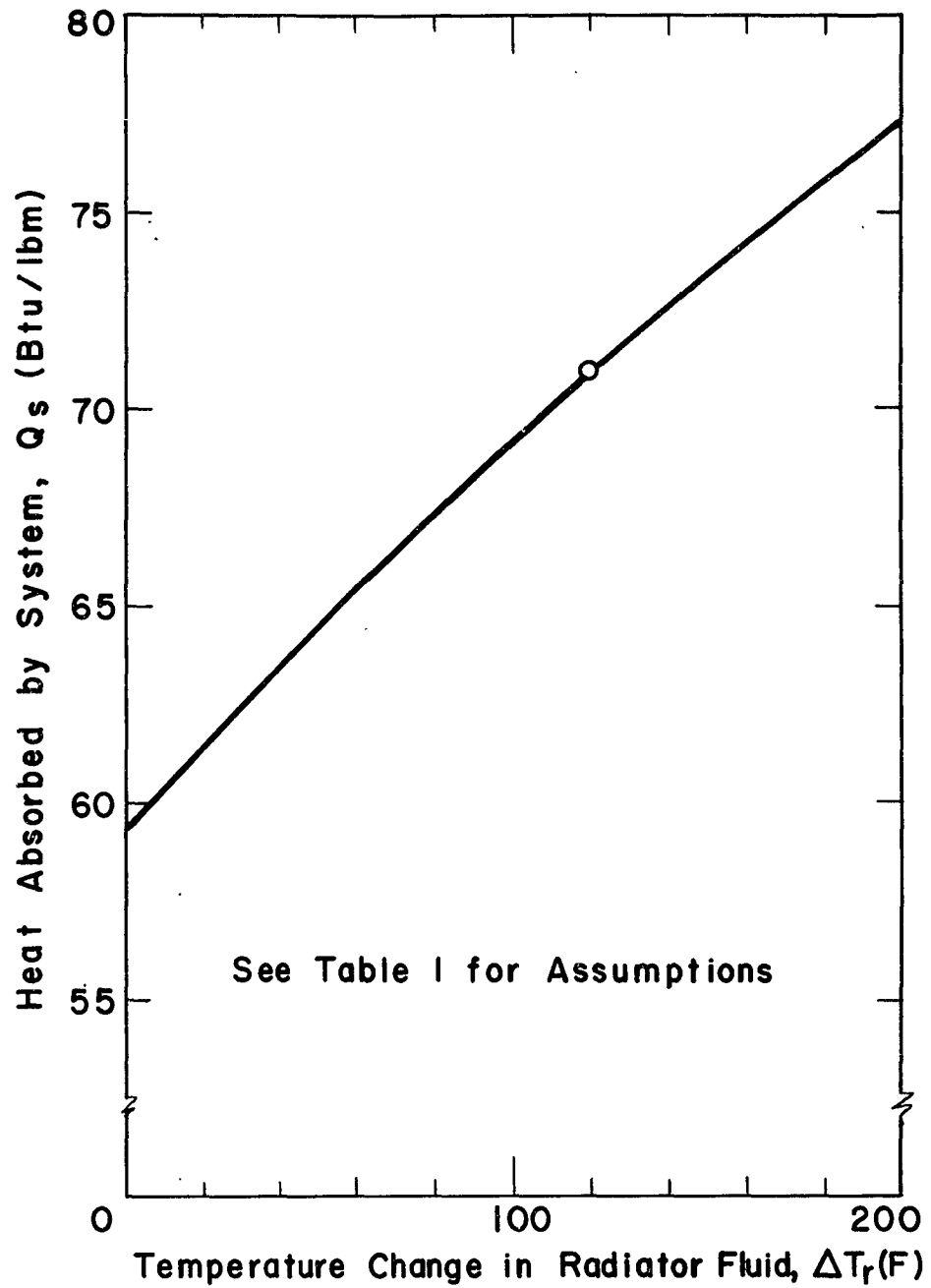


FIGURE 5 HEAT ABSORPTION CHARACTERISTICS OF CONDENSING-EJECTOR REFRIGERATION SYSTEM

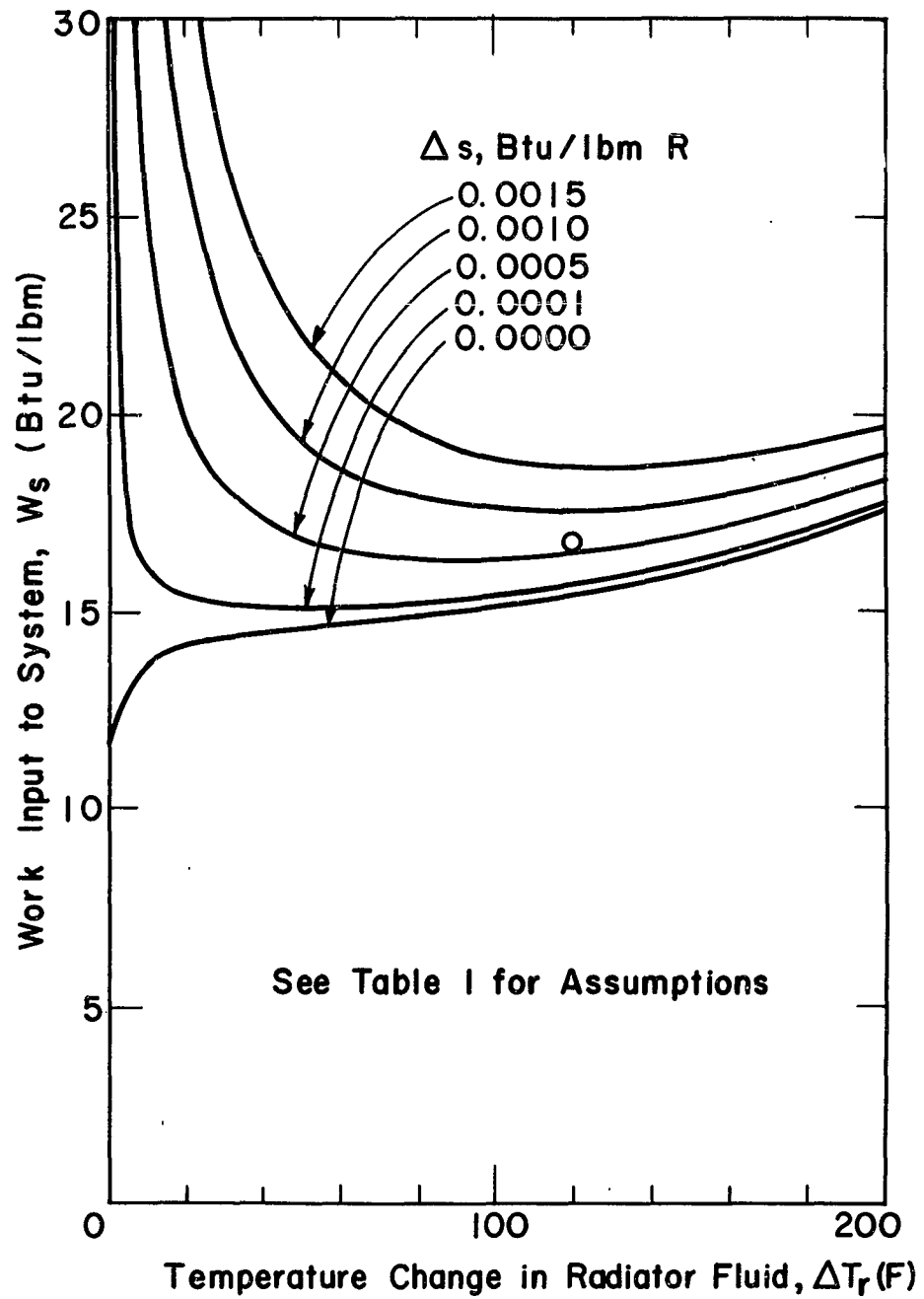


FIGURE 6 IDEAL WORK INPUT TO CONDENSING - EJECTOR REFRIGERATION SYSTEM

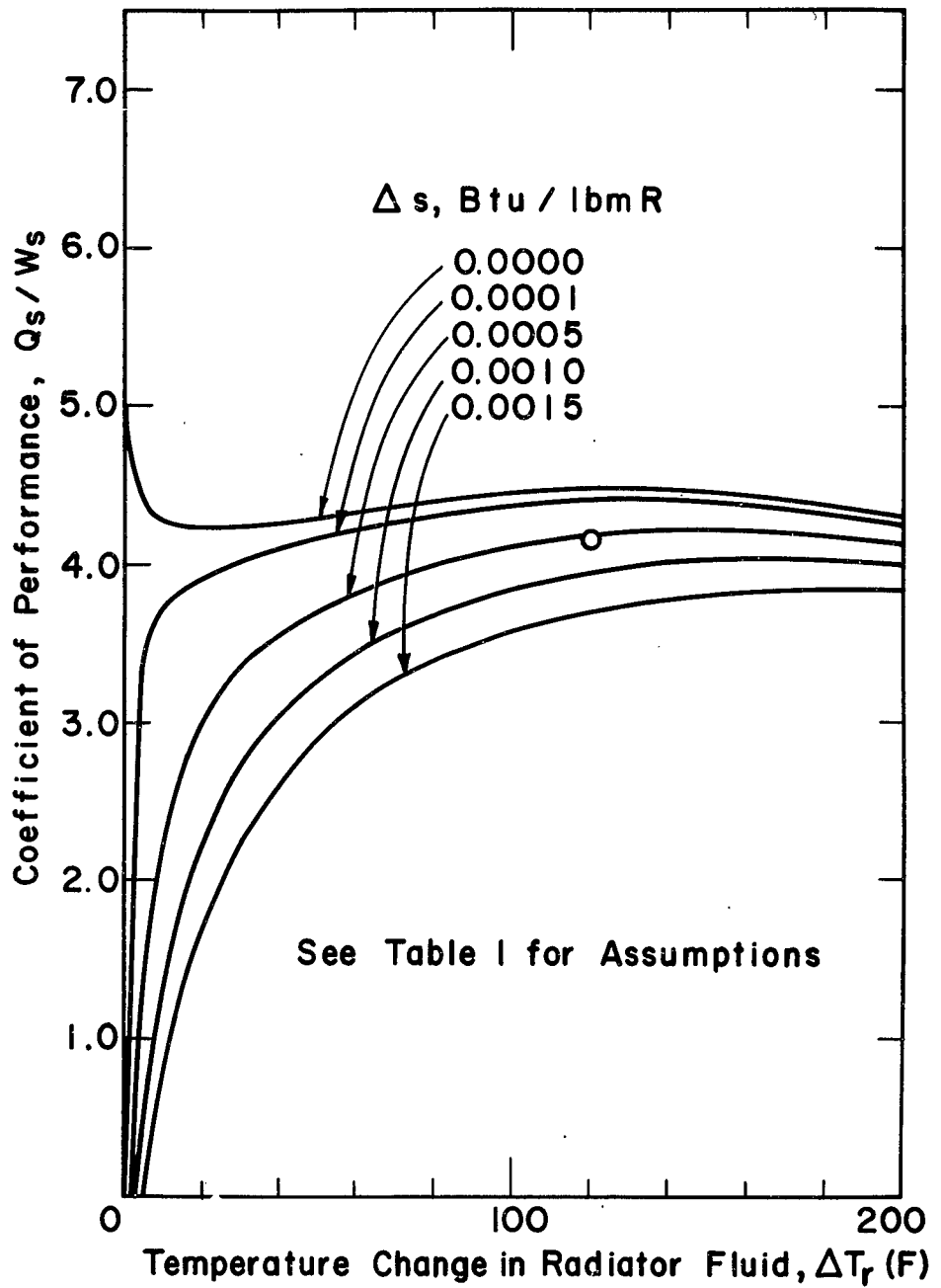


FIGURE 7 COEFFICIENT OF PERFORMANCE OF
 CONDENSING-EJECTOR REFRIGERATION
 SYSTEM

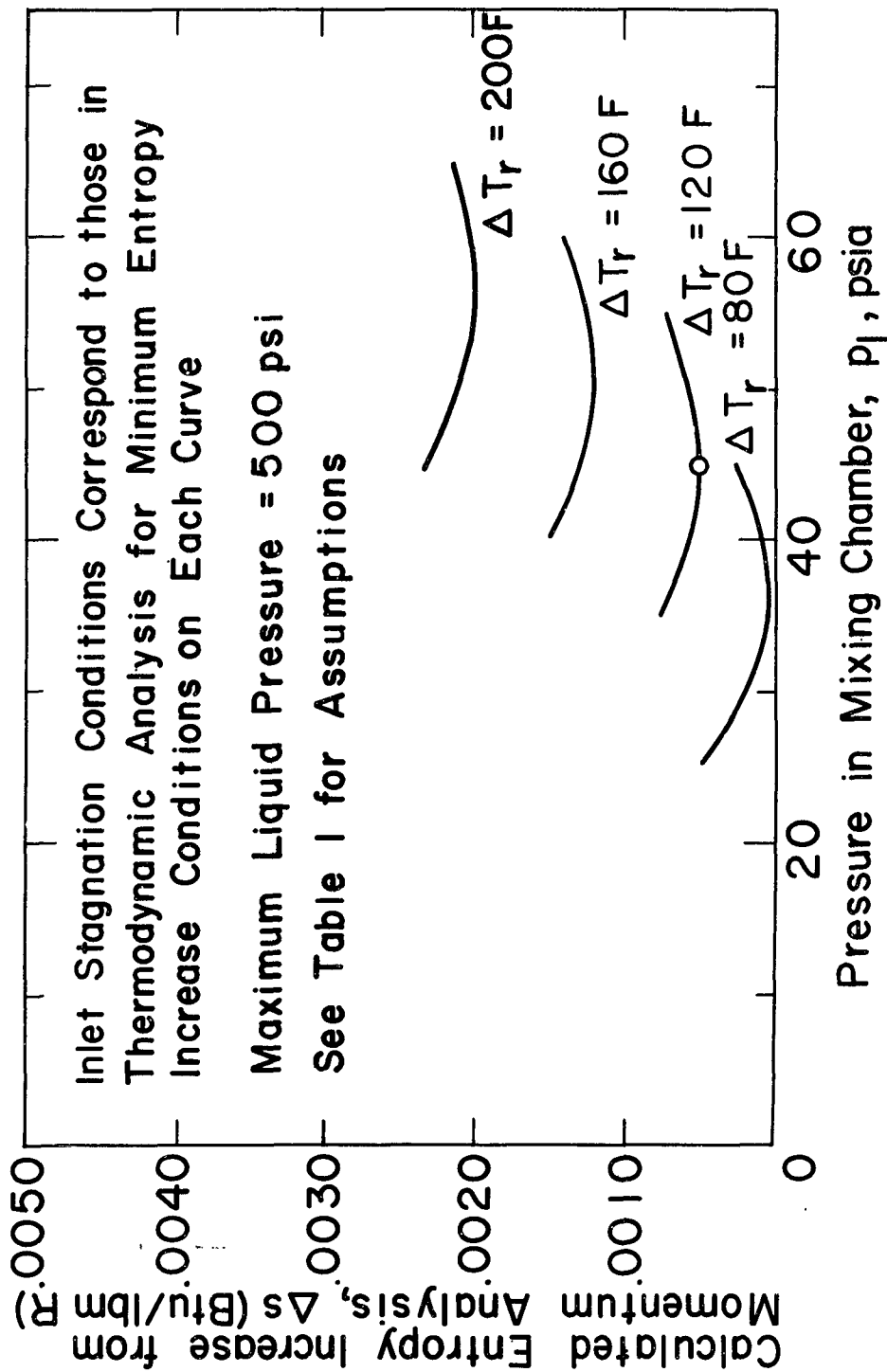


FIGURE 8 ENTROPY INCREASE IN CONDENSING EJECTOR ASSUMING CONSTANT PRESSURE MIXING SECTION

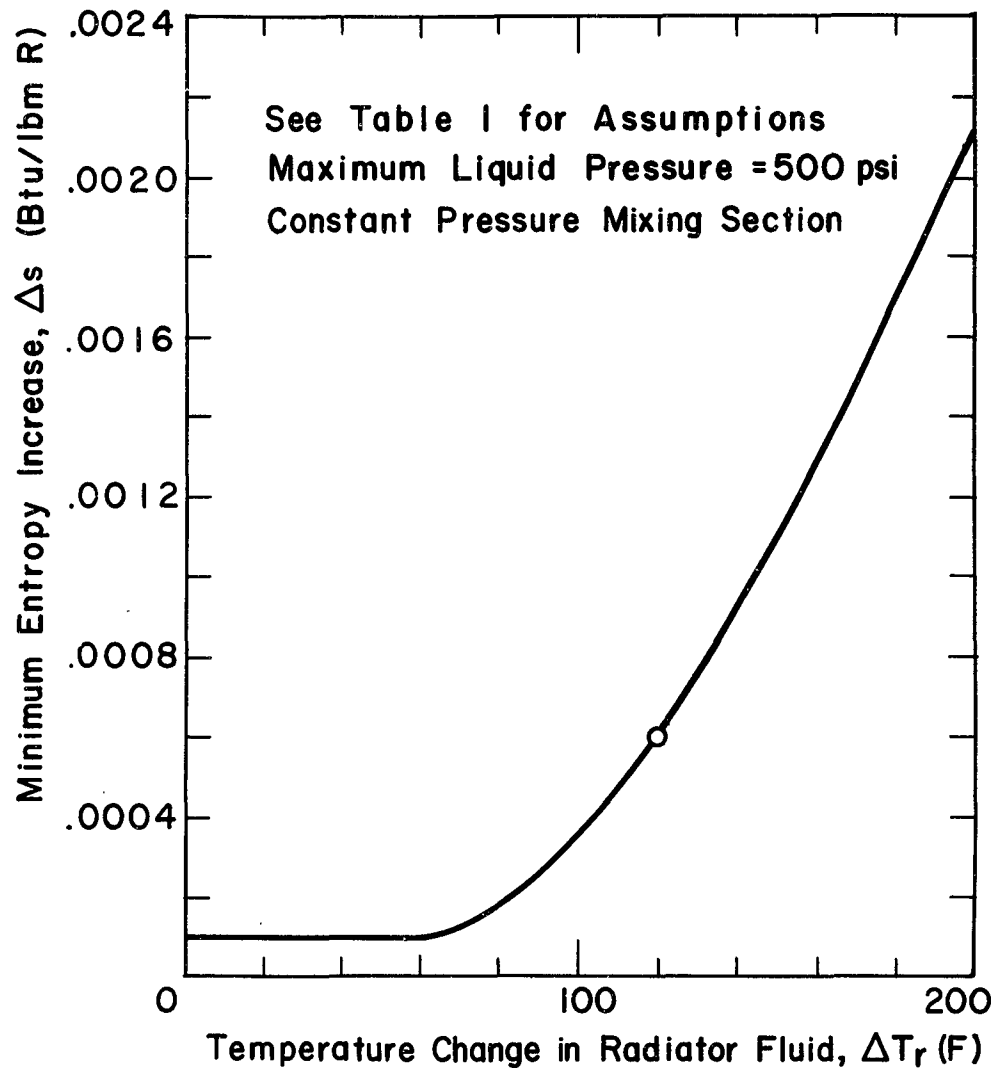


FIGURE 9 MINIMUM ENTROPY INCREASE IN CONDENSING-EJECTOR REFRIGERATION SYSTEM

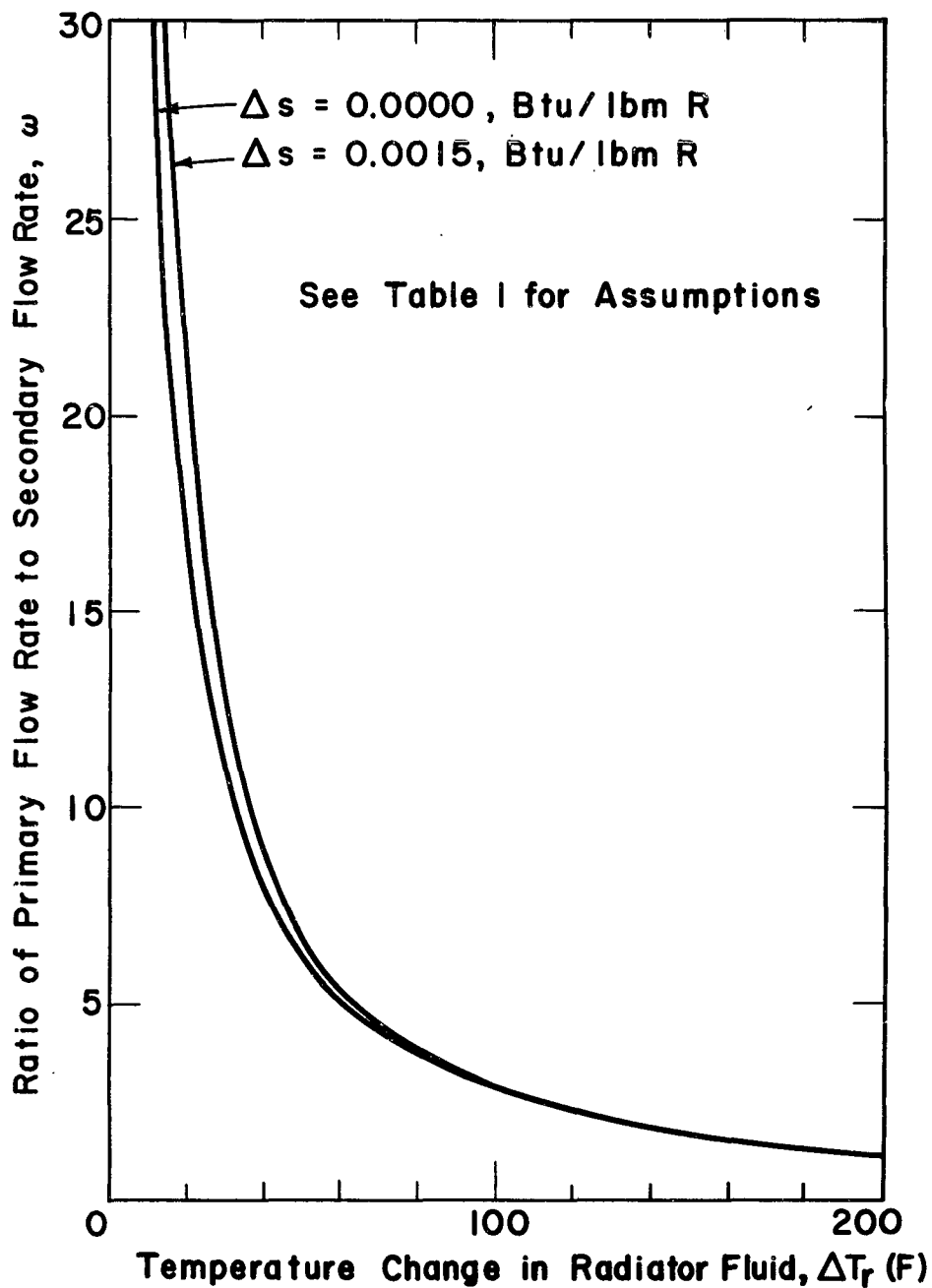


FIGURE 10 RATIO OF SECONDARY FLOW RATE TO PRIMARY FLOW RATE FOR CONDENSING-EJECTOR REFRIGERATION SYSTEM

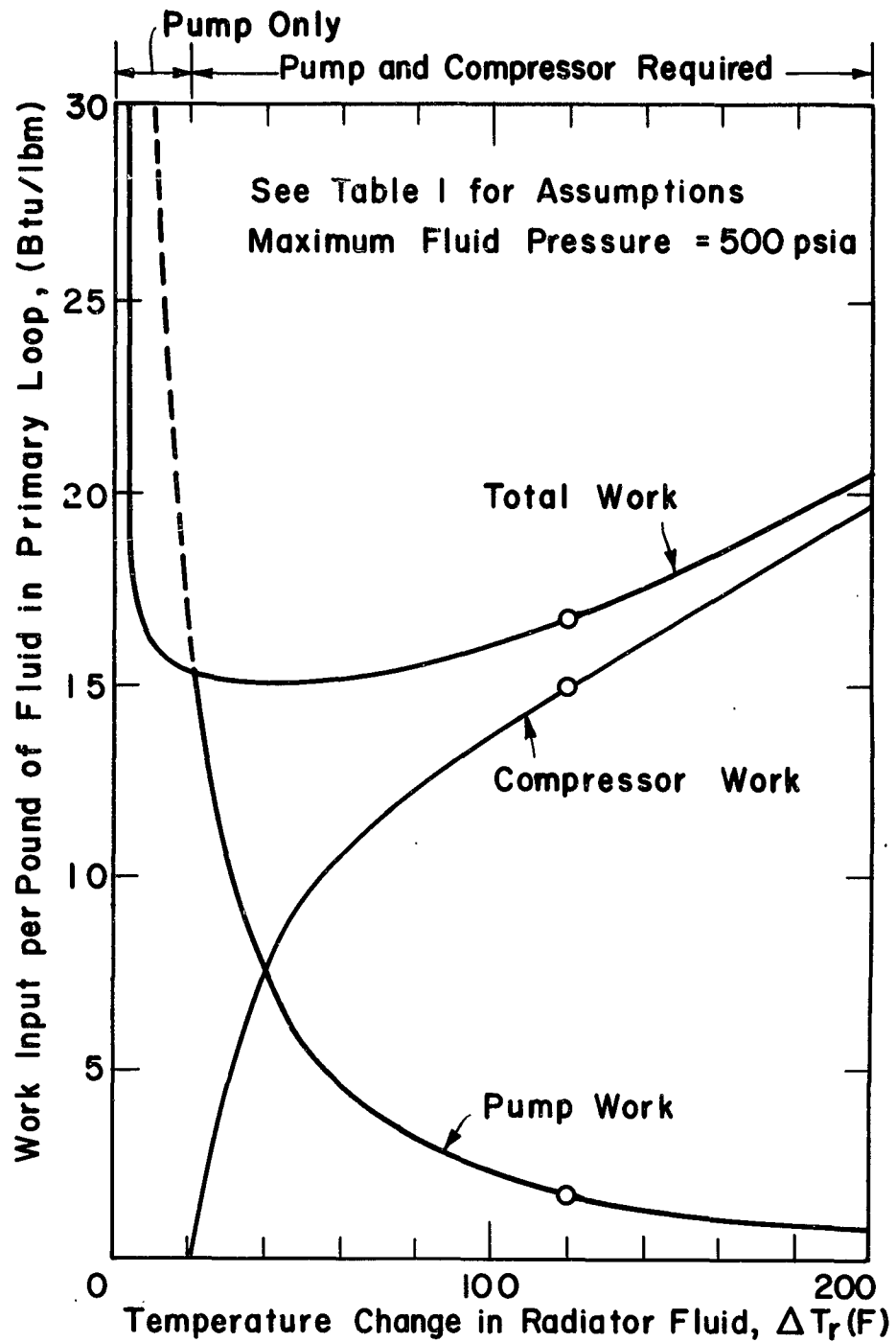


FIGURE II IDEAL WORK INPUT TO CONDENSING EJECTOR REFRIGERATION SYSTEM FOR CONSTANT PRESSURE MIXING SECTION

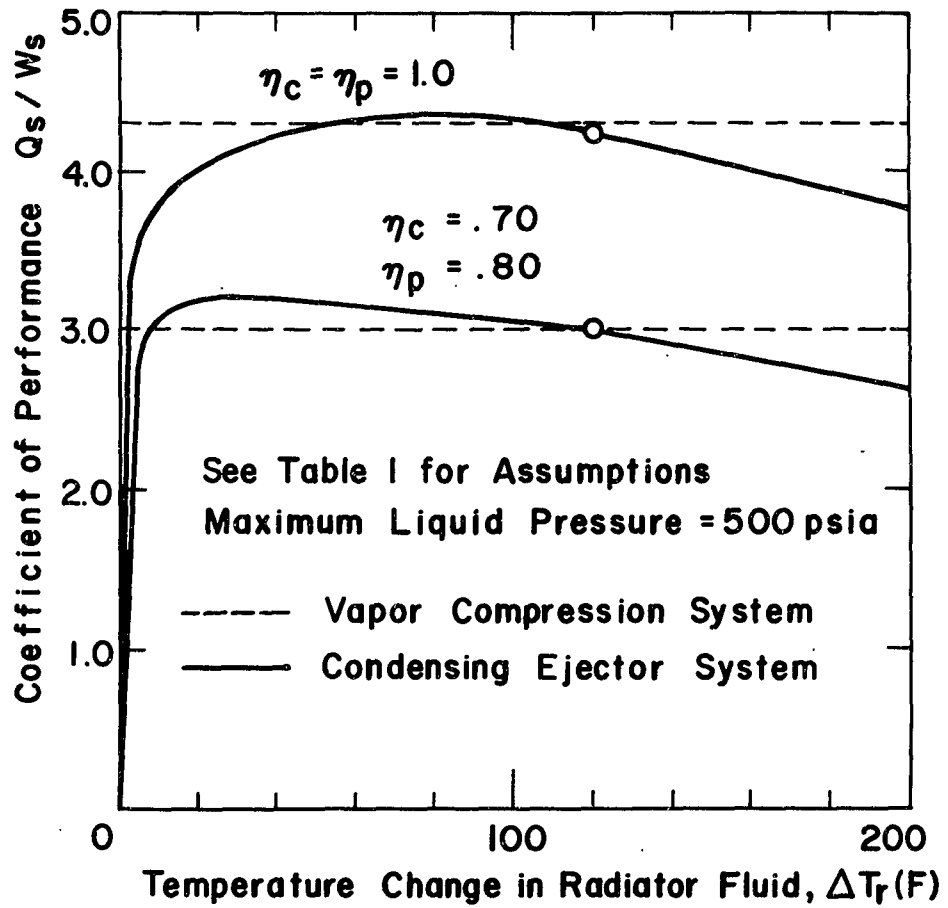


FIGURE 12 COEFFICIENT OF PERFORMANCE OF CONDENSING-EJECTOR REFRIGERATION SYSTEM AND CONVENTIONAL VAPOR-COMPRESSION REFRIGERATOR SYSTEM

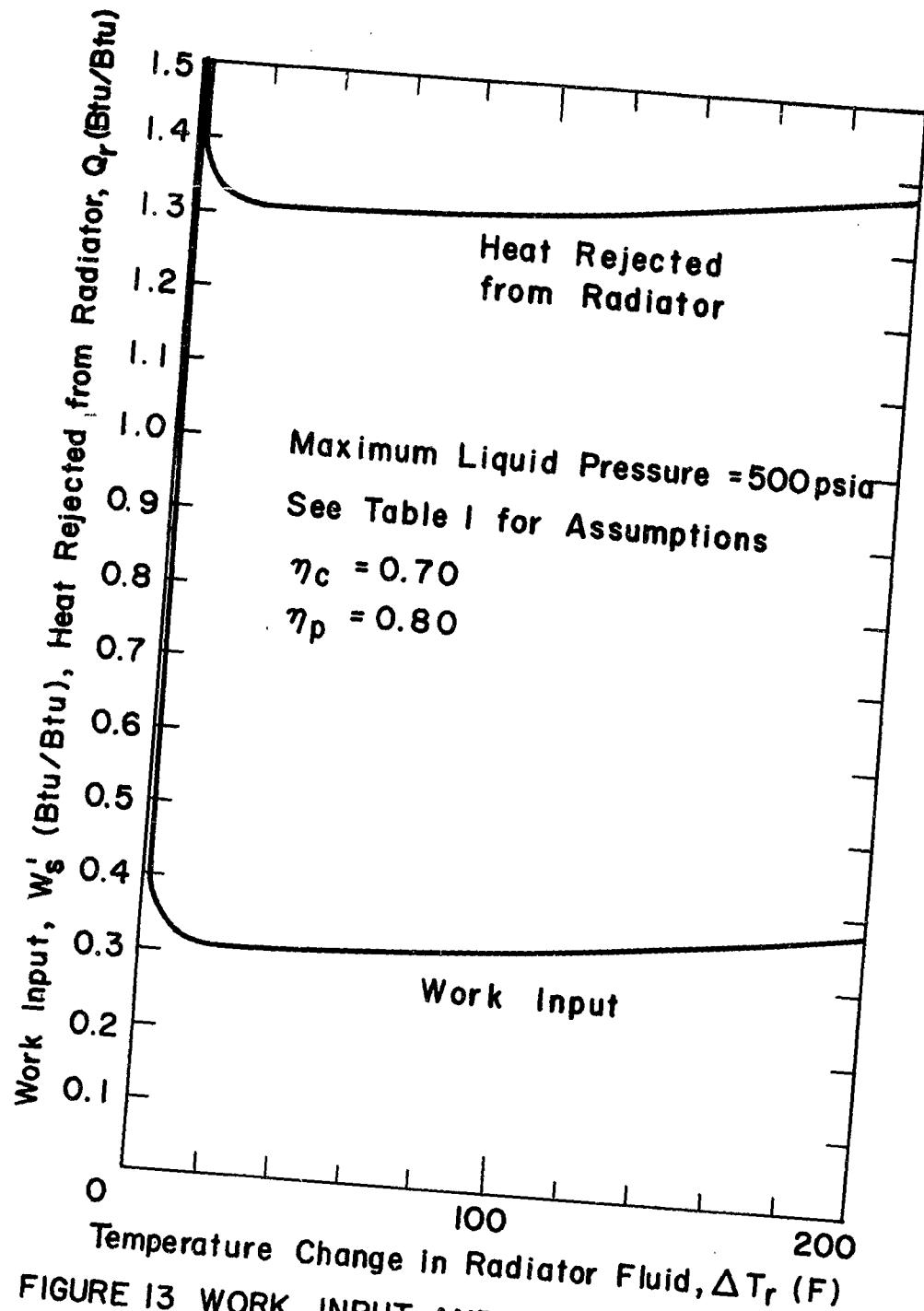


FIGURE 13 WORK INPUT AND HEAT REJECTED FROM RADIATOR FOR CONDENSING-EJECTOR REFRIGERATION SYSTEM PER BTU OF COOLING

CONTAMINATION PATTERN IN THE ENCLOSED
ATMOSPHERES OF MERCURY SPACECRAFT

by

R. A. Saunders

U. S. Naval Research Laboratory
Washington, D. C.

709

ASD-TDR-63-260

CONTAMINATION PATTERN IN THE ENCLOSED
ATMOSPHERES OF MERCURY SPACECRAFT

R. A. SAUNDERS

The problem of determining the identity of contaminants in closed atmospheres is a familiar one to the Navy. The full submergence capability of the Polaris submarine, for example, could not have been realized without the complete control of atmospheric contamination. A determination of the identity and concentration ranges of contaminants in the submarine atmosphere was important in achieving this control. Analytical techniques originally developed at the Naval Research Laboratory for this purpose are also being applied to the detection of contaminants in the atmospheres of Mercury spacecraft.

The low concentration of most atmospheric contaminants presents the first problem in a determination of this type. The contaminants must be concentrated and separated from the large volume of air or other diluent in which they are dispersed. This is accomplished in Mercury spacecraft by means of activated charcoal in the environmental control system, which completely strips the atmosphere of contaminants and serves the double purpose of pilot protection and analytical sampler. The contaminated charcoal is removed from the spacecraft after flight and returned to the laboratory for analysis.

Most of the contaminants adsorbed on the charcoal can be recovered without decomposition by heating the charcoal in a vacuum to a temperature of 300°C and condensing the desorbate in liquid nitrogen traps. The various contaminants are recovered with efficiencies which differ appreciably, however. Normal hydrocarbons, for instance, can be desorbed from charcoal with efficiencies which vary from 100 percent for compounds up to C₆ to less than 1 percent for compounds above C₁₂. Contaminants of high molecular weight and low volatility, which would exist in the

capsule atmosphere as liquid or solid particulate matter, would be strongly adsorbed on the charcoal and not recovered at all by this procedure. The recovery efficiency for high-molecular-weight material can be improved somewhat by an additional process of steam elution, although this method suffers the disadvantage of diluting the desorbed contaminants with a considerable volume of water.

Another problem in this type of analysis results from the complexity of the contaminant mixture desorbed from the charcoal. Mixtures comprising over 200 individual constituents, representing virtually every class of organic chemical, have been recovered from submarine charcoals. This number is not too surprising when one considers the multitude of sources for atmospheric contamination that exist on a submarine. Fortunately, the number of contaminant sources in the space cabin are fewer, and the contaminant mixture recovered from the environmental-control system is considerably less complex. The spacecraft atmosphere usually contains less than a dozen contaminants of measurable concentration, although more than 40 have been observed as a result of a malfunction of cabin electrical equipment. As is the case with the submarine, the space cabin contains contaminants representative of many chemical classes.

The three best instrumental methods of analysis for complicated mixtures are infrared and mass spectroscopy and vapor-phase chromatography. All of these methods are well adapted to the analysis of small quantities of material. The total amount of contaminant mixture recovered from a space cabin is fairly small and, in addition, the concentrations of the individual constituents vary widely. The major constituents of this mixture are identified easily as carbon dioxide and Freon-114 by examining its infrared spectrum. The carbon dioxide, of course, is expired by the astronaut. The bulk of this contaminant is removed from the atmosphere by lithium hydroxide packets which are located in the environmental-control system downstream from the activated charcoal.

The Freon refrigerant is used in the system for suit and cabin temperature conditioning during prelaunch operations. These two components usually constitute over 99¹/₂ percent of the contaminant mixture recovered from the spacecraft. The identities of the minor constituents of the mixture are not so easily established. Both carbon dioxide and Freon are very strong absorbers in the infrared spectral region and together mask out a large portion of the spectrum of the whole mixture, completely obscuring absorption arising from the minor constituents. The low partial pressure of the minor components also precludes the possibility of establishing their identity in the whole mixture by mass-spectral techniques.

Weak peaks attributable to the minor contaminants can be observed in a vapor-phase chromatogram of the whole mixture. Unfortunately, a chromatogram is quite useless as a means of identifying the constituents of a completely unknown and complicated mixture. Too many substances have the same retention time on a chromatographic column for a given set of conditions. The chromatograph is an excellent fractionating device, however, which permits the separation of the major components (Freon and carbon dioxide) from the remaining minor contaminants. It is possible to recover the constituents of a mixture eluted from an appropriate chromatograph, either individually or as mixtures of one of two components. When separated from the presence of interfering compounds, the identity of these single or double components can be readily determined by means of infrared and mass-spectral techniques. The quantity of a particular contaminant recovered can be adequately determined by measuring the area under the appropriate peak of the chromatogram.

The concentration of the minor contaminants in the space cabin is usually low, in the parts-per-million range or less, and hence the amount of material recovered for analysis is small. Fortunately, an analytical gas chromatograph is designed to function best with small

sample quantities. As a matter of fact, too large a sample injected onto a chromatographic column reduces the resolving power of the column. It is desirable, however, to inject as large a sample as practical, which in some cases may be all the sample available, in order to recover enough of each component eluted from the chromatograph to permit spectral identification. Gas sample injections of 50 ml or less (at S.T.P.) are customary. Since the dozen or so minor contaminants combined usually constitute less than 1/2 percent of the whole contaminant mixture, the volume of any one of these contaminants eluted from the chromatograph is small indeed. Recovered volumes of 25 microliters of gas at S.T.P. are typical. Some of these components are sharply resolved and are eluted from the chromatograph in quick succession. The smallness and uniqueness of the original sample demand an efficient high speed and easily operated fraction-collecting device to successfully recover such microquantities of material from the effluent stream of the chromatograph.

The fraction collector used for this purpose was designed around a pair of linear gas-sampling valves, together with a unique collection trap which is illustrated in Fig. 1. The trap consists of a 7-mm diameter glass tube closed at one end with a rubber serum cap and terminated at the other by a 24-gauge hypodermic needle. Two of these traps can be positioned on the fraction collector simultaneously (Fig.2). The serum cap on the end of the trap is slid over one of a pair of hypodermic needles on the fraction collector. These needles terminate the line carrying the eluted material from the chromatograph. By changing the position of one of the linear valves on the fraction collector, the effluent stream from the chromatograph can be directed through either one of the two traps. The eluted component is frozen out on the walls of the collection trap, and the helium carrier gas passes out beneath the surface of the liquid nitrogen coolant through the bottom needle. This design permits the use of liquid nitrogen,

which is the most efficient coolant, but prevents the condensation of atmospheric constituents within the trap. When the elution of a component has been completed, as indicated by the chromatogram recorded simultaneously during the fractionation, the carrier-gas stream can be instantly rerouted to an alternate collection trap to permit collection of the next component. After a trap has been used to collect an eluted component, it is removed from the fraction collector and allowed to remain in liquid nitrogen until ready for subsequent analysis.

Collected components can be spectrally examined in the infrared region as either liquids or gases by employing suitable microcells. A component to be studied in the liquid state is removed from the liquid nitrogen and allowed to melt in the collection trap. It is then transferred through the needle at the bottom of the trap into a variable-space microcell. This cell enables one to obtain a multiplicity of spectra at any desired pathlength with only one cell and one cell-filling operation. Liquid volumes as small as 1/4 of a microliter are sufficient. More volatile samples are studied in the gas phase by inserting the needle on the bottom of the trap through a serum cap on an evacuated multipath microgas cell and expanding the sample into the cell. A sample is transferred to the inlet system of a mass spectrometer in the same manner. Sample transfer from trap to cell or to inlet system is easy and complete.

Sufficient material is eluted under chromatographic peaks only 10 to 15 divisions high at maximum sensitivity to permit good spectra of components exhibiting fairly strong absorption in the infrared spectral region. Contaminants present in the cabin atmosphere at concentrations as low as a few parts per million can be identified easily by this means. Mass spectra can be obtained of components eluted under chromatographic peaks only one division high at maximum sensitivity representing concentrations in the original cabin atmosphere in the parts-per-billion range.

A chromatogram of some of the contaminants recovered during Cdr. Schirra's orbital flight is shown in Fig. 3. This chromatogram was recorded at maximum sensitivity. The compounds responsible for the three weak peaks in the middle were easily identified on the basis of their mass spectra as acetone, cyclohexane, and methyl alcohol. A half or even a fourth of the material eluted under these peaks could have been identified just as easily. Some of the peaks in this chromatogram represent more than one contaminant, each having the same retention time. Toluene and p-dioxane, for example, are both eluted under the last peak. The material eluted under the seventh peak has been identified on the basis of its infrared spectrum as hexamethylcyclotrisiloxane. Silicone oils and greases are used in some of the capsule equipment. Some of these formulations characteristically evolve straight chain and cyclic siloxane compounds of low molecular weight. This is the first time that one has been detected in a space-cabin atmosphere. The presence of formaldehyde together with the cyclic trisiloxane may indicate the actual thermal decomposition of the silicone product. Both of these compounds are eye irritants at sufficient concentration.

The component eluted under the next to last peak of this chromatogram is an interesting one. It was detected in the atmospheres of our first and third manned orbital flights. It was not detected in the atmosphere of Aurora VII, nor has it been detected in any other spacecraft atmosphere. Unhappily, this contaminant has not yet been identified, in spite of the fact that excellent infrared and mass spectra of the compound have been obtained.

The contaminants in the atmosphere of Sigma VII were relatively few in number, as indicated by the simplicity of this chromatogram. For contrast, a chromatogram of the material recovered from a capsule atmosphere in which a gyro malfunction occurred during simulated flight is shown in Fig. 4. A considerable increase in the number of contaminants is apparent. The detection of certain contaminants or an increase in the concentration of these contaminants might be useful as an

indication of certain electrical overload conditions which might not otherwise be apparent. Incidentally, this chromatogram was also recorded at maximum sensitivity. Every component in a mixture as complicated as this, even those eluted under peaks as small as some of these, can be identified by means of the analytical procedures described.

Table 1 lists all the contaminants which have been identified in the various spacecraft atmospheres examined to date. The table also lists the approximate minimum concentrations which would have ensued had all of the recovered contaminant been dispersed in the free volume of the cabin at one time. It should not be inferred, however, that these values necessarily equal actual concentrations. A dash in place of numerical values in the table indicates a lack of quantitative data.

The pattern of contamination has been similar in all of the manned spacecraft which the U.S. has orbited to date. The contaminants marked with an asterisk in Table 1 were common to all of these spacecraft, although their relative concentrations were different. Some of the more pronounced concentration differences were attributable to a minor electrical overload in one flight and the preflight use of an adhesive to install cabin equipment in another.

None of the contaminants listed are normally considered hazardous at the concentrations encountered, although some of the more toxic compounds, such as chlorinated and aromatic hydrocarbons, are certainly undesirable at concentrations only an order of magnitude higher than those reported. Naval divers and aviators have reported a few incidents of adverse physiological effects experienced from breathing an occasional batch of compressed air or oxygen. Surprisingly, analyses of these gases never revealed more than a variety of relatively innocuous hydrocarbons at rather low concentration. Presumably the contamination level in Russian spacecraft is at least as high as that in our own, and perhaps higher. It is not unlikely, therefore, that the space sickness experienced by Russian Cosmonaut Titov might have resulted from a contaminated atmosphere.

Practically all of the contaminants listed were evolved in the outer cabin atmosphere as distinct from the separate atmosphere in the pilot's pressure suit. They originate from such sources as plastics, lubricating compounds, insulations, paints, cements, and residual solvents from degreasing treatments. Most of the aliphatic and olefinic hydrocarbons listed were detected at very low concentrations in one suit atmosphere and probably originated as impurities in a batch of contaminated breathing oxygen. The presence of these compounds in compressed gases stems from the cracking of hydrocarbon compressor oils. The various Freons listed either were used as refrigerants or were present as impurities in those which were. Specific sources for most of the other contaminants can only be surmised at this time.

Table 1

A Compilation of All Contaminants Identified
in the Atmospheres of Mercury Spacecraft

<u>Contaminant</u>	<u>Formula</u>		<u>Concentration (ppm)**</u>
1. Freon-114	$\text{CF}_2\text{Cl}-\text{CF}_2\text{Cl}$	*	60-6000
2. Ethylene dichloride	$\text{CH}_2\text{Cl}-\text{CH}_2\text{Cl}$		0-40
3. Toluene	$\text{C}_6\text{H}_5\text{CH}_3$	*	3-20
4. n-Butyl alcohol	$\text{C}_4\text{H}_9\text{OH}$		0-4
5. Freon-11	CFCl_3		0-3
6. Vinyl chloride	$\text{CH}_2=\text{CHCl}$		0-3
7. Ethyl alcohol	$\text{C}_2\text{H}_5\text{OH}$	*	0-3
8. m-Xylene	$\text{C}_6\text{H}_4(\text{CH}_3)_2$		0-3
9. Vinylidene chloride	$\text{CH}_2=\text{CCl}_2$	*	0-2
10. Methylene chloride	CH_2Cl_2	*	0-2
11. o-Xylene	$\text{C}_6\text{H}_4(\text{CH}_3)_2$		0-1
12. Benzene	C_6H_6	*	0-1
13. Methylchloroform	CH_3CCl_3		0-1
14. Trichloroethylene	$\text{CHCl}=\text{CCl}_2$		0-1
15. Acetone	CH_3COCH_3		0-1
16. Methyl ethyl ketone	$\text{CH}_3\text{COC}_2\text{H}_5$		0-1
17. Methyl isopropyl ketone	$\text{CH}_3\text{COC}_3\text{H}_7$		0-1
18. Ethylene	$\text{CH}_2=\text{CH}_2$		0-1
19. n-Propyl alcohol	$\text{C}_3\text{H}_7\text{OH}$		0-1
20. Acetaldehyde	CH_3CHO		0-1
21. Ethyl acetate	$\text{CH}_3\text{COOC}_2\text{H}_5$		0-1
22. Freon-114, unsym.	CFCl_2CF_3		0-1
23. Methyl alcohol	CH_3OH	*	0-1
24. 1,4-dioxane	$(\text{CH}_2)_4\text{O}_2$	*	0-1
25. Cyclohexane	$(\text{CH}_2)_6$	*	-
26. Formaldehyde	CH_2O		-
27. Hexamethylcyclotrisiloxane	$(\text{CH}_3)_6(\text{SiO})_3$		-
28. Freon-22	CHF_2Cl		-

Table 1 - (Continued)

<u>Contaminant</u>	<u>Formula</u>	<u>Concentration (ppm)**</u>
29. Freon-23	CHF ₃	-
30. Freon-12	CF ₂ CCl ₂	-
31. Freon-125	CF ₃ CF ₂ H	-
32. Hexene-1	C ₆ H ₁₂	-
33. Propylene	C ₃ H ₆	-
34. n-Butane	C ₄ H ₁₀	-
35. Butene-1	C ₄ H ₈	-
36. iso-Pentane	C ₅ H ₁₂	-
37. n-Pentane	C ₅ H ₁₂	-
38. Propane	C ₃ H ₈	-
39. n-Hexane	C ₆ H ₁₄	-
40. 2,2-Dimethylbutane	C ₆ H ₁₄	-
41. trans-Butene-2	C ₄ H ₈	-
42. Cis-Butene-2	C ₄ H ₈	-
43. Ethylene	C ₂ H ₄	-
44. Acetylene	C ₂ H ₂	-
45. 3-Methylpentane	C ₆ H ₁₄	-
46. Carbon dioxide	CO ₂	* -

* These contaminants were common to the atmospheres of the first three U.S. manned orbital flights.

** The values listed represent the approximate minimum concentrations which would have ensued had all of the recovered contaminant been dispersed in the free volume of the cabin at one time. A dash indicates that quantitative values were not determined.

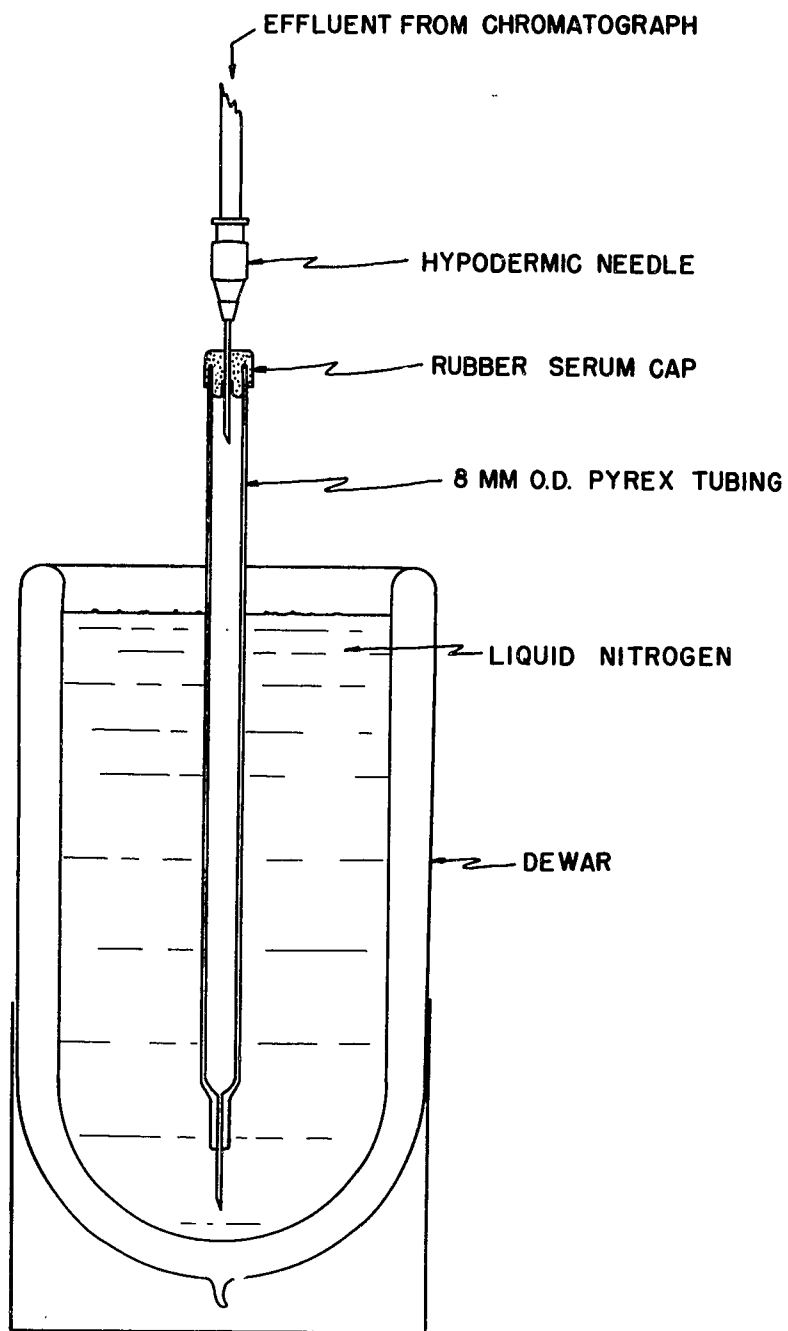


Figure 1. Fraction Collection Trap

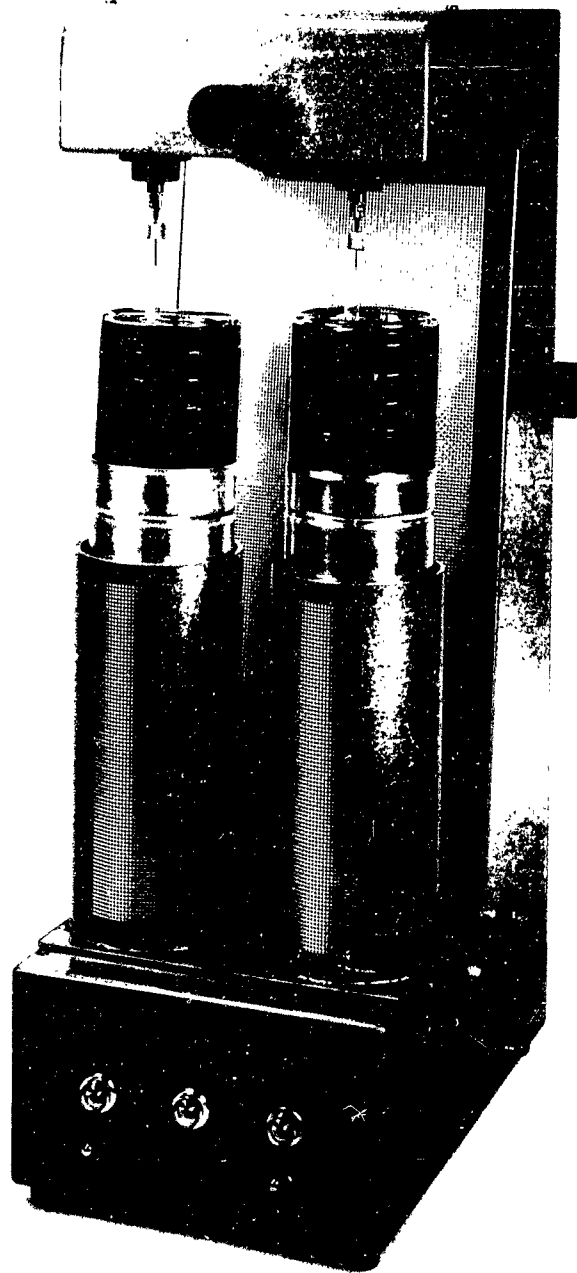


Figure 2. Fraction Collector

Fig. 3 Chromatogram of contaminants
From Sigma VII

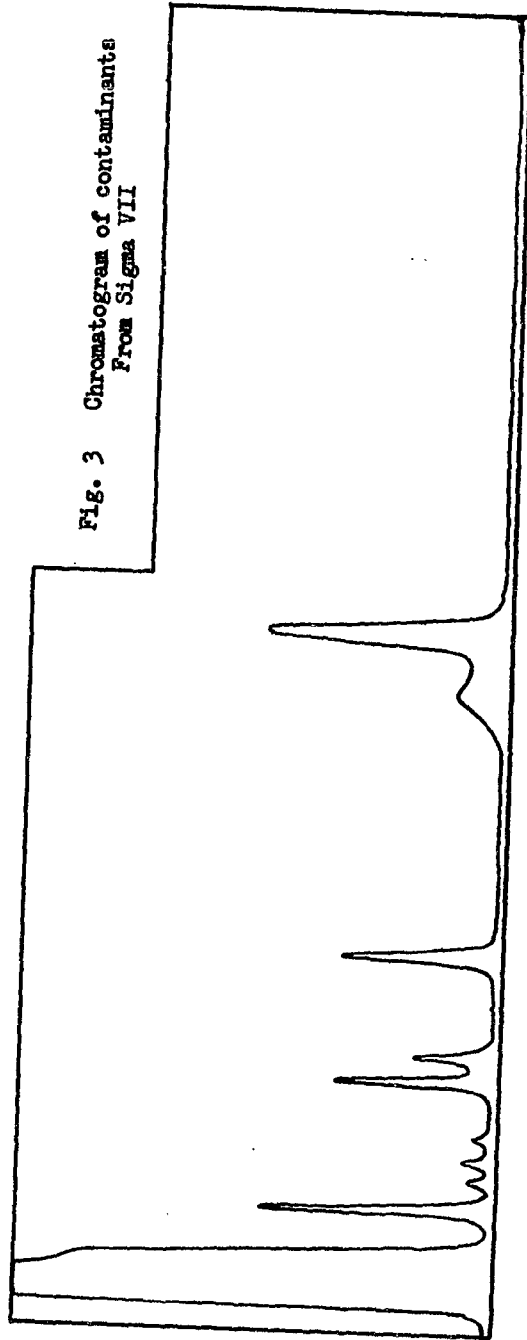
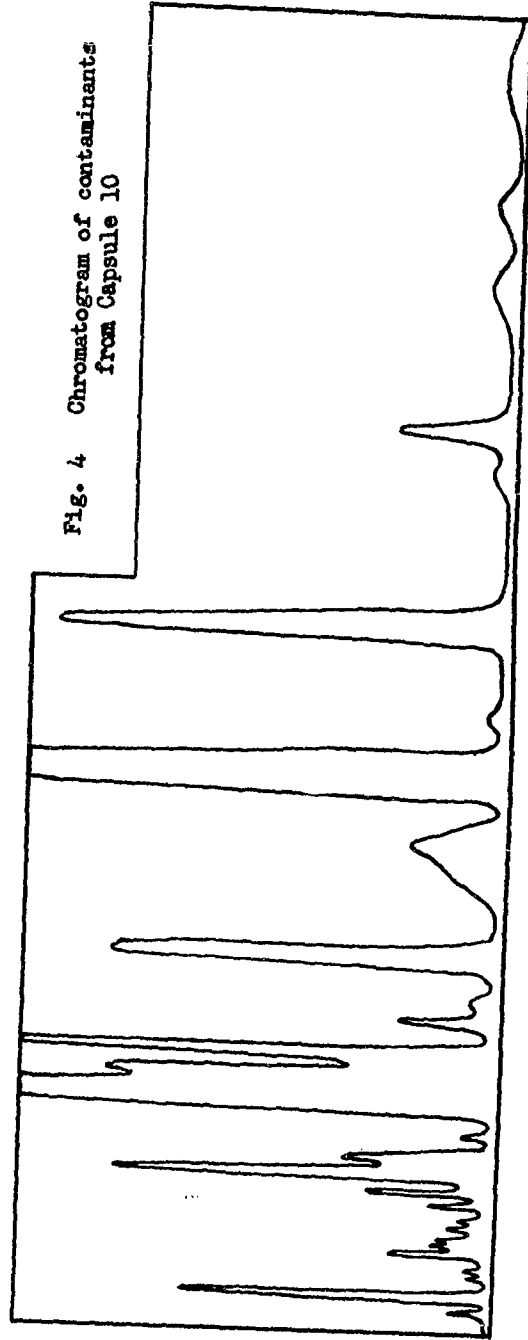


Fig. 4 Chromatogram of contaminants
from Capsule 10



CONCURRENT CATHODIC REDUCTION OF CARBON DIOXIDE AND ANODIC
PRODUCTION OF BREATHING OXYGEN

by

R. E. Shearer

J. C. King

C. A. Palladino

Mine Safety Appliances Research Corp.,
Callery, Pennsylvania

CONCURRENT CATHODIC REDUCTION OF CARBON DIOXIDE AND ANODIC
PRODUCTION OF BREATHING OXYGEN*

by

R. E. Shearer
J. C. King
C. A. Palladino

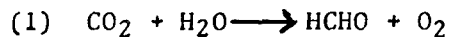
INTRODUCTION

The following is presented as a concept that is believed novel for atmosphere control for space vehicles. Included are results to date in a program sponsored by National Aeronautics and Space Administration to determine feasibility of the concept. Initial phases involved a screening program set up to determine feasibility of approaches from a large number of possible approaches. Promise of feasibility has been obtained from several approaches, which are described; and gathering of quantitative data to enable more complete assessment of feasibility is being initiated at the writing of this paper.

CONCEPT

Cathodic reduction of carbon dioxide has been reported in the literature as yielding formic acid with some formaldehyde in aqueous solution.¹ Cathodic reduction of formic acid to formaldehyde and methanol has also been claimed;² but failure to duplicate these results has also been reported.³

Since cathodic reductions can be coupled with anodic production of oxygen, an investigation was conducted to determine the degree of cathodic reducibility that could be attained with carbon dioxide. If reducibility to equimolar amounts of formaldehyde and methanol could be demonstrated, complete consumption of carbon dioxide and full production of human breathing oxygen would be attainable. This is based on the fact that production of carbon dioxide represents utilization of 82% of the human's oxygen requirement. If oxygen were produced from carbon dioxide mole per mole then, 82% of the oxygen requirement would be produced. This process would be obtained in production of formaldehyde according to the equation:

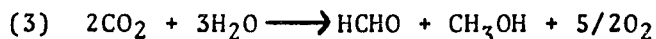


* Contribution of MSA Research Corporation, Callery, Pa. Supported by Crew Systems Division of National Aeronautics and Space Administration, Manned Space Craft Center, Houston, Texas, under Contract NASr70 monitored by D. M. Perry.

Production of 123% of the human oxygen requirement would be obtained from production of methanol according to the equation



The sum of equations 1 and 2 would then be



Thus, cathodic reduction of carbon dioxide to equimolar amounts of formaldehyde and methanol would be an interesting tool for atmosphere control, resulting in production of breathing oxygen in conversion of carbon dioxide to liquid products with consumption of water which could be obtained from recycled urine or from condensate of cabin air.

EXPERIMENTAL

An experimental program was set up to find optimum conditions for reduction of carbon dioxide. Work is still in progress; but variables screened to date include cathode materials, catalysts, electrolyte composition, pressure, temperature, current density, use of diaphragms, use of reduction promoters and modification of a dry amalgam process recently described in the literature.⁴ To date, the modified dry potassium amalgam process has given good yields of formic acid from carbon dioxide as has an H-shaped cell with an aluminum diaphragm a saturated solution of beryllium sulfate as the electrolyte and a mercury cathode with carbon dioxide bubbling through it. No significant yields of products of further reduction, such as formaldehyde or methanol, were obtained; but this may be due to failure to build up formic acid content of the electrolyte; because when more concentrated commercial formic acid solutions were electrolyzed with a beryllium sulfate electrolyte or with a sodium sulfate electrolyte at high current densities, significant yields of formaldehyde with traces of methanol were obtained.

The modified dry amalgam process involves continuous electrochemical formation of the amalgam by electrolyzing solutions of salts of alkali metals with a mercury cathode and continuously reacting the resulting amalgam in an anhydrous area with carbon dioxide. The resulting reduction product, formulated by Miller et al as MCOOM, is hydrolyzed; and the hydrolysis product can then be analyzed. In a continuous operation, the reduction product of the dry amalgam could be hydrolyzed periodically with the electrolyte; and the hydrolysis product could then be exposed to further electrochemical reduction in the electrolyte.

For analysis of reduction products, procedures involving gas chromatography and colorimetry were developed. For formaldehyde, methanol and methylal in water, a 15 foot long 1/4 inch copper column packed with 10% Ethofat 60/25 on 40-60 mesh was developed for use with a column temperature of 120°C, a sample injection temperature of 150°C, and a carrier gas flow rate of 40 cc/min.⁵ The gas phase is analyzed for methane and carbon monoxide in a 6 foot column packed with type 13X Molecular Sieves, which also separate hydrogen, oxygen and nitrogen. Helium carrier gas flow rate is 80 cc/min.

Formic acid is detected in the presence of formaldehyde and methanol by removing the formaldehyde with phenylhydrazine hydrochloride and reducing the remaining formic acid with magnesium. The resulting formaldehyde is detected with Schiff's reagent.

POSSIBLE APPROACHES TO FINAL DEVELOPMENT

Final evaluation of practicality of the proposed process will rest upon assessment of quantitative data on two processes: (1) the use of beryllium sulfate at high current densities at a large area mercury cathode and (2) the combination of dry amalgam reduction followed by electrochemical reduction. Data on material and energy balances would have to be assessed as well as estimates of overall system weight and volume.

Disposal of the products of reduction will have to be studied after these products have been fully characterized. Fractional distillation is one possibility for removal of organics from the electrolyte; while adsorption and liquid-liquid extraction are others. In case of extraction, at least five organic liquids have high enough partition coefficients that they effect separation.⁶ These liquids are listed in Table 1 together with their pertinent properties.

TABLE 1 - LIQUID EXTRACTANTS

	<u>Boiling Point</u> <u>°C</u>	<u>Solubility</u> <u>gm/100 ml H₂O</u>	<u>Partition Coef.</u> <u>K</u>
Benzyl alcohol	205.2	4	3.35
Fusel oil(mixture of amyl alcohols)	--	--	3.23
isoamyl alcohol	130.5	2.672	--
d-amyl alcohol	128	(sl. s.)	--
n-Amyl alcohol	138	2.7	3.15
n-Butyl alcohol	117.7	7.9	3.13
2-ethyl Butyl alcohol	149.5	0.63	3.09

K = $\frac{\text{gm formaldehyde per liter of organic phase}}{\text{gm formaldehyde per liter of water phase}}$

BIBLIOGRAPHY

1. Fischer, F. and Prziza, O. Ber 47 256 (1914).
2. Ellis and McElroy, U. S. Patent 867575 (1907).
3. Baur, Zeit. Elektrochem. 1919 25, 102.
4. Miller, R. M. et al J. Org. Chem. 27 2646 (1962).
5. Bombaugh, K. J. and Bull, W. C. Paper presented at The Pittsburgh Conference, 1962.
6. Johnson, H. G. and Piret, E. L., "Partition Coefficients of Formaldehyde Solution", J. Ind. and Eng. Chem., Vol. 40 p 743-746, (1948).

CHOICE OF AN ATMOSPHERE
FOR AN EXTENDED
SPACE MISSION

by

Robert S. Thomas

Lockheed Missiles and Space Company
Palo Alto, California

ASD-TDR-63-260

Choice of an Atmosphere for an Extended
Space Mission

by

Robert S. Thomas

INTRODUCTION

As the time of extended manned space missions draws closer, it becomes increasingly more important to consider the possible effects of using some atmosphere other than that common to sea level Earth conditions in spacecraft. Many of the advantages of artificial atmospheres are obvious. Some of the advantages and many of the disadvantages, particularly long term physiological effects, are less apparent.

Ideally, the atmosphere selected should: produce minimum physiological stress, minimize the danger of decompression sickness and maximize the time for action after a puncture, minimize fire and meteorite hazards, minimize leakage losses and structure stress, minimize the thermal control problem, and simplify the pressure control system.

Since no known atmosphere simultaneously does more than two or three of the above, trade-offs are necessary. In this paper, the known facts under each of the above are marshalled, limiting ranges are determined, effects on total spacecraft mass noted, and recommendations made.

Minimum Physiological Stress

The ultimate necessity for oxygen is the need of virtually every cell in the body to carry on oxidative metabolism. This need is a function partly of the involuntary housekeeping functions of the body, partly of the level of voluntary muscular activity, and partly of diet.

Assuming normal respiration and normal functioning of the oxygen transport system, the body's need for oxygen can be expressed as a requirement for a certain partial pressure of oxygen in the alveoli, i.e., in that part of the lungs containing gases effectively in equilibrium with the arterial blood.

The theoretical alveolar partial pressure of oxygen ($P_{A_{O_2}}$) is a function, not only of the partial pressure of oxygen in the external environment, but of the total pressure of the external environment (P_b), the respiratory quotient, R, and the alveolar partial pressure of carbon dioxide ($P_{A_{CO_2}}$). The relationship is the following (Ref. 1, p. 804):

$$(1) P_{A_{O_2}} = F_{I_{O_2}} (P_b - P_{A_{H_2O}}) - P_{A_{CO_2}} \left[F_{I_{O_2}} + \frac{(1-F_{I_{O_2}})}{R} \right] \quad (\text{Torr})$$

(all pressures in Torr.)

Where: $F_{I_{O_2}}$ = fractional concentration of oxygen in inspired dry gas $P_{A_{H_2O}}$ = 47 (Torr) = the vapor pressure of water at normal body temperature.

Equation (1) is an approximation based on the assumption that $P_{I_{CO_2}}$ (partial pressure of carbon dioxide in inspired air) is small relative to $P_{A_{CO_2}}$.

R is the volume ratio of carbon dioxide produced to oxygen consumed. For a person neither gaining nor losing weight, the steady state R is a function only of the percent of proteins, fats, and carbohydrates in the diet. Most healthy adults in the United States have a respiration quotient between .80 and .85.

$P_{A_{CO_2}}$ is about 39 Torr for adults at sea level. Equation (1) is frequently used to determine "physiologically equivalent atmospheres" by assuming R is about .82, $P_{A_{CO_2}}$ is about 39 Torr, and plotting P_b vs. $P_{I_{O_2}}$ for some desired

value of $P_{A_{O_2}}$. A family of such curves is plotted in Fig. 1. A similar family of curves assuming $P_{A_{CO_2}}$ is 30 Torr is plotted in Fig. 2. For both curves the vapor pressure of water in the external environment is assumed to be 10 Torr.

A $P_{A_{CO_2}}$ of 30 Torr is typical of an acclimatized person living at an altitude of 15,000 ft. (Ref. 2, p. 357). Values of $P_{A_{CO_2}}$ below 25 Torr have been observed in trained subjects breathing air at 321 Torr (22,000 ft.) for an hour. (Ref. 3, p. 152-53). It is doubtful that one would want to presuppose a $P_{A_{CO_2}}$ of less than 30 Torr for continuous exposure during a space mission.

In the case of a sudden exposure to hypoxic conditions, R rises to values over 1.0 and $P_{A_{CO_2}}$ falls to values as low as 20 depending on the exposure. Both changes are results of hyperventilation (increased rate and/or volume of respiration) and tend to maintain a higher $P_{A_{O_2}}$. After 45 minutes to an hour at reduced pressure, R returns to its steady state value; $P_{A_{O_2}}$ continues to fall slowly for several days. (Ref. 4, pp. 25-26). Fig. 3 (IBID) shows the variation between acclimatized and unacclimatized individuals with $R = .85$. Acute refers to values taken immediately after stabilization of R at the steady state value.

Acclimatization is a complex process involving changes, not only in ventilation rates, but in oxygen dissociation curves, hemoglobin count, pH, and, possibly, basic tissue structure and chemistry. (Ref. 2). While some of these adaptations take place in minutes, others require weeks. It is possible, indeed probable, that some of the adaptations found in those living their entire lives at elevated altitudes are genetically transmitted. If this is true, then a lifetime at altitude would not induce complete adaptation in sea level dwelling races.

It has been shown that 6 weeks of exposure to altitude plus exercise enables a person (1) to be free from hypoxia even while working hard at a PA_{O_2} of 50 Torr and less, (2) to resist decompression sickness much more successfully and, (3) to increase the time of consciousness after a decompression from 2 minutes to 30 minutes at 230 Torr (air) and from 30 sec. to 90 sec. at 140 Torr (air). (Ref. 5, p. 46). These advantages are lost in a few weeks of exposure to low altitudes unless maintained by breathing low oxygen mixtures for at least an hour per day. (Ref. 6, p. 139, Ref. 7, p. 160).

Training in deliberate hyperventilation has also been suggested for space crews (Ref. 15, p. 4), to avoid the symptoms of hypocapnia usually brought about in untrained subjects by emotional stress or physical stress not associated with hypoxia.

Table I (Ref. 8, p. 192) illustrates physiologic limitations associated with several altitudes. Associated alveolar oxygen pressures are shown to facilitate comparisons with non-air atmospheres where applicable. Decompression sickness limits assume prior breathing of air at sea level.

In addition to the basic physiological requirements for an artificial atmosphere already mentioned, there are a number of other important physiological effects consequent to the use of various artificial environments.

A PI_{O_2} in excess of 425 Torr produces definite toxic effects. Nitrogen and some other proposed diluents have a narcotic effect over 4 or 5

Table I.

THRESHOLD ALTITUDES AND PHYSIOLOGIC LIMITS
FOR UNACCLIMATIZED INDIVIDUALS

Altitude	Ambient Pressure (TORR)	*P _A O ₂ (TORR)	Physiologic Limitations
8,000 ft 2.43 km	565 (Air)	65	Max. altitude for prolonged flights without undue fatigue from mild hypoxia
10,000 ft 3.08 km	523 (Air)	57	Max. altitude without supplemental oxygen. The physiologic adjustments mainly respiratory and circulatory, are adequate to compensate for effects of hypoxia. Additional environmental stress or physical exertion may produce decompensation
15,000 ft 4.61 km	427 (Air)	42	The compensatory mechanisms become inadequate, and physical and mental reserves are minimal
20,000 ft 6.16 km	350 (Air)	34	There is mental and physical incapacitation leading to loss of comprehension and posture, convulsions, cessation of respiration and finally cessation of circulation
23,000 ft 7.08 km	308 (Air)		Threshold for occasional symptoms of decompression sickness
25,000 ft 7.69 km	287 (Air)		Threshold for occasional severe manifestations of decompression sickness
30,000 ft 9.22 km	226 (Air)		Critical threshold for high-incidence of decompression sickness
40,000 ft 12.32 km	140 (O ₂)	55	Max. altitude breathing pure O ₂ without additional pressure
45,000 ft 13.85 km	110 (O ₂)		Max. altitude for reasonably prolonged emergency pressure breathing of pure O ₂
50,000 ft 15.38 km	87 (O ₂)		Max. altitude for brief emergency pressure breathing of pure O ₂ with immediate descent
65,000 ft 20.00 km	54		Body fluids boil

*P_AO₂ = Alveolar oxygen partial pressure

atmospheres. Some indications of atelectasis* due to breathing pure oxygen atmospheres are in the literature but this was not noted in the recent School of Aviation Medicine tests (Ref. 10) of pure oxygen at 176 Torr. During those tests, however, drying of the upper respiratory passages, a temporary lowering of vital capacity, considerable ear pressure adjustment, and voice alterations were noted.

Such voice alterations are characteristic of any artificial atmosphere. An idea of the relative magnitude of this effect is shown below (Ref. 11).

ATMOSPHERE (Torr)			RELATIVE PITCH AIR = 1	
	$P_{I_{O_2}}$	P_I Diluent	P_b	
1.	167	593 (N ₂)	760	1.00
2.	198	370 (N ₂)	568	0.98
3.	198	138 (He)	336	1.22
4.	198	370 (He)	568	1.50
5.	258	---	258	0.95
6.	568	---	568	0.95
7.	198	370 (Ne)	568	1.15

The higher thermal conductivities of He and Ne have been said to make people feel "colder" under otherwise similar thermal conditions than mixtures of O₂ and N₂ of comparable pressures. This could be adjusted by variations in wall and gas temperatures, humidity, and ventilation rates. References 12 and 14 discuss basic respiration in some detail. Reference 13 defines the nomenclature of respiration physiology.

* The atelectasis danger might be worse during sleep or in the presence of acceleration stress.

Minimizing the Decompression Sickness Danger

When the ambient air pressure is reduced quickly enough and drastically enough from a higher level at which the body has been equilibrated, gas bubbles form in the bloodstream and in the tissues. The resulting syndrome has been called caison disease, compressed air illness, aeroembolism, dysbarism, and decompression sickness. The various names reflect occupation with various conditions of origin and/or symptoms. Decompression sickness will be used throughout this work. The symptoms include diffuse pain in the extremities and chest, itching of skin, and in severe cases, nausea, paralysis, convulsions, and coma.

Table I illustrated the decompression sickness symptoms usually associated with several altitudes for unacclimatized men breathing air. It should be stressed that this table refers only to relatively sudden exposures to the new altitude after breathing air at sea level. As previously indicated, some modification of this table is achievable through acclimatization. The symptoms can be reduced or eliminated by prebreathing gas of lower nitrogen partial pressure with the same or lower total pressure. Decompression sickness can also be prevented by changing from the higher to the lower pressure gradually by stages, e.g., no symptoms occur if the pressure is reduced from sea level to 47,000 ft. in about 10 hours by continuous and 5 hours by stage decompression. (Ref. 16, p. 184).

Decompression sickness can also be somewhat alleviated by substituting another inert gas for nitrogen, i.e., one which has lower solubility in the tissues and/or a higher diffusion rate. Helium and Neon are such. Argon is somewhat and Xenon and Krpton much worse than Nitrogen with

respect to bubble formation.

Figure 4 shows the time of useful consciousness following sudden decompression to various altitudes (Ref. 6). The times for air and oxygen converge above 15 km to about 15 sec. It is interesting that, for exposure to altitudes above 15 km, even when breathing pure O₂, loss of consciousness is unavoidable if the exposure time before recompression exceeds 5 to 6 sec. (Ref. 8). Recovery is, however, more rapid breathing high oxygen partial pressure mixtures.

Although, as mentioned, a very slow decompression will prevent decompression sickness, Ref. 16 (p. 181) indicates no "significant effect on the incidence of serious symptoms" for rates of ascent varying from 150 to 1200 meters per minute. This corresponds roughly to 10 to 80 Torr per minute. This range of values should be kept in mind when referring to Figures 5 and 6.

Figure 5 (Ref. 17) shows cabin leakage as a function of leakage area for four different atmospheres. For these curves, it is assumed that delivery of gas is sufficient to maintain cabin pressure at the original values. Under such circumstances the mass flows are approximately proportional to the first power of the pressure and the inverse 1/2 power of the molecular weight of the gas. Figure 5 shows that the mass flow for atmospheres of equal mole fractions of oxygen and nitrogen is about 4/3 that of atmospheres of equal mole fractions of oxygen and helium for the same total pressure.

The leakage rates shown in Figure 5 could be extended to normal leakage from the vehicle for holes down to the order of magnitude of the molecular diameter of the gas molecules. At that point, van der Waals forces become

important. If leakage, is, in fact, mostly from molecular diffusion through the walls, leakage will not be a serious problem.

Figure 6 shows the decay of cabin pressure with time for the same 4 atmospheres under the assumption that the gas supply is turned off immediately when the decompression starts. Alternatively, it could be considered to apply after exhaustion of the gas supply.

The horizontal arrows in Figure 6 point to the ambient pressure at which the alveolar oxygen pressure ($P_{A_{O_2}}$) equals about 30 Torr. The vertical arrows point to the ambient pressure at which symptoms of decompression sickness could be expected. Thirty Torr $P_{A_{O_2}}$ is the level at which loss of consciousness is imminent for the "normal unacclimatized man" (Ref. 15). The vertical arrows point to the pressure (for the two gas mixtures) at which about 50% of unacclimatized subjects would have some decompression sickness symptoms. The exact point of onset of these symptoms is subject to considerable variation by age, obesity, physical fitness, and experience and is modified by concurrent exercise and hypoxia. For the pure oxygen atmosphere, decompression sickness would probably occur very little before blood boiling.

Generally, it has been found that decompression sickness symptoms first appear when the ratio of initial pressure to new pressure is about 2.25, regardless of the absolute values of the pressure involved, for air mixtures. Because of the greater mechanical pressure exerted by the higher pressure of the denser bubbles upon the elastic restraining forces of the body and the greater amount of gas absorbed in the tissues, symptoms are, in fact, more severe with diving-type than with flying-type decompressions

of the same pressure ratio. (Ref. 16).

Figure 6 shows that the decompression sickness point comes later than the hypoxia point for all four atmospheres. One could conceive, however, of a mode of temporary emergency action involving the use of an oxygen mask rather than a full pressure suit in which time to reach the minimum ambient pressure for pressure breathing (87 Torr) or to reach the pressure at which body fluids boil (47 Torr) would be significant.

One of the most important considerations for emergency decompressions does not show up in Figure 6; that is, the problem of abruptly donning a full pressure suit and going from cabin pressure to suit pressure. For purposes of reliability, the suit atmosphere will probably be pure O_2 . For purposes of mobility, it will have the lowest possible pressure commensurate with physiological requirements. Assuming suit pressure to be at most 180 Torr, it would be impossible to have the cabin pressure over 400 Torr (if air) without risking decompression sickness upon abrupt change to suit pressure. The cabin pressure could be somewhat greater than 400 Torr if the nitrogen fraction were reduced or eliminated.

Minimizing the Fire and Meteorite Hazards

In addition to affecting the decompression time after a meteorite penetration, there is some interest in the choice of atmosphere with respect to other meteoritic phenomena. If there is combustion of the meteorite, the combustion will tend to be more complete for higher partial pressures of oxygen for a fixed total pressure and for lower total pressures for a fixed partial pressure of oxygen. The higher the total pressure, the

greater the molecular weight and the higher the specific heat of atmospheric gases, the lower will be the temperature rise from a given heat input.

These considerations are marginal. In spite of the fact that at least one experimenter has succeeded in cooking rats in a small enclosure by firing particles into the enclosure at meteorite-like velocities, the total kinetic energy plus energy of combustion of a one gram meteorite (probability of less than 10^{-4} of hitting a 5000 ft^2 cabin in 360 days by Whipple's 1962 distribution) moving at a typical velocity would only raise the temperature of a 1000 ft^3 cabin some 7 degrees C. A smaller cabin and/or the induced burning of other cabin materials could, however, increase the problem.

Further tests need to be made on flammability characteristics of different atmospheres. The problem is complex. Reference 18 reports that helium showed little advantage over nitrogen as a diluent. They reach this judgment on the basis of burning rates. Reference 19 (p. 355) points out, however, that the data from Ref. 18 shows that for 160 Torr O_2 , about 700 Torr N_2 was required to prevent combustion and only 400 Torr He; also for a total pressure of 600 Torr, the maximum allowable P_{O_2} which would avoid combustion was about 104 Torr with N_2 as the diluent and about 218 Torr with He. Theoretical analyses indicate that helium's advantage over nitrogen will, in the absence of natural convection be less for constant volume flow but even greater for constant mass flow.

Reference 18 also points out that spontaneous ignition temperatures tend to be higher with pure oxygen atmospheres than with the same P_{O_2} plus diluent, but that a fire once started in the pure oxygen atmosphere burns more vigorously and at a higher temperature.

Generally, atmospheres with low oxygen content moderate the severity of a fire once it starts and in some cases reduce the likelihood of a fire starting. Atmospheres which conduct heat rapidly away from a "hot spot" reduce the likelihood of a fire starting but aid the spread of a fire more than atmospheres with low thermal conductivity and/or heat capacity. The presence of natural and/or forced convection modifies the problem.

Minimizing Leakage Losses and Structural Stress

Leakage rates are difficult to predict. Very little testing has been done on leakage rates from space cabins exposed to launch vibrations, thermal cycling, vacuum degradation of seals and seal lubricants, and other space stresses for an extended space mission. In the absence of definitive data, a certain conservatism is requisite.

On the basis of experience at LMSC and elsewhere, a reasonable design objective for an interplanetary vehicle of about $5 \times 10^6 \text{ cm}^2$ surface area seems to be about $2.5 \times 10^{-10} \text{ cm}^2$ of effective leakage area per cm^2 of surface area. Actually, the amount of effective leakage area is not a function of surface area alone but a function of the number and types of seals and joints. Applying this factor to an assumed pressurized area of $5 \times 10^6 \text{ cm}^2$ gives a leakage area of $1.25 \times 10^{-3} \text{ cm}^2$. Using this leakage area and the appropriate mass flows from Figure 5, Figure 7 is constructed.

The leakage in Fig. 7 assumes a constant leakage rate. In fact, it is expected that initial leakage rates would be lowest and that leakage rates would increase with time. Predictions of the exact variation of leakage rates with time do not seem possible at present.

It is possible to compute the amount of structure necessary to withstand the pressure differential between cabin and space for various atmospheres. This consideration alone would, of course, urge the selection of the lowest possible cabin pressure. If this consideration were, in fact, the chief one in determining structure weight, it would deserve considerable attention. For applications of this type, however, the resistance of launch and re-entry stresses, elastic deformations, internal mechanical stresses, and meteorite puncture will require a structure greatly in excess of that dictated by the pressure differential alone. When operations upon the surface of Venus (5-10 earth atmospheres) are contemplated, structure mass will indeed be a strong function of internal pressure.

Minimizing the Thermal Control Problem

One of the most important problems in space flight is the elimination of heat generated within the vehicle by crew and equipment. Various methods are possible for conveying the heat from the interior to the outer surface for radiation to space. Most methods rely heavily upon initial removal of heat from crew and equipment by the atmosphere. The pressure and composition of the atmosphere determine the volume and mass flows and the consequent fan power necessary to do the job.

For a given geometry, and constant mass flow, the blower power required is roughly proportional to the inverse square power of the density. Optimization of the geometry and flow rates can sometimes reduce the dependence to the inverse 1.5 or 1.6 power. The approximate variation in power requirements for a typical space vehicle for a fixed geometry is shown in Table 2. Two weight penalties associated with possible predicted power sources, i.e., 23 Kg/Kw for solar-thermionic and 46 Kg/Kw for nuclear A.P.U.'s are shown.

TABLE 2
EFFECT OF ATMOSPHERE ON BLOWER POWER (per man)

<u>Atmosphere</u>	<u>Blower Power (watts)</u>	<u>weight penalty (Kg)</u>	
		<u>23 Kg/Kw</u>	<u>46 Kg/Kw</u>
Sea level air	400	9.2	18.4
180 Torr O ₂ + 180 Torr N ₂	1600	36.8	73.6
180 Torr O ₂ + 180 Torr He	4400	101.2	202.4
180 Torr O ₂	6400	147.2	294.4

The weight differences look insignificant when compared with, e.g., radiation shielding weight, but reducing the power requirements tends to increase the reliability of the system more than saving an equivalent weight in solid metal.

Simplifying the Pressure Control System

It is much easier to control the total pressure inside a spacecraft than to control the partial pressure of one gas in a multi-gas system. This fact alone may be important enough to cause early brief missions to turn to single gas atmospheres.

Progress in the development of partial pressure sensors has been rapid, however, in the last two years. One person working in the field (Ref. 20) predicts a probability of failure of present partial pressure control hardware (partial pressure sensor and associated servomechanisms) of .23 for a one year mission and .41 for a two year mission. The same observer stresses the importance of "...statistically oriented exploratory testing under extremes of single and combined environmental and functional stresses".

Repair capability would, of course, effectively lower the above probabilities of failure. It seems reasonable to expect considerable improvement in partial pressure sensor systems by the late 1960's.

SUMMARY

One of the most important items determining the choice of atmosphere is the necessity of keeping the suit pressure down to promote mobility. The people working in this area seem to believe this will continue to be of great importance for a number of years. Assuming this to be the case, 180 Torr of O_2 is selected as the nominal suit pressure to provide a $P_{A_{O_2}}$ of 100 Torr.

It is further assumed that, to avoid decompression sickness, the primary (cabin) pressure should not exceed 360 Torr if it contains substantial nitrogen. The 180 Torr O_2 + 180 Torr N_2 is finally selected over lower pressures to maximize time for action and minimize fire and explosion hazards, and minimize fan power. Helium is neglected because its known advantages do not seem to outweigh its known disadvantages and its long term physiologic effects are still unknown. If we are ever to operate

under conditions such as those previously mentioned as obtaining on the surface of Venus (5-10 earth atmospheres), helium may well be the only choice. There is abundant evidence of the success of this technique in deep sea diving.

Although a $P_{A_{O_2}}$ of 100 Torr is recommended, a more or less full acclimatization to altitude for the crew is urged to take advantage of reserves thereby built up against hypoxia and decompression sickness. To retain the acclimatization it would be necessary to spend some time each day at lower pressures. The increased trouble and possibly even danger involved in doing this while in flight might out-weigh the advantages, but this should not be assumed summarily.

More experimentation is needed to establish the effect of sudden decompression from an atmosphere such as that recommended for the space cabin of 180 Torr O_2 and 180 Torr N_2 to that recommended for the space suit of 180 Torr O_2 . The two factors generally considered responsible for decompression sickness, the difference in partial pressure of nitrogen between the initial and final atmospheres and the ratio of initial and final total pressures, which determines bubble size, both seem to be well under the values for, e.g., the well documented type of decompression from 160 Torr O_2 plus 600 Torr N_2 to 60 Torr O_2 plus 240 Torr N_2 . Our knowledge of the etiology of this malady is not, however, complete enough to justify complete confidence in such an analogy.

REFERENCES

1. Medical Physiology and Biophysics, ed. T. C. Ruch and J. F. Fulton, W. B. Saunders, 1960, 18th Ed.
2. A. Hurtado and R. T. Clark, Jr., "Parameters of Human Adaptation to Altitude," in Physics and Medicine of the Atmosphere and Space, ed. O. O. Benson, Jr., and H. Strughold, Wiley, New York, 1960.
3. Aeromedical Laboratory, Handbook of Respiration, ed. D. S. Dittmer, R. M. Grebe, WADC TR-58-352, Aug. 1958.
4. H. Rahn and W. O. Fenn, A Graphical Analysis of the Respiratory Gas Exchange, The American Physiological Society, Washington, D.C., 1955.
5. U. T. Slager, Space Medicine, Prentice-Hall, 1962.
6. U. C. Luft, "Altitude Sickness," in Aerospace Medicine, ed. H. G. Armstrong, Williams and Wilkins, 1961.
7. G. F. Gell, "Breathing Oxygen," Op Cit.
8. R. W. Bancroft, "Medical Aspects of Pressurized Equipment," Op. Cit.
9. U. C. Luft, "Physiological Limitations in Cabin Environments and Human Adaptations," in Physics and Medicine of the Upper Atmosphere, ed. C. S. White and O. O. Benson, Univ. of New Mexico Press, 1952.
10. T. E. Morgan et al, "Observations in the SAM Two-Man Space Cabin Simulator, II. Biomedical Aspects," Aerospace Medical Journal, July, 1961, pp. 591-602.
11. R. P. Haviland , "Air for the Space Ship," Journal of Astronautics, V. 3, p. 31, 1956.
12. J. H. Comroe Jr. and R. D. Dripps, American Journal of Physiology, V. 142, pp. 700-707, 1944.
13. J. H. Comroe, Jr. et al, Fed. Proceedings, V. 9, p. 602, 1950.
14. W. O. Fenn, et al, Am. Journal of Physiology, V. 146, p. 637 and ff., 1946.
15. B. Balke, Human Tolerances, Federal Aviation Agency, Civil Aeromedical Research Institute, Oklahoma City, Oklahoma, April, 1962.
16. H. G. Clamann, "Decompression Sickness," in Aerospace Medicine, ed. by H. G. Armstrong, Williams and Wilkins, 1961.

REFERENCES (Cont' d)

17. R. S. Thomas and Y. S. Li, Extended Lunar Operations Feasibility Study, Second Quarter, 1962, TXA 1339/LMSC A051923, 25 June 1962.
18. Klein, H. A., The Effects of Cabin Atmospheres on Combustion of Some Flammable Aircraft Materials, WADC TR 59-456, Aeronautical Systems Division, April, 1960.
19. J. L. Heldenbrand, "Selection of the Closed System Atmosphere," in Cloud Circuit Respiratory Systems Symposium, WADD TR 60-574, Aeronautical Systems Division, August, 1960.
20. Personal Communication from F. Greene, AiResearch, Los Angeles, California.

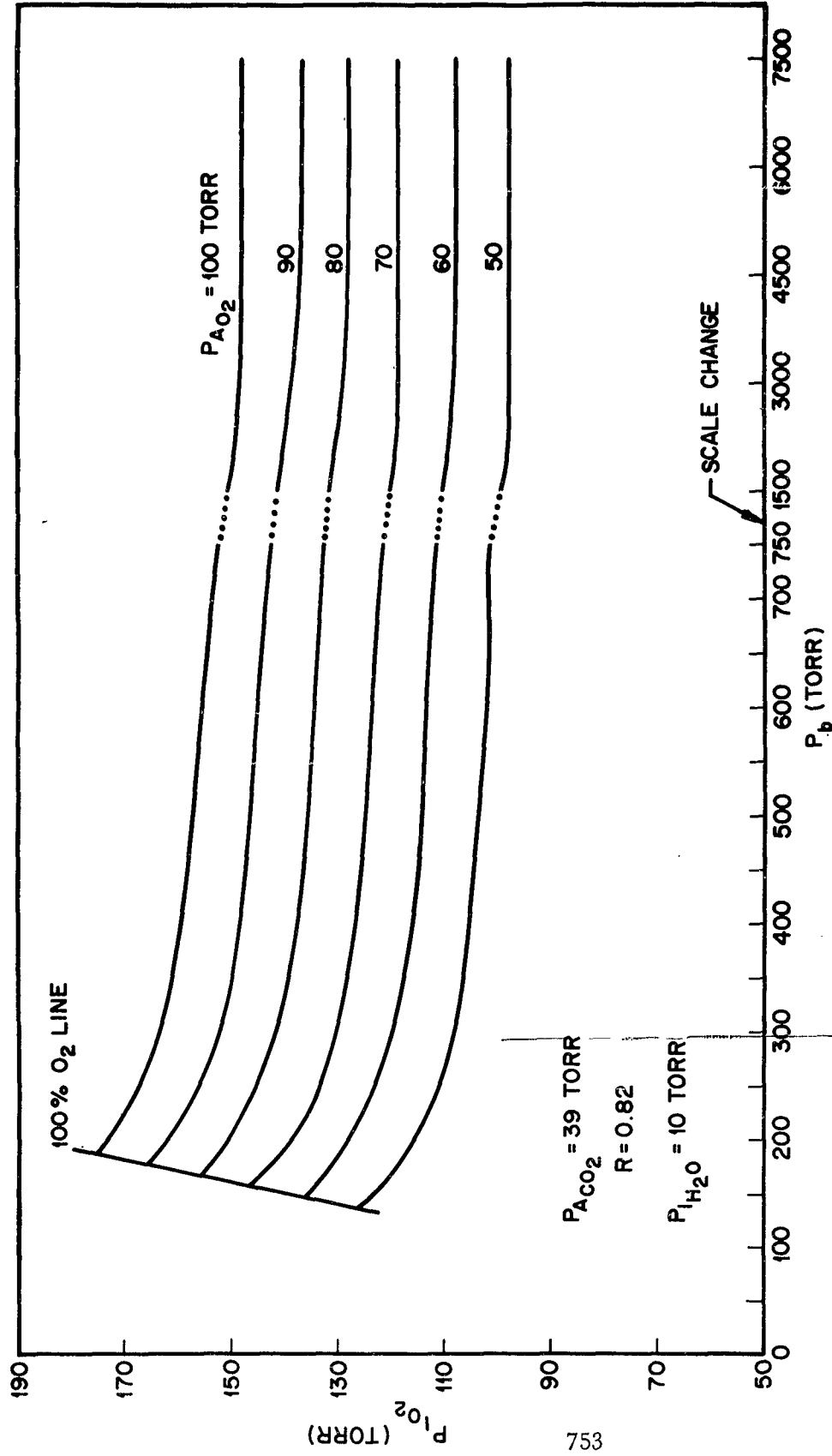


FIGURE 1. PARTIAL PRESSURE OF O₂ AS A FUNCTION OF BAROMETRIC PRESSURE TO PROVIDE
 REQUIRED $P_{A_{O_2}}$ WITH $P_{A_{CO_2}} = 39 \text{ TORR}$

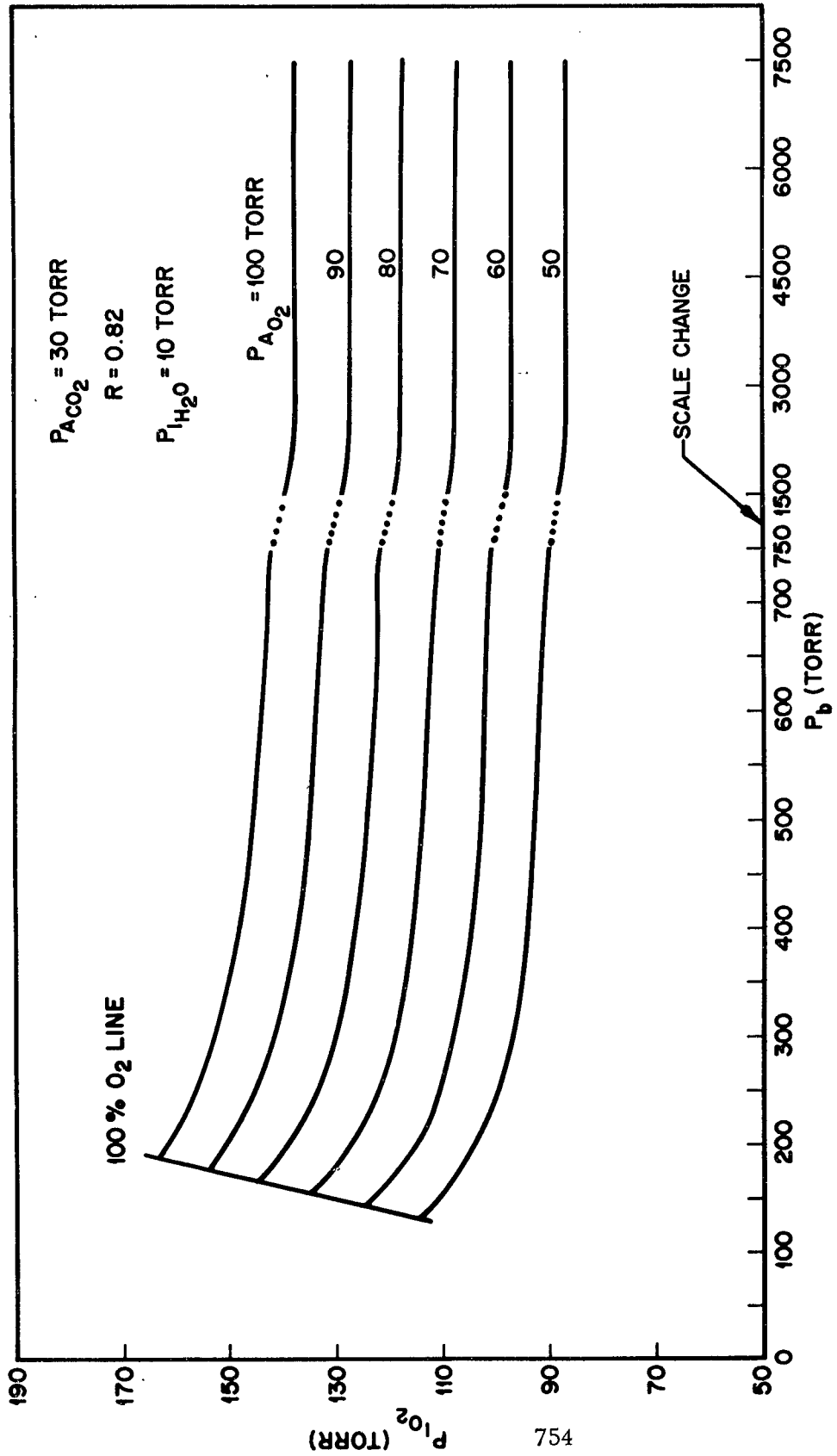
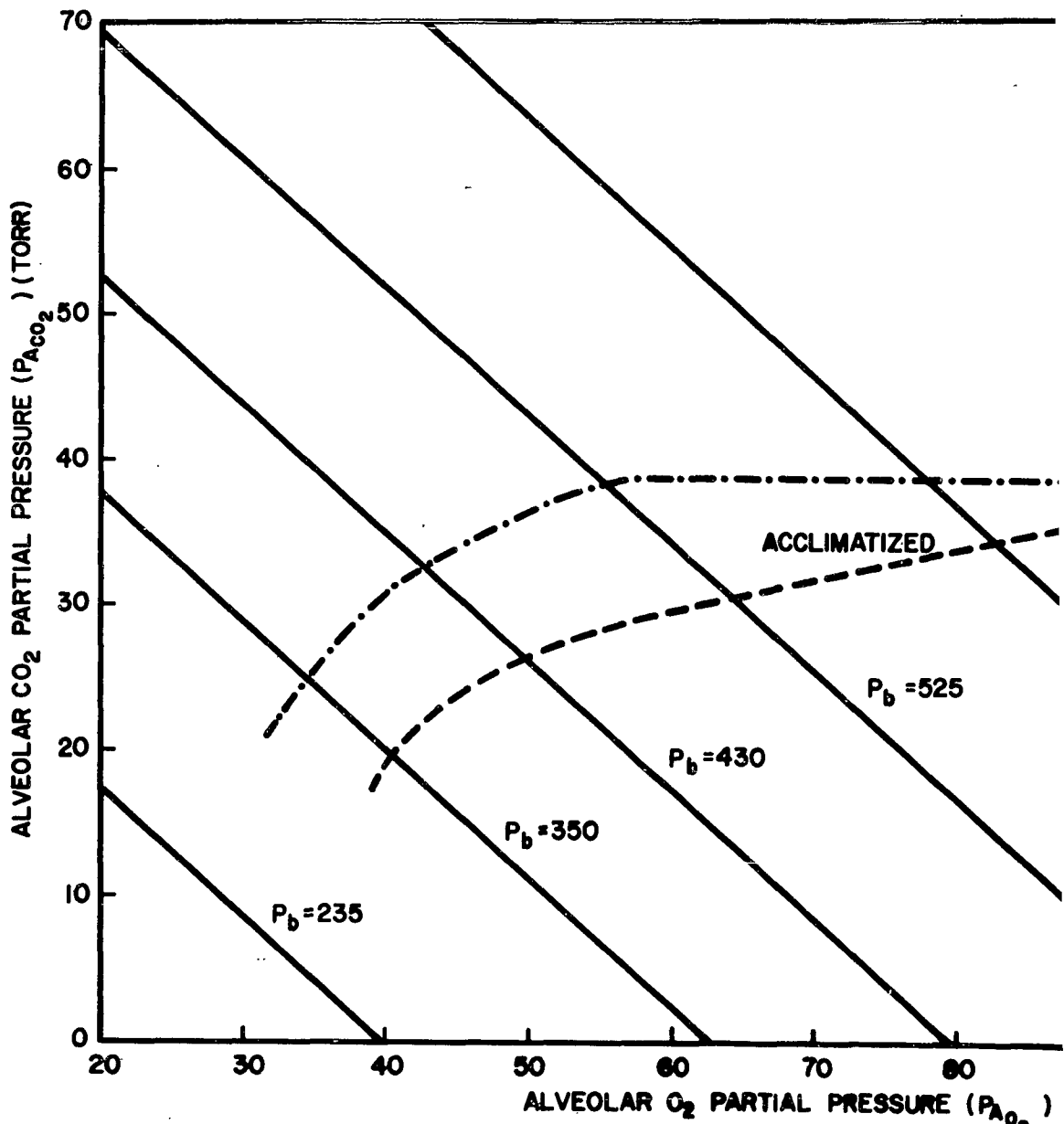


FIGURE 2. PARTIAL PRESSURE OF O₂ AS A FUNCTION OF BAROMETRIC PRESSURE TO PROVIDE
 REQUIRED $P_{A_{O_2}}$ WITH $P_{A_{CO_2}} = 30 \text{ TORR}$



1

FIGURE 3. ALVEOLAR GAS CONCENTRATIONS AT VARIOUS ALTITUDES (AIR PR ACUTE EXPOSURE AND AFTER ACCLIMATIZATION (R = 0.85))

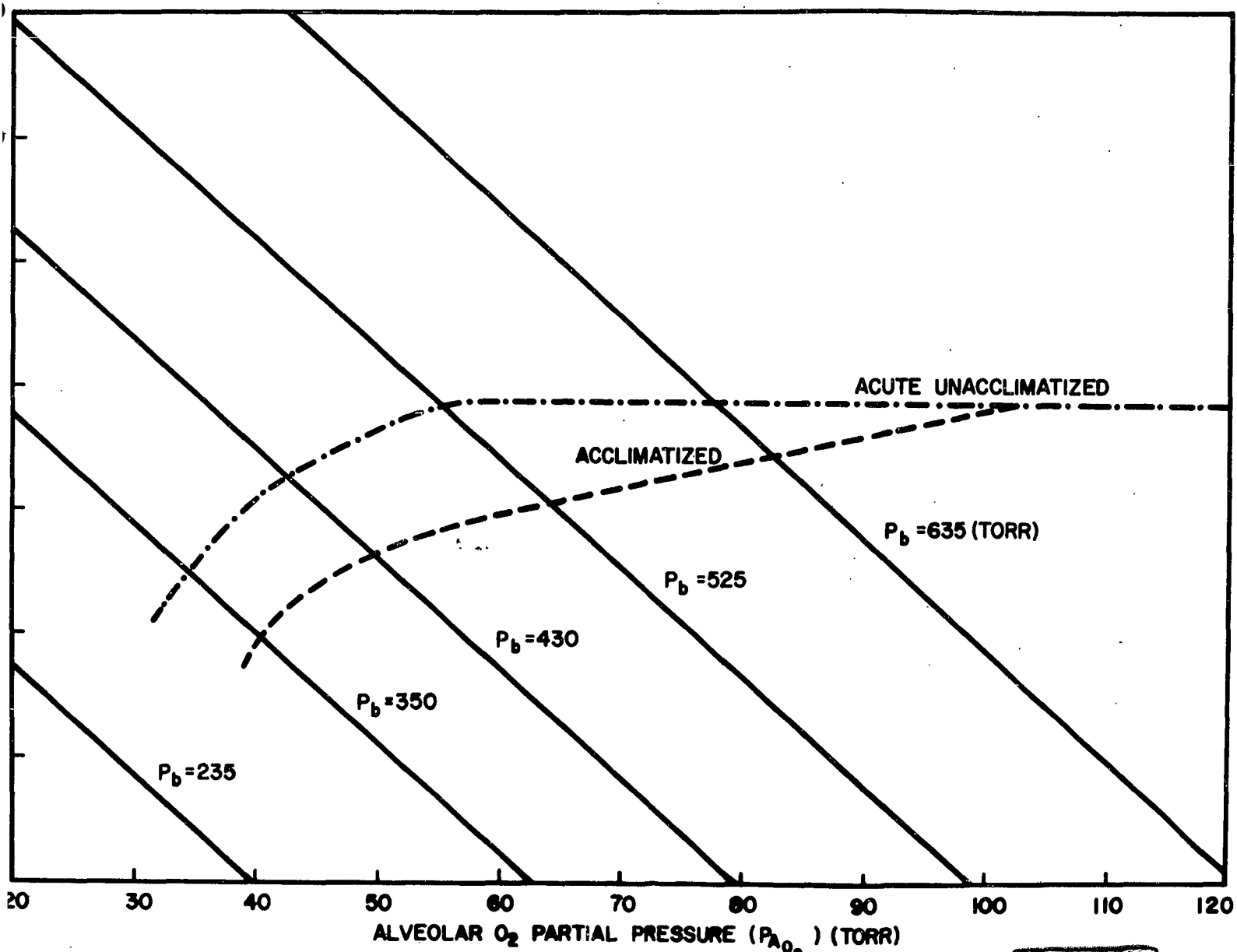


FIGURE 3. ALVEOLAR GAS CONCENTRATIONS AT VARIOUS ALTITUDES (AIR PRESSURES) DURING ACUTE EXPOSURE AND AFTER ACCLIMATIZATION (R = 0.85)

2

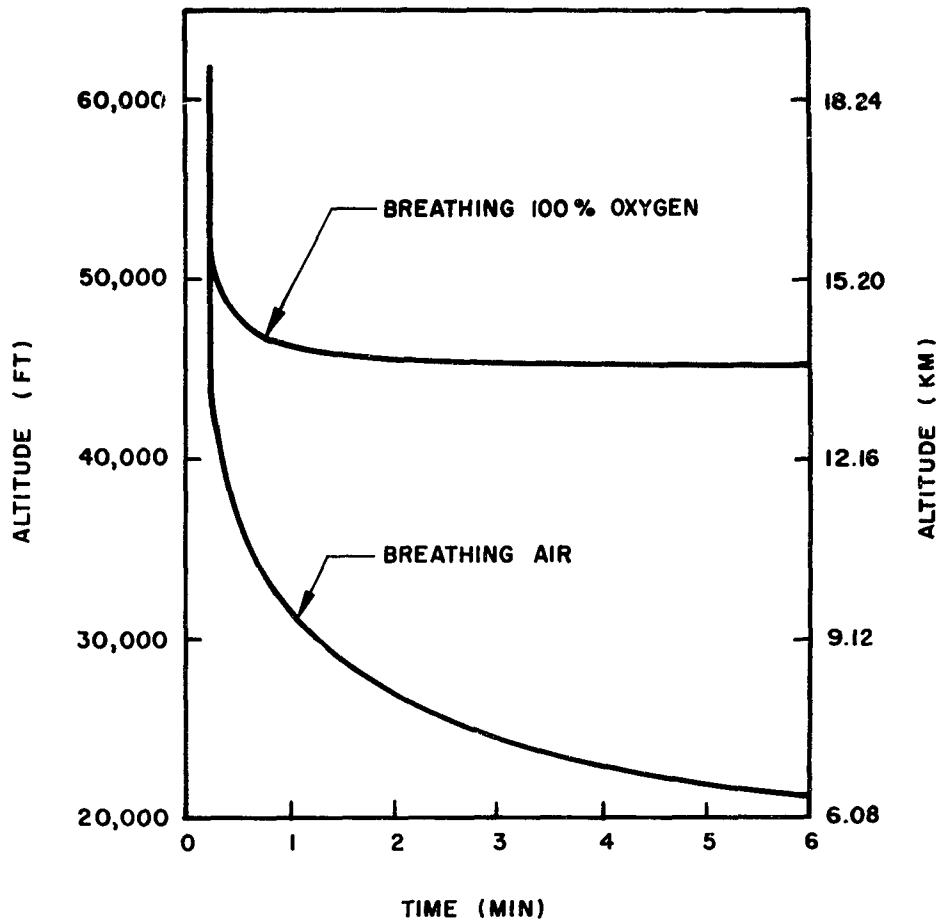


FIGURE 4. TIME OF USEFUL CONSCIOUSNESS AT ALTITUDE AFTER DECOMPRESSION OF PRESSURIZED CABIN FOR AIR (~540 TORR) AND FOR 100% O₂ (200 TORR)

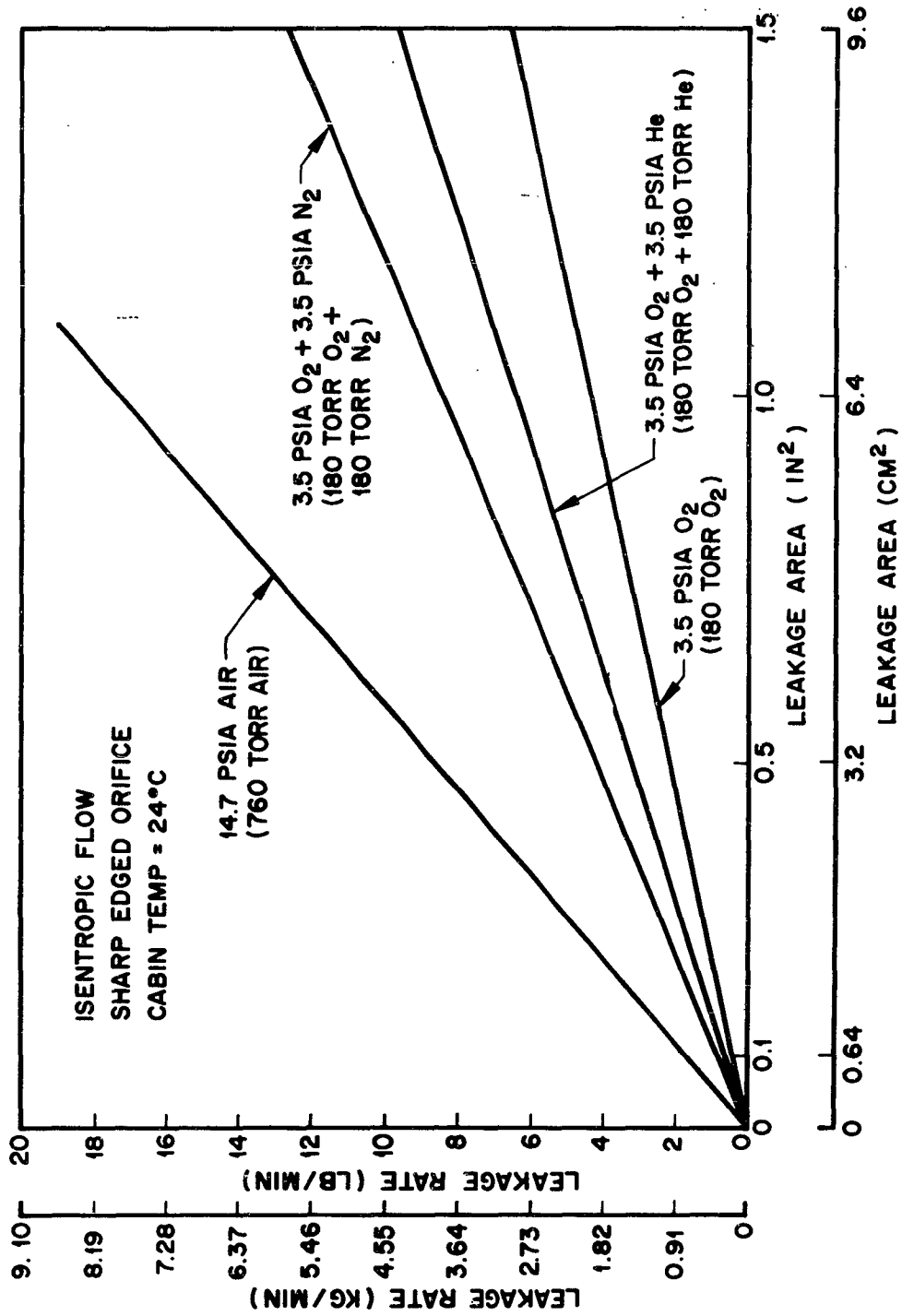


FIGURE 5. CABIN LEAKAGE AT CONSTANT PRESSURE VS LEAKAGE AREA

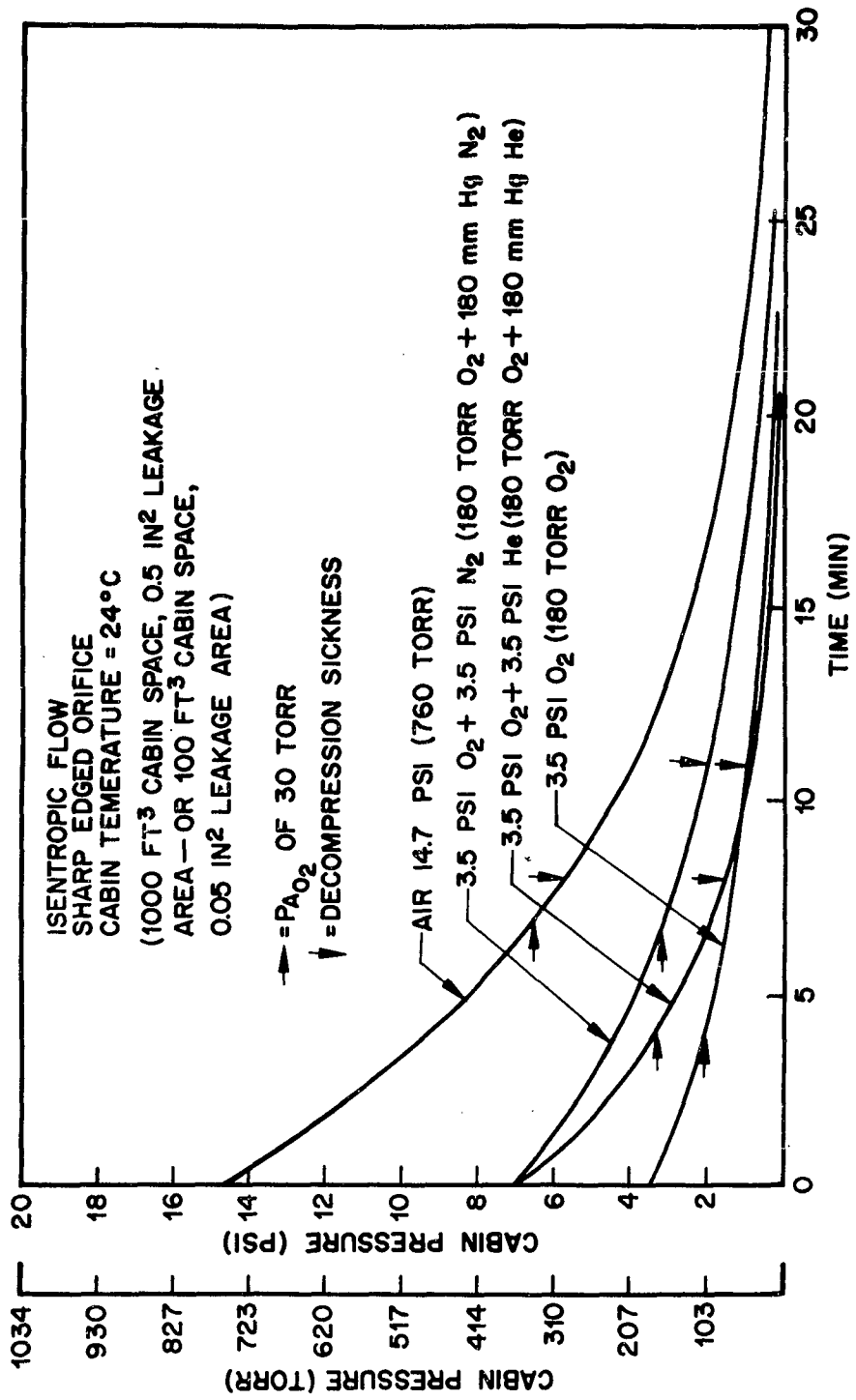


FIGURE 6. CABIN PRESSURE DECAY VS TIME

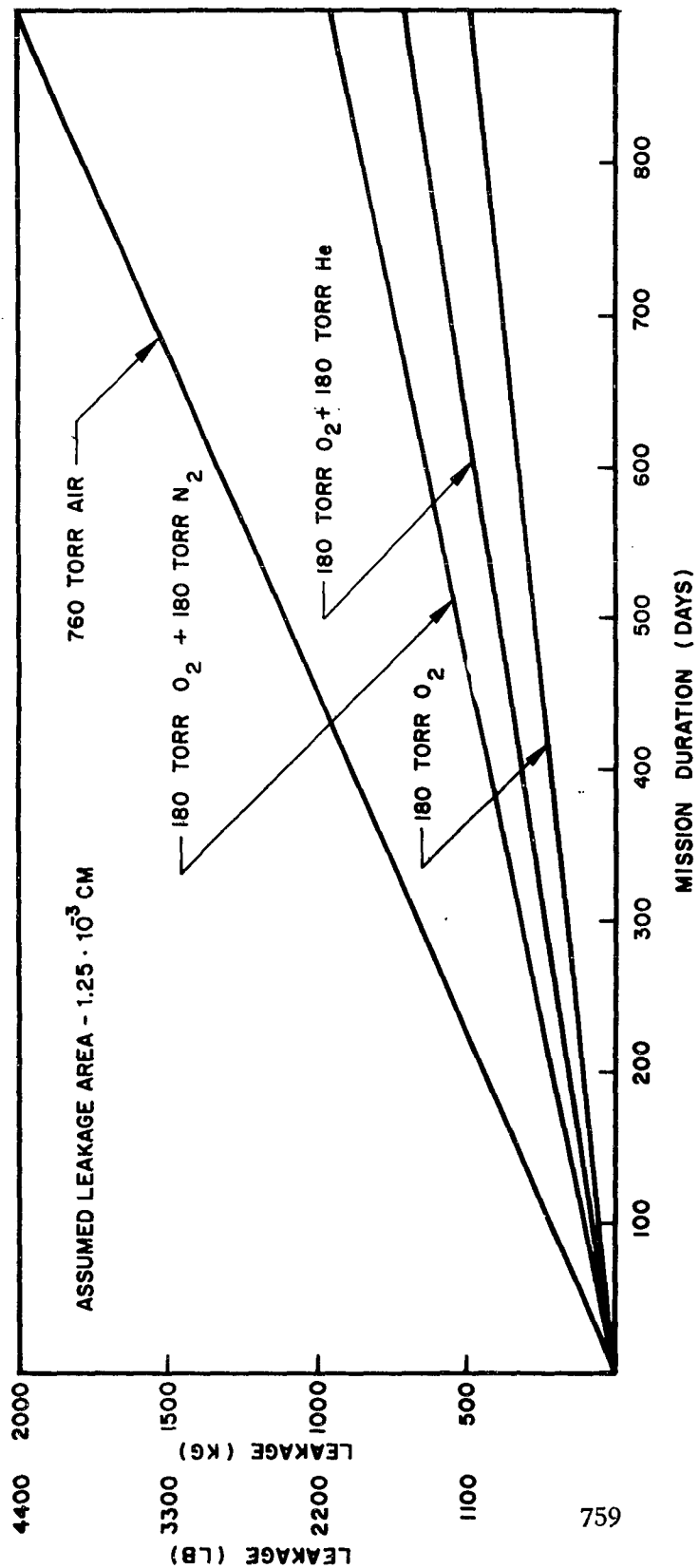


FIGURE 7. TOTAL MISSION LEAKAGE FOR VARIOUS ATMOSPHERES; MASS FLOWS FROM FIG. 5

**THERMAL ENVIRONMENT REQUIREMENTS IN
MANNED SPACECRAFT**

by

J. E. Janssen

**Minneapolis-Honeywell Regulator Company
Hopkins, Minnesota**

761

THERMAL ENVIRONMENT REQUIREMENTS IN MANNED SPACECRAFT

By

J. E. Janssen

INTRODUCTION

The recent orbital flights of project Mercury have emphasized the importance of maintaining the astronaut's environmental temperature within narrow limits. While ground tests indicated the space suit temperature control should be set at mid-range, Schirra found it necessary to adjust the control for maximum cooling in order to maintain a tolerable temperature¹. Environmental temperature control will be even more critical in the case of future flights lasting for several days or weeks. Living in a spacesuit for a week or more imposes a severe strain on the astronaut. In all probability some time will be spent outside the space suit and provision should be made for a "shirt-sleeve" environment in the spacecraft cabin. Space travel imposes severe restrictions on both weight and power consumption. The capacity of any cabin air-conditioning system must, therefore, be very limited. It is desirable that the engineer design the spacecraft cabin to operate as close to the desired environmental temperature as possible without the aid of auxiliary equipment. The question to be investigated here is, "What is the proper design temperature for thermal comfort in a spacecraft cabin?"

Comfort is a measure of the interaction that occurs between a person and his environment. Many environmental variables influence comfort; however, this discussion will be confined to the thermal interaction between a human subject and his environment and the requirements for thermal comfort will be derived.

The human body is essentially a constant-temperature heat engine. In addition to useful work, waste heat is produced by the metabolic process. This heat must be dissipated to the surrounding environment at the same average rate at which it is generated and with a constant deep-body temperature. When these rates are not in balance, the body surface temperature begins to rise or fall. The main internal mechanism for controlling body temperature is evaporative cooling of the skin. As the skin temperature rises or falls, more or less moisture in the form of perspiration is released for evaporative cooling. The body extremities

and surface layers can tolerate a considerable temperature range and their heat capacity helps to damp out the effect of environmental temperature fluctuations. However, if the skin temperature drops low enough, the body is forced to increase its metabolic rate. One way of accomplishing this is by increasing muscular activity through shivering. Psychological forces also induce the subject to modify his environment when possible by putting on or removing clothing.

Excessive adjustment to environmental conditions can be defined as thermal discomfort. Thermal comfort, on the other hand, can be defined as that set of conditions which results in an equivalence between the body heat loss rate and the body heat production rate, with the individual oblivious of the temperature level of his surrounding environment. In order to determine the relative thermal comfort level of different environments, it is necessary to know the relationship among the various factors which influence the balance between the body heat loss and heat production rates.

The heating and ventilating literature contains a great deal of information on the heat production and heat loss rates as a function of environmental conditions for earthbound conditions. Free or natural convection is an important body cooling mechanism under most conditions, but the absence of gravity in a spacecraft eliminates the buoyance force, and free convection does not exist. Radiation and evaporation are left as the main modes of heat transfer. Janssen² derived comfort equations for a "shirt-sleeve" environment with low-velocity forced convection in a spacecraft cabin and found that with air velocities of 10 to 20 ft. per min. the cabin temperature should be from 3 to 6 degrees lower than for the earth surface environment. This means that an environmental temperature specification of $75 \pm 5F$ may not give sufficient latitude. A reasonable estimate of the changes in heat transfer rates to be expected in a spacecraft would permit the environmental temperature to be specified with greater accuracy and reduce the danger of exceeding the available temperature differential. It is the purpose of this paper to inquire further into this problem and consider the case of a rotating space station where artificial

gravity is produced by the centrifugal acceleration. The discussion will be confined to the case of a "shirt-sleeve" environment, i.e. normal clothing with no heating or cooling mechanisms integral with the clothing.

HEAT BALANCE

The various modes of heat transfer to or from the human body can be separated as follows:

$$Q_g = + Q_l \pm Q_k \pm Q_r \pm Q_c \pm Q_{st} \quad (1)$$

Q_g = Heat generation rate

Q_l = Heat transfer by evaporation

Q_k = Heat transfer by conduction

Q_r = Heat transfer by radiation

Q_c = Heat transfer by convection

Q_{st} = Heat storage in surface layers

Heat Storage

Under non-steady-state conditions, the heat capacity of the surface layers of the body and the extremities is quite important, and the value of Q_{st} must be considered. An unbalance in heat production and heat loss rates cannot be maintained for a period of hours, however; and heat storage becomes insignificant for the quasi-steady-state case. Therefore, it will be neglected.

Heat Generation

The heat generation or metabolic rate varies from a low of about 250 btu per hour, when sleeping, to as high as 4800 btu per hour under maximum exertion, as shown in Table I.

Table I. Total Heat Generated by An Average Person with Various Degrees of Physical Activity³

<u>Activity</u>	<u>Heat Generated btu per hr.</u>
Seated at rest	380
"Sedentary"	400
Standing at rest	430
Moderately active worker	600
Walking 2 mph	760
Walking 4 mph	1390
Maximum exertion	3000-4800

The human body is a rather inefficient heat engine, and when the body is doing little or no external work as in the sedentary case, all of the energy released in the metabolic process must ultimately appear as heat. The experimental data available are reported for a sedentary subject of 150 pounds, 5 ft. 8 in. tall, and 19.5 sq. ft. in surface area with a total heat loss of about 400 btu per hour. The activities of subjects in a spacecraft would approximate this condition a large part of the time and it is under this condition that thermal discomfort tends to be most noticeable. Therefore, the heat transfer equations will be derived for the sedentary subject.

Latent-Heat Loss

Latent-heat loss associated with the evaporation of moisture from the skin and lungs can vary from approximately zero for an inactive person in a cool damp environment to over 3000 btu per hour under conditions of maximum exertion in a hot environment. The indications are that for a sedentary individual the body controls the latent-heat loss largely independent of the relative humidity of the environment as long as the relative humidity is below 70-80% and the temperature is in the comfort range⁴. In a report, "Man and His Thermal Environment", W. Bruce⁵ reproduced an ASHVE table showing that in an environment of 79F, the sensible heat loss remained constant at 225 btu per hour for various

activities in which the metabolic rate ranged from 384 to 661 btu per hour. At the same time the latent-heat loss rate varied from 159 to 436 btu per hour.

If it is assumed that the relative humidity is below the critical level, the latent-heat loss term can be moved to the left side of Eq. (1) and this reduces the right side to the sensible heat transfer rate. Information is available relating the sensible heat loss to the environmental temperature.

Heat Conduction

Conductive heat exchange depends on intimate body contact with solid objects and a temperature difference between the body surface and the object. In the case of a standing subject, the conduction area is so small that conduction can be ignored unless extreme conditions and a heat balance on the feet alone are considered. For the case of a subject sitting on a chair and in contact with the back of the chair, the contact area is usually less than two square feet -- less than 10% of the total body surface area. Some conduction heat occurs in this case, but if conduction prevails, convection and radiation cannot occur. The conduction heat transfer rate is probably not too different from the radiation plus convection rates. Therefore, if the chair or solid surface in contact with the body is at about the same temperature as the surrounding environment, the assumption of heat transfer by radiation and convection from body areas which are actually conduction areas is probably not grossly in error, and the conduction term in Eq. (1) can be neglected.

THERMAL COMFORT EQUATION

With the simplifications discussed above, Eq. (1) can be reduced to the sensible heat loss from the body.

$$Q_s = \pm Q_r \pm Q_c \quad (2)$$

The American Society of Heating, Refrigerating and Air Conditioning Engineers⁶ and the John B. Pierce Laboratory⁷ have published considerable data on the sensible heat loss from sedentary subjects as a function of

environmental conditions. This data was used to determine the constants for a sensible heat loss equation in an earlier paper².

$$Q_s = 2.52 [(T_b/100)^4 - (T_{mrt}/100)^4] + 5.25 (T_b - T_a)^{1.25} \quad (3)$$

Q_s = Sensible heat loss, btu per hr.

T_b = Mean clothing and exposed skin temperature, degrees Rankine

T_{mrt} = Mean radiant temperature, degrees Rankine

T_a = Air dry-bulb temperature, degrees Rankine

Using the sensible heat loss data from which Eq. (3) was derived and Eq. (3), body surface temperature was calculated as a function of environmental temperature ($T_a = T_{mrt}$)* and compared to the body surface temperature measurements of several investigators as shown in Fig. 1.

It appears then that Eq. (3) is reasonably valid for an earth surface environment. In order to apply it to spacecraft it is necessary to examine the influence of gravity. Radiation will be unaffected by gravity, but free convection is directly dependent on gravitational acceleration.

*The term "environmental temperature" will be restricted to the case where the dry-bulb and mean radiant temperature are equal. Mean radiant temperature (T_{mrt} or mrt) is that uniform surface temperature of a black-body enclosure which would result in the same net radiation heat exchange as the body experiences in the actual environment.

Free Convection

The average laminar, free-convection, heat transfer coefficient for a vertical plate with uniform wall temperature is given by⁸:

$$\bar{h} = \frac{k}{L} \frac{0.638 (\text{Pr})^{.5}}{(0.861 + \text{Pr})^{.25}} [\text{Gr}]^{.25} \quad (4)$$

- h = Heat transfer coefficient
- k = Thermal conductivity of air
- L = Characteristic vertical dimension
- Pr = Prandtl number for air

The Grashoff number, Gr, is defined as

$$\text{Gr} = \frac{g \beta (T_b - T_a) L^3}{\nu^2} \quad (5)$$

- g = Local gravitational acceleration
- β = Expansion coefficient = $\frac{1}{T}$ for perfect gas
- ν = Kinematic viscosity

The Grashoff number is the only term in Eq. (4) which is influenced by changes in the gravitational constant. Heat transfer by convection is given by:

$$Q_c = h A_c (T_b - T_a) \quad (6)$$

- A_c = Surface area of the body

Introducing Eqs. (4) and (5) into Eq. (6) and equating this to the convection term in Eq. (3) gives:

$$5.25 (T_b - T_a)^{1.25} = A_c \frac{0.638 (\text{Pr})^{.5}}{(0.861 + \text{Pr})^{.25}} \left[\frac{g \beta}{L \nu^2} \right]^{.25} (T_b - T_a)^{1.25} \quad (7)$$

Therefore:

$$A_c \frac{0.638 (\text{Pr})^{.5}}{(0.861 + \text{Pr})^{.25}} \left[\frac{\beta}{L \nu^2} \right]^{.25} = \frac{5.25}{(g)^{.25}} = 2.21 \quad (8)$$

The convection term can then be written as:

$$Q_c = 2.21(g)^{.25} (T_b - T_a)^{1.25} \quad (9)$$

And Eq. (3) becomes

$$Q_s = 2.52 \left[\left(\frac{T_b}{100} \right)^4 - \left(\frac{T_{mrt}}{100} \right)^4 \right] + 2.21(g)^{.25} (T_b - T_a)^{1.25} \quad (10)$$

g = Local gravitational acceleration, ft. per sec²

In the earlier work², equations were derived for low velocity forced convection. For an atmosphere of air at 14.7 psia, the forced convection term was given by:

$$Q_c = 1.55 v^{0.466} (T_b - T_a) \quad (11)$$

Eq. (11) has been compared with Eq. (9) in Fig. 2 to determine which mechanism gives the largest heat loss and therefore predominates. It is seen that in most cases free convection leads to the greatest convection cooling rate. Hill and Schnitzer⁹ have shown that the rotational acceleration "comfort zone" for a rotating space station extends from 0.035g to 1g depending on the rotational radius of the craft. For space craft with a radius of 50 ft., rotational comfort is limited to 0.25g. Increasing the radius to 75 ft. widens the comfort zone from 0.17 to 0.4g.

Because of the power and fans required to circulate air and the possibility of creating undesirable drafts, it probably would not be practical to use design air velocities in excess of 30 ft. per min. Free convection provides more cooling than 20 ft. per min. forced convection and almost as much as 30 ft. per min. at an acceleration of 0.25g. It appears then that an assumption of free convection with a gravitational acceleration of 0.25g would be adequate for rotating space stations. Introducing this value into Eq. (10) gives a thermal comfort equation for rotating space stations under 0.25g conditions.

$$Q_s = 2.52 \left[\left(\frac{T_b}{100} \right)^4 + \left(\frac{T_{mrt}}{100} \right)^4 \right] + 3.72 (T_b - T_a)^{1.25} \quad (12)$$

DISCUSSION

Eqs. (3), (11) and (12) have been plotted in Fig. 3. This chart provides a means for separating the influence of the dry-bulb air temperature from the mean radiant temperature and intercomparing the effect of convective heat transfer under the various conditions. For example, if it is assumed that an environmental temperature of 75F (mean radiant = dry bulb = 75F) is desirable for an earth surface environment, the mean body surface temperature (clothing plus exposed skin) would be about 85.5F. An equivalent environmental temperature for a rotating space station (0.25g) is found by determining the point where the 85.5F body surface temperature curve at 0.25g crosses the line of $T_a = T_{mrt}$. This occurs at about 73.6F. The equivalent of a 75F earth surface environment for the case of a spacecraft under weightless conditions with forced convection at 20 ft. per min. is found to be 73.3F.

A body surface temperature of 85.5F is rather high and would be valid for light clothing. A business suit, for example, usually results in a surface temperature of about 82F which occurs in a normal environment at about 70F. The equivalent environmental temperature for the 0.25g case

would be 68.3F and for the 20 ft. per min. forced convection case at 67.7F. Under zero g conditions with no forced convection the mrt would have to be lowered to 61.8F to achieve the same conditions as a 70F earth surface environmental temperature.

Spacecraft exposed to intense solar radiation on one side and the infinite heat sink of space on the other side would develop appreciable temperature gradients. The magnitude of the gradient would depend on the nature of insulation in the walls and any means present for pumping heat from the hot to the cold side. Comfort surveys in typical homes with a two-sphere radiometer¹⁴ have shown mean radiant temperatures as much as 10° below air temperature close to picture windows on winter days. Mean radiant temperatures as much as 10° above air temperature have been measured in an air conditioned room in summer. Insulation in the walls of a spacecraft will tend to reduce temperature gradients in the cabin but will tend to raise the temperature level. On the other hand, reduction of insulation will lower the temperature level but will increase the temperature gradient. Reduction or complete loss of the gravitational force will tend to increase the possible difference between the dry-bulb and mean radiant temperatures. Some difference between the dry-bulb and mean radiant temperatures can be expected and the mrt will be more effective than dry-bulb in determining the comfort level. At 1g the slope of the curves in Fig. 3 is about 1.25 indicating that the mean radiant temperature is 25% more effective than air temperature in controlling comfort. At 0.25g the mean radiant is 60% more effective than the dry bulb, and under weightless conditions with 20 ft. per min. velocity, the mrt is 140% more effective than dry-bulb. Under weightless conditions with no forced convection the constant comfort lines of Fig. 3 would be horizontal and would pass through the common points on the line of $T_a = T_b$. Thermal comfort would then be independent of dry-bulb temperature so long as the subject were motionless.

This offers an interesting possibility for controlling the comfort level. If the walls of the spacecraft cabin are painted (have an infrared emittance of about 0.9), window shades of aluminum foil can be used to

achieve thermal radiation shielding from the hot or the cold side and thus lower or raise the effective mean radiant temperature.

Atmospheres other than air at 14.7 psia have been considered for spacecraft. For the case of pure oxygen at 5 psia the convection constants in Eqs. (3) and (12) are reduced from 5.25 and 3.72 to 3.05 and 2.16 respectively. The constant for the forced convection case, Eq. (11), was found to be reduced from 1.55 to 0.932^2 . This would have the effect of reducing the desired environmental temperature even more than for the cases presented in Fig. 3. It also offers an interesting opportunity for simulation of low-gravity conditions in the laboratory. An oxygen rich atmosphere at a reduced pressure can be selected which will give the same convection constant as atmospheric air at normal pressure but at a reduced gravity. Such a laboratory environment should yield the same comfort conditions as atmospheric air in a spacecraft.

CONCLUSIONS

From this estimate of thermal comfort in spacecraft, several conclusions can be drawn.

1. In general, the environmental temperature in a spacecraft cabin should be somewhat lower than a comparable environment on earth. Artificial gravity produced by rotation would be quite effective in maintaining convective heat transfer.
2. The mean radiant temperature is more effective than air temperature in determining thermal comfort in a "shirt sleeve" environment.
3. An oxygen-rich atmosphere at reduced pressure can be used to simulate the effect of a reduced gravitational force on thermal comfort.

REFERENCES

1. "Missiles and Rockets", October 15, 1962, p. 14.
2. "Thermal Comfort in Space Vehicles", by J. E. Janssen, ASME Paper 59A207.
3. "Air Conditioning and Refrigeration", 2nd ed., by Jennings and Lewis, International Textbook Co., p. 71
4. "Environmental Research Program", by B. H. Jennings, ASHRAE Journal, November 1960.
5. "Man and His Thermal Environment", by W. Bruce, National Research Council of Canada, Division of Build Research Report, 1953.
6. "ASHAE Guide 1955", p. 116
7. "Recent Advances in Physiological Knowledge and Their Bearing on Ventilation Practice", by Winslow, et al., ASHVE Trans., V. 45, 1939, p. 111
8. Heat, Mass and Momentum Transfer, by Rohsenow and Choi, Prentice Hall, 1961
9. "A Report on the Research and Technological Problems of Manned Rotating Spacecraft", NASA TND-1504 Aug. 1962, p. 1
10. "A Method for Improving the Effective Temperature Index", by C. P. Yaglou, Heating Piping and Air Conditioning, Sept. 1947, p. 131
11. "Temperature and Human Life", by Winslow and Herrington, Princeton Univ. Press, 1949.
12. "Differences Between Men and Women in Their Response to Heat and Cold", by J. D. Hardy and E. F. DuBois, Proc. Nat. Acad. of Sci., Vol. 26, 1940, p. 389.
13. "Full-Scale Human-Body-Model Thermal Exchange Compared with Equational Condensations of Human Calorimetric Data", by L. P. Herrington, ASME, Paper No. 58-A-181.
14. "Two-Sphere Radiometer", by D. J. Sutton and P. E. McNall, Jr., Heating, Piping and Air Conditioning, Vol. 26, No. 3, March 1954, p. 157.

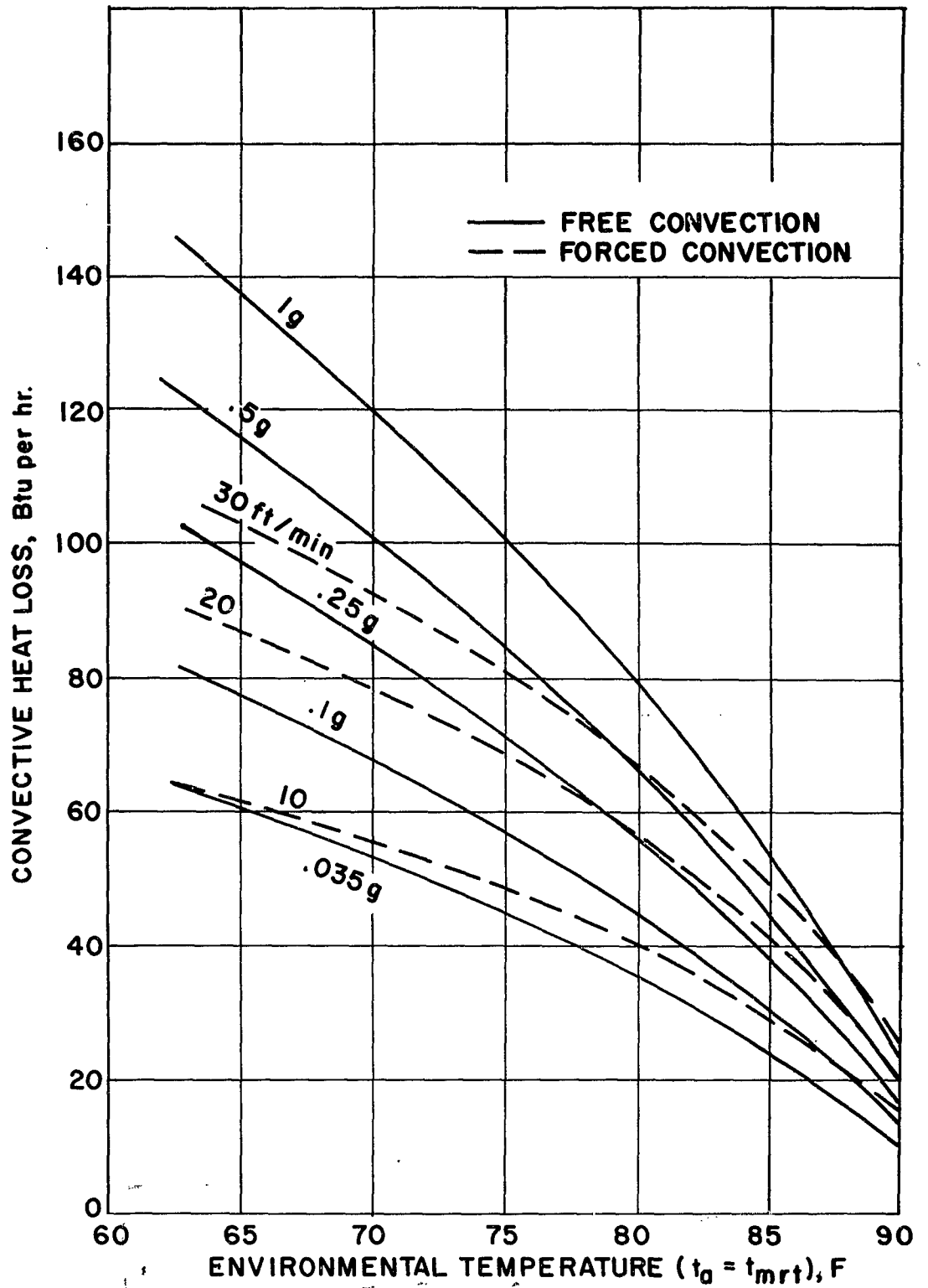


FIG. 2 - CONVECTION HEAT LOSS FROM THE HUMAN BODY

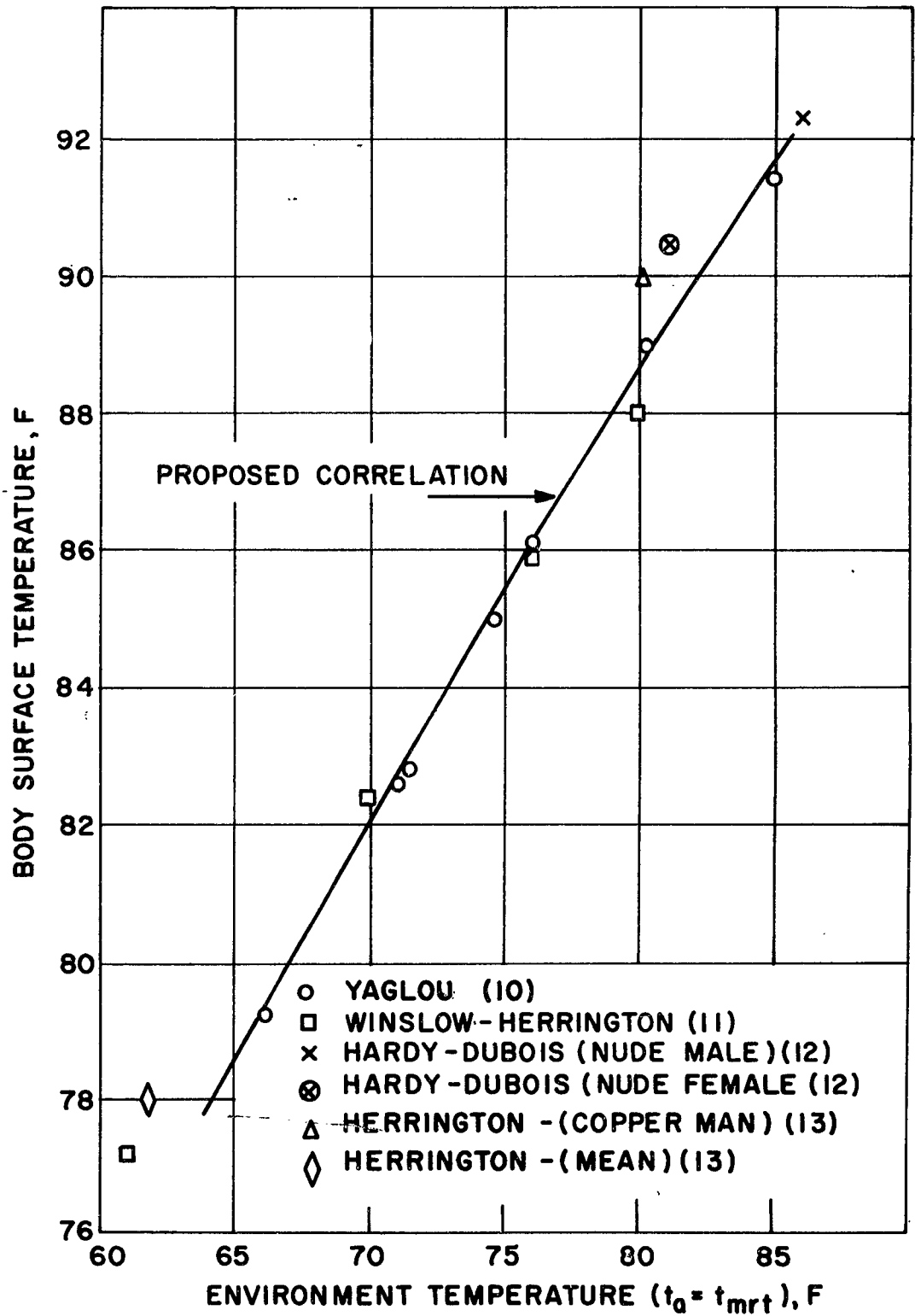


FIG. I-COMPARISON OF PROPOSED CORRELATION WITH OTHER PUBLISHED DATA

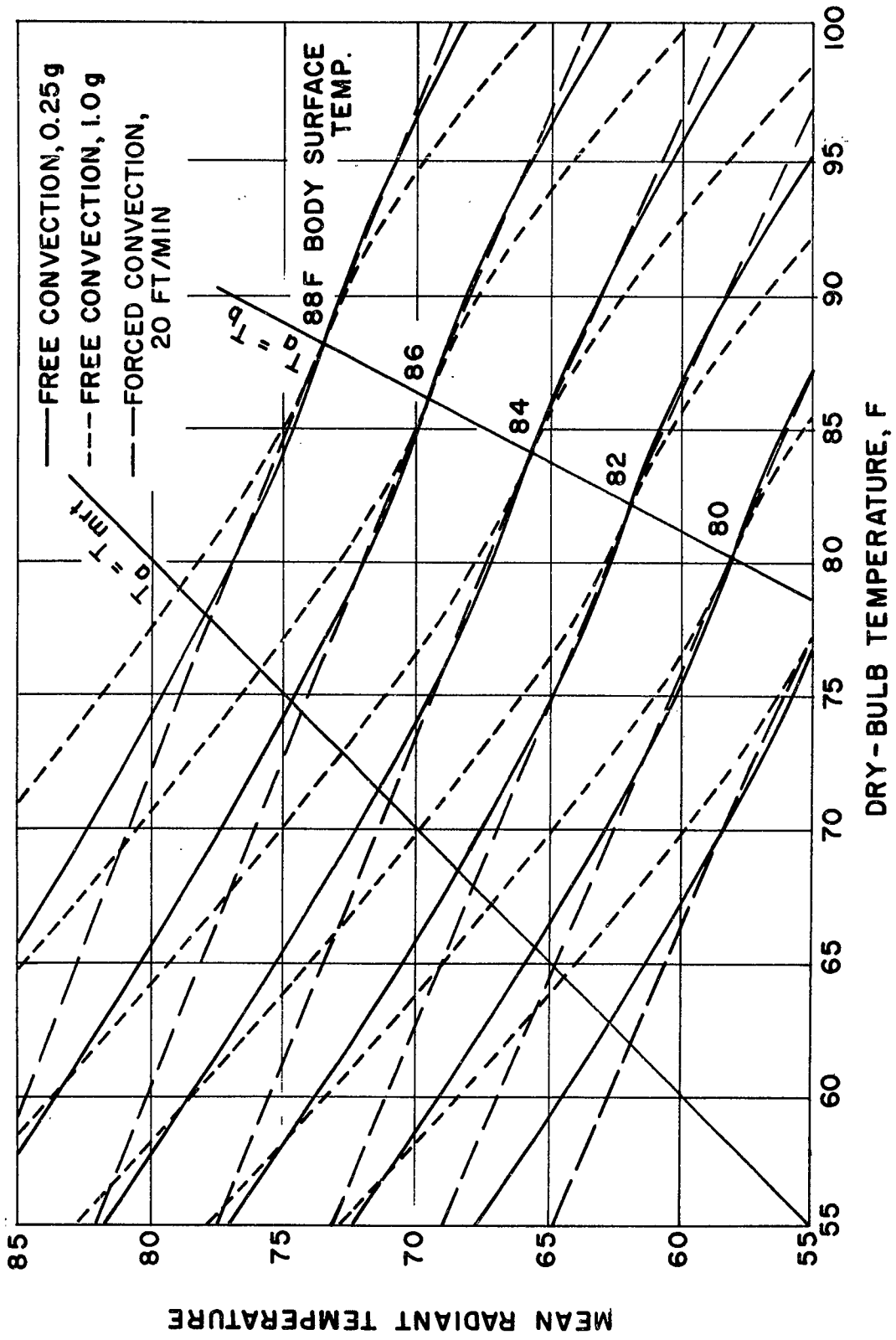


FIG. 3 - THERMAL COMFORT CHART

LITHIUM PERCHLORATE CANDLES -
A LIGHTWEIGHT SOLID CHEMICAL OXYGEN SOURCE

by

R. C. Oliver

Ford Motor Company
Newport Beach, California

LITHIUM PERCHLORATE CANDLES -
 A LIGHTWEIGHT SOLID CHEMICAL OXYGEN SOURCE
 by
 R. C. Oliver

INTRODUCTION

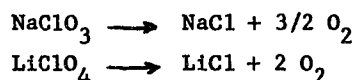
The inherent simplicity and long term storability of solid chemical oxygen sources have made such sources the object of investigation of various naval and air forces for many years. For space and aircraft application oxygen supplies must have as high a ratio of oxygen weight to total weight as possible; it is perhaps not widely appreciated how satisfactory chemical sources of oxygen appear relative to other sources when compared on this basis. Consider the following:

<u>Oxygen Source</u>	<u>Lb.Total/Lb.O₂</u>
Compressed Gas	
450 psi (2.6 lb. O ₂)	8.0 ⁽¹⁾
1800 psi (21.2 lb. O ₂)	2.7 ⁽¹⁾
7500 psi (1.1 lb. O ₂)	4.9 ⁽²⁾
LOX	
20 liters	2.1 ⁽¹⁾
25 liters	1.6 ⁽³⁾
Supercritical Cryogenic	
197 lb.	1.4 ⁽⁴⁾
Chemical	
LiClO ₄	1.66 (Ideal; Realizable about 1.9)
NaClO ₃	2.21 (Ideal; Realizable about 2.5)

The chemical sources are seen to be superior to compressed gas sources, and competitive with others. (The Garrett Corporation⁽⁵⁾ predicts that lower values than those shown can be obtained for cryogenic

sources, but the values shown are believed to be realistic at present.) In addition, chemical sources have the advantage that high pressures are not involved, with attendant explosion hazards and valve leakage possibilities. The chemical sources should be preferable for emergency sources which may need to be stored for long periods.

Sodium chlorate is presently being used by the U.S. Navy⁽⁶⁾ in chemical oxygen sources; it is instructive to compare this material to LiClO_4 . The reactions are ideally:



The materials can be compared as follows:

<u>Compound</u>	<u>Theoretical Oxygen Availability</u>	<u>Theoretical Density</u>
NaClO_3	45.1 wt. %	2.490 gm/cc
LiClO_4	60.1 wt. %	2.429 gm/cc

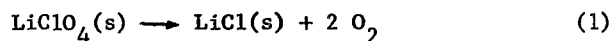
On a weight basis, LiClO_4 has 33% greater oxygen content than NaClO_3 ; on an ideal volume basis, it has 30% greater oxygen. The primary advantage of NaClO_3 lies in its much lower cost per unit of stored oxygen.

Both chemical sources require addition of a fuel material to keep the reactions proceeding. Sodium chlorate candles use iron powder, steel wool, and barium peroxide as additives, and contain about 88% sodium chlorate. The barium peroxide acts as a chlorine suppressant.

These observations indicate that LiClO_4 as a basis for a chemical oxygen source might well find application where light weight and storability are required. A program was thus initiated at Aeronutronic to determine whether such sources were feasible and to solve some of the preliminary development problems. This paper presents the results of these efforts.

THERMOCHEMISTRY OF PERCHLORATE CANDLE COMBUSTION

The overall reaction



theoretically liberates 6.69 kcal per gram mole at 298^oK, based on the latest JANAF data⁽⁷⁾. In practice, however, the decomposition kinetics are complex⁽⁸⁾, and the reaction will not proceed in the absence of added fuel materials, at least at ordinary pressures. (The sodium chlorate decomposition liberates 12.5 kcal, but it too needs added fuel.) The preferred fuel material would be the one which liberates the greatest amount of heat per unit weight of oxide formed. The necessary data for selection are given in Table I. (Carbonaceous materials are excluded because CO₂ or possible CO could not be tolerated above very low levels.) Beryllium has the highest heat release but can immediately be ruled out due to the potential toxicity hazard from BeO; lithium looks good, but is difficult to handle; boron might be satisfactory, but the oxide is fairly volatile; magnesium, aluminum and silicon appear reasonably attractive.

Magnesium and aluminum were studied in some detail from a thermodynamic standpoint to see what might theoretically be expected from their combustion with LiClO₄ at low fuel levels. Adiabatic combustion was assumed, although it was recognized that this bore little resemblance to the end-burning process expected. Results based on an Aeronutronic machine computation program are given in Table II in terms of theoretical flame temperatures and equilibrium compositions. Several points merit comment:

(1) Flame temperatures are high. With 3% Al and 97% LiClO₄, a flame temperature of 1151^oK (1612^oF) is calculated. Substantially lower temperatures may be expected in practice, however, because of heat losses and incomplete combustion.

(2) LiCl(g) and Li₂Cl₂(g) are present in surprisingly large quantities at temperatures predicted. Table III gives mole fractions at 15 psia of LiCl(g) and Li₂Cl₂(g) over LiCl(l) as a function of temperature. It is evident that excessive quantities of LiCl will be vaporized, forming smoke, and thereby tend to plug up filters, if the amount of fuel material added is such as to give flame temperatures above perhaps 1150^oK. It is obviously mandatory to minimize fuel addition in order to minimize smoke generation as well as to minimize oxygen consumption.

(3) Water cannot be tolerated in the mixture, although it is apparently not nearly as serious with magnesium as with aluminum. The

TABLE I
HEAT-RELEASING METALLIC FUELS*

<u>Metal</u>	<u>Oxide</u>	<u>Molecular Weight Oxide</u>	<u>$\Delta H_f^o, 298$</u>	<u>Heat Release, kcal/gm metal</u>	<u>Heat Release kcal/gm oxide</u>
Be	BeO	25.0	-143.1	15.9	5.72
Li	Li ₂ O	29.9	-142.6	10.3	4.77
Li	Li ₂ O ₂	45.9	-151.7	10.9	3.31
B	B ₂ O ₃	69.6	-305.3	14.2	4.39
Mg	MgO	40.3	-143.7	5.91	3.56
Al	Al ₂ O ₃	102.0	-400.4	7.40	3.92
Fe	Fe ₂ O ₃	159.7	-198.5	1.77	1.24
Ti	TiO ₂	79.9	-225.5	4.70	2.82
Si	SiO ₂	60.1	-209.9	7.47	3.49

*Sources: JANAF Tables, NBS 500, Chemical Engineers Handbook

TABLE II
THEORETICAL COMBUSTION RESULTS FOR PERCHLORATE CANDLE COMPOSITIONS

Combustion Pressure = 15 psia

	LiClO ₄ - Al - H ₂ O			LiClO ₄ - Mg - H ₂ O		
	93	95	97	93	93	95
%LiClO ₄	5	5	3	5	7	5
%Al or Mg	2	-	-	2	7	5
%H ₂ O	1375	1496	1404	1280	1438	1310
T _c , °K	2015	2233	2067	1844	2128	1898
°F Mole Fractions in Gas Phase (2)					
Gaseous Species (1)	.00086	.0024	.00115	.000069	.000004	.000006
Cl	.0339				.00034	
HCl	.000043				0.	
HClO	.0605	.1974	.0819	.0032	.0200	.1157
LiCl	.000023	.000051	.000030	.000003	0.	0.
ClO	.01335	.00179	.0015	.000595	0.	0.
Cl ₂	.01598	.04474	.0208	.00118	.0060	.0281
Li ₂ Cl ₂	.00001				.00034	.0082
LiOH	.0414				.0612	
H ₂ O	.8459	.75356	.8945	.9949	.9120	.8562
O ₂						.962

NOTES: (1) Condensed phases (assumed immiscible) with aluminum additive are LiAlO₂, Al₂O₃, LiCl; With magnesium, condensed phases are LiCl and MgO, and in the absence of H₂O, Li₂O in trace quantities.
(2) Gaseous metallic species, as well as ClO₂ and Cl₂O, are below significance level (1/2 x 10⁻⁶ mole fraction)

TABLE III
 MOLE FRACTIONS OF LiCl(g) AND Li₂Cl₂(g)
 OVER LiCl(c) at 15 PSIA

<u>TEMPERATURE</u> °K	<u>MOLE FRACTION</u> LiCl(g)	<u>MOLE FRACTION</u> Li ₂ Cl ₂ (g)
1150	.0032	.0012
1200	.0073	.0024
1250	.014	.0043
1300	.026	.0074
1350	.046	.0124
1400	.079	.020
1450	.13	.032
1500	.20	.046

equilibrium HCl content assuming 2 wt.% H₂O in the candle and 5 wt.% metal, is 3 mol % with aluminum and 0.03 mol % with magnesium.

(4) At the same wt.% metal loading, magnesium gives lower flame temperatures than aluminum, and more importantly, much lower contents of Cl, Cl₂, and ClO in the vapors. Generation of gaseous chlorine species can be attributed to the following reactions with free energy changes in kcal/reaction shown at 1300°K:

<u>Reaction</u>	<u>F^o_{f1300°K}</u>	
LiCl(l) + ½O ₂ (g) → ½Li ₂ O(c) + Cl(g)	35.697	(2)
½O ₂ + LiCl(l) + Al ₂ O ₃ (c) → LiAlO ₂ (c) + Cl(g)	20.046	(3)
2Cl(g) → Cl ₂ (g)	-22.572	(4)
Cl(g) + ½O ₂ (g) → ClO(g)	8.873	(5)

With the partial pressure of oxygen fixed (near 1 atm.) the amount of monatomic chlorine for the two cases is set by reactions (2) and (3). The free energy changes shown permit computation of the Cl₂ and ClO content by reactions (4) and (5) as

$$P_{Cl_2} = 6200 P_{Cl}^2$$

$$P_{ClO} = .032 P_{Cl} P_{O_2}^{\frac{1}{2}}$$

The total gaseous chlorine content can thus be related to the atomic chlorine content as computed from reactions (2) and (3), and since the positive free energy change for reaction (2) is much larger for reaction (2) than for reaction (3), the atomic chlorine content, and thus the total chlorine content, will be much lower with reaction (2) than with reaction(3). (Note that the Cl₂ content is related to the square of the Cl content.) With 1 atm. oxygen partial pressure, the atomic chlorine content is found to be 1 ppm (by volume) with Mg and 435 ppm (by volume), at 1300°K, with Al. Values found for the various cases can be read from Table II.

These results are of course sensitive to the thermodynamic data employed.

(5) In all cases the calculated equilibrium amount of Cl₂O and ClO₂ was less than ~ ½ppm and rejected as zero by the computer program.

With aluminum, however, as noted above, appreciable amounts of ClO were computed (30 ppm at 5% Al); with Mg, no ClO was predicted.

These calculations show that magnesium is preferable to aluminum, and that flame temperatures must be kept low in order to prevent volatilization of LiCl. Also, while no calculations were made, it would be expected that the probability of lithium metaborate formation with boron fuel would increase the chlorine and chlorine oxide content of the gas mixture in a manner similar to that with aluminum.

EXPERIMENTAL STUDIES

At the time this research was undertaken*, no candle formulations using LiClO_4 as an oxygen source had been described in the open literature, at least to our knowledge; our approach was thus Edisonian in nature. We recognized three important problem areas:

- (1) Formulation: maximum LiClO_4 , minimum fuel, catalyst possibilities.
- (2) Ignitor type.
- (3) Smoke filtration.

The experimental conditions employed to test these problems were as follows:

(1) Formulation: Some preliminary studies with aluminum and magnesium indicated that considerable difficulty could be expected in attempting to burn catalyst-free mixtures containing less than about 10% metal, and that mixtures with 10% metal gave excessive quantities of smoke and excessive flame temperatures. As a result, a large number of mixtures of these metals and other fuel materials were tried at various lower levels of fuel material, compression pressure, and with various catalysts, seeking systems with properties closer to those desired. Mixtures were generally tamped or pressed into metal cups as shown in Figure 1, these cups being $1\frac{1}{2}$ " in diameter and $\frac{5}{8}$ " deep. A few strands, as shown in the figure, were also tested, but were not investigated in detail. A number

* In January, 1962. We subsequently learned of some brief but similar studies by the Naval Research Laboratory⁽⁹⁾ some two years earlier.

of the best formulations were also formed into candles 7/8" in diameter and 5½" long. Most of the firings were into the open air, observations being made only of the combustion characteristics and smoke level resulting. The more successful formulations were fired in an enclosed apparatus, the evolved gases passing through a filter, a KI scrubber to measure contaminant level, and a wet test meter to measure gas evolution. Fuels tested at various levels (< 10% by weight) included B, Mg, Al, steel wool, Zr wool, Li, MgSi₂, KBH₄, NaN₃, LiNH₂, Si, Zn, Cd, Mn, Ni, Co, Cr, Fe powder, and somewhat academically, sawdust, silicone rubber and polyethylene.

A number of catalysts were also tried. These included the conventional solid propellant burning rate catalysts such as iron oxide and copper chromite, as well as cobaltous chloride as suggested by work at Iowa⁽¹⁰⁾, silver nitrate⁽¹¹⁾ (known to stabilize lithium perchlorate decomposition), Ag₂O, Ag, Pd, Pb(NO₃)₂, Pb₃O₄, BiCl₃ hydrate, and LiCl which was known⁽⁸⁾ to catalyze the decomposition.

Contaminant suppression additives were investigated briefly, the materials tested including the peroxides of lithium, sodium and barium. External chemical filters for removing chlorine and chlorine oxides were also investigated, it being our opinion that these represented a surer and simpler procedure for removing these contaminants. External filter materials tried included Li₂O₂, Li₂O₂ with sand, NaOH, molecular sieves, and activated charcoal.

A few firings were made with fibrous additives such as glass wool and asbestos; it was recognized that such materials would decrease the weight advantages of these candles so that their use was not investigated at length.

(2) Ignitors were investigated briefly. It was believed that a slow burning gasless type ignitor would be most suitable. Most firings were made using 95 BaCrO₄ - 5 B mixture with electrical ignition. Other ignitors tried involved use of the material in ordinary road flares, NH₄ClO₄ with Mg and Al, and LiClO₄ with Mg and Al, in higher fuel to oxidizer ratio than in the main candle.

(3) Smoke filtration: This problem was recognized to be related largely to the formulation problem, with larger amounts of fuel

material greatly increasing the smoke filtration problem. Filters were used only with the more successful mixtures which were fired to obtain gas evolution data; the filter employed was generally a glass fiber fine-pored filter. A prefilter and support of wire mesh and steel wool, or in some cases a sintered metal filter, were used to support the filter material and to knock out any entrained or condensing LiCl.

RESULTS

Results can be summarized as follows:

(1) The great majority of test formulations burned only briefly and incompletely. This was believed to be largely due to the fact that in dilute mixtures of this type the fuel particles are generally relatively widely separated so that heat liberated by the combustion of a given particle primarily goes to melt the surrounding LiClO_4 , and the molten perchlorate does not ignite the other particles. Further, metals which are denser than the melt will tend to sink away from the combustion zone.

(2) In the absence of catalyst, formulations containing Mg burned completely although too rapidly at the 10% Mg level, but samples did not burn satisfactorily at the 5% Mg level. Formulations containing carbonaceous material (2-5%) burned slowly and cleanly, although CO_2 and possible CO liberation appears to rule them out for use in manned systems. LiNH_2 at the 6% level burned satisfactorily but produced an odor of NH_3 ; this may have been due to moisture in the candle.

Most other mixtures did not burn at reasonable concentration levels. Li and KBH_4 burned explosively, spattering unreacted material from the container or, as in one case with 6% KBH_4 (pressed), detonating.

(3) Silver and lead nitrates and oxides were found to be excellent catalysts, as was bismuth chloride. Silver oxide was found to be very effective, permitting combustion to take place slowly, cleanly, at low fuel contents and low temperatures, and with relatively little smoke (LiCl) generation. One of the better formulations was

LiClO_4	94.5%
Mg	4.5%
Ag_2O catalyst	1.0%

No fibrous additive nor chlorine suppressant was used.

A typical experimental 110 gram candle of this formulation pressed at 10,000 psi (7/8" x 5 1/4"), when ignited with a 95 BaCrO₄ - 5 B mixture, burned for seven minutes and yielded 1.44 SCF O₂ (32°F 1 atm). This corresponds to 1.88 lb. candle per lb. of oxygen, as compared to 1.85 lb. candle per lb. of oxygen which this mixture should give ideally. The container is not considered in these weight figures, but the container would presumably be used repeatedly.

Quite evidently, the catalyst is critical to the process. Without it, much higher levels of fuel material are required, much higher temperatures result, and much lower oxygen yields are obtained. In addition, the low combustion temperature obtained through use of low fuel loadings with the catalyst practically eliminates the smoke problem.

(4) As with NaClO₃ candles, some chlorine (or chlorine oxides) was liberated with the evolved oxygen. This contaminant, which was found to vary all the way from 50 to 1000 ppm, was apparently completely removed (as tested by KI solution) with a bed of Li₂O₂. Cartridges of these materials could be used to remove chlorine from a large number of candles. Removal was also complete with activated charcoal. NaOH pellets and molecular sieves were not effective in the same quantities. Barium peroxide, at the 4 wt.% level, reduced chlorine evolution but did not eliminate it. Lithium peroxide as an additive appeared to have a deleterious effect on combustion properties. Much further research appeared necessary to eliminate the chlorine evolution problem through the use of additives.

(5) Smoke filtration appeared to be completely effective with the simple fine-pored glass filter "paper" used. Adequate prefiltering is necessary to remove large entrained droplets.

CONCLUDING COMMENTS

The success attained with the lithium perchlorate candle compositions tested indicate that candles of this type are indeed practical, giving near theoretical yields of oxygen and with no serious combustion properties. It is believed as a result that these candles represent a type of oxygen storage device which should be considered wherever light weight and small storage volume are required.

It is recognized that the results described in the foregoing are not sufficient to consider such candles fully developed. In particular, the following areas appear to need further investigation:

Formulation studies - maximization of oxygen yield by varying fuel and catalyst content; maximization of burning time, study of effects of contained moisture.

Development of low-mass, high capacity chlorine removal cartridge.

Packaging studies - consideration of length to diameter effects, heat loss, etc.

Fabrication techniques - consideration of cold pressing, hot pressing, extrusion.

Ignitor studies - electrical vs. hand grenade types, etc.

Zero-"g" effects - possible need for fibrous materials to prevent liquid carry over.

Solutions to all these problems, except perhaps the zero-"g" effects, are well within conventional technology.

REFERENCES

1. Konecci, E. B., "Advances in Space Science," Vol. 1, 1959, p. 192, edited by F. I. Ordway, III, Academic Press, New York and London.
2. Anon., "Closed Circuit Respiration/Ventilation System Phase I," p. 29, WADD TR-60-33, January 1960 (Air Reduction Co.)
3. Keating, D. A., "Design Study of High Pressure Oxygen Vessels," p. 15, WADD TR-59-76, February 1960.
4. Waggoner, J. N. and Burriss, W. L., "Problems and Progress in Providing an Earth Environment for Manned Space Flight," paper presented at ARS Meeting, October 9-15, 1961 (New York).
5. Anon., "Airesearch Capabilities and Experience in the Field of Aerospace Cryogenics," brochure supplied to the author by W. L. Burriss (1962).
6. Piatt, V. R. and Ramskill, E. A., "The Present Status of Chemical Research in Atmosphere Purification and Control in Nuclear-Powered Submarines," Annual Progress Report, NRL Report 5630, July 14, 1961.
7. JANAF-Thermochemical Tables, Dow Chemical Company, Midland, Michigan.
8. Markowitz, M. M. and Boryta, D. A., "The Decomposition Kinetics of Lithium Perchlorate," J. Phys. Chem., 65, 1419 (1961).
9. Miller, R. R., U.S.N.R.L., Washington, D.C., private communication, August 7, 1962.
10. O'Brien, J. F., Proc. Iowa Acad. Sciences, 66, 1949 (1959).
11. Markowitz, M. M. and Boryta, D. A., "Retardation of the Thermal Decomposition of Lithium Perchlorate," J. Phys. Chem., 66, 358 (1962).

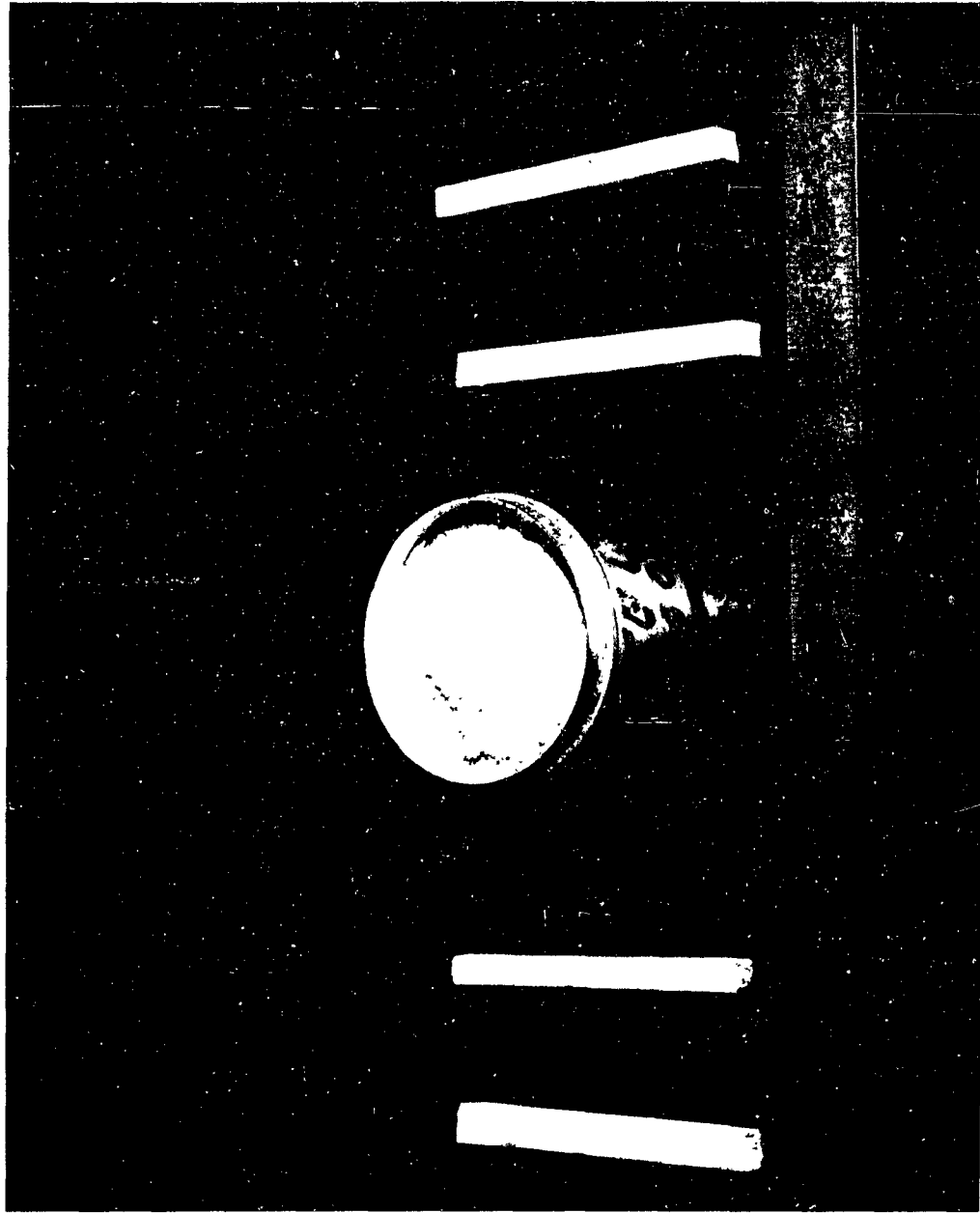


Figure 1. Experimental Candle Samples

THE USE OF ELECTRIC FIELDS TO ORIENT
DIELECTRIC LIQUIDS IN A ZERO GRAVITY
ENVIRONMENT

by

Dr. J. M. Reynolds

Dynatech Corporation
and
Massachusetts Institute of Technology
Cambridge, Massachusetts

795

NOMENCLATURE

C	constant of proportionality in Equation (2)
E	electric field strength, statvolts cm^{-1} or $\sqrt{\text{dyne}} - \text{cm}^{-1}$
F, f	force, dyne - cm^{-3}
g_0	981 $\text{cm} - \text{sec}^{-2}$
R	radius of fluid interface in cm
R_0	radius of outer electrode of the stage, cm
R_i	radius of inner
T	surface tension at the interface between two fluids, dyne - cm^{-1}
V	rms electric potential, statvolts or $\sqrt{\text{dyne}}$ except in Table 1 where volts are noted. (Note 300 volts = 1 statvolt.)
Γ	defined by Equation (6), sec^{-1}
ϵ^*	defined by Equation (7)
ρ	density, gram - cm^{-3}
Σ	surface charge density, statcoulomb - cm^{-2}
σ	electrical conductivity in esu. (Note 1 esu of conductivity = 9×10^{11} mho cm^{-1} .)
σ^*	defined by Equation (8)
ω	angular frequency of impressed field, sec^{-1}

THE USE OF ELECTRIC FIELDS TO ORIENT
DIELECTRIC LIQUIDS IN A ZERO GRAVITY ENVIRONMENT*

By

John M. Reynolds**

INTRODUCTION

The effect of electric fields on dielectric fluids forms a portion of classical Electrodynamics (Reference 1, 2, 3) in which it is demonstrated that a stress tensor exists in such fluids due to the fact that an electrostatic energy is associated with each element of the fluid. In examining fruitful areas of application for such forces, an analogy may be drawn between magnetohydrodynamics and electrohydrodynamics. In the former area forces are of the Lorentz type and result from interactions of currents flowing in the medium and magnetic fields. Consequently, MHD is appropriate for consideration in media in which the maintenance of significant current density requires a low level of energy input; that is, conductors. EHD, on the other hand, involves forces produced by gradients in very strong electric fields. Appropriate media for consideration in the area of EHD consequently involve those in which a low energy expenditure is involved in the maintenance of strong electric fields; that is, nonconductors or dielectrics.

Further comparison of the fields of MHD and EHD reveals an important practical difference between the two at the present time. EHD has suffered from a lack of obvious applications and, consequently, has not

* This work has been performed at Dynatech Corp., Cambridge, Mass. under Contract No. AF 33(657)-9423 with Aeromedical Laboratory WPAFB.

** Consulting Engineer, Dynatech Corp.; Assistant Professor of Mechanical Engineering, Massachusetts Institute of Technology.

reached a stage of development which permits a clear categorization of the physical phenomena involved. A recent review (Reference 4) indicates the scope of the EHD field which encompasses a number of separate phenomena.

The purpose here is to outline progress which has been made in one potential area of application of the EHD phenomenon which Pohl (Reference 5) has called "dielectrophoresis". This is the use of electric fields to provide a body force in a two-fluid container to assure a predictable orientation of the fluids relative to each other in a zero gravity environment. The advantages of such an orientation scheme in a liquid oxygen container, for example, are that vapor can be vented for pressure relief or use in breathing apparatus with assurance that liquid is not lost in the process. On the other hand, for systems which require liquid delivery from tanks, pump inlet lines may be located so that vapor is not ingested thus avoiding excessive cavitation or vapor lock in the pump.

Electrostatic Forces

Forces due to the presence of electric fields in fluid media ultimately reduce to the interaction of the field with charges in the medium. There are two aspects of force which are considered in EHD; body forces and forces due to charge accumulation at interfacial surfaces. The origin of both of these forces is the force $-(E)(q)$ - experienced by a charge q in an electric field of strength E .

For illustrative purposes, the physical basis of the body force may be explained as follows. Each molecule of a fluid undergoes polarization when placed in an electric field. For homogeneous fluids in uniform

fields the sum of the electrostatic forces vanishes. However, if the electric field is nonuniform, each polarized molecule will experience a net force due to the fact that the positive charges are located at a point having a different field strength than the negative charges. The action of a nonuniform field on a particle (ν) is shown in Figure 1. The derivation of the expression for the body force on a homogeneous dielectric fluid will not be reproduced here. However, the result is well established (Reference 1, 2, 3). The body force experienced by a unit volume of initially homogeneous fluid in an electric field is*

$$F = 1/2 \text{ grad } [E^2 \rho \left(\frac{\partial \epsilon}{\partial \rho} \right) t] \quad (1)$$

where E , ρ , and ϵ are the electric field strength, fluid density, and dielectric constant, respectively. Equation (1) has been derived from thermodynamic considerations with no assumption regarding the dependence of ϵ on the thermodynamic properties of the fluid. Such an assumption is, however, required if the expression is to be evaluated. A commonly used expression relating ϵ and the fluid properties is the Clausius-Mossotti equation which provides a reasonable correlation of experimental observations on nonpolar fluids (Reference 6). That is,

$$\frac{\epsilon - 1}{\epsilon + 2} = C \rho \quad (2)$$

where C is a constant depending on the particular fluid under con-

* Electrostatic units (esu) are used throughout.

sideration. Combining (1) and (2) yields

$$\vec{F} = \frac{(\epsilon - 1)(\epsilon + 2)}{6} \text{ grad } E^2 \quad (3)$$

for homogeneous fluids.

Inspection of Equation (3) reveals two important aspects of dielectrophoretic forces on homogeneous fluids:

- a. the direction of the force does not depend on the polarity of the field. Consequently, alternating fields produce a force of varying magnitude but constant direction,
- b. the force is derivable from a potential and consequently cannot be used as the basis of pumps to drive fluid through external circuits.

A discussion of surface forces will be deferred. However, it is appropriate to mention here that the force on a fluid element surrounded by another fluid is of the type considered above. In this case, however, the polarization of the entire element as an entity is considered which involves consideration of bound charges at the interface between the fluids. A spherical element of one fluid (ϵ) contained in another continuous fluid (ϵ_c) experiences a force per unit volume of

$$\vec{F} = \frac{3\epsilon_c}{2} \frac{\epsilon - \epsilon_c}{\epsilon + 2\epsilon_c} \text{ grad } E^2 \quad (4)$$

In this expression the field is evaluated on the assumption that the spherical element is not present. This procedure is valid only when the field does not vary significantly over the dimension of the sphere.

The relations discussed above form the basis of zero-gravity tank design. For the system in its normal mode of operation, with the fluids separated, Equation (3) predicts that the one having the higher

dielectric constant will be subject to the greater force. In fact, for liquid-vapor systems, the vapor will experience no force ($\epsilon \approx 1$) while the liquid will be attracted to the point of highest field strength. Consequently, for a cylindrical tank having a single axial electrode (Figure 2) the liquid will form a cylinder on the electrode while the vapor will occupy the remaining tank volume.

Equation (4) is appropriate when considering a system subjected to an inertial disturbance since it predicts the force with which a detached drop of liquid is attracted to the liquid-vapor interface.

Zero Gravity Simulator

The theoretical magnitude of the forces involved in electrostatic tanks is such that the performance of these devices can be measured only when the effects of normal gravitational forces are absent. Therefore, it is necessary to observe the performance of systems incorporating this principle in a zero gravity simulator containing two equal density, but immiscible dielectric fluids. Such requirements are difficult to satisfy, particularly in view of the fact that water, glycerol, etc. are not suitable for simulator fluids regardless of the degree of purity maintained. The fluids chosen for the present investigation were silicone oil and peanut oil. This combination satisfies the basic requirements in that both fluids are dielectrics with conductivities of the order of picomhos per cm.

This fluid combination placed in a glass cylinder having a transparent conducting film on its inner surface forms a zero gravity simulator in which various electrode geometries may be studied.

The results of investigations using the simulator are twofold;

1. The fluids do form a stable configuration as predicted by Equation (3) if the applied field is of sufficiently high frequency, 60 cps in the present case.
2. No stable separation can be accomplished with D. C. fields.

One test is shown in Figure 3 in which peanut oil is being collected on the central electrode in a cylindrical tank. The poor contrast in these photographs is due to difficulty experienced in finding coloring material which is soluble in only one of the simulator fluids.

The fact that D. C. fields cannot produce a stable interface indicates that the general question of stability is of primary importance in considering application of electric fields to operational zero gravity tankage systems. This question will be considered under a separate heading of this paper. At this point, it is sufficient to point out that if the frequency of the applied field is large compared to the reciprocal of the relaxation time σ/ϵ of the fluids, the interface can be stable.

Time to Equilibrium

The applicability of Equation (4) to the problem of predicting time to equilibrium in operational systems has also been investigated. Here, the motion of spheres of peanut oil in a continuum of silicone oil was determined photographically by taking motion pictures against a polar coordinate grid. The results of these tests are shown in Figure 4. Since the determination of accelerations from photographic data is a crude process at best, it is felt that the agreement shown satisfactorily substantiates the applicability of Equation (4) to the system under consideration.

The drag coefficients used in these computations were taken from empirical curves since most of the points shown fall outside the region of Stokes flow.

Tank Design

Operational tankage for zero gravity vehicles usually requires higher force levels than are obtainable with a single central electrode. In considering means of increasing the force levels in the tank, we note that the EHD forces do not depend on polarity. Therefore, it is possible to construct a tank of a number of stages. These stages are concentric annular spaces contained between a series of concentric cylindrical electrodes of alternating polarity. The force in each stage is radially inward.

Ideally, from an electrical viewpoint, the stage boundaries would consist of porous conductors or fine mesh screens. However, the surface tension forces in such a system would be so large that much of the liquid (assumed wetting) would be held on the stage electrodes. Consequently, a rather coarse array of conductors is envisioned as the most appropriate operational configuration. A laboratory model of such a unit is shown in Figure 5. In this unit the stage electrodes consist of a number of 1/16 " diameter rods parallel to the tank axis. Such configurations have proven to be effective in orienting laboratory fluids and provide an excellent means of increasing the energy density in the container.

The detail design of these stages depends on the particular application under consideration. Stage design may be used to shape the field into any desired shape for a specific purpose and the stage elements can be of considerably more complex geometry than the rods shown in Figure 5.

The general problem of the design of the electrostatic field can be illustrated by considering systems of the simple type shown in Figure 5. Assuming that a voltage level has been selected, a rational basis for design is to define a minimum acceptable force level which would

accelerate a detached fluid element toward the equilibrium configuration.

For example, the minimum force level within a given stage is given by Equation (4)

$$F_{\min} = 3 \frac{\epsilon - 1}{\epsilon + 2} \frac{V^2}{R_o^3 (\ln R_o/R_i)^2} \quad (4a)$$

where the continuous medium is taken as gaseous and V is the applied (rms) voltage. The radii R_o and R_i refer to the outer and inner radii of the stage, respectively. The stage radii for a given design with a specified minimum force level are shown in Figure 6. The forces shown for this design are idealized in that at the stage radii the forces change discontinuously as would be the case if the electrodes are ideal permeable electrodes. For real electrode configurations, the actual force levels are qualitatively as indicated by the solid line in Figure 6.

Some reflection on a force profile of this type will indicate that the direction of the force in the vicinity of the electrodes is such that fluid over some finite region on both sides is driven toward the electrodes. Such a design results in excessive fluid "hang-up" on the electrodes.

An alternative design scheme can be used to avoid this difficulty. This involves the use of a constant radius ratio for all the stages in the tank. In this case, the force is continuous through the system as shown in Figure 7. While this design avoids the hang-up problem, the energy level in the tank is considerably higher than for the constant minimum force design. This results in a weight penalty.

Good design practice normally indicates a compromise between these extremes. The degree of compromise is dictated by the specific applica-

tion under consideration. It must be recognized that these design procedures can only give an indication of performance since the local fields around the individual stage elements have not been considered. At present, we have only a qualitative idea of detailed stage optimization procedures. However, the above considerations provide a rational point of departure for tank design.

Stability

The stability of cylindrical interfaces under the influence of electric fields must be assured if operational devices of the type under consideration are to become a reality. This area is complex and has required a serious analytical effort in the present investigation. The details of the analysis will be presented in another paper. However, some discussion of the physics of the problem is appropriate here along with a discussion of the analytical result although it has not yet been verified experimentally.

The basis of the unstable behavior of the interface in steady fields lies in the finite conductivity of the fluids. However small, a finite conductivity results in the appearance of free charge at the interface since Ohm's law requires that the normal components of current density (σE) must be continuous while the change of the normal component of the displacement (ϵE) current is equal to the free surface charge. The Ohm's law condition cannot, in general, be satisfied without yielding a discontinuity in displacement current.

Application of an alternating field of sufficiently high frequency can, however, reduce the free interfacial charge to tolerable levels.

The nature of the frequency dependence can be seen from the expression for surface charge on a cylindrical interface of radius R between

electrodes of radii R_i and R_o .

$$\Sigma = \frac{(\epsilon_i \sigma_o - \epsilon_o \sigma_i) \left(\cos \omega t + \frac{\omega}{\Gamma} \sin \omega t \right)}{\sigma^* \left[\left(\frac{\omega}{\Gamma} \right)^2 + 1 \right]} \quad (5)$$

where

$$\Gamma \equiv \sigma^*/\epsilon^* \quad (6)$$

and

$$\epsilon^* = \epsilon_i \ln \frac{R_o}{R} + \epsilon_o \ln \frac{R}{R_i} \quad (7)$$

$$\sigma^* = \sigma_i \ln \frac{R_o}{R} + \sigma_o \ln \frac{R}{R_i} \quad (8)$$

The subscripts i and o refer to the inner and outer fluids. That is σ_i is the conductivity of the inner fluid, etc. It is apparent that for

$$\omega \gg \frac{\sigma^*}{\epsilon^*}$$

this reduces to

$$\Sigma = \frac{\epsilon_i \sigma_o - \epsilon_o \sigma_i}{\frac{\omega}{\Gamma} \sigma^*} \sin \omega t \quad (9)$$

which clearly indicates the inverse relationship between surface free charge and frequency.

The stability of these systems can be analyzed by inspecting the sign of the work done by all the forces at the interface during an assumed

perturbation. These forces are:

1. The surface component of the body force, Equation (1).
2. The force due to free charge at the interface.
3. Surface tension forces.
4. Hydrostatic pressure force.

The results of the stability analysis indicate three criteria for stability. First, as the stage approaches $R_o/R_i = 1$, the system behaves as if the stage were constructed of parallel flat plates. This configuration is always unstable for an interface parallel to the electrodes. The geometrical criterion, therefore, indicates how closely one may approach the parallel plate geometry and retain a stable interface. This condition is

$$\epsilon^* > \epsilon_i - \epsilon_o. \quad (10)$$

(Note that the system is always unstable if $\epsilon_i - \epsilon_o < 0$).

Second, for long wavelength disturbances surface tension exerts a destabilizing influence on the system which must be compensated by electrical forces. This criterion indicates that there is a lower limit for the stabilizing voltage for each stage geometry. Moreover, there is one geometry which yields a minimum value for the stabilizing voltage.

The smallest possible stabilizing voltage is given by

$$\frac{V^2}{TR} \approx 6.7 \frac{\epsilon_i - \epsilon_o}{\epsilon_i \epsilon_o}. \quad (11)$$

where T is the surface tension and R the interface radius

This minimum voltage requires a geometry which satisfies

$$\frac{\epsilon_i - \epsilon_o}{\epsilon^*} = \frac{2}{3} \quad (12)$$

Table 1 indicates values of the stage parameters for a stage having a radius of the order of three inches. Here $(R_o/R_i)_{\min}$ is from Equation (10) and is independent of the stage radius. This is the radius ratio at which it becomes impossible to stabilize the interface at any voltage. The quantity $(R_o/R_i)_{\text{opt}}$ is the radius ratio which requires the lowest voltage to stabilize and is independent of stage radius. The voltage V_{\min} is the minimum stabilizing voltage for a 3 inch effective radius (R) and $(R_o/R_i)_{\text{opt}}$.

A third criterion limits the maximum voltage across the stage. At short perturbation wavelengths, surface tension is a stabilizing factor while the electrical forces destabilize the system. Consequently, for short wavelength disturbances, there is a maximum voltage which must not be exceeded. This is given by

$$\frac{V_{\max}^2}{TR} = 9 \left(\frac{\epsilon_i + \epsilon_o}{\epsilon_i - \epsilon_o} \right)^2 \frac{\epsilon_i - \epsilon_o}{\epsilon_i \epsilon_o} \quad (13)$$

for a stage of $(R_o/R_i)_{\text{opt}}$. These levels of V_{\max} are shown in Table 1 for a three inch radius.

TABLE 1

SAMPLE VALUES OF PARAMETERS DEFINING STABLE OPERATION

Note that V_{\max} is Sensitive to the Particular Geometry Assumed

	Simulator	LOX - Vapor	LH ₂ - Vapor
T (dyne/cm)	1.3	18	2.9
ϵ (liquid)	—	1.50	1.25
$(R_o/R_i)_{\min}$	1.2	1.6	1.3
$(R_o/R_i)_{\text{opt}}$	1.3	2.2	1.45
V_{\min} (volts)	600	5200	1600
V_{\max}^* (volts)	0.6×10^4	3×10^4	1.7×10^4

*For an interface of three inch radius and $(R_o/R_i)_{\text{opt}}$.

The values given in Table 1 indicate that the tolerable voltage range is fairly broad and lies within the range of values which can be attained in practice. Since the voltage levels are proportional to the square root of the tank dimensions containers of the order of 30 inches in radius could be built for LOX and somewhat larger tanks could be built for LH₂.

This discussion of stability is not meant to be definitive since experimental confirmation is not available at this writing. The values given indicate orders of magnitude only. The important result here is that systems designed to employ electrostatic forces for zero gravity fluid orientation must be compatible with the rather broad restrictions imposed by stability considerations.

Conclusion

The results of the present investigation, indicate that it is feasible to employ the dielectrophoretic phenomenon to orient cryogenic liquids in a zero gravity environment. The orientation scheme has been shown to work in a laboratory simulator. A particular operational system can be made more flexible through the use of the staging concept as long as the geometrical restrictions imposed by stability considerations are observed.

References

1. Electromagnetic Theory, J. A. Stratton, McGraw-Hill, 1941.
2. Electrodynamics of Continuous Media, L. D. Landau and E. M. Lifshitz, Addison-Wesley, 1960.
3. Classical Electricity and Magnetism, W.K.H. Panofsky and M. Phillips, Addison-Wesley, 1955.
4. "Electrofluidmechanics; A Study of Electrokinetic Actions in Fluids", Report Number ASD-TR-61-642 WPAFB Dayton, Ohio.
5. "Some Effects of Non-uniform Fields on Dielectrics", H. A. Pohl, Journal of Applied Physics, 29, 1182 (1958).
6. Polar Molecules, P. Debye, Dover Publications

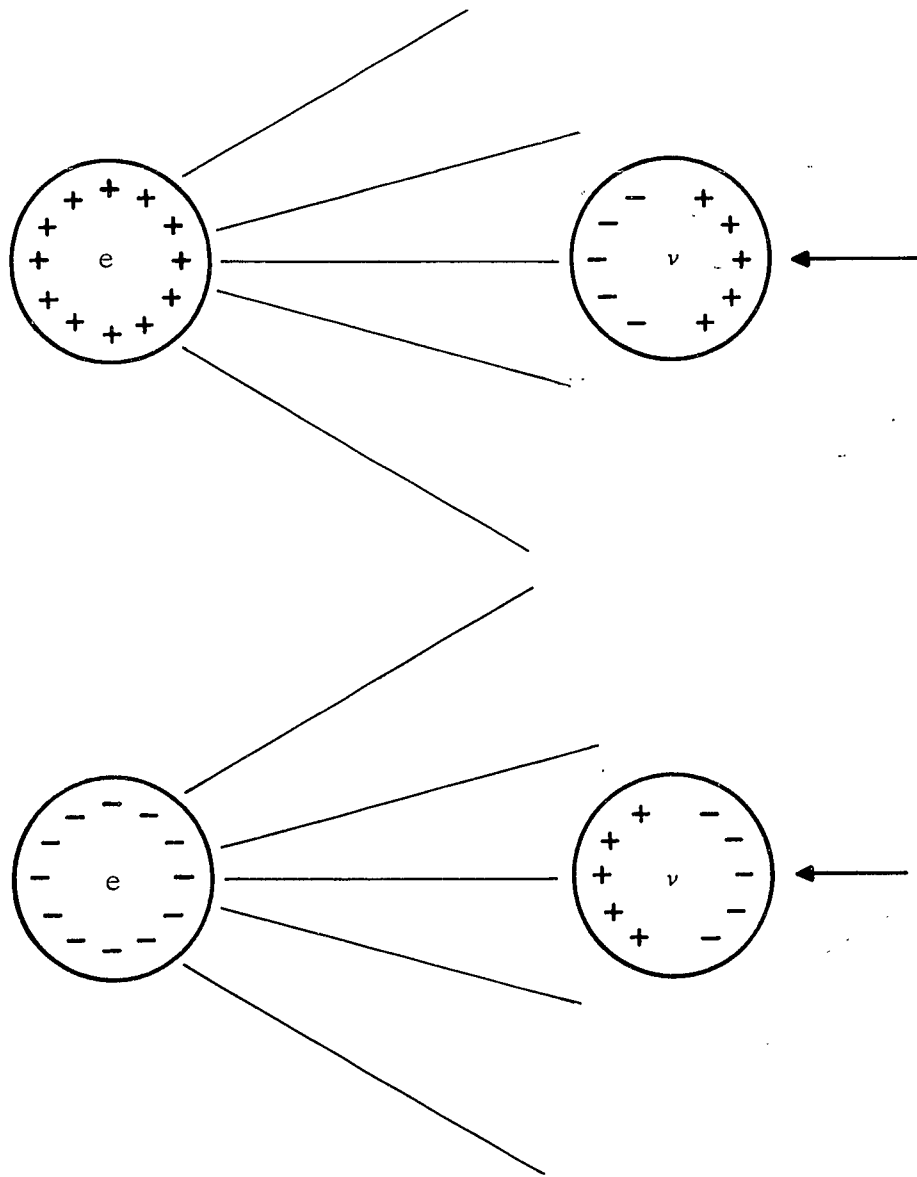


FIGURE 1
 THE ACTION OF THE FIELD AROUND AN ELECTRODE (e)
 ON A POLARIZED PARTICLE (v). ARROW INDICATES
 THE DIRECTION OF FORCE.

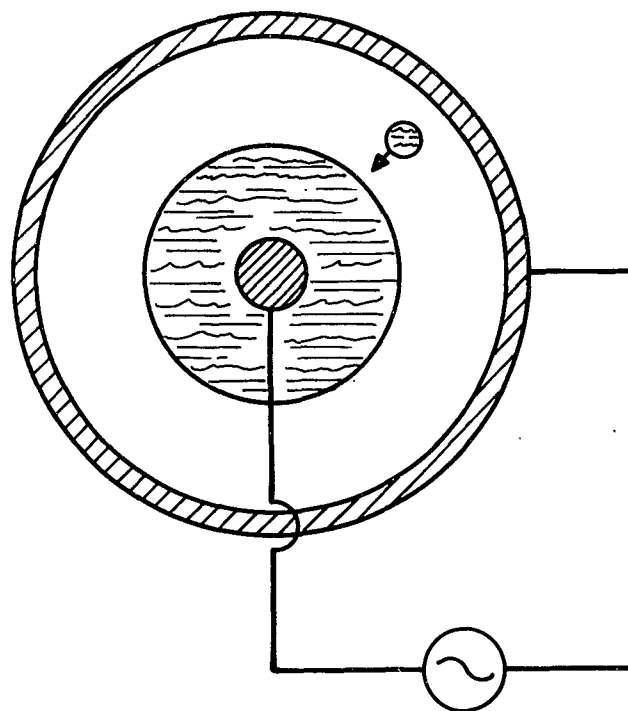
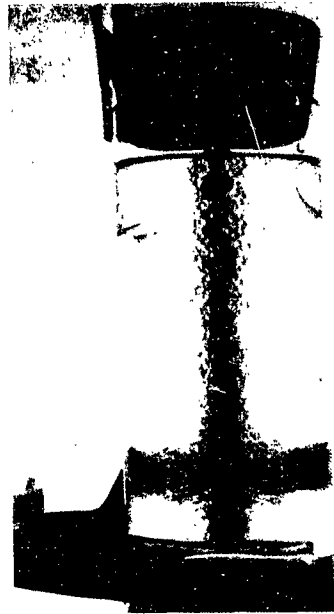


FIGURE 2
EQUILIBRIUM POSITIONS OF LIQUID AND
VAPOR IN A CYLINDRICAL CONTAINER



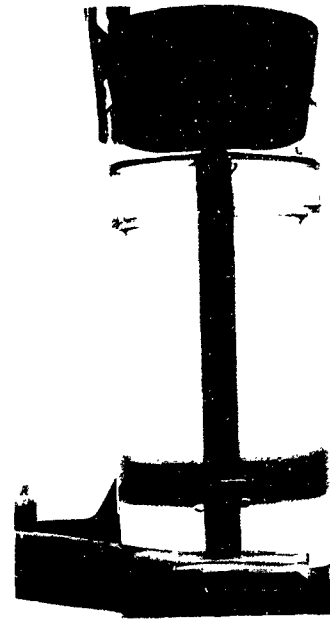
3-a
Initial Configuration, Zero Voltage



3-b
Time: 5 Seconds, 10,000 Volts



3-c
Time: 10 Seconds, 10,000 Volts



3-d
Time: 60 Seconds, 10,000 Volts

Figure 3
Orientation of (almost) Equal Density Fluids From a Well Mixed Initial Condition

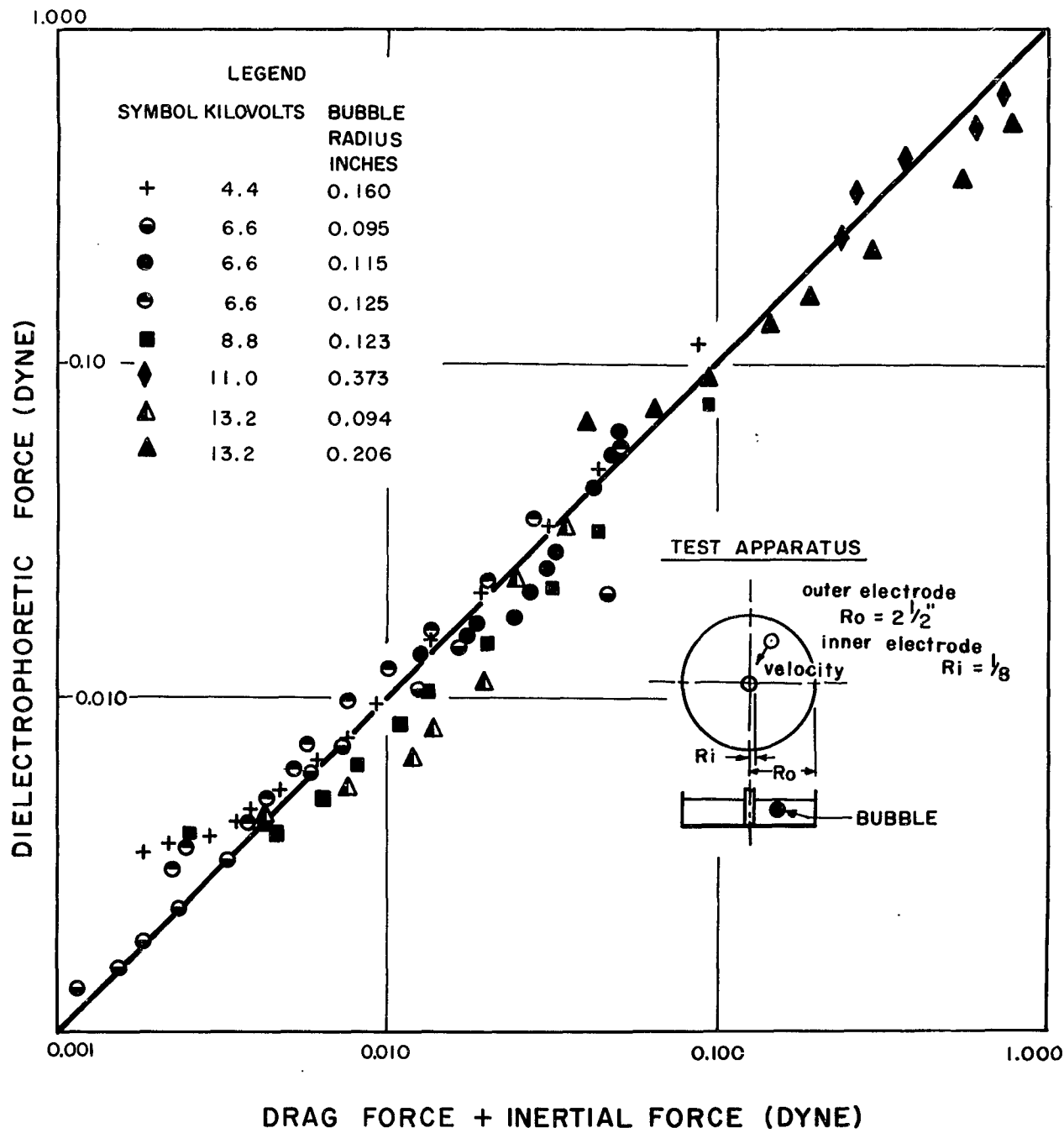


FIGURE 4
 CORRELATION OF BUBBLE MOTION DATA.
 ELECTRICAL FORCE COMPUTED FROM EQUATION (4)
 817

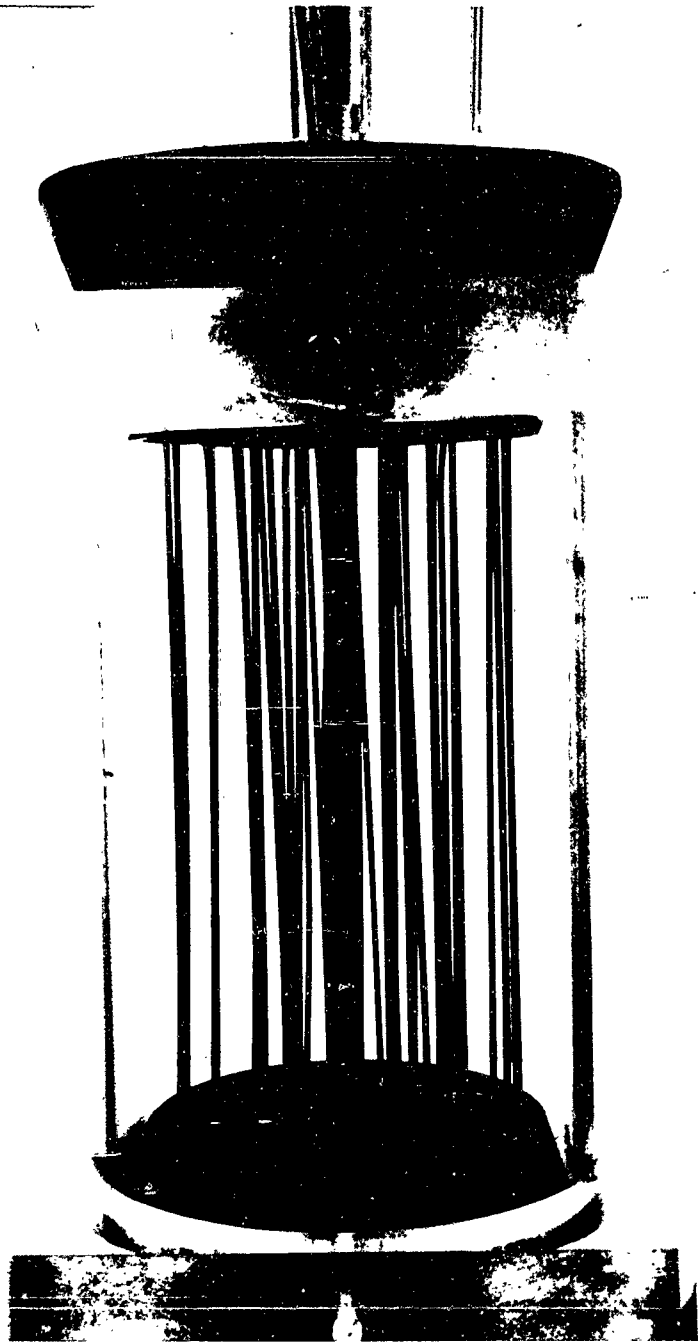


FIGURE 5
LABORATORY TEST MODEL OF MULTI-STAGE TANK DESIGN

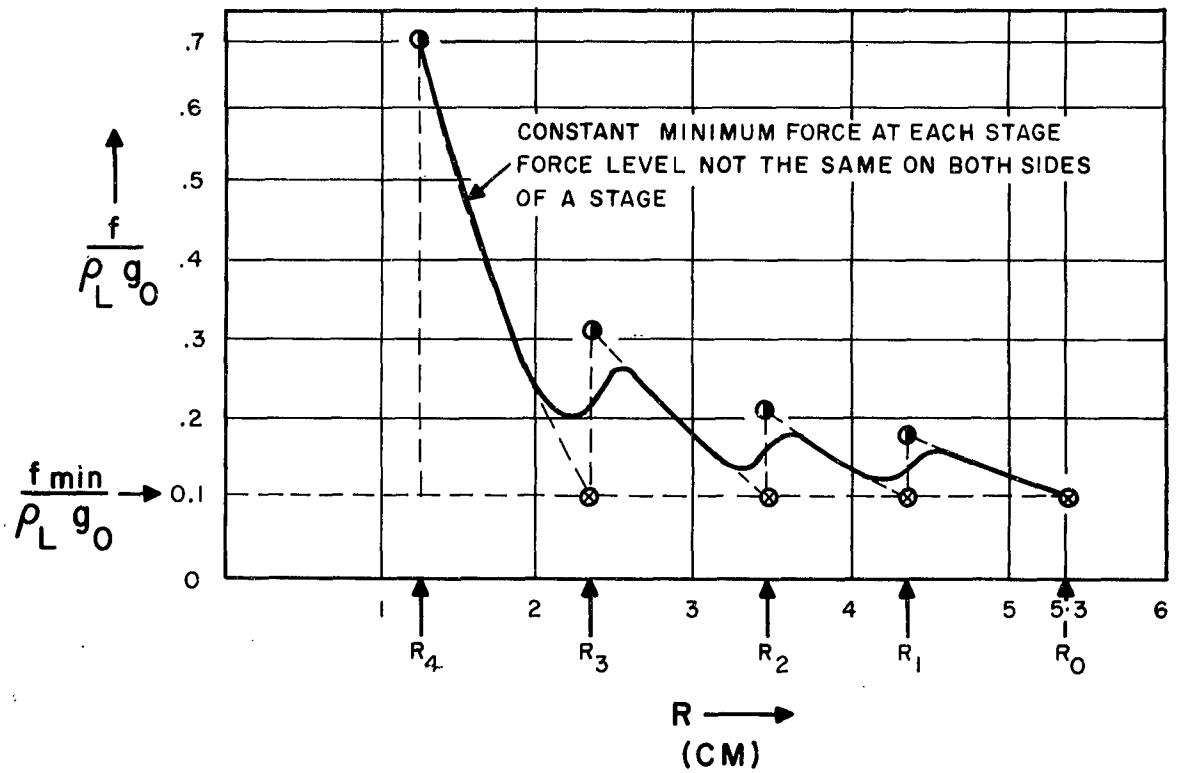


FIGURE 6

FORCE PROFILES IN A MULTI-STAGE CONTAINER
THE CONSTANT MINIMUM FORCE CRITERION

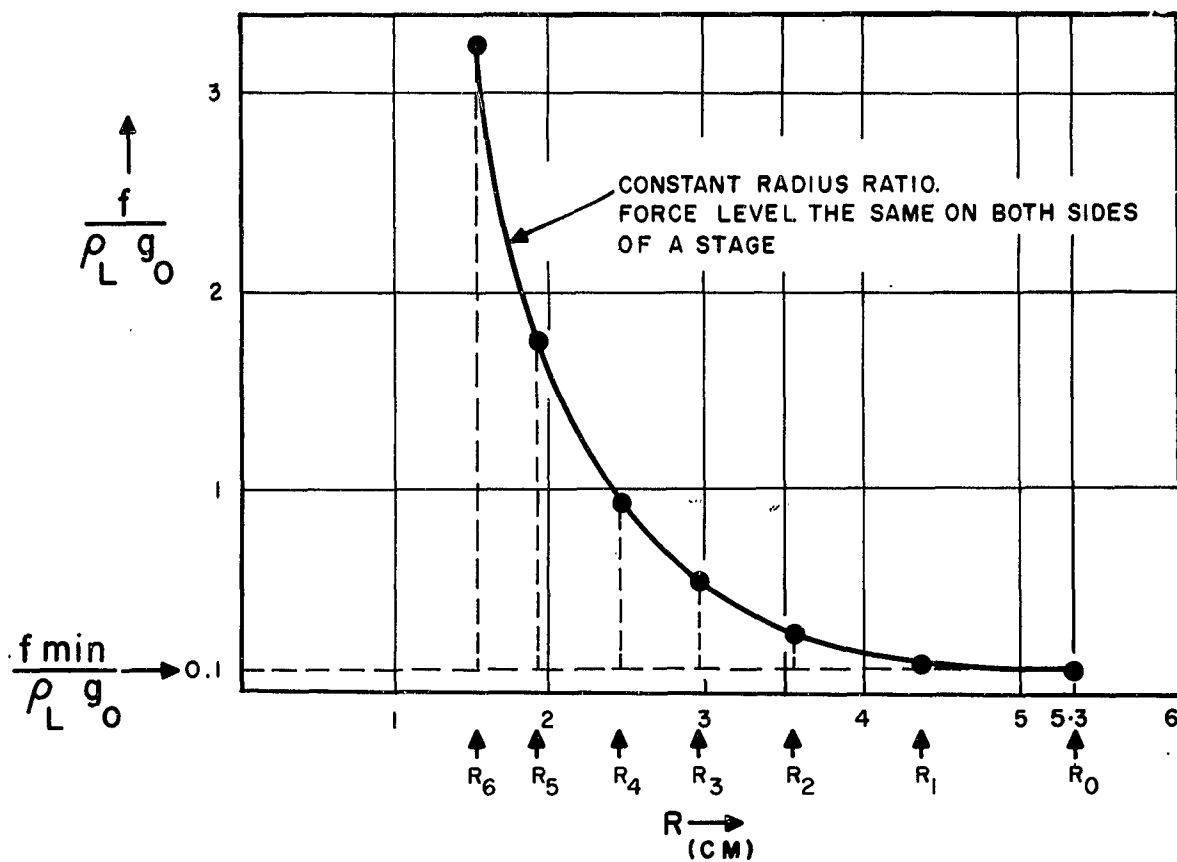


FIGURE 7
 FORCE PROFILES IN A MULTI-STAGE CONTAINER.
 THE CONSTANT RADIUS RATIO CRITERION

MEANS OF CREATING SIMULATED VARIABLE GRAVITY FIELDS
FOR THE STUDY OF FREE CONVECTIVE HEAT TRANSFER

by

David A. Kirk

Directorate of Materials & Processes
Aeronautical Systems Division
Wright-Patterson Air Force Base, Ohio

LIST OF SYMBOLS

Symbols and Their Rationalized MKS Units

English Letters

\vec{a}	acceleration, $\frac{\text{meter}}{\text{sec}^2}$, lt^{-2}
\vec{B}	Magnetic flux density, $\frac{\text{webers}}{\text{meter}^2}$, $\text{mQ}^{-1}\text{t}^{-1}$
C	constant, dimensionless
C_p	specific heat at constant pressure, $\frac{\text{joules}}{\text{Kg} \text{ } ^\circ\text{K}}$, $\text{l}^2 \text{T}^{-1}\text{t}^{-2}$
d	a Characteristic dimension of a system, meters, l
\vec{E}	electric field intensity, $\frac{\text{volts}}{\text{meter}}$, $\text{lmQ}^{-1}\text{t}^{-2}$
\vec{f}	body force, $\frac{\text{newtons}}{\text{meter}^3}$, $\text{l}^{-2}\text{nt}^{-2}$
\vec{g}	net gravitational acceleration, $\frac{\text{meters}}{\text{sec}^2}$, lt^{-2}
\vec{g}^*	equivalent gravitational acceleration produced by the imposed electromagnetic body force, $\frac{\text{meters}}{\text{sec}^2}$, lt^{-2}
\vec{g}_c	the earth's sea level acceleration, $\frac{\text{meters}}{\text{sec}^2}$, lt^{-2}
h	heat transfer coefficient, $\frac{\text{watts}}{\text{meter}^2 \text{ } ^\circ\text{K}}$, $\text{mT}^{-1}\text{t}^{-3}$
I	electric current, amperes or $\frac{\text{coulombs}}{\text{sec}}$, Qt^{-1}
\vec{j}	electric current density, $\frac{\text{amperes}}{\text{meter}^2}$, $\text{l}^{-2}\text{Qt}^{-1}$
\vec{J}_H	heat flux density, $\frac{\text{joules}}{\text{sec meter}^2}$, nt^{-3}
k	thermal conductivity, $\frac{\text{joules}}{\text{sec meter } ^\circ\text{K}}$, $\text{lmT}^{-1}\text{t}^{-3}$
k_{eff}	effective thermal conductivity, $\frac{\text{joules}}{\text{sec meter } ^\circ\text{K}}$, $\text{lmT}^{-1}\text{t}^{-3}$
L	leverage ratio, dimensionless
l	length, meters, l
m	mass, kilograms, m
Nu	Nusselt number = $\frac{k_{\text{eff}}}{k}$, dimensionless
p	pressure, $\frac{\text{newtons}}{\text{meters}}$, $\text{l}^{-1}\text{nt}^{-2}$

LIST OF SYMBOLS (CONT'D)

- Pr Prandtl number, $= \frac{\nu \Delta \rho_T}{k \Delta T}$, dimensionless
- Q electric charge, coulombs, Q
- q electric charge density, $\frac{\text{coulombs}}{\text{meter}^3}$, 1^{-3} Q
- \vec{r} position vector, meters, l
- Ra Rayleigh number $= \frac{g(\rho - \rho_0) d^3 \Delta \rho_T}{\rho \nu k \Delta T}$, dimensionless
- T temperature, degrees Kelvin, T
- t time, seconds, t
- v velocity vector, $\frac{\text{meters}}{\text{sec}}$, 1 t^{-1}

Greek Letters

- α coefficient of volumetric expansion $= \frac{-\partial \rho}{\rho_0 \partial T}$, $^{\circ}\text{K}^{-1}$, T^{-1}
- α_e temperature coefficient for electrical conductivity change $= \frac{-\partial \sigma}{\sigma_0 \partial T}$, $^{\circ}\text{K}^{-1}$, T^{-1}
- θ angle of inclination, radians, dimensionless
- λ heat of vaporization, $\frac{\text{joules}}{\text{kilogram}}$, 1^2 t^{-2}
- ν momentum diffusivity or kinematic viscosity, $\frac{\text{meter}^2}{\text{sec}}$, 1^2 t^{-1}
- ρ mass density, $\frac{\text{kilograms}}{\text{meter}^3}$, 1^{-3} m
- ρ_T heat content per unit volume, $\frac{\text{joules}}{\text{meter}^3}$, 1^{-1} mt^{-2}
- σ electrical conductivity, $\frac{1}{\text{ohm meter}}$, $1^{-3} \text{ m}^{-1} \text{ Q}^2 \text{ t}$
- $\vec{\omega}$ angular velocity, $\frac{\text{radians}}{\text{sec}}$, t^{-1}

Operators in Cartesian Coordinates

Δ difference or change in a function

$$\nabla = \vec{i} \frac{\partial}{\partial x} + \vec{j} \frac{\partial}{\partial y} + \vec{k} \frac{\partial}{\partial z}$$

$$\nabla^2 = \frac{\partial^2}{\partial x^2} + \frac{\partial^2}{\partial y^2} + \frac{\partial^2}{\partial z^2}$$

MEANS OF CREATING SIMULATED VARIABLE GRAVITY FIELDS FOR
THE STUDY OF FREE CONVECTIVE HEAT TRANSFER

by D. A. Kirk

INTRODUCTION

Present equations for predicting the rate of heat transfer by film boiling, film condensation, and single phase free convection assume that the major portion of the transport occurs by mass or fluid motion. Density changes in a gravitational field cause such motion, while viscous and inertia forces tend to inhibit this motion. Previous experimental investigators have succeeded in widely varying all parameters, except gravity, which are known functions in the various heat transfer equations. To assure applicable rate equations for extraterrestrial heat transfer problems, the effect of gravity must be experimentally verified. This paper briefly presents the theoretical reason why gravity has a predominating influence on heat transferred by the three types of free convection, the analytical relations presently used for predicting the rate of heat transfer, and an analysis of five methods for simulating variable gravity conditions.

THEORY AND PRESENT CORRELATING METHODS

Previous investigators have assumed in their hydrodynamic and heat flow equations that variations in density of a phase of the medium affect only the gravity (potential) term. Under conditions of a weak gravity field this assumption could prove to be incorrect. Since approximate solutions to these equations require additional simplification, such as elimination of non-linear terms, it seems unlikely that additional variations in density will be accounted for in the near future. An experimental investigation could be conducted to determine the interval for which present theory is applicable, if some means were devised to reduce the equivalent gravity (potential) term.

According to Archimedes' law, a buoyancy force, \vec{f}_g , will act on a fluid of density, ρ , in a medium of mean density, ρ_0 ;

$$\vec{f}_g = \vec{g} (\rho - \rho_0) \quad (1)$$

where \vec{g} is the gravitational field at the point in question. Considering only the variations in mass density as they modify gravity, the Boussinesq modification of the Navier-Stokes equation is written as,

$$\rho_0 \frac{\partial \vec{v}}{\partial t} + \rho_0 \vec{v} \cdot \nabla \vec{v} = \rho_0 \nu \nabla^2 \vec{v} - \nabla p + \rho_0 \vec{g} \quad (2)$$

where \vec{v} - velocity, ν - kinematic viscosity, and p - pressure. With no internal heat generation and constant density the Biot-Fourier law states that the rate of heat accumulation, $\frac{\partial \rho_r}{\partial t}$, must equal the conduction inward, $k \nabla^2 T$, less that carried out by convection, $\vec{v} \cdot \nabla \rho_r$

$$\frac{\partial \rho_r}{\partial t} = k \nabla^2 T - \vec{v} \cdot \nabla \rho_r \quad (3)$$

where ρ_r , k , T are the heat content per unit volume, thermal conductivity, and temperature, respectively. Equations (1-3) form the present theoretical basis used in developing analytical relations for predicting single and two phase free convection heat transfer.

The dimensionless number presently used in final heat transfer relations may be found by considering the ratio of buoyancy force to viscous force and using the convective velocity of equation (3). Neglecting the heat accumulation term in equation (3) and for relatively small disturbances, the convective velocity \vec{v} becomes

$$v = \frac{k (\Delta T/d^2)}{\Delta \rho_r/d} = \frac{k \Delta T}{d \Delta \rho_r} \quad (4)$$

as far as orders of magnitude are concerned, where d is a characteristic dimension of the system. Substituting this velocity into the viscous term the force becomes

$$f_v \propto \frac{\rho_v \Delta v}{d^2} \propto \frac{\rho_v k \Delta T}{d^3 \Delta \rho_r} \quad (5)$$

by the same line of reasoning. The criterion for convective heat transport is arrived at by dividing the buoyance force of equation (1) by the above force, thus

$$\frac{f_g}{f_v} \propto \frac{g (\rho - \rho_0) d^3 \Delta \rho_r}{\rho_v k \Delta T} = Ra \quad (6)$$

where Ra is defined as the Rayleigh number. For the processes of film boiling or film condensation the heat transferred per unit volume, $\Delta \rho_r$, is the mass density times latent heat of vaporization and the physical properties refer to the phase of greatest resistance to transport, while for single phase thermal convection the heat transfer is the product of the volumetric specific heat, ρC_p , and the temperature change, ΔT .

The first analytical solution of the convection equations was found by Lorenze in 1881 (ref 9, p 443) and later improved by Schmidt and Beckman in 1930 (ref 9, pp 444-450) for the rate of heat transport from a vertical surface to a colder gas. Rayleigh (ref 24) was the first to analytically predict the onset of convective motion for a horizontal layer of fluid when heated from below and, later Low (ref 13) and Reid and Harris (ref 25) have extended this theory to include different boundary conditions. Malkus (ref 14) has made an important contribution to our understanding of the thermal turbulence spectrum by time averaging the second order terms involving the products of fluctuations in equations (2-3).

Nusselt (ref 9, p 661) in 1916 was the first to develop a theoretical relation for predicting the rate of film condensation. Realizing that an analogy exists between film boiling and film condensation, Bromley (ref 2) arrived at a rate equation for film boiling. Bromley's equation is exactly the same as Nusselt's equation, except for the physical parameters which refer to the blanketing vapor rather than the condensate film.

Past experimental correlations; Bosworth, (ref 1) Eckert and Drake (ref 6), Jacob (ref 9), and McAdams (ref 16), for rate of heat transfer by film boiling, film condensation, and single phase free convection have been based largely on the general type equation developed by Lorenze and Nusselt. For the viscous limiting case these equations can be reduced to one general form as given by

$$Nu = C_1 (Ra)^n \quad (7)$$

where

$$Nu = \frac{hd}{k} = \frac{k_{eff}}{k} = \text{Nusselt number}$$

C_1 = constant depending on the geometry and on the type of free convection.

n = constant which is 1/4 for laminar flow and 1/3 for turbulent flow.

h = the heat transfer coefficient or the heat flux density per unit temperature difference.

k_{eff} = effective thermal conductivity (see ref 9, p 508 and pp 534-539).

For most fluids the rate of free convective heat transfer is limited to the effects of viscosity and the Rayleigh criterion is valid.

Free convective heat transfer in liquid metals requires the use of a modified equation, since these fluids have extremely high thermal conductivities and low viscosities. When the viscous drag can be neglected, the Euler non-viscous flow equation applies, thus at steady state

$$\vec{f}_p = \nabla p = \rho \vec{v} \cdot \nabla \vec{v} \propto \rho \frac{v^2}{d} \quad (8)$$

where Δp = pressure gradient.

Substituting equation (4) for the velocity

$$\vec{f}_p \propto \frac{\rho k^2 \Delta T^2}{d^3 \Delta \rho_T} \quad (9)$$

The inviscid criterion for thermal convection becomes

$$\frac{f_g}{f_p} \propto \frac{g (\rho - \rho_0) d^3 \Delta T}{k^2 \Delta \rho_T} = (Pr) (Ra) \quad (10)$$

where the Prandtl number, Pr , has been defined as the ratio of viscous diffusivity, ν , to thermal diffusivity, $\frac{k \Delta T}{\Delta \rho_T}$. LeFevre (ref 12) has derived the inviscid, single phase, transport equation.

$$Nu = C_2 (Ra Pr)^n \quad (11)$$

which is analogous to equation (7). Sparrow and Gregg (ref 27) have provided the exact (numerical) solutions in the Prandtl number range of the liquid metals where both non-viscous and viscous forces are important. Over the Prandtl number range of 0.003 to 0.73 covered by the exact solutions of Sparrow and Gregg (ref 27) and Schmidt and Beckman (ref 9, P 449), the results can be expressed by the approximate form

$$Nu = 0.562 (Ra)^{1/4} (Pr)^{0.187} \quad (12)$$

for the laminar flow over a vertical plane. Equation (12) agrees within 5 percent of these exact solutions.

Single equations have been developed semi-empirically which are applicable to liquids over an extremely wide range of Prandtl numbers. By assuming a cubic equation for the laminar velocity profile over a vertical plate Eckert and Drake (ref 6, pp 313-316) derived heat transfer equation

$$Nu = 0.508 \left[\frac{Pr}{0.952 + Pr} \right]^{1/4} (Ra)^{1/4} \quad (13)$$

which agrees to within 10 percent of the exact solutions of Ostrach (ref 22) over the Prandtl number range of 0.01 to 1000. For fully established turbulent convection between two horizontal plates Globe and Dropkin (ref 7) found the empirical equation

$$Nu = 0.069 (Ra)^{1/3} (Pr)^{0.074} \quad (14)$$

correlated within the experimental deviation of about 25 percent and over the Prandtl number range of 0.02 to 8750.

Nakagawa (ref 19) has derived the equation for the rate of convective heat transfer through a horizontal layer of fluid bound between two constant temperature surfaces. In the region of marginal stability Nakagawa's equation is

$$Nu = 1 + C_3 \frac{(Ra - Ra_c)}{Ra} \quad (15)$$

where C_3 and Ra_c are constants which are known functions of the boundary conditions. For Rayleigh numbers less than the critical value Ra_c the Nusselt number is defined as unity. Nakagawa and Goroff (ref 21) found that departure from this equation was significant when the Rayleigh number was very much above the critical value.

Considering only the case of thermal convection in a horizontal layer of fluid, one can now choose four types of relations typified by equations (7), (11), (12), and (15) to make a correlation of experiments. Which type of equation, if any, would best predict thermal convection in a reduced gravity environment is a question left to be answered. Some selectivity is possible if the Prandtl number range is restricted and it is known whether the flow will be turbulent or laminar.

METHODS CONSIDERED FOR CREATING VARIABLE GRAVITY CONDITIONS

In earth bound free convection experiments we are only able to vary naturally the buoyancy body force by changes in mass density, since the earth's gravitational acceleration is relatively constant over a wide change in altitude. An additional acceleration may be made to vary the net acceleration on a fluid mass, or a linear temperature dependent body force may be made to vary directly the net buoyancy force. By superimposing one of these two types of action on a free convection heat transfer experiment at ground level, the effect of gravity can be studied. Three acceleration methods and two body force methods have been analyzed for the study of single phase free convection heat transfer.

Centrifugal Actions

As shown in figure 1 the common centrifuge may be used to create a net acceleration normal to the plane P. For any fixed geometry the angle of inclination is determined from the angular velocity ω . In order to have a uniform acceleration through out the fluid mass, the dimensions of the test cell must be quite small compared to radius of rotation, r ; the error in assuming a constant radius can then be neglected. The resultant acceleration, a , can be varied from the ground level value, \vec{g}_c , to very large values depending on the capabilities of the centrifuge.

A large, vibration free, centrifuge is available at the Aerospace Medical Division, ASD. The main objection to a centrifuge experiment is that the important range of less than one ground level gravity can not be covered. Costello and Tuthill (ref 5) have used this method to investigate pool boiling over the range of 20 to 45 times ground level gravity, while Merti and Clark (ref 15) have investigated the range from 1 to 20.

Degrees of Free Fall

By allowing a heat transfer test cell to fall freely, and/or partially so, the effect of simulated variable gravity conditions can be studied. An acceleration, a , may be imparted to a mass, m , of the test cell apparatus when coupled to another mass, m_1 , through a pulley of leverage, L , as shown in figure 2. Neglecting pulley inertia, pulley friction, and air resistance the acceleration is

$$\vec{a} = \frac{(L m_1 - m)}{(L^2 m_1 + m)} \vec{g}_c \quad (16)$$

Thus, the acceleration can be made to vary continuously from $-\vec{g}_c$, for free fall to $\frac{\vec{g}}{L}$, when, $m_1 \gg m$.

The primary objection to this method is the short time available for an experiment. Assuming a travel distance of 30 feet and an initial velocity of equal magnitude but of opposite direction to the final velocity, the total time is 2.73 seconds for a zero gravity experiment. Usiskin and Siegel (ref 28) have performed boiling experiments lasting 0.7 seconds using complete free fall, and performed longer tests using less acceleration.

Airplane Flight Programs

To obtain a zero gravity flight a vertical parabolic path, generally called a Kiplarian trajectory, must be followed. An estimate of the time for such a zero gravity flight may be found by assuming an initial velocity, v_1 , of 400 mph inclined 50° and a final velocity, v_2 , of 600 mph declined 50° , thus

$$t = \frac{1}{g_c} (v_1 \sin \theta_1 + v_2 \sin \theta_2) = 34.9 \text{ sec} \quad (17)$$

Flights between zero and ground level gravity will proportionately increase this time. Important trends in rate data can be obtained, but, unless the system response to reaching equilibrium is at least an order of magnitude less than this time, little weight can be given to the coefficients of heat transfer obtained.

Hedgepeth (ref 8) was able to reduce extraneous plane vibrations and windage by allowing the test apparatus to free float; however, this reduced the test period available from 30 to 7 seconds. Motion pictures were taken of the flow pattern through the glass walls of the apparatus. Hedgepeth and Zara have continued the work with another apparatus instrumented to yield heat transfer rate data.

Electrostatic

According to Coulomb's law, the electrostatic body force is equal to the product of the net charge density and the electric field strength. If each particle of fluid were charged equally and the charge density was only a linear function of temperature, then a buoyancy force would create convection motion. However, obtaining a uniformly charged fluid would be quite difficult and in addition charge density tends to accumulate at the bounding surface. Unless this problem is solved, the electrostatic method appears quite unfeasible.

Electromagnetic

Ampere's Force law predicts that a current density, j , will react with the transverse

component of the magnetic field, \vec{B} , to give a body force normal to the current - magnetic field plane, thus

$$\vec{f}_{em} = \vec{j} \times \vec{B} \quad (18)$$

An impressed electromagnetic body force, $\vec{j}_{im} \times \vec{B}$, can be made to act in the plane of the gravitational body force, ρg . A portion of a fluid will experience a buoyancy force, ∂f , when its temperature, T , is greater than the mean value T_0 by ∂T ; thus,

$$\partial \vec{f} = \partial(\rho g) + \partial(\vec{j}_{im} \times \vec{B}) \quad (19)$$

which is Archimedes' buoyancy force plus an electromagnetic buoyancy force.

The only temperature dependent terms in equation (19) are the mass density, ρ , and the electric current density, j_{im} , assuming the media is a liquid metal of unit relative permeability. Applying Ohm's law and carrying out the differentiation, equation (19) becomes

$$\frac{\partial \vec{f}}{\partial T} = -\alpha \rho_0 \vec{g} - \alpha_e (\vec{j}_{im} \times \vec{B}) \quad (20)$$

where

$$\alpha = \frac{-\partial \rho}{\rho_0 \partial T} = \text{coefficient of thermal expansion}$$

$$\alpha_e = \frac{-\partial \sigma}{\sigma \partial T} = \text{temperature coefficient for electrical conductivity change.}$$

An equivalent gravitational field, \vec{g}^* , created by the electromagnetic buoyancy force may be defined by replacing the last term of equation (20) with its equivalent buoyancy, $\alpha \rho_0 \vec{g}^*$, thus

$$\vec{g}^* / g_c = \frac{\alpha_e (\vec{j}_{im} \times \vec{B})}{\alpha \rho_0 g_c} \quad (21)$$

For the experiment planned by the author (ref 10) the apparatus constructed will operate over the range from -13.6 to 15.6 times ground level gravity using a sodium - potassium eutectic alloy. Figure 3 shows the schematic of this principle for studying the effect of gravity on single phase free convection heat transfer through a horizontal layer of fluid. This principle can only be applied to single phase free convection, since electric conduction occurs quite differently in the vapor and liquid state for metals.

The electromagnetic method of producing simulated variable gravity fields does have several secondary effects which must be taken into account. The author (ref 10) has made the following conclusions concerning these effects:

- 1 An electrically conducting fluid tends to carry magnetic flux lines with the fluid, (figure 4). For the convective velocities and electrical conductivities expected, this distortion can be neglected.

- 2 For electrically conducting fluids, motion across a magnetic field produces a magnetic "viscosity" effect (figure 4). Chandrasekhar (refs 3,4) and Nakagawa (ref 20) have developed theory and Nakagawa (refs 17,18) and Lehnert and Little (ref 11) have performed experimental investigations concerning thermal convection in a magnetic field. A significant magnetic drag is expected, but may be taken into account independently of the impressed electromagnetic buoyancy force.
- 3 The impressed electric current produces a circular magnetic field causing a variation in the impressed electromagnetic body force (figure 5). This circular magnetic field causes only 0.1 percent variation and can be neglected.
- 4 Joule heating will occur within the test fluid when the impressed electric current is flowing. Already, Ostrach (ref 23) and Woodrow (ref 29) have theoretically considered the case of heat generating fluids in free convective heat transfer. A significant distortion of the temperature distribution is expected, but this may be taken into account independently of the impressed electromagnetic buoyancy force..
- 5 A total of eight galvanomagnetic and thermomagnetic effects were analyzed and were estimated to cause extremely small errors. The better known Hall, Ettingshausen, and Nernst effects are shown schematically in figures 6,7, and 8 respectively.

A properly planned experiment is, therefore, feasible and the probability of determining the effect of gravity by the electromagnetic method is very favorable. Progress to date has consisted of normal convection experiments, determination of the inhibition by the magnetic field, spectrum of temperature fluctuations, and imposing the electromagnetic body force.

CONCLUSIONS

To provide significant heat transfer rate data under simulated variable gravity conditions, a method should provide sufficient test time to yield equilibrium rate data, have minimum assumptions and complicating factors, cover 0 to 10 times the ground level value, and not require an extended development effort. Actually none of the methods analyzed completely fulfill all these requirements, (see table 1). The electromagnetic method was selected as the most favorable, because an experimental program could be undertaken to ascertain the two complicating factors of joule heating and magnetic drag. Elimination of the disadvantages encountered with the other four methods does not appear feasible.

LIST OF REFERENCES

1. Bosworth, R.C.L. 1952 Heat Transport Phenomena, John Wiley & Sons, Inc., N.Y., N.Y.
2. Bromley, L.A. 1950 "Heat Transfer in Stable Film Boiling", Chem. Eng. Prog., v 46, pp 221-27.
3. Chandrasekhar, S. 1952 "On the Inhibition of Convection by A Magnetic Field." Lond., Eding., Dublin Phil. Mag., 7th ser., v 43, pp 501-32.
4. Chandrasekhar, S. 1954 "On the Inhibition of Convection by a Magnetic Field," II, Lond., Eding., Dublin Phil. Mag. 7th ser., v 45, pp 1177-91.

LIST OF REFERENCES (CONT'D)

5. Costello, C.P. and Tuthill, W.E. 1960 "Effects of Acceleration on Nucleate Pool Boiling," presented at the 1960 Mexico City Am. Inst. Chem Engr. meeting.
6. Eckert, E.R.G. and Drake, R.M. 1959 Heat and Mass Transfer, 2nd ed, McGraw-Hill Book Company, Inc.
7. Globe, S. and Dropkin, D. 1959 "Natural Convection on Heat Transfer in Liquids Confined by Two Horizontal Plates and Heated from Below," Trans. Am. Soc. Mech. Eng., Ser. C. v 81, pp 24-28.
8. Hedgepath, L.M. 1961 "Zero Gravity Boiling and Condensing," Progress in Astronautics and Rocketry, vol III, Energy Conversion for Space Power, Academic Press, N.Y., N.Y., pp 593-611.
9. Jakob, M. 1949 Heat Transfer - Volume I, John Wiley & Sons, Inc., N.Y., N.Y.
10. Kirk, D.A. 1960 "The Effect of Gravity on Free Convection Heat Transfer - Part I: On the Feasibility of Using an Electromagnetic Body Force," WADD TR 60-303, Wright Air Development Division, Dayton, Ohio.
11. Lehnert, B. and Little, N.C. 1957 "Experiments on the Effect of Inhomogeneity and Obliquity of a Magnetic Field in Inhibiting Convection," Tellus, v 9, pp 97-103.
12. LeFevre, D.J. 1956 "Laminar Free Convection from a Vertical Plane Surface." Heat 113, Mechanical Engineering Research Laboratory, Great Britain.
13. Low, A.R. 1929 "On the Criterion of Stability of a Layer of Viscous Fluid Heated from Below," Proc. Roy. Soc., Ser. A., v 125, pp 180-195.
14. Malkus, W.V.R. 1954 "The Heat Transport and Spectrum of Thermal Turbulence," Proc. Roy. Soc., Ser. A., v 225, pp 196-212.
15. Merti, H. Jr. and Clark, J.A. 1961 "Pool Boiling in an Accelerating System," ASME Trans., v 83C, pp 233-242.
16. McAdams, W.H. 1954 Heat Transmission, 3rd ed, Mc Graw-Hill Book Co., N.Y., N.Y.
17. Nakagawa, Y. 1955 "An Experiment on the Inhibition of Thermal Convection by a Magnetic Field" Nature, Lond., v 175 pp 417-419.
18. Nakagawa, Y. 1957 "Experiments on the Inhibition of Thermal Convection by a Magnetic Field," Proc. Roy. Soc., Ser. A. v 240, pp 108-13.
19. Nakagawa, Y. 1960 "The Heat Transport by Convection," Phys. Fluids, v 3, 83-86.
20. Nakagawa, Y. 1960 "Heat Transport by Convection in Presence of an Impressed Magnetic Field," Phys. Fluids, v 3, pp 87-93.

LIST OF REFERENCES

21. Nakagawa, Y. and Goroff, I.R. 1961 "Experiments on Heat Transport by Convection in the Presence of a Magnetic Field," Phys. Fluids, v 4, pp 344-54.
22. Ostrach, Simon 1953 "An Analysis of Laminar Free - Convection Flow and Heat Transfer about Flat Plate Parallel to the Direction of the Generating Body Force," NACA Rep. 1111, Lewis Research Center, Cleveland, Ohio
23. Ostrach, Simon 1955 "Unstable Convection in Vertical Channels with Heating from Below, Including Effects of Heat Sources and Frictional Heating," NACA Tech Note 3458, Lewis-Research Center, Cleveland, Ohio.
24. Rayleigh, Lord 1916 "On Convection Currents in a Horizontal Layer of Fluid, when the Higher Temperature is on the Under Side," Lond., Eding., Dublin. Phil. Mag., 6th ser., v 32, pp 529-546.
25. Reid, W. H. and Harris, D.L. 1958 "Some Further Results on the Benard Problem," Phys. Fluids, v 1, pp 102-10.
26. Siegel, R. and Usiskin, C. 1959 "A Photographic Study of Boiling in the Absence of Gravity," Trans. Am. Soc. Mech. Engr., ser. C, v, 81, pp 230-36
27. Sparrow, E.M. and Gregg, J.L. 1959 "Details of Exact Low Prandtl Number Boundary-Layer Solutions for Forced and for Free Convection," NASA Memo 2-27-59E, Lewis Research Center, Cleveland, Ohio
28. Usiskin, C.M. and Siegel, R. 1961 "An Experimental Study of Boiling in Reduced and Zero Gravity Fields," ASME Trans., v 83c, pp 243-51
29. Woodrow, J. 1956 "Free Convection in Heat Generating Fluid (Laminar Flow), Part 2, Negative Temperature Gradient," A.E.R.E. R/R 1981, Atomic Energy Research Establishment, Harwell, Berk, (Great Britain).

TABLE I
DISADVANTAGES OF THE FIVE METHODS ANALYZED

Centrifugal Actions	Degrees of Free Fall	Airplane Flight Programs	Electrostatic	Electromagnetic
(3)	(1)	(1)	(2) (4)	(2)

Where disadvantages are:

- (1) insufficient testing time to yield equilibrium rate data
- (2) important assumptions and complicating factors
- (3) cannot perform tests at reduced gravities
- (4) cannot be constructed without an extended development effort

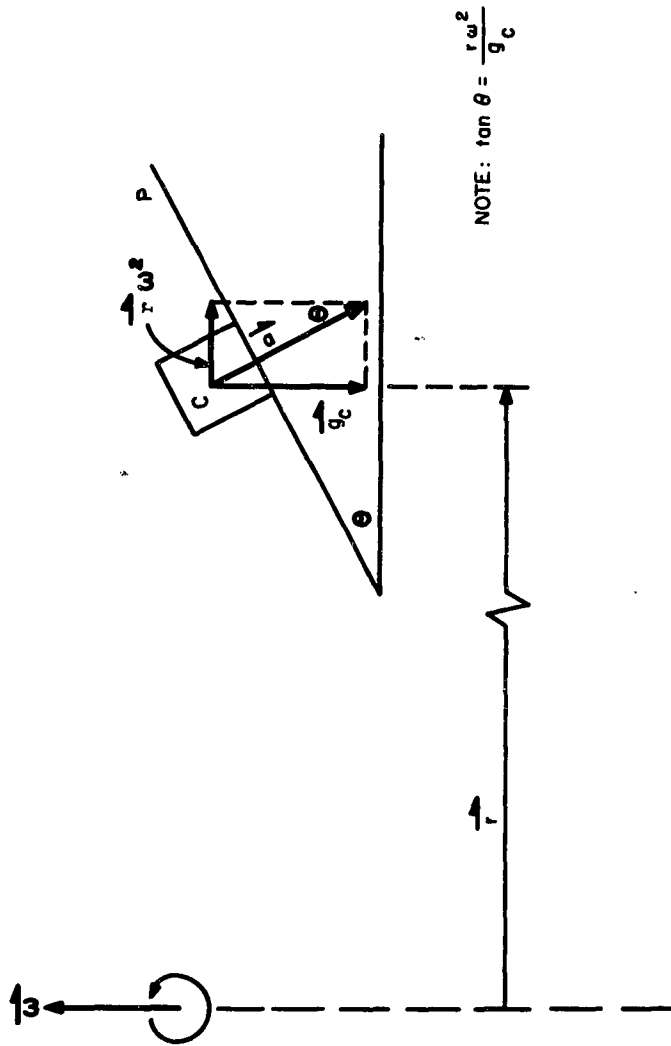


Figure 1. Schematic of Centrifuge Arrangement

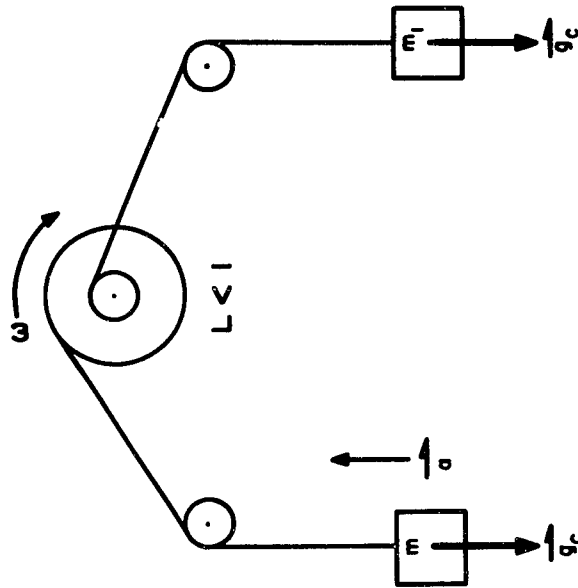
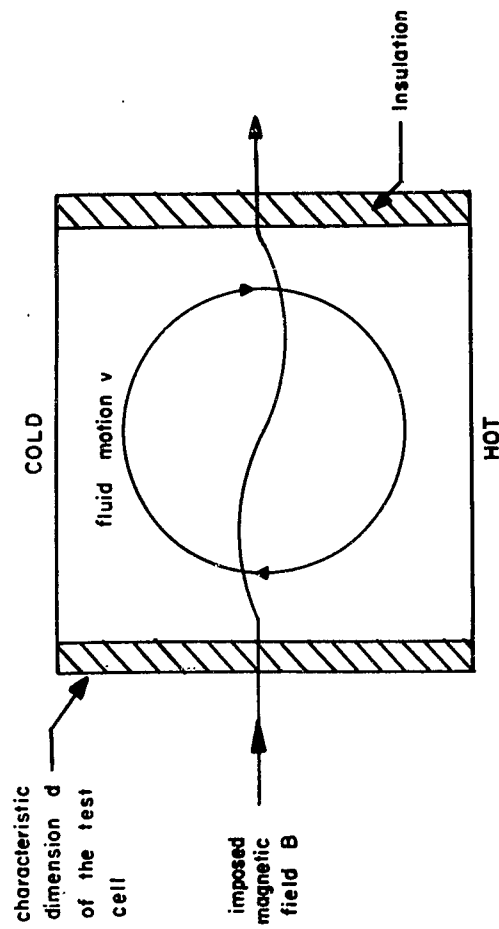
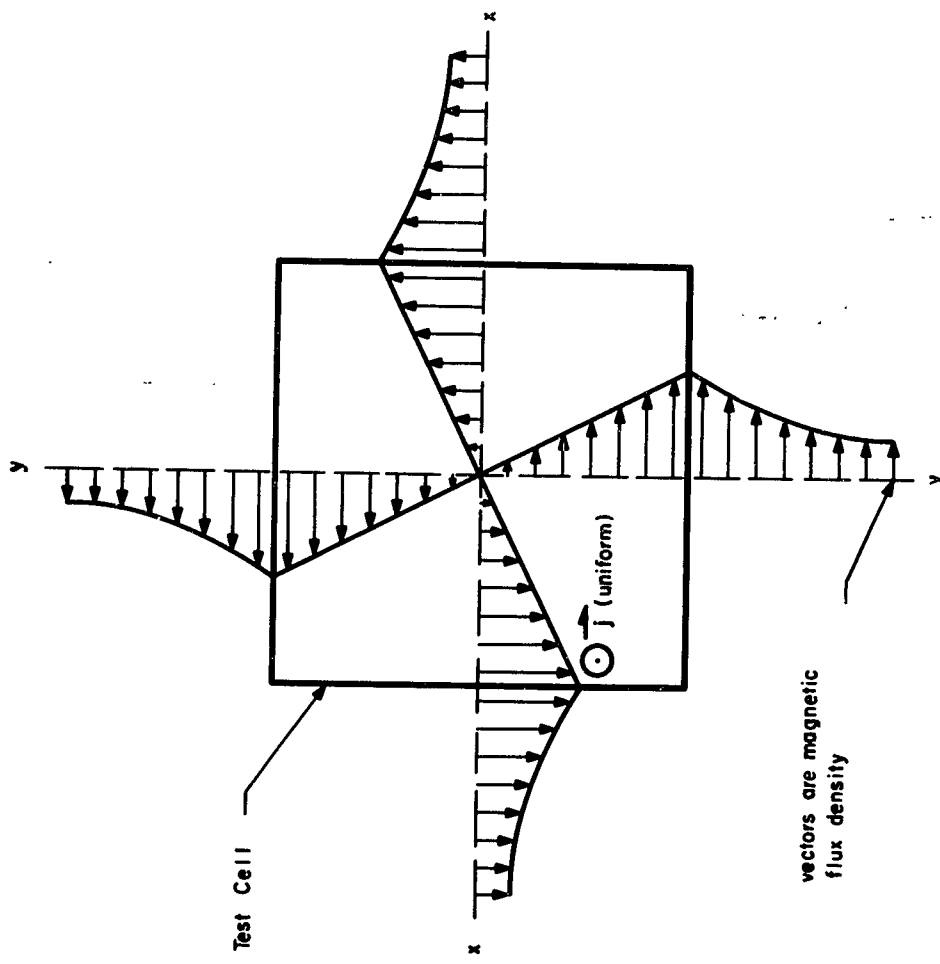


Figure 2. Schematic for Obtaining Various Degrees of Free Fall Using a Pulley Arrangement



field distortion proportional to $\sigma a v$
 field diffusion drag proportional to $\sigma B^2 v$

Figure 4. Reactions to Motion of an Electrically Conducting Fluid in a Magnetic Field



vectors are magnetic flux density

Figure 5. x and y Axis Magnetic Field Distribution Caused by the Impressed Current

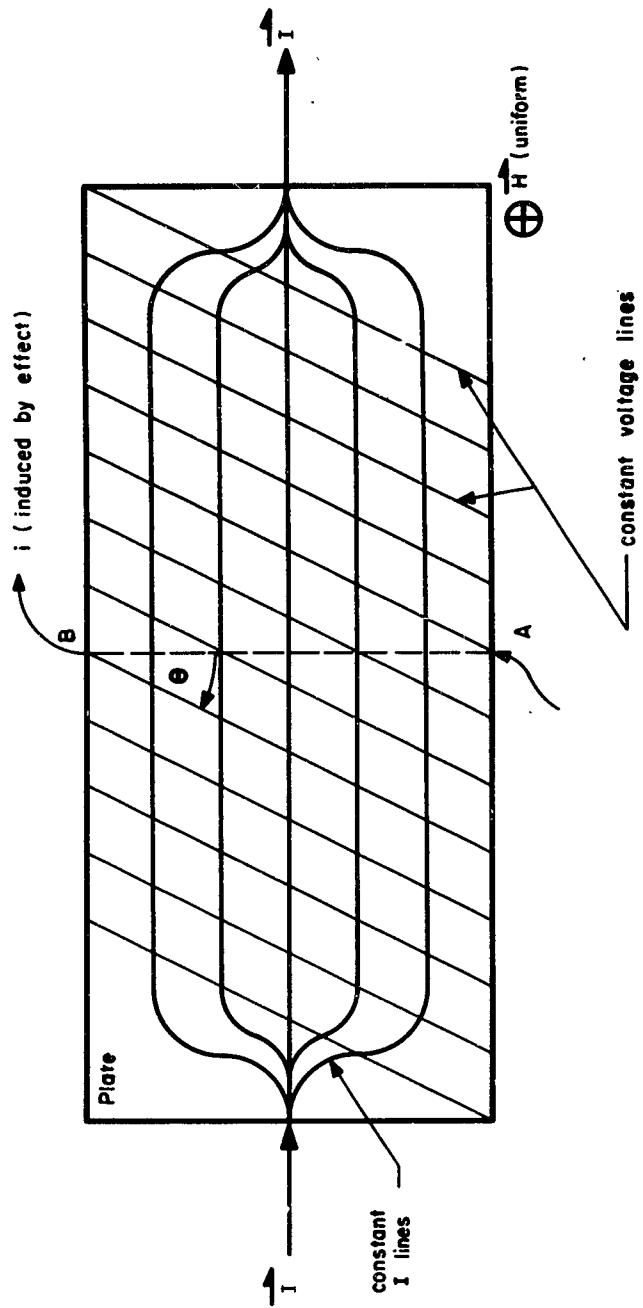


Figure 6. Hall Effect for a Negative Coefficient

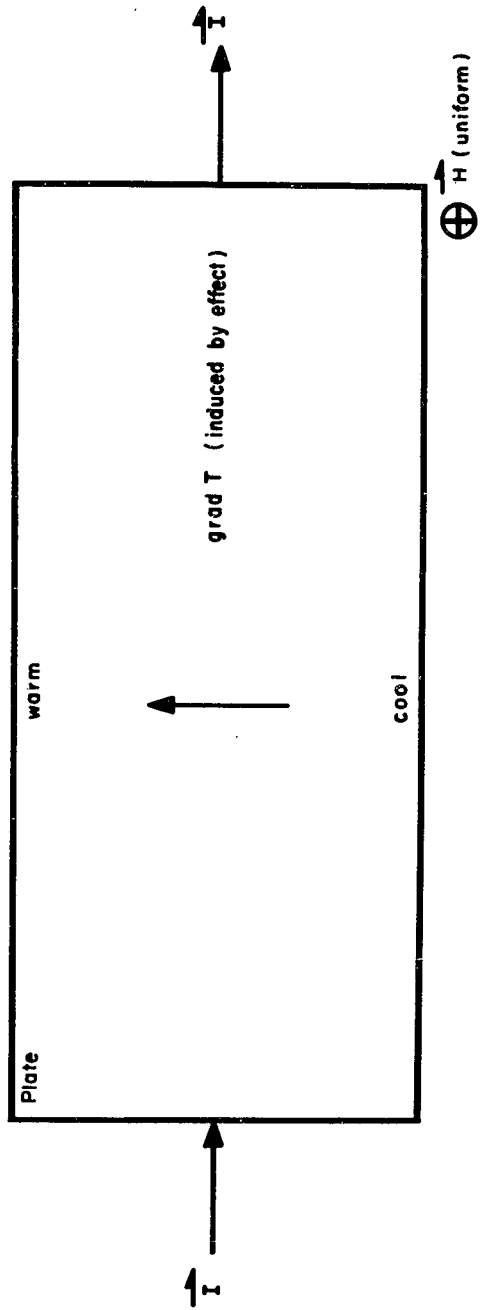


Figure 7. Ettingshausen Effect for a Positive Coefficient

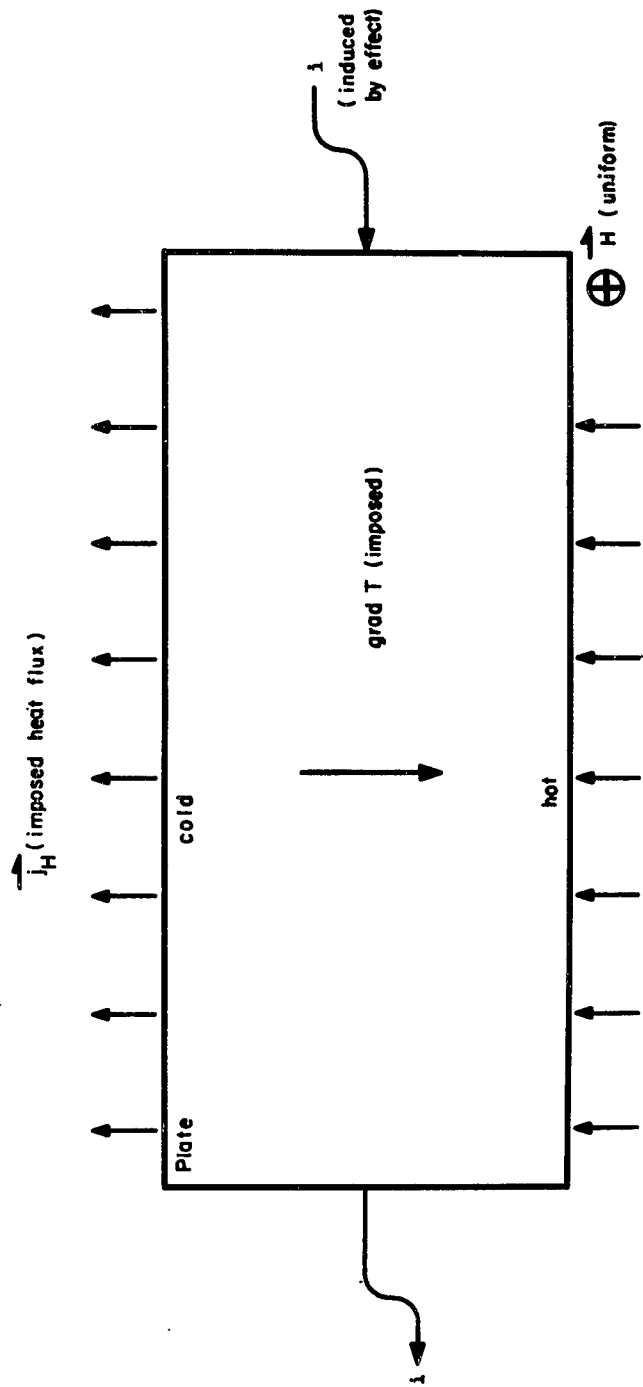


Figure 8. Nernst Effect for a Positive Coefficient

ANALYTICAL AND EXPERIMENTAL
INVESTIGATION OF
SELF-THERMOSTATIC EFFECTS

by

T. M. Olcott

M. Ratner

Lockheed Missiles and Space Company
Palo Alto, California

ASD-TDR-63-260

ANALYTICAL AND EXPERIMENTAL INVESTIGATION OF SELF-THERMOSTATIC EFFECTS

by

T. M. Olcott and M. Ratner

INTRODUCTION

Spacecraft thermal control can be accomplished thru either active or passive means. Passive systems are preferred being the simpler. The internal temperatures of passive systems are dependent upon the fixed relations between vehicle configuration, internal power dissipation, vehicle surface conditions, and orbit geometry. If the variations in internal power or the changes in orbital flux are large, then temperature excursions will be correspondingly large. Thus to insure that temperatures in the vehicle will stay within satisfactory limits it is sometimes necessary to restrict the variations in either orbit parameters or internal power dissipation. To do this, involves close scheduling at launch time, as well as possible unnecessary use of electrical power while in orbit.

Self-thermostatic effects can offer a solution to some of these problems. These effects consist of either variations in surface properties, or thermal resistance stimulated by changes in the temperature of the item to be controlled. These variations act in such a way as to increase the heat rejection rate when the vehicle temperature is rising, and to decrease the heat removal rate when the temperature is decreasing. Such variations can be either active or passive in nature. The self-thermostatic devices discussed in this paper are assumed to be non power consuming.

Temperature dependent surface properties occur in a variety of materials; and though not large in effect some of these materials are useful. Mechanical devices can also be used to bring about self-thermostatic changes in surface characteristics by varying the degree of utilization of two surfaces with different finishes. These devices produce greater effects, but entail added equipment and complexity. Thermal conductivity that varies with temperature is exhibited by many materials. However, the effect, in general, is small in comparison to the requirements for self-thermostatic control. Devices can also be used to produce large resistance changes but again the problem of weight and reliability is involved.

It is the purpose of this paper to review some of these various effects and to present an analysis of some of the requirements for self-thermostatic surfaces. An experimental investigation of a variable resistance device is then described.

A REVIEW OF SELF-THERMOSTATIC EFFECTS

Changes in Surface Properties

While little can be said about changes in solar absorptance with temperature, two techniques have been developed that can produce temperature control through changes in emittance. Friedman and Cox of the Naval Research Laboratory (Ref. 1)

have advanced the concept of utilizing absorption edge phenomena in semiconductors; while Hass et al (Ref. 2) have used the narrow band absorption characteristics of silicon monoxide for control of emittance with temperature.

Absorption edge Absorption edge characteristics are found in semiconductors, such as the infra-red type, for which a sharp transition in the spectral absorption characteristics exist in the neighborhood of 10 microns. Such semiconductors generally show a shift to longer wave lengths in the absorption edge location with increasing temperature of the order of 0.06 microns /°F. The total emittance represented by equation (1),

$$\epsilon_T = \frac{\int_0^{\infty} \epsilon_{(\lambda, T)} P_{(\lambda, T)} d\lambda}{\int_0^{\infty} P_{(\lambda, T)} d\lambda} \quad (1)$$

is a function of black body spectral distribution, $P_{(\lambda, T)}$, and the spectral emittance, $\epsilon_{(\lambda, T)}$, characteristics. Figure 1 presents an idealized curve of spectral emittance versus wave length for a surface exhibiting absorption edge characteristics, at a temperature T' and a higher temperature T . Also shown on this Figure are black body spectral distributions indicating a shift to shorter wave lengths with increasing temperature. According to Wien's displacement law this shift is of the order of 0.05 microns/°F at 10 microns. It can be seen from inspection of equation 1, and noting the shifts in $\epsilon_{(\lambda, T)}$ and $P_{(\lambda, T)}$ with temperature, that for a surface exhibiting absorption edge characteristics total emittance rises with increasing temperature.

Figure 2 shows a plot of total emittance versus temperature for several cases where the absorption edge location (λ_0) has different values. Considering a material with an absorption edge at 9 microns, the total emittance at 67°F would be 0.22 (point A on Figure 2). If the absorption edge location is unchanged with temperature the emittance would be 0.32 at 139°F (point B on Figure 2). Assuming that the material has a shift in the location of the absorption edge, of 0.06 microns/°F temperature change, the total emittance would be 0.60 at 139°F, and the absorption edge would occur at 15 microns (point C on Figure 2). Thus with no shift in the absorption edge there is a change in total emittance of 45% in 100°F; with the temperature shift present there is a 170% change in total emittance.

Narrow band absorption Another type of spectral response that is useful is the type first considered by Hass, Drummer and Schach (Ref. 2). It is found in materials with a pronounced absorption peak in the neighborhood of 10 microns. The idealization of this response is shown in Figure 3. This characteristic is also found in semiconductors and is called plasma resonance absorption. The absorption peak can be located in the neighborhood of 10 microns by suitable doping of the semiconductor. Piper and Marple (Ref. 3) have produced absorption edge peaks at 8 to 11 microns in cadmium sulphide by doping with gallium. Spitzer et al (Ref. 4) were able to locate peaks in germanium from 5 to 15 microns with heavy doping with arsenic, phosphorous, and antimony. The extent of temperature broadening has not been established for plasma resonance of this type.

When the narrow band absorption peak is located somewhat below 10 microns, at room temperature, the Wien shift of the black body spectral distribution can cause an increase in the total emittance with temperature at temperatures of practical interest. This situation is shown in Figure 3 for various peaks, each 2 microns in width with λ_0 as the center wave length. It can be seen that the rate of change of emittance with temperature is very sensitive to the location of the peak. The degree of change in total emittance with temperature appears smaller with this effect than with absorption edges.

Color changes Research into coatings whose solar absorptance changes reversibly with incident radiation and temperature is being pursued. For changes in α_s one is concerned with materials that exhibit bleaching effects with temperature, or changes of color with changes in intensity of incident solar radiation. Work on the titanates of barium and calcium show bleaching effects at 248°F and 302°F respectively. Some organics and inorganic compounds exhibit phototropism (changes of color with incident radiation) or thermotropism (changes of color with temperature). However none of these effects show immediate promise for thermal control.

Mechanical devices To date the majority of the work done on mechanical devices that produce changes in surface properties has been on the use of shutters. These shutters are actuated by bimetallic or temperature sensitive fluid filled devices. Shutters are generally designed in such a way as to produce a fairly significant change in α_s/ϵ between their open and closed

position. The position of the shutter is determined by the temperature of the actuating device. This device can sense either the shutter surface temperature or the internal equipment temperature.

Changes in Thermal Resistance

Changes in thermal conductivity A strong dependence of thermal conductivity on temperature is a necessary criteria for passive self-thermostatic resistance changes. Pyrolytic graphite shows this effect but only below room temperature. Possible extensions of present work may produce forms for which the temperature dependence is strong up to 100°F. Porous materials exhibit variations in thermal conductivity with temperature, however the values of conductivity are generally quite low.

Mechanical devices There are many ideas for devices that produce changes in thermal resistance with temperature. Among these are thermal switches that produce a large change in resistance between their open and closed position. In the open position the resistance path is radiation across the switch while contact conductance forms the resistance path in the closed position. These switches can be activated by fluid filled bellows, bimetallic elements or magnets that lose or change their holding powers markedly at a transition temperature. Such devices can produce large changes in resistance, but they involve moving parts with attendant weight and reliability problems. The anisotropic behavior of thermal conductivity in pyrolytic graphite, and thermoelectric materials offer a different approach to thermal switch design. Since

the conductivity of pyrolytic graphite may vary by a factor of 100 in two different directions, a rotating element could be utilized to vary the thermal resistance between two points.

Conclusions

Where significant changes in thermal properties are required to achieve self-thermostatic control, mechanical devices appear the best solution at present. Of the passive approaches, the absorption edge in semiconductors appears most promising. However, since α_s is high for these surfaces, their greatest usefulness occurs where no solar energy is incident on the surface.

ANALYSIS OF THE REQUIREMENTS FOR SELF-THERMOSTATIC EFFECTS

A study was performed to determine the applicability of various self-thermostatic surfaces and devices for thermal control of typical spacecraft payloads. An analysis was made considering a vehicle in a 150 n mi circular orbit with variations in internal and external loads. Conditions were investigated where close temperature control and wide temperature control limits were required. Three situations were considered where close temperature control was required. These are 1) varying internal power dissipation 2) constant internal power dissipation and 3) zero internal power dissipation. One case of varying internal power dissipation was also considered where internal temperature was allowed to vary between -30°F and $+160^{\circ}\text{F}$. As part of the variation in thermal load for each case a change in the orbit inclination angle from 30° to 0° was included.

The internal temperature of the payload is given by the following expression:

$$T_i = \left[\frac{q_i + \alpha_s \left[\overline{F_s S + F_r R} \right] + \epsilon \left[\overline{F_e E} \right]}{\sigma \epsilon} \right]^{1/4} + R q_i$$

where: q_i = internal power dissipation

α_s = solar absorptance of the vehicle surface

ϵ = infrared emittance of the vehicle surface

R = thermal resistance between the vehicle surface and the power dissipating source

T_i = temperature of the power dissipating source

$\left[\overline{F_s S + F_r R} \right]$ = average solar energy incident upon the vehicle surface.

117 BTU/hr for $\beta = 30^\circ$ and 76 BTU/hr for $\beta = 0^\circ$ for a cylinder with its axis locally horizontal and in the orbit plane.

$\left[\overline{F_e E} \right]$ = average earth emission incident on the vehicle surface which equals 23 BTU/hr for a 150 nmi orbit

σ = Boltzmann constant.

Note: All fluxes and resistance are based on a unit area and thermal storage terms are considered large.

The following studies investigate the required changes in α_s , ϵ , and R to maintain T_i within certain prescribed limits with variations in q_i and $\left[\overline{F_s S + F_r R} \right]$.

Close Temperature Control

Varying internal power A payload requiring internal temperature to be constant was considered where q_i varied from 42 BTU/hr to 11 BTU/hr and, at the same time, β varied between 30° and 0° . The vehicle surface was assumed to have an α_s of 0.26 and an ϵ of 0.86. The internal to external resistance required to maintain T_i at 80°F was $0.95 \text{ hr } ^\circ\text{F}/\text{BTU}$ at maximum load conditions. The resistance required for different combinations of α_s and ϵ required to maintain T_i at 80°F for minimum load conditions is shown in Figure 4.

At the maximum load condition the vehicle surface temperature (T_s) was 40°F . The surface temperature at minimum load conditions must be less than 40°F to provide any stimulus for self-thermostatic changes in α_s and ϵ . Therefore, it can be seen from Fig. 4 that a resistance change from 0.95 to at least 3.7 must be accomplished. This would be the case if a step change in ϵ with temperature were available (point A on Fig. 4). If a change in ϵ of $+0.0025/^\circ\text{F}$, were available, while α_s remained constant at 0.26 (point B on Fig. 4), an even greater change in R from 0.95 to 9.0, must be accomplished. This change in ϵ is as large as could be anticipated with passive self-thermostatic control of surface properties. A step change in ϵ with temperature could possibly be approached with a shutter system controlled by changes in surface temperature.

If no change occurred in the surface characteristics (point C on Fig. 4), the required resistance change would be from 0.95 to 10.2. Thus for any of these three situations (a step change in ϵ , a change in ϵ of $+0.0025/^{\circ}\text{F}$ and no change in ϵ), a resistance change is required. Since the differences in the resistance changes required is not too great it appears that for the case of varying internal power, the applicability of passive self-thermostatic surfaces or shutters controlled by surface temperature is questionable.

Constant internal power Consideration was given to the situation where close temperature control was required but no changes occurred in internal power dissipation. The same orbit parameters as the previous case were assumed; an 80°F temperature was to be maintained; and power dissipation was kept constant at 42 BTU/hr. The conditions of the surface at maximum load conditions were again taken to be an ϵ of 0.86 and an α_s of 0.26, with a required internal to external resistance of 0.95. For this situation minimum load conditions consisted only of a change to a β of 0° . The required relation between α_s , ϵ and R to maintain T_1 at 80°F at minimum load conditions is shown in Fig. 5.

Since no variation occurs in internal power no change is required in resistance if a step change in emittance with temperature is available (point A Fig. 5). Considering a change in ϵ of $+0.0025/^{\circ}\text{F}$, with α_s constant, a resistance change of 0.95 to 1.28 must be accomplished (point B Fig. 5). This would result in an emittance at minimum load conditions of 0.83 with a surface temperature of 27°F . If the surface were non self-thermostatic and α_s

remained at 0.26 and ϵ at 0.86, a resistance change of 0.95 to 1.38 would be required (point C Fig. 5). For this situation the usefulness of passive self-thermostatic surfaces appears limited, since the variation in resistance required for the passive self-thermostatic surface is similar to that required for the non self-thermostatic surface. Thus, active surface control, or a variable resistance material or device is the most suitable method of control for this situation.

Zero internal power The last case considered, requiring close temperature control, was one with no internal power dissipation. For this situation changes in thermal resistance are of no value in maintaining internal temperature control, since internal temperature is equal to surface temperature. Figure 6 presents the variation in surface temperature with α_s/ϵ for β equal to 0 and 30°. It can be seen from this figure that for a non self-thermostatic surface, changing from a β of 30° with a surface temperature of 80°F to a β of 0°, will produce a surface temperature of 33°F. If a step change in emittance with temperature were available, no change would occur in surface temperature with a change in β . However, with a surface capable of an emittance change of +0.0025/°F, changing from a β of 30° to 0° produces a temperature change from 80°F to 57°F with an α_s of 0.26 and a change of 80°F to 43°F with an α_s of 0.90.

The latter surface, with an α_s of 0.9 and an emittance changing at a rate of +0.0025/°F, is available in materials exhibiting absorption edge characteristics.

It is interesting to note that this change in ϵ , of $+0.0025/^{\circ}\text{F}$, produces a lesser degree of control with the higher α_s . This indicates that the absorption edge effects are most useful in situations where no solar energy is incident upon the surface. For surfaces facing the sun the absorption edge effects must be diluted to obtain a low effective α_s .

For this application, e.g., zero internal power dissipation, self-thermostatic surfaces are the only means by which temperature control can be realized with varying external fluxes. The excursions in surface temperature with varying fluxes could be eliminated with step changes in ϵ , and could be more than halved with a change in ϵ of $+0.0025/^{\circ}\text{F}$.

Wide Temperature Control Limits

To illustrate the situation where close temperature control is not required an equipment satellite requiring temperature control between -30°F and $+160^{\circ}\text{F}$ was considered. An analysis was performed to determine the changes in internal power that could occur without exceeding these temperature limits. The same orbit parameters were used, evaluating the change from minimum load to maximum load conditions. At minimum load the internal power dissipation was assumed to be 0 BTU/hr. The internal temperature was set at -30°F and β was assumed to be 0° . With an assumed α_s of 0.26 the internal temperature of -30°F occurs with an emittance of 0.57. Maximum load conditions were then imposed on the vehicle, and the internal power dissipation that produced an

internal temperature of $+160^{\circ}\text{F}$ was determined. R was taken to be $0.1 \text{ hr } ^{\circ}\text{F}/\text{BTU}$, α_g was held constant at 0.26 and ρ was set at 30° . For the case of a non self-thermostatic surface the internal power could rise to 90 BTU/hr where as for a self-thermostatic surface capable of an emittance change of $+0.0025/^{\circ}\text{F}$ the internal power could rise to 174 BTU/hr before the internal temperature would reach $+160^{\circ}\text{F}$.

An internal to external resistance of $0.1 \text{ hr } ^{\circ}\text{F}/\text{BTU}$ is extremely low. If a higher resistance were chosen the allowable change in power from minimum load to maximum load conditions would be less. For a resistance of $1 \text{ hr } ^{\circ}\text{F}/\text{BTU}$, changing from minimum to maximum load with non self-thermostatic surfaces produces a q_i max of 54 BTU/hr . With a passive self-thermostatic surface a q_i max of 88 BTU/hr can be achieved.

Thus it appears that for this situation that both passive and active self-thermostatic surfaces as well as variable resistance schemes could be used for thermal control.

Conclusions

An attempt has been made to investigate some of the areas of interest for self-thermostatic surfaces, materials and devices. For the case where close temperature control is required in power dissipating vehicles variable

resistance changes and active surface changes controlled by surface temperature can be used. Passive self-thermostatic surfaces have their greatest applicability where reasonably large changes in internal temperature can be allowed.

It was felt that the greatest overall potential existed with variable resistance devices such as thermal switches. An experimental program was evolved to indicate to what extent such a device would be feasible, and is described in the following section.

Experimental

A thermal switch is used to vary the thermal resistance between a power dissipating component and its heat sink. This resistance variation is stimulated by small temperature changes in the power dissipating component. For the switch to perform satisfactorily it must produce a high open switch and a low closed switch resistance. A switch of this type was built and tested to evaluate its performance.

Equipment

To achieve the design requirement of a high ratio of open to closed switch resistance the following design was used. The heat flow path in the open position was through multiple layers of reflective insulation. In the

closed position the controlling resistance consisted of contact under pressure between the same layers of insulation. Conduction paths in parallel with the controlling portion of the switch were minimized to help achieve a high open switch resistance. Conduction paths in series with the controlling portion of the switch were kept large to improve the closed switch resistance.

Switch actuation, in a small temperature range, was produced by the movement of a temperature sensitive fluid filled bellows. The bellows movement compressed the insulation when the switch closed and allowed the layers of insulation to expand when the switch opened.

One end of the switch was attached to a power dissipating component. The entire assembly was insulated and surrounded by a constant temperature heat sink. By noting the energy supplied to the power dissipating component, its temperature, and the temperature of the heat sink, the overall switch resistance was determined.

The thermal switch shown in Figure 7, consisted of a temperature sensitive fluid filled bellows that provided the controlling movement of the switch. The bellows contained Freon 11 and was sealed at both ends.

The bellows assembly was kept in compression by three biasing springs that held the bellows in contact with the upper surface of the supporting plate.

These springs were supported on one end by the lower surface of the support plate and on the other end, by retainers, and adjusting screws, that were fastened to the bellows head. The bellows was kept in compression because commercially available bellows are not designed to expand beyond their free length.

Six flexible copper straps, fastened to the support plate and bellows head, were used to reduce the thermal resistance of the bellows assembly. A resistance heater, the power dissipating component, was fastened to the bottom of the support plate.

The support plate was fastened to a cylindrical copper container which was wrapped with multiple layers of reflective insulation. Fifty layers of reflective insulation covered the entire assembly except for the area directly over the bellows head. Five layers of insulation covered this area. The reflective layers were 0.00025 inch Mylar sheets with aluminum vapor deposited on one side. Since the insulation is only coated with aluminum on one side metal to metal contact never occurs when the switch is in the closed position. This alleviates the possible problem of cold welding.

The insulated assembly was supported from the top of an outer container by 3 thin wires that passed through the insulation to the bottom of the inner

container. The wires did not contact any part of the bellows and were supported from the lid of the outer container by thin walled stainless steel tubes. This support method minimized the heat leak in parallel with the bellows assembly.

The outer container had two lids. The inner lid supported the insulated assembly and the outer lid provided a bearing surface for the bellows. A hole in the center of the inner lid allowed the bellows to bear against the outer lid, and simplified adjusting the position of the inner container. The bellows head and outer lid surfaces were lapped to achieve good contact when the switch was closed. Copper tubing for liquid nitrogen cooling was fastened to the surface of the outer container.

Thermocouples were attached to the bellows head, the heater, and the outer container. The power leads and the heater and bellows head thermocouples were routed through the bottom of the insulated assembly. The leads were attached to the outer container to insure that any energy leaving through the leads would be absorbed by the constant temperature heat sink. Fine gauge wires were used to minimize this heat leak.

The entire assembly was installed in a vacuum facility capable of 10^{-5} mm of Hg.

When the assembly was exposed to a vacuum, and the outer container cooled, the switch operated in the following manner. When the heater temperature increases the Freon temperature in the bellows also increases. This increases the pressure in the bellows causing it to expand and compress the layers of reflective insulation directly over it. Normally the layers of this type of insulation are kept separated by the numerous wrinkles in each layer. This type of separation produces a relatively small contact area. When pressure is exerted on the insulation the contact area increases as the Mylar sheets are moved together, decreasing the thermal resistance through the insulation. As the thermal resistance is lowered, more energy is able to leave; and a point is reached where the heater and Freon temperature start to decrease. When this occurs the bellows pressure decreases, causing the bellows to move away from the top of the outer container. This allows the insulation to expand causing an increase in thermal resistance. This movement continues until the bellows assumes a position that allows the energy leaving the device to equal the power dissipated in the heater.

Procedure

The tests were performed in the following manner.

The bellows was placed on the support plate, in the inner container. The biasing springs, retainers, and adjusting screws were then assembled. The adjusting screws were tightened compressing the biasing springs and bellows.

This initial compression was made to prevent the bellows from expanding beyond its free length when placed in the vacuum chamber. The bellows was then charged with Freon 11 and sealed. The inner container containing the bellows assembly was wrapped with insulation. Multiple layers of insulation were used alternately covering the sides and the ends of the container. Additional wrinkles were put in the Mylar insulation prior to application.

After being insulated, the inner container was placed in the outer container and the first lid was installed. The length of the support wires was adjusted so that the bellows would make contact with the outer lid. After installing the outer lid, the electrical leads and the liquid nitrogen lines were connected.

The assembly was exposed to a vacuum. When most of the condensable vapors had been removed, liquid nitrogen cooling was initiated.

When the outer can reached -280°F power was supplied to the heater. The temperature of the outer can was controlled to $-280^{\circ}\text{F} \pm 10^{\circ}\text{F}$ with a thermocouple controller and solenoid valve that regulated the flow of liquid nitrogen to the cooling coils. The temperature of the heater, bellows head and outer container were recorded continuously. After temperature stabilization was achieved a new power setting was made. Data were taken at several different power settings to indicate the degree of control of the switch.

Discussion of Test Results

The results discussed in this section are from preliminary data from a test that is being conducted presently.

For each of the power settings made the overall resistance of the switch was determined by the following relation using steady state temperatures.

$$R = \frac{T_{\text{heater}} - T_{\text{outer container}}}{Q_{\text{heater}}}$$

A plot of this resistance as a function of the heater temperature is shown in Figure 8. This variation in resistance occurred with power dissipations ranging from 5 watts ($R = 30 \text{ hr } ^\circ\text{F}/\text{BTU}$) to 0.15 watts ($R = 530 \text{ hr } ^\circ\text{F}/\text{BTU}$). The heater temperature varied between 240°F and -10°F for the range of data taken. In the steeper portion of the resistance versus heater temperature curve a resistance change of 2.5 to 1 occurs between 80°F and 100°F .

Even though a large resistance change of 18 to 1 occurred, the temperature excursion of the heater was too great to be acceptable. Another problem was that the closed switch resistance of $30 \text{ hr } ^\circ\text{F}/\text{BTU}$ was too high.

The excessive temperature change required to actuate the switch could possibly

be eliminated by either a more energetic fluid than the Freon 11, which has a change in vapor pressure of 1.7 percent /°F at room temperature, or a different bellows and biasing spring configuration.

The variation in bellows movement with pressure is dependent upon the total allowable stroke of the bellows. The bellows chosen had one of the largest allowable strokes of those commercially available.

The closed switch resistance was limited by the contact resistance between the bellows head and the outer lid. As was mentioned before the surface of the bellows head and outer lid were lapped to provide flat surfaces and to improve surface finish. However no measurements were made to determine quantitatively the roughness and flatness of these two surfaces. The pressure developed by the bellows when constrained was dependent upon the fluid choice and the ratio of the internal and external diameters of the bellows head. For a given internal diameter a reduction in the external diameter would increase contact pressure but decrease contact area. No effort was made to optimize this aspect of the device.

The effect of the layers of Mylar between the bellows head and lid when the switch is closed is questionable. The Mylar could be deformed to some extent to accommodate the irregularities in the two metal surfaces, but the wrinkles in the Mylar could cause high spots that would tend to reduce the contact area.

The open switch resistance was limited by the conduction leaks penetrating the insulation. It would be fairly difficult to increase the resistance of these leaks since minimum gauge wires were used both for supporting the inner container and for the instrumentation and power leads. Care was taken in wrapping the inner container with insulation in order to achieve high insulation efficiency.

Since the testing of the switch has not been completed, no experimental data has been taken to evaluate the performance with the switch locked open. This data would be useful to indicate the self-thermostatic qualities of the insulation and would indicate precisely to what degree the switch was affecting the observed resistance change. An estimate was made to determine what the self-thermostatic qualities of the multiple layers of reflective insulation would be. It was calculated that if the switch were locked open a temperature change from 0°F to 100°F would produce a resistance change of 528 to 495 hr °F/BTU. This small change in the resistance occurred because even with the switch open the overall resistance is affected far more by conduction than by radiation. Thus it can be seen that essentially all of the resistance change shown in Fig. 8 was brought about by the action of the bellows.

Conclusions

The thermal switch performed satisfactorily in that it produced a resistance

change of 18 to 1. Two things, however, must be improved before this particular design could be considered useful. First as was mentioned before, the temperature change required to actuate the switch would need to be reduced. The examples presented in the analysis of the requirements for self-thermostatic effects indicate that a thermal switch would be quite useful if it were capable of a 10 to 1 resistance change in a 10^oF temperature span. This could possibly be achieved with this type of design if a better selection of bellows were made.

The second problem associated with this device was the value of the closed switch resistance. This resistance, of 30 hr ^oF/BTU, should be reduced by a factor of 10 or more before the device could be considered practical for most applications.

The key to reducing the closed switch resistance lies with the problem of achieving a low contact resistance. Since this aspect of the switch is most important further efforts will be to explore quantitatively the characteristics required to achieve low contact resistance.

REFERENCES

1. D. Friedman and J. E. Cox, "A Novel Method for Temperature Control for Satellites and Space Vehicles", USNRL Memo Report 1179, June 1961.
2. G. Hass, L. F. Drummeter Jr., and M. Schach, "Temperature Stabilization Of Highly Reflecting Spherical Satellites", Journal of the Optical Society of America Vol. 49, page 918, 1959.
3. W. W. Piper and D. T. F. Marple, "Optical Properties of Free Electrons in Cadmium Sulphide". Journal of Applied Physics, Supplement to Vol. 32, page 2237, October 1961.
4. W. G. Spitzer, F. A. Trumbore and R. A. Logan, "Properties of Heavily Doped N Type Germanium", Journal of Applied Physics, Vol. 32, page 1822, 1961.

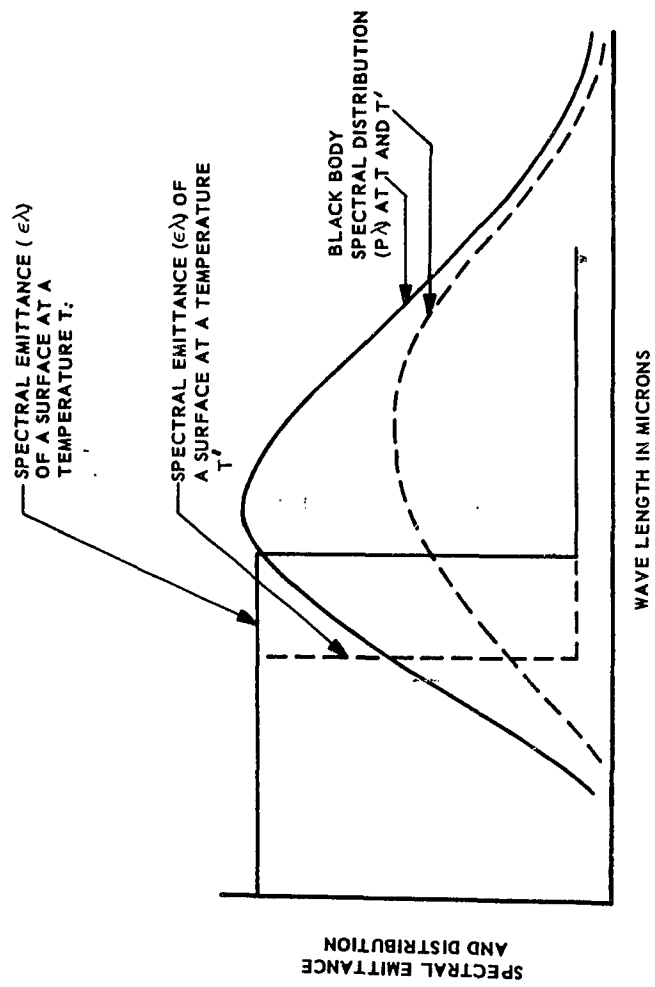


Figure 1 Variation in the Spectral Emittance of an Absorption Edge and the Black Body Spectral Distribution Between Temperature T and T'

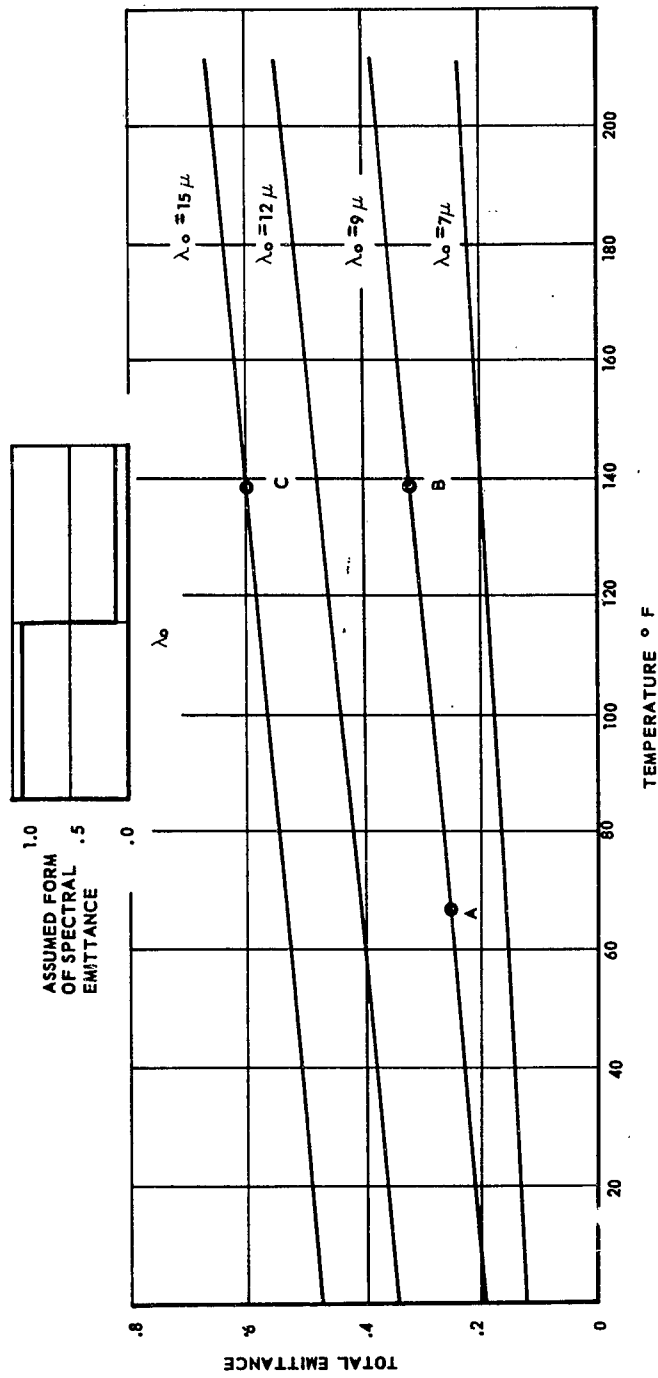
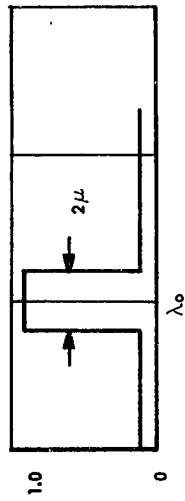


Figure 2 Variation in Total Emittance with Temperature for Various Absorption Edges



ASSUMED
FORM OF
SPECTRAL
EMITTANCE

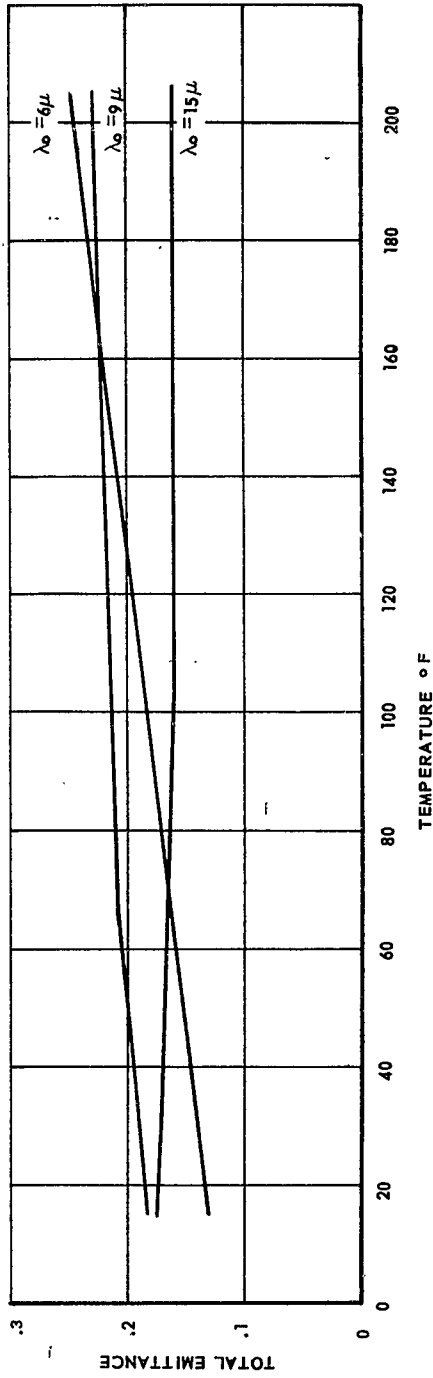


Figure 3 Variation in Total Emittance With Temperature for Various Narrow Band Absorption Peaks

MINIMUM LOAD: $q_i = 11$ BTU/HR, $\beta = 0^\circ$,

POINTS A, B AND C INDICATE THE ϵ THAT WOULD RESULT IN CHANGING FROM MAXIMUM TO MINIMUM LOAD CONDITIONS MAINTAINING T_i AND α_s CONSTANT.

POINT A: A STEP CHANGE IN ϵ WITH TEMPERATURE

POINT B: A CHANGE IN ϵ OF $+0.0025/^\circ\text{F}$

POINT C: NO CHANGE IN ϵ

MAXIMUM LOAD: $\alpha_s = 0.26$, $\epsilon = 0.86$, $R = 0.95$, HR $^\circ\text{F}$ /BTU, $\beta = 30^\circ$

$q_i = 42$ BTU/HR

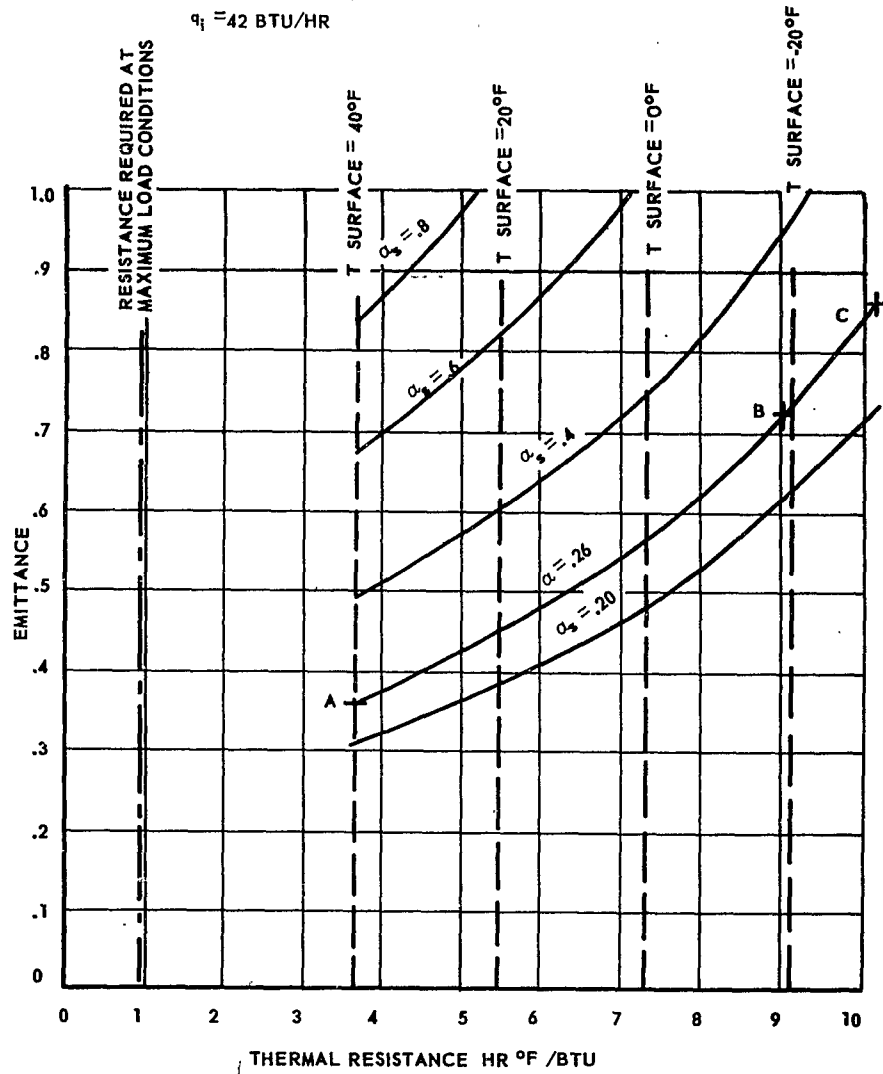


Figure 4 Relation Between α_s , R and ϵ to Maintain T_i at 80°F for Minimum Load Conditions

MINIMUM LOAD: $q_i = 42 \text{ BTU/HR}$ $\beta = 0^\circ$,
 POINTS A, B, AND C INDICATE THE ϵ THAT WOULD RESULT IN CHANGING
 FROM MAXIMUM TO MINIMUM LOAD CONDITIONS MAINTAINING T_i AND, α_s CONSTANT

POINT A: A STEP CHANGE IN ϵ WITH TEMPERATURE
 POINT B: A CHANGE IN ϵ OF $+0.0025/^\circ \text{F}$
 POINT C: NO CHANGE IN ϵ

MAXIMUM LOAD: $\alpha_s = 0.26$, $\epsilon = 0.86$, $R = 0.95 \text{ HR } ^\circ \text{F/BTU}$, $\beta = 30^\circ$,

$q_i = 42 \text{ BTU/HR}$

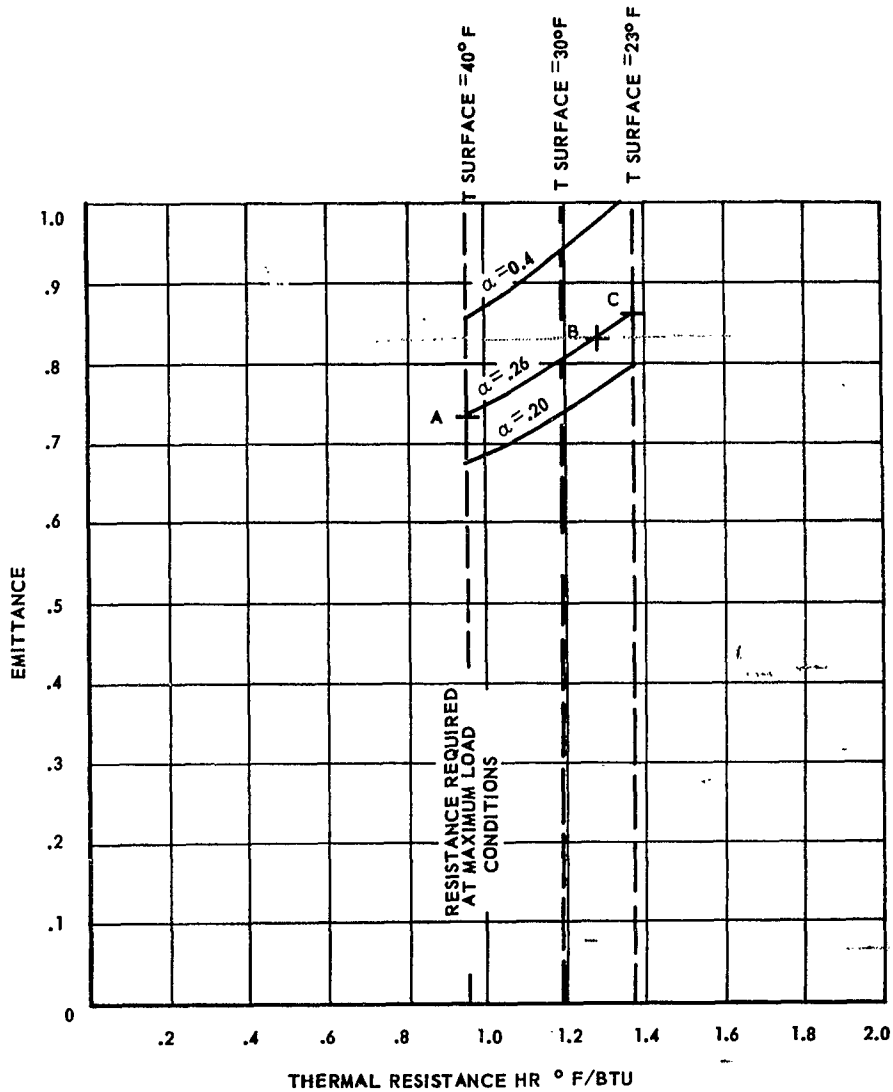


Figure 5 Relation Between α_s , R and ϵ to Maintain T_i at 80°F for Minimum Load Conditions

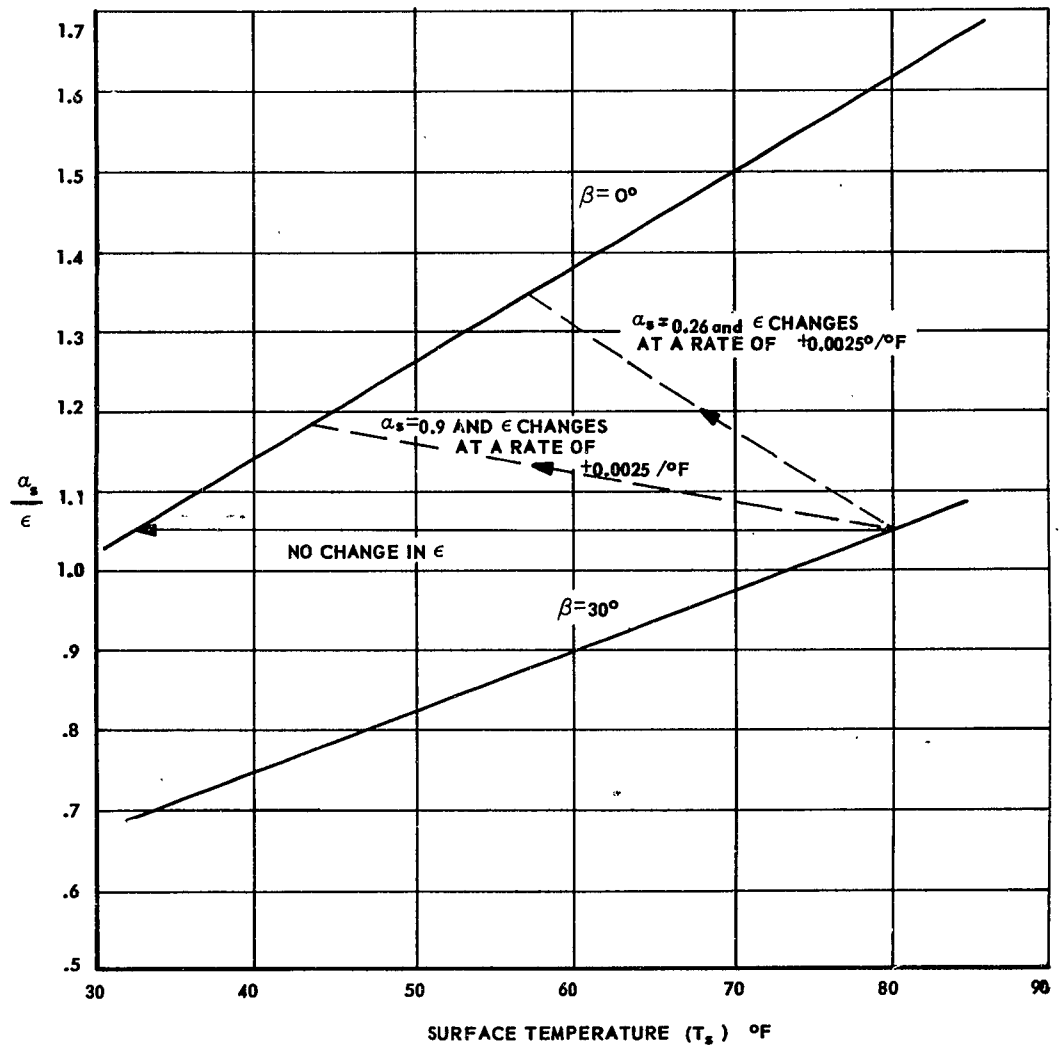
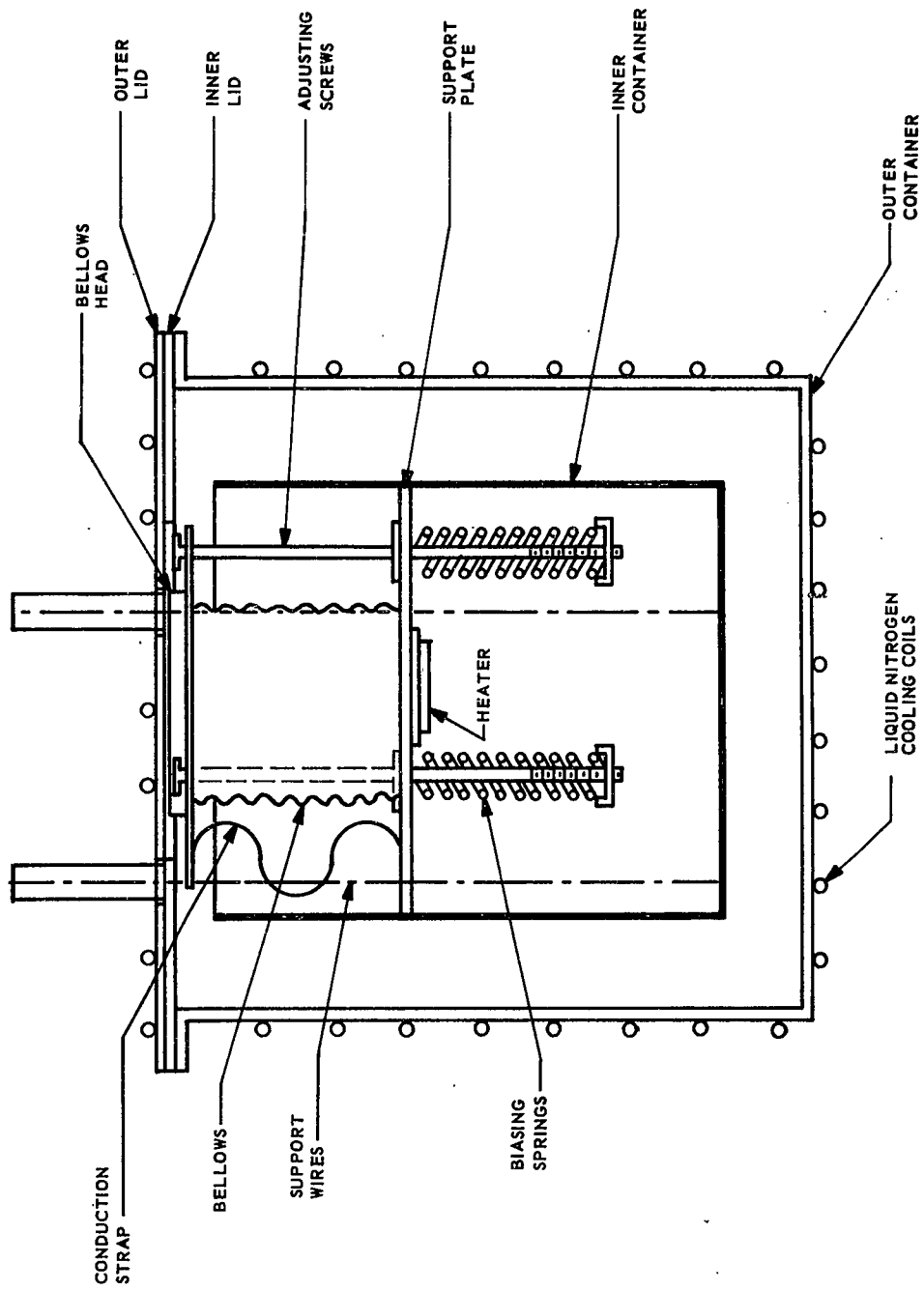


Figure 6 Requirements for Self-Thermostatic Control of a Non Power Dissipating Payload With a Change in β From 30° to 0°



NOTE: INSULATION NOT SHOWN
 BELLOWS IN EXPANDED POSITION

Figure 7 Thermal Switch Configuration

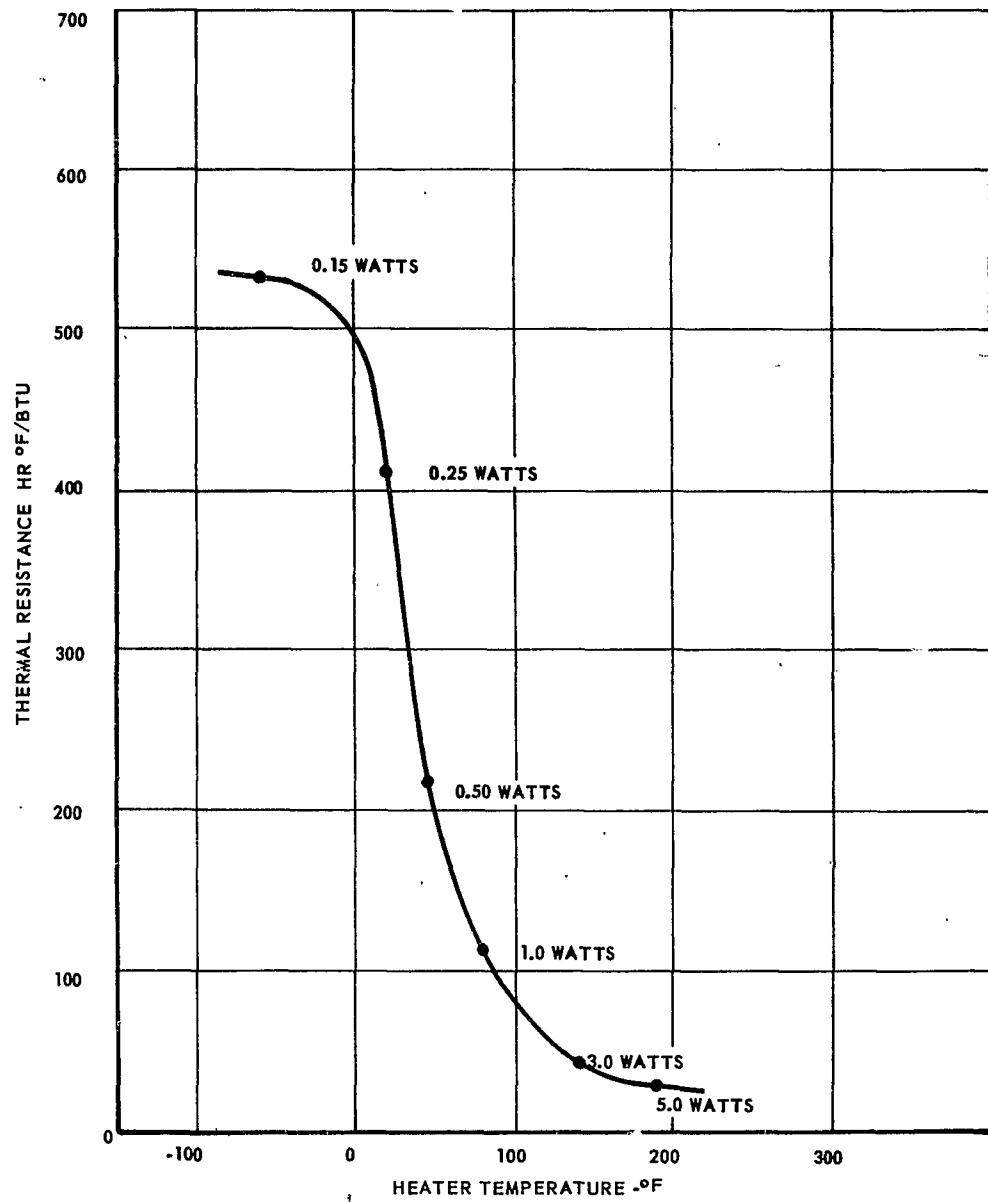


Figure 8 Thermal Switch Performance With 5 Layers of Aluminized Mylar Between the Bellows Head and Outer Lid

SPACECRAFT THERMAL CONTROL USING
CRYOGENIC HYDROGEN

by

G. M. Hall

A. F. Knights

Walter Kidde and Company, Inc.,
Belleville, New Jersey

SPACECRAFT THERMAL CONTROL USING CRYOGENIC HYDROGEN

by

G. M. Hall and A. F. Knights

Introduction

Practical environmental control of manned spacecraft requires "on board" heat sink capability. The heat sink may be water in a nonintegrated environmental control system or cryogenic hydrogen in an integrated environmental control system (ECS). Studies conducted indicate a significant weight saving in favor of the integrated system. Consequently, a breadboard test program was undertaken to demonstrate the operation of an integrated environmental control system.

The breadboard contains electrical heaters to simulate the vehicle heat loads. Power for the heaters is generated by the integrated accessory power system (APS). Sulfur hexafluoride (SF_6) is circulated in a series loop through the heaters and the tubes of the primary heat exchanger. Cold hydrogen flowing through the shell of the exchanger absorbs the environmental heat load. Some of the warm hydrogen leaving the primary exchanger is recirculated to the inlet side of the primary exchanger where it is mixed with cryogenic hydrogen entering the ECS. The remainder of the warm hydrogen is combusted with oxygen in the APS to generate the power used for heat load simulation.

The ECS design selected for breadboard testing has 2 basic features which make it attractive:

- (1) Warm hydrogen is recirculated through the primary heat exchanger between hydrogen and sulfur hexafluoride.
- (2) A gaseous series flow heat transport loop is used resulting in the simplest most reliable environmental control system.

The recirculation feature eliminates the freezing problem encountered with any heat transport fluid at cryogenic temperature. The single loop heat transport technique used eliminates a secondary gaseous cooling loop required by a liquid heat transport technique. As a result, fewer operating and control components are required for operation of the ECS.

Tests conducted on the breadboard system described above demonstrated the feasibility of this design. The following text and schematics describe the basis for selection of the breadboard design as well as discuss the results of the initial tests on this system.

Design Discussion

The design of the breadboard system tested was based upon a study sponsored by the USAF Aeronautical Systems Division (ASD) (1). This investigation determined that the use of cryogenic hydrogen as a heat sink and a fuel aboard a manned spacecraft was entirely feasible. As part of the over-all study of integrated environmental control and accessory power systems, considerable analysis was devoted to selection of the best environmental control techniques. The following factors were considered in the analysis:

- (1) The temperature limitations of the heat sources

Cabin air	60°F minimum to 80°F maximum
Electronic equipment	0°F to 300°F
Electrical equipment	0°F to 500°F
Hydraulic system	250°F to 550°F

- (2) The heat transfer regimes at the heat sources and sink

Four modes of heat transfer were considered; radiation vaporization, forced convection using a gas, and forced convection using a liquid. Radiation to an "on-board" heat sink proved impractical due to low heat transfer rates and limitations on component location with respect to the heat sink. The use of a vapor cycle could provide high heat transfer coefficients resulting in the smallest heat transfer surfaces. However 2-phase flow and heat transfer characteristics in a zero-gravity environment are not well established. For this reason, the vapor cycle is considered unattractive at this time. Forced convection

using a gas or liquid heat transport fluid proved to be a practical heat transfer technique. This was examined in greater detail before selection of the best approach.

(3) The fluids used as coolants

Seven gases and six liquids were investigated for use in forced convection systems. The influence of their thermal and physical properties on system pressure, temperature, weight, pumping power, and safety were analyzed. The dielectric strength of each gas was considered to determine the suitability of an electrical or electronic coolant. Based upon findings, sulfur hexafluoride was selected as the best gaseous coolant and a 70% ethylene glycol-water solution as the best liquid coolant. Freon C-318 was selected for secondary coolant loops in the liquid cooling system.

(4) The arrangement of the heat loads in the cooling circuit

Series and parallel arrangements of the heat sources in the cooling circuit were analyzed. The size of heat transfer surfaces, pumping losses and their effect on weight were considered for each arrangement. The simple series arrangement was selected as best. Heat transfer surfaces required and pumping losses encountered were determined comparable between series and parallel arrangements. However, the series circuit permits a higher maximum coolant temperature and therefore requires about 10% less hydrogen flow than the best series-parallel arrangement.

(5) The fluid process conditions

Based upon the selection of heat transport fluid and series arrangement of heat loads, process conditions in the primary heat exchanger were selected. Expressions were developed for determining the influence of coolant flow

rate on heat transfer surface area and pumping power. These expressions were used to determine the tradeoff between primary heat exchanger weight and hydrogen flow rate with its attendant weight penalties.

(6) The weight of systems analyzed

System weights for the gaseous and liquid environmental control techniques defined by the above design selections were determined. Results indicated no significant weight difference when all direct and indirect weight penalties are considered. Therefore, the greater simplicity of the gaseous heat transport techniques proved to be the key factor in the selection of the single loop gaseous cooling technique as the best system for spacecraft application.

The system defined by the design selections described above is shown schematically in Figure 1. Gaseous sulfur hexafluoride acts as both a heat transport fluid and a compartment atmosphere in the electronic equipment bays. It absorbs heat from the sources in series, in ascending order of source temperature. This arrangement allows rejection of heat to hydrogen in the primary heat exchanger at the highest possible temperature level. Direct cooling of the sources with hydrogen was considered to be impractical, (1). The gas temperature at the exit from the primary heat exchanger is maintained within limits by controlling the flow of hydrogen through the exchanger. Using recirculation of warm hydrogen from the exchanger outlet, the hydrogen inlet temperature is maintained at a safe level to prevent condensation of the SF_6 . Thermal control of the heat sources is achieved by varying the flow rate of SF_6 in response to signals from temperature sensors TS1, TS2, TS3, and TS4. The SF_6 circulation system is sized to provide thermal control under all conditions of heat generation in the sources.

temperature in excess of 260°F will cause the dual thermal switch TS3 to open both control valves. As the temperature drops from 260°F, due to the higher flow rate, control valve "A" will close at 255°F, and control valve "B" will close if the temperature drops to 250°F. If at any time the temperature of the SF₆ leaving the "electrical" heater exceeds 455°F, thermal switch TS4 will open control valve "A". The temperature of the SF₆ at the outlet of the primary heat exchanger is controlled by temperature sensor TS2. This sensor actuates the vent valve in the hydrogen circuit whenever the SF₆ temperature exceeds +10°F.

The primary heat exchanger is of conventional shell and tube type construction. A double tube sheet is used to avoid leakage of hydrogen into the SF₆ stream. Sulfur hexafluoride flows inside U tubes. Hydrogen flows in the shell. The shell is divided by a longitudinal baffle, so that the hot and cold streams move essentially in counterflow throughout.

Finally, consider the accessory power system. Oxygen expelled from the storage dewar at cryogenic temperature is warmed in a preliminary heat exchanger with hydrogen, and regulated to system pressure by sensing hydrogen pressure. Subsequently both gases flow through a temperature equalizing heat exchanger. The fuel and oxidizer leave this exchanger at comparable temperature and pressure. Flow control is achieved with a proportional area bipropellant valve. The gases leaving the valve are mixed and burned in the combustion chamber. The combustion products form the working fluid for the turbine-alternator power package. Power generated by the alternator is returned to the heaters simulating electronic and electrical equipment in the sulfur hexafluoride loop.

Test Procedure

The complete system fabricated contains 4 discrete fluid circuits; the hydrogen tankage, the hydrogen system other than tankage, the oxygen system including tankage, and the SF₆ circulation loop. Each of these circuits were purged of air using a gas-fill, vacuum-purge cycle before filling

System Description

A breadboard model of an integrated environmental control and accessory power system was built. This system consists of 3 subsystems:

- (1) Cryogenic storage and expulsion
- (2) Environmental control
- (3) Accessory power generation

First, consider the cryogenic storage and expulsion system. Initially, liquid hydrogen and liquid oxygen are stored in dewars. (Figure 2). Supercritical pressures of 315 psia in the hydrogen dewar and 900 psia in the oxygen dewar are attained and maintained by addition of thermal energy, through heating coils. The heating agent is warm hydrogen which has absorbed heat from the environmental control system. Flow of hydrogen through the heating coil in each dewar is controlled to expel the cryogen, at constant pressure, in response to demands by the environmental control or accessory power subsystems.

Changes in demand for hydrogen and oxygen normally come from the APS. An increase in propellant flow rate in response to an increased load causes the pressures in the dewars to drop. A pressure switch in each dewar then operates a valve to admit more hydrogen to the heating coil, restoring the pressure. The demand for cryogenic hydrogen may also be increased by the environmental control system. If the flow required by the APS is not sufficient for cooling purposes, the SF₆ loop tends to over heat. This condition is sensed by a thermal switch which opens a vent in the hydrogen line. Venting increases the flow through the primary heat exchanger. Maintaining supercritical pressure in the hydrogen and oxygen lines eliminates 2-phase flow with its attendant problems in a zero-gravity field.

Second, consider the environmental control system. The ECS consists of 3 parts:

- (1) The hydrogen circuit
- (2) The sulfur hexafluoride loop
- (3) The primary heat exchanger, in which heat is transmitted from the SF₆ to the hydrogen

The hydrogen circuit is shown in Figure 2. Cryogenic hydrogen expelled from the dewar passes first to a primary mixer where it is combined with warm hydrogen recirculated from the outlet of the primary heat exchanger. A positive displacement, vane-type pump recirculates the warm hydrogen. The hydrogen mixture enters the primary heat exchanger. After leaving the exchanger, part of the hydrogen flows to the dewar heating coils, part is recirculated, and the remainder flows downstream to the APS. If the hydrogen flow required by the APS exceeds that required for cooling, the hydrogen temperature entering the primary heat exchanger could fall below the acceptable limit. To avoid this condition, a bypass valve is provided in the cryogenic line. When the inlet temperature at the exchanger drops below -64°F, sensor TSI opens the bypass valve. The hydrogen which bypasses the exchanger enters the bypass mixer, where it is mixed with the warm hydrogen leaving the exchanger and the dewar heating coils. The mixed stream then flows to the APS.

The sulfur hexafluoride loop is shown in Figure 3. The gas, circulated by a centrifugal blower, flows through 3 electrical heaters in series. The first 2 of these simulate electronic equipment aboard the spacecraft. The third simulates electrical equipment capable of operating at relatively high temperatures. The heat loads due to the cabin atmosphere and the hydraulic system (Figure 1) were not simulated.

After passing through the heaters, the SF₆ enters the primary heat exchanger, where it is cooled before returning to the blower. The flow rate of SF₆ is controlled by an orifice and 2 control valves, operating in parallel. This combination allows circulation at 3 discrete flow rates. The valves are actuated by temperature sensors located at the exit of the second "electronic" heater and at the exit of the "electrical" heater. An SF₆

with the gas to be used in each circuit. After purging, the cryogenics were pumped into the respective tankage at atmospheric pressure.

Initial system startup was achieved with gaseous hydrogen and oxygen. The system was run on gaseous propellants until the environmental system was warmed up to prevent freezing of the environmental coolant during the transient starting conditions. Tankage vent valves were then closed and the automatic pressurizing system actuated to obtain operating pressure in the tanks. Subsequently, the cryogenic supply valves were opened to begin operation on the cryogenics.

Constant load and transient load tests were conducted during the test series. During these tests, system pressures, temperatures, and flows were measured and recorded. Critical parameters were monitored during the test for a continuous indication of the system operating condition. Shutdown in each test was achieved without difficulty. APS on-off solenoid valves were closed to stop propellant flow and system vent valves actuated to bleed out system pressure. Tankage pressure was vented or maintained depending upon how soon the next test was anticipated. Restart required a repetition of the above procedure with the exception of the purging cycles.

Test Discussion

The test program successfully demonstrated the operation of an integrated cryogenic accessory power and environmental control system. On the basis of these tests, the system was accepted by ASD for installation at their facility, where more exhaustive tests, including longer duration testing will be accomplished. The performance of the environmental control system during transient testing in which the heat load was varied between 2.5 and 16.5 KW is described below.

Fluid temperatures in the sulfur hexafluoride loop are presented in Figure 4. The lower solid line, labelled TC4, is the gas temperature at the outlet from the primary heat exchanger. Throughout the test, this bulk temperature remained above -25°F , which is well above the condensation point of the gas at 2 psig (-84°F). The line (TC5), representing the SF_6 temperature at the outlet from the flowrator, shows the small but measurable effect of the thermal capacity of the lines and flowrator; these transfer heat to the gas in the first 20 minutes of the test, and tend to cool the gas when the SF_6 temperature leaving the primary heat exchanger rises near the end of the test. The line labelled TC6 is the temperature leaving the first "electronic" heater. This particular heater was not activated during this test. The temperature rise from TC5 to TC6 is caused by the power input at the centrifugal blower, plus heat transferred from piping and the heater during cool-down from their initial temperatures of 110°F at the start of the test. The line TC7 is the temperature at the outlet of the active "electronic" heater. This temperature is monitored by a thermal switch set to open both SF_6 flow control valves if the gas reached 260°F at this point. This did not occur. The upper solid line, TC8, is the gas temperature at the exit from the "electronic" heater. This temperature is monitored by a thermal switch set to open one of the SF_6 flow control valves if the exit temperature exceeds 455°F . This condition did not occur. Since neither of the temperatures, TC7 or TC8, reached their allowable maxima, the SF_6 flow rate was not varied during the test.

The effect of the thermal capacity of the active electric heaters is shown explicitly in Figure 5. Here heat absorption curves for the environmental cooling loop are plotted as functions of time. The upper curve is the amount of heat transferred to the sulfur hexafluoride by the active heaters. The lower heat absorption curve represents the heat addition to the SF_6 between the outlet of the primary heat exchanger and the inlet to the active heater section. This heat input is composed of heat transferred from the lines plus the circulation blower power which is absorbed by the gas flowing through it. The net alternator power outlet is also shown. Time lags of the order of 4 to 6 minutes in

absorption of heat loads after a step increase in power generation can be seen. The blower, piping, and inactive heater section contributed significant energy to the SF_6 throughout the test.

Temperatures in the hydrogen circuit during the tests are plotted in Figure 6. The temperature at the inlet to the primary heat exchanger gives an indication of the effectiveness of the primary mixer. In this unit, cryogenic hydrogen from the dewar is mixed with warm hydrogen recirculated from the exchanger outlet before entering the primary heat exchanger. The performance of the recirculation and mixing process was satisfactory. There was a malfunction of the thermal switch to hold the mixture temperature above $-64^{\circ}F$. This required the disabling of the cryogenic hydrogen bypass valve, allowing the mixture to reach $-110^{\circ}F$ during the test. This excursion from the selected minimum had no apparent effect on the system operation.

The temperature of the hydrogen leaving the primary heat exchanger remained relatively constant during the run. This characteristic was expected and resulted from the interaction of 2 factors. First, flow and heat load change in unison tending to maintain the equilibrium. Secondly, the heat capacity of the system acts against any rapid temperature changes, also tending to maintain the equilibrium condition. The upper dotted curve in Figure 6 is the temperature of the recirculated hydrogen at the exit from the recirculation pump. This is the temperature of the recirculated hydrogen mixed with the cryogen in the primary mixer. (Figure 2).

The effect of the heat capacity of the material in the primary heat exchanger is seen in Figure 7. For this figure, heat absorbed by the hydrogen stream in the heat exchanger at any time during the run is calculated from the measured inlet and outlet temperatures, the heat capacity of the gas, and the flow rate. High frequency variations in the temperatures were smoothed out before calculating points for this curve. The instantaneous heat loss of the SF_6 in the primary heat exchanger was calculated in a similar manner. When the power load on the

turbine is changed, the total hydrogen flow to the heat exchanger changed immediately. At the same time, the temperature of the hydrogen at the exchanger inlet changes rapidly (see Figure 6). Consider the step changes from 2.5 KW to 9.6 KW, and from 9.6 KW to 16.6 KW, as shown in Figure 7. The effect of the sudden changes in hydrogen flow rate and inlet temperature in each case is a sudden rise in the heat absorption of the hydrogen stream in the exchanger. This rise in heat absorption by the hydrogen continues for about 2 minutes in each case, even though the heat rejected by the SF_6 stream is considerably less. The lag in the heat rejection by the SF_6 stream is due to the thermal capacity of the components in the environmental control loop.

At the end of the 2-minute period following the step increase in alternator power input, the heat absorption by the hydrogen stream reaches a maximum and in the case of the change from 9.6 KW to 16.6 KW tends to drop off. During this period, hydrogen has absorbed heat from the tubes and from the shell of the heat exchanger. Because of the relatively large mass of material exposed to the hydrogen stream in this nonflight type heat exchanger, the exchanger structure cools slowly. By the time a significant drop in the shell and tube wall temperatures is experienced, as shown by a tendency for the heat absorption by the hydrogen stream to decrease, the heat absorbed by the SF_6 due to the higher power level in the environmental control loop is beginning to be rejected in the heat exchanger. The thermal capacity of the heat exchanger structure, then, causes the hydrogen heat absorption rate to rapidly reach a quasi-steady state condition after a step change in environmental heat load.

If a flight type heat exchanger were employed in this system, the fluctuations in hydrogen heat absorption and in hydrogen temperature leaving the primary heat exchanger would be larger. The extent of the fluctuation depends on the net effect of lags in absorption of heat in the SF_6 circuit and the thermal capacity of the primary heat exchanger. The former tends to increase fluctuations in hydrogen temperature; the latter tends to decrease them.

Conclusions

One of the important questions answered by the test results reported here is the feasibility of exchanging heat between a warm gaseous coolant and a cryogenic heat sink without experiencing a condensation of the warm gas. The method of controlling the hydrogen inlet temperature at the heat exchanger by recirculation of warm hydrogen from the exchanger outlet has proven to be entirely satisfactory as indicated by the data in Figure 6. A properly sized constant flow recirculation loop and a relatively simple mixing exchanger suffice to raise the temperature of supercritical hydrogen, flowing from the storage dewar at a nominal -400°F up to temperatures of -110° or higher at the inlet to the primary heat exchanger. Hydrogen inlet temperatures were maintained at a satisfactory level during an increase of up to 50% in the cryogen flow rate.

The primary heat exchanger operated satisfactorily during all of the tests performed. Though the unit was not operated at its maximum design rating, it was operated under steady state conditions at 20 KW (total heat transferred) during the test described. This is 70% of rated load. At this load level, test performance was within 10% of the theoretical performance. Although the temperature of the hydrogen entering the primary heat exchanger fell below the selected minimum of -64° , no evidence of condensation of the sulfur hexafluoride gas was noted.

The tests discussed herein are the first tests conducted on the integrated system to demonstrate its operation. Considerable future testing is planned for this system to explore its full capabilities and accumulated operating characteristics which may form the basis for design of future spacecraft control systems.

REFERENCES

- (1) Study of Integrated Cryogenic Fueled Power Generating and Environmental Control Systems, ASDTR 61-327, November 1961

- Volume I - ASTIA No. 270471 - Summary Report,
K. Traynelis, A. Jennings, and G. Hall
- Volume II - ASTIA No. 270474 - Cryogenic Tankage Investigation
C. W. Spieth et al
- Volume III - ASTIA No. 270472 - Power Generating Equipment
Study
G. Hall and E. Treirat
- Volume IV - ASTIA No. 270491 - Environmental Control and
Attitude Control Studies
A. Knights, A. Jennings, M. Forte
- Volume V - ASTIA No. 270473 - Integration and Control
Studies
A. Jennings and G. Hall

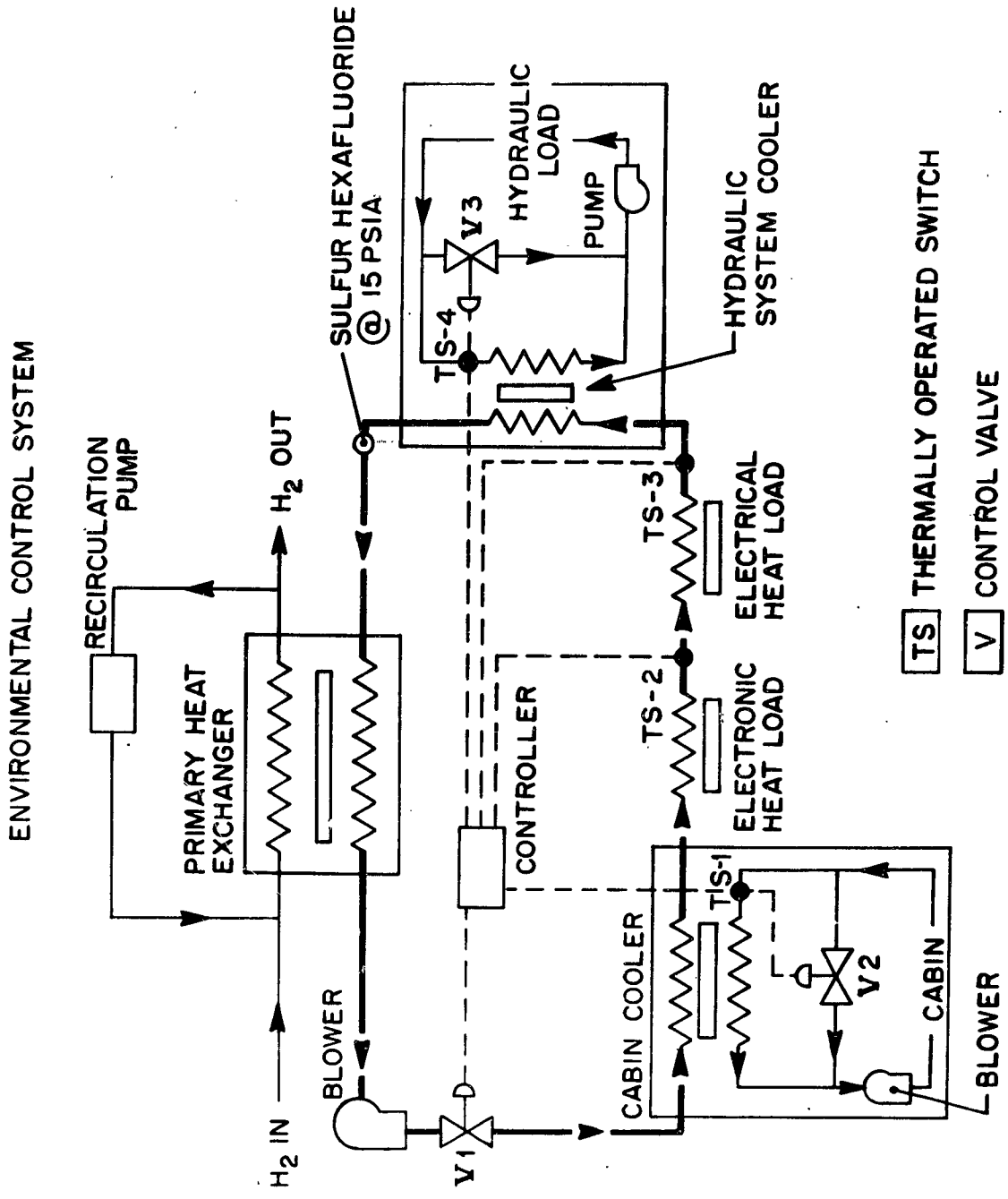
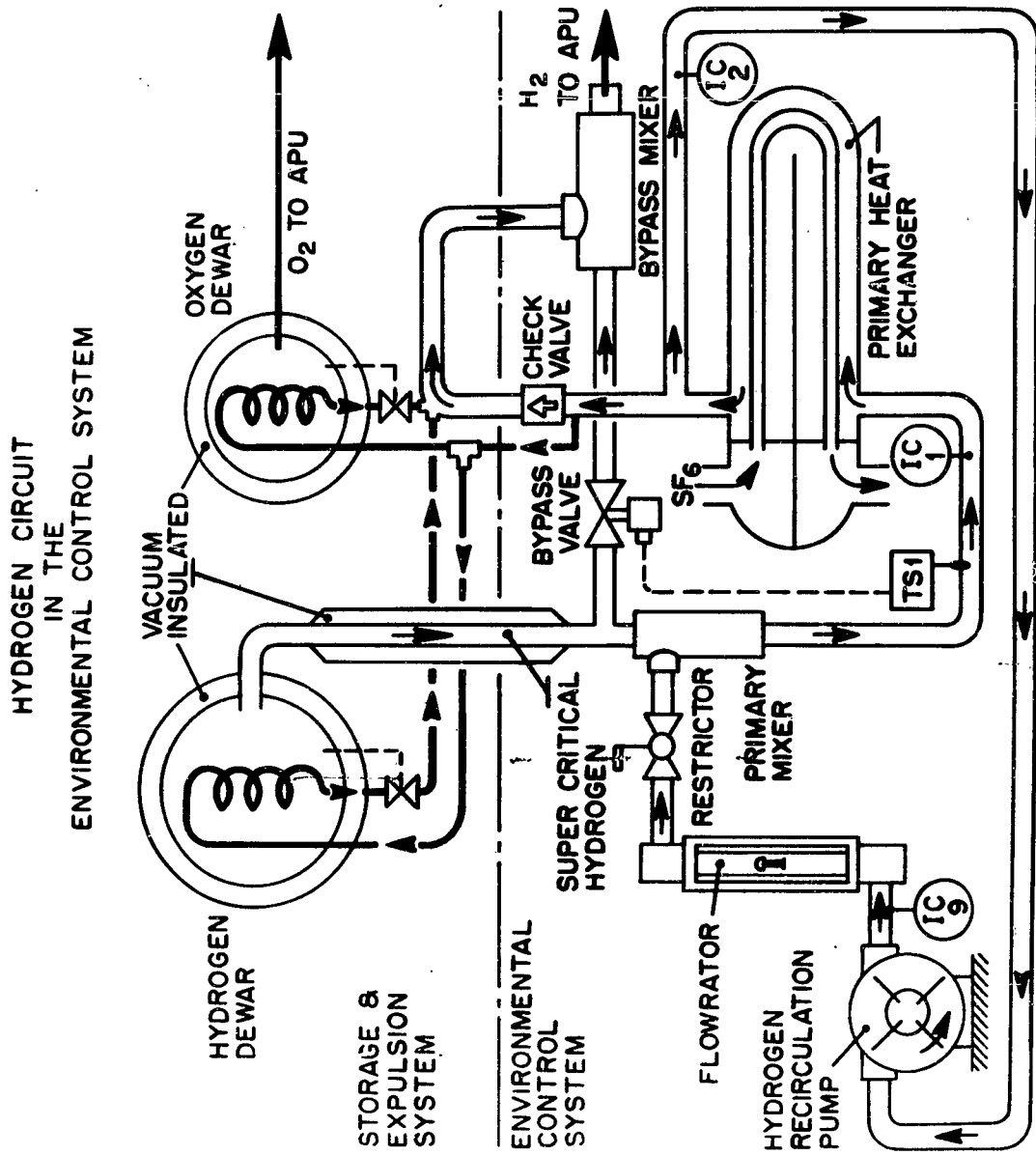


Figure 1. Cryogenic Heat Sink ECS With a Gaseous Primary Coolant Loop



- Ⓢ IRON-CONSTANTIN THERMOCOUPLE
- ⓉS THERMALLY OPERATED SWITCH

Figure 2. Breadboard Equipment Cooling Loop with Vehicle Heat Load Simulation.

SULFUR HEXAFLUORIDE CIRCUIT IN ENVIRONMENTAL CONTROL SYSTEM

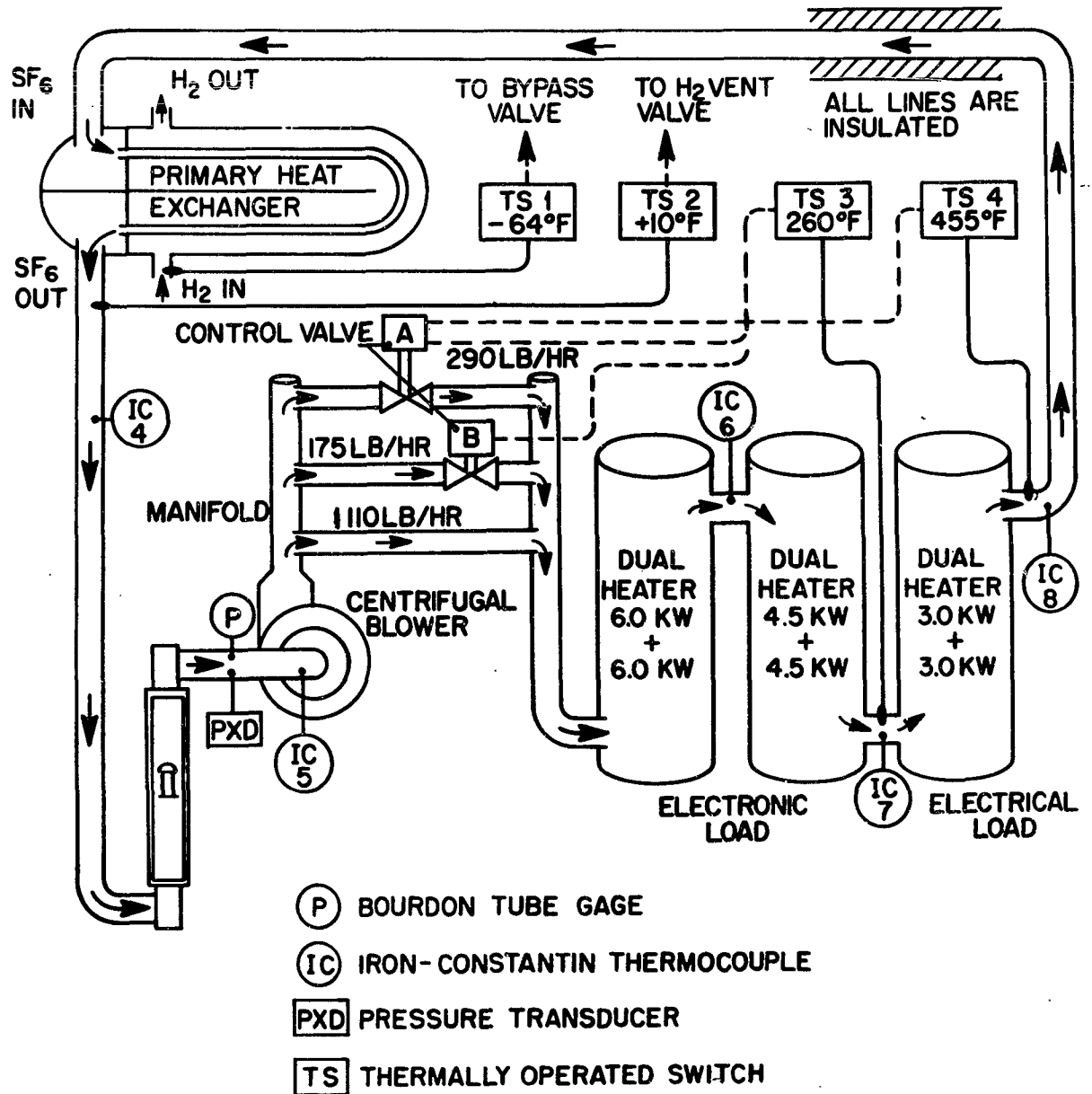
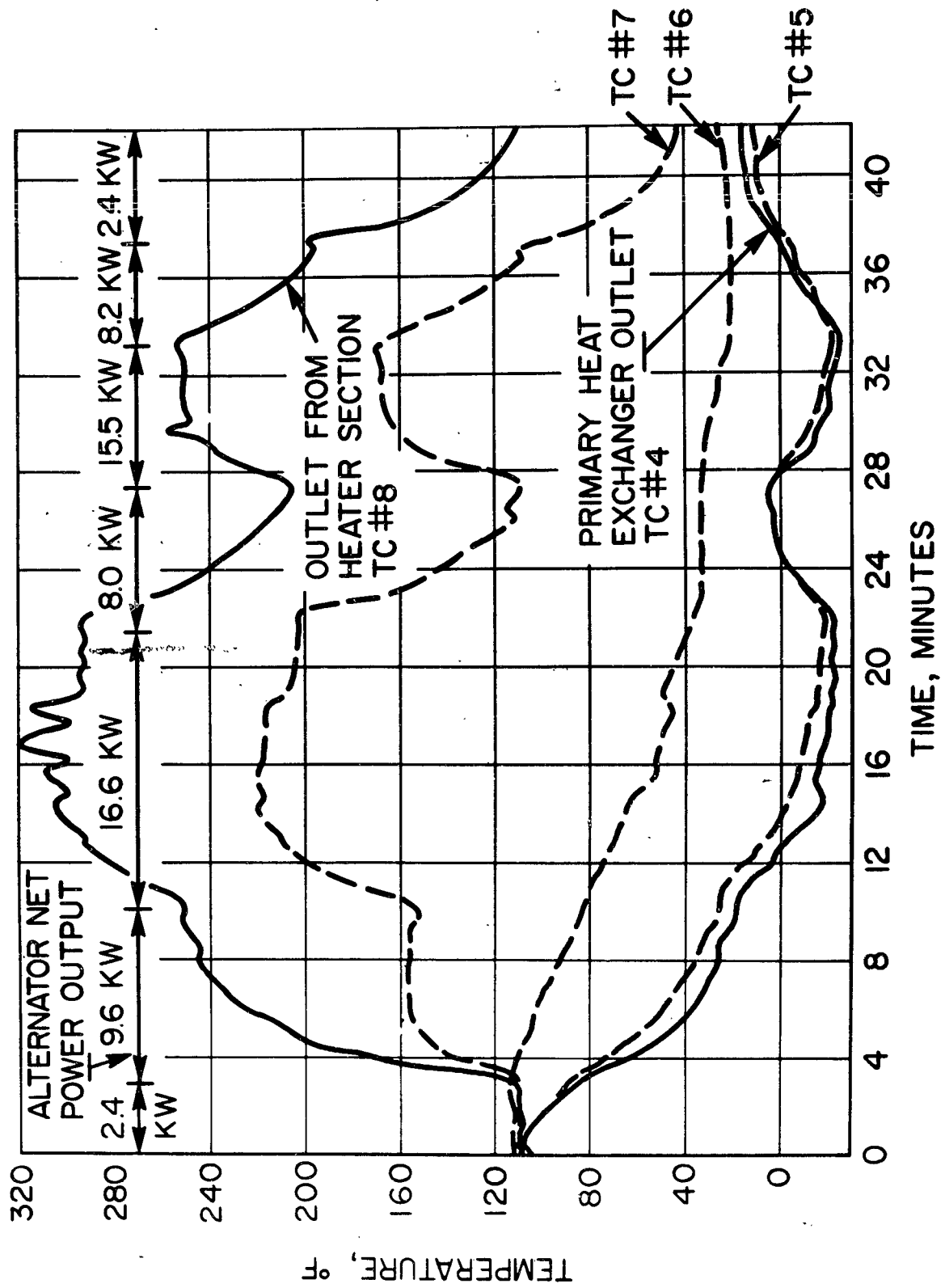


Figure 3. Cryogenic Hydrogen Supply System with Recirculation for Temperature Control

SF₆ BULK TEMPERATURES IN THE EQUIPMENT COOLING LOOP



895

Figure 4. Primary Coolant Loop Test Temperature Comparison

HEAT ABSORPTION IN THE EQUIPMENT COOLING LOOP

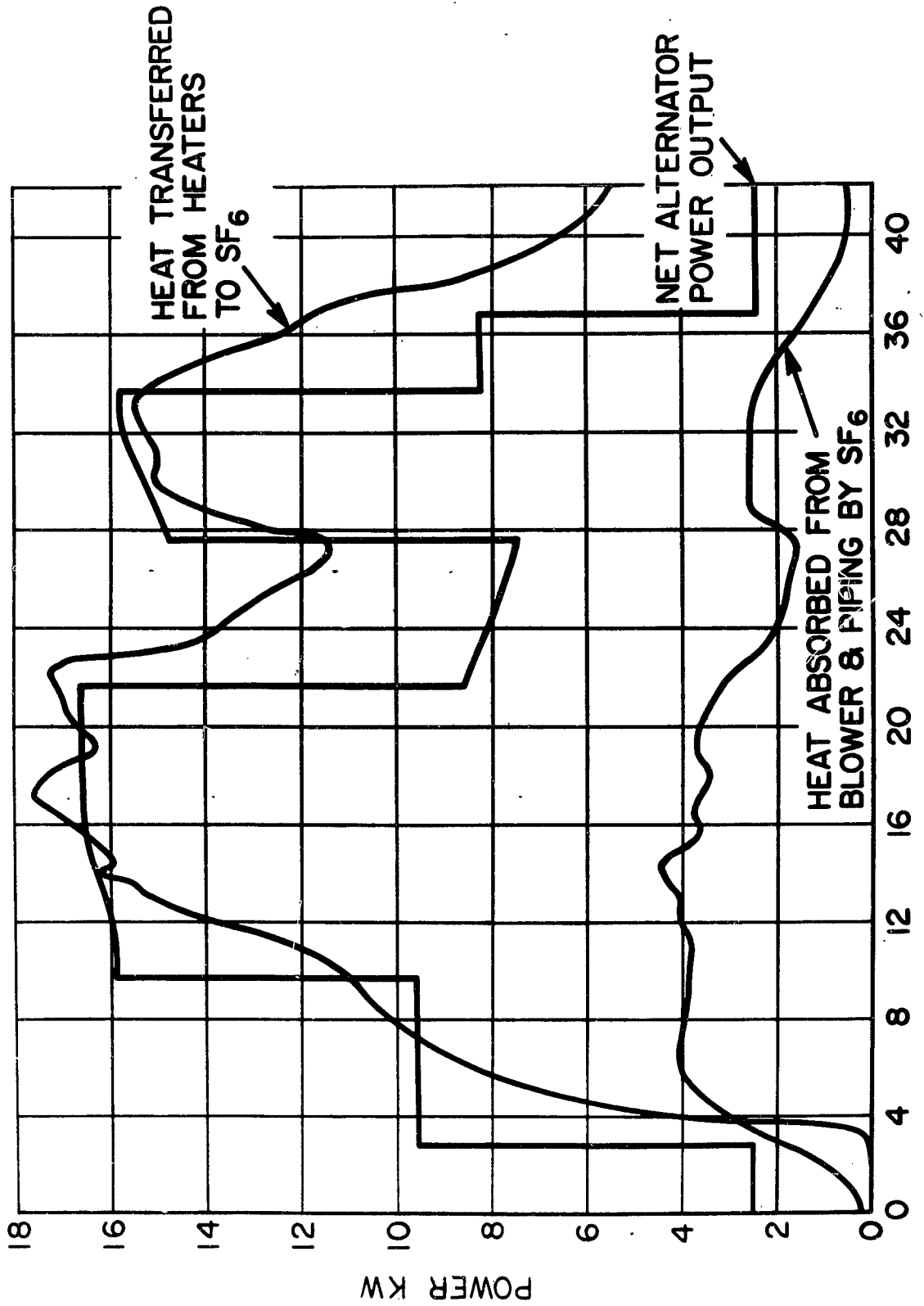
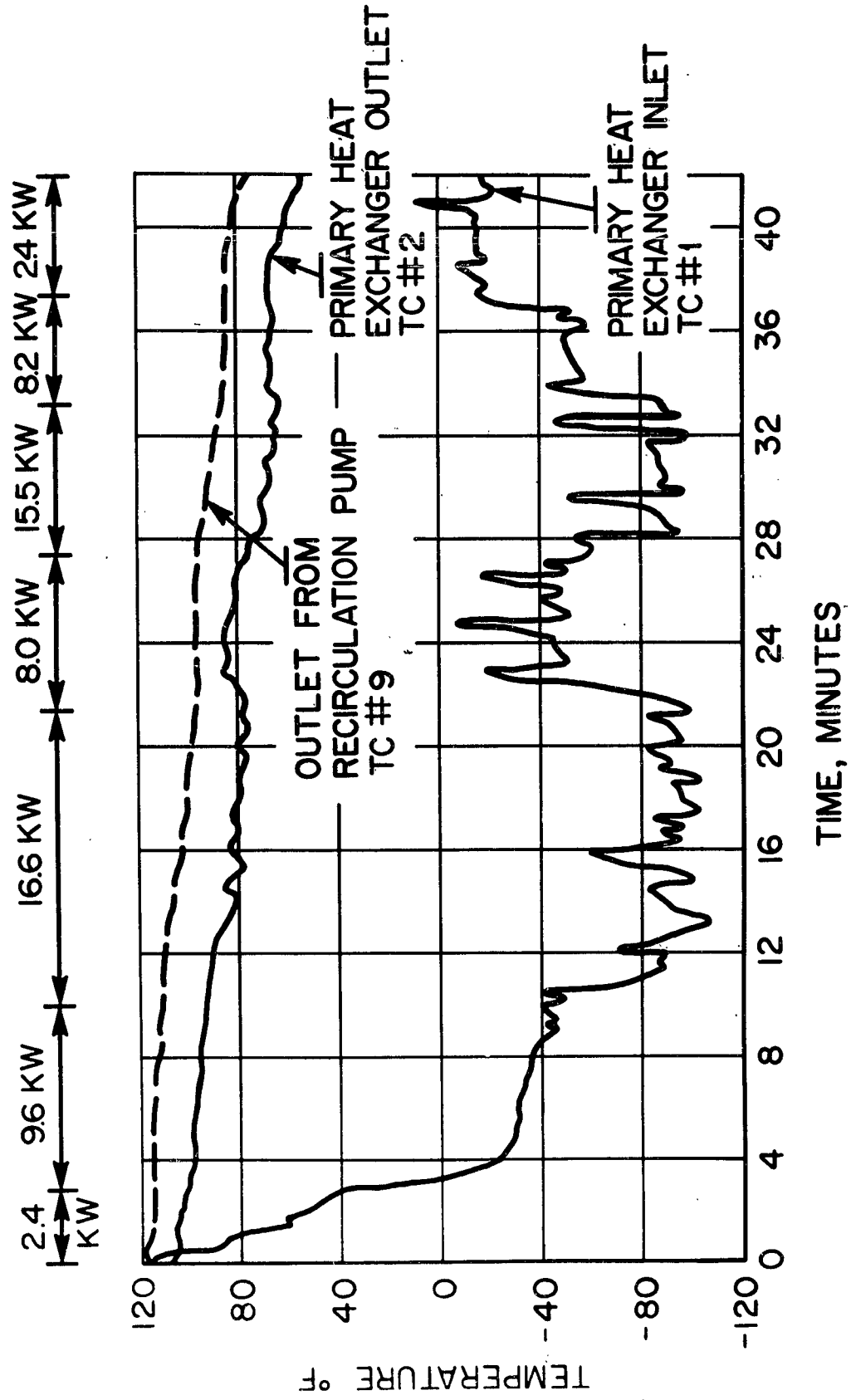


Figure 5. Comparison of ECS Heat Input and Absorption Rates

FLUID BULK TEMPERATURES IN THE HYDROGEN CIRCUIT



897

Figure 6. Hydrogen Circuit Test Temperature Characteristics

INSTANTANEOUS HEAT FLOW IN PRIMARY EXCHANGER

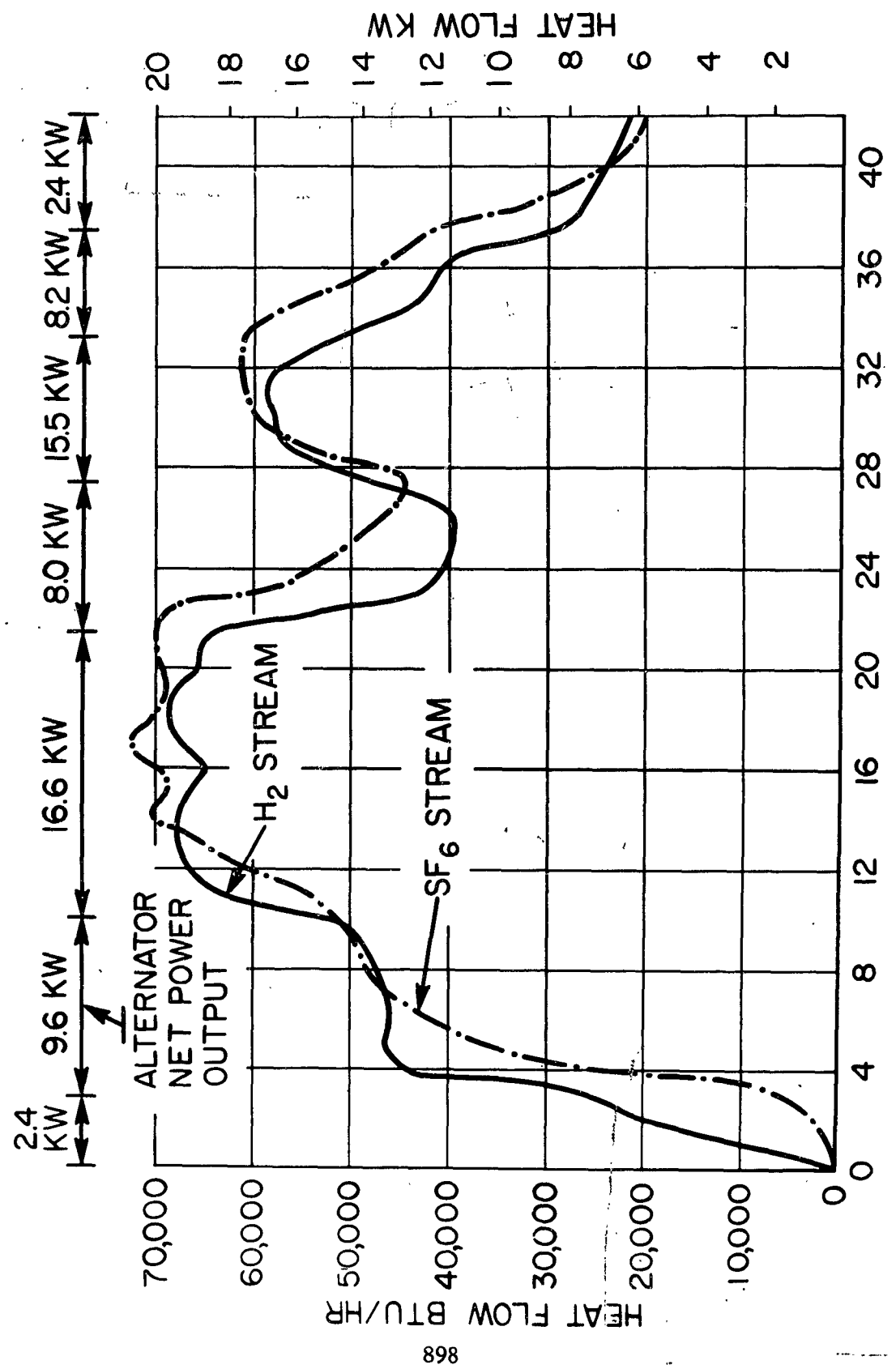


Figure 7. Transient Heat Flow Characteristics in the Primary Heat Exchanger

SECTION III
LIST OF ATTENDEES

List of Attendees

Non-Government Individuals and Organizations

Aeronca Manufacturing Corporation
Middletown, Ohio

R. Criss
R. Kievit
W. Niehaus

Aerospace Corporation
P. O. Box 95085
Los Angeles 45, California

J. Krisilas
K. R. Printiss
J. Smylie

Aeronutronics
Division of Ford Motor Co.
Ford Road
Newport Beach, California

Dr. R. C. Oliver

AiResearch Manufacturing Co.
9851 Sepulveda Boulevard
Los Angeles 45, California

W. Burriss
S. Coe
F. Green
J. Rousseau
R. Rydelek
A. Shaffer

AiResearch Manufacturing Co.
Dayton, Ohio

D. Derbes

Air Preheater Company
Four Gateway Center
Pittsburg 22, Pennsylvania

J. Arnold
T. Evans

Allied Research, Aracon Labs.
Virginia Road
Concord, Massachusetts

L. Wilkie

Amoco Chemicals Company
Seymour, Indiana

W. Proell

Arde, Inc.
100 West Century Road
Paramus, New Jersey

G. McKee

Avco Corporation
RAD Division
201 Lowell St.
Wilmington, Massachusetts

D. Grunditz
M. Rand

Armour Research Foundation
10 West 35th St.
Chicago 16, Illinois

D. Boies
A. Dravnieks
E. Fochtman
A. Gaynor

Atlantic Research Corporation
Alexandria, Virginia

B. Bartholomew
M. Markels
E. Schmitt, Jr.

Atlantic Research Corporation
379 W. First St.
Dayton, Ohio

J. Raney

Non-Government Individuals and Organizations (Cont'd)

Baird-Atomic, Inc.
95 Second Ave.
Waltham 54, Massachusetts

J. Wisentaner

Battelle Memorial Institute
505 King Ave.
Columbus 1, Ohio

J. Beach
R. Duffee

Beckman Instruments
2500 Harbor Boulevard
Fullerton, California

J. Dubin
Dr. T. Weber

Bell Aerosystems Company
131 North Ludlow St.
Dayton 2, Ohio

H. Dow

Bellcomm, Inc.
1737 L. St. NW
Washington 6, D. C.

T. Bottomley, Jr.

Bendix Systems Division
3300 Plymouth Road
Ann Arbor, Michigan

H. Collicott

Bendix Corporation
Pioneer-Central Division
Hickory Grove Road
Davenport, Iowa

W. Schelar
Dr. B. Sollami

The Boeing Company
Box 3707, Internal Box 22-68
Seattle, Washington

R. Ames
R. Evans

The Boeing Company
3801 South Oliver Road
Wichita 1, Kansas

D. Glaspie

The Boeing Company
3838-94th Ave., NE
Bellevue, Washington

W. Jahn

Brooks and Perkins, Inc.
1950 W. Fort St.
Detroit 16, Michigan

H. Young, Jr.

Chance Vought Corporation
Vought Astronautics
Dallas 1, Texas

R. Knezek
G. Whisenhunt

Chrysler Corporation
Airtemp Division
Dayton, Ohio

A. Ebert

Chrysler Corporation
P. O. Box 1827
Detroit 31, Michigan

R. Lower
R. Palmer

Non-Government Individuals and Organizations (Cont'd)

Douglas Aircraft Company
Thermo-Mechanical Section
Long Beach, California

R. Barker
W. Thayer

Douglas Aircraft Company
3000 Ocean Park Boulevard
Santa Monica, California

R. Byke
G. Fredrickson
R. Krueger
E. Mills
Dr. L. Rutz

-- Dynatech Corporation
Cambridge 39, Massachusetts

W. Welsh

Dynatech Corporation
P. O. Box 57
Centerville, Ohio

N. Wright

Fiberite Corporation
Winona, Minnesota

P. Fina

General American Trans. Corp.
MRD Division
Niles 48, Illinois

G. Remus
J. Zeff

General American Trans. Corp.
722 Maple Hill Drive
West Carrollton, Ohio

H. Thorpe

General Dynamics
Zone 594-70 Kearney Villa Road
San Diego, California

C. King

General Dynamics
West 5th St.
Pomona, California

D. Roberts

General Dynamics
R&D Dept.
Groton, Connecticut

H. Wallman

General Dynamics
Grants Lane
Ft. Worth, Texas

A. Warner, Jr.

General Electric
MSD
3198 Chestnut St.
Philadelphia, Pennsylvania

C. Dohner

General Electric Company
P. O. Box 8555
Philadelphia, Pennsylvania

E. Fried
A. Okamoto

General Electric Company
MSD
P. O. Box 8444
Philadelphia, Pennsylvania

A. Little

Non-Government Individuals and Organizations (Cont'd)

General Electric Company
King of Prussia, Pennsylvania

P. Petty

Goodyear Aircraft Corporation
Akron 15, Ohio

M. Braun
L. Cerreta
F. Whitmire

Grumman Aircraft Corporation
OAO Plant 5
Bethpage L. I. , New York

A. Bartilucci

Hamilton Standard Division
United Aircraft Corporation
Windsor Locks, Connecticut

C. Beal
D. Jennings
F. Morris
D. Putnam
Mr. Rennenger
C. Steinhagen
R. Trusch

International Electric Company
425-13th St. NW
Washington, D. C.

F. Fuller

Ionics, Inc.
1426 G. Street, N. W.
Washington 5, D. C.

S. McGriff

Isomet Corporation
433 Commercial Ave.
Palisades Park, New Jersey

F. Pollara

Itek, Corporation
10 Maguire Road
Lexington 74, Massachusetts

S. Berliner

Janitrol
Aero Division
Columbus 4, Ohio

M. Decker
P. Schumann
R. Troy

Jet Propulsion Laboratory
4800 Oak Grove Drive
Pasadena 3, California

B. Hagenmeyer
J. Flamondon

Joseph Kaye and Company
49 Hampshire Street
Cambridge 39, Massachusetts

C. Kemper

Kaman Aircraft
333 W. First St.
Dayton 2, Ohio

H. Stoodly

Lear Siegler, Inc.
Power Equipment Division
Elyria, Ohio

C. Eian

Lear Siegler, Inc.
Power Equipment Division
2640 St. Charles Ave.
Dayton, Ohio

I. Noland

Non-Government Individuals and Organizations (Cont'd)

Little, A. D., Inc.
Acorn Park
Cambridge, Massachusetts

C. Walker

Lockheed Missile and Space Co.
Sunnyvale, California

J. Baxter
H. Cohan
R. Jagow

Lockheed Georgia Company
Marietta, Georgia

R. Bready
L. Knight, Jr.

Lockheed Missile and Space Co.
Palo Alto, California

T. Olcott
J. Smith

Lockheed California Company
Pacoima, California

J. Werner

Mallory Metallurgical Co.
3029 E. Washington St.
Indianapolis, Indiana

R. Lmes

Martin Company
Baltimore 3, Maryland

R. Berner
E. Schumacher

Martin Company
Mail No. C-231
Denver, Colorado

E. Gebhardt

Martin Marietta
Aerospace Physics Laboratory
Orlando, Florida

J. Gonzalez

McDonnell Aircraft Company
Dept. 242, Lambert Field
St. Louis, Missouri

A. Bay
M. Peeples

Melpar, Inc.
Falls Church, Virginia

D. Rice

MSA Research Corporation
Callery, Pennsylvania

Dr. J. Mausteller
J. McDonough
M. McGoff
C. Palladino
R. Shearer

Minneapolis-Honeywell
2600 Ridgeway Road
Minneapolis 13, Minnesota

Mr. Janssen

North American Aviation, Inc.
Los Angeles International Airport
Los Angeles, California

A. Adkins
G. Campbell
R. Paselk

Non-Government Individuals and Organizations (Cont'd)

North American Aviation, Inc.
12214 Lakewood Boulevard
Downey, California

H. Nordwall
I. Saldinger
R. Sexton
K. Toups
R. Wallace
B. Wendrow
D. Woody

Northern Research & Engineering
Cambridge 39, Massachusetts

R. Bilger
T. Blatt
K. Ginwala

Northrop Space Laboratories
Hawthorne, California

A. Shlosinger

Nuclide Corporation
State College, Pennsylvania

D. Marshall

Perkin-Elmer Corporation
Electro-Optical Division
Norwalk, Connecticut

J. McCalla
W. McNeill
Dr. R. Noble
E. Watson

Pratt and Whitney Aircraft
1000 Asylum Ave.
Hartford, Connecticut

H. Johnson

Radio Corporation of America
Dayton 2, Ohio

M. Filcik

Radio Corporation of America
Camden, New Jersey

E. Lynch
J. Panas

Radio Corporation of America
Moorestown, New Jersey

P. Marsello

Radio Corporation of America
Princeton, New Jersey

H. Munson

Radio Corporation of America
Burlington, Massachusetts

P. Sacramone

Radio Corporation of America
7 Bearfort Way
Trenton 8, New Jersey

C. Usiskin

Raytheon Company
Bedford, Massachusetts

R. Joachim
L. Rayburn

Republic Aviation Corporation
Farmingdale, New York

T. Cuerou
R. Fiore
E. Kaplan
P. Markell
L. Rose
A. Schmidt
D. Ting

Non-Government Individuals and Organizations (Cont'd)

Reynolds Metals Company
Richmond 18, Virginia

B. Halcombe

Sanders Associates, Inc.
Nashua, New Hampshire

C. Skillas

Space Technology Laboratories
Redondo Beach, California

E. Bender
A. Optican
N. Richardson

Stewart-Warner Corporation
1514 Drover St.
Indianapolis, Indiana

D. Keener

Sundstrand Aviation
2480 West 70th Ave.
Denver 21, Colorado

R. Bailey

Thompson-Ramo Wooldridge
Cleveland 17, Ohio

A. Babinsky

United Aircraft Corporation
East Hartford 8, Connecticut

G. Peters
W. Biedler
H. Johnson

United Aircraft Corporate Systems Center
Farmington, Connecticut

J. Hanks

United Control Corporation
Redmond, Washington

G. Limberg

United Aircraft Products, Inc.
Dayton 8, Ohio

R. Campbell
W. Klank

U.S. Rubber Research Center
Wayne, New Jersey

E. Percarpio

United Nuclear Corporation
384 West First St.
Dayton 2, Ohio

H. Lake

United Nuclear Corporation
5 New Street
White Plains, New York

L. Malin

Vitro Laboratories
Silver Spring, Maryland

M. Koplou

Walter Kidde and Company, Inc.
Belleville 9, New Jersey

G. Hall
A. Rakowski
K. Traynelis

Webb Associates
Yellow Springs, Ohio

Dr. J. Fletcher
Dr. P. Webb

Other Department of Defense Activities

Navy

U. S. Naval Research Laboratories
Washington 25, D. C.

J. Christian
R. Saunders

Hq SSD (SSZB)
Los Angeles 45, California

Col. E. Cole
1/Lt. R. Kabel

Capt. George M. Elwinger
69 Beaumont St.
Sheppard AFB, Texas

Army

USAEROL
Sanitary Sciences Branch
Fort Belvoir, Virginia

D. Lindsten

Other Government Agencies

The Library of Congress
Washington 25, D. C.

E. Wise

National Aeronautics and Space Administration
NASA Manned Spacecraft Center
Houston, Texas

J. Ballinger
R. Frost
W. Guy
D. Derry

National Aeronautics and Space Administration
Flight Systems
Langley Field, Virginia

F. Booth

National Aeronautics and Space
Administration
1512 H Street
RBB
Washington 25, D. C.

A. L. Ingelfinger
C. Mook

National Aeronautics and Space
Administration
Langley Research Center
Hampton, Virginia

E. Mason
I. Shiflet
C. Wilson

National Aeronautics and Space
Administration
Lewis Research Center
Cleveland, Ohio

T. Mroz

Universities

Massachusetts Institute of
Technology
Cambridge, Massachusetts

G. Brown

Tufts University
Cambridge 39, Massachusetts
Dr. H. Choi

WPAFB Activities

ASBLCS (H. Seeler)	ASRMF (Col. Winebrenner)
ASNDGS (L. Bridge)	ASRMFE (W. Savage)
ASNDSA (D. Barnett)	ASRMFE (F. Thompson)
ASNDSA (C. Beatty)	ASRMFE-3 (T. Trumble)
ASNOSA (D. McLane)	ASRMFE-2 (W. Uhl)
ASNGI (L. Larson)	ASRMFE-2 (E. Thompson)
ASNGS (L. Lomas)	ASRMFE-2 (E. Zara)
ASNGS (A. Owen)	ASRMFE-2 (C. Feldmanis)
ASNPFE (W. Beyerlein)	ASRMFE-2 (J. Allen)
ASNSPT (G. Letton)	ASRMFE-2 (W. Fox)
ASNRP (E. Koepnick)	ASRMFE-2 (A. Gross)
ASNVCE (F. Humphrey)	ASRMFE-2 (F. Stidham)
ASNVCE (H. Wood)	ASROO (J. Schauweker)
ASNXXH (V. Clarke)	ASRSSV (H. Kasten)
ASR (Col. Hood)	ASRSSV (M. Talley)
ASR (P. Murray)	ASTEES (R. Noble)
ASRCEM (J. Charlesworth)	MCLI (G. Bowman)
ASRCNE (R. VanVliet)	MCLI (M. Franke)
ASRMD (H. Magrath)	MCLI (J. Hitchcock)
ASRMDD (R. Gatenbee)	MCLI (A. Shine)
ASRMDS (G. Maddux)	MRMPB (A. Prince)
ASRMFS (C. May)	MRMPR (J. Bowen)
ASRMPE (H. Velkoff)	MRMPR (L. Rock)
ASRMPR (J. Miller)	MRMPT (N. Poulos)

WPAFB Activities (Cont'd)

MRV (W. McCandless)

MROO (S. Birnbaum)

MRVSA (C. Metzger)

MRVSR (R. Bennett)

MRVSR (C. Roach)

TDES (E. Comfort)

1. Environmental control
2. CO₂ regeneration
3. Atmosphere control processes
4. IBM general heat transfer programs
5. Radiation heat transfer

- I. AFSC Project 6146
- II. Symposium Monitor:
E. B. Thompson
- III. Not avail fr OTS
- IV. In ASTIA collection

Aeronautical Systems Division, Dir/Aeromechanics, Flight Accessories Lab, Wright-Patterson AFB, Ohio. Rpt Nr. ASD-TDR-63-260. PROCEEDINGS OF THE FIRST SPACE VEHICLE THERMAL AND ATMOSPHERIC CONTROL SYMPOSIUM. Apr 63, 910p. incl illus, tables.

Unclassified Report

This report presents various papers concerning Space Vehicle Thermal and Atmospheric Control Systems. Papers include those presented or submitted by both industry and Governmental Agencies for the first Space Vehicle Thermal and Atmospheric Control Symposium held 12 and 13 February 1963. The symposium was sponsored by the Flight Accessories Laboratory, Aeronautical Systems Division of the Air Force Systems Command. The specific areas include: (1) Analysis of

(over)

1. Environmental control
2. CO₂ regeneration
3. Atmosphere control processes
4. IBM general heat transfer programs
5. Radiation heat transfer

- I. AFSC Project 6146
- II. Symposium Monitor:
E. B. Thompson
- III. Not avail fr OTS
- IV. In ASTIA collection

Aeronautical Systems Division, Dir/Aeromechanics, Flight Accessories Lab, Wright-Patterson AFB, Ohio. Rpt Nr. ASD-TDR-63-260. PROCEEDINGS OF THE FIRST SPACE VEHICLE THERMAL AND ATMOSPHERIC CONTROL SYMPOSIUM. Apr 63, 910p. incl illus, tables.

Unclassified Report

This report presents various papers concerning Space Vehicle Thermal and Atmospheric Control Systems. Papers include those presented or submitted by both industry and Governmental Agencies for the first Space Vehicle Thermal and Atmospheric Control Symposium held 12 and 13 February 1963. The symposium was sponsored by the Flight Accessories Laboratory, Aeronautical Systems Division of the Air Force Systems Command. The specific areas include: (1) Analysis of

(over)

environmental control systems by application of digital computer techniques, (2) Methods for Synthesizing Environmental Control Systems, (3) Atmosphere Control Problems in long duration space vehicle missions, (4) Control of contaminants present in closed atmospheres, (5) Various techniques for recovering oxygen from carbon dioxide, such as carbon dioxide reduction by hydrogen and photosynthesis, (6) Heat transfer in pool boiling as affected by an electric field, (7) Various techniques of thermal analysis of structures, (8) A general computer program for the determination of radiative interchange geometric configuration factors, and (9) Temperature control systems for satellites and probe vehicles.

environmental control systems by application of digital computer techniques, (2) Methods for Synthesizing Environmental Control Systems, (3) Atmosphere Control Problems in long duration space vehicle missions, (4) Control of contaminants present in closed atmospheres, (5) Various techniques for recovering oxygen from carbon dioxide, such as carbon dioxide reduction by hydrogen and photosynthesis, (6) Heat transfer in pool boiling as affected by an electric field, (7) Various techniques of thermal analysis of structures, (8) A general computer program for the determination of radiative interchange geometric configuration factors, and (9) Temperature control systems for satellites and probe vehicles.